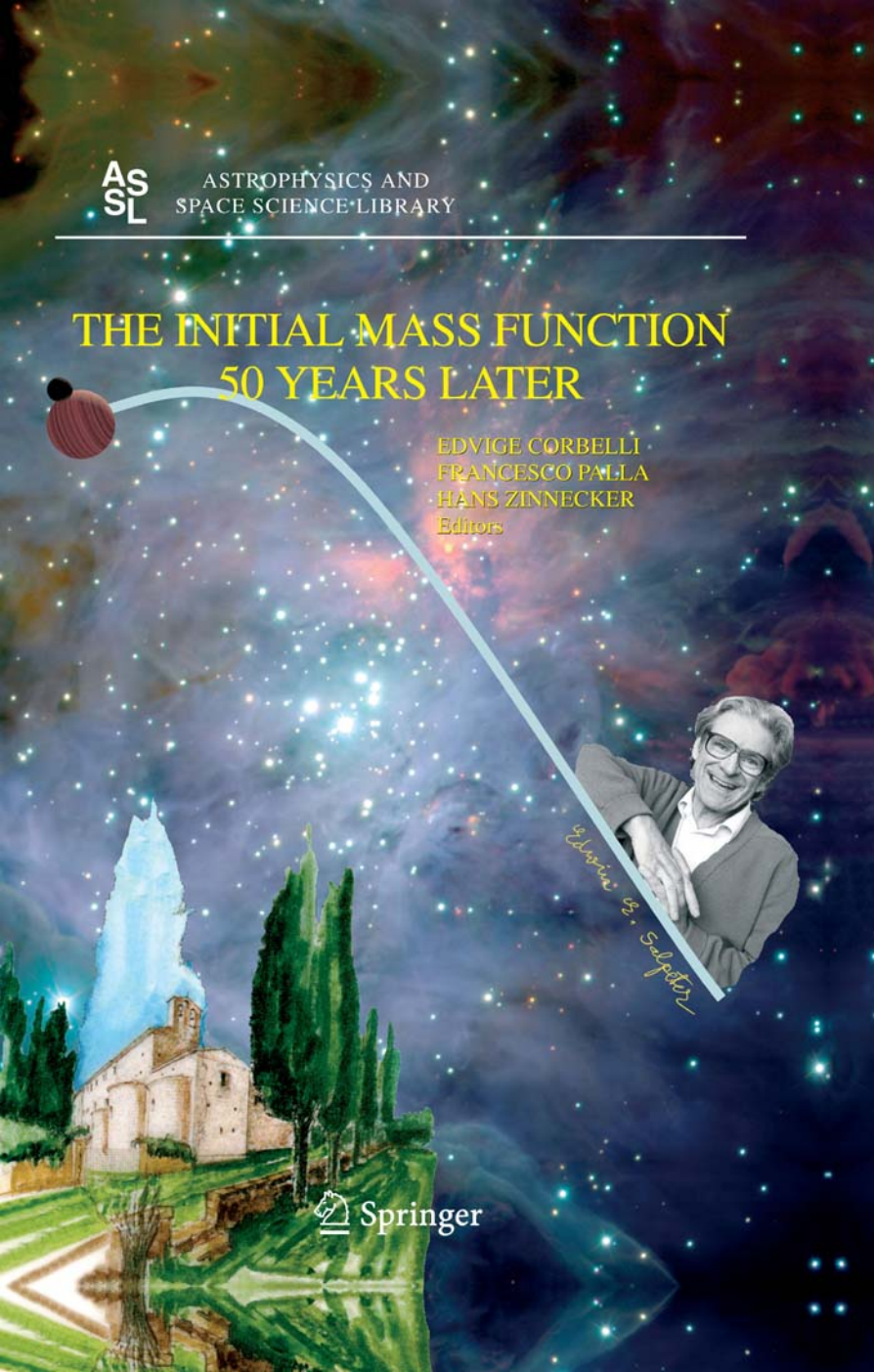
ASTROPHYSICS AND
SPACE SCIENCE LIBRARY
THE INITIAL MASS FUNCTION
50 YEARS LATER
EDVIGE CORBELLI
FRANCESCO PALLA
HANS ZINNECKER
Editors
Springer

THE INITIAL MASS FUNCTION 50 YEARS LATER

ASTROPHYSICS AND SPACE SCIENCE LIBRARY

VOLUME 327

THE INITIAL MASS FUNCTION 50 YEARS LATER

Edited by

EDVIGE CORBELLI
INAF Osservatorio Astrofisico di Arcetri, Firenze, Italy

FRANCESCO PALLA
INAF Osservatorio Astrofisico di Arcetri, Firenze, Italy

and

HANS ZINNECKER
Astrophysikalisches Potsdam, Germany

Springer

A C.I.P. Catalogue record for this book is available from the Library of Congress.

ISBN-10 1-4020-3406-7 (HB) Springer Dordrecht, Berlin, Heidelberg, New York
ISBN-10 1-4020-3407-5 (e-book) Springer Dordrecht, Berlin, Heidelberg, New York
ISBN-13 978-1-4020-3406-0 (HB) Springer Dordrecht, Berlin, Heidelberg, New York
ISBN-13 978-1-4020-3407-7 (e-book) Springer Dordrecht, Berlin, Heidelberg, New York

---

Published by Springer,
P.O. Box 17, 3300 AA Dordrecht, The Netherlands.

Printed on acid-free paper

springeronline.com

Printed in the Netherlands.

This book is dedicated to Ed,
from whom we have learned
so much, to his insight and
friendship.

Contents

Figure 1. Amazing view of a Spineto farmhouse.

Preface

The idea to celebrate 50 years of the Salpeter IMF occurred during the recent IAU General Assembly in Sydney, Australia. Indeed, it was from Australia that in July 1954 Ed Salpeter submitted his famous paper "The Luminosity Function and Stellar Evolution" with the first derivation of the empirical stellar IMF. This contribution was to become one of the most famous astrophysics papers of the last 50 years. Here, Ed Salpeter introduced the terms "original mass function" and "original luminosity function", and estimated the probability for the creation of stars of given mass at a particular time, now known as the "Salpeter Initial Mass Function", or IMF. The paper was written at the Australian National University in Canberra on leave of absence from Cornell University (USA) and was published in 1955 as 7 page note in the Astrophysical Journal Vol. 121, page 161.

To celabrate the 50th anniversary of the IMF, along with Ed Salpeter's 80th birthday, we have organized a special meeting that brought together scientists involved in the empirical determination of this fundamental quantity in a variety of astrophysical contexts and other scientists fascinated by the deep implications of the IMF on star formation theories, on the physical conditions of the gas before and after star formation, and on galactic evolution and cosmology.

The meeting took place in one of the most beautiful spots of the Tuscan countryside, far from the noise and haste of everyday life. Located south of Siena, the Abbazia di Spineto and its rural environs are still one of the few unspoiled venues in Tuscany, ideal for a few days of retreat and exchange. The setting of the farmhouses scattered around the Abbey allowed a full immersion in the unique landscape of Val d'Orcia, a land of hot springs, vineyards, ancient villages and solitary churches. Soon after this meeting, the Val D'Orcia has been inscribed on UNESCO's World Heritage.

The meeting was attended by some 110 participants from all over the world. The response from the community was overwhelming, a tribute to Ed Salpeter's unique combination of great science and personality. The sheer size of the present volume testifies to the desire to contribute both in the oral presentations and in print to the problem of the IMF after 50 years since Ed's seminal paper. All aspects of current research in this field have been thoroughly cov-

ered in extended reviews and in shorter contributions. The book starts with historical reviews of the development of the concept of the IMF from 1955 to 2005. Then, current determinations of the IMF in the galactic context, in the field, in stellar clusters and in star forming regions, are discussed with emphasis on fundamental issues such as the independence of the IMF on the environment and the completeness down to substellar masses - a field that has developed enormously in the last decade or so. Investigations of the properties of the IMF in nearby and more distant galaxies are presented in Part IV. The issue of the origin of the IMF starting from the physical conditions prevailing in atomic and molecular clouds and their subsequent fragmentation and collapse is reviewed both from the observational and theoretical point of view. The last section deals with the characteritistics of the IMF in the extreme conditions of the early Universe, a topic that is becoming more and more relevant for direct observations.

The spirit of the Conference is conveniently summarized by the expression "Chuzpah", a Hebrew word applied in Yiddish to Chuzpe and used in general to express the attitude of taking risks, with a little bit of impudence added on. This spirit comes directly from the beautifully written essay by Ed Salpeter and published in the Ann. Rev. Astron. Astrophys. (2002, Vol.40, p.1) where we find that Ed adopted this approach when he first attacked the problem of determining the stellar initial luminosity and mass functions. Many participants gave their own interpretation of the meaning of Chuzpah and its relevance for current studies of the IMF. As an illustration, we collect in the final Part of the book four Chuzpah talks that deal with matters not directly linked to the IMF, but in which Ed gave his usual basic contribution. It is an example that Chuzpah can be very useful at times!

The conference included a tour to the hot springs of Bagno Vignoni, a visit to the Abbey of Sant'Antimo, and to the fortress of Montalcino, home of the renowned Brunello wine. The *Confinensamble* performed a memorable concert inside the Spineto Abbey. The book contains many pictures of these special moments that we hope will convey the spirit. Apart from Hans, we like to thank Yuri Beletsky, Bernhard Brandl, Dimitris Gouliermis, and Manuela Zoccali for providing us with such beautiful shots.

The meeting would not have been successful without the charm, competence and efficiency of Mrs. and Mr. Cuccia-Tagliaferri and their staff. Special thanks to Beatrice and Cristina who helped us greatly before and during the conference. Finally, we wish to thank the support of INAF-Osservatorio Astrofisico di Arcetri and the skills of our system managers, Roberto Baglioni and Lorenzo Falai.

Edvige Corbelli, Francesco Palla & Hans Zinnecker

Firenze, November 2004

List of Participants

Adams Fred, *University of Michigan, USA* fca@umich.edu
Allen Anthony, *Academia Sinica, Taiwan*, tony@asiaa.sinica.edu.tw
Andersen Morten, *AIP-Potsdam, Germany*, mandersen@as.arizona.edu
André Philippe, *CEA-Saclay, France*, pandre@discovery.saclay.cea.fr
Barrado y Navascués David, *LAEFF/INTA, Spain*, barrado@laeff.esa.es
Basu Shantanu, *Univ. of West. Ontario, Canada*, basu@astro.uwo.ca
Bate Matthew, *University of Exeter, UK*, mbate@astro.ex.ac.uk
Beckwith Steven , *Space Telescope ScI, USA*, svwb@stsci.edu
Bessell Mike, *Australia Nat. Univ.-Weston, Australia*, bessell@mso.anu.edu.au
Beuther Henrik, *Harvard Smithsonian CfA, USA*, hbeuther@cfa.harvard.edu
Beletski Yury, *ESO-Garching, Germany*, ybialets@eso.org
Blitz Leo, *Univ. of California-Berkeley, USA*, blitz@astro.berkeley.edu
Bonnell Ian, *St Andrews University, UK*, iab1@st-andrews.ac.uk
Bouvier Jerome, *Obs. de Grenoble, France*, Jerome.Bouvier@obs.ujf-grenoble.fr
Brandl Bernhard, *Sterrewacht Leiden, The Netherlands*, brandl@strw.leidenuniv.nl
Brandner Wolfgang, *MPIA-Heidelberg, Germany*, brandner@mpia.de
Braun Robert, *ASTRON, The Netherlands*, rbraun@astron.nl
Bresolin Fabio, *Inst. for Astronomy-Hawaii, USA*, bresolin@ifa.hawaii.edu
Bromm Volker, *Harvard Observatory, USA*, vbromm@cfa.harvard.edu
Brunt Christopher, *UMass-FCRAO, USA*, brunt@fcrao1.astro.umass.edu
Burningham Ben, *University of Exeter, UK*, bgb@astro.ex.ac.uk
Calura Francesco, *Università di Trieste, Italy*, fcalura@ts.astro.it
Cartwright Annabel, *Cardiff University, UK*, Annabel.Cartwright@astro.cf.ac.uk
Chabrier Gilles, *Ecole Normale Lyon, France*, chabrier@ens-lyon.fr
Chen Hui-Chen, *Institute of Astr.-Taoyuan, Taiwan*, s8229003@cc.ncu.edu.tw
Chernoff David, *Cornell University, USA*, chernoff@astro.cornell.edu
Chiosi Cesare, *Università di Padova, Italy*, chiosi@pd.astro.it
Clarke Cathie, *Institute of Astr.-Cambridge, UK*, cclarke@ast.cam.ac.uk
Corbelli Edvige, *Osservatorio di Arcetri, Italy*, edvige@arcetri.astro.it
D'Antona Francesca, *Osservatorio di Roma, Italy*, dantona@mporzio.astro.it
De Marchi Guido, *ESA-Noordwijk, The Netherlands*, gdemarchi@rssd.esa.int
Dickey John, *University of Minnesota, USA*, John.Dickey@utas.edu.au
Elmegreen Bruce, *IBM Watson Res. Center, USA*, bge@watson.ibm.com
Falai Lorenzo, *Osservatorio di Arcetri, Italy*, falai@arcetri.astro.it
Feigelson Eric, *Penn State University, USA*, edf@astro.psu.edu

Ferrara Andrea, *SISSA/ISAS, Italy*, ferrara@sissa.it
Figer Donald, *Space Telescope ScI, USA*, figer@stsci.edu
Flaccomio Ettore, *Osservatorio di Palermo, Italy*, ettoref@oapa23.astropa.unipa.it
Glassgold Al, *Univ. of California-Berkeley, USA*, aglassgold@astro.berkeley.edu
Goodwin Simon, *Cardiff University, UK*, Simon.Goodwin@astro.cf.ac.uk
Gouliermis Dimitrios, *MPIA-Heidelberg, Germany*, dgoulier@mpia.de
Grebel Eva, *University of Basel, Switzerland*, grebel@astro.unibas.ch
Haardt Francesco, *Università dell'Insubria, Italy*, haardt@mib.infn.it
Harayama Yohei, *MPIE-Garching, Germany*, yohei@mpe.mpg.de
Hartmann Lee, *Smithsonian Astrophysical Obs., USA*, lhartmann@cfa.harvard.edu
Hennebelle Patrick, *Observatoire de Paris, France*, patrick.hennebelle@ens.fr
Heyer Mark, *University of Massachusetts, USA*, heyer@astro.umass.edu
Hoffman Lyle, *Lafayette College, USA*, hoffmang@lafayette.edu
Hollenbach David, *NASA Ames Res.C., USA*, hollenba@ism.arc.nasa.gov
Hony Sacha, *ESA/ESTEC, The Netherlands*, shony@rssd.esa.int
Houck James, *Cornell University, USA*, jrh13@cornell.edu
Inutsuka Shu-ichiro, *Kyoto University, Japan*, inutsuka@tap.scphys.kyoto-u.ac.jp
Klessen Ralf, *AIP-Potsdam, Germany*, rklessen@aip.de
Kroupa Pavel, *Sternwarte Bonn, Germany*, pavel@astro.uni-bonn.de
Lada Charles, *Smithsonian Astrophysical Obs., USA*, clada@cfa.harvard.edu
Larson Richard, *Yale University, USA*, larson@astro.yale.edu
Leitherer Claus, *Space Telescope ScI, USA*, leitherer@stsci.edu
Lucatello Sara, *Osservatorio di Padova, Italy*, lucatello@pd.astro.it
Luhman Kevin, *Harvard Smithsonian CfA, USA*, kluhman@cfa.harvard.edu
Martín Eduardo, *Inst. Astr. de Canarias, Spain*, ege@ll.iac.es
Massi Fabrizio, *Osservatorio di Arcetri, Italy*, fmassi@arcetri.astro.it
McCaughrean Mark, *AIP-Potsdam, Germany*, mjm@aip.de
Melnick Gary, *Harvard-Smithsonian CfA, USA*, gmelnick@cfa.harvard.edu
Meyer Michael, *University of Arizona, USA*, mmeyer@as.arizona.edu
Monin J.-L., *Obs. de Grenoble, France*, Jean-Louis.Monin@obs.ujf-grenoble.fr
Myers Phil, *Smithsonian Astrophysical Obs., USA*, pmyers@cfa.harvard.edu
Nakamura Fumitaka, *Niigata University, Japan*, fnakamur@ed.niigata-u.ac.jp
Oey Sally, *Lowell Observatory, USA*, Sally.Oey@Lowell.edu
Omukai Kazu, *NAO, Osawa, Japan*, omukai@th.nao.ac.jp
Onishi Toshikazu, *Nagoya University, Japan*, ohnishi@a.phys.nagoya-u.ac.jp
Pacini Franco, *Università di Firenze, Italy*, pacini@arcetri.astro.it
Padoan Paolo, *University of California-San Diego*, USA, ppadoan@ucsd.edu
Palla Francesco, *Osservatorio di Arcetri, Italy*, palla@arcetri.astro.it
Panagia Nino, *ESA/Space Telescope ScI, USA*, panagia@stsci.edu
Persi Paolo, *IASF/CNR-Roma, Italy*, persi@rm.iasf.cnr.it
Petr-Gotzens Monika, *ESO-Garching, Germany*, mpetr@eso.org
Portinari Laura, *Tuorla Observatory, Finland*, lportina@tac.dk

Prisinzano Loredana, *Osservatorio di Palermo, Italy*, loredana@astropa.unipa.it
Prusti Timo, *ESA/ESTEC, The Netherlands*, Timo.Prusti@rssd.esa.int
Reid Neill, *Space Telescope ScI, USA*, inr@stsci.edu
Renzini Alvio, *ESO-Garching, Germany*, arenzini@eso.org
Riddick Fiona, *University of Oxford, UK*, fcr@astro.ox.ac.uk
Robberto Massimo, *Space Telescope ScI, USA*, robberto@stsci.edu
Romaniello Martino, *ESO-Garching, Germany*, mromanie@eso.org
Romano Donatella, *Osservatorio di Bologna, Italy*, romano@bo.astro.it
Salpeter Edwin, *Cornell University, USA*, ees12@cornell.edu
Salvati Marco, *Osservatorio di Arcetri, Italy*, salvati@arcetri.astro.it
Scalo John, *University of Texas, USA*, parrot@astro.as.utexas.edu
Schaerer Daniel, *Geneva Observatory, Switzerland*, daniel.schaerer@obs.unige.ch
Schneider Raffaella, *Osservatorio di Arcetri, Italy*, raffa@arcetri.astro.it
Shaviv Giora, *Technion, Israel*, gioras@physics.technion.ac.il
Shang Hsien, *Academia Sinica, Taiwan*, shang@asiaa.sinica.edu.tw
Shu Frank, *National Tsing Hua University, Taiwan*, shu@mx.nthu.edu.tw
Silk Joe, *University of Oxford, UK*, silk@astro.ox.ac.uk
Stamatellos Dimitris, *Cardiff University, UK*, D.Stamatellos@astro.cf.ac.uk
Stauffer John, *California Insitute of Technology, USA*, stauffer@ipac.caltech.edu
Stolte Andrea, *University of Florida, USA*, stolte@astro.ufl.edu
Tantalo Rosaria, *Università di Padova, Italy*, tantalo@pd.astro.it
Terzian Yervant, *Cornell University, USA*, terzian@astrosun.astro.cornell.edu
Testi Leonardo, *Osservatorio di Arcetri, Italy*, lt@arcetri.astro.it
Tosi Monica, *Osservatorio di Bologna, Italy*, tosi@bo.astro.it
Vazquez-Semadeni Enrique, *UNAM-Morelia, Mexico*, e.vazquez@astrosmo.unam.mx
Vreeswijk Paul, *ESO-Santiago, Chile*, pvreeswi@eso.org
Walterbos René, *New Mexico St. Univ., USA*, rwalterb@nmsu.edu
Weidner Carsten, *Sternwarte-Bonn, Germany*, weidner@astrophysik.uni-kiel.de
Whitworth Anthony, *Cardiff University, UK*, ant@astro.cf.ac.uk
Wong Tony, *CSIRO Australia Telescope, Australia*, Tony.Wong@csiro.au
Wyse Rosemary, *Johns Hopkins University, USA*, wyse@pha.jhu.edu
Zinnecker Hans, *AIP-Potsdam, Germany*, hzinnecker@aip.de
Zoccali Manuela, *Pontificia Universidad Catolica, Chile*, mzoccali@astro.puc.cl

I

THE IMF CONCEPT THROUGH TIME

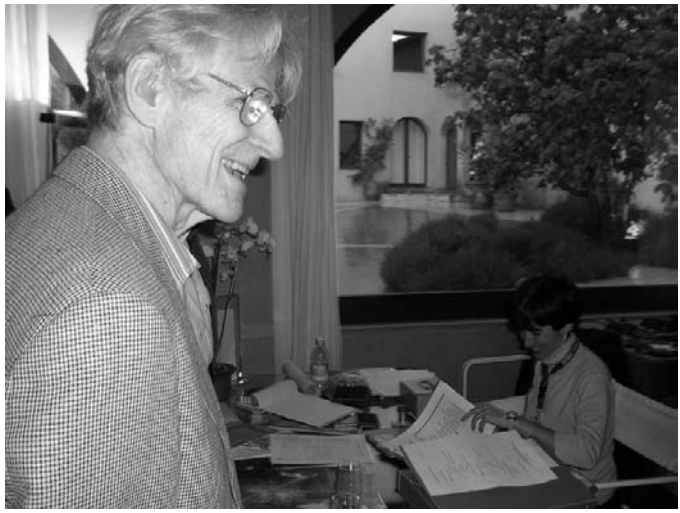

Figure 2. Ed Salpeter and Edvige at registration desk.

Figure 3. Ed Salpeter giving the historical talk.

INTRODUCTION TO IMF@50

Edwin E. Salpeter
Department of Astronomy, Cornell University, U.S.A.
ees12@cornell.edu

Abstract I submitted my IMF paper in 1954 from a stay in Australia , but the seeds of the paper stem from the Ann Arbor Astrophysics Summer School in 1953. After reminiscing about the pros and cons of that paper, I also mention an aftermath at a Vatican Conference in 1957. I conclude with my advice to young scientists that they should NOT separate science and politics, but should be involved in national issues.

1. The 1953 Ann Arbor Summer School

I submitted my IMF paper almost exactly 50 years ago and I want to give some background to that paper. I should distinguish between "motivation" (why do you want to do it?) and "technique" (how can you do it?), but the two get mixed up and have multiple sources. The paper was written in 1954 during a one year stay at the (then almost brand-new) Australian National University in Canberra, Australia. However, I mainly have to talk about the beginnings in 1953 in the U.S.A. and a little about the aftermath at a Vatican Conference in 1957.

Early in 1953 I was preparing to write a book on "Energy Production in Stars" for Wiley/Interscience (I have missed the deadline of 1955 by a little already). At the time I considered myself purely as a theoretical nuclear physicist, not an astrophysicist, and the book was to be mainly on thermonuclear reactions plus nuclear photo-disintegrations. I expected that real astrophysicist would apply the results to real astronomy, but I also hoped that some physicists might read the book. For that purpose I felt I had to put some elementary astronomy in the book, including stellar structure and statistics, even though I knew little of that myself at the time. Learning some astronomy at the ripe old age of 28 was made easier by Martin Schwarzschild of Princeton giving patient and insightful answers to my many naive questions. Schwarzschild and Hoyle, both separately and together, had recently started to calculate stellar evolution away from the main sequence and into the red giant branch. It would take a

E. Corbelli et al. (eds.), The Initial Mass Function 50 Years Later, 3–10.

while before the calculations became fully quantitative, but it was already clear that stars leave the main sequence rapidly when they have burned roughly 12% of their hydrogen, almost independent of the mass.

My incentive to give myself a crash course in stellar astronomy in early 1953 was enhanced by the fact that I had to give a course that summer on "energy production in stars", with similar aims to my planned book. My lectures were at the Ann Arbor Astrophysics Summer School at Michigan University. This summer school was probably the most important educational experience in my whole career, with brilliant and trustworthy "bigshots" like Walter Baade and George Gamow, but also youngsters like myself (see Fig. 1).

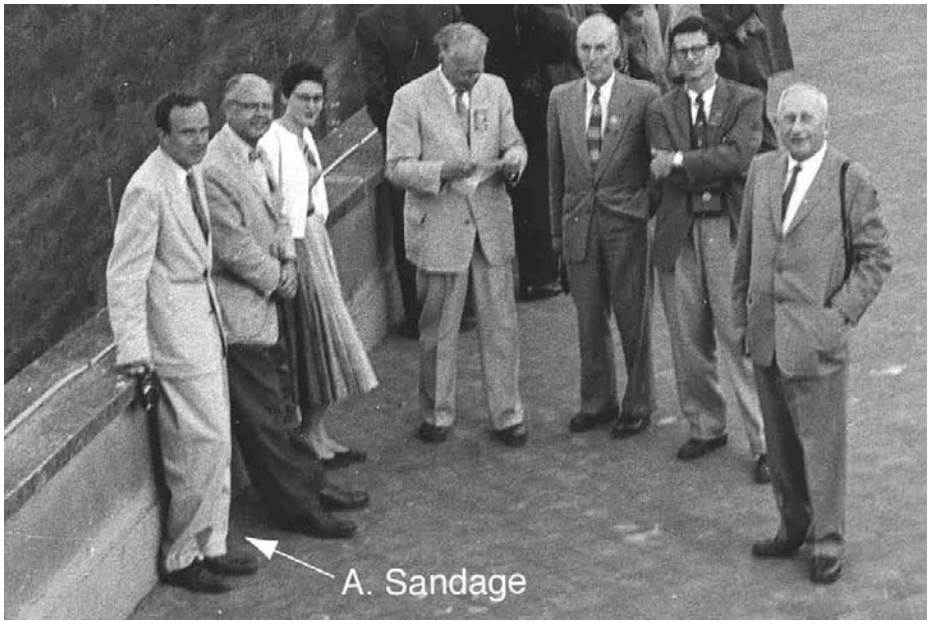

Figure 1. Some participants at the Ann Arbor summer school, 1953. Ed Salpeter is the second one from the right.

As Oppenheimer once said in a different context: "What we don't understand, we explain to each other". That summer school was instrumental for my IMF paper the following year in at least two ways. One pedagogical impetus came from my wanting to put together in one enormous Table, both for the book and the lectures, all the properties of main sequence stars as a function of mass M from the smallest to the largest. These properties had to include both visual and bolometric luminosity, central and surface temperature, and the radius. I used the observations and calculations then available, but I mainly had to use *Chuzpah*, or gall or guts, or unashamed guesswork. The real experts in the field would not have wanted to publish such a Table, since they knew the

enormous uncertainties at the time. As a mere outsider I did not mind making enormous extrapolations and guesses. Another quantity I put in that Table in 1953 was τ_H(M), the hypothetical lifetime a star of mass M would have if it could burn 100% of its H-mass at constant luminosity. It was not difficult for me to postulate, one year later, that the actual main sequence lifetime τ_{MS}(M) is simply $0.12 \times \tau_H$(M).

Walter Baade explained to us simply and forcefully about the two stellar populations, with all population II stars of the same age, essentially equal to the age T_0 of our Galaxy, which was then estimated to be about 6 billion years old. The uniqueness of the stellar ages explained the sudden upper turnoff of the population II main sequence, but Baade told us that population I stars had all ages from zero to T_0. I had also vaguely wanted to teach myself about stellar statistics for Ann Arbor, but had not gotten around to this yet. However, I now got a very strong impetus and motivation, even though in a negative way, from George Gamow.

Gamow was giving a course of lectures at the Ann Arbor summer school, talked about almost anything in any branch of science (even on the genetic code) and was most stimulating throughout. He (and his younger colleagues Alpher and Hermann) had already elucidated how to make the very light elements early after "The Big Bang". He was still hoping to make all the elements up to iron in a big bang scenario, although he knew it was difficult. In particular he did not believe that these elements were made in population I stars. The following is the most relevant paragraph of Gamow's lecture notes, verbatim but with my underlining: "Gamow considered the possibility that population II stars have original abundances of elements, and that population I stars have a mixture of elements which includes the original abundances and the abundances of elements formed in stars. This theory is excluded, however, by the observation that not enough stars have contributed much to interstellar matter during the age of the universe. The interstellar matter is of original pre-stellar composition".

Of various kinds of motivations, a powerful one happens when an expert, whom you otherwise trust, makes an assertion which you do not believe. I just did not believe that the birthrate of massive main sequence stars (which are needed to make medium and heavy elements) over the last 6 billions was negligibly small. For my big main sequence Table I had already estimated (also very approximately) the main sequence lifetime as a function of mass and it was quite short for the very massive stars. However, to calculate an Initial Mass Function, I also needed observational data on the main sequence luminosity function.

2. The 1954 IMF Paper

Very soon after the Ann Arbor summer school I flew to Australia, with my wife Mika and new-born daughter Judy, to spend a year at the Australian National University (ANU) in Canberra. This new University was located in down-town Canberra, did not have an Astronomy Department and I was in the Physics Department. Fortunately, the Mt. Stromlo Observatory, although not officially associated with the ANU, was fairly close geographically and I made many trips to its library to learn about stellar statistics.

One curious bottleneck was the confusion between the main sequence (MS) luminosity function and the red giant (RG) luminosity function. The visual luminosity function was already known fairly well observationally, for MS and RG combined. The colors of the two types of stars are radically different, so two-wavelength photometry could distinguish them easily, but combining this with painstaking statistics counts was tedious. One frightening warning came from observations of stellar population II, where photometry had already shown a sharp upper cut-off to the MS (not counting the small number of blue stragglers): The *total* visual luminosity function for population II above the cut-off, although coming purely from RG (plus the horizontal branch), was qualitatively similar to that for population I, which included the MS! It took a particularly large dose of *Chuzpah* for me to estimate what fraction of the population I luminosity came from main sequence stars, but that estimate was not too far from the actual fraction.

I am somewhat ashamed of two other pieces of Chuzpah, or plain sloppiness:

1 Although it was already known that the distribution of stars perpendicular to the galactic plane depends on stellar mass, I ignored that fact. I simply made no real distinction between the luminosity function within a fixed distance from the Galactic plane and that for the extended galactic disk.

2 My worst sloppiness was to assume that the absolute rate of star formation has been constant over the last T_0 years. Assuming a constant rate per existing gas mass would have been more reasonable, even at the time, and would have led to a gas mass exponentially decreasing with time. The later discussions by Maarten Schmidt and others that the star formation rate may depend on an even higher power of gas column density was “beyond the scope” of my paper, but I could easily have handled an exponentially decreasing gas supply. For that calculation, I would have needed an observational value for the present-day ratio of gas to star masses, but again I was scared about not knowing how things changed with distance from the Galactic Plane.

There was a third piece of *Chuzpah* I was proud of 50 years ago and I am even prouder of today: As mentioned, the age of the Galaxy T_0 was then thought to be about 6 billion years, more than a factor of two too small. With τ_{MS}(M) the main sequence lifetime as a function of mass M, the values of mass and the "turn-off magnitude" where τ_{MS}(M)=T_0 was obviously important for my calculation. The main idea of my paper was to say that, for brighter population I stars, the total initial luminosity function is larger than the observed one by the factor of T_0/τ_{MS}(M). Of course I was worried that the 1954 value for T_0, as well as my function τ_{MS}(M), were inaccurate, so I invented a "fudge factor". This fudge factor effectively eliminated the numerical value of T_0 from the calculation and instead took an empirical "turn-off magnitude" from the observational data for stellar population II.

For comparison with theories of star formation the shape of the IMF itself is most important, but I was more interested in two applications. The most important for me involved the integral of IMF times stellar mass, which showed that the mass from all stars that have died (presumably now in the interstellar medium) almost equals (about 80%) the mass in existing stars. Although I did not mention George Gamow, this near equality was my negation of the paragraph I quoted above. The other result involved the integral of the IMF itself and showed that the number of stars that have died is about 12% of the number of existing stars. We did not think of neutron stars or black holes in those days, so I identified those "dead stars" with present day white dwarfs. Since white dwarfs were estimated to constitute about 10% of all existing stars, I was rather pleased with this result.

3. The 1957 Vatican Conference

A definitive aftermath to my 1954 IMF work was a conference at the Vatican in May 1957 on "Stellar Populations". The theoretical discussion was dominated by Fred Hoyle, but the observational half was more important in my opinion. Much of what the conference did was to vindicate Walter Baade's general ideas on the two stellar populations, but the most important observational talks were by Allan Sandage (see Fig. 2).

Sandage himself had done much definitive work over the previous few years and some of this impinged directly on the IMF. The main sequence and its turn-off for stellar population II globular clusters was of course well known already in 1953, but by now it had also been observed for a number of population I star clusters of various shorter ages. Fig. 3 is a modification of one of Sandage's figures at the Vatican conference.

Once we had the main sequence for a young cluster, the observed luminosity function for the cluster of course gave the initial luminosity function up to a certain mass. Compilations for many young clusters thus gave fairly direct

Figure 2. Inside the Vatican, May 1957. Ed Salpeter is in the center of the front row.

evidence that my IMF was correct at least in a very qualitative way, but now opened up the possibility for more quantitative work. The related question of the dependence of the star formation rate on interstellar gas abundance was also discussed.

I did not pay much attention to theories of star formation after 1957, partly because it was - and still is - such a difficult problem. Partly, my reluctance to tackle the theory stemmed from my belief that more progress would come from observations. In particular, although I was hoping that my IMF was roughly

right on the average, I expected that it would vary extremely strongly with varying conditions. For instance, I (and others) thought that massive stars would be strongly favored in regions of strong turmoil and possibly in regions of high gas column density in general and the young Galaxy in particular. These are just the controversies which we will be debating here, and there surely will be variations but just what is still not clear. This uncertain state of affairs has been good for me personally over the last 50 years - in the absence of clearcut answers, my IMF still gets quoted! However, this absence has been bad for the theorists - we need clearcut variations to decide between rival theories.

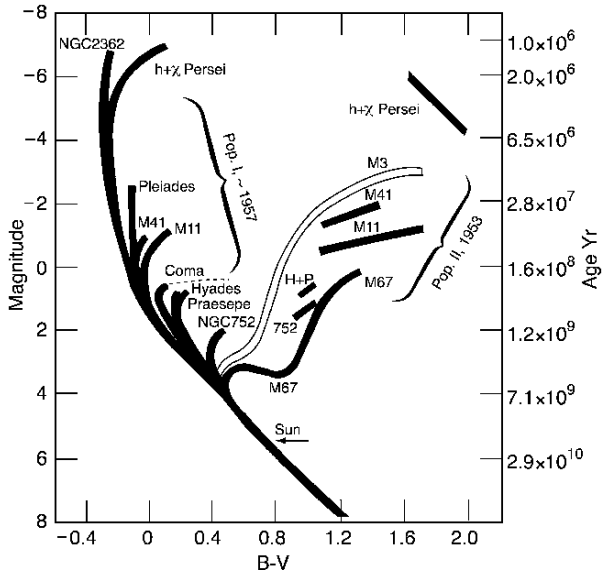

Figure 3. Adapted from a slide by A. Sandage, May 1957.

4. The ANU versus Cornell and the threat of fascism

During my year 1953/54 in Canberra I had to decide between two Universities. I had been offered the newly established Chair of Theoretical Physics at the Australian National University, but I had also been offered tenure back at Cornell University. Although I submitted my IMF paper from the ANU, this paper actually pushed me towards Cornell: Theoretical physics meant quantum electrodynamics and High Energy Theory in those days and as the chairman of a department (albeit a small one) I just could not goof off into Astronomy. As I mentioned earlier, I had thought of my previous nuclear astrophysics work as basically theoretical physics, to be applied to astronomy by others. My IMF

work, on the other hand, was getting me into real astronomy and by now I was hooked. At Cornell I was also in a physics department, but the atmosphere was more flexible for branching out into other fields.

There were other considerations besides my own purely academic ones. My late wife, Mika, had just gotten her Ph.D. in psychobiology, so she was at the beginning of her career. Unfortunately, male chauvinism was pretty bad at the time both at the ANU and at Cornell, but a little bit less so at Cornell. There was also real politics, with Joe McCarthyism pretty rampant in the U.S.A. just before we came to Australia. There was no equivalent political hysteria in Australia in the early fifties, but the "White Australia Policy" sounded pretty racist. In the middle of 1954 I judged that McCarthyism was on the way out, but the White Australia Policy was likely to last a long time. So, on the political side also we opted for the USA and we returned permanently to Cornell.

The political decision in favor of the USA is not so clearcut with 50 years of hindsight: Joe McCarthyism did indeed disappear fairly quickly, but the disaster of Vietnam took its place and, on the other hand, Australia's immigration policies became more benign surprisingly quickly. Although I am still not sure of my wisdom 50 years ago, I am sure of my advice to young US scientists for the future :

Work hard on star formation, but work even harder on getting involved on science policy and national technical issues, which will help to maintain democracy. I may be a minority of one in advocating that one should NOT separate science and politics—partly because I am old enough to remember the Weimar Republic before 1934: Citizens there were not against democracy, they just did not want to get involved in politics, so they lost democracy and gained World War II. The end result was particularly disastrous for science: Germany's industry recovered surprisingly quickly after the war, but basic science took very, very much longer to recover. Let us not allow politics to demolish democracy and basic science now or in the future.

ED, ME, AND THE INTERSTELLAR MEDIUM

Steven V.W. Beckwith
Space Telescope Science Institute, 3700 San Martin Drive, Baltimore, MD 21204, USA
svwb@stsci.edu

Abstract Many of the young scientists at Cornell have had the unique privilege of working with Ed Salpeter in research and teaching. But working with genius has its unique challenges as well. His profound influence on several generations of scientists came from a special approach that shaped our department, our science, and our lives and can be described only by those who experienced it first hand.

Ed and I first met in the winter of 1977. I had come to Cornell to interview for a job as an assistant professor of astronomy. It was one of those famous Ithaca winters where an unusually deep snowfall created drifts over 8 feet high, and the temperature had dropped close to 0 °F during the time of my visit. I had flown out from Los Angeles, my blood thin after five years in the desert climate of the southwest. It was my first job interview. The bleak weather added strongly to the sense of dread that I felt approaching the illustrious faculty in astronomy, a task for which I was completely unsuited.

Before my colloquium, Jim Houck took me aside to tell me what to expect and how to comport myself before his colleagues. My biggest worries were Tommy Gold and Ed Salpeter, both of whom I was sure knew much more about the subject matter of my colloquium than I did.

"Tommy's alright," Jim said. "He will come up with his own theory to explain your observations. Just make sure you don't contradict him right away."

"What about Ed?" I asked.

"Oh, Ed would never embarrass you publicly," Jim assured me. "He will get you in private."

Although not quite the assurance I was hoping for, his predications turned out to be right on the money. Tommy had a novel explanation for my data, somewhat at odds with Occam's razor but still entirely consistent with observation, and Ed asked a softball question at the end. Later in the privacy of his office, Ed probed gently to see if I had really done my homework and, apparently satisfied, left me alone. It turned out that he had already thought about the subject five years previously in some detail and had no need to undercut

E. Corbelli et al. (eds.), The Initial Mass Function 50 Years Later, 11–18.

me while I was under great pressure. When I arrived at the department later in the year—the interview having gone well enough, it seems—he was quick to engage me in conversations about my research revealing insight that I had not encountered among any of the other pundits who commented on the work.

The approach of quiet confidence belied a temperament perfectly suited to Cornell setting the tone for what turned out to be a very collegial department despite the enormous accomplishments and rivalries of the senior faculty. Ed guided the younger scientists gently but firmly, never letting us getting away with sloppy reasoning or intellectual dishonesty but making sure to be supportive of us who had a true passion for science. His own passion for ideas and raw creativity was magnetic. It raised the level of performance of all who were around him.

A few years later, Ed generated a second terrifying moment that turned out to be a fairly typical rite of passage for those of us on the tenure track and, incidentally, sets up one of the science areas discussed below. In the fall semester of 1984, Ed and I co-taught the graduate course on the Interstellar Medium, Astronomy 555. The rules were such that we figured out Ed's travel schedule first, I filled in on the dates he was out of town, and we split whatever lectures were remaining (not many, as I recall.)

Early in the course, Ed delivered a long, erudite lecture on the formation of dust in the atmospheres of evolved stars, a lecture filled with equations I struggled to understand, explained in a manner that I could not follow. One thing I did grasp is that his complex theory for creating dust in winds coming from the stars was spherically symmetric, meaning the matter came off the stellar surfaces in shells. Later in the lecture, he said that he did not really believe the winds were spherically symmetric but were more likely to be clumpy and irregular as might result from convective overshoot in the layers beneath the photospheres. Immediately following the lecture, he left for an extended trip to another continent.

I was terrified. I had almost no idea how to explain the details of what he said. I did not even follow several of his explanations, and it was obvious that none of the students did either. Yet, they were going to come to me for help, thus forcing me, an instructor in the course, to admit that I was lost. I struggled with my notes for a while before finally deciding to fess up, admit to the students that they would have to wait for Ed's return if they had any questions about the material, and ask their forgiveness. My friend and fellow faculty member, Ira Wasserman, had the same experience teaching stellar structure with Ed but having greater pride in his abilities worked a 20 hour weekend to understand every detail from first principles for the students' questions when Ed left after his lecture on a Friday.

Ed was the primary glue that held the department together at the senior level. He took great care to match people as potential collaborators and introduced

me early on to Antonella Natta, who was to become a collaborator for more than 10 years and a friend for life. He stimulated our interest in the interstellar medium, started us out on two nice problems that we worked out together and published. He eventually turned us loose when he was satisfied we were ready to venture forth on our own. A second signature of his style was his ability to sense who would make good intellectual partners and how those collaborations would maintain the collegiality at Cornell we younger scientists prized. Rank was not so important; ability and ideas counted. Most importantly, he softened the potential friction that could develop between the strong personalities of Tommy, Carl Sagan, and Frank Drake, an intimidating group for the junior faculty, one that could easily have made our work more difficult than it already was.

Ed's science, of course, was nothing short of phenomenal. Its combination of breadth and depth are unequalled by all but a handful of 20th century astronomers and astrophysicists. The subject of this conference, the Initial Mass Function, is perhaps the best known of Ed's enduring legacy. Despite the 50 years since the publication of his seminal paper on the subject, the Salpeter IMF (Salpeter 1955) is still the function of choice for models of stellar distributions in the local and distant universe.

To highlight Ed's remarkable impact, I will take two examples from work done with the Hubble Space Telescope (HST). The first example concerns interpretations of the Hubble Ultra Deep Field (HUDF), a dataset taken this year. A primary motivation for these observations was to search for the epoch of reionization experienced by the universe when the first stars and galaxies were born from neutral hydrogen and helium in the first billion years after the Big Bang. The exact age of the universe at this epoch is still not known, but it is thought to be between about 300 and 900 million years, corresponding to observable redshifts between 15 and 6. The HUDF produced good data on the luminosity density of young stars between redshifts of 6 and 7 at a rest wavelength of 1400 Å.

There are currently three different papers that take essentially the same data –luminosity density at λ_{rest} =1400 Å– and extrapolate to λ_{rest} =912 Å to see if the observed population could ionize the universe at that epoch. The three papers reach different conclusions. Yan and Windhorst (2004) and Stiavelli, Fall, and Panagia (2004) conclude that the observed stars could ionize the universe; Bunker et al. (2004) conclude the opposite. One of the essential differences between the authors is the assumption they use about the stellar population needed to extrapolate from one wavelength to another. Bunker et al. and Yan and Windhorst assume a Salpeter IMF; Stiavelli, Fall, and Panagia assumed a previously unobserved top-heavy IMF of the sort generated from a theoretical Population III of stars created from pure hydrogen and helium. Ed

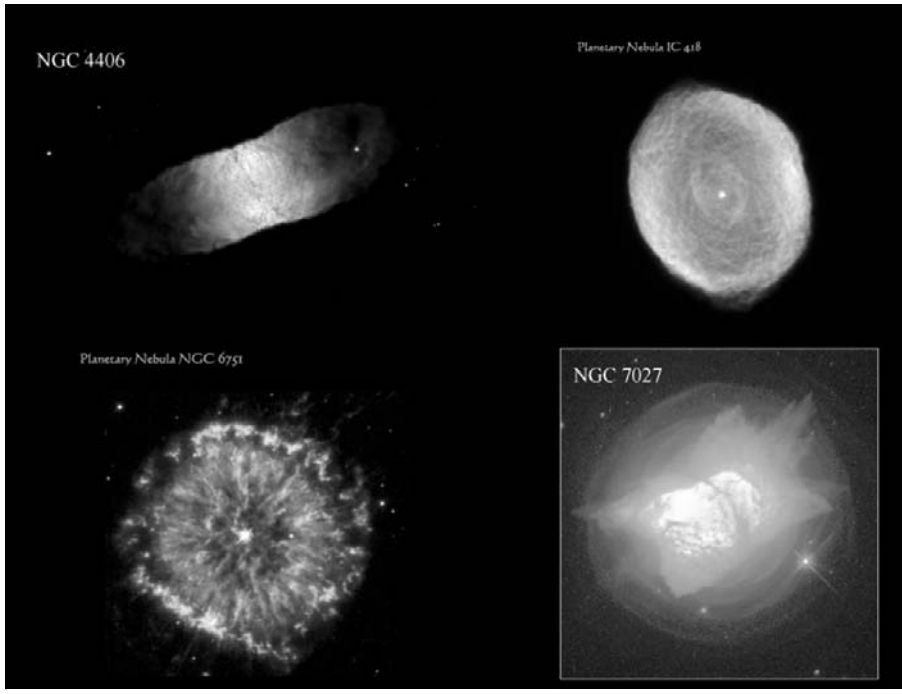

Figure 1. These four images of planetary nebula show deviations from spherical symmetry including clumping and substructure within the envelopes around these dying stars. Clockwise from upper left: NGC 4406 (C. R. O'Dell; Heritage 2002/14); IC 418 (R. Sahai & A. R. Hajian; Heritage 2000/28), NGC 7027 (H. Bond, STScI), NGC 6751 (NASA/Heritage Team; Heritage 2000/12). To view the Hubble Heritage pictures in color, go to URL: http://heritage.stsci.edu/**year**/**#**, where the year/# are cited parenthetically.

established the Salpeter IMF in 1955, and his work with Palla and Stahler in the 1980s laid the groundwork for the Population III IMF.

The second example is the remarkable morphology of planetary nebulae, an example that relates to the lecture referred to earlier that Ed delivered in Astronomy 555 in 1984. The resolution of HST combined with its sensitivity at ultraviolet wavelengths produced pictures of planetary nebulae that are both wondrous and counter to the idea that mass loss from evolved stars is spherically symmetric. The nebulae are the result of mass loss from the stars, matter subsequently ionized when the star's photospheric temperature becomes high enough to generate ionizing photons.

Figures 1–3 provide many examples to underscore this point. The structures around these stars often exhibit symmetry but rarely spherical symmetry. All variety of shapes is seen. Several are helically symmetric, many examples look like the mass is concentrated in clumps (although we do not know if they condensed after mass ejection or as part of the process), and some are bipolar.

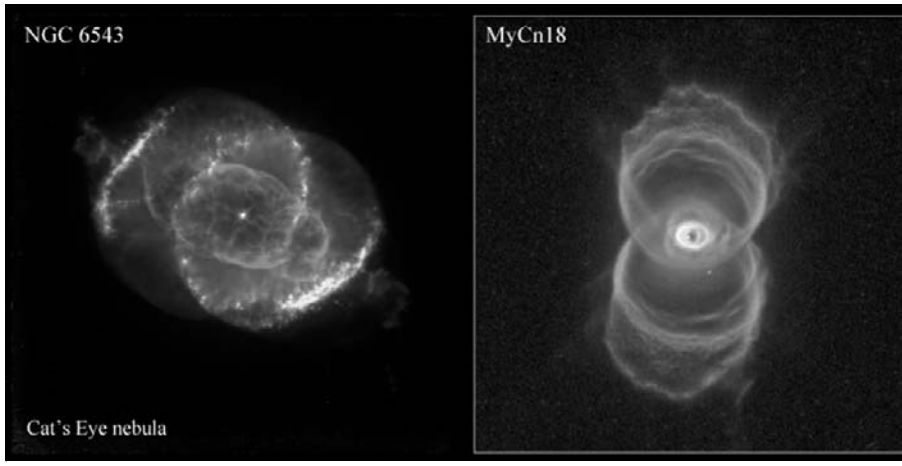

Figure 2. These two planetary nebulae display helical and bipolar symmetry. A more recent image of The Cat's Eye Nebula, NGC 6543 shown in figure 4, also shows the mass loss in waves prior to the formation of the nebula itself. To view these Hubble press release images in color, go to URL: http://hubblesite.org/newscenter/newsdesk/archive/release/**year**/**#**, where the year/# are 1995/49 for NGC 6543 (J. P. Harrington & K. J. Borkowski) and 1996/07 for MyCn18 (R. Sahai & J. Trauger.)

Whatever mechanism creates mass loss in these stars, it cannot rely on strict spherical symmetry to operate.

One of the other new discoveries made possible by these high resolution images is the presence of shells surrounding some planetary nebulae indicating periodic mass loss with a characteristic time scale of $\sim$1000 years (Figure 4.) This remarkable discovery adds to the mystery of just how these dying stars shed their outer layers, a process that supplies much of the interstellar matter necessary to create new stars and planetary systems with the heavy-element enriched ashes of evolved stars.

You will hear a great deal more about recent science stimulated by Ed's work over the last 50 years. All will demonstrate the remarkable impact of his great mind, and it will leave us humbled perhaps to the point of wondering if Ed has any weaknesses of the sort that we ordinary scientists might have. During my long friendship with Ed, I was able to discover only two.

The first was Ed's approach to the politics of advisory committees. Ed resisted serving on committees throughout most of his career until he was asked to serve on the National Science Board, a very influential appointment. He agreed and began attending the meetings to give his sage advice. After a few months, he confessed to me that he really was not very good at it and felt somewhat at sea amongst the other members.

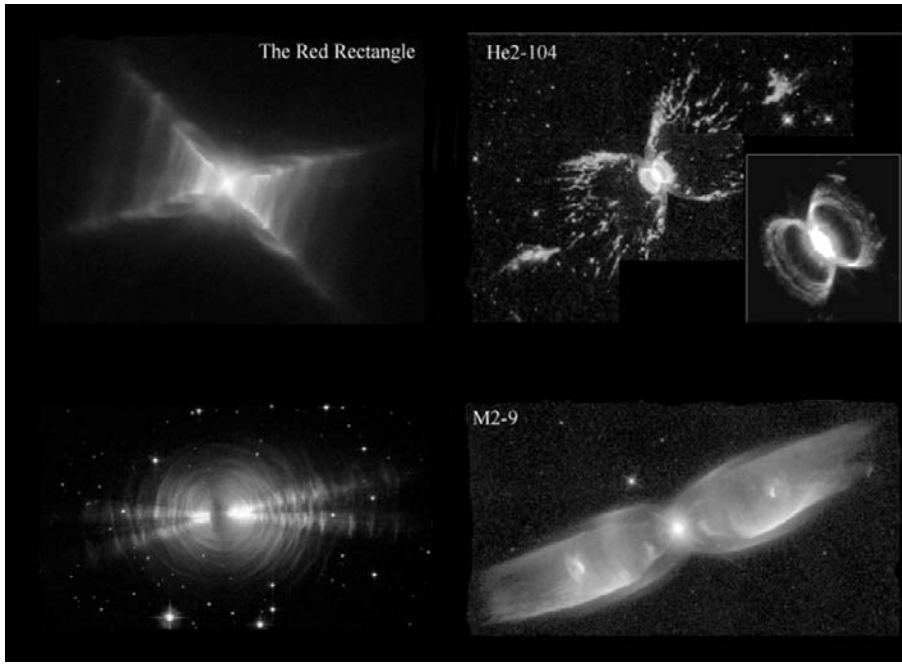

Figure 3. These four nebulae show striking bipolar symmetry and a remarkable channeling of the mass loss into narrow directions. Clockwise from the upper left: The Red Rectangle (H. Van Winkel & M. Cohen; Hubble release 2004/11), He2-104 (R. Corradi et al.; Hubble release 1999/32), M2-9 (B. Balick, V. Icke, & G. Mellema; Hubble release 1997/38) and The Egg Nebula (W. Sparks & R. Sahai; Heritage 2003/09). See notes to Figures 1 & 2 to find the URLs for these images.

"It really drives me crazy," he said to me one day over coffee. "I sit through each meeting paying close attention to the topics, even though most of it is pretty boring and concerns topics I don't know much about. It seems like a big waste of time. But the university administrators miss most of the meetings, showing up just when we start a topic of interest to them, only to vanish 5 minutes after we settle the issues in their favor. And I cannot figure out how they do it!"

The administrators, I now know, figured it out by trial and error: attend hundreds of meetings and understand the chairman's style each time until you develop the skill to show up at the right moments. For someone with Ed's talent, that would have been a terrible waste.

His other self-confessed regret was that he tended to forget some of his early work, understandable given the broad scope of his contributions. One summer, just before the award of the Nobel Prize later that year, Subrahmanyan Chandrasekhar visited Cornell to give some lectures and spend time with us

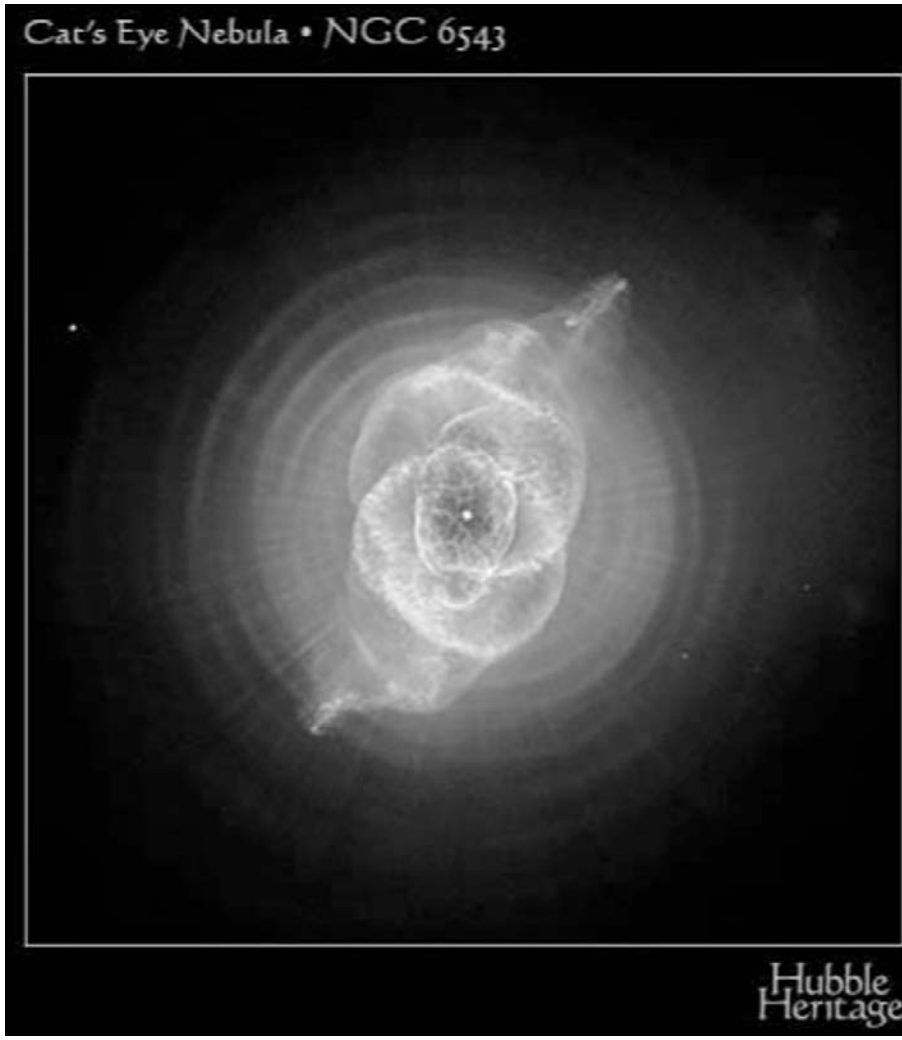

Figure 4. The Cat's Eye Nebula, NGC 6543, in a more recent image with the Advanced Camera for Surveys on HST (R. Corradi & Z. Tsvetanov; Hubble release 2004/27 and Heritage 2004/27). The waves of mass loss that preceded the formation of the ionized nebula are seen clearly surrounding the nebula as circular rings with radial striations. The time between the peaks of the early mass loss events was of order 1000 years, different from any known dynamical time scale in evolved stars.

informally talking about science. A group of us were at a bag lunch with him in Newman Hall when one of the students asked him to explain a subtlety of stellar evolution that he had published 30 years earlier. He admitted that he had not thought about the subject in 30 years then got up and worked out every

detail perfectly on the blackboard to the amazement of everyone in the group. It was truly a tour de force.

After lunch, Ed came up to me and remarked that he recently invented an elegant solution to a problem that had been on his mind for quite some time. He wrote it up in a draft paper and handed it to one of his students, who did a brief literature search only to discover that Ed had already published the exact same solution to this old problem 20 years earlier!

For a person with such deep humanity, these very human characteristics only make Ed more charming and endear him to those of us who learned so much at his side.

References

Bunker, A. J., Stanway, E. R., Ellis, R. S., and McMahon, R. G. 2004, MNRAS, in press, astro-ph/0403223

Salpeter, E. E. 1955, ApJ, 123, 666

Stiavelli, M., Fall, S. M., and Panagia, N. 2004, ApJ, 610, L1

Yan, H. and Windhorst, R. A. 2004, ApJ, 612, L93

Figure 5. Steve Beckwith and Joe Silk.

THE IMF CHALLENGE – 25 QUESTIONS

Hans Zinnecker
Astrophysical Institute Potsdam, An der Sternwarte 16, D-14482 Potsdam, Germany
hzinnecker@aip.de

Abstract I list 25 basic questions (15 from observations, 10 from theory) related to the stellar IMF, as a reference to a general discussion on the origin of the IMF and its possible variation with changes in the star formation environment.

1. Introduction

The IMF is the principal result of the star formation process, and a good theory of star formation must predict the correct IMF as its endproduct, including its variation as a function of environmental conditions. However, one can also turn the question around and ask what we can infer from the observed IMF about the star formation process. A particularly challenging question is whether the IMF is universal, and if so, why. How can it be that the initial and environmental conditions don't have much of an effect on the final outcome (on average)?

It is in this spirit that I have compiled a number of basic questions, breaking down the IMF challenge into smaller and more tractable pieces.

2. Observations

Here I give a first set of questions related to determine the IMF from various observations.

1 How to determine the Pop I field star IMF? Which mass-luminosity relation to use (metallicity spread), which history of the star formation rate?

2 How to determine the Pop II field star IMF? How to measure the local halo population in the Hubble deep fields (HDF/UDF)?

3 Any chance to learn something about Pop III? where to look? (in the outer or inner Galaxy?)

E. Corbelli et al. (eds.), The Initial Mass Function 50 Years Later, 19–22.

4 Examples and problems of the open cluster IMF (Pleiades, alpha Per, Hyades; stellar age spread?)

5 Examples and problems of the globular cluster IMF (e.g. implications of milli-sec pulsars in M15?)

6 The IMF in the youngest embedded clusters? what can be said on the Orion Trapezium Cluster? Rho Oph? IC348?

7 Different IMFs in T associations vs. OB associations? (Taurus/Cham vs. Sco-Cen/Orion) Is the IMF bimodal?

8 IMF in Orion Trapezium, N3603, and 30 Dor? Is the IMF a function of the increasing number of O-stars?

9 How is the build-up of the IMF in young clusters? high mass first or last? need for time-resolved mass spectra?

10 What do we know about the bottom end and the top end of the IMF? Does it vary from region to region?

11 Measure the primary and secondary mass distribution in binary systems: is the pairing random or correlated?

12 How certain is the proposition of a universal IMF? How can we get accurate IMF slopes (to 0.1 dex)?

13 What is the best evidence for an abnormal (truncated) IMF? Are there isolated O-stars? Is the IMF top-heavy in starburst clusters (30 Dor) or starburst galaxies (M82)?

14 The IMF as a spatial average (cluster core and cluster halo): what is the effect of stellar mass segregation on IMF slopes?

15 How to infer the IMF indirectly, e.g. from chemical evolution constraints or mass-to-light ratios?

3. Theory

I continue with a second set of questions, related to the origin of the IMF and star formation theory.

1 IMF from turbulent or other hierarchical fragmentation?

2 IMF from competitive or other types of gas accretion?

3 IMF from a mixture of fragmentation and accretion (low-mass end vs. high-mass end, respectively)?

4 IMF from fractal statistics of clouds (dense packing)?

5 Is the origin of stellar masses regulated by feedback? e.g. winds and jets (at low-mass), winds and radiation-pressure (at high-mass)?

6 Is the IMF an ensemble average, due to the central limit theorem (thus log-normal)?

7 What is the physics of the maximum-mass and the minimum mass? any metallicity-dependence? gravitational dynamics (collisions and ejections, respectively)?

8 Is there a different mass distribution in case of triggered star formation compared to spontaneous evolution?

9 Does the IMF depend on the star formation rate or star formation efficieny? Is the rate and/or the efficiency self-regulated? dynamically or radiatively (supernovae, winds, turbulence, or ionisation)?

10 Which is currrently the "best" theory of the IMF? which observations does it explain? which predictions does it make?

4. Discussion

The IMF is important to interpret the properties of distant galaxies with unresolved stellar populations (dynamics, colors, chemistry). This is why we try so hard to understand its shape and origin.

If I were to summarise my main expectations of the present IMF meeting, I would hope that we can at least address and advance three major issues: (1) Whether the IMF is by and large universal? To decide we need more convincing IMF observations and a better theoretical understanding of why the IMF should be so robust. (2) Whether the dominant mode of star formation is triggered or spontaneous? Can we convince ourselves that there are regions with a top-heavy IMF? Also, can we find out whether the stellar content of dense young clusters is different from loose young associations? (3) Whether all stars form in binary systems or "clusterings"? If so, the effect of multiplicity corrected IMFs (where multiplicity often goes unresolved in distant star clusters) and the effect of dynamical mass segregation on the IMF must be given more attention than up to now. Most astronomers treat galaxies as if they consist of a collection of single stars which seems to be far from the truth.

I wish an enjoyable meeting!

Figure 1. Hans puzzled at crossroads.

Figure 2. Hans and Wolfgang Brandner.

FIFTY YEARS OF IMF VARIATION: THE INTERMEDIATE-MASS STARS

John Scalo
University of Texas, Austin Texas, USA
scalo@astro.as.utexas.edu

Abstract I track the history of star count estimates of the Milky Way field star and open cluster IMFs, concentrating on the neglected mass range from 1 to 15 $M_\odot$. The prevalent belief that the IMF is universal appears to be without basis for this mass range. Two recent estimates of the field star IMF using different methods and samples give values of the average logarithmic slope Γ between -1.7 and -2.1 in the mass range 1.1 to 4 $M_\odot$. Two older estimates between 2 and 15 $M_\odot$, using much smaller samples, disagree severely; the field IMF in this range is essentially unknown from star counts. Variations in Γ among open cluster IMFs in this same mass range have not decreased despite numerous detailed studies, with a rather uniformly distributed spread of about 1.0 to 1.4, even for studies using homogeneous data and reduction procedures and including only clusters with a significant mass range. These cluster variations *might* be accommodated by the combined effects of sampling, systematic errors, stellar evolution uncertainties, dynamical evolution, and unresolved binaries. If so, then the cluster data are consistent with a universal IMF, but are also consistent with sizeable variations. The data do not allow an estimate of an average IMF or Γ because the average depends on the choice of weighting procedure and other effects. There is little basis for claims that the field star IMF is steeper or flatter than the cluster IMF in this mass range. If the spread in cluster IMFs is in excess of the effects listed above, real IMF variations must occur that do not depend much on environmental physical conditions explored so far. The complexity of the star formation process seen both in observations and in simulations of turbulent cluster formation suggests that large realization-to-realization differences might be expected. In this case an individual cluster IMF would be in part the product of evolutionary contingency in star formation, and the significant function of interest is the probability distribution of IMF parameters. In either case an average IMF can probably be better determined from the field star IMF using data from future space astrometric missions, or from combinations of indirect constraints using integrated light or chemical evolution applied to whole galaxies.

E. Corbelli et al. (eds.), The Initial Mass Function 50 Years Later, 23–40.

1. Introduction

When Salpeter (1955) first derived the “Original Mass Function," now known as the “Initial Mass Function" or IMF, for field stars, his primary result was an empirical demonstration of certain fundamental aspects of stellar evolution theory. As it turned out, the IMF became a fundamental datum for understanding the formation of stars and the evolution of galaxies, and spawned diverse techniques for its estimation, from star counts to integrated properties of galaxies, and a bewildering variety of theories to account for its empirical form.

The purpose of this review is to outline some of the major developments in the field over the past decades, concentrating on recent empirical results using star counts in the mass range between about 1.2 and 15-20 $M_\odot$ for Galactic field stars and open clusters. It is in this range that the field star IMF can be best compared with young- to medium-age open cluster IMFs, and it is arguably the best mass range for determining a large number of cluster IMFs. The IMF in this mass range has been neglected in the past two decades as attention has turned almost entirely to subsolar-mass stars. While some studies have claimed some convergence on the cluster and field star subsolar IMF (see papers in this volume), there are certainly examples of differences that are so large they are difficult to understand as observational or dynamical effects (e.g. Jeffries et al. 2001 and Fig. 4a in Kroupa 2002, Fig. 2 in Kroupa & Weidner, this volume). Recent reviews emphasizing the IMF of subsolar stars in the field and clusters can be found in Kroupa (2002) and Chabrier (2003a), while the IMF in star-forming regions is reviewed by Meyer et al. (2000), Luhman (2002), and Hillenbrand (2004). Useful reviews of more general IMF constraints are given by Kennicutt (1998) and Elmegreen (1999b); for earlier work see Scalo (1986). Surprisingly, the IMF above 1 $M_\odot$ has not been critically examined, although statements that the stellar IMF in this range is invariant are now common in the literature. The present paper aims to examine the question of universality for this restricted but accessible mass range.

In order to focus the discussion, I omit the wealth of studies of globular clusters, the Galactic bulge, center, or halo, clusters or field stars in other galaxies, theories of the IMF, and the numerous indirect lines of evidence on the IMF based on, for example, integrated light and chemical evolution constraints (see other papers in this volume; Scalo 1986 for older work and more methods). I also omit discussion of the important mass range above 15-20 $M_\odot$ for a number of reasons. Due to the degeneracy in mass at a given luminosity, the IMF for very massive stars requires spectroscopy to interpolate masses among evolutionary tracks, as claimed by Garmany et al. (1982, see Massey 1985), and demonstrated convincingly by Massey et al. (1995). Unfortunately the Milky Way study of Garmany et al. (1982) has not been repeated using improved data and evolutionary tracks, and sample sizes for clusters where most of these

stars are found are very small (typically a few dozen stars), giving large uncertainties, and an undersampling bias that yields an IMF that is too flat (Kroupa 2001). Combined with the unknown sensitivity of the results to the effective temperature scale (see Massey et al. 2004), uncertainties in massive star evolutionary tracks, and details of extinction and reddening corrections for Milky Way stars (Van Buren 1985), I omit discussion of existing massive star IMF results (see Scalo 1998, Kroupa 2002 for references). The IMF of massive stars is so important for galaxy evolution studies that a re-evaluation is urgently needed.

In what follows, "IMF" refers to the frequency distribution of stellar masses per unit logarithmic interval of mass, dN/dlogM. The parameter Γ is the slope of a log-log power-law fit to some portion of this IMF, without implying that the IMF can be well-represented by a power-law or a piecewise power law; indeed other forms may give better fits to the data in some mass ranges (e.g. Chabrier 2003a).

Salpeter's (1955) original estimate of the field star IMF was not a power law, but had a logarithmic slope Γ of about -1.7 below 1 $M_\odot$, -1.2 from 1 to 10 $M_\odot$, and strong steepening above that mass (see Fig. 1). Salpeter suggested that if a power law were to be applied to the whole function, a line of slope -1.35 would give an adequate representation, and this slope became known as the "Salpeter IMF." Of course we know today that if the input were updated to modern values the resulting IMF would look considerably different; in particular, it is usually believed that the IMF is steeper at intermediate and large masses than at subsolar masses. Nevertheless, it has become common in the last decade to interpret various data as consistent with the Salpeter slope for masses above 1 $M_\odot$; as will be seen below, there is currently little basis for assigning a given average, let alone universal, value, at least from star counts.

Soon after the publication of Salpeter's paper, remarkable consistency of his IMF result with open cluster data was found by Sandage (1957) using five clusters, Jaschek & Jaschek (1957) using three clusters, and van den Bergh (1957) using nine clusters plus Orion, although Jaschek & Jaschek had to assume an unrealistically large evolutionary correction (not used in the other two studies) in order to obtain agreement with Salpeter. Van den Bergh's result is shown in Fig. 1 (as the distribution per unit mass, dN/dM) where Salpeter's original field star IMF can also be seen. Considering the large uncertainties in cluster IMFs that are recognized today, the agreement was amazingly good, certainly much better than nearly any contemporary comparison of field and cluster IMFs!

The fundamental question of IMF universality was first emphasized by van den Bergh & Sher (1960) who, in a pioneering study of 20 open clusters, claimed evidence for different low-mass turnovers in the IMF. Although much of this turned out to be incompleteness, this paper was pivotal in raising the issue of cluster IMF universality, a question that remains open today: Para-

phrasing Kennicutt (1998), the answer has seemed paradoxical because: 1. It is extremely difficult to imagine that the observed complexity of star formation results in a universal IMF; 2. The uncertainties in empirical IMF estimates may be so large that all evidence is consistent with a universal IMF. Unfortunately this latter statement, even if true, does not help us establish whether the IMF *is* universal, or, assuming it is, even on average, what that universal IMF may be. Alternatively, real variations may contribute to the scatter in cluster IMFs. Partly because of its appeal and simplicity (and because the physicist's need for universality runs deep), the former interpretation is nearly always adopted. Here I emphasize the point of view that we simply do not know the answer to this question yet.

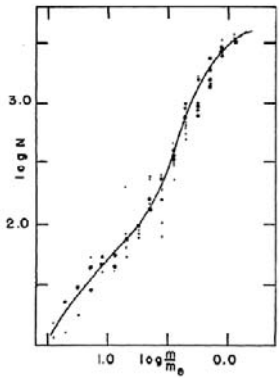

Figure 1. IMF per unit mass combining nine clusters plus Orion compared with Salpeter's (1955) field star IMF estimate (van den Bergh 1957).

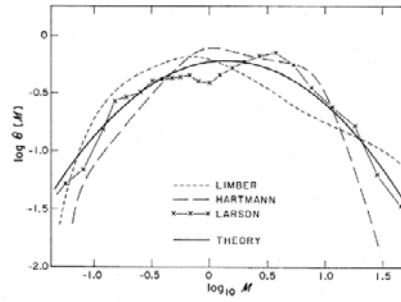

Figure 2. Empirical estimates of the field star IMF by Limber (1960), Hartmann (1970), and Larson (1973) as presented by Larson (1973). The solid line is Larson's hierarchical fragmentation model.

2. Historical Divergence: Field Star IMF

By the 1970s estimates of the IMF for field stars began to diverge from Salpeter's original estimate and from each other, a situation that has not changed much to the present day. Fig. 2 shows three empirical estimates for field stars compared with Larson's (1973) probabilistic hierarchical fragmentation model. We note that Larson was the first to suggest a lognormal IMF. All the field star IMFs in Fig. 2 turn over below around 1 $M_\odot$, but we now know that these data were very incomplete for the smaller masses. More important is that these IMFs do not agree with each other even above 1 $M_\odot$, showing large variations in shape and slope.

Motivated by this state of affairs, Miller & Scalo (1979) reassesed the field star IMF, which they found could be fit with half of a lognormal function,

emphasizing a number of uncertain transformations and corrections to the observed luminosity function that are needed to construct the field star IMF. A thorough analysis of more and updated observational data and theoretical input by Scalo (1986) gave a very different result. In the mass range 1.4 to 15 $M_\odot$, where the shape of the IMF is not affected much by uncertainties in long-term SFR variations, the IMF was “convex," rather than "concave" as in Miller & Scalo, with a very steep slope of Γ = -2.6 for 1.4-3.5 $M_\odot$ and -1.8 for 2-12 $M_\odot$. Kroupa et al. (1993) used a fit of Γ = -1.7 to Scalo’s (1986) IMF over the entire mass range above 1 $M_\odot$, but this includes the massive stars from 15 to 60 $M_\odot$, where the field star IMF was (and still is) particularly uncertain.

Around the same time it was recognized that the construction of the mass function from the luminosity function depends very sensitively on the mass-luminosity (M-L) relation because it is the derivative of this relation that enters the conversion. This is particularly important for the low-mass IMF (D’Antona & Mazzitelli 1983, Kroupa et al. 1990, Kroupa et al. 1993). Useful comparisons of empirical and theoretical M-L relations are given in Kroupa (2002) and deGrijs et al (2002a). This development, along with the reconciliation of the long-standing discrepancy between IMFs derived from the local photometric and trigonometric parallax samples as due mostly to unresolved binaries (Kroupa et al. 1991; Chabrier 2003b) and significant advances in instrumentation, initiated a large and ongoing research effort by many groups to establish the general form of the subsolar IMF (although not well enough to decide on a functional form; see Chabrier 2003a). Unfortunately there was no corresponding progress in the 1-15 $M_\odot$ range: the IMF derived by Yuan (1992) is essentially that of Scalo (1986), and the “KTG" IMF of Kroupa et al. (1993) is a joining of their new result below 1 $M_\odot$ with a single power law fit to Scalo (1986) for larger masses, and so contained no new information above 1 $M_\odot$.

Until very recently, the only semi-independent rederivation of the IMF in the mass range of interest here was by Rana (see Rana 1991, Fig. 3) and Basu & Rana (1992a,b). Rana’s IMF shows evidence for flat plateaus at around 2.5 and 5 $M_\odot$, but if these features are ignored, the best fit power law IMF between 1.4 and 100 $M_\odot$ has Γ = -1.3, very similar to the Salpeter value. Since the results above 15-20 $M_\odot$, based on a (very uncertain) luminosity function, should receive little weight for the reasons explained by Massey et al. (1995), the corresponding single power-law fit in the 1-15 $M_\odot$ range would be significantly flatter, with Γ around -1. An updated version of this field star estimate was given by Basu & Rana (1992a,b), using the same luminosity function and mass-luminosity relation as adopted by Rana. These papers find Γ = -1.5 to -1.7 for masses from 1.4 $M_\odot$ to 100 $M_\odot$, but they note again that a single power law does not seem to give a good fit. Exclusion of the higher-mass stars because of the mass degeneracy of the luminosity function would give a much

flatter $\Gamma \approx$ -1.2. These results are flatter by about 0.6 to 1.0 in Γ compared to Scalo (1986) for reasons that remain unexplained.

Unfortunately there is little hope of disentangling the field star IMF from the history of the Galactic star formation rate for masses around 0.9 to 1.3 $M_\odot$. To make things worse, this is just the mass range over which the uncertain stellar scale height correction varies the most (Scalo 1986), and approaches the mass where main sequence lifetimes are still uncertain. Open clusters are required to study this mass range.

Two decades of technical advances and data accumulation, primarily Hipparcos and infrared surveys like DENIS and 2MASS, have resulted in significantly more trustworthy field star counts, at least for masses below about 4 $M_\odot$. Advances in interferometry, radial velocity techniques, and astrometry, have yielded many more accurate binary star masses (see Anderson 1998, Segransan et al. 2004), improving our understanding of the M-L relation.

These advances have not cleared up the situation much. There have been only two recent determinations of the field star IMF at masses above 1 $M_\odot$, although none that go beyond about 4 $M_\odot$. Reid et al. (2002) combined their previous data with Hipparcos astrometry for a 25 parsec sample of AFGKM stars in order to construct the present-day luminosity function, and then followed the classic procedure used by Salpeter and most subsequent work to derive the IMF. Adopting a segmented power law to fit the results, they found IMF slopes of Γ = -1.8 (or -1.5) between 1.1 (or 0.6) $M_\odot$ and 3 $M_\odot$, depending on the choice of M-L relation. It is not clear how the results around 1 $M_\odot$ are affected by the adopted star formation rate history and dependence of scale height on mass. The Reid et al. results can be compared with the steeper IMF found by Scalo (1986) and the flatter IMF found by Basu & Rana (1992a,b) in this mass range.

An alternative method for field stars is to match synthetic populations from evolutionary tracks to counts from Hipparcos in the color-magnitude diagram, greatly enlarging the stellar sample and eliminating some uncertainty due to the M-L relation and star formation history. Schroder & Pagel (2003) matched counts in seven regions along the main sequence in the HR diagram with simulated populations generated with a given IMF and SFR history. Applying this technique to thin disk stars out to 100 pc with $M_V < 4$, their best fit IMF had Γ = -1.7 for 1.1 to 1.6 $M_\odot$, and -2.1 for 1.6 to 4 $M_\odot$. Schroder & Pagel (2003) avoided many of the considerable sources of uncertainty and bias discussed in detail by Pont & Eyer (2004) by matching counts in horizontal cuts through the HR diagram rather than assigning individual masses.

These most recent studies by Reid et al. (2002) and Schroder & Pagel (2003) use much larger samples than earlier work, and could be optimistically interpreted as consistent with Γ = -1.9 $\pm$0.4 in this limited mass range from 1.1 to

4 $M_\odot$, although the dependence on SFR history and scale height variation with mass is not clear.

What about intermediate mass stars 3-4 to 15-20 $M_\odot$? Unfortunately determination of the luminosity function, and hence present-day mass function, for stars in this mass range has been eclipsed by the availability of improved and enlarged data for lower-mass stars. For this reason there apparently has been little improvement in the field star IMF in this mass range since the compilation of luminosity functions by Scalo (1986), which simply adopted a subjective average of the various LFs available. A different choice of luminosity functions (and other input) in this range by Rana (1991; Basu & Rana 1992a,b) gave a much different result. It is probably safe to say that the field star IMF in the 3-20 $M_\odot$ mass range is unknown, or at least extremely uncertain. Presumably future space astrometric surveys will provide trustworthy IMF estimates to at least 10-20 $M_\odot$. For more massive stars spectroscopy and interpolation between evolutionary tracks in the HR diagram is required (Massey et al. 1995), with the attendant difficulties mentioned earlier.

3. Historical Divergence: Open Cluster IMFs

Studies of cluster IMFs are difficult but crucial: they offer the best opportunity to understand the nature of the IMF and to test for universality. The primary advantage of clusters is of course that the stars were all born at approximately the same time and have the same distance and metallicity. Many of the problems mentioned above in connection with field stars can be avoided by studying star clusters of various ages.

However clusters come with their own set of problems. These include: 1. There are few nearby clusters whose stars cover a wide range in masses, so age and limiting magnitude restricts the range of masses that can be studied in each cluster. 2. Most clusters studied have only 50-200 objects to the completeness limit, leading to a small number of stars per mass bin or a very small number of bins (assuming a histogram is used for the estimate); the associated uncertainties in estimates of Γ are surprisingly large (Elmegreen 1999a, Kroupa 2001). 3. Mass segregation, with more massive stars concentrated to the cluster center, occurs even in young clusters, so that it may be primordial (see Sirianni et al. 2002 and references therein), although post-formation dynamical evolution is also important (e.g. de la Fuente Marcos 1997). Recent detailed studies of the effect in fairly young clusters can be found in Sung & Bessell (2004, NGC 3603), de Grijs et al. (2002a, b, LMC clusters), Sirianni et al. (2002, SMC cluster NGC 330), and Littlefair et al. (2003, NGC 2547). The ubiquity of mass segregation means that clusters must be observed to large radii. But then there is a severe problem with: 4. Membership: proper motions and radial velocities are needed, but this is possible only for very nearby clusters. There

are also difficult corrections that must be made for foreground and background contamination and incompleteness. Undercorrection for field star contamination artificially steepens the IMF, while undercorrection for incompleteness flattens it. All these corrections become more important in the outer cluster regions, just the regions that must be included in order to avoid effects due to mass segregation. 5. Unresolved binaries: this is an important effect that hides lower-mass stars in both field and cluster samples; see Sagar & Richtler (1991), Phelps & Janes (1993); Malkov & Zinnecker (2001), Kroupa (2001, 2002) and references therein. 6. Adopted cluster properties: distance, age, metallicity, extinction, and differential reddening estimates can all make a difference in the derived IMF. 7. Uncertainties in evolutionary tracks and isochrones; this is especially important for pre-main sequence stars in very young clusters (e.g. Hillenbrand & White 2004) and very massive stars, where photometry is degenerate with respect to mass (Massey et al. 1995). An example is shown in Kroupa (2002, Fig. 4b). Uncertainties in the T_{eff} scale enter here also. The estimation of masses for stars from evolutionary tracks may be subject to the same types of insidious and large uncertainties that plague the estimation of ages of field stars near the main sequence by interpolation in isochrones, and need to be addressed in detail using an approach along the lines of Pont & Eyer (2004). 8. Cluster IMFs could also be affected by preferential escape of low-mass stars during dispersal of residual gas in initially virialized clusters (Kroupa & Boily 2002).

Many of these effects increase with cluster distance. It is important to notice that mass segregation, unresolved binaries, and ejection during residual gas dispersal all tend to give a cluster IMF that is too flat relative to the true or original cluster IMF; for that reason *every estimate of* Γ *derived for clusters should be considered an upper limit* (i.e. the IMF could be significantly steeper).

There were many numerous post-1960s estimates of IMFs in open clusters. Most of this early work was reviewed and reproduced using a uniform mass-luminosity relation in Scalo (1986). Some highlights include: 1. Taff's (1974) composite IMF for 62 clusters that could be well-fit by a single power law of slope -1.7 from 1 $M_\odot$ to at least 20 $M_\odot$; unfortunately Taff did not comment on the variations among clusters, and his procedure for combining cluster data has never been re-examined. 2. The IMFs for five young clusters and OB associations using evolutionary tracks combined with Stromgren photometry in the mass range 2.2 to 10 $M_\odot$ by Claudius & Grosbel (1980) was a model for future studies of young clusters. Their Γ values were estimated using a maximum likelihood method rather than least squares fitting to histograms. The results gave Γ from -1.6 to -2.0, but most of the samples were small; combining the Orion subgroups using 135 stars gave Γ = -1.9, similar to that derived independently by Brown et al. (1994). 3. A study of 75 clusters with a range of ages by

Tarrab (1982) found logarithmic slopes that varied enormously, from near zero to about -3, although most were in the range -1 to -2. Her study necessarily used inhomogeneous and old sources of data, many of the clusters only have about 20-50 members used in the IMF determination, and a few of these clusters have been studied more recently with different results (although Sanner & Geffert 2001 find good agreement for four of five clusters in common).

The spread in Γ found by Tarrab (1982) has, surprisingly, not decreased much in later comparisons of clusters (see Fig. 5 in Scalo 1998, reproduced with a few additions above 1 $M_\odot$ in Kroupa 2002; also Kroupa & Weidner, this volume; and more recent Milky Way cluster studies summarized below). According to Tarrab, only a small part of the scatter could be attributed to sampling fluctuations. However a careful study of this problem by Kroupa (2001) suggests that much of the spread can be due to a combination of sampling noise (see Kroupa's Fig. 3), dynamical effects, and (for low-mass stars) unresolved binaries. The question of how much of the spread in IMF slopes among clusters is real remains central question today, and is discussed further below.

Since the 1980s there have been significant instrumental, observational, and theoretical advances that have opened up new ground for cluster IMF studies. CCD arrays on large telescopes allowed accurate, deep photometry. Multi-object spectrographs allowed IMF determinations in very young clusters where interpolation between isochrones is necessary (e.g. Luhman 2002 for a review). Sensitive near-IR cameras allowed the study of IMFs of embedded star clusters using near-IR luminosity functions, an approach that has been greatly refined in the past few years (see Lada & Lada 2003, Muench et al. 2003), especially in combination with spectroscopic surveys (e.g. Hildebrand & Carpenter 2000, Luhman et al. 2003, Wilking et al. 2004). These efforts concentrate on subsolar- and substellar-mass stars. New generations of stellar evolutionary models use improved input physics, cover a broad range of masses and metallicities, include pre-main sequence and brown dwarf evolutionary tracks, and are often publicly available. However the theoretical models and the empirical effective temperature scale still have considerable uncertainties, even for main sequence stars (e.g. Hillenbrand & White 2004, Pont & Eyer 2004).

What do Milky Way open cluster studies using these improved techniques and models tell us? I will concentrate on masses above 1 $M_\odot$ and the issue of universality, and except for a few cases only cite papers later than 1998; most earlier work is discussed at length in Scalo (1998). In nearly all the cases listed below the number of objects used is of order 100 or larger and the quoted fitting uncertainties are less than ± 0.25.

One of the best examples of a cluster-to-cluster IMF variation remains the two clusters NGC 663 and NGC 581, part of a study of eight youngish clusters

by Phelps & Janes (1993). Both clusters have similar ages, number of members, and limiting magnitude, the raw data were obtained and reduced by the same authors in the same way, and both show exceptionally fine power-law forms for their IMFs, yet Γ = -1.1 for NGC 663 while Γ = -1.8 for NGC 581, each with very small fitting uncertainties.

An increasing fraction of studies find a steep Γ around -2 in the mass range (1-2) to (4-10) $M_\odot$. These include NGC 2422 (Prisinzano et al. 2003, corrected for dynamical evolution), Stock 2 (Sanner & Geffert 2001), NGC 2323 (Kalirai et al. 2003), NGC 4815 (Prisinzano et al. 2001), NGC 6631 (Sagar et al. 2001), the Pleiades (Sanner & Geffert 2001; see also Moraux et al. 2004 and the comparisons in Prizinzano et al. 2003 and Kroupa 2002; Kroupa & Weidner, this volume, Fig. 2), and the Orion Nebula Cluster for masses above about 2.5 $M_\odot$ in the spectroscopic survey of Hillenbrand (1997, Hillenbrand & Carpenter 2000) when stars out to 2.5 pc are included.

Examples of much flatter IMFs with $\Gamma \approx$ -0.9 in similar mass ranges include: NGC 2244 (Park & Sung 2004), NGC 2451A (Sanner et al. 2001, although the sample size is very small), the starburst cluster NGC 3603 (Sung & Bessell 2004), and several earlier studies listed in Scalo (1998). Some of these flat IMFs could be due to mass segregation, but some of these studies tried to include those effects in their estimates. Of course there are examples everywhere in between, including many that are around -1.1 to -1.6, so could be consistent with the Salpeter value considering uncertainties; e.g. Sanner et al. (2000) for NGC 1960 and NGC 2194, Slesnick et al. (2002) for h and χ Persei, Yadav & Sagar (2004) for NGC 2421, Yadav & Sagar (2002) for Tr 1 and Be 11. One of the best cases appears to be NGC 7510 with Γ = -1.1 for 1 to 13 $M_\odot$ (Sagar & Griffiths 1998, see Fig. 4 below). The comprehensive study of the Upper Scorpius OB association by Preibisch et al. (2002) gave $\Gamma \approx$ -1.6 between 2 and 20 $M_\odot$.

Perhaps the spread is due to different reduction procedures, M-L conversions, evolutionary tracks, even binning procedures, etc. used by different groups, as suggested by Massey (2003). If we look at studies that compare a number of clusters using homogenous data and the same reduction procedures, the degree of variation seems just as large. In various mass ranges spanning 1 to 15 $M_\odot$, the ranges in Γ for some such programs come out -1.1 to -1.8 (Phelps & Janes 1993, seven clusters); -0.7 to -2.3 (Sanner & Geffert 2001, seven clusters, although sample size is small in all but three cases; the IMFs for six of these clusters are reproduced in Fig. 3; see their Fig. 4 for the Pleiades); and -0.8 to -1.9 (De Marchi et al., this volume, including only the five clusters with sufficient data above 1 $M_\odot$). Using a sample of six very young but distant clusters (with correspondingly large uncertainties), Piskunov et al. (2004) obtained a range of Γ from -1.0 to -1.5, suggesting consistency with a single Γ close to -1.3, given the very large quoted fitting uncertainties. However Sagar

and coworkers (see Sagar 2002 for a review) have studied a large number of distant clusters, and found an extremely large range in Γ, even including only the clusters that have IMF fitting errors of less than about ±0.25, from -0.3 to -2.5 (e.g. Sagar & Griffiths 1998, Subramaniam & Sagar 1999, Sagar, Munari, & de Boer 2001), although they tend to cluster around -0.8 to -1.8, and the authors summarize their results as being consistent with the Salpeter value for the mean, implying that the actual uncertainties are very large. The IMFs for the five clusters studied by Sagar & Griffiths (1998) are shown in Fig. 4.

It appears that the range in Γ among clusters is not decreased when we only consider homogeneous open cluster studies.

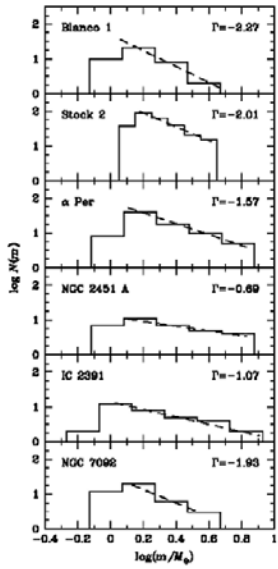

Figure 3. IMFs for six clusters studied by Sanner & Geffert (2001).

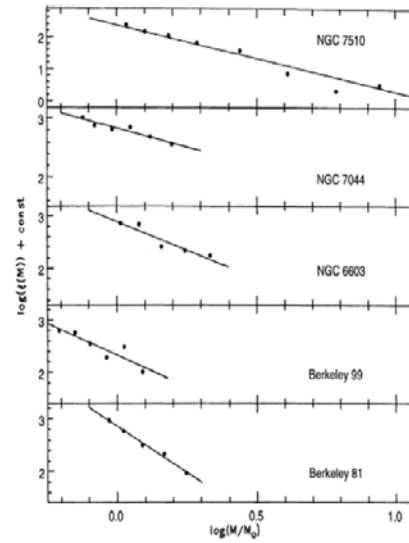

Figure 4. IMFs for five clusters studied by Sagar & Griffiths (1998). The older clusters are dynamically evolved but have similar richness and ages ∼ 1 Gyr.

Porras et al. (2003 and references therein) have nearly completed the J-band luminosity-function modeling of 40 young embedded clusters along the Perseus Arm. Although there is considerable spread in the individual Γ values (the individual IMFs are fairly noisy), perhaps the most interesting result is that most of the cluster IMFs, which extend considerably above 1 $M_{\odot}$, give a mean value of Γ = -1.0 ±0.14, significantly flatter than other studies discussed above.

There are many other intriguing cases of IMF variations in clusters that are not easy to dismiss, including low-mass cutoffs well above the limiting

magnitude of the study, e.g. the 3 $M_\odot$ turnover in NGC 6231 (Sung et al. 1998) and "dips" at certain masses that are difficult to ascribe to random sampling effects (NGC 3293, Baume et al. 2003; NGC 6231, Sung et al. 1998; NGC 2571, Georgi et al. 2002; NGC 2580, Baume et al. 2004; and the Orion Nebula Cluster, see Hillenbrand & Carpenter 2000). There may even be an example of a cluster with different IMFs in different subregions (NGC 7654, Pandey et al. 2001).

Altogether the spread in these studies is about 1.4 in Γ. It is difficult to ascribe this spread primarily to sampling noise, as proposed by Kroupa (2001), since there is no discernible correlation between the departure from the straight mean cluster value and the sample size (Scalo, in preparation). Strong *differential* effects of dynamical evolution, even among clusters with similar richness and age, could be important, since the areal coverage (say relative to the half-mass radius) of different clusters varies significantly. Differential unresolved binary effects would also need to be invoked, which should give an apparent flattening with distance.

The standard approach in the past decade has been to ascribe all variation to noise, errors, and systematic effects, and take a straight mean of the cluster Γ values as representative of a universal IMF (see Kroupa 2002). When carried out for the enlarged sample described here, the average Γ is about Ð1.6 in the range 2 to 15 $M_\odot$, but there are various problems with such a procedure. The most severe problem is how the various determinations of Γ in clusters should be weighted or even included in taking an average; for example, if weights are assigned according to total sample size or average number of stars per mass bin, or cluster distance, the resulting averages differ from the straight unweighted average. An extreme example is: should we include the Perseus arm clusters with flat IMFs studied by Porras et al. as 38 points with low weight, or a single point?

In principle it is possible to estimate the pdf of the cluster Γ values to see if it peaks at some value that could be regarded as the most likely, or average (Kroupa 2002). This pdf, constructed by combining the Galactic sample of clusters in Scalo (1998) and enlarging it to include more recent studies (many of which were cited above), does not resemble a Gaussian as might be expected for pure sampling errors when only clusters with mean (log) masses from 1.5 to 15 $M_\odot$ and clusters younger than about 0.5 Gyr (to avoid main sequence turnoff problems) are included. However such a pdf estimate is jeopardized by the almost certain need for segregation and unresolved binary corrections, and especially the subjective choice of studies to be included. That the pdf above about 2 $M_\odot$ is consistent with a Gaussian (Kroupa 2002) is not supported for this enlarged sample; Kroupa's (2002, Fig. 5b, also Kroupa & Weidner, this volume) sample in this mass range is identical with Scalo (1998) except for the addition of two more recent Milky Way studies, and was influenced by

the inclusion of several studies of massive star IMFs both in the Milky Way and Magellanic Clouds, which were omitted from the present sample. Nevertheless, the pdf of Γ values as used by Kroupa (2002) provides an important approach to the universality problem, and needs to be reconsidered in detail.

Even if the IMF varies from cluster to cluster, an average IMF might be meaningful, and it is of interest to ask whether this average, if universal, is the same as the field star IMF. It was recognized by Reddish (1978) and Vanbeveren (1982, 1983) that a potential problem in such a comparison is that if the upper stellar mass limit in *most* clusters is limited by the available cluster mass, the field star IMF will be too steep compared to the "true" cluster IMF because the mass distribution of clusters gives a smaller probability for obtaining more massive stars. Kroupa & Weidner (2003, also this volume) independently examined this problem in more detail, concluding that there should be a significant difference between the field and cluster IMF. However the effect depends on the assumed lower limit of cluster masses; the field-cluster IMF difference basically sets in at the lower limit assumed for the cluster mass function (see the case chosen in Goodwin & Pagel 2004). Empirically it is not at all clear that the field and average cluster IMFs differ, or in what direction. This is an important question, since the effect could significantly alter the appropriate IMFs for galaxy evolution studies (Weidner & Kroupa 2004).

4. Conclusions

The surprisingly good agreement between the field star and cluster IMF found in the late 1950s had changed to divergence by the 1970s. The main point of this review is that re-convergence has not yet occurred in the mass range 1 to 15 $M_{\odot}$, despite claims to the contrary. Different determinations of the field star IMF above 1-2 $M_{\odot}$ have continued to disagree, and the field star IMF above about 4 $M_{\odot}$ has not been throroughly reinvestigated in nearly two decades, despite large differences between existing studies. The differences in Γ between open cluster IMFs found in the 1980s have not decreased despite advances on several fronts; values of Γ appear rather uniformly distributed with a spread of around 1.0 to 1.4, even for groups of clusters with about the same age studied using the same reduction procedures.

These cluster variations might still be accommodated by the combined effects of sampling, systematic errors, dynamical evolution, and unresolved binaries, as suggested by Kroupa (2001; also Kroupa & Boily 2002). In that case the necessary importance of the latter two effects implies that the cluster mass functions are steeper than determined, and that the observations are only consistent with a universal IMF because these uncertainties are so large; the observations do *not* imply that the IMF *is* universal. In fact, given the evidence and problems discussed earlier, it should be clear that just about any hypoth-

esis concerning the field star and cluster IMFs could be accommodated in the 1-15 $M_{\odot}$ mass range. Appeals to Occam's Razor appear forced in this case. A balance must be struck between convenient interpretations of disparate results, and attention to uncertainties, physical effects, and convincing evidence, mirroring the cautions discussed by Brandl & Anderson (this volume) in the context of starbust IMF estimates.

In spite of these results, the prevalent notion about the IMF remains that the IMF is approximately universal. A key reason for this confluence of opinion, besides its simplicity, is that there is no evidence for a *systematic* dependence of the IMF on gas or star density, metallicity, galactocentric radius, or time in our own or any other galaxy (with the possible exception of starburst galaxies and the Galactic center; but see Figer 2004, Brandl & Andersen 2004, Leitherer 2004, this volume), a point that has been made for both the high-mass and low-mass IMF by many authors (e.g. Massey & Hunter 1998; see Luhman 2002, Kroupa 2002 for more discussion). Since these are the types of variations that astrophysicists might have expected, the default position became universality, with a corresponding projection of this belief onto interpretation of the observations.

However, complex physical processes can exhibit variations in their statistical properties not coupled primarily to average environmental conditions. Variations can be due to sensitivity to initial conditions, or contingency in complex evolutionary processes, as suggested for massive stars by Bonnell et al. (2004). If the high-mass IMF is stochastic, and is coupled to the formation of the rest of the IMF, e.g. through disk photoevaporation or other feedback (see Silk, this volume), the whole IMF would be expected to show large "tail wagging the dog" variations (see Robberto et al., this volume). Even without such feedback, the final mass of a gas clump destined to become one or more stars is a chancy matter in a turbulent star-forming region. It will be interesting to investigate the level of IMF variations between realizations of MHD turbulence simulations when such calculations have the resolution and physical realism to actually describe the formation of individual stars. See Jappsen et al. (2004; Klessen et al., this volume) for an example. In this case the significant empirical function of interest is the probability distribution of individual IMF parameters, as recognized by Kroupa (2002). However if the average IMF is the quantity of interest, field star results from future astrometric missions and careful combinations of integrated light (see Kennicutt 1998; Leitherer, this volume) and chemical evolution constraints (e.g. Renzini, this volume) may be less problematic.

References

Anderson, J. 1998, in Fundamental Stellar Properties: The Interaction between Observation and Theory, IAU Symp. 189, ed. T. R. Bedding, A. J. Booth, J. Davis (Kluwer: Dordrecht), p. 99.

Basu, S. & Rana, N. C. 1992a, ApJ, 393, 373.

Basu, S. & Rana, N. C. 1992b, A & A, 265, 499.

Baume, G., Vazquez, R. A., Carraro, G., & Feinstein, A. 2003, A&A, 402, 549.

Baume, G., Moitinho, A., Giorgi, E. E., Carraro, G., & Vazquez, R. A. 2004, A&A, 417, 961.

Bonnell, I. A., Vine, S. G., & Bate, M. R. 2004, MNRAS, 349, 735.

Brown, A. G. A., de Geus, E. J. & de Zeeuw, P. T. 1994, A & A, 289, 101.

Chabrier, G. 2003a, Publications of the Astronomical Society of the Pacific, 115, 763.

Chabrier, G. 2003b, ApJL, 586, L133.

Claudius, M. & Grosbel, P. J. 1980, A&A, 87, 339.

D'Antona, F. & Mazzitelli, I. 1983, A&A, 127, 149.

De Grijs, R., Gilmore, G. F., Johnson, R. A. & Mackey, A. D. 2002a, MNRAS, 331, 245.

De Grijs, R., Gilmore, G. F., Mackey, A. D., Wilkinson, M. I., Beaulieu, S. F., Johnson, R. A., & Santiago, B. X. 2002b, MNRAS, 337, 597.

de la Fuente Marcos, R. 1997, A&A, 322, 764.

Elmegreen, B. G. 1999, ApJ, 515, 323.

Elmegreen, B. G. 1999, in The Evolution of Galaxies on Cosmological Timescales, ASP Conf. Ser. Vol. 187, ed. J. E. Beckman & T. J. Mahoney, p. 145.

Garmany, C. D., Conti, P. S. & Chiosi, C. 1982, ApJ, 263, 777.

Giorgi, E. E., Vazquez, R. A., Baume, G., Seggewiss, W., & Will, J.-M. 2002, A&A, 381, 884.

Goodwin, S. P. & Pagel, B. E. J. 2004, MNRAS, in press (astro-ph/0410068).

Hartmann, W. K. 1970, Memoires de la Societe Royale des Sciences de Liege, 59, 49.

Hillenbrand, L. A. & Carpenter J. M. 2000, ApJ, 540, 236.

Hillenbrand, L. A. & White, R. J. 2004, ApJ 604, 741.

Hillenbrand, L. A. 2004, in The Dense Interstellar Medium in Galaxies, ed. S. Pfalzner, C. Kramer, C. Straubmeier, A. Heithausen (NY: Springer-Verlag), in press, astro-ph/0312187.

Jappsen, A. ĐK., Klessen, R. S., Larson, R. B., Li, Y., & Mac Low, M. M. 2004, A&A, in press, astro-ph/0410351.

Jaschek, C. & Jaschek, M. 1957, PASP, 69, 337.

Jeffries, R. D., Thurston, M. R., & Hambly, N. C. 2001, A&A, 375, 863.

Kalirai, J. S., Fahlman, G. G., Richer, H. B., & Ventura, P. 2003, ApJ, 126, 1402.

Kennicutt, R. C. 1998, in The Stellar Initial Mass Function, ASP Conf. Ser. 142, ed. G. Gilmore & D. Howell (ASP Press: San Francisco), p. 1.

Kroupa, P. 2001, MNRAS, 322, 231.

Kroupa, P. 2002, Science, 295, 82.

Kroupa, P. & Boily, C. M. 2002, MNRAS, 336, 1188.

Kroupa, P., Gilmore, G., & Tout, C. A. 1991, MNRAS, 251, 293.

Kroupa, P., Tout, C. A. & Gilmore, G., 1990, MNRAS, 244, 76.

Kroupa, P., Tout, C. A. & Gilmore, G., 1993, MNRAS, 262, 545.

Kroupa, P. & Weidner, C. 2003, ApJ, 598, 1076.

Lada, C. J. & Lada, E. A. 2003 ARAA, 41, 57

Larson, R. B. 1973, MNRAS, 161, 133.

Limber, D. N., 1960, Astrophys.J., 131, 168.
Littlefair, S. P., Naylor, T., Jeffries, R. D., Devey, C. R., & Vine, S. 2003, MNRAS, 345, 1205.
Luhman, K. L. 2002, in Modes of Star Formation and the Origin of Field Populations, ASP Conf. Proc., Vol. 285, ed. E. K. Grebel, W. Brandner (San Francisco, ASP), p. 74.
Luhman, K. L., Stauffer, J. R., Muench, A. A., Rieke, G. H., Lada, E. A., Bouvier, J. & Lada, C. J. 2003, ApJ, 593, 1093.
Malkov, O. & Zinnecker, H. 2001, MNRAS, 321, 149.
Massey, P. 1985, PASP, 97, 5.
Massey, P. 2003, ARAA, 41, 15.
Massey, P. & Hunter, D. A. 1998, ApJ, 493, 180.
Massey, P., Lang, C. C., Degioia-Eastwood, K. & Garmany, C. D., 1995, ApJ., 438, 188.
Massey, P., Puls, J., Kudritzki, B., Puls, J. & Pauldrach, A. W. A. 2004, ApJ, 608, 1001.
Meyer, M. R., Adams, F. C., Hillenbrand, L. A., Carpenter, J. M. & Larson, R. B. 2000, in Protostars and Planets IV, ed. V. Mannings, A. P. Boss, S. S. Russell (Tucson: Univ. Ariz. Press), p. 121.
Miller, G. E. & Scalo, J. M. 1979, ApJS, 311, 406.
Moraux, E., Kroupa, P. & Bouvier, J. 2004, A&A, in press (astro-ph/0406581)
Muench, A. A. et al. 2003 AJ, 125, 2029.
Pandey, A. K., Nilakshi, Ogura, K., Sagar, R. & Tarusawa, K., 2001, A&A, 374, 504.
Phelps, R. L. & Janes, K. A., 1993, AJ, 106, 1870.
Piskunov, A. E., Belikov, A. N., Kharchenko, N. V., Sagar, R., & Subramaniam, A. 2004, MNRAS, 349, 1449.
Pont, F. & Eyer, L. 2004, MNRAS, 351, 487.
Porras, A., Cruz-Gonzalez, I. & Salas, L. 2003, in Galactic Star Formation Across the Stellar Mass Spectrum, ASP Conf. Series, Vol. 287, ed. J. M. De Buizer, N. S. van der Bliek (San Francisco: ASP), p. 98.
Preibisch, T., Brown, A. G. A., Bridges, T., Guenther, E., & Zinnecker, H. 2002, AJ, 124, 404.
Prisinzano, L., Carraro, G., Piotto, G., Seleznev, A. F., Stetson, P.B. & Saviane, I., 2001, A & A, 369, 851.
Prisinzano, L., Micela, G., Sciortino, S. & Favata, F. 2003, A & A, 404, 927.
Rana, N. C. 1991, ARAA, 29, 129.
Reddish, V. C. 1978, Stellar Formation (Oxford: Pergamon).
Reid, I. N., Gizis, J. E. & Hawley, S. L. 2002, AJ, 124, 2721.
Sagar, R. 2002, in Extragalactic Star Clusters, IAU Symp. 207, ed. E. K. Grebel, D. Geisler, D. Minniti (San Francisco: ASP), p. 515.
Sagar, R. & Richtler, T. 1991, A & A, 250, 324.
Sagar, R. & Griffiths, W. K. 1998, MNRAS, 299, 777.
Sagar, R., Munari, U., & de Boer, K. S. 2001, MNRAS, 327, 23.
Sagar, R., Naidu, B. N., & Mohan, V. 2001, Bull. Astr. Soc. India, 29, 519.
Salpeter, E. E. 1955, ApJ, 121, 161.
Sandage, A., 1957, Astrophys.J., 125, 422.
Sanner, J., Brunzendorf, J., Will, J. -. & Geffert, M., 2001, A&A, 369, 511.
Sanner, J. & Geffert, M. 2001, A & A, 370, 87.
Sanner, J., Altmann, M., Brunzendorf, J. & Geffert, M. 2000, A & A 357, 471.
Scalo, J. M. 1986, Fund. Cos. Phys., 11, 1.

Scalo, J. M. 1998, in The Stellar Initial Mass Function, ASP Conf. Ser. 142, ed. G. Gilmore & D. Howell (ASP Press: San Francisco), p. 201.
Schroder, K.-P. & Pagel, B. E. J. 2003, MNRAS, 343, 1231.
Segransan, D., Delfosse, X., Forveille, T., Beuzit, J. L., Perrier, C., Udry, S., & Mayor, M. 2003, in Brown Dwarfs, Proc. IAU Symp. 211, ed. E. Martin (San Francisco: ASP), p. 413.
Sirianni, M., Nota, A., De Marchi, G., Leitherer, C., & Clampin, M. 2002, ApJ, 579, 275.
Slesnick, C. L., Hillenbrand, L. A., & Massey, P. 2002, ApJ, 576, 880.
Subramaniam, A. & Sagar, R. 1999, AJ, 117, 937.
Sung, H. & Bessell, M. S. 2004, AJ, 127, 1014.
Sung, H., Bessell, M. S., & Lee, S.-W. 1998, AJ, 115, 734.
Taff, L. G., 1974, AJ, 79, 1280.
Tarrab, I. 1982, A & A, 109, 285.
Van Buren, D. 1985, ApJ, 294, 567.
van den Bergh, S., 1957, ApJ., 125, 445.
Vanbeveren, D. 1982, A&A, 115, 65.
Vanbeveren, D. 1983, A&A, 124, 71.
Weidner, C., Kroupa, P., & Larsen, S. S. 2004, MNRAS, 350, 1503.
Wilking, B. A., Meyer, M. R., Greene, T. P., Mikhail, A. & Carlson, G. 2004, AJ, 127, 1131.
Yadav, R. K. S. & Sagar, R., 2002, MNRAS, 337, 133.
Yadav, R. K. S. & Sagar, R., 2004, MNRAS, 351, 667.
Yuan, J. W., 1992, A &A, 261, 105.

Figure 5. John Scalo leading the group under the storm.

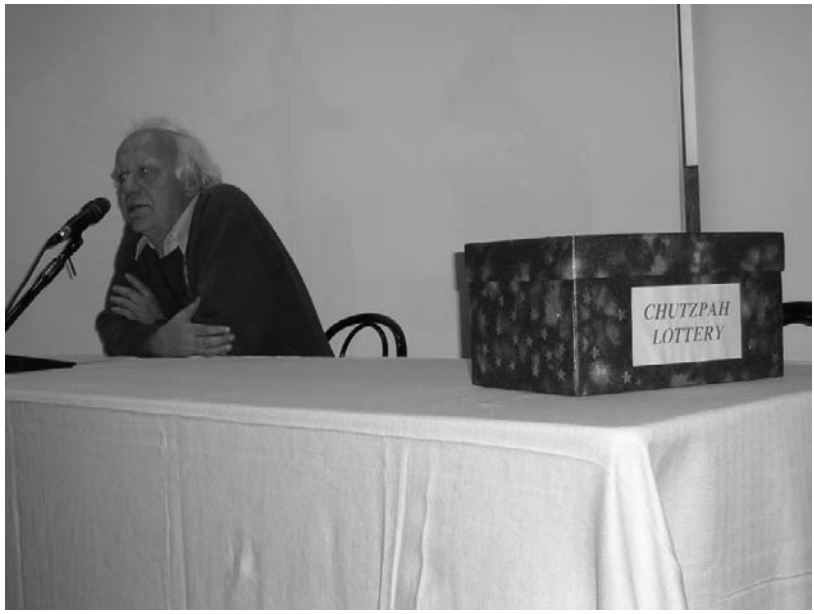

Figure 6. Franco Pacini: the founder of the Arcetri-Salpeter connection.

Figure 7. The attentive audience.

THE INITIAL MASS FUNCTION: FROM SALPETER 1955 TO 2005

Gilles Chabrier
Ecole Normale Supérieure de Lyon, CRAL, Lyon, France
chabrier@ens-lyon.fr

Abstract Fifty years after Ed Salpeter's seminal paper, tremendous progress both on the observational and theoretical sides allow a fairly accurate determination of the Galactic IMF not only down to the hydrogen-burning limit but into the brown dwarf domain. The present review includes the most recent observations of low-mass stars and brown dwarfs to determine this IMF and the related Galactic mass budget. The IMF definitely exhibits a similar behaviour in various environments, disk, young and globular clusters, spheroid. Small scale dissipation of large scale compressible MHD turbulence seems to be the underlying triggering mechanism for star formation. Modern simulations of compressible MHD turbulence yield an IMF consistent with the one derived from observations.

1. Introduction

The determination of the stellar initial mass function (IMF) is one of the Holy Grails of astrophysics. The IMF determines the baryonic content, the chemical enrichment and the evolution of galaxies, and thus the universe's light and baryonic matter evolution. The IMF provides also an essential diagnostic to understand the formation of stellar and substellar objects. In this review, we outline the current determinations of the IMF in different galactic environments, measuring the progress accomplished since Salpeter (1955) seminal paper 50 years ago. We also examine this IMF in the context of modern theories of star formation. A more complete review can be found in Chabrier (2003a) but very recent results are included in the present paper.

2. Mass-magnitude relations

Apart from binaries of which the mass can be determined eventually by use of Kepler's third law, the determination of the MF relies on the transformation of the observed luminosity function (LF), $\Phi = dN/dM$, i.e. the number of stars N per absolute magnitude interval dM. This transforma-

E. Corbelli et al. (eds.), The Initial Mass Function 50 Years Later, 41–50.

tion involves the derivative of a mass-luminosity relationship, for a given age τ, or preferentially of a mass-magnitude relationship (MMR), $\frac{dn}{dm}(m)_\tau = (\frac{dn}{dM_\lambda(m)}) \times (\frac{dm}{dM_\lambda(m)})^{-1}_\tau$, which applies directly in the observed magnitude M_λ and avoids the use of often ill-determined bolometric and $T_{\rm eff}$-color corrections.

Fig. 1 displays the comparison of the Andersen (1991) and Ségransan et al. (2003) data in the V band with different theoretical MMRs, namely the parametrizations of (KTG), Reid et al. (2002) for $M_V < 9$ complemented by Delfosse et al. (2000) above this limit and the models of Baraffe et al. (1998) (BCAH) for two isochrones. The KTG MMR gives an excellent parametrization of the data over the entire sample but fails to reproduce the flattening of the MMR near the low-mass end, which arises from the onset of degeneracy near the bottom of the main sequence (MS), yielding too steep a slope. The Delfosse et al. (2000) parametrization, by construction, reproduces the data in the M_V=9-17 range. For $M_V < 9$, however, the parametrization of Reid et al. (2002) misses a few data, but more importantly does not yield the correct magnitude of the Sun for its age. The BCAH models give an excellent representation for $m \gtrsim 0.4 M_\odot$. Age effects due to stellar evolution start playing a role above $m \sim 0.8\,M_\odot$, where the bulk of the data is best reproduced for an age 1 Gyr, which is consistent with a stellar population belonging to the young disk ($h < 100$ pc). Below $m \sim 0.4\,M_\odot$, the BCAH MMR clearly differs from the Delfosse et al. (2000) one. Since we know that the BCAH models overestimate the flux in the V-band, due to still incomplete molecular opacities, we use the Delfosse et al. (2000) parametrization in this domain. The difference yields a maximum $\sim$ 16% discrepancy in the mass determination near $M_V \sim 13$. Overall, the general agreement can be considered as very good, and the inferred error in the derived MF is smaller than the observational error bars in the LF. The striking result is the amazing agreement between the theoretical *predictions* and the data in the K-band (Figure 2), a more appropriate band for low-mass star (LMS) detections.

3. The disk and young cluster mass function

3.1 The disk mass function

A V-band nearby LF Φ_V can be derived by combining Hipparcos parallax data (ESA 1997), which are essentially complete for $M_V < 12$ at r_{comp}=10 pc, and the sample of nearby stars with ground-based parallaxes for $M_V > 12$ with r_{comp}=5.2 pc (Dahn et al. 1986). Such a sample has been reconsidered recently by Reid et al. (2002), and extended to r=8 pc by Reid et al. (2004). The revised sample agrees within $\sim 1\sigma$ with the previous one, except for $M_V \gtrsim 14$, where the 2 LFs differ at the $\sim 2\sigma$ limit. The 5-pc LF was also obtained in the H and K bands by Henry & McCarthy (1990).

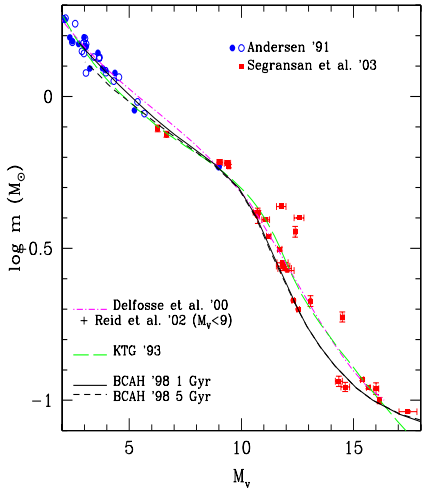

Figure 1. Comparison of the observed and theoretical m-M$_V$ relation.

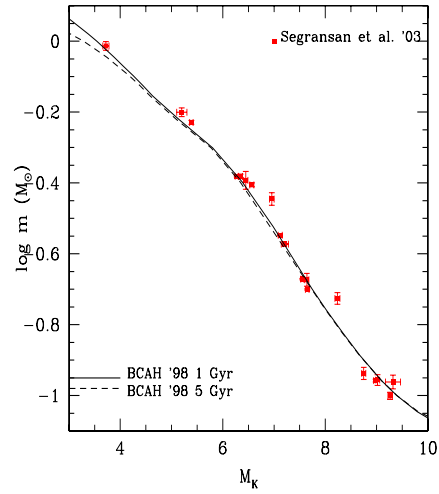

Figure 2. Same for the m-M$_K$ relation.

The IMFs, $\xi(\log\ m) = \frac{dn}{d\log m}$, derived from the Φ_V and Φ_K LFs are portrayed in Figure 3 below 1 M$_\odot$. Superposed to the determinations is the following analytical parametrization (in $(\log \mathrm{M}_\odot)^{-1}\,\mathrm{pc}^{-3}$):

$$\begin{aligned} \xi(\log\ m) &= 0.093 \times \exp\Big\{-\frac{(\log\ m\ -\ \log\ 0.2)^2}{2\times(0.55)^2}\Big\}, \quad m \leq 1\,\mathrm{M}_\odot \\ &= 0.041\, m^{-1.35\pm0.3} \qquad\qquad\qquad\qquad\quad , m \geq 1\,\mathrm{M}_\odot \end{aligned} \tag{1}$$

This IMF differs a bit from the one derived in Chabrier (2003a) since it is based on the revised 8-pc Φ_V. The difference at the low-mass end between the two parametrizations reflects the present uncertainty at the faint end of the disk LF, near the H-burning limit (spectral types $\gtrsim$ M5). Note that the field IMF is also representative of the bulge IMF (triangles), derived from the LF of Zoccali et al. (2000).

A fundamental advantage of the nearby LF is the identification of stellar companions. It is thus possible to merge the resolved objects into multiple systems, to calculate the magnitude of the systems and then derive the *system* IMF. The following parametrization, slightly different from the one derived in Chabrier (2003a) is displayed in Figure 4 (normalyzed as eqn.(1) at 1 M$_\odot$, where all systems are resolved):

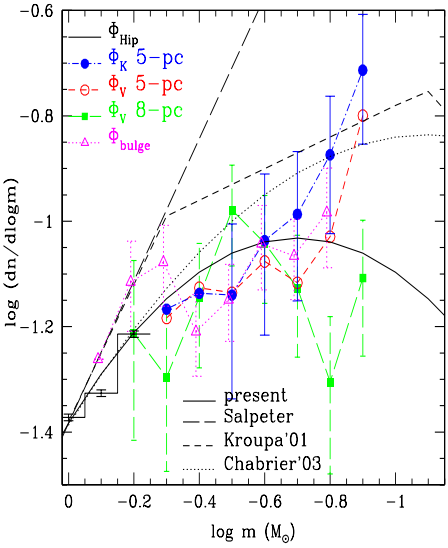

Figure 3. Disk IMF for individual objects.

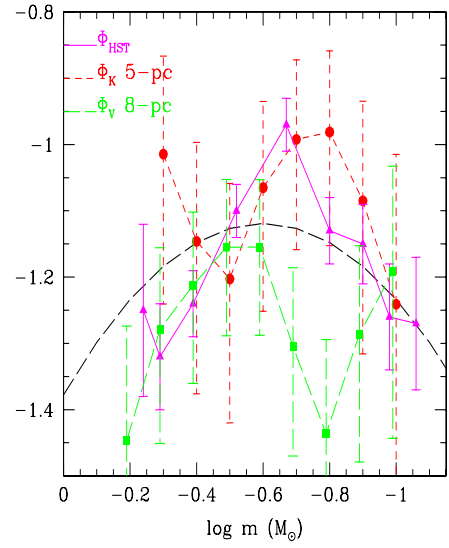

Figure 4. Disk IMF for unresolved systems.

$$\xi(\log\, m) = 0.076 \times \exp\Big\{-\frac{(\log\, m\ -\ \log\, 0.25)^2}{2 \times 0.55^2}\Big\},\ \ m \leq 1\,\mathrm{M}_\odot \qquad (2)$$

As shown by Chabrier (2003b) and seen on the figure, this system IMF is in excellent agreement with the MF derived from the revised HST phometric LF (Zheng et al. 2001), showing that the discrepancy between the MF derived from the nearby LF and the one derived from the HST stemmed primarily from unresolved companions in the HST field of view.

The brown dwarf regime.

Many brown dwarfs (BD) have now been identified down to a few jupiter masses in the Galactic field with the DENIS, 2MASS and SDSS surveys. Since by definition BDs never reach thermal equilibrium and keep fading with time, comparison of the predicted BD LFs, based on a given IMF, with observations requires to take into account time (i.e. formation rate) and mass (i.e. IMF) probability distributions. In the present review, we proceed slightly differently from the calculations of Chabrier (2003a). We start from the *system* IMF (2) and we include a probability distribution for the binary frequency which decreases with mass. Indeed, various surveys now show that the binary fraction X_{bin} (and orbital separation) decreases with mass, varying from $X_{bin} \approx 60\%$ for G and K-stars to $\approx 40\%$ for early (M0-M4) M-dwarfs, to $\approx 20\%$ for later

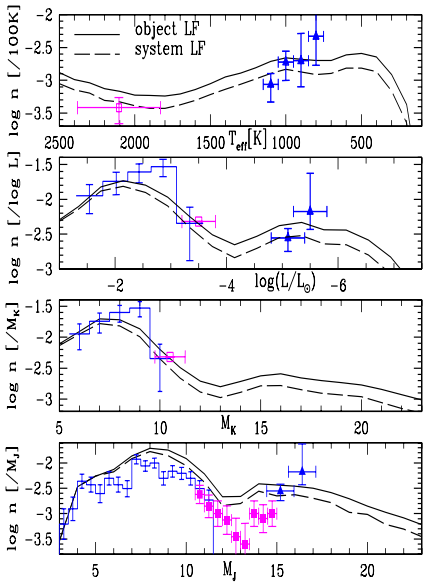

Figure 5. Comparison of the observed and theoretical LMS, L-dwarf (■) and T-dwarf (▲) distributions.

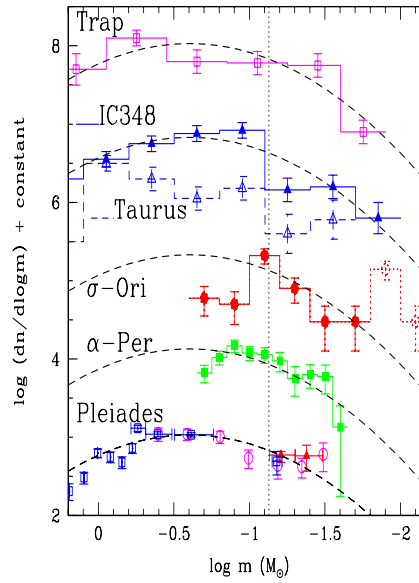

Figure 6. IMF for young clusters. Dash-line: field system IMF (2). Vertical dotted line: H-burning limit.

M and L-dwarfs, correcting for undetected short period binaries, to $\approx 10\%$ for T-dwarfs.

Figure 5 displays the calculated BD density distributions as a function of $T_{\rm eff}$, L, M_K and M_J, based on the BD cooling models developed in the Lyon group, and the most recent estimated LMS and BD densities (Gizis et al. 2000, Burgasser 2001, Cruz 2004[1]). The dash-line displays the distributions obtained with the system IMF (4) while the solid line corresponds to the IMF (1) for individual objects. As mentioned above, the distributions obtained with this latter IMF are consistent with a binary frequency decreasing from $\sim 50\%$ to $\sim 20\%$. The agreement between the theoretical calculations and the observations is very satisfactory, keeping in mind the remaining uncertainties in BD cooling theory and in accurate determinations of the observed BD $T_{\rm eff}$, M_{bol} and number densities. The predicted dip around $M_J \sim M_K \sim 13$, $M_{bol} \sim 15$ (Chabrier (2003a)) is confirmed by the recent L-dwarf observations.

[1]Unpublished data in the J-band were kindly provided by N. Reid

3.2 The young cluster mass function

Figure 6 displays the MFs derived from the observed LFs of several young clusters, with ages ranging from ~ 1 Myr to ~ 150 Myr, down to the substellar domain (see references in Chabrier (2003a)). Note that some of the faintest objects in σ-Or have been shown recently to be field star contaminations (McGovern et al. 2004, Burgasser et al. 2004). We used the MMRs from BCAH for the appropriate age in the appropriate observational filters. Accuracy of the BCAH models for young clusters has been examined carefully by Luhman et al. (2003). These observational surveys do not resolve multiple systems, so the derived MFs reflect the system MFs. Superposed to these IMFs is the field system IMF (2). Figure 6 clearly points to a similar underlying IMF between young clusters and the Galactic field, except for the significantly less dense Taurus cluster.

4. The globular cluster and spheroid mass function

Globular clusters provide a particularly interesting test-bed to investigate the stellar MF. They provide a homogeneous sample of MS stars with the same age, chemical composition and reddening, their distance is relatively well determined, allowing straightforward determinations of the stellar LF. From the theoretical point of view, the Baraffe et al. (1997) evolutionary models accurately reproduce the observed color-magnitude diagrams of various clusters with metallicity $[\mathrm{M/H}] \leq -1.0$ both in optical and infrared colors, down to the bottom of the main sequence, with the limitations in the optical mentioned in §2 for more metal-rich clusters. As mentioned above, however, the consequences of this shortcoming on the determination of the MF remain modest. The IMFs derived by Chabrier (2003a) for several globular clusters, from the LFs observed with the HST, corrected for dynamical evolution, by Paresce & DeMarchi (2000) are displayed in Fig.7. Superimposed on the derived IMFs is the spheroid IMF given by eqn.(20) of Chabrier (2003a) (short-dash line), with the characteristic mass shifted by 1 to 2 σ's ($m_c = 0.22$ to 0.32 $\mathrm{M}_\odot$), similar to the IMF derived by Paresce & DeMarchi (2000). The disk IMF (2) is also superimposed for comparison. We note the relative similarity of the these two IMFs, but a deficiency of very-low-mass objects, including BDs, in the cluster IMFs.

5. Galactic implications : mass budget and mass to light ratio

Integrating the IMF (1) yields the stellar and brown dwarf number- and mass-densities given in Table I, and the relative contributions $\mathcal{N} = N(\Delta m)/N_{tot}$ and $\mathcal{M} = M(\Delta m)/M_{tot}$, where N and M denote re-

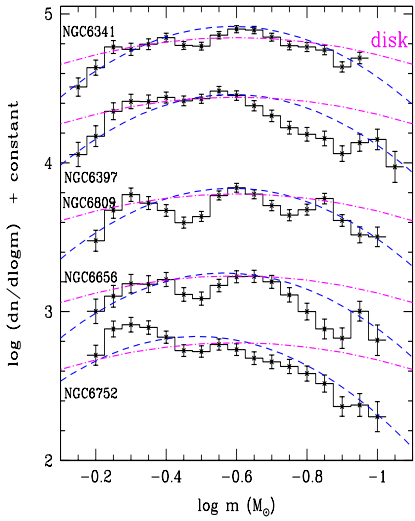

Figure 7. IMF for several globular clusters. Dot-dash line: disk system IMF (2)

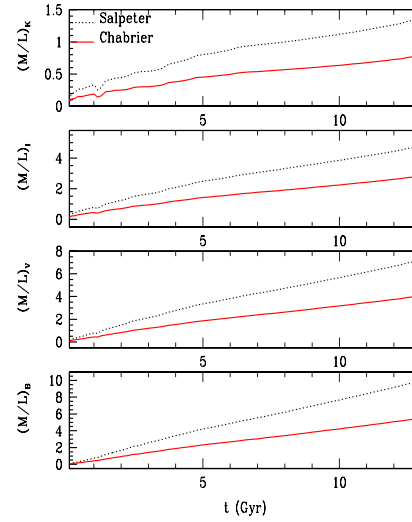

Figure 8. Mass-to-light ratio for single stellar population in optical and NIR bands.

spectively the number and mass of objects in the mass range Δm. Adding up remnant densities (Chabrier (2003a)) yields the stellar+substellar contributions to the Galactic mass budget. These new determinations give a BD-to-star number ratio of $n_{BD}/n_\star \sim 1/3$.

Figure 8 compares the M/L ratio obtained with the present IMF (1) and with the Salpeter IMF (see also Bruzual & Charlot 2003). The present IMF yields M/L ratios in good agreement with observations and with expectations from CDM hierarchical simulations of spiral disk galaxies or from dynamical arguments (e.g. from Tully-Fischer relation), whereas a Salpeter IMF yields too large values (Portinari et al. 2004).

6. Star formation theory

Although we are still far from a general paradigm for star formation, some general properties can be considered as robust : (1) star formation extends well below the H-burning limit, (2) the shape of the IMF seems to be very similar in very diverse environments, (3) star formation is a rapid process, comparable to the dynamical timescale $\tau_{dyn} = (3\pi/32G\rho)^{1/2}$ $\approx$1-5$\times10^5$ yr for typical star-forming molecular clouds, (4) the stellar IMF seems to be reminiscent of the prestellar core mass spectrum, suggesting that the IMF is already determined by the cloud clump mass distribution (see André and Myers, this conference),

Table 1. Present day stellar and brown dwarf Galactic budget[a,b].

Parameter		*Disk*	Spheroid	Dark halo
n_{BD}		2.6×10^{-2}	3.5×10^{-5}	
ρ_{BD}		1.0×10^{-3}	$\lesssim 2.3 \times 10^{-6}$	
$n_\star$		$(9.3 \pm 2) \times 10^{-2}$	$\leq (2.4 \pm 0.1) \times 10^{-4}$	
$\rho_\star$		$(3.4 \pm 0.3) \times 10^{-2}$	$\leq (6.6 \pm 0.7) \times 10^{-5}$	$\ll 10^{-5}$
n_{rem}		$(0.7 \pm 0.1) \times 10^{-2}$	$\leq (2.7 \pm 1.2) \times 10^{-5}$	
ρ_{rem}		$(0.6 \pm 0.1) \times 10^{-2}$	$\leq (1.8 \pm 0.8) \times 10^{-5}$	$< 10^{-4}$
n_{tot}		0.13 ± 0.03	$\leq 3.0 \times 10^{-4}$	
ρ_{tot}		$(4.1 \pm 0.3) \times 10^{-2}$	$\leq (9.4 \pm 1.0) \times 10^{-5}$	$< 10^{-4}$
BD:	$\mathcal{N}$; $\mathcal{M}$	0.20; 0.02	0.10; 0.03	
LMS($\leq 1 M_\odot$):	$\mathcal{N}$; $\mathcal{M}$	0.71; 0.68	0.80; 0.77	
IMS(1-9$M_\odot$):	$\mathcal{N}$; $\mathcal{M}$	0.03; 0.15	0.; 0.	
WD+NS:	$\mathcal{N}$; $\mathcal{M}$	0.06; 0.15	0.10; 0.20	

[a] The number densities n are in [pc^{-3}], the mass densities ρ are in [$M_\odot$ pc^{-3}].

(5) on large scales, the spectral line widths in molecular clouds indicate supersonic, super-Alfvénic conditions. All these observations point to a common driving mechanism for star formation, namely turbulence-driven fragmentation. Figure 10 compares the mass spectrum obtained from MHD simulations done recently by Padoan & Nordlund (2002) and Li et al. (2004) with the *system* IMF (2) (indeed, the prestellar cores correspond to multiple systems, which eventually will fragment further into individual objects). Although such comparisons must be considered with due caution before drawing any conclusion, the agreement between the simulations and the IMF representative of the field is amazing. Note that such hydrodynamical simulations form BDs in adequat numbers from the same fragmentation mechanism as for star formation. Various observations of disk accreting BDs indeed show that BDs and stars form from the same underlying mechanism. Motivation for invoking the formation of BDs by ejection thus no longer seems to be necessary. Moreover, the recent observation of a wide binary BD (Luhman 2004) definitely contradicts the predictions of such a scenario as a dominant formation mechanism for BDs. This new picture thus combines turbulence, as the initial driving mechanism for fragmentation, and gravity, providing a natural explanation for a (scale free) power-law IMF above a critical mass, namely the mean thermal Jeans mass $\langle m_J \rangle$, and a lognormal distribution below, due to the fact that only the densest cores, exceeding the local Jeans mass, will collapse into bound objects. Note that in these simulations of supersonic turbulence, only a few percents of the total mass end up into the collapsing cores after one dynamical time, solving naturally the old high efficiency problem associated with turbulence-driven star

formation. Recent similar simulations by Li & Nakamura (2004), on the other hand, suggest enhanced ambipolar diffusion to occur through shock compression.

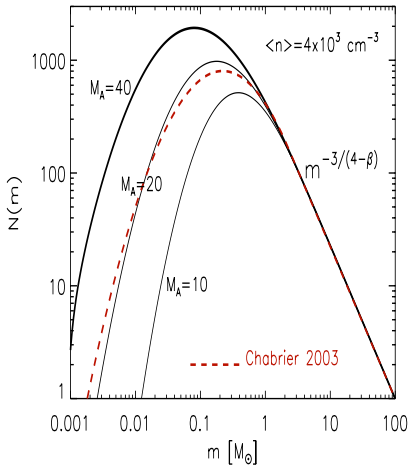

Figure 9. Comparison of the system IMF (2) with the one obtained by Padoan & Nordlund (2002)

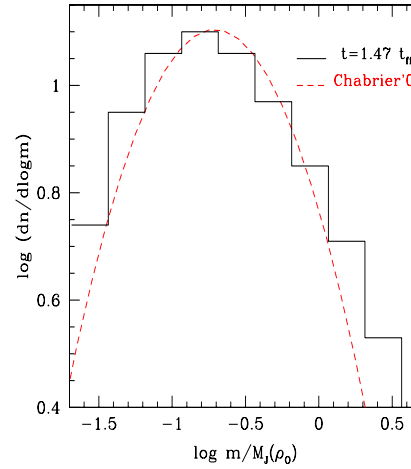

Figure 10. Same with the one obtained from MHD simulations by Li et al. (2004).

7. Conclusion and perspective

In this review, we have examined the most recent determinations of the Galactic stellar IMF. Thanks to tremendous progress both in observational techniques and in the theory of low-mass stars and brown dwarfs, the IMF can now be determined down to a few jupiter masses, two orders of magnitude below the $\sim 0.5 M_\odot$ limit of accuracy of the Salpeter (1955) IMF. This IMF adequately reproduces various observational constraints, star and BD counts, binary frequencies, galactic mass-to-light ratios. It is well described by a Salpeter power-law above $\sim 1 M_\odot$ rolling down into a lognormal form below this mass, with a characteristic mass around 0.2 $M_\odot$, although more data is needed to really nail down this issue. Only for nearly zero-metal environments in the early universe do we expect a significantly larger characteristic mass, due to the lack of efficient cooling mechanism in the cloud (see Bromm, this conference). The universality of the IMF in various environments, disk, young and globular clusters, spheroid, points to a universal triggering mechanism and a dominant cooling process for star formation. Small scale dissipation of large scale supersonic MHD turbulence provides an appealing solution for this mechanism.

References

Andersen, J., 1991, A&ARv, 3, 91
Baraffe, I., Chabrier, G., Allard, F., & Hauschildt, P., 1997, A&A, 327, 1054
Baraffe, I., Chabrier, G., Allard, F., & Hauschildt, P., 1998, A&A, 337, 403
Bruzual & Charlot 2003, MNRAS, 344, 1000
Burgasser, A., 2001, PhD thesis
Burgasser, A., et al., 2004, ApJ, 604, 827
Chabrier, G., 2003a, PASP, 115, 763
Chabrier, G., 2003b, ApJ, 585, L133
Cruz, K., 2004, PhD thesis
Dahn, C.C, Liebert, J., Harrington, R.S, 1986, AJ, 91, 621
Delfosse, X., et al., 2000, A&A, 364, 217
Gizis, J., et al. 2000, ApJ, 120, 1085
Henry, T.J., & McCarthy, D.W., 1990, ApJ, 350, 334
Kroupa, P., 2001, MNRAS, 322, 231
Li, P.S.,Norman, M., Mac Low, M.-M., & Heitsch, F., 2004, ApJ, 605, 800
Li, Z.-Y., & Nakamura, F., 2004, ApJ, 609, L83
Luhman, K., et al. 2003, ApJ, 593, 1093
Luhman, K., 2004, ApJ, 614, 398
McGovern, J., et al. 2004, ApJ, 600 1020
Padoan, P., & Nordlund, Å, 2002, ApJ, 576, 870
Reid, I.N., Gizis, J.E. & Hawley, S.L., AJ, 2002, 124, 2721
Reid, I.N., et al., 2004, in preparation
Paresce, F., & De Marchi, G., 2000, ApJ, 534, 870
Portinari, Sommer-Larsen & Tantalo, 2004, MNRAS, 347, 691
Salpeter, E.E., 1955, ApJ, 121, 161
Ségransan, D., et al., 2004, IAU Symposium 211, Astr. Soc. Pacific, 2003, p. 413
Zheng, Z, Flynn, C., Gould, A., Bahcall, J.N., & Salim, S., 2001, ApJ, 555, 393
Zoccali, M. et al., 2000, ApJ, 530, 418

Figure 11. Hans, Francesco and Edvige introducing the conference.

II

THE IMF IN OUR GALAXY: CLUSTERS AND FIELD STARS

"I am proud, rather than ashamed, of the sloppy approximations I made in that paper, but I was also lucky that several errors mostly canceled each other, rather than adding up. The result was also a particularly simple powerlaw for the IMF, which is close to the predicting log scale invariance for the distribution of mass among different stars (a similar but not identical, relation holds for the distribution of people into villages, town and cities). Developments in 50 years has been good for me but bad for science: I had hoped that my IMF was only an average for today and that the actual function would vary strongly from quiescent to active regions and would also vary from the young galaxy to the galaxy today. Some such variations probably exist but are too weak for universal agreement, so "the Salpeter function" is still of some use today and gets quoted, but the theory of star formation has suffered greatly by not having clear-cut observational variations, which would have to be predicted by a correct theory." – Ed Salpeter (Ann. Rev. Astron. Astrophys. 2002)

Figure 12. Ed proudly showing the universality of the IMF.

Figure 13. Participants arrival at Spineto.

THE FIELD IMF ACROSS THE H-BURNING LIMIT

I. Neill Reid
STScI, 3700 San Martin Drive, Baltimore, MD 21218, USA
inr@stsci.edu

Abstract I review recent progress in constraining the form of the substellar mass function in the field. Using 2MASS, we have compiled the first infrared luminosity function extending through the L dwarf régime. Our results show a clear minimum space density at ∼L4, with a subsequent rise toward lower luminosities; the local ratio of M dwarfs to L dwarfs is $\sim 20:1$. Theoretical models show that these data offer only weak constraints on $\psi(M)$, with significant α-dependent differences only emerging in the predicted T (and Y) dwarf densities. Current observational estimates suggest a flattening in $\psi(M)$ at substellar masses($\alpha < 0.8$), broadly consistent with results from studies of young open clusters.

1. Introduction

Over the last decade we have been able to establish a firm observational foundation for the mass function, $\psi(M)$, at stellar masses. While the exact functional form, and the underlying physical processes, remain obscure to a certain extent (Chabrier, this conference), new surveys coupled with improved astrometry and mass-luminosity data give reliable densities for field stars between 0.1 and $\sim 1.5 M_{\odot}$. The situation is less solid at lower masses. While recent follow-up observations of near-infrared survey data, notably 2MASS, have produced the first reliable statistics for substellar objects, there are significantly more problems in converting those measurements to $\psi(M)$. This talk reviews the current status of the subject, and highlights a number of caveats concerning the derivation of $\psi(M)$ at stellar masses.

2. The field mass function at stellar masses

The traditional method of deriving $\psi(M)$ for the Galactic field is as follows:

1 Identify a well-defined, well-characterised sample of nearby stars;

2 Estimate distances, multiplicity and luminosities using the available data (astrometry, photometry, high-resolution imaging, spectroscopy);

E. Corbelli et al. (eds.), The Initial Mass Function 50 Years Later, 53–60.

3 Define a distance-limited sample by assigning appropriate distance limits, usually as a function of stellar luminosity, and derive space densities (the luminosity function, $\Phi(M_V)$);

4 Use a mass-luminosity relation to estimate masses for individual objects, and hence derive the present-day mass function;

5 Adjust for evolutionary effects and the disk star formation history to derive an estimate of the initial mass function.

Reid, Gizis & Hawley (2002 - PMSU4) provide a recent example of this type of analysis at stellar masses. However, steps 4 and 5 become significantly more complicated in the substellar régime, as discussed further below.

Sample completeness is the key to the reliability of these studies, and, as a result, a high premium is placed on accurate distance determination. For early- type stars, the availability of the Hipparcos catalogue has revolutionised matters, providing precise trigonometric parallax data for over 110,000 stars. Even so, the Hipparcos magnitude limits restrict complete late-G and K dwarf samples to distances of 25-30 parsecs, while complete M dwarf samples are drawn from increasingly smaller volumes and must rely on combinations of astrometric, photometric and spectroscopic distance estimates. Fortunately, orbital diffusion over the history of the Milky Way means that those stars can still be taken as characteristic of the outer Galactic disk - stars currently in the immediate Solar Neighbourhood may have originated from regions 1-3 kpc inside or outside the Solar Radius. As discussed elsewhere in this volume, applying standard mass- luminosity relations to the resultant distance-limited catalogue gives a mass function broadly consistent with a power-law, $\alpha \sim 1$ (where $\alpha = 2.35$ for the Salpeter function), although a log-normal distribution can also be used to (better?) represent the data.

An issue of mild contention in these studies is the appropriate distance limit to apply for late-type M dwarfs (>M5). Some argue for a boundary as close as 5 parsecs and use an all-sky sample (eg Henry et al. 2004); I prefer to set a distance limit of 8 parsecs but limit analysis to regions accessible from northern hemisphere observations, $\delta > -30^o$. The original northern 8- parsec (N8-pc) sample was defined in 1997 (Reid & Gizis, 1997), comprising 140 main-sequence stars, 9 white dwarfs and one brown dwarf. Since then, we have added two brown dwarfs (Gl 570D and 2M1507-1627) and 14 main-sequence stars in 10 systems, while eliminating (through improved parallax measurements) 13 main-sequence stars in 10 systems (Reid et al. 2003; Reid et al. 2004 - NStars8)[1]. All save 5 of the 109 systems have accurate trigono-

[1]Henry et al. (2004) have recently estimated a photometric distance of 7.3 pc to LP 775-31 (M7); our distance estimate for that star is 8.3 pc (NStars5).

metric parallax data, while at least 85% have been scrutinised thoroughly for low-mass companions.

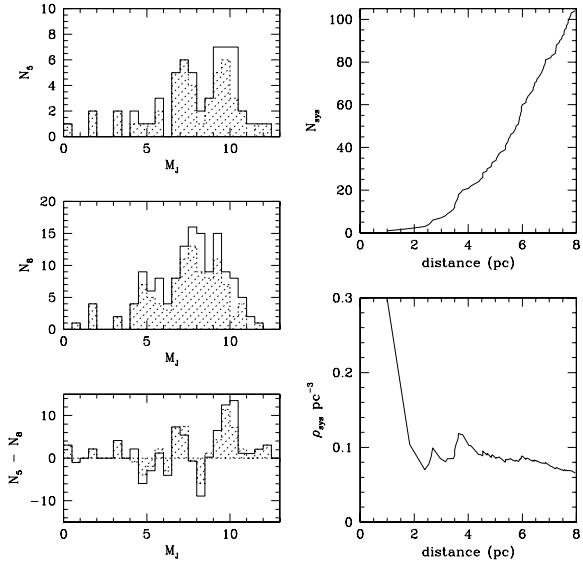

Figure 1. The left-hand panels compare the J-band luminosity functions of the 5-pc (uppermost panel) and Northern 8-pc (middle panel) samples; the lower panel plots the difference between the observed N8-pc sample and predicted numbers, extrapolated from the 5-pc sample. The right-hand panels plot the cumulative distribution of systems within 8-parsecs (all M_J) and the corresponding run of number density with distance.

The N8-pc luminosity function is compared against data for the 5-pc sample in Figure 1, where we also show the run of total number density with increasing distance. The latter shows a shallow decline at $d > 6.5$pc, but differencing the luminosity function shows that most of the discrepancy lies with relatively bright mid-type M dwarfs. As Chabrier notes (this conference), there is also an offset in number densities at the faintest magnitudes, albeit only $\sim 1.5\sigma$. I shall return to this issue later in this paper.

3. A local substellar census

Both the N8-pc and 5-pc samples are based almost exclusively on systems identified using conventional photographic techniques, notably proper motion surveys. Late-type dwarfs are notoriously faint at optical wavelengths. With the completion of the DENIS and 2MASS near-infrared sky surveys, we have a much more effective technique for discovering nearby cool dwarfs. Over the last three years, we have exploited this advantage in carrying out a thorough survey for late-type dwarfs within 20-parsecs of the Sun (Reid & Cruz, 2001;

Cruz et al. 2003 - NStars5). Following a two-pronged approach, we have combined data from the 2MASS Second Incremental Release (2M2nd, 48% sky coverage) with the NLTT catalogue (Luyten, 1980) to search for nearby early- and mid-type M dwarfs, while using 2MASS data directly to search for ultracool dwarfs (spectral types M8 and later). The former study has so far netted three additions to the N8-pc sample (NStars8).

Figure 2 illustrates our basic technique for finding ultracool dwarfs. The main sequence is effectively vertical in (J-K_s) between spectral types M0 and ∼M7, with all dwarfs having colours between 0.8 and 0.9 magnitudes; as a result, infrared surveys must be combined with optical data to derive useful photometric parallaxes for those stars. Later than M7, however, the main sequence turns redward in (J-K), and we can utilise infrared data alone to estimate luminosities and distances. Capitalising on that, we have used photometry of late-M and L dwarfs with known parallax to outline the (J, (J-K_S)) colour-magnitude limits expected for systems within 20 parsecs (Figure 2): systems falling above and to the right of the selection criteria are likely to have d≤20 pc.

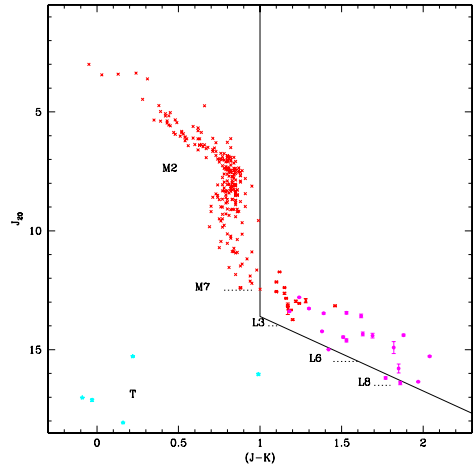

Figure 2. Identifying nearby ultracool dwarfs: the figure plots (J, (J-K_s)) for late-type dwarfs with accurate photometry and reliable parallaxes, with all objects placed at a distance of 20 parsecs. The full lines identify our selection criteria: sources lying above and to the right of the selection limit are likely to be within 20 parsecs of the Sun. Note that a few late-type L dwarfs fall below our selection criteria, so we expect $\sim 25-40\%$ incompleteness later than ∼L5.

There are $\sim 2 \times 10^8$ sources in the 2M2nd catalogue, and 1% of those sources meet the colour-magnitude limits outlined in Figure 2. Using an array of additional criteria, including (R-J) colour, location in the (J-H)/(H-K_S) plane and proximity to nearby galaxies (LMC, SMC, M31) and known star-forming regions, that daunting list can be trimmed to manageable proportions

(~ 1670 candidates - NStars5). We have since expanded coverage to the full 2MASS survey, excluding regions within 15^o of the Galactic Plane. Follow-up optical and infrared spectroscopic classification is almost complete, and we have identified over 200 new ultracool dwarfs, besides recovering almost all previously-known systems, allowing us to derive the first reliable luminosity function for this spectral domain (Cruz et al. 2004). The resultant function has a clear minimum at $M_J \sim 13.25$ ($\sim$L4), with a sharp increase in number densities at lower luminosities. Only ~ 80 L dwarfs (all-sky) reside within 20 parsecs of the Sun. This should be compared with an expected total of approximately 1600 M dwarfs. As will be discussed further below, this apparent paucity is in broad accord with expectations.

4. The substellar mass function

The L dwarf régime encompasses both very low-mass stars and brown dwarfs, with the balance switching from the former to the latter as one moves from L0 to L8. As a result, turning the L dwarf luminosity function into a mass function is complicated, because brown dwarfs follow near-identical cooling tracks in the (L, T_{eff}) plane at rates that depend inversely on the mass. Thus, all brown dwarfs look the same as each other (just at different ages) and there is no simple, single-valued mass-luminosity relation. Consequently, studies of the substellar mass function tend to invert the process outlined in §2. Rather than using the luminosity function to compute $\psi(M)$, one starts with an estimate of $\psi(M)$ and the star-formation rate, and predicts $\Phi(M_J)$, adjusting the input data until suitable agreement is obtained with the observations. We note that this is similar in some respects to the techniques adopted by Kroupa, Tout & Gilmore (1993) at stellar masses.

Figure 3 presents an example of this type of analysis, taken from work by P. Allen (Allen, Koerner & Reid 2004). Theoretical predictions, modeling $\psi(M)$ as a power-law (index α_1) for $M < 0.1M_\odot$ coupled with a constant star formation rate, are matched against the NStars late-M/L dwarf luminosity function and T dwarf space densities from Burgasser (2004). There are two main conclusions: first, almost all theoretical models match the L dwarf data, regardless of the value of α_1; second, the T dwarf data favour $\alpha_1 < 0.5$, significantly flatter than the best-fit power-law at stellar masses. In an independent analysis, Burgasser (2004) arrives at very similar conclusions. The former result reflects the rapid evolution of brown dwarfs through the L dwarf temperature régime, coupled with a predominance of higher- mass ($> 0.05M_\odot$) systems. L dwarf statistics therefore provide poor constraints on the form of the mass function.

On the other hand, the T dwarf densities suggest a turnover or flattening in the mass function as masses decrease below the substellar limit, a result broadly consistent with studies of $\psi(M)$ in young star clusters (eg Luhman,

this conference). That is, there is no strong conflict between results for clusters and for the field[2] (see also Chabrier, 2003). Figure 3 also shows that the best prospect of further constraining $\psi(M)$ in the field rests with extending observations to lower luminosities and temperatures, through late T dwarfs to room-temperature Y dwarfs.

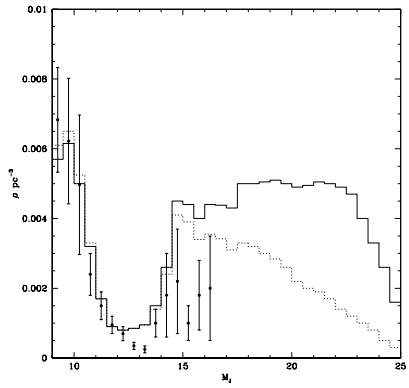

Figure 3. Comparison between observed and predicted luminosity functions for ultracool dwarfs - the solid line plots predictions for a power-law mass function with $\alpha_1 = 0.8$ at $M < 0.1M_\odot$; the dotted line shows predictions for $\alpha_1 = 0.4$ (models from Allen et al. 2004).

5. Caveats and concerns

The results presented at this conference suggest broad agreement in the overall form of the initial mass function below $\sim 1.5M_\odot$, even if the underlying physical mechanism(s) remain unclear. However, there are some issues that still deserve attention.

Photometric parallaxes: As surveys expand to include stars at larger distances, we have to rely more on indirect distance estimators, such as photometric and spectroscopic parallaxes. It is important to hold in mind that those calibrations must be well matched to the intrinsic structure in the main sequence, such as the (still theoretically-unexplained) break at (V-I)$\sim$2.9. Systematic errors in mean colour-magnitude relations *will* introduce systematic errors in both $\Phi(M_V)$ and $\psi(M)$ (see Reid & Gizis 1997).

[2]One of the driving questions behind studies of $\psi(M)$ in the 70s, 80s and 90s was whether low-mass stars and brown dwarfs could provide sufficient mass density to make a significant contribution to dark matter. The latter requires a slope near the Salpeter value. As a result, studies tended to be conservative in setting limits on α, emphasising the steepest value that might be consistent with the data.

The mass-luminosity relation: Substantial progress has been made in calibrating this relation at lower masses, but there are two caveats. First, there are still relatively few stars between 0.6 and 1.5$M_{\odot}$, and small offsets in the mean relation in this mass range systematically affect $\psi(M)$ at the transition between the low-mass ($\alpha = 1$) and high-mass (Salpeter) régimes (see PMSU4). More calibrators would be very useful. Second, there may be an intrinsic width to the mass-luminosity distribution - that is, mass calibrations may need to include a second parameter beyond luminosity.

Multiplicity: Stellar (and brown dwarfs) multiplicity affects analyses in several ways. First, as Kroupa has emphasized (2002, this meeting), unrecognised binaries bias $\Phi(M_V)$ and hence $\psi(M)$. That bias is mass dependent, since it is now widely acknowledged that the multiplicity fraction (and perhaps the mass ratio distribution) is mass dependent (Burgasser et al. 2004). Second, and more important, it remains unclear how to account properly for binary components in constructing $\psi(M)$. In simple terms, is there a distinction between wide and close binaries? If so, where do we draw the line (1 au? 10 au? 50 au?)? Is that distinction mass dependent? High mass stars might well be expected to have a greater sphere of influence during formation than low-mass stars and brown dwarfs. We need a better understanding of this issue before we can directly link the fragmentation process of molecular clouds to the final product, the mass spectrum of star-like bodies.

Finally, a word on completeness and the N8-pc sample: Taken at face value, Figure 1 suggests that there are almost 30 M dwarfs with $9 < M_J < 10.5$ missing from the 8-parsec sample. There undoubtedly is some incompleteness, but note that most of these 'missing' stars are not ultracool dwarfs, but relatively bright mid-type dwarfs with V< 16, well within the scope of Luyten's proper motion surveys. I have been involved in combing through those datasets for the last decade, netting only a handful of discoveries. I suspect that ≤ 6 new *systems* remain to be found with $M_J < 10.5$ and $\delta > -30^o$ - and I will be happy to provide a modest reward to the first astronomer to prove me wrong by discovering system #7[3].

Acknowledgments The other members of our NSTars team are Kelle Cruz, Jim Liebert, Davy Kirkpatrick, Adam Burgasser, John Gizis, Patrick Lowrance and Peter Allen. Much of the observational data summarised here were acquired by Kelle Cruz for her thesis work, while the theoretical models are due to Peter Allen. This work was supported by a grant awarded as part of the

[3]There is a time limit - the discovery must be made before May 31 2008

NASA Space Interferometry Mission Science Program, administered by the Jet Propulsion Laboratory, Pasadena.

References

Allen, P., Koerner, D.W., Reid, I.N. 2004, AJ, submitted
Burgasser, A. J. 2004, ApJ, in press
Chabrier, G., 2003, PASP, 115, 763
Cruz, K. L., Reid, I. N., Liebert, J., Kirkpatrick, J. D., & Lowrance, P. J. 2003, AJ, 126, 2421
Cruz, K.L. et al., 2004, in prep.
Henry, T.J., Subasavage, J.P., Brown, M.A., Beaulieu, T.D., Jao, W.-C., Hambly, N.C. 2004, AJ, 128, 2460
Kroupa, P., Tout, C. A., & Gilmore, G. 1993, MNRAS, 262, 545
Kroupa, P. 2002, Science, 295, 82
Luyten, W.J., 1980, The NLTT Catalogue, Univ. of Minnesota, Minnesota
Reid, I. N. & Cruz, K. L. 2002, AJ, 123, 2806
Reid, I. N., et al. 2003, AJ, 125, 354
Reid, I. N., et al. 2004, AJ, 128, 463
Reid, I. N. & Gizis, J. E. 1997, AJ, 113, 2246
Reid, I. N., Gizis, J. E., & Hawley, S. L. 2002, AJ, 124, 2721

Figure 4. Neil Reid and Mike Bessel circle.

THE 0.03–10 $M_{\odot}$ MASS FUNCTION OF YOUNG OPEN CLUSTERS

J. Bouvier[1], E. Moraux[2] and J.R. Stauffer[3]
[1]*LAOG, Grenoble, France*
[2]*IoA Cambridge, UK*
[3]*IPAC, Caltech, USA*

Abstract We report the present day mass functions (PDMFs) of 3 young open clusters over a mass range from 30 Jupiter masses to 10 $M_{\odot}$. The PDMFs of the 3 clusters are remarkably similar, suggesting little impact of specific conditions (stellar density, metallicity, early dynamical evolution) on the mass distribution. Functional forms are provided to allow quantitative comparison with MFs derived in other environments.

1. Introduction

Now that hundreds of brown dwarfs have been discovered, one can start to address quantitatively such issues as the continuity of the mass function across the stellar/substellar boundary, the overall shape of the IMF over several decades of mass, its invariance or, on the contrary, its dependency on local conditions (metallicity, stellar density, ionizing flux, etc.), and to search for the lower mass cutoff corresponding to the fragmentation limit below which a condensed object cannot form in isolation. Such a complete characterization of the IMF would provide definite constraints on theories of star and brown dwarf formation.

The determination of bias-corrected mass functions over nearly 3 decades of masses, from 0.03 to 10 $M_{\odot}$, is presented in this contribution for young open clusters (YOCs). The benefits of young clusters and the resulting reliability of the derived MF are outlined in Section 2. Deep wide-field optical surveys performed at CFHT uncovered several tens of brown dwarfs in 3 nearby YOCs and are briefly presented in Section 3. The resulting mass functions we derive for the 3 clusters are presented in Section 4 and analytical fits are obtained, which permit quantitative comparison with model predictions and/or mass distributions derived in other environments (SFRs, field, extragalactic).

E. Corbelli et al. (eds.), The Initial Mass Function 50 Years Later, 61–66.

2. The promise of young open clusters

Deriving a reliable estimate of the mass function especially in the substellar domain is an intrincate multistep process. A proper sample of confirmed brown dwarfs must first be built, usually from an initial photometric selection of candidates followed by a spectroscopic assessment of their substellar nature. The distribution of absolute magnitudes (or luminosities) is derived, provided that the distance to each object is known and a correction for foreground extinction is made. Then, the knowledge of the age of each object is required to convert its luminosity to a mass, with the help of age-dependent mass-luminosity relationships delivered by evolutionary models. The reliability of the resulting mass distribution thus largely depends on the precision attached to the distance, age and extinction of each object in the sample. Uncertainties in any of these quantities will most likely skew the resulting mass function, as will any sytematic error in the theoretical models. In addition, scatter in the mass function estimate may result from low number statistics, which can only be beaten by the construction of large samples, and by intrinsic variations in the properties of the objects in the sample, such as age or metallicity.

In young open clusters, all these sources of uncertainties are reduced. Rich nearby clusters harbor large populations of stars and brown dwarfs whose distance and age are known, usually to better than 20% and sometimes to within a few percent. Extinction is most often insignificant and scatter in the intrinsic properties of the cluster members (age, distance, metallicity) minimal. Spectroscopic diagnostics of youth, such as lithium or gravity sensitive features, serve to distinguish between bona fide substellar cluster members and intervening field dwarfs. A property specific to a nearby young cluster, the common proper motion shared by all its members also offers an additional criterion to build homogeneous samples of confirmed cluster members. Hence, with distance and age accurately known, and membership assessed in several independent ways, observed magnitudes of cluster members are directly converted to mass with the help of theoretical models. The resulting mass function pertains to an homogeneous population of objects spanning several decades of mass from low mass brown dwarfs to the most massive cluster members, all of which were born together under the same conditions and have shared the same evolution.

Another advantage is the concentration of cluster populations over restricted areas on the sky, which can now be mapped in a very efficient way with the new generation of wide-field CCD mosaics. Owing to their youth and proximity, substellar cluster members are still relatively bright and easily detectable from intermediate size telescopes. Hence, deep large scale surveys can be devised which cover a large fraction of the cluster area, as is required to characterize the spatial distribution of cluster members as a function of mass. How the

cluster's present day mass function (PDMF) relates to the IMF is, in principle, a matter of concern. However, numerical simulations suggest that it is not until a few 100 Myr that clusters start to preferentially lose low mass members as they relax dynamically. By 100 Myr, the typical age of the clusters studied in the next section, only 10% of the stars (and brown dwarfs) are expected to have been removed from the cluster (e.g. de la Fuente Marcos & de la Fuente Marcos 2000). Primordial ejection of brown dwarfs from their protostellar cradle, as advocated by Reipurth & Clarke (2001), does not appear to be an issue either since recent numerical simulations indicate that ejection velocities are similar for brown dwarfs and stars, and are usually smaller than the velocity required to escape the cluster's potential (e.g. Delgado, Clarke & Bate 2004, Moraux & Clarke 2004).

Thus, young open clusters offer a ground to build statistically robust mass functions from volume limited and physically homogeneous samples of coeval stars and brown dwarfs. At an age of about 100 Myr, the derived mass function is predicted to be quite similar to the IMF, i.e., prior to any dynamical evolution of the cluster. Due to the distance of the clusters, multiple systems are unresolved. *System* mass functions are thus derived, which can nevertheless be statistically corrected for binarity to yield single star (and brown dwarf) mass distributions (see, e.g., Moraux et al. 2003).

3. Brown dwarfs in young open clusters

We performed deep, wide area photometric surveys at CFHT of 3 nearby open clusters whose properties are summarized in Table 1. Beyond their proximity and richness, they have also been selected as having a similar age, between 100 and 150 Myr, but possibly differing in metallicity. The photometric survey covers a large enough area in each cluster so as to derive the spatial distribution of cluster members as a function of mass and hence take spatial segregation into account when estimating the cluster's mass function. The depth of the survey (I$\sim$z$\sim$24.0) corresponds to a mass limit between 30 and 50 Jupiter masses. On the bright side, saturation occurs on the images for $\sim$0.4 $M_{\odot}$stars. Mass functions are therefore derived in the mass range 0.030-0.40$M_{\odot}$, and completed by literature data for more massive cluster members. Binaries and higher order multiple systems are not resolved at the distance of the clusters.

The photometric selection in (I, I-z) color magnitude diagrams yields from several tens to several hundred low mass member candidates in each cluster (e.g. Moraux et al. 2003). The candidates were followed up and their membership assessed (or rejected) based on a combination of diagnostics : proper motion, lithium absorption, spectroscopic gravity index, infrared photometry and/or spectroscopy. As an illustration of the method and the results, Fig-

Table 1. Deep wide-field surveys of young open clusters.

Cluster	*Age (Myr)*	*[Fe/H]*	*Richness (known members)*	*Distance (pc)*	*Surveyed area (sq.deg.)*
Blanco 1	100	+0.1/0.2	> 200	260	2.5
Pleiades	120	0.0	~ 1200	130	6.4
NGC 2516	150	-0.3/0.0	~ 2000	350	2.0

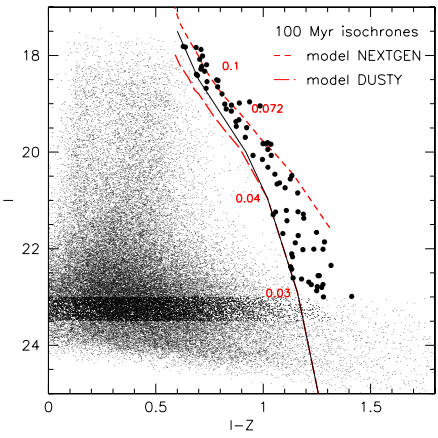

Figure 1. Optical CMD of the Blanco 1 cluster : 100 Myr NextGen and Dusty isochrones (dashed) from the Lyon group are labelled with mass. The cluster sequence, on the red side of our selection line (solid), is shown by filled dots. (From Moraux et al. 2004).

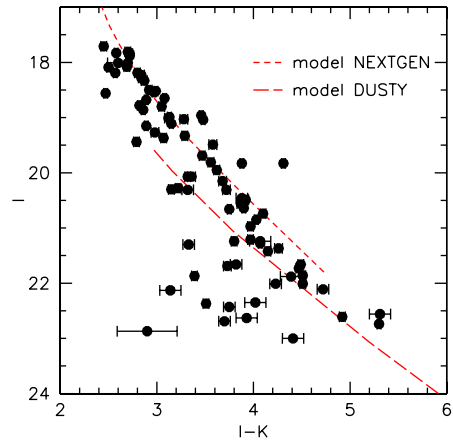

Figure 2. Infrared CMD of the Blanco 1 cluster candidates : optically-selected candidates lying on the blue side of the isochrones in this diagram are rejected as non members. (From Moraux et al. 2004).

ures 1 & 2 show the optical and infrared color magnitude diagrams of the Blanco 1 cluster from which bona fide very low mass stars and brown dwarfs are identified.

4. The mass function of young open clusters

The present day mass functions (PDMFs) of 3 young clusters were thus derived from unbiased samples of probable cluster members, taking into account mass segregation and not attempting to correct for unresolved binaries.

In a Salpeter-like power-law representation,

$$\xi(m) = \frac{dn}{dm} \propto m^{-\alpha}$$

we derive $\alpha = 0.6 \pm 0.1$ for the mass distribution of Pleiades and Blanco 1 members over the 0.03–0.50M$_\odot$mass range (Fig. 3). This is broadly consistent with Kroupa's (2001) field IMF for systems, though we find no evidence for a discontinuity at the stellar/substellar boundary.

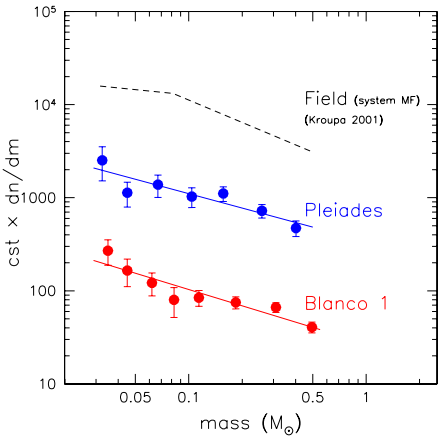

Figure 3. The mass function of young clusters derived from the CFHT survey in the mass range 0.03-0.50M$_\odot$. The field system MF from Kroupa (2001) is shown for comparison (α_0=0.2 for $m \leq 0.08$M$_\odot$, α_1=0.8 for $0.08 < m \leq 0.5$M$_\odot$).

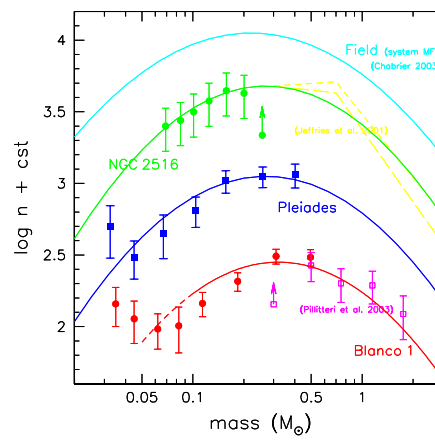

Figure 4. The mass function of young open clusters from low mass brown dwarfs to the most massive stars. Field system MF from Chabrier (2003) is shown for comparison. Parameters of the lognormal functional forms are given in Table 2.

On a broader mass range, from 30 Jupiter masses up to the most massive stars, the mass function of young clusters is resonably well fitted (Fig. 4) by a Scalo-like lognormal form :

$$\xi_{\rm L}(m) = \frac{dn}{d\log m} \propto \exp\left[-\frac{(\log m - \log m_0)^2}{2\sigma^2}\right] \qquad (1)$$

with (m_o, σ) values listed in Table 2. The high mass part of the MFs in Fig. 4 was built from published data (Pillitteri et al. 2003, Jeffries et al. 2001, Stauffer & Prosser database, see Moraux et al. 2003).

From Fig. 4 and Table 2, the PDMF of the 3 young open clusters appear quite similar, with a characteristic system mass around 0.3M$_\odot$. The fraction of brown dwarfs in each cluster compared to stars is 10-15%, which amounts to a substellar mass of $\sim$1% of the total cluster mass. Hence, to first order, the cluster MFs appear invariant under various probably different initial conditions (stellar density, metallicity, etc.).

The cluster PDMFs are also similar to the field system MF (Chabrier 2003, Moraux, Kroupa & Bouvier 2004). Small differences may exist, with a char-

Table 2. Cluster PDMFs lognormal functional fits : $\frac{dn}{d\log m} \propto \exp \frac{-(\log m - \log m_o)^2}{2\sigma^2}$

Region	m_o *($M_\odot$)*	σ	n_{BD}/n_{tot}	$n_\star/n_{tot}$	$\Sigma(m_{BD})/m_{tot}$
Blanco 1	0.32	0.50	0.11	0.89	1%
Pleiades	0.27	0.52	0.15	0.85	1.5%
NGC 2516	0.27	0.51	0.15	0.85	1.5%
Field[a]	0.22	0.57	0.21	0.79	2%

[a] Chabrier's (2003) lognormal galactic *system* MF.

acteristic mass possibly slightly higher in clusters than in the field and, consequently, a larger BD-to-star fraction in the field. Whether these differences result from the early dynamical evolution of the cluster, with a preferential loss of low mass members, or from remaining uncertainties in the field and clusters MF estimates requires more detailed studies.

References

Chabrier, G. 2003, PASP, 115, 763
Delgado-Donate, E. J., Clarke, C. J., & Bate, M. R. 2004, MNRAS, 347, 759
de la Fuente Marcos, R. & de la Fuente Marcos, C. 2000, APSS, 271, 127
Jeffries, R. D., Thurston, M. R., & Hambly, N. C. 2001, A&A, 375, 863
Kroupa, P. 2001, MNRAS, 322, 231
Moraux, E., & Clarke, C. J. 2004, A&A, in press
Moraux, E., Bouvier, J., Stauffer, J. R., & Cuillandre, J.-C. 2003, A&A, 400, 891
Moraux, E., Kroupa, P., & Bouvier, J. 2004, A&A, 426, 75
Moraux, E., Bouvier, J., Stauffer, J. R., & Cuillandre, J.-C. 2004, A&A, submitted
Pillitteri, I., Micela, G., Sciortino, S., et al. 2004, A&A, 421, 175
Reipurth, B. & Clarke, C. 2001, AJ, 122, 432

THE TIME SPREAD OF STAR FORMATION IN THE PLEIADES

John R. Stauffer
Spitzer Science Center, Caltech, Pasadena, CA 91024, USA
stauffer@ipac.caltech.edu

Abstract It is at least reasonable to believe that the time spread of star formation in a cluster could influence the resultant (averaged) IMF. If so, then we would expect a "universal" IMF within clusters only if the time spread of star formation was sensibly the same for all clusters. Alternatively, if the time spread of star formation is highly variable in clusters, it would seem likely that their IMF's should also be fairly variable. In fact, there have been a number of claims for large time spreads of star formation in open clusters, most notably the Pleiades. I will review the various claims of an age spread in the Pleiades and attempt to reconcile them.

1. Introduction

Open clusters should serve as useful laboratories for the study of the initial mass function. They can provide, for example, a good measure of how "universal" the IMF is, by comparison of the IMF one derives for a sample of well observed clusters. Another useful observable that is at least in principle possible to determine is the time spread of star-formation within a cluster - that is, the age difference between the oldest and the youngest star in a given cluster. If that age spread is large (tens of Myr of longer), one must conclude that the molecular clouds from which the cluster forms must also be long-lived. One could also speculate that this could lead to significant variations of the IMF between clusters (e.g. if external events caused truncated star-formation in a given cluster prior to when that would have happened "naturally").

The Pleiades has been one of the favorite clusters for claims of a large time spread of star formation. Herbig (1962) originally estimated an age spread in the Pleiades of more than 100 Myr, with the low mass stars being oldest. More recently, Siess, Forestini and Dougados (1997) and Belikov et al (1998) - have claimed detection of an age spread in the Pleiades of order 30 Myr.

E. Corbelli et al. (eds.), The Initial Mass Function 50 Years Later, 67–72.

It is my belief, however, that the attempts to determine the age spread in the Pleiades are flawed, and that in fact it is very difficult to derive an accurate estimate of the time spread of star formation for the Pleiades. My argument for why this is so is detailed in the next section.

2. Color-Magnitude Diagrams and the Age of the Pleiades

2.1 Previous Papers Claiming a Large Age Spread

To my knowledge, Herbig (1962) was the first paper to attempt to derive a quantitative estimate of the time spread of star formation in an open cluster. Herbig used photometry of Pleiades members from Johnson and Mitchell (1958) as his observational data. He compared photometry of the high mass cluster members to Henyey model predictions for post-main sequence evolution, and derived an upper-main sequence turnoff age for the cluster of order 60 Myr. He based his contraction age for the cluster on NOT finding a clear PMS turn-on down to $M_V \sim 8.5$ - corresponding to an age > 200 Myr using the Kelvin-Helmholtz contraction age formula (detailed PMS isochrones were not yet available). This large apparent age spread led Herbig to propose a model for star-formation in open clusters where low-mass star formation begins first and continues for a long period, with high mass stars forming in a burst at a later time. A theoretical basis for this type of time history of star-formation in clusters was later proposed by Norman & Silk (1982). Unfortunately, several sources of error resulted in Herbig getting what I believe was the wrong answer. The most important error source was the relative immaturity of the theoretical models used to infer the UMS and PMS ages for the cluster. If exactly the same inputs were used with modern tracks to provide the inferred ages, one instead would obtain an UMS age of about 100 Myr (using Meynet et al. 1993 models) and a lower limit for the PMS contraction also of order 100 Myr (using Baraffe et al. 1998 low-mass evolutionary models). That is, using modern tracks and the same input data used by Herbig, the data are consistent with the high and low mass stars being coeval.

Two new claims of relatively long time periods for star-formation in the Pleiades have recently been published. Siess, Forestini & Dougados (1997) looked at the dispersion about the main sequence in an M_V vs. B-V CMD, and noticed that the dispersion about the locus increased below $M_V \sim 7.0$ for the Pleiades. In order to explain that increased dispersion, they required an age spread of about 30 Myr (and a mean age of about 90 Myr). Belikov et al. (1998) also used an M_V vs. B-V CMD as their input. In their case, they converted that CMD into a luminosity function and compared the luminosity function (LF) to models for a range of cluster ages and age spreads. In order to fit a local peak and an immediately following (at lower luminosity) dip in the

LF, their models required an age spread. Depending on what fraction of the stars were involved, the age spread required was of order 20-60 Myr.

2.2 Why CMDs Do Not Provide an Accurate PMS Contraction Age for the Pleiades

There is a fatal flaw in using an M_V vs. B-V CMD to estimate the PMS contraction age for the Pleiades which is easily illustrated by showing three figures (provided here as Figures 1, 2 and 3). All three figures are CMD's for low mass stars in the Pleiades compared to similar data for low mass stars in the 600 Myr old Praesepe cluster. Praesepe is chosen as a reference to indicate the location of the single star main sequence and the effects of photometric binaries for a cluster with similar distance and richness as the Pleiades. For a more detailed discussion, see Stauffer et al. (2003). Figure 1 shows an M_V vs. B-V CMD for the two clusters, where the distance moduli and reddening values are from Pinsonneault et al (1998) and are designed to align the single star loci for the two clusters in the late-F and G dwarf regime. Figures 2 and 3 use the same assumptions and basically the same stars, but with instead V-I_K and V-K as the x-axis.

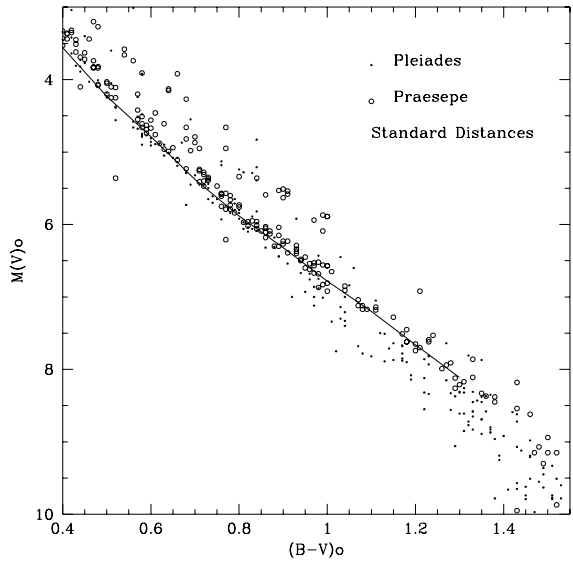

Figure 1. B-V based CMD for the Pleiades and Praesepe. We assume m-M_o = 5.53 and A_V=0.12 for the Pleiades, and m-M_o=6.05 and A_V=0.00 for Praesepe. The solid line is an empirical main sequence curve derived from field stars.

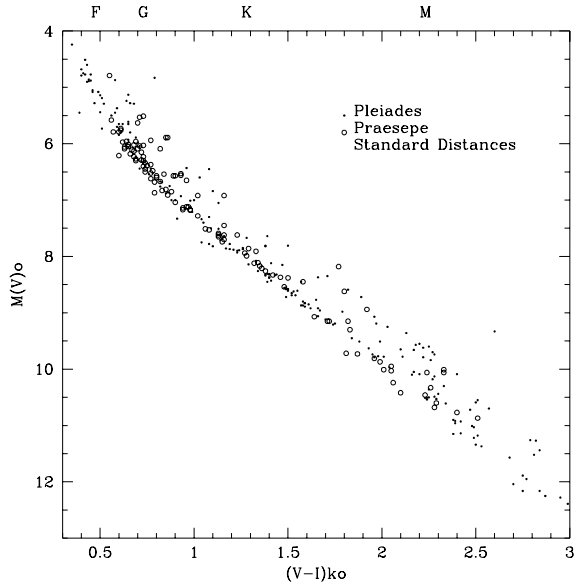

Figure 2. Same as Figure 1, except Kron V-I as the x-axis.

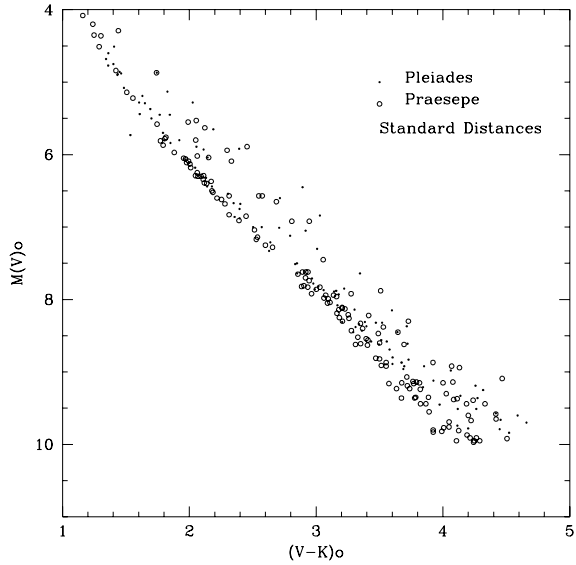

Figure 3. Same as Figure 1, except V-K as the x-axis.

The three figures show radically different behaviors in terms of identifying the pre-main sequence turn-on point in the Pleiades. Figure 1 shows a prima facie impossible result - beginning at Mv $\simeq$ 7, the Pleiades K and early M dwarfs fall systematically about 0.5 mag below the main-sequence defined by the Praesepe stars. Figure 2 shows the Pleiades and Praesepe stars coinciding down to $M_V \sim 11.0$ - implying an age for the Pleiades in excess of 200 Myr. Figure 3, finally, does show an apparent PMS turn-on point in the Pleiades at $M_V \sim 8.5$, corresponding approximately to an age of 100 Myr. At minimum, these figures indicate that any PMS age estimate for the Pleiades based on a single CMD should be viewed with extreme caution. In particular, the B-V based CMD clearly cannot provide a simply interpreted age estimate for the cluster - and that was the input data for both Belikov et al. and Forestini et al.

3. Why Are the Pleiades K Dwarfs So Blue?

The anomalous behavior shown by the three CMD's are best interpreted as indicating that the Pleiades K dwarfs have spectral energy distributions (SED's) that differ significantly from older, inactive dwarfs of the same mean effective temperature. Compared to older K dwarfs, the Pleiades K dwarfs are bluer in the blue, and redder in the red. They also have wavelength dependent spectral types (spectra obtained at shorter wavelengths yielding earlier spectral types). The effective temperature inferred from B-V for the most affected K dwarfs are 300-400 K warmer than that inferred from their V-K colors. The spectral region in the Pleiades where the SED's become anomalous (spectral type $>$ K2; $M_V > 7$; B-$V_o > 0.95$) is also where:

a) One finds the largest amplitude photometric variability in the Pleiades;

b) Hα is found in emission;

c) Coronal emission peaks at Log(L_x/L_{Bol}) = -3;

d) Flare stars have been identified (the brightest flare star in the Pleiades has $M_V \sim 7$; a large fraction of the known members fainter than that have been observed to flare at least once).

The stars with the largest blue excesses are generally the most rapidly rotating for that mass.

The explanation which we favor for the above set of behaviors is simply that the Pleiades dwarfs later than K2 are simply very "active" and very spotted. It is possible to fit the Pleiades K dwarf SED's with two-component spot models with very large spot filling factors ($>$ 30% in area for the cool spots). Because many of these stars do not have large amplitude light curves, much of the spot area must be in spots which are well distributed in longitude. See Stauffer et al. (2003) for more details.

4. Conclusions and Inferences

The abnormal SEDs for Pleiades K and M dwarfs prevents using any single CMD to derive a quantitatively accurate age for the cluster. It may eventually be possible to combine all available photometry to estimate accurate T(eff)'s for these stars, and hence derive a useful PMS age estimate - but that is work for the future.

It is logical to believe that all young K dwarfs will share the Pleiades disease to some degree, leading to spectral energy distributions different from older K dwarfs. Gullbring et al (1998) in fact have presented evidence for this type of anomaly in WTT's. If one uses color-T(eff) relations derived from old K dwarfs, or even if one uses theoretical tracks whose model atmospheres are meant to emulate "normal" (i.e. old) stars, the age one infers from pre-main sequence isochrone fitting will depend on the color used to infer T(eff). Assuming there is a range of spottedness for stars in a given cluster, even if one uses the same observable to infer T(eff), the dispersion in spottedness would lead to a spurious apparent age spread. Determining ages and age spreads in star forming regions is therefore even more difficult than believed previously.

References

Baraffe, I., Chabrier, G., Allard, F., & Hauschildt, P. 1998, A&A, 337, 403
Belikov, A., Hirte, S., Meusinger, H., Piskunov, A., & Schilbach, E. 1998, A&A, 332, 575
Gullbring, E., Hartmann, L., Briceno, C., and Calvet, N. 1998, ApJ, 492, 323
Herbig, G. 1962, ApJ, 135, 736
Johnson, H. & Mitchell, R. 1958, ApJ, 128, 31
Meynet, G., Mermilliod, J.-C., & Maeder, A. 1993, A&A, 265, 513
Norman, C. & Silk, J. 1980, ApJ, 238, 158
Pinsonneault, M. et al. 1998, ApJ, 504, 170
Siess, L., Forestini, M., & Dougados, C. 1997, A&A, 324, 556
Stauffer, J., et al. 2003, AJ, 126, 833

Figure 4 John Stauffer and wife at arrival in Spineto.

AGE SPREADS IN CLUSTERS AND ASSOCIATIONS: THE LITHIUM TEST

Francesco Palla and Sofia Randich
INAF–Osservatorio Astrofisico di Arcetri, L.go E. Fermi 5, 50125 Firenze, Italy
palla@arcetri.astro.it,randich@arcetri.astro.it

Abstract We report the evidence that several low-mass stars ($<$0.4 $M_\odot$) of the Orion and Upper Scorpius clusters have lithium abundances well below the interstellar value. Due to time-dependent depletion, our result implies stellar ages greater than $\sim$5 Myr, suggesting that star formation has been proceeding for a long time in these systems.

1. How long does star formation last in clusters?

A central debate on star formation (SF) concerns the time scale during which a molecular cloud complex can sustain the production of new stars. Two competing views exist: a *slow mode* regulated by the quasi-static evolution of magnetized clouds (e.g., Palla & Stahler 2000), and a *fast mode* driven by the dissipation of turbulence followed by prompt gravitational collapse (e.g., Hartmann, this conference). Whether or not SF can last for an extended period of time ($\sim 10^7$ yr), longer than the dynamical time (1–2 Myr), is still unclear. Age dating based on isochrones in the HR diagram of nearby SF regions yields age distributions in the range 1–3 Myr with evidence for a significant population of older stars ($>$5 Myr). However, given the uncertainties of the isochronal method, it is important to find independent ways of gauging stellar ages and age spreads.

2. Using Li-depletion to estimate age spreads

The age dating method based on Li abundances rests on the ability of low-mass stars to burn their initial Li content during the early phases of PMS contraction. Lithium depletion time scales vary with stellar mass, being $\sim$10 Myr for 0.2–0.4 $M_\odot$ stars. The Li-based method has been successfully applied to relatively young open clusters ($>$30 Myr; e.g., Stauffer 2000), but never to

E. Corbelli et al. (eds.), The Initial Mass Function 50 Years Later, 73–74.

SFRs in the assumption that their low-mass members are too young and too cold for nuclear burning.

We have measured the Li I 6708 Å line in a sample of ∼90 ONC members with mass 0.4–0.8 $M_\odot$ and isochronal ages greater than ∼1 Myr using FLAMES+Giraffe on ESO-VLT2. As shown in Fig. 1, we find a decrease of the Li-abundance by a factor 5-10 in the coldest (T∼3700 K) and faintest objects. Comparison with PMS evolutionary models indicates that the observed Li-depletion corresponds to stellar ages greater than ∼5 Myr.

In Upper Scorpius we have determined the EW(Li)-isochronal age relation using the low-mass stars observed by Preibisch & Zinnecker (1999): the oldest stars appear to have a much lower EW(Li) than the bulk of the younger stars. The most Li-poor stars are also the least massive objects (∼0.2 $M_\odot$), setting an age estimate greater than ∼10 Myr.

We conclude that differences in Li-abundance are present among low-mass members of very young clusters. Due to the time dependence of Li-depletion, these variations can be interpreted as a substantial spread in stellar ages. This finding offers an independent evidence for a slow mode of star formation. In the near future, we will extend our observations to stars of lower mass with the goal of detecting the Li-depletion boundary, thus setting an absolute age for very young clusters.

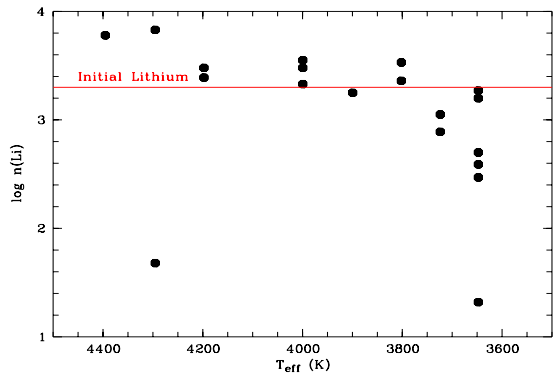

Figure 1. Li-abundances in low-mass stars of the Orion Cluster

References

Palla, F. & Stahler, S.W. 2000, ApJ, 540, 255
Preibisch, T. & Zinnecker, H. 1999, AJ, 117, 238
Stauffer, J. 2000 in Stellar Clusters and Associations, ASP Conf. Vol. 198, p. 255

THE INITIAL MASS FUNCTION OF THREE GALACTIC OPEN CLUSTERS

L. Prisinzano[1], G. Micela[1], S. Sciortino[1], F. Favata[2] and F. Damiani[1]
[1]*INAF–Osservatorio Astronomico di Palermo "G. Vaiana", P.za del Parlamento 1, Palermo, Italy,*
[2]*Astrophysics Division–Space Science Department of ESA, Estec, The Netherlands*
loredana@astropa.unipa.it

Abstract We studied three Galactic open clusters (OC) spanning a range of age of 1 Gyr in order to compare their Mass Function (MF). In all cases, we analyzed optical multi-band images to obtain the color-magnitude diagrams (CMD). Several theoretical stellar evolution models were considered to determine distance and age of the OCs and to convert the Luminosity Function (LF) into MF. Different membership criteria were used for each OC based on cluster properties and X-ray data and/or photometric IR data available in literature. The adopted methods and the comparison of the Initial Mass Functions (IMF) derived for the three OCs are presented.

1. The clusters

NGC 6530 is a very young OC (age 0.3–10 Myr), located in front of the molecular cloud M8. Cluster stars with $V \leq 13$ are on the Main Sequence (MS), while fainter cluster stars are still in pre-MS phase, as shown in Prisinzano et al. (2004). We used very recently published Chandra ACIS-I X-ray data by Damiani et al. (2004) in order to select probable cluster members.

NGC 2422 (d= 500 pc) is a young OC with age of about 100 Myr, directly comparable to the Pleiades. The cluster MS locus was identified in the CMD using X-ray counterparts by Barbera et al. (2002). Based on the available CMDs, a sample of 1277 photometric candidate cluster members was selected. The IMF of the whole cluster was obtained after correcting for mass segregation effects, as described in Prisinzano et al. (2003).

With an age of about 1.2 Gyr, NGC 3960 (d=1850 pc) is an old OC affected by relevant effects of differential reddening.

To empirically identify the cluster MS locus in the CMD, we built a CMD density map of the cluster using optical and IR data and statistically subtracting the CMD density map of field stars. This map allowed us to derive age and

E. Corbelli et al. (eds.), The Initial Mass Function 50 Years Later, 75–76.

distance of the cluster. The LF and MF were obtained after correcting for field star contamination, as shown in Prisinzano et al. (2004).

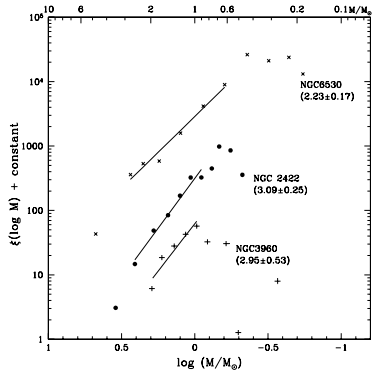

Figure 1. IMF (arbitrarily normalized) of the three open clusters.

2. Results

The IMF obtained for the three OCs are shown in Fig. 1; in the mass range covered by each line, the MF was represented by a power law whose index is indicated in figure. The two older OCs (NGC 2422 and NGC 3960) have slope consistent within errors, while the very young OC NGC 6530 shows a power law index consistent with the Salpeter value 2.35. It is slightly flatter likely because the fraction of massive stars is larger than that of the other two OCs. All the IMFs show a peak at a mass that increases with the cluster age, and this could reflects different physical conditions of the environments where the three OCs formed. Such result supports recent observational results suggesting a time variable IMF (e.g. Chabrier, 2003).

References

Damiani, F., Flaccomio, E., Micela G., & Sciortino, S., 2004, ApJ 608, 781
Barbera, M., Bocchino, F., Damiani, F., et al. 2002, A&A, 546, 1006
Chabrier, G. 2003, ApJ, 586, L133
Prisinzano, L., Micela G., Sciortino, S. & Favata, F. 2003, A&A, 404, 927
Prisinzano, L., Micela G., Sciortino, S. & Favata, F. 2004, A&A, 417, 945
Prisinzano, L., Damiani, F., Micela G. & Sciortino 2004, A&A, in press

THE STELLAR IMF OF GALACTIC CLUSTERS AND ITS EVOLUTION

Guido De Marchi[1], Francesco Paresce[2] and Simon Portegies Zwart[3]
[1]*European Space Agency, Keplerlaan 1, 2200 AG Noordwijk, The Netherlands*
[2]*European Southern Observatory, Karl-Schwarzschild-Str 2, 85748 Garching, Germany*
[3]*Instituut Anton Pannekoek, Kruislaan 403, 1098 SJ Amsterdam, The Netherlands*
gdemarchi@rssd.esa.int, fparesce@eso.org, spz@science.uva.nl

Abstract We show that one can obtain a good fit to the measured main sequence mass function (MF) of a large sample of Galactic clusters (young and old) with a tapered Salpeter power law distribution function with an exponential truncation. The average value of the power law index is very close to Salpeter (~ 2.3), whereas the characteristic mass is in the range $0.1 - 0.5\,\mathrm{M}_{\odot}$ and does not seem to vary in a systematic way with the present cluster parameters such as metal abundance and central concentration. However, a remarkable correlation with age is seen, in that the peak mass of young clusters increases with it. This trend does not extend to globular clusters, whose peak mass is firmly at $\sim 0.35\,\mathrm{M}_{\odot}$. This correlation is due to the onset of mass segregation following early dynamical interactions in the loose cluster cores. Differences between globular and younger clusters may depend on the initial environment of star formation, which in turn affects their total mass.

1. Introduction

Conflicting claims exist as to the universality of the IMF (see e.g. Gilmore 2002) or lack thereof (e.g. Eisenhauer 2002). This unsatisfactory state of affairs has its most likely origin in the lack of uniformity of the experimental data used to infer the stellar IMF. The comparison of different data-sets, obtained by different authors in different environments (see e.g. the reviews of Scalo 1998, Kroupa 2001 and Chabrier 2003) is unfortunately hampered by systematic uncertainties. Therefore, our only hope to assess observationally whether the star formation process and its end result, namely the IMF, are the same everywhere rests on our ability to secure a statistically complete and physically homogeneous sample of stars. This is presently possible for Galactic clusters thanks to the recent advancements in the instrumentation (HST, VLT, etc.) and in our

E. Corbelli et al. (eds.), The Initial Mass Function 50 Years Later, 77–82.

understanding of the dynamical evolution of stellar systems (Meylan & Heggie 1997).

In Paresce & De Marchi (2000, hereafter PDM00) we studied the luminosity function (LFs) of a homogeneous sample of globular clusters (GCs) and showed that, within the present uncertainties, they can all be traced back to the same global MF and, most likely, the same IMF. That work suggests that the latter has a log–normal form below $1\,M_\odot$, with a characteristic mass $m_c = 0.33 \pm 0.03\,M_\odot$ and width $\sigma = 0.34 \pm 0.04$, independently of the cluster physical parameters or dynamical history. In a subsequent paper (De Marchi et al. 2004) this analysis has been extended to a homogeneous sample of young Galactic clusters (YCs), with ages ranging from a few Myr to a Gyr, by comparing their MF to one another and to that of GCs. Here follows a summary of the main results.

2. The sample

While the GCs in the sample have all been observed with the same instrument and band, and the data reduced with the same reproducible processing (see PDM00 for details), the YCs data come from several different sources. To enforce the highest degree of uniformity, we have searched the literature on YC LFs with specific guidelines, namely: the availability of recent, high quality photometry to supplement Schmidt plate material; a clear indication of which portion of the cluster has been studied; a solid membership selection; a reliable conversion from magnitude to mass; a detailed explanation of any correction to the MF to account for stellar multiplicity. The list of YCs selected in this way and the respective references are given in Figure 1.

Since the YC data span a wide wavelength range, it is not possible to directly compare to one another their LFs. Instead, we have concentrated on their MFs, which most authors approximate with a segmented power law, as done for instance by Kroupa (2001). The MFs are shown in Figure 1 (thick solid lines). Since most authors converted magnitudes to masses using the relationships of D'Antona & Mazzitelli (1994), the differences in the MFs should reflect those in the LFs.

In order to compare the MFs of the YCs in Figure 1 to one another and to that of GCs, it is useful to define some parameters that describe the MF shape. A log–normal distribution offers a suitable parametric description of the MF of GCs (PDM00). However, when extended to masses above those currently observable in GCs, a log–normal MF would fall off far more rapidly than the MF of YCs. In fact, the latter is in most cases very close to a Salpeter power law above $1\,M_\odot$. For this reason, we have looked for a different functional form which would accurately reproduce the observed MF of GCs and which,

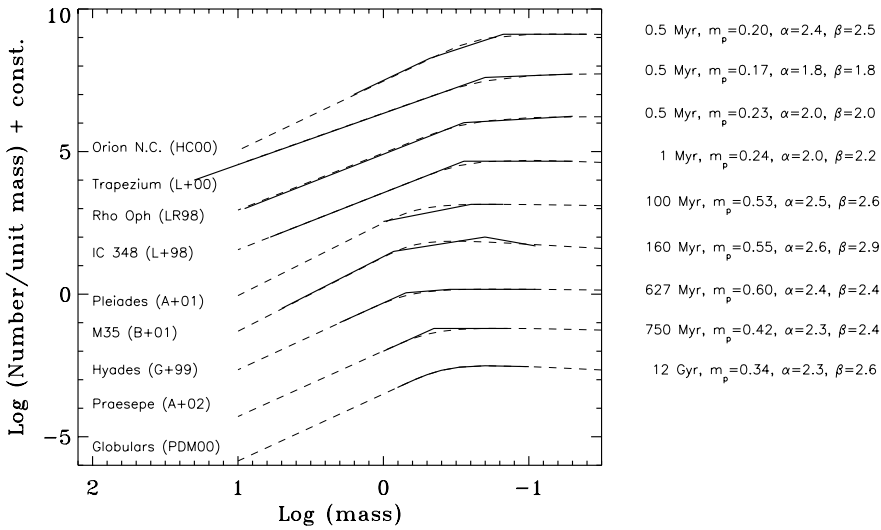

Figure 1. Observed MFs (solid lines) are fitted with a TPL (dashed lines). Cluster age increases from top to bottom.

once extended above $1\,\mathrm{M}_\odot$, would still be compatible with the MF of YCs. Following the notation of Elmegreen (1999), one can write the MF as:

$$f\,(m) = \frac{d\,N}{d\,m} \propto m^{-\alpha}\left[1 - e^{(-m/m_p)^{\beta}}\right] \qquad (1)$$

where m_p is the peak mass, α the index of the power law portion for high masses and β the tapering exponent which causes the MF to flatten at low masses. The values of the tapered power law (TPL) parameters providing the best fit (dashed lines) to the observations are shown on the right-hand side of Figure 1, together with the cluster age. The typical uncertainty on m_p is $< 0.1\,\mathrm{M}_\odot$.

Since the index α has an almost negligible effect on the shape of the MF around m_p, its value cannot be constrained for GCs. We have simply assumed in this case $\alpha = 2.3$ (the Salpeter value). Space limitations do not allow us to show here the TPL fit to the MF of each individual GC, so in Figure 1 we show the average MF (for more details, see De Marchi et al. 2004). Nevertheless, both m_p and β span a very narrow range around their average values, with $m_p = 0.35 \pm 0.04\,\mathrm{M}_\odot$ and $\beta = 2.6 \pm 0.3$ for the whole GC sample.

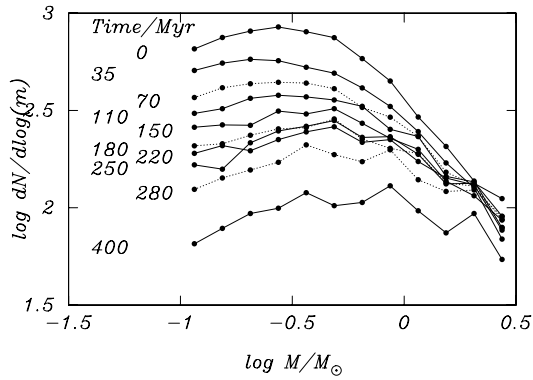

Figure 2. Temporal evolution of the MF inside the half-mass radius.

3. The evolution of the mass function

Figure 1 reveals that the shape of the MF can change considerably from cluster to cluster, with the peak varying widely in mass (although α and β span a range of values fully consistent with that of GCs). The cluster MFs in Figure 1 are arranged with age increasing from top to bottom and even a casual inspection reveals immediately a strong trend, with the MF peak shifting to higher masses.

The most likely origin of this trend is the combined effect of mass segregation and the limited cluster area covered by the observations. In the absence of tidal interactions with the Galaxy, one expects the global MF of a cluster to vary slowly with time due to evaporation. For massive GCs this process can take several tens or hundreds of Gyr (Gnedin & Ostriker 1997) but, in YCs, mass segregation and the resulting evaporation proceed more rapidly (Raboud & Mermilliod 1998). Portegies Zwart et al. (2001) have shown that the global MF of a 600 Myr old cluster with a mass of $1600\,\mathrm{M}_\odot$ differs only marginally from its IMF, even when the enhanced erosion induced by the Galactic potential is included in the calculations. However, the same simulations show that the local MF changes dramatically in the inner cluster regions, inside the half-mass radius. This is perfectly in line with the YC data of Figure 1, since all the MFs shown there were obtained in the inner cluster regions.

Without addressing here the details of a complete quantitative analysis (see Portegies Zwart et al. 2001; De Marchi et al. 2004), Figure 2 shows the temporal evolution of the stellar MF inside the half-mass radius of a $1600\,\mathrm{M}_\odot$ model cluster. The IMF is assumed to be that of Scalo (1986) with an initial peak at $\sim 0.4\,\mathrm{M}_\odot$. The peak mass clearly grows with time, much in the same way as we observe in Figure 1. Since the average stellar mass increases towards the cluster center, due to mass segregation, the location of the MF peak depends steeply on the fraction of cluster area sampled by the data: the wider the latter,

the lower the peak mass. Thus, although not specific to any one of the clusters in our sample, the simulation shown in Figure 2 proves rather convincingly that mass segregation, combined with limited sampling of the cluster population, can explain much of the variation noticed in Figure 1.

4. Conclusions

It is, thus, likely that the YCs in Figure 1 share a rather similar IMF, since the progressive difference among their shapes grows with age in the same sense expected from dynamical evolution. Such an IMF would have to be very similar to the MF of the youngest clusters ($\sim$ 1 Myr old) with a peak mass $m_p \simeq 0.2\,\mathrm{M}_\odot$ or, more likely, $m_p \simeq 0.15\,\mathrm{M}_\odot$ when account is taken of binaries (see Kroupa 2001). The latter is very similar to the IMF of the disc (Chabrier 2003). As discussed by PDM00, the similarity among the MF of GCs suggests that they as well could all share the same IMF.

An obvious question is whether the IMF is the same for both GCs and YCs. More precisely, one could ask whether dynamical evolution in GCs might have proceeded in such a way that the peak of their MF has moved from an initial value of $m_p \simeq 0.15\,\mathrm{M}_\odot$ to the presently observed $\sim 0.35\,\mathrm{M}_\odot$. The lack of correlation between the past dynamical history of GCs and their current global MF argues against this hypothesis (PDM00). If, however, GCs are indeed the naked cores of disrupted dwarf galaxies, as suggested e.g. by Martini & Ho (2004), one cannot exclude that their mass structure has been considerably altered and the properties of their IMF homogenised by the stripping process. Evidence of on-going GC disruption has been recently found in NGC 6712 (De Marchi et al. 1999) and NGC 6218 (Pulone et al. 2004). Since any low-mass stars lost by GCs should populate the halo, if the IMF of GCs was originally similar to that of YCs, the halo MF should also be peaked at $\sim 0.15\,\mathrm{M}_\odot$. If, however, the MF of the halo turns out to be similar to that currently observed in GCs, it will indicate that their present day MF does not substantially differ from the IMF. Unfortunately, the current uncertainties on the actual properties of the halo MF (Graff & Freese 1996; Gould et al. 1998) do not presently allow us to test this hypothesis.

Regardless as to whether the IMF has a peak at $\sim 0.15\,\mathrm{M}_\odot$ or $\sim 0.35\,\mathrm{M}_\odot$, it appears that its functional form is well matched by a TPL, at least for a large sample of clusters with widely different properties. This lends support to the theoretical predictions of Adams & Fatuzzo (1996), Larson (1998), Elmegreen (1999; 2004) and Bonnell et al. (2001) who suggest high- and low-mass stars form through different processes and/or in different environments. Thus, it is probably not premature to suggest that the difference between the peak mass of globular and younger clusters also results from their initial star formation environment, which in turn affects the total mass of these systems. In spite of

the many uncertainties still affecting this investigation, the very fact that the IMF seems to have a characteristic scale mass will hopefully soon allow us to characterize the star formation process from the properties of the IMF itself.

References

Adams, F., Fatuzzo, M. 1996, ApJ, 464, 256
Adams, J., Stauffer, J., Monet, D., et al. 2001, AJ, 121, 2053
Adams, J., Stauffer, J., Skrutskie, M. et al. 2002, AJ, 124, 1570
Barrado y Navascués, D., Stauffer, J., Bouvier, J., Martín, E. 2001, ApJ, 546, 1006
Bonnell, I., Clarke, C., Bate, M., Pringle, J. 2001, MNRAS, 324, 573
Chabrier, G. 2003, PASP, 115, 763
D'Antona, F., Mazzitelli, I. 1994, ApJS, 90, 467
De Marchi, G., Paresce, F., Leibundgut, B., Pulone, L. 1999, A&A, 343, L9
De Marchi, G., Paresce, F., Portegies Zwart, S. 2004, in preparation
Eisenhauer, F. 2001, in Starburst Galaxies: Near and Far, Ed. L. Tacconi & D. Lutz (Heidelberg: Springer), 24
Elmegreen, B. 1999, ApJ, 515, 323
Elmegreen, B. 2004, MNRAS, 354, 367
Gilmore, G. 2001, in Starburst Galaxies: Near and Far, Ed. L. Tacconi & D. Lutz (Heidelberg: Springer), 34
Gizis, J., Reid, I., Monet, D. 1999, AJ, 118, 997
Gnedin, O., Ostriker, J. 1997, ApJ, 474, 223
Gould, A., Flynn, C., Bahcall, J. 1998, ApJ, 503, 798
Graff, D., Freese, K. 1996, ApJ, 467, L65
Hillenbrand, L., Carpenter, J. 2000, ApJ, 540, 236
Kroupa, P. 2001, MNRAS, 322, 231
Larson, R. 1998, MNRAS, 301, 569
Luhman, K., Rieke, G. 1999, ApJ, 525, 440
Luhman, K., Rieke, G., Lada, C., Lada, E. 1998, ApJ, 508, 347
Luhman, K., Rieke, G., Young, E., Cotera, A. et al. 2000, ApJ, 540, 1016
Martini, P., Ho, L. 2004, ApJ, 610, 233
Meylan, G., Heggie, D. 1997, A&ARv, 8, 1
Paresce. F, De Marchi, G. 2000, ApJ, 534, 870 (PDM00)
Portegies Zwart, S., McMillan, S., Hut, P., Makino, J. 2001, MNRAS, 321, 199
Pulone, L., De Marchi, G., Paresce, F. 2004, in preparation
Raboud, D., Mermilliod, J. 1998, A&A, 333, 897
Scalo, J. 1986, Fundamentals of Cosmic Physics, 11, 1
Scalo, J. 1998, in ASP Conf. Ser. 142, Ed. G. Gilmore & D. Howell (San Francisco: ASP), 201

TWO STAGES OF STAR FORMATION IN GLOBULAR CLUSTERS AND THE IMF

Francesca D'Antona
INAF-Osservatorio di Roma, Monteporzio, Italy
dantona@mporzio.astro.it

Abstract I summarize recent ideas on the necessity of two separate events of star formation in many Globular Clusters to explain the star-to-star variations in elemental abundances, and show the consequences of this suggestion on the initial mass function of their stars.

1. Introduction

Contrary to a substantial uniformity of abundance of heavy elements, the light elements that are susceptible to abundance changes from proton-capture reactions (as the pp, CN, ON, NeNa, and MgAl cycles) exhibit star-to-star abundance variations in many GCs, far in excess of the modest variations seen in halo field stars –see, e.g., Smith (1987), Kraft (1994), and Sneden (1999). These abundance spreads are present also at the turnoff and among the subgiant stars (e.g. Gratton et al. 2001), so that these anomalies must be attributed to some process of self–enrichment occurring at the first stages of the life of the cluster, starting as soon as all the supernovae have already exploded, expelling from the clusters their high velocity ejecta. At an epoch starting $\sim 5 \times 10^7$yr from the birth of the first stellar generation, the massive asymptotic giant branch (AGB) stars lose mass through low velocity winds, so that it can be reasonably speculated that these winds remain inside the cluster. In addition, the massive AGB envelopes are the ideal place to manufacture elements through nuclear reactions in which proton captures are involved, as they are subject to hot bottom burning (HBB) (e.g. Ventura et al. 2001, Ventura, D'Antona, & Mazzitelli 2002), although a quantitative reproduction of the observed abundance spreads, e.g., of the oxygen vs. sodium anticorrelation (Denissenkov & Herwig 2003, Ventura et al. 2004), is still far from being available. The most appealing suggestion is that such ejecta continuously form second generation stars for a time lasting about 200 Myr. This hypothesis was put forward by D'Antona et al. (2002) as the simplest way of interpreting

E. Corbelli et al. (eds.), The Initial Mass Function 50 Years Later, 83–88.

the horizontal branch (HB) morphology, which typically shows extended blue tails in those GCs having the most prominent abundance spreads. The HB morphology in fact can be due to the mixture of stars belonging to a first stellar generation, having cosmological helium abundance, and the stars belonging to a second stellar generation and having larger –and variable– helium abundance. These latter stars have a mass smaller than average at the giant tip at present age and, for similar mass loss along the red giant (RG) branch, will have a smaller mass (and bluer location) on the HB. Helium enrichment is a natural outcome of the AGB evolution – Ventura et al. (2001), together with other chemical anomalies which can help to explain the observed abundance spreads. Thus, examining the properties of HBs in GCs showing CNO and Na–Mg anomalies we can try to understand which are the requirements (especially on the Initial Mass Function –IMF) needed to reproduce the data.

We have approached this problem – D'Antona & Caloi (2004) – by studying the GC NGC 2808, which has a marked dichotomy of the HB, and the result shows that the IMF needed to reproduce the HB morphology is very peculiar indeed, and may teach us a lot about the star formation and dynamical evolution of GCs.

2. The IMF of NGC 2808

Which are the HB morphologies which may derive from a two stage star formation process? There are clusters in which the HB is clearly bimodal: in NGC 2808 the RR Lyrae region is almost completely devoid of stars; in NGC 1851 it is much less populated than both the blue and red side of the HB. We then have interpreted the dichotomy in the HB of NGC 2808 as due to the differing helium contents of the clump (red HB) stars and blue HB stars. This assumption is certainly parametric and has no pretence of uniqueness, but it has three attractive features: i) we know from the RG branch that the stars in this cluster show a dispersion in the abundances linked to the hot CNO cycle (Carretta et al. 2003, 2004); ii) if we accept that the massive AGB stars are responsible for this abundance dispersion, all AGB models predict that the AGB winds are helium enriched; iii) the epoch of star formation from the AGB winds must necessarily end when massive AGBs are still evolving, and *this will naturally produce a helium content gap*.

The data on NGC 2808 by Bedin et al. (2000) include 565 red clump stars, and 580 stars in the blue HB. Simple simulations show that it is possible to interpret the red part of the HB as formed by stars with helium content Y=0.24, and the blue part as due to a population with enrichment in helium. By adopting a unique average mass loss, and dispersion of mass loss, along the red giant branch evolution, we fit at the same time the red and blue side of the HB: along the blue HB, the location of the stars is reproduced by attributing increasingly

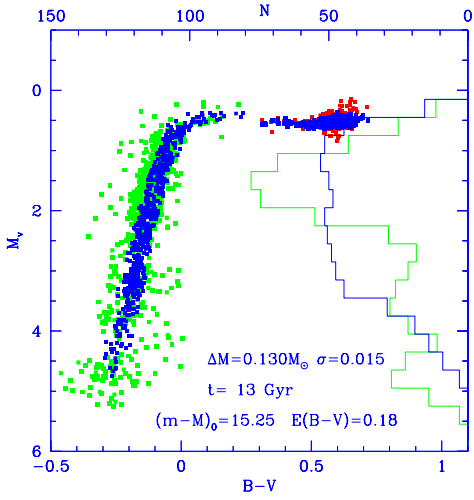

Figure 1. Typical simulation, superimposed on the HB data for NGC 2808, obtained assuming an age of 13 Gyr. An average 0.13 $M_\odot$ lost on the RGB reproduces the red clump. The corresponding blue HB distribution, assuming random helium content between 0.27 and 0.32 is shown, compared to the observed (dotted) distribution.

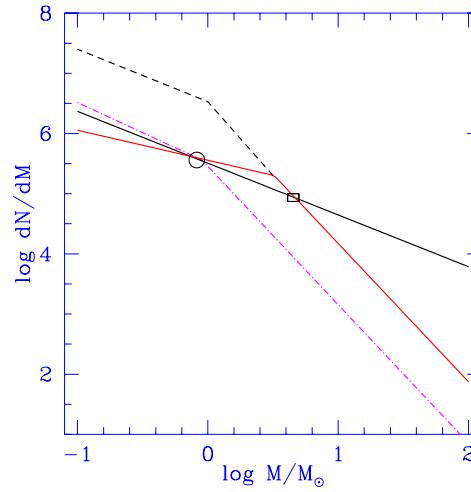

Figure 2. Sketch of possible IMFs for NGC 2808. A normal IMF would either pass through the open circle representing the population of the HB red clump (at mass $\simeq 0.8M_\odot$, dash-dotted line), or through the rectangle at 4–5 $M_\odot$ (dashed-continuous line). An IMF passing through both points would have a slope x$\simeq 0$, or a small number of low mass stars compared to the larger mass stars.

larger helium content. In other words, *the mass along the blue HB varies mainly through the variation of M_{RG}(Y)*. Thus, to obtain the lack of stars in the RR Lyrae region we need to suppose that the helium content on the reddest side of the blue HB is discontinuously larger than the helium content of the red clump. One full simulation for a metallicity Z=1×10^{-3} and an age of 13 Gyr is shown in Figure 1, where, for the blue side, we assume that the helium content is randomly distributed between Y=0.27 and Y=0.32. The minimum Y=0.27 is necessary in order for the RR Lyr region to remain unpopulated. If the metallicity is Z=2×10^{-3}, the minimum helium gap for the blue HB is reduced to Y=0.26.

If NGC 2808 is made up by a first stellar population having standard helium content Y=0.24, from which, today, the stars populating the red clump of

the HB evolve (and not considering for the moment the loss of stars from the cluster), the number of clump stars provide a point of calibration of the IMF at $\sim 0.8M_{\odot}$, which is shown as an open circle in Fig. 2. In addition, as we know the helium content of the ejecta as function of the progenitor mass (Ventura 2002) we also know which are the progenitor masses of the ejecta from which the blue HB stars were born, and we can derive another point of the IMF at M$\simeq 4-5\ M_{\odot}$ (rectangle in Fig. 2), as shown in detail by D'Antona & Caloi (2004).

Kroupa (2001) makes the case for an universal IMF for stellar systems of different metallicities, at intermediate and high masses. His reassessment of the IMF is made for many stellar populations and different mass ranges— and shows that the typical IMF can be schematized by segments of power law having the form: $\frac{dN}{dM} = c \times M^{-(1+x)}$. For masses larger than the solar mass, the index is $x\ \simeq$1.3, that is Salpeter's index, or a larger value, while the smaller masses have much milder slopes. In the whole range up to $0.7M_{\odot}$, Piotto & Zoccali (1999) find that the MFs of many GCs have very mild slopes (x from ~ -0.5 to ~ 0.2). The MF above $0.7M_{\odot}$ is steeper, and although it is difficult to determine it with care, it can be assumed close to Salpeter's slope (x=1.3). Simplifying Kroupa's results, we describe the IMF of GCs as made up of a power law with index x=0 below 0.9 $M_{\odot}$, connected to a power law with index x=1.3 above $0.9M_{\odot}$. This IMF can be fit to the points we have derived for NGC 2808 at M$\simeq\ 0.8M_{\odot}$ and at M$\simeq\ 4-5M_{\odot}$. Looking at Figure 2, we recognize that the mass function at masses 4–5 $M_{\odot}$ is *much larger* than predicted if the IMF of the GC had been "normal", as described above, and fits the point representing the red clump. In order to fit both the red clump IMF and the intermediate mass stars IMF, we need to use two very different slopes: we may adopt Salpeter's slope (or a larger slope) for the masses which include our normalization point at 4–5 $M_{\odot}$, and slopes which can fit the red clump for small masses as exemplified in Fig. 2. Obviously, it is also possible to satisfy both constraints by using a unique IMF, but it must have an index x=–0.14! Such an IMF can not be extrapolated too much, as it predicts an unrealistic high mass for the cluster and is not consistent with all the evidence concerning the IMFs derived from many different stellar environments.

3. Discussion

Figure 2 summarizes the schematic IMFs based on our interpretation of the morphology of the HB in NGC 2808. We find that, based on the number of red clump stars, the original IMF of NGC 2808 can not be similar to the "universal" IMF by Kroupa (2001), otherwise the matter lost by the intermediate mass stars would be a factor $\sim$10 smaller than the mass necessary to be consistent with the blue HB. In order to have enough stars in the main blue clump, we need a

very flat IMF, that is x~ 0. This could imply that the GC intermediate mass stars could be born preferentially in the central regions of the cluster, or could be dynamically segregated there. Evidence for clustering of massive stars in the central parts of young clusters is accumulating – Panagia et al. (2000), Stolte et al. (2002), Brocato et al. (2003). It is possible that the ejecta of the intermediate mass stars gave birth to the second generation, and the external parts of the cluster, containing all the other first generation low mass stars, were lost, leaving the present proportion of first and second generation stars. The IMFs shown in Fig. 2 can be considered then simple examples of what actually should be obtained by considering the proper dynamic evolution of the cluster, including the loss of low mass stars from it. What seems to be clear is that, if the true IMF of the first stellar population of GCs was similar to the field IMF, we *need that most of the low mass stars, today progenitors of the HB red clump, has been lost from the cluster*.

A final consequence of the proposed IMF is that we expect about a factor 10 more neutron stars and black holes to be born in the cluster, if it can be extrapolated to higher masses. This would be consistent with the large number of millisecond pulsars (MSPs) present in many GCs. In particular the 20 MSPs discovered in the cluster 47 Tuc by Camilo et al. (2000) indicate that the richest GCs may contain more than ~ 1000 NSs (e.g. Pfahl et al. (2003)) a number embarassingly large. In fact, the number of NSs predicted by a normal IMF in NGC 2808 would be between 2600 and 14000, implying a retention factor from 7 to 40%, at variance with the characteristic kick speeds of single radiopulsar in the Galaxy, which have an average $< v > \sim 250 - 300$Km/s – Hansen & Phinney(1997), much larger than the escape velocity from typical clusters (~ 25Km/s). Pfahl et al. (2003) have shown that the retention factor is between 1% and 8%, even including consideration of binarity, but it would have been much smaller if they had taken into account a number of other effects. The retention problem becomes less severe if we assume that the IMF of intermediate mass stars, necessary to interpret the blue HB morphology, can be extended to the masses which form neutron stars, even if the slope is larger than Salpeter's.

Acknowledgments I thank Edvige Corbelli and Francesco Palla for inviting me to share with the other participants the pleasure to be with Edwin Salpeter in the occasion of the 50 years of the IMF and in the celebration of Ed's birthday.

References

Bedin, L. R., Piotto, G., Zoccali, M., Stetson, P. B., Saviane, I., Cassisi, S., & Bono, G. 2000, A&A, 363, 159

Brocato, E., Castellani, V., Di Carlo, E., Raimondo, G., & Walker, A. R. 2003, AJ, 125, 3111

Camilo, F., Lorimer, D. R., Freire, P., Lyne, A. G., & Manchester, R. N. 2000, ApJ, 535, 975

Carretta E., & Gratton R.G. 1997, A&AS, 121, 95

Carretta, E., Bragaglia, A., Cacciari, C., & Rossetti, E. 2003, A&A, 410, 143
Carretta, E., Bragaglia, A., & Cacciari, C. 2004, ApJ, 610, L25
D'Antona, F. & Caloi, V. 2004, ApJ, 611, 871
D'Antona, F., Caloi, V., Montalbán, J., Ventura, P., & Gratton, R. 2002, A&A, 395, 69
Denissenkov, P. A. & Herwig, F. 2003, ApJ, 590, L99
Gratton, R. G. et al. 2001, A&A, 369, 87
Hansen, B. M. S. & Phinney, E. S. 1997, MNRAS, 291, 569
Kraft, R. P. 1994, PASP, 106, 553
Kroupa, P. 2001, MNRAS, 322, 231
Panagia, N., Romaniello, M., Scuderi, S. & Kirshner, R.P. 2000, ApJ 539, 197
Pfahl, E., Rappaport, S. & Podsiadlowski, P. 2003, ApJ, 573, 283
Piotto, G. & Zoccali, M. 1999, A&A, 345, 485
Smith G. H. 1987, PASP, 99, 67
Sneden C. 1999, Ap&SS, 265, 145
Stolte, A., Grebel, E. K., Brandner, W., & Figer, D. F. 2002, A&A, 394, 459
Ventura, P., D'Antona, F., Mazzitelli, I., & Gratton, R. 2001, ApJ, 550, L65
Ventura, P., D'Antona, F., & Mazzitelli, I. 2002, A&A, 393, 215
Ventura, P., Mazzitelli, I. & D'Antona, F. 2004, Proceedings of the Joint Discussion 04 of the XXIV IAU General Assembly, Sydney, Astrophysical Impact of Abundances in Globular Cluster Stars, eds. F.D'Antona and G. Da Costa, Mem.S.A.It. 75, n. 2, in press
Zoccali, M., Cassisi, S., Piotto, G., Bono, G., & Salaris, M. 1999, ApJ, 518, L49

Figure 3. Close encounter between Eva Grebel and Franca D'Antona.

THE STELLAR INITIAL MASS FUNCTION IN THE GALACTIC CENTER

Donald F. Figer
STScI, 3700 San Martin Drive, Baltimore, MD 21218, USA
figer@stsci.edu

Abstract Massive stars define the upper limits of the star formation process, dominate the energetics of their local environs, and significantly affect the chemical evolution of galaxies. Their role in starburst galaxies and the early Universe is likely to be important, but we still do not know the maximum mass that a star can possess, i.e."the upper mass cutoff." I will discuss results from a program to measure the upper mass cutoff and IMF slope in the Galactic Center. The results suggest that the IMF in the Galactic center may deviate significantly from the Salpeter value, and that there may be an upper mass cutoff to the initial mass function of $\sim 150\ M_{\odot}$.

1. Motivating Questions

Two simple, yet still unanswered, questions motivate this paper. First, is the stellar initial mass function (IMF) universal? Second, what is the most massive star that can form? These questions are related, as they concern primary output products of the star formation process. The IMF is observed to be roughly constant, within errors, although outliers to the value of the slope do exist. The data at the high mass end are woefully incomplete for determining the upper limit for which the IMF essentially becomes zero, i.e. an upper mass cutoff.

There are several properties of stellar clusters that are required for estimating the high mass IMF slope and, in particular, an upper mass cutoff:

1 the associated star formation event must produce a large amount of mass in stars, at least $10^4\ M_{\odot}$,

2 the resultant cluster must be young enough, certainly no older than 3 *Myr*, so that its most massive members are pre-supernovae,

3 the cluster must be old enough for its stars to have emerged from their natal cocoons,

4 the cluster must be close enough to be resolved into individual stars, and

E. Corbelli et al. (eds.), The Initial Mass Function 50 Years Later, 89–94.

5 the stellar surface number density must be low enough to allow one to separate light from individual stars.

Given this rather long list of requirements, it is perhaps not surprising that, as of yet, an upper mass cutoff has not been identified; although, recent work might have identified a cutoff in R136, a starburst cluster in the LMC (Weidner & Kroupa 2004). There is only one cluster in the Galaxy that can satisfy these requirements, the Arches cluster near the Galactic center. There are two other clusters massive enough, the Quintuplet and Central clusters, also both in the Galactic center, but those clusters are both too old, $\sim$4 *Myr*, and their most massive members have dimmed as WR stars or compact objects.

2. The Galactic center environment and its young clusters

The Galactic center occupies a very small volume, $\sim$0.04% of the Galaxy, yet it contains 10% of all Galactic molecular material and a similar proportion of newly formed stars. The extreme tidal forces in the center shred molecular clouds having densities less than about 10^4 cm^{-3}; therefore, the clouds in the region necessarily have relatively high densities compared to those in the disk. The cloud temperatures are also about a factor of three higher, and the magnetic field strength may be as much as 1 mG. This environment may favor the formation of massive stars (Morris 1993). See Morris & Serabyn (1996) for a review.

There are three massive young clusters within a projected radius of 30 pc of the Galactic center: the Arches, the Quintuplet, and the Central cluster. Their properties have been reviewed (Figer et al. 1999a, Figer et al. 1999c, Figer et al. 2002, Figer 2003). In brief, all three have about equal mass, $\sim 10^4$ $M_\odot$; but the first is only 2-2.5 *Myr* old, or about half the age of the other two. These older clusters are too old for an accurate determination of their initial mass functions using photometry alone, as their most massive members have likely progressed to the supernovae stage, or, at the least, have dimmed substantially and are lost amongst the background population of red giants. Even when they are distinguished from the background, as Wolf-Rayet stars, it is impossible to infer their original masses.

3. The Arches cluster and the IMF in the Galactic center

The Arches cluster is located just 30 pc, in projection, from the Galactic center (Cotera et al. 1992, Nagata et al. 1995, Figer 1995, Cotera 1995, Cotera et al. 1996, Blum et al. 2001). It contains 160 O-stars, and is the most massive young cluster in the Galaxy (Serabyn, Shupe, & Figer 1998, Figer et al. 1999a). Given its youth, its members have not yet advanced to their end states, and they still follow a linear relationship between mass and magnitude (Figer et al. 2002). The brightest members have masses $\sim$120 $M_\odot$, and are enriched

in helium and nitrogen (Najarro, Figer, Hillier, & Kudritzki 2004). They are commensurately luminous, up to $10^{6.3}\ L_{\odot}$, and have prodigious winds that carry a significant amount of mass, up to $10^{-5}\ M_{\odot}\ yr^{-1}$. Some of these winds have been individually identified through radio observations of their free-free emission (Lang, Goss, & Rodríguez 2001), and there are several point-like and diffuse x-ray emission sources centered on the cluster (Yusef-Zadeh et al. 2002).

The IMF in the Galactic center has been measured in one location, the Arches cluster (Figer et al. 1999a, Stolte, Grebel, Brandner, & Figer 2002), and it is somewhat shallow compared to the Salpeter value (Salpeter 1955). Figure 1 shows the mass function, as observed using HST/NICMOS. It was constructed by converting magnitudes into masses using the Geneva stellar evolution models (Schaller, Schaerer, Meynet, & Maeder 1992). The counts have been corrected for contamination by the background population. The slope appears to be shallow with respect to the Salpeter value. Such a cluster is likely to have experienced significant dynamical evolution in the strong tidal field of the Galactic center; however, Kim et al. (2000) find that this effect is unlikely to have produced such a flat slope.

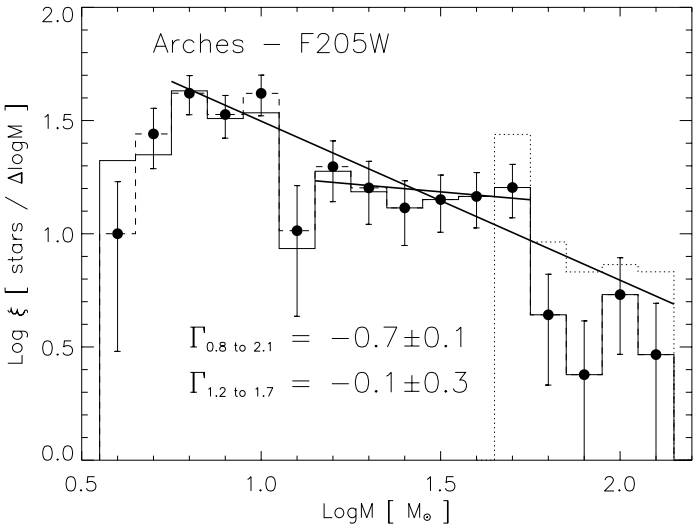

Figure 1. Present-day mass function of the Arches cluster in the F205W NICMOS filter (bold). Incompleteness corrected data are shown with a dashed line. The dotted line shows concurrence with earlier observations using Keck for the highest mass stars. The average IMF slope is -0.7, although Stolte et al. (2002) found a slightly steeper slope of -0.9 after correcting for differential extinction.

4. An upper mass cutoff

The Arches cluster appears to have an upper mass cutoff (Figer 2003, Figer 2004, Figer et al. 2005). Figure 2 shows the mass function extended to very high masses and computed out to a radius of 12 arcseconds from the center of the Arches cluster. In this plot, we see that one might expect massive stars up to 500−1,000 $M_{\odot}$, yet none are seen beyond ∼120 $M_{\odot}$. Taking account of errors, and the unreliable mass-magnitude relation at the highest masses, one can safely estimate an upper mass cutoff of ∼150 $M_{\odot}$. The most important caveat to this result relates to the youth of the cluster. An age >3 *Myr* would mean that the most massive stars have progressed to their end states and would not be observed. Several analyses suggest an age of 2-2.5 *Myr* (Figer et al. 1999a, Blum et al. 2001, Figer et al. 2002, Najarro, Figer, Hillier, & Kudritzki 2004). Note that an age <1 *Myr* would give a deficit of roughly twice that shown in the figure and a predicted maximum stellar mass of 600−1,700 $M_{\odot}$. A similar analysis was done for R136 in the LMC that also found a cutoff of 150 $M_{\odot}$ (Weidner & Kroupa 2004).

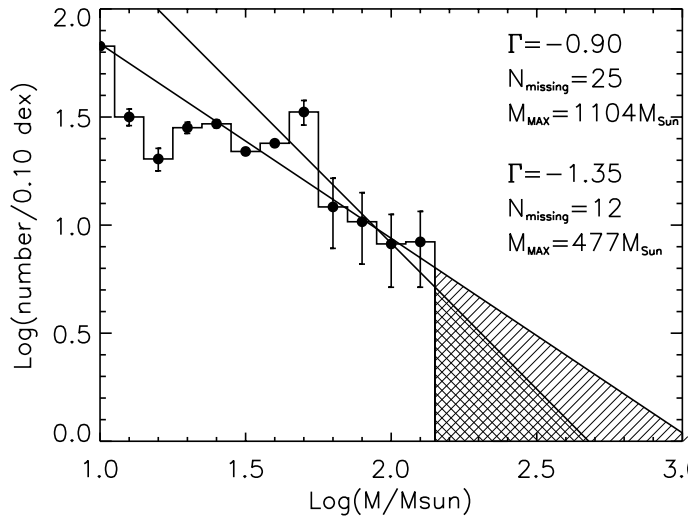

Figure 2. Present-day mass function of the Arches cluster in the F205W NICMOS filter with lines overplotted for the inferred mass function and the Salpter mass function. The hatched regions demonstrate that one would expect there to be many very massive stars in the cluster (Figer 2005).

5. Supermassive stars in violation of the cutoff?

There are several stars in apparent violation of the cutoff estimated in the Arches cluster. The Pistol star, in the Quintuplet cluster, has an estimated initial mass of 150−200 $M_{\odot}$ (Figer et al. 1998, Figer et al. 1999b). Star #362 in the Quintuplet cluster is a near-twin to the Pistol star (Figer et al. 1999c, Geballe, Najarro, & Figer 2000), so it likely had a similar initial mass. Both stars are roughly equally bright, although they are also both variable (Glass, Matsumoto, Carter, & Sekiguchi 2001). It is interesting to note that these two stars, if as massive as we think, should only live for $\sim$3 *Myr*, yet they reside in a cluster that is at least 4 *Myr* old. LBV1806−20 is another high mass star that may violate the limit, but it is likely binary (Figer, Najarro, & Kudritzki 2004). η Car, with a system mass that may be higher than the limit, is also a likely binary (Damineli et al. 2000). A promising resolution to the apparent paradox of a limit and systems with higher masses could be that all such systems are either binary or have been built through recent mergers (Figer & Kim 2002).

References

Blum, R. D., Schaerer, D., Pasquali, A., Heydari Malayeri, M., Conti, P. S., & Schmutz, W. 2001, AJ, 122, 1875

Cotera, A. S., Erickson, E. F., Simpson, J. P., Colgan, S. W. J., Allen, D. A., & Burton, M. G. 1992, American Astronomical Society Meeting, 181, 8702

Cotera, A. S. 1995, Ph.D. Thesis, Stanford University

Cotera, A. S., Erickson, E. F., Colgan, S. W. J., Simpson, J. P., Allen, D. A., & Burton, M. G. 1996, ApJ, 461, 750

Damineli, A., Kaufer, A., Wolf, B., Stahl, O., Lopes, D. F., & de Araújo, F. X. 2000, ApJ, 528, L101

Figer, D. F. 1995, Ph.D. Thesis, University of California, LosăAngeles

Figer, D. F. 2003, IAU Symposium, 212, 487

Figer, D. F. 2004, in proceedings of The Formation and Evolution of Massive Young Star Clusters, ed. Lamers

Figer, D. F., et al. 2002, ApJ, 581, 258

Figer, D. F. et al. 2005, in preparation

Figer, D. F. & Kim, S. S. 2002, in Stellar Collisions, Mergers and their Consequences, ASP Conf. Ser. 263, 287

Figer, D. F., Kim, S. S., Morris, M., Serabyn, E., Rich, R. M., & McLean, I. S. 1999a, ApJ, 525, 750

Figer, D. F., McLean, I. S., & Morris, M. 1999, ApJ, 514, 202

Figer, D. F., Morris, M., Geballe, T. R., Rich, R. M., Serabyn, E., McLean, I. S., Puetter, R. C., & Yahil, A. 1999b, ApJ, 525, 759

Figer, D. F., Najarro, F., Morris, M., McLean, I. S., Geballe, T. R., Ghez, A. M., & Langer, N. 1998, ApJ, 506, 384

Figer, D. F., Najarro, F., & Kudritzki, R. P. 2004, ApJ, 610, L109

Geballe, T. R., Najarro, F., & Figer, D. F. 2000, ApJ, 530, L97

Glass, I. S., Matsumoto, S., Carter, B. S., & Sekiguchi, K. 2001, MNRAS, 321, 77

Kim, S. S., Figer, D. F., Lee, H. M., & Morris, M. 2000, ApJ, 545, 301
Lang, C. C., Goss, W. M., & Rodríguez, L. F. 2001, ApJ, 551, L143
Morris, M. 1993, ApJ, 408, 496
Morris, M. & Serabyn, E. 1996, ARA&A, 34, 645
Nagata, T., Woodward, C. E., Shure, M., & Kobayashi, N. 1995, AJ, 109, 1676
Najarro, F., Figer, D. F., Hillier, D. J., & Kudritzki, R. P. 2004, ApJ, 611, L105
Salpeter, E. E. 1955, ApJ, 123, 666
Schaller, G., Schaerer, D., Meynet, G., & Maeder, A. 1992, A&AS, 96, 269
Serabyn, E., Shupe, D., & Figer, D. F. 1998, Nature, 394, 448
Stolte, A., Grebel, E. K., Brandner, W., & Figer, D. F. 2002, A&A, 394, 459
Weidner, C. & Kroupa, P. 2004, MNRAS, 348, 187
Yusef-Zadeh, F., Law, C., Wardle, M., Wang, Q. D., Fruscione, A., Lang, C. C., & Cotera, A. 2002, ApJ, 570, 665

Figure 3. Volker Bromm, Don Figer and Pavel Kroupa.

THE INITIAL MASS FUNCTION IN THE GALACTIC BULGE

Manuela Zoccali
P. Universidad Católica de Chile, Av. Vicuña Mackenna 4860, Macul, Santiago, Chile; and Princeton University Observatory, Peyton Hall, Princeton, NJ 08544, USA
mzoccali@astro.puc.cl

Abstract We measured the IMF of the Galactic Bulge, down to $\sim 0.15 M_{\odot}$ through NICMOS observations of a field near (l,b)=(0,-6). The derived IMF, the deepest measured to date in the Bulge, follows a power-law slope of $\alpha = -1.33 \pm 0.07$ (where Salpeter has $\alpha = -2.35$). This result has negligible dependence on the adopted Bulge metallicity and distance modulus. A detailed description of the data analysis, together with an extended discussion of the implications is in Zoccali et al. (1999). Here we just briefly summarize the result and compare with more recent observations about the mass-luminosity relation and the Disk IMF.

1. Introduction

Knowing the Initial Mass Function (IMF) at $M \lesssim 1 M_{\odot}$ in spiral Bulges and elliptical galaxies is of special interest because these spheroids contain a large fraction, perhaps a majority, of all the stellar mass of the universe (e.g., Fukugita, Hogan & Peebles 1998). However, there is presently no way to directly determine the IMF of spheroids except by measuring the luminosity function (LF) of our own Bulge as the only surrogate for the unresolvable population in other galaxies. Although the low mass end of the stellar IMF has been determined for the solar neighborhood (Kroupa, Tout & Gilmore 1993; Dahn et al. 1995; Gould, Bahcall & Flynn 1997; Reid et al. 2002) and in young open clusters (e.g., Muench et al. 2002; Prisinzano et al., 2003; Jeffries et al., 2004; Barrado y Navascués et al., 2004) it is only in the Galactic Bulge that one can be confident that the stellar population is old, largely coeval, and metal rich (Whitford 1978; Ortolani et al. 1995; McWilliam & Rich, 1994), i.e., the closest we can come in a nearby, resolved stellar population to what prevails in other spiral Bulges and elliptical galaxies (Renzini 1999).

E. Corbelli et al. (eds.), The Initial Mass Function 50 Years Later, 95–100.

2. The Bulge IMF

The details about the data reduction and analysis have been presented in Zoccali et al. (1999). Figure 1 summarizes the result: the obtained IMF can be represented by a power-law with slope $\alpha = -1.33 \pm 0.07$ over the entire mass range. There is an indication for the IMF to steepen above $0.5M_{\odot}$. A two slope IMF gives indeed a marginally better fit, with $\alpha = -2.00 \pm 0.23$ for $M > 0.5M_{\odot}$, and $\alpha = -1.43 \pm 0.13$ for $M < 0.5M_{\odot}$. However, caution must be taken in overinterpreting the kink around 0.5 $M_{\odot}$, since a change in the adopted distance modulus and/or metallicity, while not changing the overall slope, would change the shape of this kink (see Fig. 2).

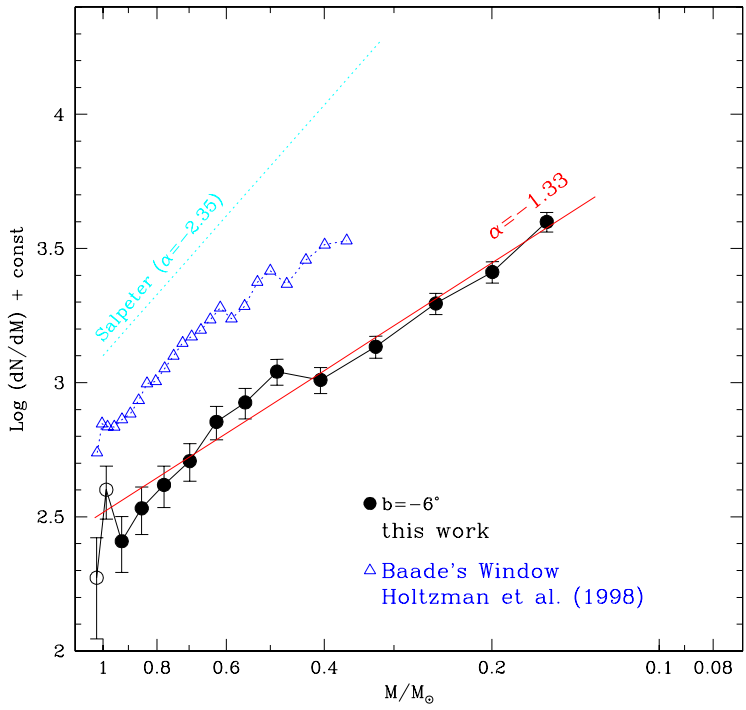

Figure 1. The IMF in the Galactic Bulge

Also shown in Fig. 1 is the IMF of a Bulge field in Baade's Window, as measured by Holtzmann et al. (1998). In the common mass range the two results are almost almost identical. Both IMF are however significantly flatter than the Salpeter slope, shown as a dotted line.

The Bulge IMF has been obtained by deconvolving the observed LF with a theoretical mass luminosity relation (MLR) from Cassisi et al. (2000). The

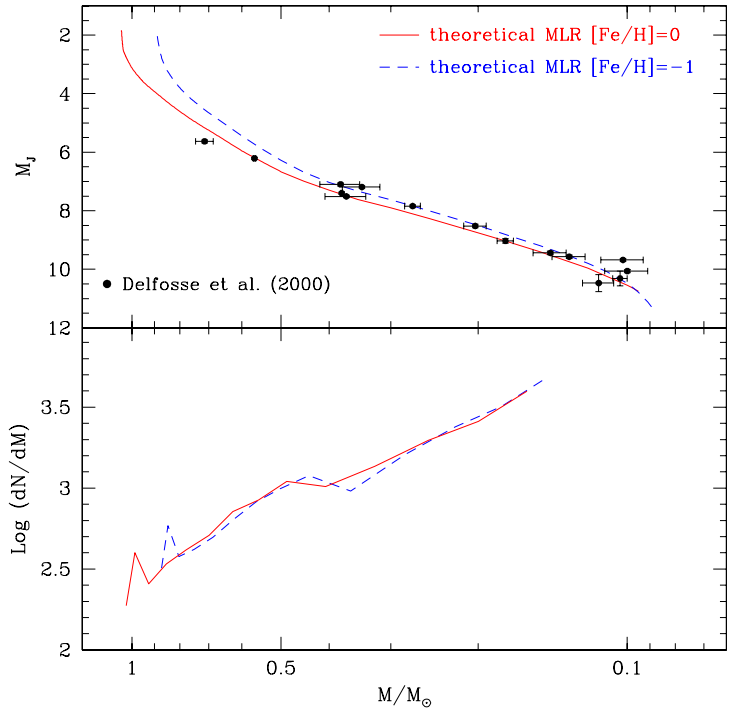

Figure 2. Top: The MLR by Cassisi et al. (2000) compared with the empirical data by Delfosse et al. (2000). Bottom: the Bulge IMF obtained with the MLR for [M/H]=0 (solid) and [M/H]=−1 (dashed).

adopted MLR was compared with the available empirical constraints in Zoccali et al. (1999). New observations have been made available since then: Fig. 2 (upper panel) shows that the adopted models follow extremely well the new empirical data from Delfosse et al. (2000). The lower panel of the same Figure shows the impact of a change in metallicity on the resulting IMF. Most Bulge stars have metallicity around solar, but the spread around this value is not negligible, especially towards low metallicities (McWilliam & Rich, 1994). However, even adopting a MLR appropriate for a [M/H]=−1 population, the overall slope would not change.

3. Bulge versus Disk IMF

Figure 3 shows the comparison between the Bulge IMF and several IMF measured in the Galactic Disk. In Zoccali et al. (1999) the Bulge IMF was compared with the Disk IMF by Gould et al. (1997) and by Reid & Gizis

(1997), which were both significantly flatter ($\alpha = -0.54$ and $\alpha = -0.8$, respectively). We are now aware of the new Disk LF by Reid et al. (2002), which superseedes the Reid & Gizis (1997) one, and of two further Disk LF by Henry & McCarthy (1990) and Dahn et al. (1995). The above mentioned Disk LFs, deconvolved with the same MLR adopted for the Bulge, give a IMF in perfect agreement with the Bulge one. This evidence, together with the similarity between the Bulge IMF and the IMF of Galactic Globular Cluster in external orbits (Zoccali et al. 1999) and with external spheroids (Wyse et al. 2000) points towards a universal IMF, at least for $M < 1 M_{\odot}$.

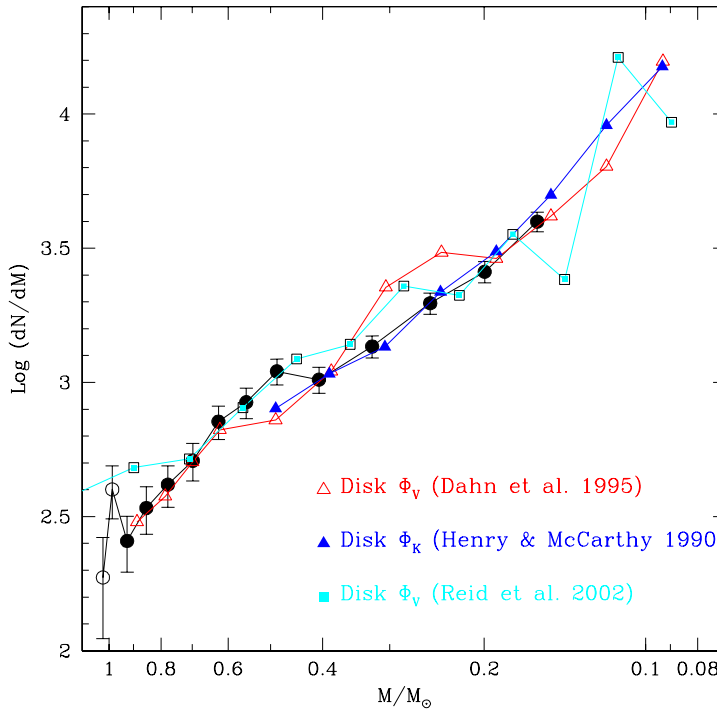

Figure 3. Comparison between the Bulge and the Disk IMF from several authors.

References

Barrado y Navascués, D., Stauffer, J. R., Bouvier, J., Martín, E. L., 2001, ApJ, 546, 1006
Cassisi, S., Castellani, V., Ciarcelluti, P., Piotto, G., Zoccali, M. 2000, MNRAS, 315, 679
Dahn, C. C., Liebert, J., Harris, H. C., Guetter, H. H. 1995, in Proc. ESO Astrophys. Symp., The Bottom of the Main Sequence and Beyond, ed. C. Tinney (Berlin: Springer), p. 239
Delfosse, X., Forveille, T., SÃl'gransan, D., Beuzit, J.-L., Udry, S., 2000, A&A, 364, 217

Fukugita, M., Hogan, C. J., Peebles, P. J. E., 1998, ApJ, 503, 518
Gould, A., Bahcall, J. N., Flynn, C. 1997, ApJ, 482, 913
Kroupa, P., Tout, C. A., Gilmore, G., 1993, MNRAS, 262, 545
Jeffries, R. D., Naylor, T., Devey, C. R., Totten, E. J., 2004, MNRAS, 351, 1401
Mc William, A., Rich, R. M., 1994, ApJS, 91, 749
Muench, A. A., Lada, E. A., Lada, C. J., Alves, J., 2002, ApJ, 573, 366
Ortolani, S., Renzini, A., Gilmozzi, R., Marconi, G., Barbuy, B., 1995, Nature, 377, 701
Prisinzano, L., Micela, G., Sciortino, S., Favata, F., 2003, A&A, 404. 927
Reid, I. N., Gizis, J. E. 1997, AJ, 113, 2246
Reid, I. N., Gizis, J. E., Hawley, S. L., 2002, AJ, 124, 2721
Renzini, A. 1999, in When and How do Bulges Form and Evolve, ed C.M. Carollo, H.C. Ferguson, R.F.G. Wyse, Cambridge University Press, p. 9
Whitford, A. E. 1978, ApJ, 226, 777
Wyse, R. F. G., Gilmore, G., Houdashelt, M. L., Feltzing, S., et al. 2002, NewA, 7, 395
Zoccali, M., Cassisi, S., Frogel, J.A., Gould, A., Ortolani, S., et al. 2000, ApJ, 530, 418

Figure 4. Manuela Zoccali witnessing the final agreement between Hartmann and Renzini.

Figure 5. Charlie Lada and Mark McCaughrean.

Figure 6. Neill Reid and Jerome Bouvier at poster session.

HALO MASS FUNCTION

Low-mass stars in deep fields

Wolfgang Brandner
Max-Planck-Institut für Astronomie, Königstuhl 17, D-69117 Heidelberg, Germany
brandner@mpia.de

Abstract Deep fields are unique probes of the Galactic halo. With a limiting magnitude of, e.g., I = 30 mag, all stars down to the hydrogen-burning limit are detected out to distances of 10 kpc, while stars with 0.5 solar masses could be traced out to distances of 400 kpc. Thus deep fields provide an opportunity to study both the structure of the Galactic halo and the mass function of population (Pop) II and Pop III stars. I summarize previous work on the Galactic stellar halo utilizing the Hubble Deep Fields North and South, supplemented by a preliminary analysis of the recently released Hubble Ultra-Deep Field.

1. Motivation

The structure and stellar content of the Galactic Halo directly points back to the formation of the Milky Way. Initial studies naturally focused on the Pop II main-sequence stars in the solar neighbourhood. These limits have been gradually extended towards fainter (i.e. lower mass and/or more distant) halo stars, including evolved stars, white dwarfs and a search for the baryonic dark matter component (e.g. Paczynski 1986, Alfonso et al. 2003, and references therein).

Studies of stellar populations in deep fields aim at addressing the following issues:

- Stellar Content and Origin of the Galactic Halo
- (Global) Structure of the Galactic Halo
- Search for a (still self-luminous) baryonic component of the ”dark matter” halo
- Fraction of Pop III stars in the Galactic Halo, in particular stars with [Fe/H] < -4 (see, e.g., Oey 2003)

E. Corbelli et al. (eds.), The Initial Mass Function 50 Years Later, 101–106.

1.1 Galactic Structure

The stellar population of the Milky Way is arranged into three dynamically distinct components. Bahcall & Soneira (1981, 1984) provided evidence for a thin disk of Pop I stars, and a halo composed of Pop II stars. Gilmore & Reid (1983) and Gilmore (1984) identified the thick disk as a third distinct component. Figure 1 illustrates the 3-component composition of the Milky Way stellar population as evidenced by SDSS data (Chen et al. 2001). Chen et al. (2001), Larsen & Humphreys (2003), and Lemon et al. (2004) all derive a flattened halo density distribution with c/a $\approx$ 0.55, following a density law $\rho(\mathrm{r}) \propto \mathrm{r}^{-2.5\pm0.3}$.

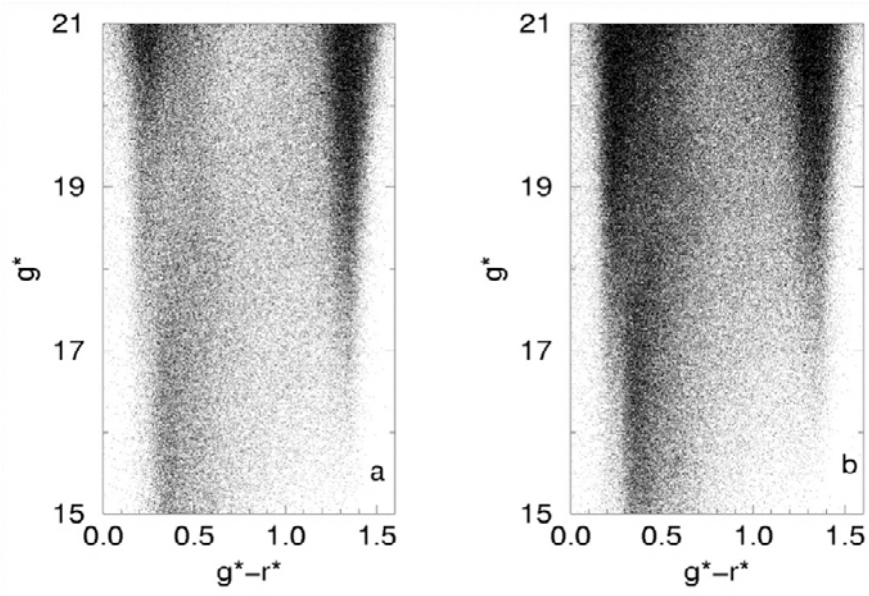

Figure 1. Colour-Magnitude Diagram based on SDSS data for high Galactic latitudes of b$> +48^\circ$ (left) and b$< -48^\circ$ (right). The three component structure of the Milky Way with the halo at $g^* - r^* \approx 0.2$ mag, the thick disk at $g^* - r^* \approx 0.33$ mag and a turn-off magnitude of $g^* \leq 18$ mag, and the thin disk at $g^* - r^* \approx 1.4$ mag is clearly evident (Chen et al. 2001).

It should be noted, however, that the results quoted above are based on the assumption of a uniform, global Salpeter-type (Salpeter 1955) luminosity function.

1.2 Subdwarf Luminosity Function

Over the past 15 years, a number of studies with increasingly fainter magnitude limits and larger field coverage aimed at the derivation of the subdwarf luminosity function. Gould et al. (1998) report a discrepancy between the lu-

minosity functions for the inner and the outer halo. If confirmed, this would constitute a case of a radially varying mass function in the halo of the Milky Way. A more recent study by Digby et al. (2003), however, reaching out to $M_V \leq 12$ mag for heliocentric distances of 2.5 kpc, did not find any indication for a variation in the mass function (see Figure 2).

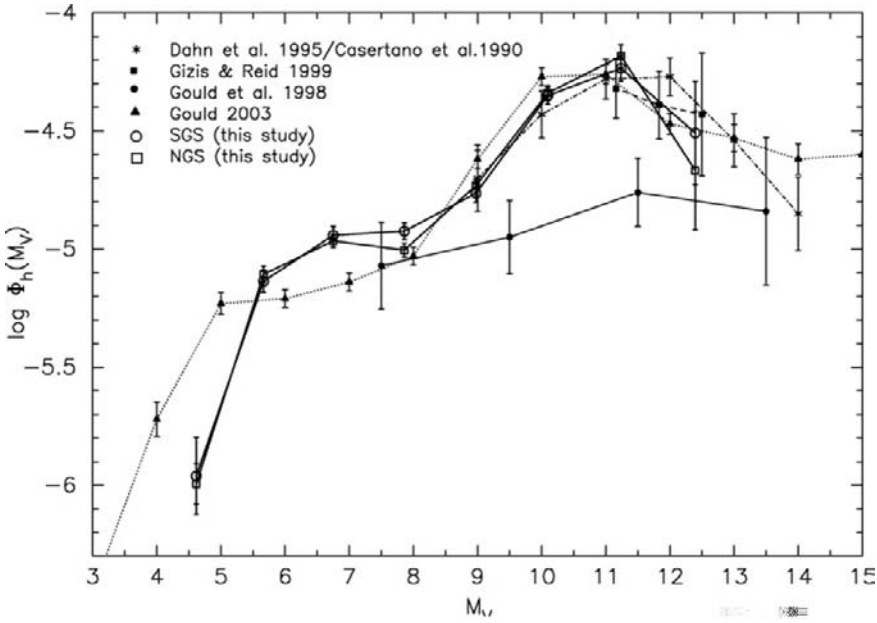

Figure 2. Compilation of estimates of the luminosity function for subdwarfs from Digby et al. (2003).

2. Hubble Deep Fields and the Halo IMF

The Hubble Deep Fields North (HDF-N) and South (HDF-S) were observed in December 1995 and October 1998, respectively, with the aim to obtain the most detailed view of distant field galaxies in order to study various aspects of galaxy evolution and cosmology based on galaxy number counts, luminosity functions and morphology (Williams et al. 1996, 2000). In order to minimize contamination by Galactic stars, the fields were centered far from the Galactic plane at latitudes of $b = +54^\circ$ and $b = -49^\circ$, respectively. The Hubble Ultra-Deep Field (UDF), obtained in late 2003, represents an even deeper image of a high-Galactic latitude field (Beckwith et al. 2004). Table 1 summarizes the basic properties of HDF-N/S and UDF.

Figure 3 shows colour-magnitude diagrams for the UDF based on the ACS/WFC source catalogue version 1.

Table 1. Properties of HDF-N/S[a] and UDF[b]

Field	*l*	*b*	*Filters*	*5σ limit (AB mag)*	*# of MS stars*
HDF-N	126°	+54°	UBVI	I ≈ 29.1	9
HDF-S	328°	-49°	UBVI	I ≈ 29.1	29
UDF	223°	-54°	BVIz	I ≈ 30.5	9 (11)

[a] Williams et al. 1996, 2000
[b] Beckwith et al. 2004

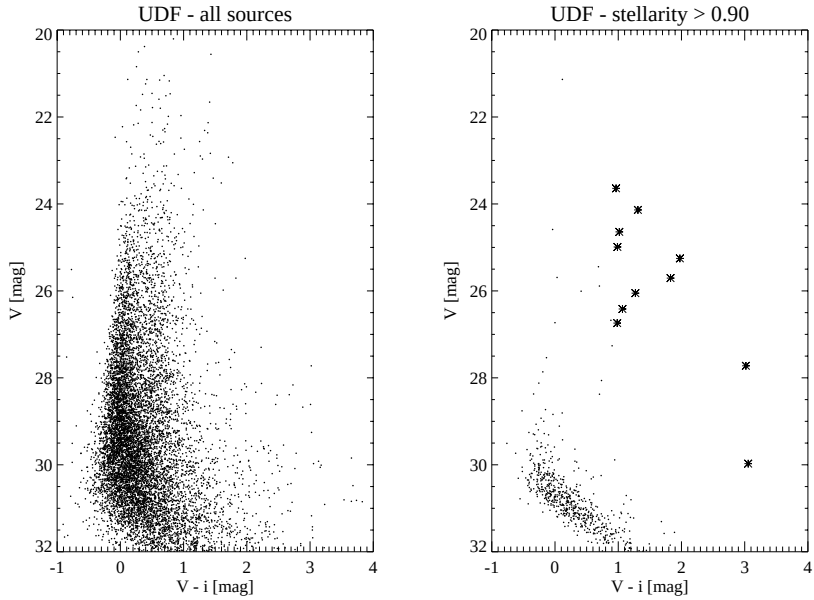

Figure 3. Colour-magnitude diagram for UDF. The diagram on the left shows all sources, whereas the diagram on the right only includes sources with a stellarity index > 0.90. Candidate main-sequence stars are marked by "star" symbols.

A pioneering study of the *stellar* content of HDF-N/S was carried out by the late Rebecca Elson and collaborators (Elson et al. 1996; Johnson et al. 1999). The number of main-sequence stars in both fields (see Figure 4) turned out to be in good agreement with models. In particular, they found no evidence for an extended, cD-like stellar halo around the Galaxy. Johnson et al. (1999) argue that the compact blue sources identified in HDF-S most likely constitute unresolved (extragalactic) star forming regions, rathern than Pop III white dwarfs.

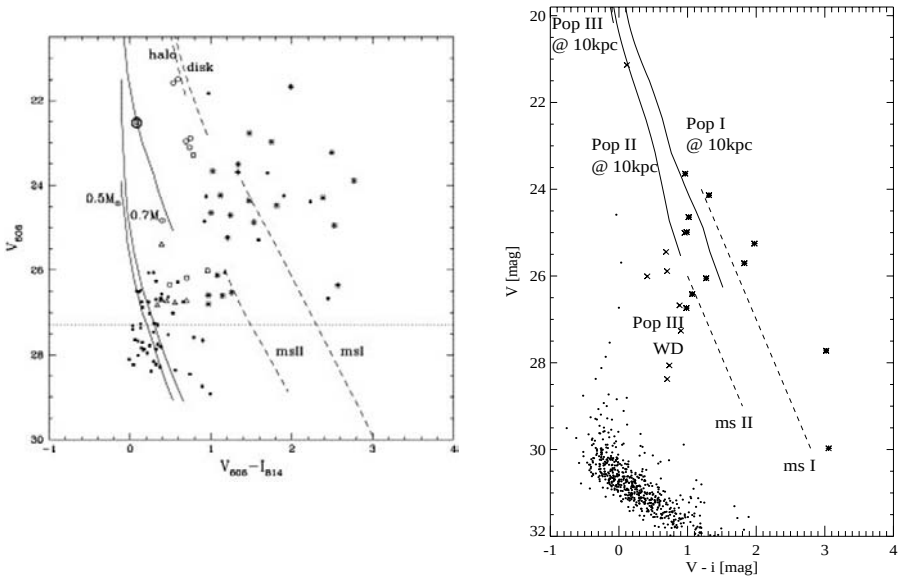

Figure 4. Colour-magnitude diagram for HDF N and S (left) and UDF (right). The locations of Pop I, II and III main-sequence stars (for a distance of 10 kpc), and cooling curves for white dwarfs with masses of 0.5 and 0.7 $M_{\odot}$ are shown as well.

In a related study, Ibata et al. (1999) and Kalirai et al. (2004) analysed deep, multi-epoch HST images of the inner halo in the direction of M4 (l = 351°, b = 16°). Down to a limiting magnitude of V = 29 mag, the observed numbers of thin-disk, thick-disk and Pop II halo white dwarfs are in good agreement with Galactic models. Based on a Chabrier IMF (Chabrier 1999) they expected to find 2 to 3 Pop III white dwarfs, but found none. While there is no need to invoke Pop III white dwarfs in order to fit the data, the small number statistics also does not yet rule out the existence of Pop III white dwarfs.

3. Open Questions

The following questions still need to be answered:

- Are all the red, low-mass candidates identified in HDF-N/S and UDF indeed stars?
- What is the nature of the compact blue sources? Are they Pop III white dwarfs or unresolved star forming regions?
- What is the exact shape of the outer halo luminosity function?

To address these questions, a spectroscopic follow-up of the brighter Pop II and Pop III candidates should be carried out. Spectroscopy of the fainter candidates is a science case for the next generation of Extremely Large Telescopes with apertures in the range 30 m to 100 m.

Second epoch imaging of HDF-N (S) in Cycle 14 (15) would provide an epoch difference of 10 (8) years. Assuming an astrometric precision of 5 mas, it would be possible to confirm proper motions as small as 0.5 mas/yr. This should be sufficient to distinguish Pop II and Pop III white dwarfs from unresolved, extragalactic star forming regions, and might lead to the first identification of Pop III objects.

Acknowledgments Discussions with Dimitrios Gouliermis and Bertrand Goldman are gratefully acknowledged.

References

Alfonso, C., Albert, J.N., Andersen, J. et al. 2003, A&A 400, 951
Bahcall, J.N., Soneira, R.M., 1981, ApJ 246, 122
Bahcall, J.N., Soneira, R.M., 1984, ApJS 55, 67
Beckwith, S.V.W., et al. 2004, in preparation
Chabrier, G., 1999, ApJ 513, L103
Chen, B., Stoughton, C., Smith, J.A., et al., 2001, ApJ 553, 184
Digby, A.P., Hambly, N.C., Cooke, J.A., Reid, I.N., Cannon, R.D., 2003, MNRAS 344, 583
Elson, R.A.W., Santiago, B.X., Gilmore, G.F. 1996, New Astro. 1, 1
Gilmore, G., Reid, N., 1983, MNRAS 202, 1025
Gilmore, G., 1984, MNRAS 207, 223
Gould, A., Flynn, C., Bahcall, J.N., 1998, ApJ 503, 798
Ibata, R.A., Richer, H.B., Fahlman, G.G. et al., 1999, ApJS 120, 265
Johnson, R.A., Gilmore, G.F., Tanvor, N.R., Elson, R.A.W. 1999, New Astro. 4, 431
Kalirai, J.S., Richer, H.B., Hansen, B.M. et al., 2004, ApJ 601, 277
Larsen, J.A., Humphreys, R.M., 2003, AJ 125, 1958
Lemon, D.J., Wyse, R.,F.G., Liske, J., Driver, S.P., Horne, K., 2004, MNRAS 347, 1043
Oey, M.S. 2003, MNRAS 339, 849
Paczynski, B. 1986, ApJ 304, 1
Salpeter, E. E. 1955, ApJ, 123, 666
Williams, R.E., Blacker, B., Dickinson, M. et al. 1996, AJ 112, 1335
Williams, R.E., Baum, S., Bergeron, L.E. et al. 2000, AJ 120, 2735

III

THE IMF IN OUR GALAXY: STAR FORMING REGIONS

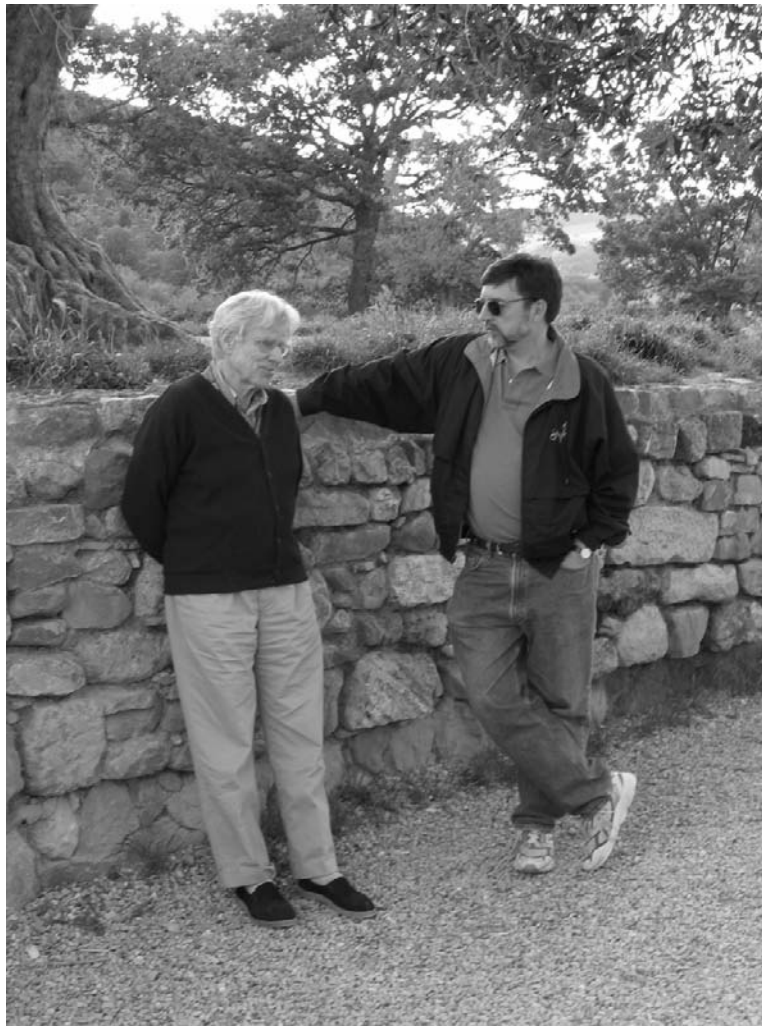

Figure 5. Theory and oservations under the olive trees: Ed and Charlie Lada.

Figure 6. Neil Reid and Eric Feigelson under the trees.

Figure 7. Hans and Morten Andersen at Banditaccia.

EMBEDDED CLUSTERS AND THE IMF

Charles J. Lada
Smithsonian Astrophysical Observatory, 60 Garden St., Cambridge, MA USA
clada@cfa.harvard.edu

Abstract Despite valiant efforts over nearly five decades, attempts to determine the IMF over a complete mass range for galactic field stars and in open clusters have proved difficult. Infrared imaging observations of extremely young embedded clusters coupled with Monte Carlo modeling of their luminosity functions are improving this situation and providing important new contributions to our fundamental knowledge of the IMF and its universality in both space and time.

1. Introduction

A fundamental consequence of the theory of stellar structure and evolution is that, once formed, the subsequent life history of a star is essentially predetermined by one parameter, its birth mass. Consequently, detailed knowledge of the initial distribution of stellar masses at birth (i.e., the IMF) and how this quantity varies through time and space is necessary to predict and understand the evolution of stellar systems, such as galaxies and clusters. Unfortunately, stellar evolution theory is unable to predict the form of the IMF. This quantity must be derived from observations. Stellar clusters have played an important role in IMF studies because they present equidistant and coeval populations of stars of similar chemical composition. Compared to the disk population, clusters provide an instantaneous sampling of the IMF at different epochs in galactic history (corresponding to the different cluster ages) and in different, relatively small volumes of space. This enables investigation of possible spatial and temporal variations in the IMF. Extremely young embedded clusters are particularly useful laboratories for IMF measurements because these clusters are too young to have lost significant numbers of stars due to stellar evolution or dynamical evaporation, thus their present day mass functions are, to a very good approximation, their initial mass functions. Embedded clusters are also particularly well suited for determining the nature of the IMF for low mass stars and substellar objects. This is because low mass stars in embedded

E. Corbelli et al. (eds.), The Initial Mass Function 50 Years Later, 109–114.

clusters are primarily pre-main sequence stars, and thus are brighter than at any other time in their lives. At these early ages brown dwarfs are similarly bright as low mass stars. Indeed, infrared observations of modest depth are capable of detecting objects spanning the entire range of stellar mass from 0.01 to 100 $M_{\odot}$ in clusters within 0.5 – 1.0 Kpc of the sun.

2. From Luminosity to Mass Functions

The monochromatic brightness of a star is its most basic observable property and infrared cameras enable the simultaneous measurement of the infrared monochromatic brightnesses of hundreds of stars. Thus, complete luminosity functions, which span the entire range of stellar mass, can be readily constructed for embedded stellar clusters with small investments of telescope time. The monochromatic (e.g., K band) luminosity function of a cluster, $\frac{dN}{dm_K}$, is defined as the number of cluster stars per unit magnitude interval and is the product of the underlying mass function and the derivative of the appropriate mass-luminosity relation (MLR):

$$\frac{dN}{dm_K} = \frac{dN}{dlogM_*} \times \frac{dlogM_*}{dm_K} \tag{1}$$

where m_k is the apparent stellar (K) magnitude, and M_* is the stellar mass. The first term on the right hand side of the equation is the underlying stellar mass function and the second term the derivative of the MLR. With knowledge of the MLR (and bolometric corrections) this equation can be inverted to derive the underlying mass function from the observed luminosity function of a cluster whose distance is known.

This method is essentially that originally employed by Salpeter (1955) to derive the field star IMF. However, unlike main sequence field stars, PMS stars, which account for most of the stars in the an embedded cluster, cannot be characterized by a unique MLR. Indeed, the MLR for PMS stars is a function of time. Moreover, for embedded clusters the duration of star formation can be a significant fraction of the cluster's age. Consequently, to invert the equation and derive the mass function one must model the luminosity function of the cluster and this requires knowledge of both the star formation history (i.e., age and age spread) of the cluster as well as the time-varying PMS mass-luminosity relation. The age or star formation history of the cluster typically can be derived by placing cluster stars on an HR diagram. This, in turn, requires additional observations such as multi-wavelength photometry or spectroscopy of a representative sample of the cluster members. PMS models must be employed to determine the time varying mass-luminosity relation. The accuracy of the derived IMF therefore directly depends on the accuracy of the adopted

PMS models which may be inherently uncertain, particularly for the youngest clusters ($\tau < 10^6$ yrs) and lowest mass objects ($m < 0.08\ M_\odot$).

Despite these complexities, Monte Carlo modeling of the infrared luminosity functions of young clusters (Muench, Lada & Lada 2000) has demonstrated that *the functional form of an embedded cluster's luminosity function is considerably more sensitive to the form of the underlying cluster mass function than to any other significant parameter* (i.e., stellar age distribution, PMS models, etc.). In particular, despite the significant differences between the parameters that characterize the various PMS calculations (e.g., adopted convection model, opacities, etc.), model luminosity functions were found to be essentially insensitive to the choice of existing PMS mass-to-luminosity relations. This indicated that, given smoothly varying mass-luminosity relations and knowledge of their ages, the monochromatic luminosities of PMS stars can provide very good proxys for their masses. *This is a direct result of the steepness of the mass-luminosity relation for PMS stars.*

The top panel of Figure 1 shows the K luminosities (magnitudes) for million-year-old PMS stars predicted by a suite of the best known PMS models in the literature. The excellent agreement between the various models reflects the steep dependence of luminosity on stellar mass, a consequence of the basic stellar physics of Kelvin-Helmholtz contraction. Any intrinsic variations or uncertainties in the models are dwarfed by the sensitivity of luminosity to stellar mass. This is in contrast to the situation for the predicted stellar effective temperatures as a function of mass. The bottom panel of Figure 1 shows that the predicted effective temperatures are much less sensitive to stellar mass. The intrinsic variations in the models are roughly similar in magnitude to the overall variation in effective temperature with mass.

3. The IMF from OB stars to Brown Dwarfs

The rich Trapezium cluster in Orion represents the best nearby target for determining the IMF of a young stellar population. Muench et al. (2002) obtained deep infrared images of the Trapezium cluster and derived its IMF by using a suite of Monte Carlo calculations to model the cluster's K-band luminosity function (KLF). The observed shape of a cluster luminosity function depends on three parameters: the ages of the cluster stars, the cluster mass-luminosity relation, and the underlying IMF (i.e., Equation 1). With the assumptions of a fixed age distribution, derived from an existing spectroscopic study of the cluster by Hillenbrand (1997), a composite theoretical mass-luminosity relation adopted from published PMS calculations and an empirical set of bolometric corrections, Muench et al. varied the functional form of the underlying IMF to construct a series of synthetic KLFs. These synthetic KLFs were then compared to the observed, background corrected, Trapezium KLF in a

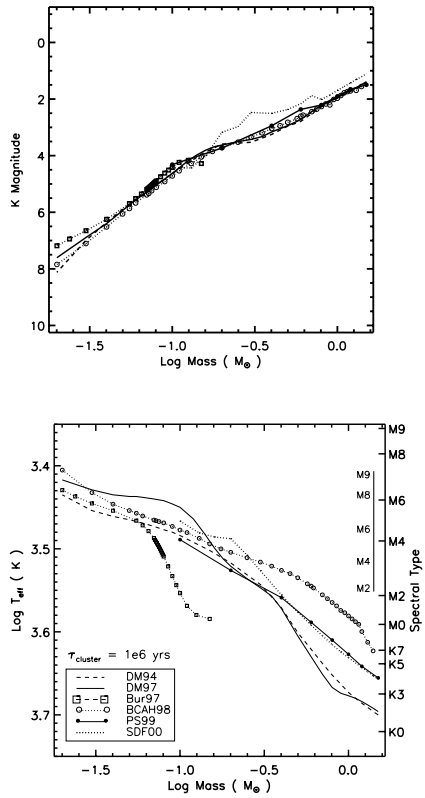

Figure 1. Comparisons of theoretical predictions for the infrared luminosities and effective temperatures of million-year-old PMS stars as a function of mass from a suite of standard PMS models (Burrows et al. 1997; Baraffe et al. 1998; D'Antona & Mazzitelli 1994; 1997; Palla & Sthaler 1999; Seiss et al. 2000). Note that the predicted PMS K magnitudes (top) appear to be in excellent agreement across the entire mass range whereas the predicted PMS effective temperatures (bottom) are not. This is a result of the steepness of the infrared mass-luminosity relation and clearly demonstrates how sensitive PMS luminosity is to variations in stellar mass.

Chi-Squared minimization procedure to produce a best-fit IMF. As part of the modeling procedure, the synthetic KLFs were statistically corrected for both variable extinction and infrared excess using Monte Carlo probability functions for these quantities that were derived directly from multi-color observations of the cluster.

The derived mass function is displayed in Figure 2 in the form of a histogram of binned masses of the stars in the best-fit synthetic cluster. This model mass function represents the IMF of the young Trapezium cluster. This mass function agrees very well with Trapezium IMFs derived from a number of other different deep infrared imaging surveys using a variety of methods (Lucas &

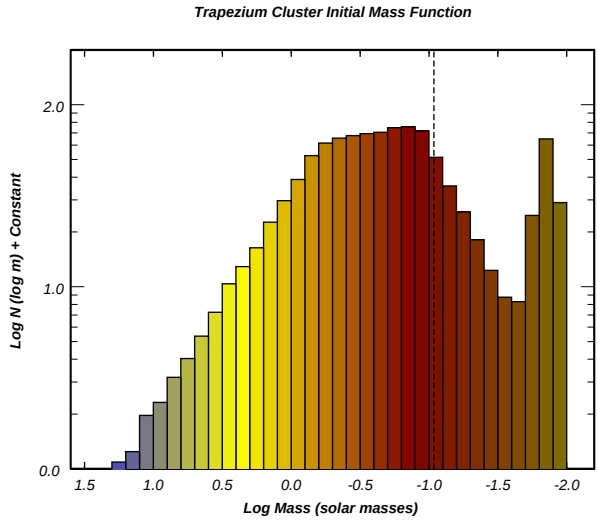

Figure 2. The IMF derived for the Trapezium cluster from Monte Carlo modeling of its luminosity function (Muench et al. 2002). This plot displays the binned mass function of the synthetic cluster whose luminosity function was found to best fit the observed KLF of the Trapezium cluster. A vertical dashed line marks the approximate location of the hydrogen burning limit. The derived IMF extends deep into the substellar regime.

Roche 2000; Hillenbrand and Carpenter 2000; Muench et al. 2000; Luhman et al. 2000). The main characteristics of this IMF are: 1) the sharp power-law rise of the IMF from about 10 $M_{\odot}$ (OB stars) to 0.6 $M_{\odot}$ (dwarf stars) with a slope (i.e., β = –1.2) similar to that of Salpeter (1955), 2) the break from the single power-law rise at 0.6 $M_{\odot}$ followed by a flattening and slow rise reaching a peak at about 0.1 $M_{\odot}$, near the hydrogen burning limit, and 3) the immediate steep decline into the substellar or brown dwarf regime.

The most significant characteristic of this IMF is the broad peak, extending roughly from 0.6 to 0.1 $M_{\odot}$. This structure clearly demonstrates that **there is a characteristic mass produced by the star formation process in Orion.** That is, the typical outcome of the star formation process in this cluster is a star with a mass between 0.1 and 0.6 $M_{\odot}$. The process produces relatively few high mass stars and relatively few substellar objects. *Indeed, no more than* $\sim$ *22% of all the objects formed in the cluster are freely floating brown dwarfs.* The overall continuity of the IMF from OB stars to low mass stars and across the hydrogen burning limit strongly suggests that the star formation process has no knowledge of the physics of hydrogen burning. Substellar objects are produced naturally as part of the same physical process that produces OB stars.

The derived IMF of the Trapezuim cluster spans a significantly greater range of mass than any previous IMF determination whether for field stars or other clusters (e.g., Kroupa 2002). Its statistically meaningful extension to substellar masses and the clear demonstration of a turnover near the HBL represents an important advance in IMF studies. For masses in excess of the HBL the IMF for the Trapezium is in good agreement with the most recent determinations for field stars (Kroupa 2002). This is to some extent both remarkable and surprising since the field star IMF is averaged over billions of years of galactic history, assuming a constant star formation rate, and over stars originating from very different locations of galactic space. The Trapezium cluster, on the other hand, was formed within the last million years in a region considerably less than a parsec in extent. Taken at face value this agreement suggests that the IMF and the star formation process that produces it are very robust in the disk of the Galaxy.

References

Baraffe, I., Chabrier, G., Allard, F. & Hauschildt, P.H. 2002, *A&A*, 382, 563

Burrows, A., Marley, M., Hubbard, W., Lunine, J., et al. 1997, *ApJ*, 491, 856

D'Antona, F. & Mazzitelli, I. 1994, *ApJS*, 90, 467

D'Antona, F. & Mazzitelli, I. 1997, *Mem.Soc.Astron.Italiana*, 68, 807

Hillenbrand, L.A. 1997, *AJ*, 113, 1733

Hillenbrand, L.A. & Carpenter, J.M. 2000, *ApJ*, 540, 236

Kroupa, P. 2002, *Science*, 295, 82

Lucas, P.W. & Roche, P.F. 2000, *MNRAS*, 314, 858

Luhman, K.L., Rieke, G.H., Young, E.T., Cotera, A.S., Chen, H., Rieke M.J., Schneider, G. & Thompson, R.I. 2000, *ApJ*, 540, 1016

Muench, A.A., Lada, E.A. & Lada, C.J. 2000, *ApJ*, 553, 338

Muench, A.A., Lada, E.A., Lada, C.J. & Alves, J.F. 2002, *ApJ*, 573, 366

Palla, F. & Stahler, S.W. 1999, *ApJ*, 525, 772

Salpeter, E.E. 1955, ApJ, 121, 161

Seiss, L., Dufour, E., Forestini, M. 2000 *A&A*, 358, 593

THE IMF OF STARS AND BROWN DWARFS IN STAR FORMING REGIONS

K.L. Luhman
Harvard-Smithsonian Center for Astrophysics, Cambridge, MA 02138, USA
kluhman@cfa.harvard.edu

Abstract I present recent measurements of the initial mass function and spatial distribution of stars and brown dwarfs in nearby star-forming regions.

1. IMF Peak Mass: Higher in Taurus

Because of the vertical nature of the mass tracks for low-mass stars on the H-R diagram, the spectral types of young objects should be well-correlated with their masses. Very little evolution in temperature is expected between the ages of Taurus (1 Myr), Chamaeleon I (2 Myr), and IC 348 (2 Myr), implying virtually identical relations between spectral types and masses for these two populations. In addition, a spectral type is a simple, observable quantity that can be measured to good accuracy with relative ease, particularly at M types. Therefore, I use the distributions of spectral types for IC 348, Chamaeleon I, and Taurus as IMF proxies that can be compared in a straightforward, reliable fashion without the involvement of evolutionary models. The IMF samples for Taurus (Briceño et al. 2002; Luhman et al. 2003a; Luhman 2004), Chamaeleon I (K. L. Luhman, in preparation), and IC 348 (Luhman et al. 2003b) are unbiased in mass down to 0.02 $M_{\odot}$, respectively, which correspond to types of $\sim$M9 for young ages. The numbers of objects as a function of spectral type in these samples are plotted in Figure 1. The distributions for IC 348 and Chamaeleon I reach a maximum at M5, while primary and secondary peaks appear at K7 and M5 in Taurus. Spectral types of M5 and K7 correspond to masses near 0.15 and 0.8 $M_{\odot}$ for ages of a few million years by the models of Baraffe et al. (1998). The difference in spectral type distributions between Taurus and the two denser clusters represents clear, unambiguous evidence for a significant variation of the IMF with star-forming conditions. Previous studies have noted that a difference of this kind might be present between Taurus and clusters like Orion (e.g., Hillenbrand 1997). However, most previous samples of mem-

E. Corbelli et al. (eds.), The Initial Mass Function 50 Years Later, 115–120.

bers of star-forming regions have been derived by combining disparate surveys that utilized biased selection techniques (e.g., Hα, IR excess). It was unclear whether the predominance of K7 and M0 stars in Taurus was an accurate reflection of the region or simply a result of incompleteness at later types. The new magnitude-limited membership surveys have enabled the first comparison of spectral type distributions in which the samples are complete down to late spectral types and contain relatively large numbers of members.

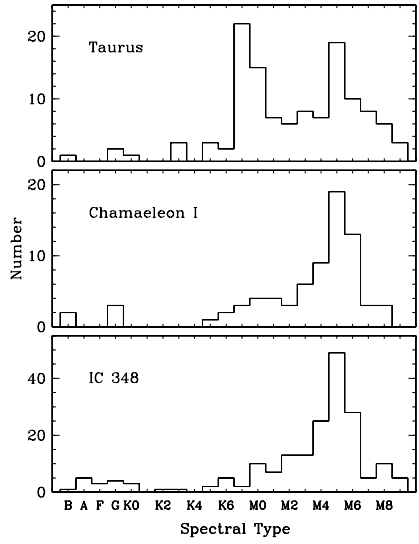

Figure 1. Distributions of spectral types for objects in the IMFs for Taurus (Luhman 2004), Chamaeleon I (K. L. Luhman, in preparation), and IC 348 (Luhman et al. 2003b) that are shown in Figures 2 and 3. These samples are extinction-limited ($A_V \leq 4$) and are nearly 100% complete for spectral types of $\leq$M9.

When the data for the samples in IC 348, Chamaeleon I, and Taurus are transformed to individual masses with evolutionary models, the IMFs in Figures 2 and 3 are produced. Because the same techniques and models were employed in converting from data to masses for each population, one can be confident in the validity of any differences in these IMFs. I also include in this comparison the IMF derived for the Trapezium Cluster in Orion through IR luminosity function modeling by Muench et al. (2002). The spectroscopically determined IMF for IC 348 agrees well with the IMF derived by Muench et al. (2003) through such luminosity function modeling, which suggests that the Trapezium IMF from Muench et al. (2002) can be reliably compared to the spectroscopic IMFs for IC 348, Chamaeleon I, and Taurus. The IMF for Taurus peaks near 0.8 $M_\odot$ and steadily declines to lower masses. Meanwhile, the

mass functions for IC 348, Chamaeleon I, and the Trapezium rise from high masses down to a solar mass in a roughly Salpeter fashion, rise more slowly down to a maximum at 0.1-0.2 $M_{\odot}$, and then decline into the substellar regime. Luhman et al. (2003b) quantified the significance of the differences in the distributions of spectral types and masses for Taurus and IC 348 by performing a two-sided Kolmogorov-Smirnov test between the distributions. In terms of both spectral types and masses, the probability that the samples for Taurus and IC 348 are drawn from the same distribution is $\sim 0.01\%$.

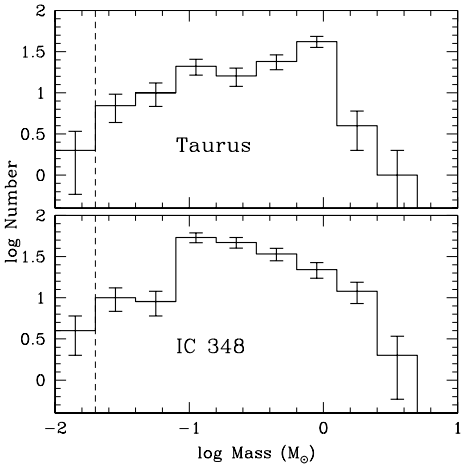

Figure 2. IMFs for Taurus (Luhman 2004) and IC 348 (Luhman et al. 2003b).

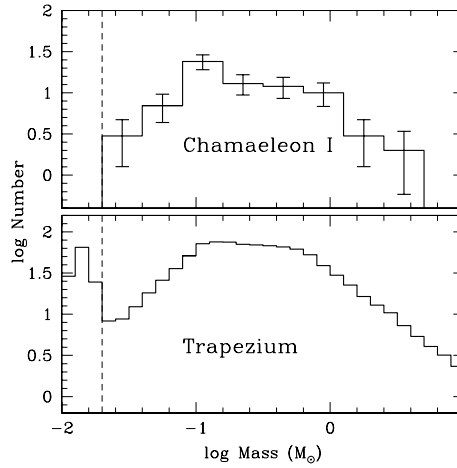

Figure 3. IMFs for Chamaeleon I (K. L. Luhman, in preparation) and the Trapezium Cluster (Muench et al. 2002). In the units of this diagram, the Salpeter slope is 1.35.

2. Brown Dwarf Fraction: Higher in Trapezium

Recent spectroscopic surveys of Taurus (Briceño et al. 2002; Luhman et al. 2003a; Luhman 2004) and IC 348 (Luhman et al. 2003b) have reported brown dwarf fractions that are a factor of two lower than the values derived from luminosity function modeling in the Trapezium Cluster in Orion (Luhman et al. 2000; Hillenbrand & Carpenter 2000; Muench et al. 2002). However, upon spectroscopy of a large sample of brown dwarf candidates in the Trapezium, Slesnick et al. (2004) found a population of faint objects with stellar masses, possibly seen in scattered light, which had contaminated previous photometric IMF samples and resulted in overestimates of the brown dwarf fraction in this cluster. After they corrected for this contamination, the brown dwarf fraction in the Trapezium was a factor of ~ 1.8 higher than the value in Taurus from

Luhman et al. (2003a). This difference would is reduced further (~ 1.4) if the new brown dwarf fraction for Taurus from Luhman (2004) is adopted. In summary, according to the best available data (Figure 4), the brown dwarf fractions in Taurus and IC 348 are lower than in the Trapezium, but by a factor (1.4-1.8) that is smaller than that reported in earlier studies.

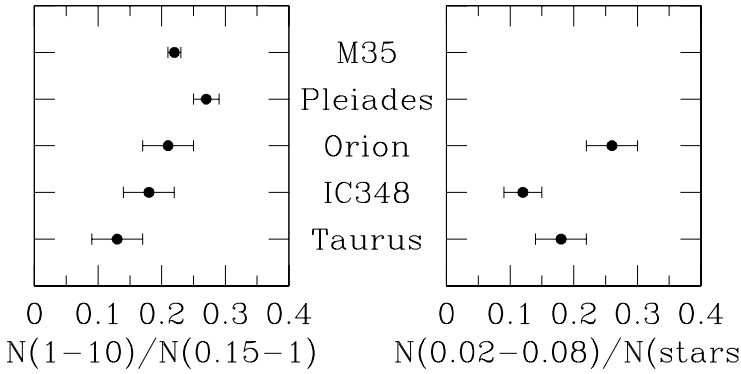

Figure 4. Ratios of the numbers of high-mass and low-mass stars (left) and brown dwarfs and stars (right) for the Taurus, IC 348, and Orion Trapezium star-forming regions and the Pleiades and M35 open clusters.

In Figure 4, I include the ratio of high-mass and low-mass stars for IC 348 (Luhman et al. 2003b), Taurus (Luhman 2004), and the Trapezium (Luhman et al. 2000) and for the open clusters of the Pleiades (Bouvier et al. 1998) and M35 (Barrado y Navascués et al. 2001). Four of these populations exhibit comparable relative numbers of high- and low-mass stars, while Taurus produces fewer high-mass stars.

3. Spatial Distribution of Young Brown Dwarfs: Same as Stars

Reipurth & Clarke (2001), Boss (2001), and Bate et al. (2002) have suggested that brown dwarfs could form as protostellar sources whose accretion is prematurely halted by ejection from multiple systems. The resulting spatial distributions of the ejected brown dwarfs might differ from those of the stellar members. Alternatively, if brown dwarfs and stars form in the same manner, then they should exhibit similar spatial distributions. Kroupa & Bouvier (2003a,b) have investigated these scenarios in detail through dynamical modeling of Taurus-like aggregates of stars and brown dwarfs. In the model in which stars and brown dwarfs form in the same manner, they found that most of the brown dwarfs indeed shared the same spatial distributions as the stars and a high binary fraction, while a small tail of higher velocity ($v > 1$ km s^{-1})

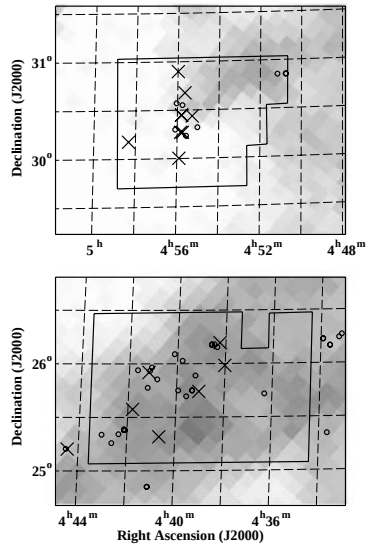

Figure 5. Spatial distribution of the previously known, high-mass members of the Taurus star-forming region (circles) and the new, low-mass members from Luhman (2004) (crosses) shown with emission in ^{12}CO (grayscale, T. Megeath, private communication). The regions surveyed by Luhman (2004) are indicated by the solid boundaries.

brown dwarfs were distributed more widely than the stars and were predominantly single. In comparison, the ejection model also produces widely distributed single brown dwarfs, but they are the dominant population among the brown dwarfs and thus exhibit a shallow density distribution Kroupa & Bouvier (2003a). Based on their interpretation of measurements of the IMF in Taurus, the Trapezium, and the field, Kroupa & Bouvier (2003b) tended to favor the ejection model. However, Briceño et al. (2002) found no statistically significant differences in the distribution of the high- and low-mass members of Taurus. Similarly, I find that the spatial distribution of the newest low-mass members from Luhman (2004) closely matches that of the previously known, more massive young stars, as demonstrated in Figure 5. Thus, the available data are better reproduced by the model in which stars and brown dwarfs have a common formation mechanism (Kroupa & Bouvier 2003a) than the ejection model (Kroupa & Bouvier 2003b). A definitive test of the two models will require measurements of the density distribution of young brown dwarfs on larger size scales. Nevertheless, from the surveys of Taurus to date, there is no evidence for different spatial distributions between stars and brown dwarfs.

4. Summary

In summary, the IMFs of IC348, Orion, and Chamaeleon peak at 0.15 $M_{\odot}$ while the IMF for Taurus peaks at 0.8 $M_{\odot}$. This difference could be a reflection of the different average Jeans masses in Taurus and the other clusters. Meanwhile, the Trapezium has a higher brown dwarf fraction than other star-forming regions, but the difference is smaller than previously reported. This could be a true variation in the IMF, or due to a high rate of disruption of companion brown dwarfs in the Trapezium, as suggested by Kroupa et al. (2003). Finally, stars and brown dwarfs in star-forming regions share similar spatial distributions, which is contrary to the predictions of some models in which brown dwarfs form through ejection (Reipurth & Clarke 2001), but not others (Bate et al. 2003).

References

Baraffe, I., Chabrier, G., Allard, F., & Hauschildt, P. H. 1998, A&A, 337, 403

Bate, M. R., Bonnell, I. A., & Bromm, V. 2002, MNRAS, 332, L65

Bate, M. R., Bonnell, I. A., & Bromm, V. 2003, MNRAS, 339, 577

Boss, A. 2001, ApJ, 551, L167

Briceño, C., Luhman, K. L., Hartmann, L., Stauffer, J. R., & Kirkpatrick, J. D. 2002, ApJ, 580, 317

Hillenbrand, L. A. 1997, AJ, 113, 1733

Hillenbrand, L. A., & Carpenter, J. M. 2000, ApJ, 540, 236

Kroupa, P., & Bouvier, J. 2003a, MNRAS, 346, 343

Kroupa, P., & Bouvier, J. 2003b, MNRAS, 346, 369

Kroupa, P., Bouvier, J., Duchêne, G., & Moraux, E. 2003, MNRAS, 346, 354

Luhman, K. L. 2004, ApJ, in press

Luhman, K. L., et al. 2000, ApJ, 540, 1016

Luhman, K. L., et al. 2003a, ApJ, 590, 348

Luhman, K. L., et al. 2003b, ApJ, 593, 1093

Muench, A. A., Lada, E. A., Lada, C. J., & Alves, J. 2002, ApJ, 573, 366

Muench, A. A., et al. 2003, AJ, 125, 2029

Reipurth, B. & Clarke, C. 2001, AJ, 122, 432

Slesnick, C. L., Hillenbrand, L. A., & Carpenter, J. M. 2004, ApJ, 610, 1045

THE SUBSTELLAR IMF OF THE TAURUS CLOUD

New young brown dwarfs in the Taurus SFR

Jean-Louis Monin[1,2], Sylvain Guieu[1], Catherine Dougados[1], Eduardo L. Martín[3] and Eugene Magnier[4]

[1] *Laboratoire d'Astrophysique de Grenoble, BP 53, France*
[2] *Institut Universitaire de France*
[3] *Instituto de Astrofisica de Canarias, Institute, C/ Via Lactea, s/n E38200 - Tenerife, Espana*
[4] *Canada-France-Hawaii Telescope Corporation, P.O Box 1597, Kamuela, Hawaii, USA*

Abstract

Recent studies have found a deficit of substellar objects in the Taurus cloud (Briceño et al. 1998; Luhman 2000). If confirmed, the higher low-mass cut-off in Taurus could have strong implications on IMF and substellar formation models. However, these previous studies have sampled the highest density regions of the Taurus cloud, and if brown dwarfs are ejected during their formation (Reipurth & Clarke 2001), a significant fraction of the substellar content of the cloud may have been missed. In order to enlarge the Taurus study, we have performed an optical (I,z) large photometric survey using the CFH12K camera on the Canada-France-Hawaii Telescope (CFHT). In this poster, we present new substellar candidates obtained from our (I,z) survey and further FORS1/VLT and LRIS/Keck spectroscopic analysis. We then compare our results with previous studies of Briceño et al. (2002) and Luhman et al. (2003).

1. Candidate selection and observations

Substellar candidates were selected from an optical $3.6\,\mathrm{deg}^2$ survey, conducted between Dec 99 and Jan 01 with the CFHT12K camera at the CFHT (Dougados et al., 2004 in prep.). Optical photometry was combined with 2MASS data (using I/I-K, I/I-z and J-H/H-K color-magnitude and color-color diagrams) to select 45 pre-main sequence candidates having colors compatible with late dwarfs (>M5). Moderate resolution (R $\simeq$ 1000) spectroscopic follow-up was recently performed on selected sources with the VLT FORS1 and the Keck LRIS spectrographs in the visible range ($\approx 6400 - 11000\,$Å).

E. Corbelli et al. (eds.), The Initial Mass Function 50 Years Later, 121–122.

Table 1. New brown dwarfs in Taurus

Name	RA	DEC	SpT	A_V	EW(H_α)
CFHT-BD-Tau 5	04:33	24:22	M7.5	9.3	-29
CFHT-BD-Tau 6	04:39	25:44	M7.25	0.6	-63.7
CFHT-BD-Tau 7	04:32	24:22	M6.5	0.0	-8.6
CFHT-BD-Tau 8	04:41	25:55	M6.5	1.8	-25.2

2. Results and discussion

Out of 45 candidates, we find 1 new Taurus Very Low Mass Stars, with spectral types M5.25, M5.5 and M6. We also find 4 new brown dwarfs (see Table 1). This new result does not significantly change the conclusions on the substellar IMF derived by Briceño et al. (2002). To compare our result with previous studies, we derive the ratio of substellar to stellar objects in our fields: $R_{ss} = N(0.02 \leq M/M_\odot \leq 0.08)/N(0.08 \leq M/M_\odot \leq 10)$. Combining the results from this study and from previous works by Martin et al. (2001), Briceño et al. (2002), Luhman et al. (2003), we derive a ratio: $R_{ss} = 15/106 = 0.15 \pm 0.04$, where only sources with $A_V < 4$ have been included. This reddening-limited sample corresponds to our detection limit of a 0.02 $M_\odot$ objects at an age of 5 Myr. We thus confirm the result from Briceño et al. (2002): the Taurus R_{ss} value is $\approx 2\times$ fewer than the one in Trapezium (0.26 ± 0.04). However we must temper this result, because the total region covered by Briceño et al. (2002) and the present study do not exceed $10.3\,\mathrm{deg}^2$, in an $\approx 100\,\mathrm{deg}^2$ region. Moreover, previously observed fields are mostly placed towards strong stellar density regions. We must now study a larger area in the Taurus cloud to test if BDs have scattered around the high density regions, as predicted by Reipurth & Clarke (2001). To this purpose, we have performed a $25\,\mathrm{deg}^2$ complementary large scale survey in regions surrounding the highest stellar density spots in Taurus. We will present these results in a forthcoming paper (Guieu et al., in prep.).

References

Briceño, C., Hartmann, L., Stauffer, J., Martin, E. 1998, AJ, 115, 2074
Briceño, C. et al. 2002, ApJ, 580, 317
Luhman, K. L. 2000, ApJ, 544, 1044
Luhman, K. L. et al. 2003, ApJ, 590, 348
Martin, E. et al. 2001, ApJ, 561, 195
Reipurth, B. & Clarke, C. 2001, AJ, 122, 432

THE LOW-MASS END OF THE IMF IN CHAMAELEON I

Timo Prusti and Sacha Hony
ESA/ESTEC, Noordwijk, The Netherlands
Timo.Prusti@rssd.esa.int,Sacha.Hony@rssd.esa.int

Abstract We have compared the low mass and brown dwarf samples of Cha I deduced by optical and infrared techniques. We conclude that optical methods tend to lead to an underestimation of the number of brown dwarfs at least by 15 % but possibly by 40 %. Highly complete samples can be constructed by combining optical and mid-infrared samples.

1. Introduction

The flattening of the Salpeter power law of IMF toward lower masses is a well established fact. Due to the flattening the mass locked into low mass stars and brown dwarfs (BDs) is not significant despite the fact that the number counts of these objects are. In the BD mass domain not only the flattening but also the turnover of the IMF can be observed. However, due to the faintness of targets and low number statistics the precise shape of the IMF in the BD mass range is poorly constrained. Simple estimates of number count ratios of stars against BDs vary from 8:1 in Taurus (Luhman et al. 2003) to 3:2 in Chamaeleon I (López Martí et al. 2004). Part of the variation may be due to different observing, selection and analysis methods, but Luhman et al. (2003) claim a true difference between Taurus (8:1) and Orion (4:1) as both regions were studied with the same methodology.

A truly different IMF at the BD mass domain between two different regions is an interesting result as it may give a handle to a better understanding of the physics determining the IMF. The turnover of the IMF is observed with diagnostics at the optical wavelengths. At infrared wavelengths different diagnostics, namely infrared excess, is used and e.g. in the ISO study of the ρ Oph cluster one cannot see any turnover in the BD mass domain (Bontemps et al. 2001). This suggests a stars to BDs number count ratio to be closer to 1:1. As ISO studies were typically conducted in the most embedded clusters and optical studies tend to be performed in less extinguished regions, it is difficult

E. Corbelli et al. (eds.), The Initial Mass Function 50 Years Later, 123–126.

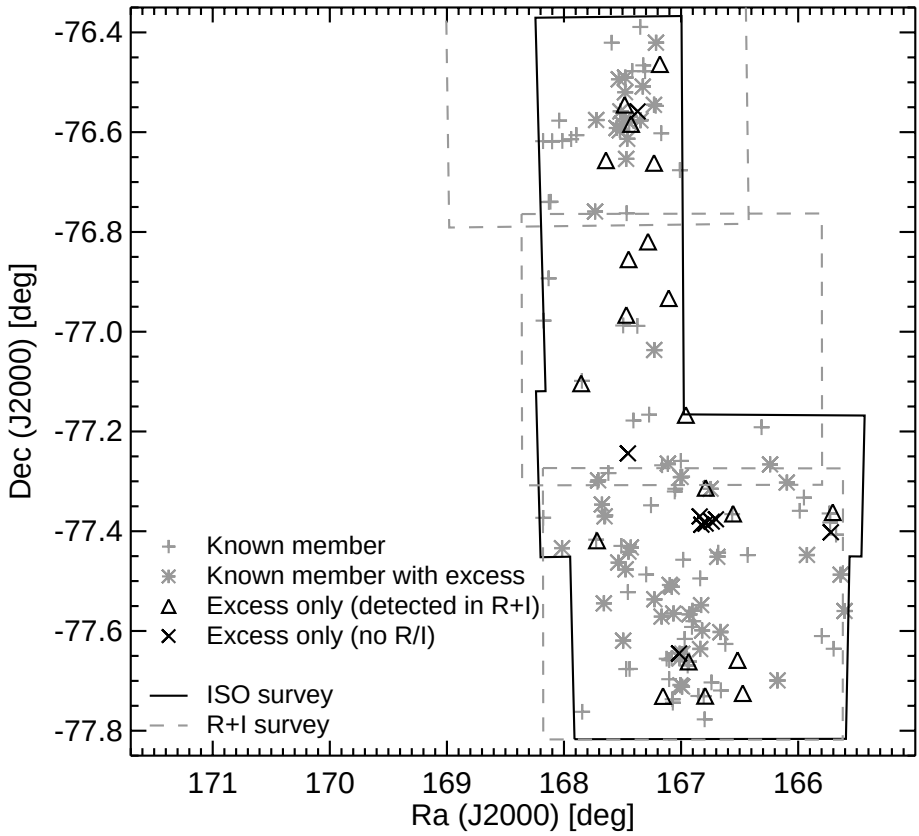

Figure 1. Spatial distribution of examined Chamaeleon I members and candidates.

to assess the significance of the large discrepancy of the deduced IMF between different studies.

Recently, López Martí et al. (2004) published an optical study of the Chamaeleon I star forming region with statistically significant number of BD candidates. Earlier, Persi et al. (2000) had published the ISO deduced sample of low mass member candidates. Between these studies there is a discrepancy of a factor of 1.5 in the relative numbers of stars to BDs. When limiting the sample to the region of Chamaeleon I which was covered both by the optical and the ISO study, we are left with a sufficient number of objects for a statistical assessment of the discrepancy between the two different IMFs (Fig. 1).

2. Results

The primary selection criterion for optically discovered BD candidates is their location in a colour magnitude plot. The confirmed BDs of Chamaeleon I

occupy a well defined region which is separated from the field stars. López Martí et al. (2004) had an additional requirement of Hα emission detection in narrow band filter before accepting an object with BD colour to be accepted as a BD candidate. In the ISO/optical overlap area 41 BD candidates are identified against 60 stars.

In the ISO study of Persi et al. (2000) there are in the overlap region 21 BD candidates against 28 stars. The numbers are lower than in the optical study simply due to the fact that ISO candidates are selected on the basis of mid-infrared excess. This in turn exists only when the object has a disk around it. The pre-main sequence disk lifetime is of the order of few million years and therefore in Chamaeleon I one expects about half of the members to have lost their disks already. Consequently, the lower number of ISO detected members is not surprising while the discrepancy exists in their relative number of stars and BDs. This ratio is 1:1 while the optical sample suggests a ratio of 3:2 as mentioned above.

Except for a few deeply embedded sources concentrated in the Ced 110 region (166.8,-77.35 in Fig. 1) there are hardly any sources without optical detection in the ISO mid-infrared excess selected sample. This suggests that extinction is not influencing the statistics based on the optical sample. The key is to examine the optical properties of the ISO excess sources which are not suffering from high extinction i.e. which can be placed in the optical colour magnitude diagram.

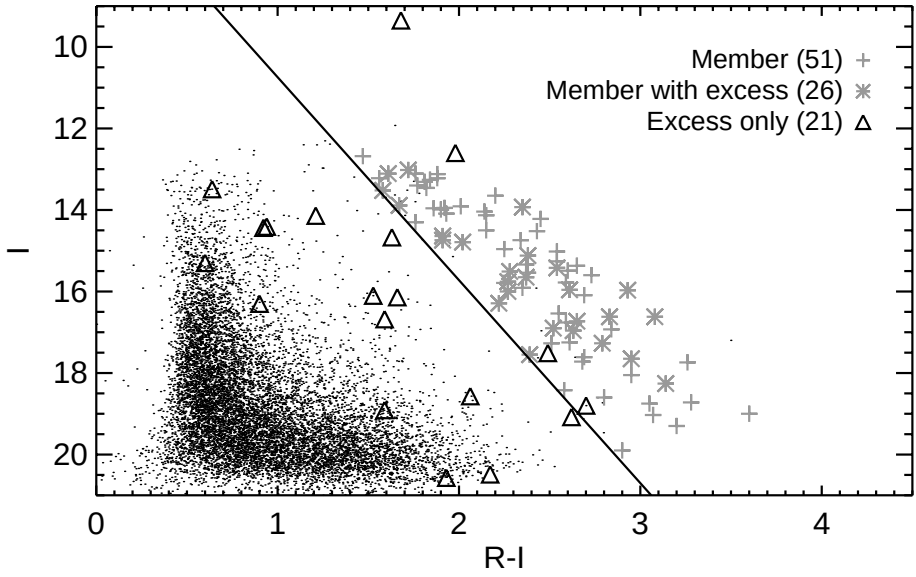

Figure 2. Colour-magnitude diagram of Chamaeleon I member candidates.

The optical sample is selected to the right hand side of the diagonal in the colour magnitude plot (Fig. 2). One can see that the ISO detected member candidates have a much wider distribution in the colour magnitude diagram. There is a population of blue stars and BDs omitted by most optical studies.

The optically and ISO based samples contain 41 and 21 BD candidates respectively. There are 15 objects common to both samples. If we assume the ISO sample being biased only by the disk dispersal and the optical sample being only biased by the colour magnitude criterium, then the total number of BDs is 57 (10 optically blue diskless members missed). This is, however, an upper limit as it is possible that the bluer colours are related to the disk i.e. *only* objects with a(n accretion) disk possess a blue R−I colour. If we assume the blue colours being associated only to disk sources, then the total number of BDs is 47 (the optical and ISO samples combined). In the former case the optical BD counts need to be corrected by 40 % while in the latter case the optical samples need a 15 % correction to the number counts of the BDs.

3. Conclusions

We have shown that in the young star forming region Chamaleon I extinction has a very limited impact on statistical studies of IMF based on optical studies. However, there is a significant population of bluer low mass stars and BDs leading to a need to correct the BD counts from optical studies by 15 upto 40 %. A more precise correction factor can be estimated when the physical reason behind the blue colours of some BDs is understood. This will allow the construction of a highly complete census of low mass members in a star forming region with a combination of optical and mid-infrared data.

References

Bontemps, S., André, P., Kaas, A. A., et al. 2001, A&A, 372, 173
López Martí, B., Eislöffel, J., Scholz, A. & Mundt, R. 2004, A&A, 416, 555
Luhman, K. L., Briceño, C., Stauffer, J. R., et al. 2003, ApJ, 590, 348
Persi, P., Marenzi, A. R., Olofsson, G., et al. 2000, A&A, 219,357

LIMITATIONS OF THE IR-EXCESS METHOD FOR IDENTIFYING YOUNG STARS

Sacha Hony and Timo Prusti
ESA/ESTEC, Keplerlaan 1, NL-2201 AZ Noordwijk, The Netherlands
shony@rssd.esa.int,tprusti@rssd.esa.int

Abstract The (mid-)IR excess due to circumstellar disks has been previously used to identify new member candidates of young stellar clusters. We apply the same method to a deep ISOCAM survey of TMC-2. The luminosities of the detected sources match those expected for the lowest mass brown dwarfs and planetary mass objects. However, comparison with number-counts of background sources from the ELAIS survey shows that the detections in the TMC-2 field are consistent with them having an extragalactic nature. The number of extragalactic sources rises steeply with decreasing IR flux. Moreover, these background sources span a wide range in both near- and mid-IR colours. These effects combined hamper the identification of faint members with disks based on IR photometry.

1. Introduction

Nearby ($<$200 pc) young ($<5\,10^6$ yr) star-forming regions are excellent laboratories for studying the initial mass function (IMF). For these young regions dynamical effects are expected to be unimportant and therefore *all* the stars that initially formed are believed to be still present in the close vicinity of their birth place. One crucial steps in determining the IMF of a young cluster is establishing its members. Observational membership criteria are often heavily biased to the brightest objects and hampered by extinction. Mid-IR surveys have been successful in overcoming some of these biases. The method relies on detecting the IR excess due to the disk around the young stellar object (YSO). The main advantages of the method are: *i*) insensitivity to extinction, *ii*) less biased to massive objects and *iii*) efficiency because it relies solely on photometry.

2. TMC-2

The Taurus molecular cloud (TMC) is of special interest because surveys indicate a deficit of brown dwarfs (BDs) compared to other regions (Briceño et al. 2002 and references therein). We have obtained 6.75 and 15 μm im-

E. Corbelli et al. (eds.), The Initial Mass Function 50 Years Later, 127–130.

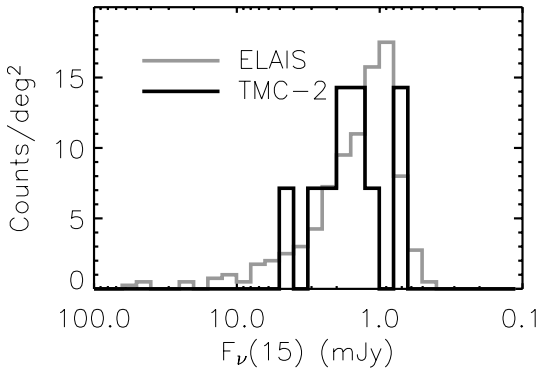

Figure 1 Source counts in TMC-2 and the ELAIS field. Both are scaled to one square degree. The counts are consistent with **all** detections in TMC-2 being of extragalactic nature.

ages of TMC-2. We have identified 40 point sources in a region of $\sim$0.25 square degree at 15 μm. 22 sources match with 2MASS and optical detections, 4 have a 2MASS counterpart, 4 are detected only at 6.75 μm and 10 lack a shorter-wavelength counterpart. Perusal of the colours shows that 20 sources are consistent with stellar photospheric emission, while 10 exhibit a clear IR excess. The spectral energy distributions (SEDs) of the excess sources are like those expected from a disk excess. Comparison with model SEDs of BDs with a disk (Natta & Testi 2001) would place them at the low-mass end (5-10 M_{jup}) of the BD domain.

The new TMC excess sources are all very faint with a 15 μm flux of $\sim$1 mJy which makes background contamination a real concern. Therefore, we have compared our data with the data of the ELAIS 15 μm survey (Lari et al. 2001). The ELAIS survey is extremely valuable, because it is obtained using the same instrument reaching a very similar depth in a field devoid of star formation. We show the number of sources per flux bin at 15 μm as found in the ELAIS survey in Fig. 1. The number rises steeply towards lower flux-levels and it is clear from the figure that (most of) the TMC-2 detections are due to the extragalactic background.

3. Separating BDs from the background

The extent to which the background dominates the counts is exemplified by Fig. 1; the field contains only 2 known young members while the number of background sources in the low-mass BD domain is $\sim$10. We investigated whether it is possible to distinguish between YSOs and galaxies based on currently available data. In Fig. 2 we show the near-IR colours of the ELAIS and TMC-2 samples. The brightest galaxies show some clustering, but the fainter galaxies exhibit a wide spread in colours. The diagram demonstrates how difficult it is to determine the nature of a source in this brightness range on the basis of near or mid-IR photometry.

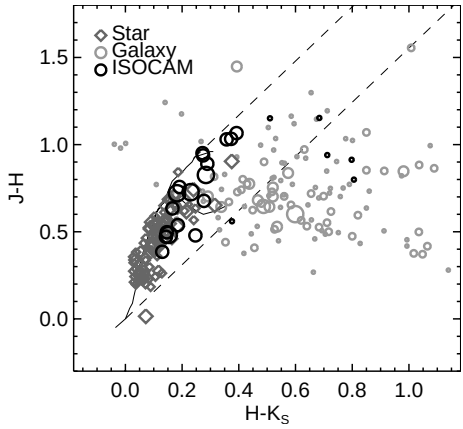

Figure 2 Near-IR colours of the sources detected in ELAIS and TMC-2. The symbol size is proportional to the K_S magnitude. The black drawn lines represent the main sequence and the giant branch. The dashed lines give the direction of interstellar reddening. The galaxies exhibit a large range of colours which overlaps the TMC-2 excess sources (small black circles).

4. Conclusions

i) We have performed a mid-IR photometric survey of a part of TMC-2. We find 10 mid-IR excess sources with a 15 μm flux of $\sim$1 mJy, which is compatible with the number of expected background sources.
ii) The number of extragalactic sources rises steeply in the flux range expected for low-mass BD.
iii) The mid-IR selected galaxies exhibit a large spread in colours, which renders it impossible to identify the young stellar objects.
iv) This limits the application of the IR-excess method to those regions (dense) and the brightness range where the number of members clearly exceeds the number of background objects.
v) For the nearest star-forming regions, one quickly reaches the background-confusion limit with the sensitivity and mapping efficiency provided by *Spitzer*.

References

Briceño, C., Luhman, K. L., Hartmann, L. et al. 2002 ApJ, 580, 317
Lari, C., Pozzi, F., Gruppioni, C. et al. 2001, MNRAS, 325, 1173
Natta, A. & Testi, L. 2001, A&A, 376, L22

Figure 3. Timo Prusti and Morten Andersen pondering over a bottle of Chianti above the Val D'Orcia valley.

THE IMF OF CLASS II OBJECTS IN THE ACTIVE SERPENS CLOUD CORE

A.A. Kaas[1], P. Persi[2], G. Olofsson[3], S. Bontemps[4], P. André[5], T. Prusti[6], A.J. Delgado[7] and F. Motte[5]

[1]*Nordic Optical Telescope, Santa Cruz de La Palma, Spain,*
[2] *Instituto Astrofisica Spaziale e Fisica Cosmica, CNR, Rome, Italy*
[3]*Stockholm Observatory, Stockholm, Sweden*
[4]*Observatoire de Bordeaux, Floirac, France*
[5]*Service d'Astrophysique, CEA Saclay, Gif-sur-Yvette, France*
[6]*Research and Scientific Support Department of ESA, Noordwijk, the Netherlands*
[7]*Instituto de Astrofísica de Andalucia, Granada, Spain*

akaas@not.iac.es, persi@rm.iasf.cnr.it, olofsson@astro.su.se, bontemps@obs.u-bordeaux1.fr, pandre@cea.fr, tprusti@rssd.esa.int, delgado@iaa.es, motte@cea.fr

Abstract Based on ISOCAM mid-IR photometry and Arnica/NOT near-IR photometry we find two separate generations of Young Stellar Objects (YSOs) in the Serpens Cloud Core. The youngest generation consists of several sub-clusters (0.12 pc diameter) of Class I and flat-spectrum sources, probably formed in a microburst of star formation within the last 10^5 yrs. The population of Class II sources, which are spatially more distributed, has a luminosity function (LF) for which an age of 2 Myr is the best fit to models.

The Serpens Cloud Core is an active star formation region of mainly low mass stars (Eiroa & Casali, 1992) located at b^{II}= 5 deg, l^{II}= 32 deg, and a distance of 260 pc. It is known for its rich collection of Class 0 sources (Casali et al. 1993). Based on LW2 (6.7 μm) and LW3 (14.3 μm) photometry obtained with ISOCAM and J (1.25 μm), H (1.65 μm), and K (2.2 μm) photometry with the ARcetri Near-Ir CAmera (ARNICA) at the 2.56 m Nordic Optical Telescope, La Palma, we have doubled the sample of IR-excess YSOs in the Serpens Cloud Core and classified them as Class I sources, flat-spectrum sources, or Class II sources based on the spectral energy distribution from near- to mid-IR.

We find a strong tendency of clustering of the Class I and flat-spectrum sources towards the NW-SE oriented ridge of dense cores traced by the mm data. These protostar candidates are most likely found close to their birth place. Each sub-cluster is typically 0.12 pc in diameter and contains between 6 and

E. Corbelli et al. (eds.), The Initial Mass Function 50 Years Later, 131–132.

12 protostar candidates. All must have formed from the same core at about the same time, and it is highly unlikely that these sources are older than a few 10^5 yrs. The surface density in these sub-clusters is in the range 500-1100 pc^{-2}, and the *local* star formation efficiency is found to be $\sim$ 9 % by hypothesizing that the protostar candidates follow the same IMF as the Class II sources (see Kaas et al. 2004). These results could put important constraints on models of cloud fragmentation and core formation inside gas clumps.

The Class II sources cluster at a scale of about 0.25 pc, but have also a relatively scattered distribution. For the Class IIs we have estimated the stellar luminosities and searched for the best fit of synthetic luminosity functions (LFs) based on three different input IMFs and various star formation (SF) histories (see Kaas et al. 2004). Taking into account the relatively coarse LF and the fact that we can not put too much confidence on the observed peak at 0.09 $L_\odot$ since it is practically at the completeness limit, we can conclude that ages less than 2 Myr are implausible both in the case of coeval and continuous SF histories. Both the Scalo (1998) and the Kroupa, Tout & Gilmore (1993) IMFs are compatible with our data down to the completeness limit for the age of 2 Myr, as is the Salpeter (1955) IMF at the high luminosity end.

The observed Class II LF fits a roughly co-eval star formation scenario about 2 Myr ago with an underlying IMF of the three-segment power-law type, which is similar to the Class II mass function for ρ Ophiuchi (Bontemps et al. 2001). For this age 20 % of the Class II objects in our study should be young brown dwarfs, although spectroscopic confirmation remains. This means only about 3 % of the mass. It seems likely that the compact clusters of Class I and flat-spectrum sources will evolve into the looser clusters of 0.25 pc found for the Class II objects over a few 10^6 yrs. It is highly plausible that the current Class II population formed in a similar fashion about 2 Myr ago. These results support the suggestion of Casali et al. (1993) that the star formation history in Serpens has proceeded in several phases.

References

Bontemps, S., Andre, P., Kaas, A.A., et al. 2001, A&A 372, 173

Casali, M.M., Eiroa, C., Duncan, W.D., 1993, A&A 275, 195

Eiroa, C., Casali, M.M., 1992, A&A 262, 468

Kaas, A.A., Olofsson, G., Bontemps, S., et al. 2004, A&A 421, 623

Kroupa, P., Tout, C., Gilmore, G.F., 1993, MNRAS 262, 545

Salpeter, E. E. 1955, ApJ, 121, 161

Scalo, J., 1998, In: The Stellar Initial Mass Function, eds. Gilmore, G., Howell, D., Astronomical Society of the Pacific, vol 142, p. 201

λ ORIONIS: A 0.02–50 $M_\odot$ IMF

D. Barrado y Navascués[1], J.R. Stauffer[2] and J. Bouvier[3]
[1]*LAEFF-INTA (ESA tracking Station), Madrid, Spain*
[2]*IPAC, Caltech, USA,*
[3]*Observatoire de Grenoble, France*
barrado@laeff.esa.es, stauffer@ipac.caltech.edu, Jerome.Bouvier@obs.ujf-grenoble.fr

Abstract We derive the initial mass function for the Collinder 69 cluster (5 Myr), covering several orders of magnitude in mass (50 – 0.02 $M_\odot$).

1. The λ Orionis Star Forming Region

One of the most amazing areas in the northern, winter sky is Orion and its myriads of star forming regions (SFR). One of the most prominent, albeit not very well studied, is the SFR dominated by the O8 III star λ^1 Ori, the λ Orionis SFR (LOSFR). Among other structures, it includes a CO and a dust ring whose diameter is about nine deg, the S264 HII region, a large number of IRAS sources, the Barnard 30 and 35 dark clouds and a cluster associated with the central star, the λ Ori cluster (Collinder 69). As a laboratory for the star formation process (or processes), the LOSFR represents a unique environment due to its diversity, its proximity (400 pc), its age range ($\sim$5 Myr) and low extinction in the internal area of the ring (A_V=0.37). Prior to our study, several groups have published studies focused on different aspects of the SFR, such as the initial discovery by Wade (1957), the photometric properties of the high mass members by Murdin & Penston (1977; hereafter M&P77), a Hα survey by Duerr, Imhoff & Lada (1982), the analysis of the IRAS data (Zhang et al. 1989) and the photometric and spectroscopic search by Dolan & Mathieu (1999, 2001, 2002; hereafter D&M). This last set of studies reached I_C=14.5, about 0.5 $M_\odot$. Our aim is to carry out a comprehensive study in the LOSFR, reaching well below the hydrogen burning limit (HBL, the substellar border line at $\sim$0.072 $M_\odot$, as derived by the Lyon models, Baraffe et al. 1998). Here, we present some initial results mainly concerning the central area of this fascinating SFR.

E. Corbelli et al. (eds.), The Initial Mass Function 50 Years Later, 133–136.

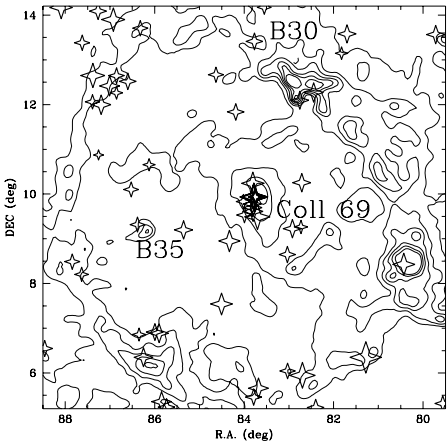

Figure 1. An IRAS image at 100 μ, showing the LOSFR.

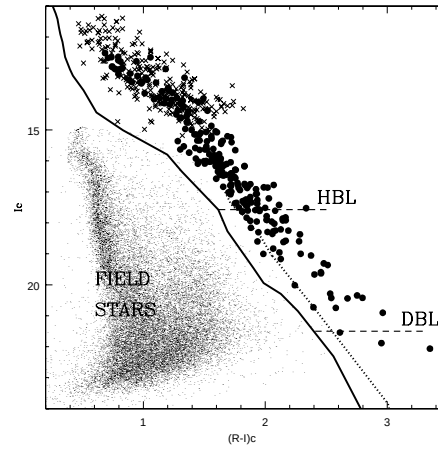

Figure 2. A deep color-magnitude diagram in the core of the LOSFR.

2. The λ Orionis cluster, Collinder 69

The star cluster associated with the star λ Orionis is clearly identified in Figure 1 by the overdensity of B stars (four point stars). In order to identify low mass members of this association, we have conducted several photometric and spectroscopic campaigns, both in the optical and the near infrared. Details regarding the first of them, an optical search –Figure 2– with the CFHT and the 12K mosaic, supplemented with 2MASS JHK data and spectroscopy from Keck and Magellan, can be found in Barrado y Navascués et al. (2004, Paper I). Note that for a 5 Myr age, and based on NextGen and Cond (Chabrier et al. 2000) models, the hydrogen and deuterium burning limits are located at I_C=17.6 and I_C=22, i.e., we have sampled the complete brown dwarf domain.

Based on this wealth of data, we have found 170 candidate members in the range I_C=12.5–22.0, which translates to 1.2–0.01 $M_\odot$ for bona fide members. Of these 170, 33 have been spectroscopically observed at low-resolution (I_C=15.2–20.7, M4.5–M8.5 spectral types), whereas another 25 have medium resolution spectra (I_C=13.7–17.6, M4–M6.0). The analysis of the optical-IR information –see color-magnitude and color-color diagrams in Paper I– indicates that the contamination rate should be about 30%. A similar value is derived from the spectroscopy.

We have also studied other properties of the low mass stellar and substellar population of the λ Orionis cluster –Coll 69– and compare those properties with previous results from the LOSFR and other young associations. In particular, we have measured the strength of the lithium doublet at 6708 Å (see Palla

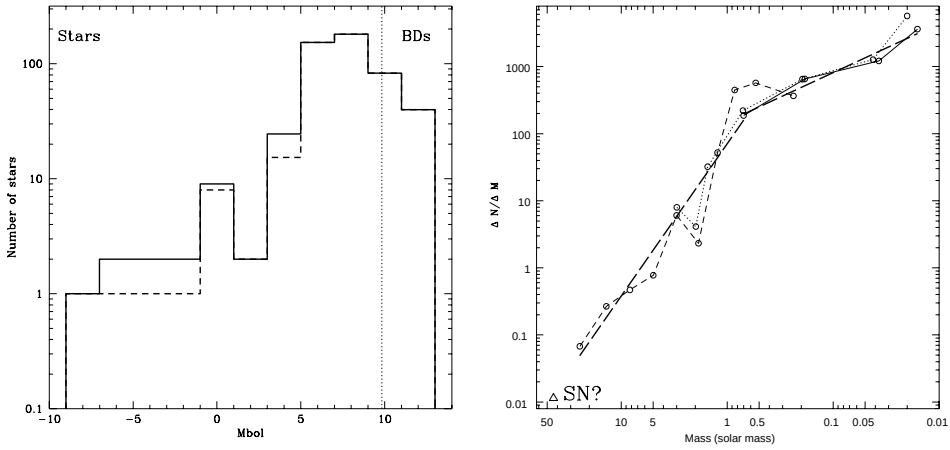

Figure 3. The Coll 69 Luminosity and Mass Functions.

& Randich, this volume) and Hα, another signpost of youth and accretion. Our targets show lithium in their medium-resolution spectra, clearly indicating that they are PMS objects. On the other hand, by comparison with the criterion for Hα defined in Barrado y Navascués & Martín (2003), we find that Coll 69 has a paucity of CTT stars compared with the clusters associated with the dark clouds Barnard 30 and 35 (as already noted by D&M). This might be related to the obvious richness of hot, high mass stars in the first association, compared with the other two, as is easily appreciated in Figure 1. D&M suggested a scenario to explain these differences, with the episodes of star formation in B30 and B35 (and eventually in the ring in the LOSFR) triggered by a supernova in Coll 69. This catastrophic event is speculated to have removed most of the disk material around the young stars in Coll 69. If this scenario is true, Coll 69 should be older than the other two clusters, and have a different history of star formation - possibly leading to a different IMF.

2.1 The IMF of the λ Orionis cluster

We have derived a Luminosity and Initial Mass Functions (LF and IMF) for the bona fide members of Coll 69. We emphasize that our IMF characterize only the central part of the cluster. For more massive stars, we used data from D&M and M&P77, scaling the areas in the appropriate way. Regarding the LF (Figure 3a), the solid and dashed lines were computed including all possible members (solid line) and removing the photometric binaries (possible members, dashed line), respectively.

The IMF is displayed in Figure 3b. In order to extend the IMF to the high mass domain, we have included data from M&P97. We have faced three important problems: the in-homogeneity of the photometric data (we have derived bolometric magnitudes from V and Ic), the paucity of massive stars –i.e., the validity of the LF in that range– and the selection of a theoretical model. We have used models by Girardi et al. (2002), D'Antona & Mazzitelli (1997) and Baraffe et al. (1998), for massive, intermediate- and low-mass objects (dashed, dotted and solid lines), respectively. The dip at about 2 $M_{\odot}$ is due to incompleteness in the sample. The last point (open triangle) at the massive end corresponds to the possible SN. Note that the binning in the LF is arbitrary, although the results do not change much by selecting other values. The slopes of the IMF (bold, dashed segments) are α=2.27$\pm$0.08, and α=0.73$\pm$0.05, for the mass ranges 25–0.70 and 0.70-0.02 $M_{\odot}$, respectively. The figure indicates that the SN hypothesis is compatible with the IMF of the cluster. To the best of our knowledge, this IMF is one of the most complete and accurate –due to the reduced internal reddening of the cluster– IMF published in the literature, covering more than three orders of magnitude in mass.

Acknowledgments DByN is indebted to the Spanish "Programa Ramón y Cajal", PNAyA AYA2001-1124-C02 and PNAyA AYA2003-05355.

References

Baraffe I., Chabrier G., Allard F., Hauschildt P. H., 1998, A&A, 337, 403
Barrado y Navascués D., et al. 2004, ApJ 610, 1064
Barrado y Navascués D., Martín E.L., 2003, AJ 126, 2997
Chabrier G., Baraffe I., Allard F., Hauschildt P., 2000, ApJ, 542, L119
D'Antona, F., & Mazzitelli, I., 1997, Mem.S.A.It. 68, 807
Dolan C.J & Mathieu R.D., 1999, AJ 118, 2409
Dolan C.J & Mathieu R.D., 2001, AJ 121, 2124
Dolan C.J & Mathieu R.D., 2002, AJ 123, 387
Duerr R., Imhoff C.L., Lada C.J., 1982, ApJ 261, 135
Girardi L., et al. 2002, A&A 391, 195
Murdin P., & Penston M.V., 1997, MNRAS 181, 657
Wade C.M., 1957, AJ 62, 148
Zhang C.Y., et al. 1989, A&A 218, 231

DOES THE "STELLAR" IMF EXTEND TO PLANETARY MASSES?

Eduardo L. Martín
Instituto de Astrofísica de Canarias, 38200 La Laguna, Tenerife, Spain
ege@iac.es

Abstract Despite the claims made by Burgasser et al. (2004) that SOri70, the coolest candidate member known in any open cluster, is a foreground brown dwarf, I argue that this object still remains a strong candidate for being a genuine cluster planet. SOri70 has different spectral energy distribution and different colors than field T dwarfs of similar spectral type (T5-T7). In a J-H versus H-K diagram, SOri70 lies in the region where models of ultracool dwarfs predict that low gravity objects should be located. The existence of planetary-mass member candidates down to about 3 Jupiter masses (detection limit of current surveys) in the Sigma Orionis open cluster suggests that the formation of giant planets may not be very different from that of stars.

1. Introduction

An indication of our poor understanding of the formation and properties of brown dwarfs (BD) and planets is the lack of consensus in the community about the best terminology (Boss et al. 2003). Some argue that the boundary between BDs and planets could be placed at the deuterium burning limit (13 Jupiter masses for solar composition). Some prefer a planet upper mass limit at around 10 Jupiter masses, where there appears to be a sharp rise in the number of extrasolar planets detected by high-precision radial velocity surveys around main-sequence stars. Finally, it has also been proposed to use a limit at 5 Jupiter masses where the mass-radius relationship of substellar objects changes its sign. In this paper we continue to use the deuterium limit as the mass boundary between brown dwarfs and planets because we do not have any strong reason to change the nomenclature adopted in our previous papers.

Since 1997, two new ultracool spectral classes have been adopted to extend the classical OBAFGKM system into cooler temperatures. The L dwarfs are characterized by weak or absent TiO bands, and very broad NaI and KI lines in the optical spectrum (Kirkpatrick et al. 1999, 2000; Martín et al. 1997, 1999). The T dwarfs are characterized by methane bands in the near-infrared spectra

E. Corbelli et al. (eds.), The Initial Mass Function 50 Years Later, 137–140.

(Burgasser et al. 2002; Geballe et al. 2002; Oppenheimer et al. 1995). Current estimates of the temperatures of ultracool dwarfs range from 2500 K to 1400 K for L dwarfs, and from 1400 K to 700 K for T dwarfs (Vrba et al. 2004).

Most of the known ultracool dwarfs have been identified in the general field by the wide area surveys 2MASS and SDSS. These objects consist of a mixed population of brown dwarfs and free-floating planets formed in different star-formation events during the lifetime of the Milky Way. Their individual ages, chemical compositions and masses are not known. It is difficult to derive their initial mass function. Our best chance to study a population of ultracool dwarfs of known age, chemical composition, and uniform distance is to find them in open clusters where the stellar populations are well characterized.

2. The IMF of the Sigma Orionis open cluster

The Sigma Orionis open cluster has been a region where our group has concentrated many efforts to reveal the substellar population (see Zapatero Osorio et al. 2003 for a recent review). It offers several advantages: (1) It is young (3-8 Myr) and thus the substellar objects are relatively bright and hot, but not so young that the theoretical models cannot be reliably used to obtain masses (Baraffe et al. 2001). (2) It has very little extinction, probably because the parental cloud has been blown away by the O-type star at the center of the cluster. (3) It is relatively nearby (distance 350 pc). (4) It is moderately rich and dense. Béjar et al. (2004, in preparation) estimate a central density of 0.2 members per square arcminute. All these advantages of the Sigma Orionis cluster have allowed us to extend the IMF, originally proposed by Ed Salpeter (1955), from stellar to planetary masses (Zapatero Osorio et al. 2000, 2003; Béjar et al. 2001; Barrado y Navascués et al. 2003).

So far the coolest and faintest candidate member that we have found in the Sigma Orionis cluster is the T dwarf candidate SOri70. It was found in a pencil-beam deep mini-survey of only 55 square arcminutes with a sensitivity of 21 magnitude in the J and H-bands carried out with the 4.2-meter William Herschel Telescope in the Observatorio del Roque de los Muchachos. Follow-up near-infrared photometry and low-resolution spectroscopy were obtained with NIRC at the 10-meter Keck I telescope. We found that SOri70 displays methane bands in the near-infrared spectrum and we classified it as T6.5. Martín & Zapatero Osorio (2003) obtained a mid-resolution J-band spectrum with NIRSPEC and obtained a best fit using synthetic spectra from Allard et al. (2001) with a surface gravity of log g=3.5, which is consistent with an age of 3 Myr and a mass of 3 Jupiters, as expected for a cluster member of such a low luminosity. However, Burgasser et al. (2004) challenged this interpretation using our own data. They claimed that both the NIRC and NIRSPEC spectra of SOri70 are indistinguishable from spectra of field T dwarfs obtained with

the same instruments. Furthermore, Burgasser et al. showed that the spectral synthesis analysis may produce unrealistic results for some field T dwarfs of known age. However, all the field T dwarfs for which they obtained unrealistically low gravities have spectral subtypes cooler than SOri70.

Knapp et al. (2004) proposed that the spread of H-K colors observed among the known T dwarfs in the solar neighborhood could largely be due to differences in surface gravities arising from a heterogeneous mix of ages and masses. Particularly, red H-K colors are strong indicators of low surface gravity due to decreased H_2 opacity (collisionally induced) in the K-band. Martín (2005) has noted that the H-K color of SOri70 is redder than those of all known field T dwarfs. In fact SOri70 occupies a unique place in the J-H versus H-K color-color diagram, separated from the other T dwarfs. The status of SOri70 remains undecided, we will obtain further imaging and spectroscopic data in the future to measure, or put an upper limit, on its proper motion and to decrease the errors bars in the photometry and the spectroscopy.

SOri70 is just the most extreme example of a population of planetary-mass objects in the Sigma Orionis cluster, which also appears to be present in the Trapezium (Lucas et al. 2001). These objects may have formed by gravitational collapse of very low-mass cores, suggesting that the "stellar" IMF may continue into planetary masses. Theoretical modeling indicates that rapid planet formation may take place by gravitational instabilities in discs (Boss 2004; Rice et al. 2004). An analogous process could also happen in filamentary molecular clouds. Planets around stars may form in a "stellar" way, i.e. the binary formation mechanisms may also apply to planetary systems. This could provide a natural explanation for the similarities in the eccentricity distributions of binary stars and giant planets (Santos et al. 2003, 2004). The higher frequency of giant planets among metal-rich stars could be interpreted as a dependence with the environment. Metal-rich stars likely form in regions with a very high rate of star formation. It will be interesting to study the IMF of brown dwarfs and planets in metal-rich star forming regions in our own Milky Way. Such regions may be more prolific in forming not only stars, but also substellar-mass objects.

References

Allard, F., Hauschildt, P. H., Alexander, D. R., Tamanai, A., Schweitzer, A. 2001, ApJ, 556, 357
Barrado y Navascués, D. et al. 2003, AA, 404, 171
Béjar, V. J. S. et al. 2001, ApJ, 556, 830
Boss, A. P. et al. 2003, in IAUS 211: Brown Dwarfs, p. 529
Boss, A. P. 2004, ApJ, 610, 456
Burgasser, A. J. et al. 2000, ApJ, 531, L57
Burgasser, A. J. et al. 2004, ApJ, 604, 827
Kirkpatrick, J. D. et al. 1999, ApJ, 519, 802
Kirkpatrick, J. D. et al. 2000, AJ, 120, 447

Knapp, G. R. et al. 2004, AJ, 127, 3553
Lucas, P. W., Roche, P. F., Allard, F., Hauschildt, P. H. 2001, MNRAS, 326, 695
Martín, E. L., Basri, G., Delfosse, X., Forveille, T. 1997, AA, 327, L29
Martín, E. L. et al. 1999, AJ, 118, 2466
Martín, E. L. & Zapatero Osorio, M. R. 2003, 593, L113
Martín, E. L. 2005, in "The Young Local Universe", in press
Geballe, T. R. et al. 2002, ApJ, 564, 466
Oppenheimer, B. R. 1995, Science, 270, 1478
Rice, W. K. M., Lodato, G., Pringle, J. E., Armitage, P. J., Bonnell, I. A.. 2004, MNRAS, in press
Salpeter, E. E. 1955, ApJ, 123, 666
Santos, N. C., Israelian, G., Mayor, M., Rebolo, R., Udry, S. 2003, AA, 398, 363
Santos, N. C., Israelian, G., Mayor, M. 2004, AA, 415, 1153
Saumon, D. et al. 1996, ApJ, 460, 993
Vrba, F. J. et al. 2004, AJ, 127, 2948
Zapatero Osorio, M. R. et al. 2000, Science, 290, 103
Zapatero Osorio, M. R. et al. 2002, ApJ, 578, 536
Zapatero Osorio, M. R. et al. 2003, in IAUS 211: Brown Dwarfs, p. 111

ESTIMATING THE LOW-MASS IMF IN OB ASSOCIATIONS: σ ORIONIS

Ben Burningham[1], T. Naylor[1], S.P. Littlefair[1] and R.D. Jeffries[2]
[1]*School of Physics, University of Exeter, Stocker Road, Exeter, EX4 4QL, UK*
[2]*Dept. of Physics, Keele University, Keele, Staffordshire, ST5 5BG, UK*
bgb@astro.ex.ac.uk

Abstract We investigate the issues of contamination and exclusion in photometric membership selection techniques when applied to OB associations. We use radial velocities to calculate membership probabilities for a sample of very low-mass candidate members of the σ Orionis young group. We find that significant numbers of bona members are not excluded by photometric selection techniques, and for I brighter than 17 there is not significant contamination in the expected PMS region.

1. Introduction

The high and variable extinction found along sight-lines toward the youngest clusters gives rise to large uncertainties in deriving masses and ages for low-mass members. Whilst this can be avoided by looking at low extinction regions, reliably assessing membership without the background blocking effect of a molecular cloud can bring its own issues. Here we investigate the use of radial velocity, measured from high resolution spectra of the 8183, 8195 Å Na I doublet, as a membership discriminator in the σ Ori young group. We have selected candidates from a broad region of colour-magnitude space (see figure 1), to investigate if an appreciable number of bona fide members would be neglected as part of a tight photometric selection on a RI colour-magnitude diagram (CMD).

2. Radial Velocities and Membership

Sufficient signal-to-noise was attained to detect NaI with an EW = 3Å at a significance of 2σ for all 54 objects in our sample. We chose this EW as our guide as most brown dwarfs detected by Martin et al. (2004) in the Upper Scorpius OB association displayed an EW(NaI) above this value. We detected

E. Corbelli et al. (eds.), The Initial Mass Function 50 Years Later, 141–142.

NaI above this significance threshold in the spectra of 38 of our targets. We have calculated upper limits for EW(NaI) for most of the failed detections. We find that find that these, and the values for EW(NaI) measured for the good detections are consistent with low-mass members of σ Ori displaying weaker EW(NaI) than were measured by Martin et al. (2004) for Upper Scorpius. It is not clear why this should be so, and this is discussed further in Burningham et al. (2004). We cross correlated the spectra with detected NaI against that of a velocity standard to obtain radial velocities. These velocities were then used to calculate probabilities of objects being radial velocity members of the σ Ori young group, P_{vel}. This process is described in detail in Burningham et al. (2004). We have plotted the positions of likely members and non-members on an RI CMD (see Figure 1) in order to assess the issues of contamination and exclusion.

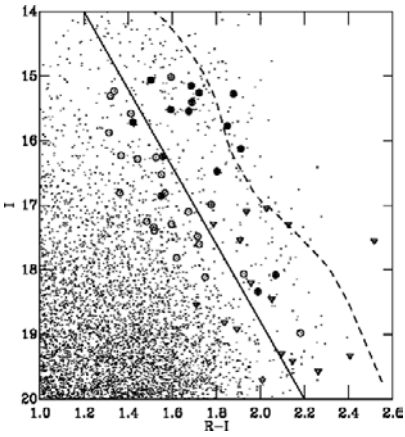

Figure 1. The CMD of 4 WFC fields centered on σ Ori (catalogue taken from Kenyon 2004). Objects with detected NaI are open circles. Objects with $P_{vel} >$ 80% are circles filled with asterisks, whilst circles filled with crosses are objects with $P_{vel} >$60%. Objects for with no detected NaI are open triangles. The dotted line is a NextGen 5 Myr isochrone (Chabrier & Baraffe 1997, Baraffe et al. 2002). Our expected PMS region is defined as redward of the solid line.

3. Conclusions

Inspection of Figure 1 allows us to draw the following conclusions. 1) Photometric selection techniques do not miss significant numbers of bona fide association members. 2) At I brighter than 17 the expected PMS region of the CMD does not contain a significant number of contaminants.

References

Baraffe et al. 2002, A&A, 382, 563
Burningham et al. 2004, MNRAS submitted.
Chabrier, G. & Baraffe, I. 1997, A&A, 327, 1039
Kenyon et al. 2004, in preparation.
Martín et al. 2004, AJ, 127, 449

YOUNG BROWN DWARFS IN ORION

Fiona Riddick[1], Patrick Roche[1] and Phil Lucas[2]
[1]*Astrophysics, University of Oxford, DWB, Keble Road, OX1 3RH, UK*
[2]*Centre for Astrophysics Research, School of Physics, Astronomy & Maths, University of Hertfordshire, College Lane, Hatfield, AL10 9AB, UK*
fcr@astro.ox.ac.uk, pfr@astro.ox.ac.uk, pwl@star.herts.ac.uk

Abstract We have obtained optical spectra of 60 low-mass stars and brown dwarfs in Orion's Trapezium cluster. Spectral types have been determined using a combination of narrowband indices derived from the spectra.

1. Observations

Multi-object optical spectroscopy in the red region was carried out using TAURUS on the AAT and GMOS on Gemini-N on objects selected from the near-IR photometry of Lucas & Roche (2000). A field to the southwest of the bright core was chosen as the nebulosity is fainter here, although the object density is still high.

2. Spectral Features

A subset of the spectra is shown from 6800-9500Åin Fig. 1. The spectra have been dereddened, normalised to 7500Åand a constant added to separate them vertically. They show the expected signatures of mid to late M dwarfs with strong TiO near 7000, 7600, 8400 and 8800Åand also VO near 7400Å. The uppermost spectrum shows the CaII triplet at around 8500Å; this is clear evidence of circumstellar line emission. The highly spatially-structured nebular background was not able to be removed from the spectra completely and appears as a series of lines in either emission or absorption, depending on the local gradient, e.g. the [SIII] line at 9069Å.

3. Spectral Typing Using Narrowband Indices

For M dwarfs, spectral indices may be defined which rely on the variation of the slope of the spectra with spectral type. Those which increase monoton-

E. Corbelli et al. (eds.), The Initial Mass Function 50 Years Later, 143–144.

ically with spectral type can be used for typing purposes, using a relationship calibrated by the indices of standard stars at each spectral type.

For initial spectral typing we have used a combination of 3 of these colour indices from Martin et al. (1996) and 4 from Kirkpatrick et al. (1999). The indices were calibrated using M-dwarf standards from Delfosse et al. (1997), Gizis et al (2000a, 2000b), Kirkpatrick et al. (1999, 2000) and Reid et al. (2000).

The spectral types obtained from the indices will be compared with types obtained from a comparison of the spectra with model spectra and with other young sources. Final spectral types will then be converted to effective temperatures in order to place the objects on the HR diagram.

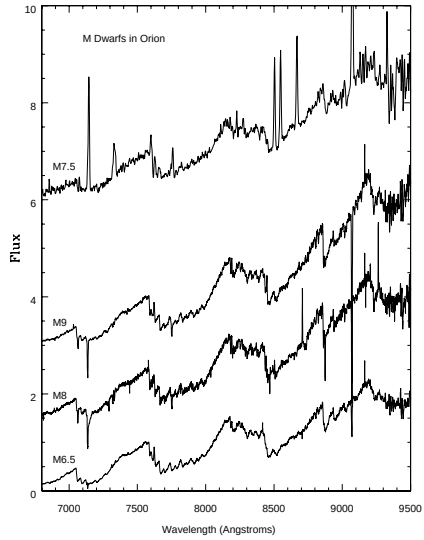

Figure 1. Optical Spectra of M Dwarfs in Orion

References

Delfosse, X. et al. 1997, A&A, 327, L25
Gizis, J.E. et al. 2000a, AJ, 120, 1085
Gizis, J.E. et al. 2000b, MNRAS 311, 385
Kirkpatrick, J.D. et al. 1999, ApJ, 519, 802
Kirkpatrick, J.D. et al. 2000, AJ, 120, 447
Lucas, P. & Roche, P. 2000, MNRAS, 314, 858
Martin, E. et al. 1996, ApJ, 469, 706
Reid, I.N. et al. 2000, AJ, 119, 369

THE FORMATION OF FREE-FLOATING BROWN DWARVES & PLANETARY-MASS OBJECTS BY PHOTO-EROSION OF PRESTELLAR CORES

Anthony Whitworth[1] and Hans Zinnecker[2]
[1]*School of Physics & Astronomy, Cardiff University, Wales, UK*
[2]*Astrophysikalisches Institut, Potsdam, Germany*
ant@astro.cf.ac.uk,hzinnecker@aip.de

Abstract We explore the possibility that, in the vicinity of an OB star, a prestellar core which would otherwise have formed an intermediate or low-mass star may instead form a free-floating brown dwarf or planetary-mass object, because the outer layers of the core are eroded by the ionizing radiation from the OB star before they can accrete onto the protostar at the centre of the core. We find that the mechanism is robust, in the sense that it operates under a wide range of conditions, but it is also inefficient, in the sense that a rather massive core is required to produce a single brown dwarf.

We model a core as a truncated singular isothermal sphere, and we presume that it is initially static. If the isothermal sound speed in the neutral gas of the core is $a_{\rm I}$, and the ambient density is $n_{\rm O}$, the core mass is

$$M_{\rm C} \simeq \left[\frac{2\,a_{\rm I}^6}{\pi\,G^3\,n_{\rm O}\,m}\right]^{1/2} .$$

Now suppose that an OB star (or association of OB stars) forms nearby, and emits hydrogen-ionizing photons at the rate $\dot{\mathcal{N}}_{\rm LyC}$. The core is immediately engulfed by an HII region.

The sudden increase in external pressure drives a compression wave into the core. At the same time the ionization front at the core boundary starts to photo-erode the core. The final mass of the protostar which forms at the centre of the core is determined by a competition between accretion and photo-erosion. The evolution divides into three phases:

Phase I. The compression wave propagates in towards the centre of the core (outside-in), and this sets up a subsonic inward velocity field. Phase I ends when the compression wave hits the centre.

E. Corbelli et al. (eds.), The Initial Mass Function 50 Years Later, 145–146.

Phase II. When the compression wave hits the centre, a protostar forms, and subsequently grows by accretion (at an approximately constant rate $\sim a_{\rm I}^3/G$). At the same time an expansion wave is reflected and propagates outwards, setting up an approximately freefall inward velocity field. Meanwhile, the ionization front has been eating into the core from the start of Phase I. Phase II ends when the inward propagating ionization front meets the outward propagating expansion wave.

Phase III. The ionization front continues to propagate inwards, but now it encounters material which is infalling quite rapidly. Phase III ends when the material flowing through the ionization front cannot escape the gravity of the protostar.

By making several simplifying assumptions and approximations, we can show that the final protostellar mass is given by

$$M_* \simeq 0.01 M_\odot \, \left(\frac{a_{\rm I}}{0.3\,{\rm km\,s^{-1}}} \right)^6 \left(\frac{\dot{\mathcal{N}}_{\rm LyC}}{10^{50}\,{\rm s^{-1}}} \right)^{-1/3} \left(\frac{n_{\rm O}}{10^3\,{\rm cm^{-3}}} \right)^{-1/3}, \quad (1)$$

where $a_{\rm I}$ is the isothermal sound speed in the neutral gas of the core, $\dot{\mathcal{N}}_{\rm LyC}$ is the rate of emission of Lyman continuum photons from the OB star (or stars), and $n_{\rm O}$ is the number-density of protons in the HII region surrounding the core. Eqn. (1) shows that photo-erosion can form brown dwarves (notionally $0.012 M_\odot \lesssim M_* \lesssim 0.078 M_\odot$) and planetary-mass objects ($M_* \lesssim 0.012 M_\odot$) under a wide variety of conditions.

However, we can also relate M_* to the initial core mass $M_{\rm C}$ and the radius of the HII region $R_{\rm HII}$:

$$\frac{M_*}{M_{\rm C}} \simeq 10^{-4} \left(\frac{M_{\rm C}}{M_\odot} \right) \left(\frac{R_{\rm HII}}{\rm pc} \right)^{-1}. \quad (2)$$

This shows that the process is very inefficient, in the sense that only a small fraction of the initial core mass survives. We conclude that brown dwarves and planetary-mass objects can form by photo-erosion of pre-existing cores, but the mechanism only works in the immediate vicinity of OB stars. Details of these calculations are given in Whitworth & Zinnecker (2004, A&A, 427, 299).

IMF IN SMALL YOUNG EMBEDDED STAR CLUSTERS

Fabrizio Massi[1], Leonardo Testi[1] and Leonardo Vanzi[2]
[1]*INAF-Osservatorio Astrofisico di Arcetri, Largo E. Fermi 5, I–50125 Firenze, Italy*
[2]*ESO, Alonso de Cordova, 3107 Santiago, Chile*
fmassi@arcetri.astro.it,lt@arcetri.astro.it,lvanzi@eso.org

Abstract Using near-infrared photometry, we have constrained the IMFs of 6 young embedded star clusters in the cloud D of the Vela Molecular Ridge. We show that they are consistent with that of field stars.

We selected a sample of 6 clusters, all associated with a CO(1–0) emission peak in the cloud D of the Vela Molecular Ridge. Massi et al. (2000) found them to be compact (~ 0.1 pc) structures with < 100 members whose most massive objects are intermediate-mass (proto)stars (M $\sim$2–10 $M_{\odot}$). Most of them are embedded in molecular gas, suggesting an age < 3 Myrs (Lada & Lada 2003). The estimated distance is 700 pc.

The observations were carried out through the $JHK_{\rm s}$ near-Infrared bands using SOFI at the NTT (ESO, La Silla, Chile). The completeness limit is $K_{\rm s} \sim$ 17–18, i. e., more than 1.5 mag deeper than Massi et al. (2000). This allows us to probe pms stars of 10^6 yrs old down to 0.1 $M_{\odot}$ at $A_V \sim 30$ mag. More details on the photometry can be found in Testi et al. (2001).

Our aim was to constrain the clusters' IMFs based on their K Luminosity Functions (KLFs). Hence, for each field we constructed both a cluster KLF, by using the photometry of sources within a radius of 2 arcmin from the cluster centre, and a reference KLF, by using all the photometry outside such radius. Noting that the clusters are likely to be younger than 3 Myrs and that the isochrones of pms stars in a $K_{\rm s}$ vs. $H - K_{\rm s}$ diagram all lie in a strip only few tenths of a magnitude in colour, we constructed dereddened KLFs by projecting each point in the $K_{\rm s}$ vs. $H - K_{\rm s}$ diagram back along the reddening vector onto a mean locus (see Fig. 1). Once normalized each outer KLF to the area of the corresponding inner one, it was subtracted from the latter to obtain a KLF free from field star contamination. We performed several tests to check that the dereddened KLFs (see Fig. 2) are good representations of the real ones, in spite of the presence of near-infrared excess emission.

E. Corbelli et al. (eds.), The Initial Mass Function 50 Years Later, 147–148.

If the clusters are coeval, the KLFs can be analitically converted into IMFs once the mass-luminosity relation is known. We recovered the mass-luminosity relation by fits to the evolutionary tracks of Palla & Stahler (1999) for ages of 1, 3 and 6 Myrs. In all cases, the obtained IMFs appear consistent with that of field stars (e.g. Scalo 1998) at least in the range 3–0.1 $M_{\odot}$.

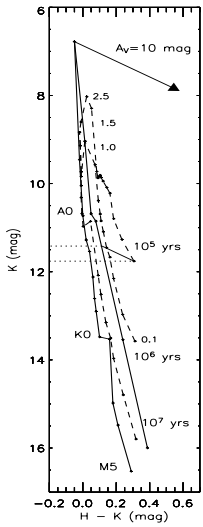

Figure 1. Mean locus in the $K_{\rm s}$ vs $H - K_{\rm s}$ diagram for the dereddening of the KLFs (thick line). Also drawn are pms isochrones from Palla & Stahler (1999; dashed lines) and the ZAMS (solid line).

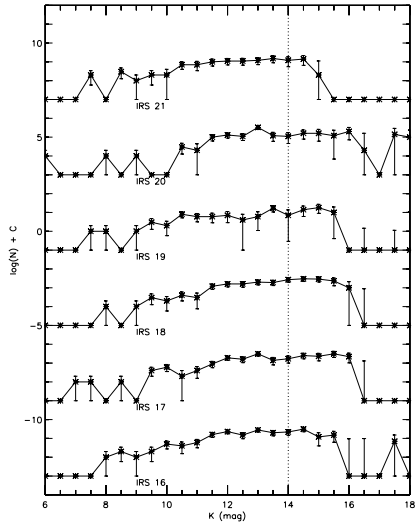

Figure 2. Dereddened KLFs for the 6 clusters. The vertical dashed line marks the estimated "dereddened" completeness limit.

References

Lada, C. J. & Lada, E. A. 2003, ARA&A, 41, 57

Massi, F., Lorenzetti, D., Giannini, T., & Vitali, F. 2000, A&A, 353, 598

Palla, F. & Stahler, S. W. 1999, ApJ, 525, 772

Scalo, J. 1958, in The Stellar Initial Mass Function, ed. G. Gilmore, & D. Howell (ASP Conf. Series Vol. 142), p. 201

Testi, L., Vanzi, L., & Massi, F. 2001, ESO Mess., 103, 28

THE ARCHES CLUSTER - A CASE FOR IMF VARIATIONS?

Andrea Stolte
Department of Astronomy, University of Florida, Gainesville, USA
stolte@astro.ufl.edu

Abstract In my thesis, I analysed the two Milky Way starburst clusters Arches and NGC 3603 with respect to their present-day mass functions (MFs), and local as well as global spatial variations in the MF slope. I present the results of the comparison of the Arches MF, indicative of the dense Galactic Center (GC) environment, and of NGC 3603, a more moderate star-forming environment in the Carina spiral arm.

1. Introduction

The Arches and NGC 3603 starburst clusters were observed using high-spatial resolution NIR imaging (Fig. 1). The aim was to resolve the clusters in such detail that local variations in the MF would become apparent. If the dense Galactic Center environment is capable of shapeing the MF in starburst clusters differently than a more moderate environment characteristic for present-day

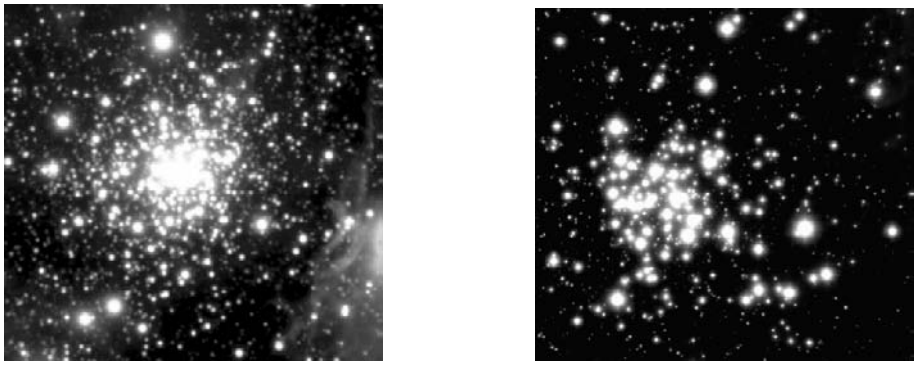

Figure 1. High-angular resolution images of the starburst clusters NGC 3603 in JHK with ISAAC (left) and Arches in HK with NAOS-CONICA (right).

E. Corbelli et al. (eds.), The Initial Mass Function 50 Years Later, 149–152.

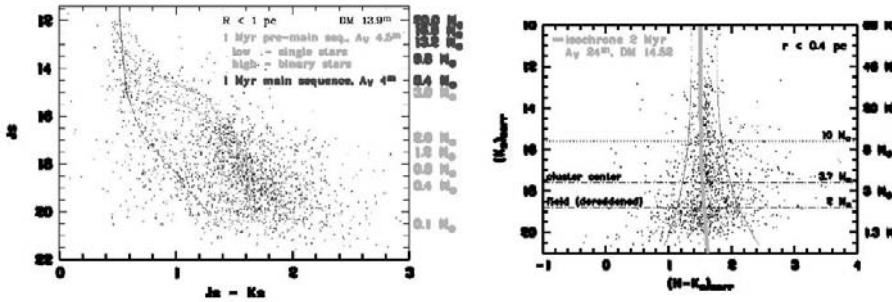

Figure 2. NGC 3603 (left) and Arches (right) colour-magnitude diagrams.

star formation in the Milky Way, this has severe consequences for our understanding of star and cluster formation in extragalactic systems, and in particular in the early Universe.

2. Starburst Cluster Mass Functions

The MFs were created from the colour-magnitude diagrams (Fig. 2) using Geneva main sequence models to transform magnitudes into stellar masses (Lejeune & Schaerer 2001). In the case of the Arches cluster, a systematic radial increase in visual extinction was corrected, and a red and blue colour cut was applied to reject background and foreground stars to avoid field contamination. This provides a conservative estimate for the flattened Arches MF, as the field star contribution increases with decreasing luminosity and mass. In NGC 3603, stars were individually dereddened, and the field star contamination was subtracted statistically. The hydrogen burning turn-on in NGC 3603 occurs at $4\,M_{\odot}$, and for lower masses a Palla & Stahler (1999) 1 Myr pre-main sequence isochrone was employed. A secondary sequence observed at the high-mass end in NGC 3603 was modelled as equal-mass binaries, and a comparable statistical binary contribution of 30% equal-mass systems was assumed to be hidden in the low-mass PMS population.

The core of both clusters shows a heavy bias to high-mass stars (see Fig. 1), while the outer cluster regions appear closer to a standard Salpeter (1955) IMF. The integrated MFs for Arches and NGC 3603 are shown in Fig. 3. These MFs are radially limited to 1 pc in NGC 3603 and 0.4 pc in Arches both due to increasing field contamination, which is more severe in the GC environment. The present-day MF in NGC 3603 displays a slightly flattened, remarkably continuous power-law from the highest to the lowest masses (note that saturation limits us to $M < 20\,M_{\odot}$) with a slope of $\Gamma = -0.9 \pm 0.1$ for $0.4 < M < 20\,M_{\odot}$, in-

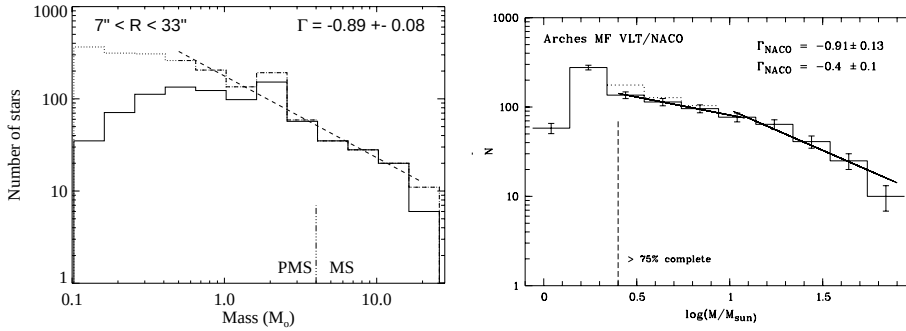

Figure 3. Present-day mass functions of NGC 3603 (left) and Arches (right).

fluenced by the high-mass core causing the integrated slope to flatten. Beyond the core radius, the slope steepens to $\Gamma = -1.1 \pm 0.1$. A similar behaviour is seen in Arches, where the MF increases from -0.6 to -1.0 to -1.3 in subsequent annuli for $10 < M < 65\,M_\odot$. However, below $10\,M_\odot$ a distinct gap occurs in the Arches CMD, indicating a turn-over between 6 and $10\,M_\odot$. This turn-over manifests itself in a change in MF slope in the integrated MF around $\log m \sim 1$. While the integrated slope at the high-mass end agrees remarkably well with NGC 3603, both with $\Gamma = -0.9 \pm 0.1$ despite the different analysis methods emploid to derive the MF, the intermediate-mass MF in Arches flattens to $\Gamma = -0.4$.

3. The Arches cluster - a case for (I)MF variations?

While the turn-over in the Arches MF is very suggestive of an altered mass function, and Frank Shu has shown arguments during the meeting that suggest a turn-over mass around $10\,M_\odot$ in the Galactic Center, we cannot say with certainty today that the Arches *initial* MF was different as well. Tidal disruption of GC clusters occurs incredibly fast, on time scales of only a few Myr (Kim et al. 2000), and may have stripped off low- and intermediate mass cluster members already at an age as young as 2 Myr. Even if dynamical evolution is responsible for the weird MF, we expect a similar behaviour in the nuclei and tidal interaction regions of other galaxies. Such a behaviour was invoked indirectly for starburst clusters in M82 (Smith & Gallagher 2001), but the Arches cluster provides the first direct evidence for a truncated MF.

Both in the case of primordial as well as dynamical segregation, we expect stellar population synthesis, the derivation of star-formation histories, and integrated cluster properties from observed light profiles to be affected by a depleted or truncated low-mass MF. In particular, a top-heavy IMF would alter the history (or future) deduced with respect to metal enrichment and remnant

stellar populations in starburst environments. Dynamical simulations have to reveal whether a truncated MF due to the depletion in low- and intermediate-mass stars can be caused purely by dynamical segregation. A varying *initial* MF would clearly challenge our picture that the outcome of the star-forming process is similar for a wide range of environmental conditions, and thus of a universal, Salpeter-like IMF.

Acknowledgments A deep thanks to Francesco and Hans, but more than to everyone to Edvige, who has done a wonderful (and exhausting!) job in creating such an exciting meeting. Very special thanks to Ed Salpeter for providing me and so many others with a wealth of stimulating research topics lasting for half a century without loosing their excitement - I am grateful for this opportunity to meet the person behind the scenes!

References

Kim, S. S., Figer, D. F., Lee, H. M., Morris, M. 2000, ApJ, 545, 301

Lejeune, T., Schaerer, D. 2001, A&A, 366, 538

Palla, F., Stahler, F. W. 1999, ApJ, 525, 772

Salpeter, E. E. 1955, ApJ, 121, 161

Smith, L. J, Gallagher, J. S. III 2001, MNRAS, 326, 1027

Stolte, A. 2003, PhD *"Mass functions and mass segregation in young starburst clusters"*, Ruperto-Carola University of Heidelberg, Germany

Figure 4. Wolfgang Brandner, Andrea Stolte, Dimitris Gouliermis and Yuri Beletski.

THE IMF AND MASS SEGREGATION IN YOUNG GALACTIC STARBURST CLUSTERS

Eva K. Grebel
Astronomical Institute of the University of Basel, CH-4102 Binningen, Switzerland
grebel @ astro.unibas.ch

Abstract The pronounced mass segregation in very young rich Galactic starburst clusters like NGC 3603 and Arches may be due to their extremely short relaxation times and high densities, which appear to lead to rapid dissolution. To what extent mass segregation in these systems is primordial as opposed to evolutionary cannot easily be distinguished. While flat in their centers, the total mass functions of these rich clusters seem close to a Salpeter slope, supporting a universal IMF.

1. Introduction

Star formation usually does not occur in isolation, but in clusters and associations. Star clusters may contain a few thousand to a million stars. Measurements of the initial mass function (IMF) are best carried out in young, rich clusters in order to minimize effects of statistical fluctuations. Ideally one would like to observe clusters that are sufficiently young to still contain the full range of stellar masses and that are as little as possible affected by dynamical evolution. These clusters may allow us to test the universality of the IMF in little evolved systems, to constrain age spreads, to measure the impact of massive stars on low-mass stars still in formation, to identify radial variations in the IMF, and to distinguish between primordial and evolutionary mass segregation.

One would preferably like to derive the mass function of a cluster on a star-by-star basis. The highest accuracy can be achieved when the distances to individual stars are known, their membership in the cluster has been established (e.g., via velocities or proper motions), and the stars' physical parameters such as luminosity, effective temperature, surface gravity, and metallicity are derived via photometry and spectroscopy down to the lowest stellar masses. Obviously, such comprehensive studies would be limited to the closest clusters

E. Corbelli et al. (eds.), The Initial Mass Function 50 Years Later, 153–158.

since at larger distances crowding and the faintness of low-mass stars prevent such measurements.

However, we do not have young, massive starburst clusters in our vicinity. While the Milky Way hosts a large number of young open clusters, rich young massive clusters are rare. Super star clusters that could be progenitors of future globular clusters are lacking. The young massive clusters in the Milky Way have masses of a few 10^4 $M_\odot$ and ages of a few Myr. Three are located near the Galactic center: Arches, Quintuplet, and the Galactic Center Cluster. The NGC 3603 cluster is the only presently known cluster of this class that lies well away from the Galactic center in the Carina spiral arm. Because it is evolving without experiencing the strong tidal fields near the Milky Way's center, and is observable also in the optical (in contrast to the clusters around the Galactic center), this relatively isolated cluster may be one of the best objects to study the IMF with present-day instrumentation. These studies mainly rely on on photometry with high angular resolution and massive-star spectroscopy as the clusters are at distances of $\sim 7 - 8$ kpc.

2. The young massive NGC 3603 cluster

Many studies have targeted the NGC 3603 cluster (e.g., Melnick, Tapia, & Terlevich 1989; Moffat, Drissen, & Shara 1994; Sagar, Munari, & de Boer 2001; Sung & Bessell 2004; Stolte et al. 2004). Its lower-mass stars have not yet reached the main sequence (e.g., Eisenhauer et al. 1998; Brandl et al. 1999). Spectroscopic studies revealed the presence of three Wolf-Rayet (W-R) and up to 50 O stars, including six O3 stars (Drissen et al. 1995 and references therein). The W-R stars are main-sequence stars with pronounced Balmer absorption features (Conti et al. 1995), supporting a cluster age of ~ 1 Myr. We obtained high-resolution imaging of NGC 3603 with the Hubble Space Telescope (HST) in the programs GO 6763 (PI: Drissen) and GO 7373 (PI: Grebel). The resulting color-magnitude diagrams (CMDs) show a fairly well-defined pre-main-sequence to main-sequence transition indicative of very little age spread (see Grebel & Gallagher 2004, their Figure 1). The CMDs are consistent with an age of ~ 1 Myr (Grebel et al. 2004). This young age should yield an IMF that is little altered by evolutionary effects.

The HST images show a wind-blown cavity around the NGC 3603 cluster, which is powered by its massive stars. Their winds and radiation pressure are eroding the giant molecular cloud in which the cluster is embedded, leaving giant pillars of denser material that evaporate more slowly. Within the cavity a few proplyd-shaped objects have been found whose cometary evaporation tails point away from the massive stars (Brandner et al. 2000). At the foot of one of the pillars, deeply embedded within the molecular cloud, a small star cluster is forming (IRS 9), and Bok globules mark potential sites of future star formation

(Grebel, Brandner, & Chu 1999). The detection of evolved stars in the giant molecular cloud (e.g., Brandner et al. 1997a, 1997b) lends further support to the scenario of multi-generation star formation.

Figure 1 shows the mass function of the NGC 3603 cluster measured using the approach of Grebel & Chu (2000) by converting completeness-corrected star counts into masses via isochrones. No corrections were made for binaries, rotation, etc. (e.g., Grebel, Roberts, & Brander 1996). The slope of the mass function becomes steeper with increasing distance to the cluster center. The high-mass bins are populated only in the innermost annulus around the cluster center. In spite of its young age, the NGC 3603 cluster thus shows significant effects of mass segregation.

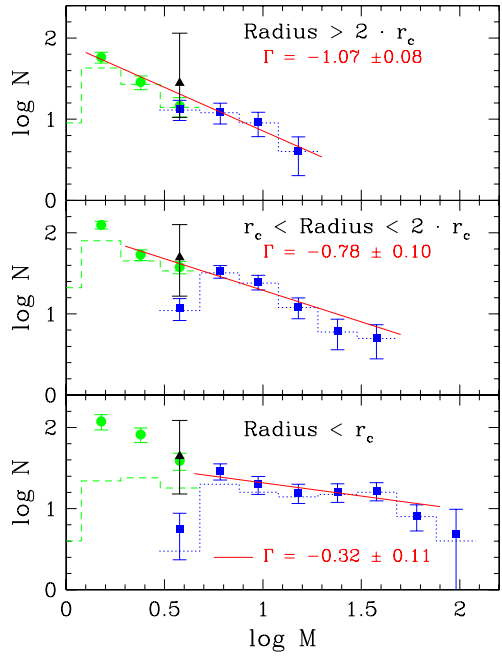

Figure 1. Mass function of the NGC 3603 cluster as a function of core radius r_c. Squares denote main-sequence stars and circles pre-main-sequence stars, both corrected for incompleteness. The triangle combines the completeness-corrected pre-main-sequence and main-sequence star counts. The dashed histogram lines show the mass function prior to completeness corrections. The solid line represents an error-weighted fit yielding the slope of the mass function, Γ ($\Gamma = -1.35$ is the canonical Salpeter 1955 slope). Γ becomes increasingly flatter toward the cluster center. Massive stars are absent at larger distances from the center. Masses were derived without making corrections for the possible contribution from binaries. Figure taken from Grebel et al. (2004); see also Grebel & Gallagher (2004).

This present-day mass function (PDMF) is not necessarily identical to the original IMF. Somewhat unexpectedly, a simple back-of-the-envelope calculation shows that dynamical evolution may already have played a role in NGC 3603: the resulting relaxation time is only ~ 2 Myr, an extremely short time of the same order of magnitude as its young age. This is because NGC 3603 is a very compact, dense cluster with a core radius of 0.25 pc and a half-light radius of 0.22 pc, leading to a crossing time of only ~ 0.02 Myr and an evaporation time of ~ 240 Myr. NGC 3603 appears to destroy itself by two-body encounters and loss of stars. Preliminary N-body simulations by P. Kroupa indicate that primordial and evolutionary mass segregation cannot easily be distinguished.

The PDMF slope approaches a Salpeter slope in the outer regions of NGC 3603. Nürnberger & Petr-Gotzens' (2002) ground-based K-band study suggests a very extended low-mass stellar content for the cluster out to 5 pc, which may support the above dissolution scenario.

3. Other young clusters

Due to high dust obscuration the clusters near the Milky Way center are best studied in the infrared. HST and ground-based adaptive optics data of the Arches cluster indicate a flat PDMF (slope ~ -0.8) and mass segregation (Figer et al. 1999; Stolte et al. 2002, 2003). As does NGC 3603, Arches has a high central density ($\sim 3 \cdot 10^5$ $M_\odot$) and a short relaxation time. — Less massive, less dense clusters like the Orion Nebula Cluster (ONC) also show mass segregation. Considering the youth of the ONC (< 1 Myr) and its long relaxation time this may indicate primordial mass segregation (Hillenbrand & Hartmann 1998).

The PDMFs of Magellanic and Galactic OB associations down to ~ 5 $M_\odot$ show good agreement with a Salpeter slope (Massey et al. 1995a,b). Compact young massive clusters like R136 and sparse clusters like its neighbor Hodge 301 in 30 Doradus agree with the Salpeter value as well (Hunter et al. 1997; Grebel & Chu 2000). Mass segregation was found in young populous Magellanic Cloud clusters (e.g., de Grijs et al. 2002), but these clusters are at least 10 times older and less dense than the massive Galactic starburst clusters. Considering the comparatively long time scales for two-body relaxation in these clusters, purely dynamical mass segregation appears unlikely, and primordial mass segregation has been proposed. While core radii tend to increase with age, the relative similarity of the PDMFs supports a universal IMF (de Grijs et al. 2002).

Sanner & Geffert (2001) measured the PDMFs of Galactic open clusters with proper motion membership. Within ~ 5 to ~ 1 $M_\odot$ slopes ranging from $-0.7 > \Gamma > -2.3$ were found. This wide range of PDMF slopes may either

be due to true IMF variations or due to the small number of member stars and the small mass range covered.

Massey et al. (1995b) found steep slopes with Γ between ~ -3.4 and ~ -4.1 for massive field stars in the Magellanic Clouds and in the Milky Way. Considering the difficulties in interpreting mixed populations and the problems of small-number statistics in the poorly populated high-mass region, it is unclear whether this is evidence for true IMF variations. Even in rich, compact clusters like NGC 3603 the PDMF slope appears rather steep when only very massive stars are considered: Eisenhauer et al. (1998) found $\Gamma = -1.7$ for stars with masses > 15 $M_\odot$.

4. Summary

Very few young, rich starburst clusters exist in the Milky Way. These should in principle permit us to study the IMF of unevolved systems in great detail. One of these clusters, NGC 3603, has an age of ~ 1 Myr and contains an essentially coeval stellar population. It shows pronounced mass segregation with an increasingly flattened mass function slope as the distance to the cluster center increases. The unusually high density of NGC 3603 leads to frequent stellar encounters and a crossing time of only a few ten thousand years. Hence the relaxation time is extremely short (similar to the present cluster age). Contrary to the assumption that very young clusters are probably also dynamically unevolved, NGC 3603 has very likely already undergone considerable dynamical segregation, which makes it difficult to distinguish between the magnitude of primordial versus dynamical mass segregation. NGC 3603 may have started with a normal IMF and an "unbiased" mass distribution, and its PDMF may be the consequence of rapid relaxation processes. A similar scenario seems to apply to the compact massive Arches cluster near the Galactic center. Hence the flat PDMFs should not be taken as evidence *per se* against a universal IMF. Attempts to derive "total" mass functions for the clusters reveal steeper slopes closer to the Salpeter value.

The survival times for the few very dense young Galactic clusters appear to be extremely short, which may explain why there are no older populous clusters in the Milky Way. This behavior is not observed in the less dense Magellanic Clouds populous clusters, which have much longer internal dynamical time scales, which survive over much longer time scales, and which show indications of primordial mass segregation with overall "normal" IMF slopes.

Acknowledgments Various people are involved in the work presented here, including my former graduate students D. Harbeck and A. Stolte and other colleagues (W. Brandner, Y.-H. Chu, L. Drissen, D.F. Figer, J.S. Gallagher, P. Kroupa, A.F.J. Moffat, & M. Odenkirchen).

References

Brandl, B., Brandner, W., Eisenhauer, F., Moffat, A.F.J., Palla, F., & Zinnecker, H. 1999, A&A, 352, L69

Brandner, W., Chu, Y.-H., Eisenhauer, F., Grebel, E.K., & Points, S.D. 1997a, ApJ, 489, L153

Brandner, W., Grebel, E. K., Chu, Y.-H., & Weis, K. 1997b, ApJ, 475, L45

Brandner, W., et al. 2000, AJ, 119, 292

Conti, P. S., Hansen, M. M., Morris, P. W., Willis, A. J., & Fossey, S. J. 1995, ApJ, 445, 35

de Grijs, R., Gilmore, G. F., Mackey, A. D., Wilkinson, M. I., Beaulieu, S. F., Johnson, R. A., & Santiago, B. X. 2002, MNRAS, 337, 597

Drissen, L., Moffat, A. F. J., Walborn, N. R., & Shara, M. M. 1995, AJ, 110. 2235

Eisenhauer, F., Quirrenbach, A., Zinnecker, H., & Genzel, R. 1998, ApJ, 498, 278

Figer, D.F., Kim, S.S., Morris, M., Serabyn, E., Rich, R.M., & McLean, I.S. 1999, ApJ, 525, 750

Grebel, E. K., Brandner, W., & Chu, Y.-H. 1999, BAAS, 31, 931

Grebel, E.K., & Chu, Y.-H. 2000, AJ, 119, 787

Grebel, E. K., Roberts, W. J., & Brandner, W. 1996, A&A, 311, 470

Grebel, E.K., & Gallagher, J.S. 2004, in The Formation and Evolution of Massive Young Star Clusters, ASP Conf. Ser. 322, eds. H.J.G.L.M. Lamers, A. Nota, & L. Smith (San Francisco: ASP), 101

Grebel, E.K., et al. 2004, in preparation

Hillenbrand, L. A. & Hartmann, L. W. 1998, ApJ, 492, 540

Hunter, D.A., Vacca, W.D., Massey, P., Lynds, R., & O'Neil, E.J. 1997, AJ, 113, 1691

Massey, P., Johnson, K.E., & Degioia-Eastwood, K. 1995, ApJ, 454, 151

Massey, P., Lang, C.C., Degioia-Eastwood, K., & Garmany, C.D. 1995b, ApJ, 438, 188

Melnick, J., Tapia, M., & Terlevich, R. 1989, A&A, 213, 89

Moffat, A. F. J., Drissen, L., & Shara, M. M. 1994, ApJ, 436, 183

Nürnberger, D.E.A., & Petr-Gotzens, M.G. 2002, A&A, 382, 537

Sagar, R., Munari, U., & de Boer, K. S. 2001, MNRAS, 327, 23

Salpeter, E. E. 1955, ApJ, 121, 161

Sanner, J. & Geffert, M. 2001, A&A, 370, 87

Stolte, A., Grebel, E.K., Brandner, W., & Figer, D. 2002, A&A, 394, 459

Stolte, A., Brandner, W., Grebel, E. K., Figer, D. F., Eisenhauer, F., Lenzen, R., & Harayama, Y. 2003, The Messenger, 111, 9

Stolte, A., Brandner, W., Brandl, B., Zinnecker, H., & Grebel, E.K. 2004, AJ, 128, 765

Sung, H. & Bessell, M. S. 2004, AJ, 127, 1014

A 2.2 MICRON CATALOGUE OF STARS IN NGC 3603

M.G. Petr-Gotzens[1], H.R. Ledo[2] and D.E.A. Nürnberger[3]
[1]*European Southern Observatory, Karl-Schwarzschild Str. 2, 85748 Garching, Germany*
[2]*Universidade do Porto, Praca Gomes Teixeira, 4099 - 002 Porto, Portugal*
[3]*European Southern Observatory, Casilla 19001, Santiago 19, Chile*
mpetr@eso.org,hugoledo@hotmail.com,dnuernbe@eso.org

Abstract We present a photometric catalogue of ∼11,500 stellar objects identified in the field of the Galactic starburst cluster NGC 3603. The catalogue is based on high quality K_s-band data obtained at the *Very Large Telescope* (VLT). We extract from the catalogue the K_s-band luminosity function and evaluate the underlying IMF. We do not find any evidence for a lower mass cut-off down to approximately $0.5 M_\odot$. The slope of the K_s-band luminosity function is consistent with a Miller-Scalo type IMF.

1. Observations and photometry

Near-infrared images at K_s-band (2.16μm) have been taken of the Galactic starburst cluster NGC 3603 and its southern surrounding, using the ISAAC instrument at the VLT. The atmospheric conditions during the observations were very good, resulting in an image quality of $0.4'' - 0.6''$ FWHM on point-sources. The telescope was offset to several different positions in order to cover a total field of $3.3' \times 6.5'$ (see Nürnberger & Petr-Gotzens 2002, for an outline of the surveyed field).

After standard data reduction, photometry was performed on 20 selected (best quality), individual ISAAC images. PSF-photometry using DAOPHOT under IRAF was applied, since severe stellar crowding in the NGC 3603 cluster makes aperture photometry less reliable. Comparing the results of PSF-photometry to our aperture photometry, carried out on a stacked mosaic and presented in Nürnberger & Petr-Gotzens (2002), shows a decrease in the mean photometric error for cluster stars by $\sim 3\,\%$. Absolute photometric calibration was achieved by calculating the nightly zero point from observations of two different standard stars, taken just before, in between and just after our observations of NGC 3603.

E. Corbelli et al. (eds.), The Initial Mass Function 50 Years Later, 159–160.

2. Composing the final catalogue

In order to avoid as much as possible artifacts and non-stellar sources in the final catalogue, we further selected and rejected entries from each of the photometry lists, before merging the photometry of the 20 individual fields. This selection/rejection process was done on a statistical basis using various parameters that characterized the quality of the psf-photometry, followed by final visual inspections of sources in the images. Finally, all photometry lists were merged. For those sources for which more than one measurement existed (identified by common x/y coordinate positions in the photometry lists) error-weighted mean magnitudes and uncertainties were calculated.

The resulting catalogue contains $\sim$ 11,500 entries. The overall 5σ detection limit is K_s $\sim$19 mag, while the completeness limit (90%) is at $\sim$17.3 mag. These magnitude limits, however, exclude the central $30''$ of the cluster, because of the high stellar crowding.

3. KLF and IMF

We then used our photometry of NGC 3603 in order to extract the K_s band luminosity function of the cluster for a region outside the central $30''$. After having applied field star corrections to each bin of the luminosity function (LF) we measured a slope of the KLF over the range K_s=13-17 mag, of $\alpha = 0.35$. The predicted slope from modelling of KLFs, assuming a log-normal IMF of Miller & Scalo (1979), a cluster age of 1-2 Myr and incorporating PMS stellar evolutionary tracks, is $\alpha = 0.36$ (Lada & Lada 1995). This is in very good agreement with our result. More recent, sophisticated modelling of KLFs will be used in our forthcoming paper. Furthermore, we see that there is no deficiency of lower mass stars down to $0.5M_{\odot}$, and even down to $0.3M_{\odot}$ after incompleteness correction.

Acknowledgments H.R. Ledo thanks the ESO Office for Science for supporting his stay at ESO Garching in 2004 through DGDF funding.

References

Nürberger, D. E. A., & Petr-Gotzens, M. G. 2002, A&A, 382, 537
Miller, G. E., & Scalo, J. M. 1979, ApJS, 41, 513
Lada, E. A., & Lada, C. J. 1995, AJ, 109, 1682

THE IMF OF THE MASSIVE STAR FORMING REGION NGC 3603 FROM VLT ADAPTIVE OPTICS OBSERVATIONS

Yohei Harayama and Frank Eisenhauer
Max Planck Institute for Extraterrestrial Physics, 85748 Garching, Germany
yohei@mpe.mpg.de, eisenhau@mpe.mpg.de

Abstract We present our preliminary results of the IMF of the central star-forming cluster HD 97950 in NGC 3603 focussing particularly on low-mass regions. NGC 3603 is the best-studied template for extragalactic starbursts so far, and our recent high resolution data in the H and K bands have shown us the deepest sources in the cluster. The IMF have revealed the existence of low-mass stars down to 0.1 $M_{\odot}$ or even below, towards the hydrogen burning limit of 0.08 $M_{\odot}$. The IMF continues to increase towards $\sim$0.1 $M_{\odot}$, but the flat slope indicates the significant deficiency of subsolar mass stars in the cluster core.

1. Observations and data reduction

Observations were carried out on 18-20 March 2003 with the NAOS / CONICA at the ESO VLT (UT4) on Paranal, Chile. Data were obtained in three bands with NACO - J (1.27 μm), H (1.66 μm) and Ks (2.18 μm) filters. Each frame in all data sets is reduced by standard data reduction procedures. Total integration times are $\sim$8 min. in J $\sim$15 min. in H and $\sim$13 min. in Ks band mosaic frames respectively, and those on outward regions become shorter. Photometry is performed by the STARFINDER package in IDL, which applies the PSF fitting technique. Photometry results were combined with the results from observations with ESO ADONIS at the 3.6 m telescope (Eisenhauer et al. 1998) in order to derive the absolute magnitudes, and to deal with saturated sources. Sources in the central region of $22'' \times 28''$ which overlap with ADONIS data were used for data analysis. We performed a completeness correction by estimating the fraction of stars missed due to blending effects of each star to fainter stars. Field star correction is not performed in the present analysis.

E. Corbelli et al. (eds.), The Initial Mass Function 50 Years Later, 161–162.

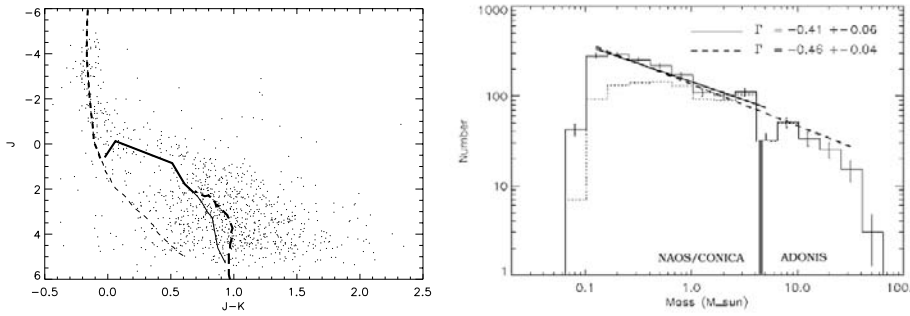

Figure 1. CMD (left) and the IMF (right). The isochrone in the CMD is created from three evolutionary models. A dotted and a dashed lines are derived from Geneva 3 Myr isochrone in Lejeune & Shaerer (2001) and 1 Myr isochrone in Baraffe et al. (2002) respectively. A solid line is derived from 0.5 and 1 Myr isochrones in Palla & Stahler (1999) by means of interpolation. In the IMF a solid histograms shows the mass distribution after the completeness correction, and a dotted one shows the original mass distribution. The slopes in solid and dashed lines are derived from the mass ranges of 0.1-6 $M_{\odot}$ and 6-40 $M_{\odot}$ respectively.

2. CMD and IMF

Figure 1 (left) shows the CMD (J-K, J) measured from 1086 stars detected simultaneously in the three bands. A distance modulus of 13.9 mag and a uniform interstellar extinction A_V = 4.5 are applied. In order to cover the full mass range, we apply several evolutionary models for different mass ranges. The IMF is shown in Figure 1 (right). The mass of every individual star was measured from its three bands magnitudes. The power law index is $\sim$0.41 in the mass range from 0.1 $M_{\odot}$ up to 6 $M_{\odot}$, and $\sim$0.46 in the range from 6 $M_{\odot}$ up to 40 $M_{\odot}$. In the IMF there is no clear turn-over up to our detection limit. The slope is even flatter than what has been reported for the outer region of the core ($7'' < R < 20\ ''$) in a previous study which indicates a presence of mass segregation (Stolte 2003). The flatter slope is consistent with mass segregation, and would suggest that formation of subsolar mass stars would be strongly inhibited in such a violent environment in the central core.

References

Baraffe, I., Chabrier, G., Allard, F., & Hauschildt, P. H. 2002, A&A, 382, 563
Eisenhauer, F., Quirrenbach, A., Zinnecker, H., & Genzel, R. 1998, ApJ, 498, 278
Lejeune, T., & Schaerer, D. 2001, A&A, 366, 538
Palla, F., & Stahler, S. W. 1999, ApJ, 525, 772
Stolte, A. 2003, PhD Thesis, University of Heidelberg

X-RAYS AND YOUNG CLUSTERS

Membership, IMFs and distances

E.D. Feigelson and K.V. Getman
Department of Astronomy & Astrophysics, Pennsylvania State University, 525 Davey Laboratory, University Park, PA 16802, USA
edf@astro.psu.edu, gkosta@astro.psu.edu

Abstract

Sensitive imaging X-ray observations of young stellar clusters (YSCs, ages ≤ 10 Myr) are valuable tools for the acquisition of an unbiased census of cluster members needed for Initial Mass Function (IMF) studies. Several dozen YSCs, both nearby and across the Galactic disk, have been observed with the Chandra and XMM-Newton satellites, detecting $> 10,000$ low-mass cluster members. Many of these samples should be nearly complete down to $\simeq 1$ $M_\odot$. An important additional benefit is that the YSC X-ray luminosity function appears to be universal with a lognormal shape, providing a new standard candle for measurement of YSC distances.

1. Measuring IMFs in young stellar clusters

Measuring the stellar Initial Mass Function (IMF) requires complete and unbiased samples which are often sought in young stellar clusters (YSCs) that have not undergone significant dynamical evolution. We consider here YSCs with ages ≤ 10 Myr where most of the lower mass stars are on the convective Hayashi pre-main sequence (PMS) evolutionary tracks.

A major difficulty in obtaining a reliable census of YSCs is that the few lying at distances $d < 400$ pc are spatially extended and not strongly concentrated. The richest is the Sco-Cen OB Association with several thousand members, but it subtends several thousand square degrees in the southern sky. Others like the Corona Australis, Perseus or Chamaeleon clouds have dozens of members and typically subtend ≥ 1 square degree. Individual Taurus-Auriga clouds or Bok globules may be smaller, but their stellar populations are too poor for IMF studies.

E. Corbelli et al. (eds.), The Initial Mass Function 50 Years Later, 163–170.

These large angular sizes require that cluster members of nearby clouds must be efficiently discriminated from the large, often overwhelming, number of unrelated foreground and background stars. This discrimination is traditionally achieved using surveys for stars with Hα emission and/or near-infrared photometric excesses. These methods efficiently select protostars and 'classical T Tauri' (CTT) stars, but often undersample the large 'weak-lined T Tauri' (WTT) population (Feigelson & Montmerle 1999). As the mass-dependency of disk evolution is not well known, correction to the full PMS population for IMF study is uncertain. Analysis of the K-band star counts towards YSCs can give a more complete census but in an indirect fashion (Lada & Lada 1995). It often requires major corrections for unrelated stars and, as individual members are not individually identified, the IMF is derived by a model-dependent conversion of the K-band distributions to mass distributions.

IMF studies may be advantageous in more distant YSCs, but here additional problems present themselves. The members are fainter than in closer clusters, so that large telescopes with low-noise detectors become necessary to detect the lowest mass cluster members. As distance increases, it becomes increasingly difficult to resolve multiple systems. Both observational and theoretical studies suggest that most stars form in binary or multiple systems. A complete census is also hindered by the wide range of extinctions often exhibited by YSC members.

In light of these constraints, one YSC has unique merits for IMF studies: the Orion Nebula Cluster (ONC). The ONC lies at $d \simeq 450$ pc, sufficiently close that the best available near-infrared instrumentation can detect objects down to a few Jupiter masses. With $\simeq 2000$ members concentrated in $\simeq 0.1$ square degrees, it is easily studied and rich enough to populate the IMF up to ~ 45 M$_\odot$. Unlike other YSCs in the Orion molecular cloud complex, it lies on the near side of the cloud and has evacuated most of the intervening molecular material, so line-of-sight absorptions are low. While the ONC census suffers some difficulties – mild contamination from unrelated young stars in the background cloud and from foreground dispersed young clusters, incomplete enumeration of multiple systems – it provides a standard for stellar IMF studies that is far above that achieved for other YSCs.

2. The role of X-ray surveys

X-ray emission from PMS was initially predicted from shocks associated with their stellar wind, but studies with the Einstein and ROSAT observatories indicated an origin more closely associated with solar-like magnetic activity (Feigelson & Montmerle 1999). The emission is $1-4$ orders of magnitude stronger than typical main sequence levels, exhibits high-amplitude flares and hotter plasmas than expected from wind shocks, and is mostly uncorrelated

with the presence or absence of an infrared-excess disk. X-ray surveys discovered many WTTs whose population is comparable to the CTT population even in YSCs associated with active star forming clouds. Although useful, surveys with these early satellites were limited by detector technology: low-resolution gas proportional counters or low-efficiency solid state microchannel plates.

The Chandra X-ray Observatory and XMM-Newton missions are much better adapted to YSC studies with their high-efficiency low-noise CCD detectors. Chandra is particularly useful with its high-precision mirrors giving arcsecond imaging capability, though its field of view is limited to 0.08 square degrees. Together, these telescopes have imaged several dozen YSC populations across the Galactic disk. These include the ρ Ophiuchi, Chamaeleon, CrA, Mon R2, L1551, L1448, Serpens, Cep B and Sgr B2 clouds; populations associated with the Orion, Trifid, Rosette and Carina HII regions; the Cyg OB2 association, η Cha cluster, and various isolated Herbig Ae/Be stars with their companions; star forming regions NGC 1333, IC 348, M 8, M 16, M 17, NGC 281, NGC 1579, NGC 2078, NGC 2024, NGC 2264, IC 1396, RCW 38, RCW 49, RCW 108, NGC 6334, NGC 6530, NGC 6383, NGC 3603, W 3, W 1, W 49, W 51, and IRAS 19410+2336; several Galactic Center YSCs; and 30 Dor in the Large Magellanic Cloud. The most comprehensive study underway is the Chandra Orion Ultradeep Project (COUP) based on a nearly-continuous 10-day pointing towards the ONC and embedded sources in OMC-1. An introduction to COUP, and references for the other regions published through mid-2003, are given in Feigelson (2003a). Figure 1 shows a portion of the COUP image, and some preliminary COUP results are presented here.

X-ray surveys are subject to selection effects which must be carefully considered in the effort to achieve a well-defined YSC census. Most importantly, PMS X-ray luminosities are strongly correlated with a tangle of interrelated stellar properties: bolometric luminosity, mass, stellar surface area and volume. The $L_x - L_{bol}$ correlation has been known for many years, but the linkage with other variables only emerged clearly in pre-COUP studies of the ONC (Flaccomio et al. 2003a; Feigelson et al. 2003b). Though quantitative analysis of the scatter in these relations by the COUP has not yet been completed, we can roughly say that a Chandra observation of a nearby YSC with limiting sensitivity $\log L_x(\mathrm{lim}) \simeq 28.0$ erg/s ($0.5 - 8$ keV band) will detect $> 90\%$ of PMS stars with masses $M > 0.2$ M$_\odot$, and an observation of a more distant YSC with $\log L_x(\mathrm{lim}) \simeq 29.5$ erg/s will detect $> 90\%$ of PMS stars with $M > 0.8$ M$_\odot$ (Preibisch et al., in preparation).[1]

[1] A second selection effect in PMS X-ray luminosities must be considered: the subpopulation of CTT stars tends to be a factor of $2 - 3$ weaker the subpopulation of WTT stars leading to, opposite to traditional methods, a selection bias against accreting stars (Flaccomio et al. 2003b). But this effect is relatively small compared to the 4 orders of magnitude range in PMS X-ray luminosities.

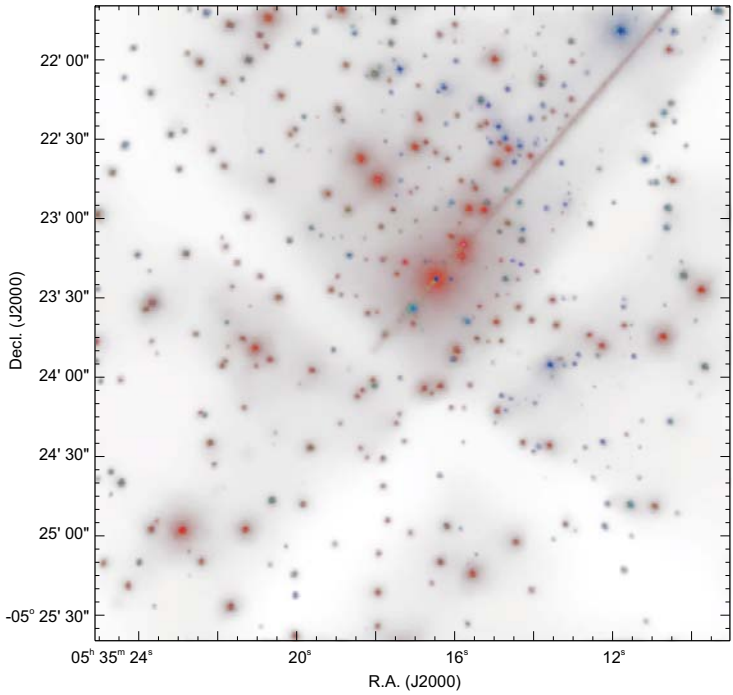

Figure 1. The central $4' \times 4'$ region of the $17' \times 17'$ Chandra ACIS image of the Orion Nebula Cluster, obtained in a $\simeq 10$-day exposure in early 2003 (Getman et al. 2004). Moderate-resolution spectra over the $0.5 - 8$ keV band, giving an independent measure of line-of-sight absorption, and temporal information on variability are available for each of the 1616 COUP sources. This dataset is the foundation of a wide range of studies comprising the Chandra Orion Ultradeep Project (COUP).

This result immediately indicates the power of Chandra studies for improving our knowledge of stellar populations in a wide variety of YSCs, and thus studying the IMF in a wide variety of conditions. In most YSCs beyond $d \simeq 1$ kpc, cluster membership is currently limited to a small number of bright spectroscopically-confirmed OB stars and lower mass stars with K-band excesses. Consider, for example, the cluster illuminating the HII region M 17 and its the surrounding molecular cloud. Only a few dozen have optical spectra and while >20,000 have JHK measurements, most of these stars are unrelated to the cloud (Hanson et al. 1997; Jiang et al. 2002). A Chandra image with $\log L_x(\mathrm{lim}) = 29.7$ erg/s shows 877 sources nearly all of which are cluster members (Getman et al., in preparation). Such X-ray selected samples should be $> 90\%$ complete above a well-defined mass limit, usually around $0.5 - 1.5$ $\mathrm{M}_\odot$ for the more distant YSCs under study.

Analysis of these fields is difficult with hundreds of faint X-ray stars often embedded in structured diffuse emission from large-scale OB wind shocks (Townsley et al. 2003). But sophisticated data analysis methods have been developed (Getman et al. 2004), careful studies are underway and within a few years $> 10,000$ Chandra-discovered YSCs members should be published. Followup optical/near-infrared photometry and spectroscopy will be needed to place these stars on the HR diagram to estimate masses for IMF analysis. Chandra should thus provide an important boost to comparative IMF studies for many of the YSC clusters listed above.

We caution that it is still unclear whether even the most sensitive X-ray surveys can efficiently detect substellar PMS objects which will evolve into L- and T-type brown dwarfs. Two YSC studies with sensitivities of $\log L_x(\lim) \simeq 27.0$ erg/s performed to date give inconsistent results. A deep Chandra image of the Chamaeleon I North cloud found all 27 known cloud members including 3 probable substellar objects (Feigelson & Lawson 2004). This suggests the X-ray census is complete and gives an IMF deficient in stars with $M < 0.3$ $M_\odot$ compared to the ONC or field star IMFs. But this may be due to mass segregation favoring higher mass stars in the small 0.6 pc^2 region covered by the Chandra imager, rather than intrinsically different IMF. The second study with $\log L_x(\lim) \simeq 27.0$ erg/s is the COUP observation of the ONC. Here, most of the spectroscopically confirmed brown dwarfs (Slesnick et al. 2004) are not detected, indicating that X-ray surveys will probably be incomplete in this low mass regime.

3. A new distance estimator for YSCs

Techniques for measuring distances to YSCs and their natal molecular clouds have hardly changed in a half-century. When a OB population can be studied spectroscopically and individual stellar absorptions are found, then main sequence fitting provides a reliable distance. But when they are too obscured or unavailable, then distance estimation methods are varied, unreliable and inconsistent. Consider, for example, the YSC surrounding the Herbig AeBe star LkHα 101, one of the brightest infrared sources in the sky, which illuminates the nebula NGC 1579. The cluster distance has variously been estimated to be 140 pc, >800 pc, $\simeq 340$ pc, and $\simeq 700$ pc (Tuthill et al. 2002, Herbig et al. 2004). If it lies at the nearer end of this range, it is one of the closest YSCs.

The X-ray luminosity function (XLF) of YSCs has two remarkable empirical characteristics that should render it an effective and accurate distance estimator for clusters such as this. First, the shapes of different YSC XLFs appear to be remarkable similar to each other, once a richness-linked tail of high luminosity O stars is omitted (Figure 2). Second, the shape of this 'universal' XLF

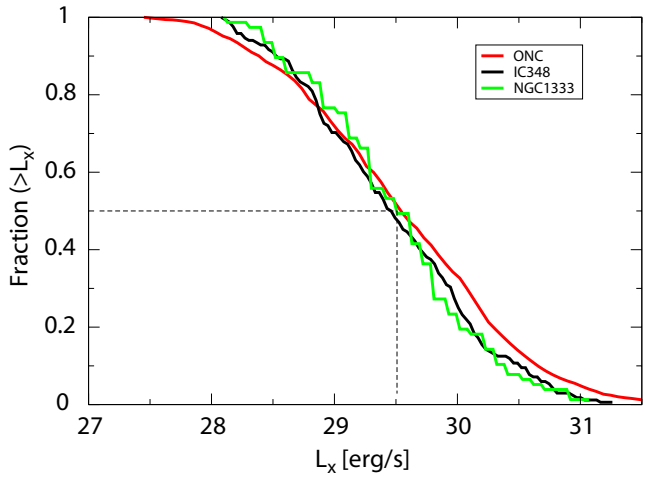

Figure 2. The universal cluster X-ray luminosity function (XLF) found in Chandra YSC studies. NGC 1333 (77 stars from Getman et al. 2002), IC 348 (168 stars from Preibisch & Zinnecker 2002), and the ONC (1508 stars from COUP data truncated at $\log L_x = 31.5$ erg/s, Getman et al. 2004).

strongly resembles a lognormal with mean $< \log L_x > \simeq 29.5$ erg/s ($0.5 - 8$ keV band) and standard deviation $\sigma(\log L_x) \simeq 0.9$ (Figure 3).

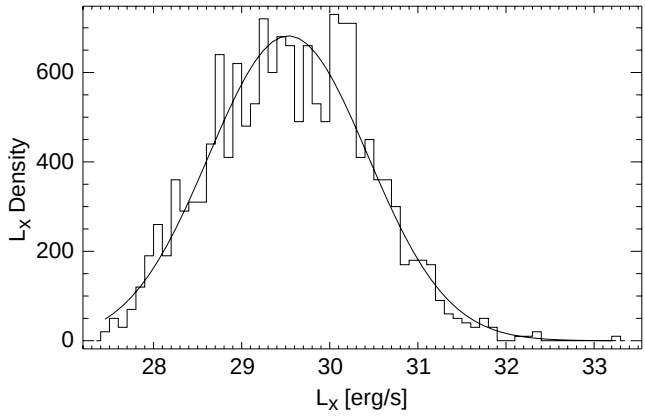

Figure 3. The Orion Nebula Cluster (ONC) XLF with lognormal fit given in the text. COUP sample of 1528 sources with absorption corrected 0.5-8 keV luminosities (Getman et al. 2004). All X-ray luminosities are in the $0.5 - 8$ keV band corrected for absorption measured from the X-ray spectrum.

While we do not have astrophysical explanations for either of these YSC XLF properties, the shape of the XLF can be roughly understood as a convo-

lution of the IMF which breaks from the Salpeter powerlaw below $\simeq 0.5$ $M_\odot$ (and itself is sometimes modeled with a lognormal curve) and the correlation between L_x and mass. These two effects result in a steep falloff in the number of fainter X-ray stars in a YSC. This was dramatically demonstrated in the Chandra studies of the ONC where a factor of 10 increase in limiting sensitivity from $\log L_x(\mathrm{lim}) \simeq 28.0$ erg/s in the early observations to $\simeq 27.0$ erg/s in the deep COUP observation led to only a very small rise in detected lightly absorbed ONC stars.

The peak of the XLF at $< \log L_x > \simeq 29.5$ erg/s can be used as a standard candle for distance estimation, much as the lognormal distribution of globular cluster optical luminosities is used as an extragalactic distance estimator (Harris 1991). One counts cluster members in flux units (this is the X-ray $\log N - \log S$ curve), matches the observed $\log N - \log S$ to the universal XLF, and reads off the distance from the offset. The table below gives a simple example for a hypothetical cluster at various assumed distances observed with Chandra for 100 ks. The tabulated values are the fraction of sources seen in broad count rate bins assuming typical PMS X-ray spectra and negligible absorption.

Table 1. Simulated X-ray source counts for young stellar clusters

$\log L_x(\mathrm{lim})$ (erg/s)	28.0	28.5	29.0	29.5	30.0
Distance (pc)	400	710	1270	2250	4000
Flux bin (cts)			Percent of sources		
$5-50$	22	46	60	76	86
$50-500$	46	42	34	22	14
$500-5000$	28	12	6	2	0
$5000-50000$	4	0	0	0	0

The table shows that the observed $\log N - \log S$ shape will differ dramatically for YSCs at different distances. For close distances or unusually long exposures (as in COUP), most cluster members are quite bright and few faint ones are seen. For far distances or short exposures, most cluster members are near the detection limit which is $3-10$ photons for typical Chandra fields. The principal challenges are corrections for absorption, which can be derived (except for the faintest sources) for individual sources from the X-ray spectrum, and the elimination of extragalactic background sources, which can be achieved by the absence of a stellar counterpart in sensitive K-band images. Accurate distances and error analysis would not be performed in broad flux bins as in the table above, but would be based on unbinned sources fluxes using a maximum likelihood method as described by Hanes & Whittaker (1987) and Cohen (1991).

Acknowledgments We thank Thomas Preibisch (MPIfR) for use of unpublished COUP results. This work was supported by NASA contract NAS8-38252 (Garmire, PI) and COUP grant SAO GO3-4009A (Feigelson, PI).

References

Cohen, A. C. 1991, Truncated and censored samples: theory and applications. New York: M. Dekker

Feigelson, E. D. & Montmerle, T. 1999, ARAA, 37, 363

Feigelson, E. 2003, in Stars as Suns: Activity, Evolution and Planets, IAU Symposium 219, 27

Feigelson, E. D., Gaffney, J. A., Garmire, G., Hillenbrand, L. A., & Townsley, L. 2003, ApJ, 584, 911

Feigelson, E. D. & Lawson, W. A. 2004, ApJ, 614, 267

Flaccomio, E., Damiani, F., Micela, G., Sciortino, S., Harnden, F. R., Murray, S. S., & Wolk, S. J. 2003, ApJ, 582, 398

Flaccomio, E., Micela, G., & Sciortino, S. 2003, A&A, 397, 611

Getman, K. V., Feigelson, E. D., Townsley, L., Bally, J., Lada, C. J., & Reipurth, B. 2002, ApJ, 575, 354

Getman, K. V. and 23 coauthors, 2004, ApJS, in press

Hanes, D. A. & Whittaker, D. G. 1987, AJ, 94, 906

Hanson, M. M., Howarth, I. D., & Conti, P. S. 1997, ApJ, 489, 698

Harris, W. E. 1991, ARA&A, 29, 543

Herbig, G. H., Andrews, S. M., & Dahm, S. E. 2004, AJ, 128, 1233

Jiang, Z., et al. 2002, ApJ, 577, 245

Lada, E. A. & Lada, C. J. 1995, ApJ, 109, 1682

Slesnick, C. L., Hillenbrand, L. A., & Carpenter, J. M. 2004, ApJ, 610, 1045

Townsley, L. K., Feigelson, E. D., Montmerle, T., Broos, P. S., Chu, Y., & Garmire, G. P. 2003, ApJ, 593, 874

Tuthill, P. G., Monnier, J. D., Danchi, W. C., Hale, D. D. S., & Townes, C. H. 2002, ApJ, 577, 826

NGC 2264: A *CHANDRA* VIEW

E. Flaccomio[1], G. Micela[1], S. Sciortino[1], F.R. Harnden[2] and L. Hartmann[2]
[1]*INAF-Osservatorio Astronomico di Palermo, P. Parlamento 1, 90134 Palermo, Italy*
[2]*Smithsonian Astrophysical Observatory, 60 Garden St., Cambridge, MA 02138, USA*
ettoref(giusi,sciorti)@astropa.unipa.it, frh(lhartmann)@cfa.harvard.edu

Abstract We present first results from a *Chandra* ACIS-I observation of the star forming region NGC 2264. Using the X-ray data to select members, we estimate the NGC 2264 stellar Initial Mass Function (IMF).

NGC 2264 is a $\sim$3 Myr old Star Forming Region located at $\sim$760 pc in the Monoceros. Compared to the ONC and Taurus, NGC 2264 has intermediate stellar density and total population, making it an interesting target for investigating the dependence of star formation on the environment. Its study is eased by the presence of an optically thick background cloud, effectively obscuring unrelated background objects, and by the low and uniform extinction of the foreground population (Walker, 1956, ApJS, 2, 365; Rebull et al. 2002, AJ, 123, 1528).

We have observed NGC 2264 with the *Chandra* ACIS-I in October 2002. We detect 420 sources in the 17'x17' FOV. Because of the higher X-ray luminosity of PMS stars respect to field objects, we expect the majority of detected sources to be associated with low mass and/or embedded young members of NGC 2264. This interpretation is supported by the I vs. R-I color magnitude diagram (CMD, Figure 1a) clearly showing that X-ray detected stars are preferentially found in the same locus of NGC 2264 members with an age of 1-10Myr. We then assume that X-ray detections are cluster members, with the exception of an handful of possible X-ray detected foreground objects that lie, in the optical CMD, outside the *cluster locus*, here defined as the region above the $10^{7.1}$yr isochrone or to the left of the $0.8M_{\odot}$ track, both highlighted in Figure 1a. We estimate masses from the CMD in Figure 1a and the Siess et al. (2000, A&A 358, 593) PMS tracks. The R and I magnitudes should be little affected by non photospheric excesses and reddening is uniform for the large majority of X-ray members, as inferred from the J-H vs. H-K diagram (not shown) in which the majority of our sample lie close to the theoretical loci. Masses estimated for a few very reddened objects may be significantly underestimated. Figure 1b shows the mass distribution of the X-ray selected

E. Corbelli et al. (eds.), The Initial Mass Function 50 Years Later, 171–172.

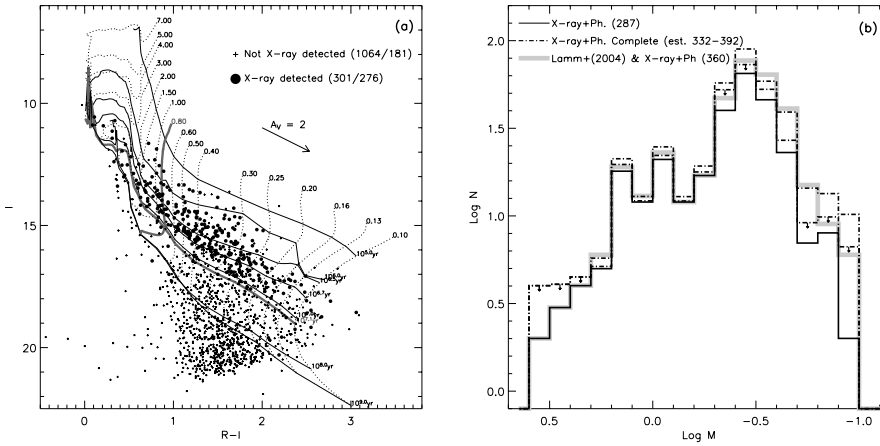

Figure 1. (*a*) Optical CMD for X-ray detected/undetected objects in the ACIS FOV. Photometry is from Lamm et al. (2004), PMS tracks from Siess et al. (2000) transformed to the I,(R-I) plane using Kenyon & Hartmann (1995, ApJS, 101, 117) and reddened by $< A_V >$=0.5 (Rebull et al., 2002). Figures in the legend report the number of objects in the whole diagram and those lying in the *cluster locus.* (*b*) Solid line: raw IMF from the X-ray selected sample; dot-dashed lines: same, corrected for completeness with two different assumptions (see text); gray line: IMF of the union of our X-ray based sample and one selected following Lamm et al. (2004).

sample (solid black line). Given the L_X-mass relation and the sensitivity of our X-ray data, our sample is likely incomplete at low masses. We estimate the completeness fraction vs. mass assuming that the NGC 2264 X-ray luminosity function in each mass bin is the same as in the ONC (Flaccomio et al., 2003, ApJ, 582, 398). Taking the actual range for the minimum detectable L_X ($10^{28.5}$-10^{29} erg/s) we compute, as a function of mass, two limiting completeness fractions which we then use to derive completeness corrected IMFs, shown in the figure as two dot-dash lines. The completeness corrected IMF is similar to that resulting from the union of our X-ray based sample and that selected following Lamm et al. (2004, A&A 417, 557) using photometric and optical variability criteria (gray line in Fig. 1b). The two samples are indeed complementary: Lamm's is expected to be deficient in WTTS, while ours in low mass CTTS (Flaccomio et al. 2003). Note that these IMFs do not include an additional X-ray discovered population of deeply embedded members: out of the $\sim$100 ACIS sources not identified with optically visible objects, a significant fraction is likely associated with a member, having the same spatial distribution of NGC 2264 members.

IV

THE EXTRAGALACTIC IMF

Figure 2. Hans presenting Ed's favorite book.

Figure 3. Some more gifts for Ed!

Figure 4. Happy birthday Ed!

VARIATIONS OF THE IMF

Pavel Kroupa and Carsten Weidner
Sternwarte, University of Bonn, Auf dem Hügel 71, D-53121 Bonn, Germany
pavel@astro.uni-bonn.de, cweidner@astro.uni-bonn.de

Abstract The *stellar IMF* has been found to be essentially invariant. That means, any detailed observational scrutiny of well resolved populations of very young stars appears to show the IMF to be of more or less the same shape independent of the metallicity and density of the star-forming region. While some apparent differences are seen, the uncertainties inherent to this game do not allow a firm conclusion to be made that the IMF varies systematically with conditions. The IMF integrated over entire galaxies, however, is another matter. Chemical and photometric properties of various galaxies do hint at *galaxial IMFs* being steeper than the stellar IMF, as is also deduced from direct star-count analysis in the MW. These results are however sensitive to the modelling of stellar populations and to corrections for stellar evolution, and are thus also uncertain. However, by realising that galaxies are made from dissolving star clusters, star clusters being viewed as *the fundamental building blocks of galaxies*, the result is found that galaxial IMFs must be significantly steeper than the stellar IMF, because the former results from a folding of the latter with the star-cluster mass function. Furthermore, this notion leads to the important insight that galaxial IMFs must vary with galaxy mass, and that the galaxial IMF is a strongly varying function of the star-formation history for galaxies that have assembled only a small mass in stars. Cosmological implications of this are that the number of SNII per low-mass star is significantly depressed and that chemical enrichment proceeds much slower in all types of galaxies, and particularly slowly in galaxies with a low average star-formation rate over what is expected for an invariant Salpeter IMF. Using an invariant Salpeter IMF also leads to wrong M/L ratios for galaxies. The detailed implications need to be studied in the future.

1. The shape of the stellar IMF

The number of stars in the mass interval $m,\ m+dm$ is $dN \equiv \xi(m)\,dm$, where $\xi(m)$ is the stellar initial mass function (IMF). The logarithmic slope is $\Gamma(\log_{10} m) = d\log_{10}\xi_{\rm L}(\log_{10} m)/d\log_{10} m$ such that $\log_{10}\xi(m) = \log_{10} k - \alpha\log_{10} m$ for the power-law form, $\xi(m) = km^{-\alpha}$, and $\alpha(m) = -d\log_{10}\xi(m)\,/d\log_{10} m = 1-\Gamma(m)$. The *logarithmic IMF* is

E. Corbelli et al. (eds.), The Initial Mass Function 50 Years Later, 175–186.

$\xi_{\rm L}(m) = m \ln(10)\, \xi(m)$, which is useful when counting stars in logarithmic mass intervals.

The *stellar IMF* is the distribution of stellar masses that results from a single star-formation burst. Because essentially all stars form in clusters (Lada & Lada 2003) we expect to measure the stellar IMF in young star clusters before they disperse to the field of a galaxy.

The stellar IMF is one of the most fundamental distribution functions of astrophysics, and consequently a huge effort has been invested into constraining its shape since its first formulation in 1954 by Salpeter (1955) (at the Australian National University in Canberra) as a single power-law with $\alpha = 2.35$ for $0.4 < m/M_\odot < 10$, based on an early analysis of star-counts in the solar neighbourhood. A further milestone in this remarkable scientific enterprise is given by Miller & Scalo (1979) who made a large effort in constraining the IMF to mass ranges outside the Salpeter limits and who deduced that the stellar IMF flattens below $0.5\,M_\odot$. Scalo (1986) re-considered this problem in what today remains the most significant piece of work in this topic by studying all of the then available observational constraints on local star counts, the shape of the stellar luminosity function, the mass-luminosity relation, stellar evolution for early-type stars and the vertical structure of the Milky Way (MW), and suggested the IMF to turn-down below about $0.4\,M_\odot$, which had important implications in trying to understand the nature and occurrence of unseen matter in the disk of the MW. An important improvement in understanding the shape of the IMF for low-mass stars was contributed by Kroupa, Tout & Gilmore (1993 and two prior papers) who proposed that the strong maximum near $M_{\rm V} \approx 12$ in the luminosity function of solar-neighbourhood stars stems from an inflection in the mass–luminosity relation, which in turn results from the association of H_2 molecules and the onset of full convection below about $0.4\,M_\odot$. This revised the IMF to be essentially flat below $0.4\,M_\odot$, but the inclusion of corrections for unresolved multiple systems and detailed modelling of star-counts with Malmquist bias and galactic-disk structure solved the disagreement between local and deep star counts and thereby increased the slope of the IMF below $0.5\,M_\odot$. The resulting form of the two-part power-law IMF for late-type stars ($\alpha_1 \approx 1.3 : 0.08 \lesssim m/M_\odot \lesssim 0.5; \alpha_2 \approx 2.3 : 0.5 \lesssim m/M_\odot \lesssim 1$) has been verified by Reid, Gizis & Hawley (2002) using revised local star-counts that incorporate HIPPARCOS distances. For $m \gtrsim 1\,M_\odot$ the IMF is proposed by Reid et al. to have $\alpha_3 = 2.5 - 2.8$, while Scalo (1986) derived $\alpha_3 \approx 2.7$, which is supported by the work of Yuan (1992). Written out,

$$\xi(m) = k \begin{cases} \left(\frac{m}{m_{\rm H}}\right)^{-\alpha_0} & m_{\rm low} \le m < m_{\rm H} \\ \left(\frac{m}{m_{\rm H}}\right)^{-\alpha_1} & m_{\rm H} \le m < m_0 \\ \left(\frac{m_0}{m_{\rm H}}\right)^{-\alpha_1} \left(\frac{m}{m_0}\right)^{-\alpha_2} & m_0 \le m < m_1 \\ \left(\frac{m_0}{m_{\rm H}}\right)^{-\alpha_1} \left(\frac{m_1}{m_0}\right)^{-\alpha_2} \left(\frac{m}{m_1}\right)^{-\alpha_3} & m_1 \le m < m_{\rm max}, \end{cases} \quad (1)$$

with exponents

$$\begin{array}{ll} \alpha_0 = +0.3 \pm 0.7 & 0.01 \leq m/M_\odot < 0.08 \\ \alpha_1 = +1.3 \pm 0.5 & 0.08 \leq m/M_\odot < 0.50 \\ \alpha_2 = +2.3 \pm 0.3 & 0.50 \leq m/M_\odot < 1.00 \\ \alpha_3 = +2.7 \pm 0.7 & 1.00 \leq m/M_\odot, \end{array} \quad (2)$$

is the KTG93 IMF after extension to the sub-stellar mass range (Kroupa 2001; 2002). This IMF is the *galaxial IMF* as it is derived from galactic field stars, and, as we will see further below, differs from the *stellar IMF*. The multi-power-law description is used merely for convenience, as it allows us to leave the low-mass part of the IMF unchanged while experimenting with different slopes above, say, $1\,M_\odot$. Other functional forms have been suggested (Miller & Scalo 1978; Larson 1998; Chabrier 2001), but these bear the disadvantage that the whole functional form reacts to changes in the parameters. Such parametrisations are useful for studying possible changes of the stellar IMF with cosmological epoch.

To constrain the stellar IMF we need detailed observations of young populations in star clusters and OB associations. The hope is that young clusters are not yet dynamically evolved so that the initial stellar population becomes evident. However, as dynamical modelling of young clusters containing O stars shows, significant dynamical evolution is already well established at an age of 1 Myr as a result of (i) the dense conditions before gas removal such that the binary-star population changes significantly away from its primordial properties, and (ii) rapid cluster expansion as a result of violent gas expulsion (Kroupa, Aarseth & Hurley 2001). This would lead to a systematic biasing of the observed stellar IMF against low-mass members if the cluster was significantly mass-segregated prior to gas expulsion (Moraux, Kroupa & Bouvier 2004). In addition to these difficulties come obscuration by natal gas and dust and the large uncertainties in deriving ages and masses given inadequate theoretical models of stars that are still relaxing from their accretion history, rotating rapidly, are variable and active, and have circum-stellar material.

The task of inferring the stellar IMF is thus terribly involved and uncertain. Nevertheless, substantial progress has been achieved. Given that there are many star clusters and OB associations, a large body of literature has been amassing over the decades, and Scalo (1998) compiled the then available IMF slope vs mass data.

An updated form of this plot is shown in Fig. 1, and as can be seen, the stellar IMF essentially follows the above galaxial IMF below $1\,M_\odot$ (after correcting the observations for unresolved multiple systems), whilst having a Salpeter slope above $1\,M_\odot$. Striking is that Large and Small Magellanic Cloud data (solid triangles) are not systematically different to the more metal rich MW data (solid circles). A systematic difference between dense clusters and sparse OB associations is also not evident (Massey 1998). Notable is that the scatter is large above $1\,M_\odot$ but constant and that it can be fitted by a Gauss distribu-

tion of α values centred on the Salpeter index (Kroupa 2002). The scatter can be understood to result from statistical fluctuations and stellar-dynamical evolution of the clusters and the dynamically evolved OB associations (Elmegreen 1999; Kroupa 2001). These observations on the α-plot thus point to a remarkable uniformity of the stellar IMF, which can thus be summarised by the multi-power-law form of eq. 2 but with

$$\alpha_3 = 2.3. \tag{3}$$

Some apparently significant deviations from this *standard* or *canonical* IMF do occur though (Fig. 2), and it will be the aim of observers and modellers alike to try to understand why the two clusters of similar age, the Pleiades (Hambly et al. 1999) and M35 (Barrado y Navascués et al. 2001), appear to have such different mass functions below $0.5\,M_\odot$.

The existence of a universal canonical stellar IMF is therefore supported by the majority of data. It has a Salpeter index above about $0.5\,M_\odot$. But this result uncovers a possibly unsettling discrepancy between this stellar IMF (eq. 3) and the galaxial IMF (eq. 2) which was found to be steeper for $m > 1\,M_\odot$.

2. The galaxial IMF

The distribution of stellar masses in an entire galaxy results from the addition of all star-forming events ever to have occurred,

$$\xi_{\rm IGIMF}(m) = \int_{M_{\rm ecl,min}}^{M_{\rm ecl,max}} \xi(m \leq m_{\rm max})\, \xi_{\rm ecl}(M_{\rm ecl})\, dM_{\rm ecl}. \tag{4}$$

This is the integrated *galaxial IMF* (IGIMF), i.e. the IMF integrated over space and time. Here $\xi_{\rm ecl}$ is the MF of embedded clusters, and $M_{\rm ecl,min} = 5\,M_\odot$, $M_{\rm ecl,max} \lesssim 10^6\,M_\odot$ are the minimum and maximum cluster masses, respectively. Note that the IGIMF becomes indistinguishable to the field-star IMF in galaxies in which presently on-going star-formation contributes insignificantly to the already present stellar population, and also that $\xi_{\rm IGIMF}$ does not correspond to the shining matter distribution for $m \gtrsim 1\,M_\odot$. To evaluate this we need to consider only the recently formed stars.

Within each cluster stars are formed following the canonical IMF. However, small star-forming cloud cores, similar to the individual groups containing a dozen $M_\odot$ in gas seen in Taurus–Auriga, for example, can never from O stars. Since the stellar IMF has been found to be essentially invariant, even when comparing the small groups of dozens of pre-main sequence stars in Taurus–Auriga with the rich Orion Nebula Cluster (Kroupa et al. 2003), constructing a young cluster population is mathematically equivalent to randomly sampling the canonical IMF. However, sampling without a mass constraint would in principle allow small star-forming regions to form very massive stars, which

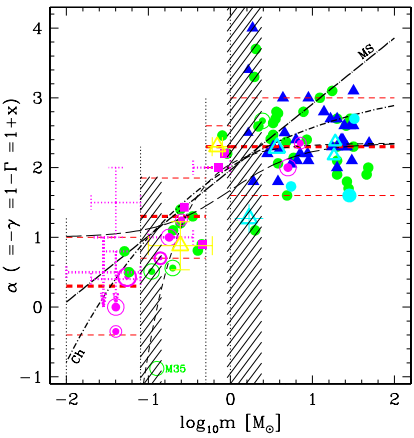

Figure 1. The alpha plot compiles measurements of the power-law index, α, as a function of the logarithmic stellar mass and so measures the shape of the MF. The canonical IMF (eq. 3) is represented by the thick short-dashed horizontal lines, and other functional forms are shown using other line-types (MS indicates the Miller & Scalo (1979) log-normal form; and the thin short- and long-dashed lines are from Larson (1998), while the thick short-dash-dotted curve is the Chabrier (2001) form labelled by Ch). Shaded regions indicate mass-ranges over which derivation of the MF is particularly hard. For details see Kroupa (2002).

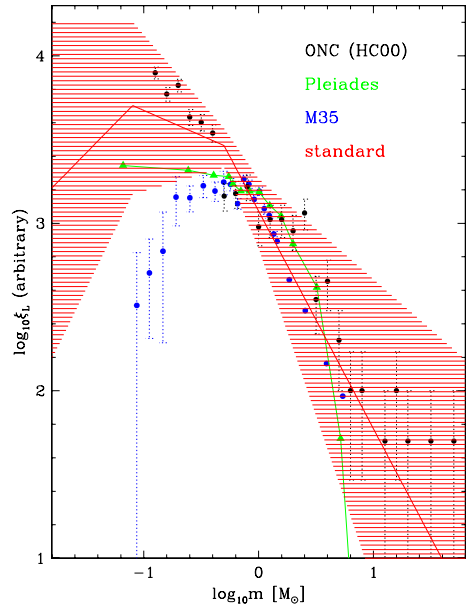

Figure 2. The measured logarithmic stellar mass functions, $\xi_{\rm L}$, in the Orion Nebula Cluster [ONC, solid circles], the Pleiades [triangles] and the cluster M35 [lower solid circles]. The average Galactic field single star-star IMF (eq. 2) is shown as the solid line with the associated uncertainty range. For details see Kroupa (2002).

would be in violation to the observations according to which massive stars are formed in rich clusters. We therefore choose stars randomly from the canonical IMF but impose a mass-limit on the mass in stars that can form from a molecular cloud core with mass $M_{\rm core} = M_{\rm ecl}/\epsilon$, where $\epsilon \lesssim 0.4$ is the star-formation efficiency (Lada & Lada 2003),

$$M_{\rm ecl} = \int_{m_{\rm low}}^{m_{\rm max}} m \cdot \xi(m)\, dm, \qquad (5)$$

where $m_{\rm low} = 0.01\, M_\odot$. In each cluster there is one single most-massive star with mass $m_{\rm max}$,

$$1 = \int_{m_{\rm max}}^{m_{\rm max*}} \xi(m)\, dm, \qquad (6)$$

where $m_{\max *} \approx 150\,M_\odot$ is the fundamental upper stellar mass limit (Weidner & Kroupa 2004a, this volume). This set of two equations needs to be solved numerically to obtain $m_{\max} = m_{\max}(M_{\rm ecl})$ that enters eq. 4. We note that our usage of an $m_{\max}(M_{\rm ecl})$ correlation disagrees with Elmegreen's (2004) conjecture that no such relation exists. This problem is dealt with further by Weidner & Kroupa (2004b, this volume).

The slope, β, of the star cluster IMF, $\xi_{\rm ecl} \propto M_{\rm ecl}^{-\beta}$, is constrained by observations:

- $20 \leq M_{\rm ecl}/M_\odot \leq 1100$: $\beta \approx 2$ locally (Lada & Lada 2003);
- $10^3 \leq M_{\rm ecl}/M_\odot \leq 10^4$: $\beta \approx 2.2$ for LMC and SMC (Hunter et al. 2003)
- $10^4 \leq M_{\rm ecl}/M_\odot \leq 10^6$: $\beta \approx 2 \pm 0.08$ for Antennae clusters (Zhang & Fall 1999).

Assuming $\beta \approx 2.2$ and the canonical IMF slope $\alpha \equiv \alpha_3 = 2.35$ for stars above $1\,M_\odot$ we get the resulting IGIMF shown in Fig. 3 which is considerably steeper than the Salpeter IMF (see Kroupa & Weidner 2003 for more details).

In Fig. 4 the slope of the IGIMF, $\alpha_{\rm IGIMF}$ for $m > 1\,M_\odot$, is studied for various values of β and α. The effect is more pronounced the steeper (larger β) the cluster mass function is.

This has a profound impact on the evolution of galaxies as can be deduced from Fig. 5. In the upper panel is shown the number of white dwarfs per star relative to the Salpeter IMF. For β values above 2 it drops considerably, and in the lower panel, were the number of supernovae of type II (SNII) per star is plotted, the effect is even stronger. For $\alpha = 2.35$ and $\beta = 2.2$ there are 89% of white dwarfs but only 35% of SNII compared to a Salpeter IMF.

3. Variations among galaxies

The star-formation rate (SFR) of a galaxy is given by

$$SFR = M_{\rm tot}/\delta t, \tag{7}$$

where $M_{\rm tot} = \int_{M_{\rm ecl,min}}^{M_{\rm ecl,max}} M_{\rm ecl}\,\xi_{\rm ecl}(M_{\rm ecl})\,dM_{\rm ecl}$ is the mass in clusters assembled in time interval δt. Lets assume for the moment that the cluster IMF, $\xi_{\rm ecl}$, is also invariant, and that $M_{\rm ecl,min} = 5\,M_\odot$ is fixed while $M_{\rm ecl,max}$ may vary. Then the $M_{\rm ecl,max}$ vs SFR relation can be calculated for different δt. A comparison of this simple theory with empirical data is provided in Fig. 7. The figure plots empirical maximum star-cluster masses vs galaxial global SFRs, and a fit to these data yields

$$\log_{10}(M_{\rm eclmax}) = \log_{10}(k_{\rm ML}) + (0.75(\pm 0.03) \cdot \log_{10} SFR) + 6.77(\pm 0.02), \tag{8}$$

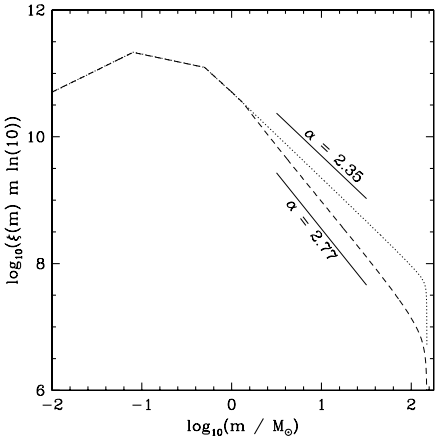

Figure 3. The dotted line is the canonical stellar IMF, $\xi(m)$, in logarithmic units and given by the standard four-part power-law form (eq. 3). The dashed line is $\xi_{\rm IGIMF}(m)$ for $\beta = 2.2$. The IMFs are scaled to have the same number of objects in the mass interval $0.01 - 1.0\,M_\odot$. Note the turn down near $m_{\rm max*} = 150\,M_\odot$ which comes from taking the fundamental upper mass limit explicitly into account (Weidner & Kroupa 2004; 2004a, this volume). Two lines with slopes $\alpha_{\rm line} = 2.35$ and $\alpha_{\rm line} = 2.77$ are indicated.

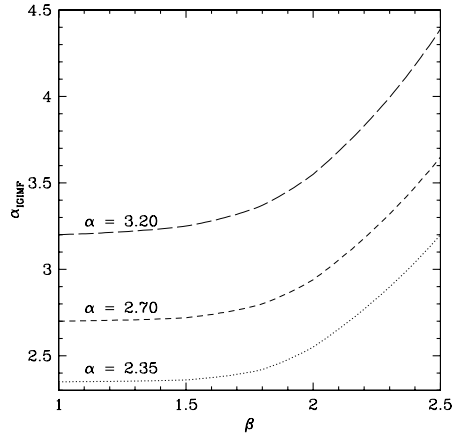

Figure 4. The IGIMF power-law index $\alpha_{\rm IGIMF}$ ($m > 1\,M_\odot$) as a function of the star-cluster MF power-law index β for $\alpha = 2.35, 2.7, 3.2$.

where $k_{\rm ML}$ is the mass-to-light ratio. Fig. 6 shows this relation. Interestingly, the theory is nicely consistent with the data for $\beta \approx 2.2$ and $\delta t \approx 10$ Myr, which suggests that the cluster IMF may indeed be quite invariant, and that a galaxy is able to assemble complete star-cluster systems within typically 10 Myr independent of the SFR (Weidner, Kroupa & Larsen 2004).

With the use of eq. 8 the time-dependent IGIMF of galaxies of different types can be calculated: On specifying a SFR, $M_{\rm ecl,max}$ follows (eq. 8) and from eq. 4 the galaxial IMF can be computed in dependence of the star-formation history by adding up all galaxial IMFs generated in each multiple-δt-epoch until the present. As a straight-forward result we expect the galaxial IMF to be steeper (larger $\alpha_{\rm IGIMF}$) for low-mass galaxies than for massive galaxies because the average SFR is lower for the former. We also expect a dependence of the galaxial IMF on the star-formation history (SFH) of a galaxy.

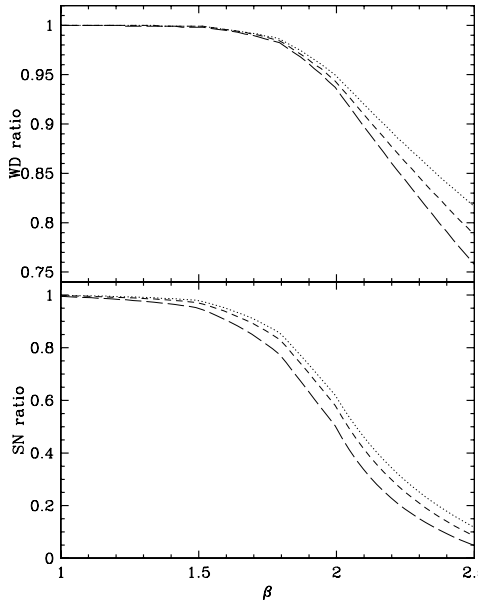

Figure 5. Upper panel: The ratio of the number of stars in the IGIMF (for input stellar IMFs with $\alpha = 2.35, 2.7, 3.2$, dotted, short-dashed and long-dashed lines, respectively) relative to the canonical IMF (Salpeter above $0.5\,M_\odot$) in the mass interval $0.8 \leq m/M_\odot \leq 8$ (the relative number of white dwarfs) in dependence of the cluster mass-function power-law exponent β. Lower panel: The same except for $8 \leq m/M_\odot \leq m_{\rm max*} = 150\,M_\odot$ (the relative number of SNII per star). The normalisation of the IMFs is as in Fig. 3. Note that the panels have different vertical scales.

These expectations are born out. The final IGIMF of a dwarf or low-surface brightness galaxy with a stellar mass of $M_{\rm gal} = 10^7 M_\odot$ assuming a stellar IMF slope $\alpha = 2.35$ is shown in Fig. 7, and in Fig. 8 for $\alpha = 2.70$. In the case with $\alpha = 2.35$ three SFHs are considered. A single burst of star-formation followed by no further formation (solid line), an episodic SFR with 100 Myr long peaks every 900 Myr (long-dashed line) and a constant SFR over 14 Gyr (dotted line). The influence of the SFH on the IGIMF is significant for galaxies with a small mass in stars. For a steeper input IMF (Fig. 8) this effect is even more pronounced. Such a steep IMF slope may possibly be the true value if the observationally derived stellar IMFs for massive stars are corrected for unresolved binaries (Sagar & Richtler 1991). In galaxies with a large stellar mass, $M_{\rm gal} = 10^{10} M_\odot$ (Fig. 9), the sensitivity of $\alpha_{\rm IGIMF}$ on the SFH becomes negligible because the average SFR is always large enough to sample the star-cluster IMF to the fundamental stellar upper mass limit. In summary, the IGIMF slope, $\alpha_{\rm IGIMF}$, is shown as a function of $M_{\rm gal}$ in Fig. 10. The

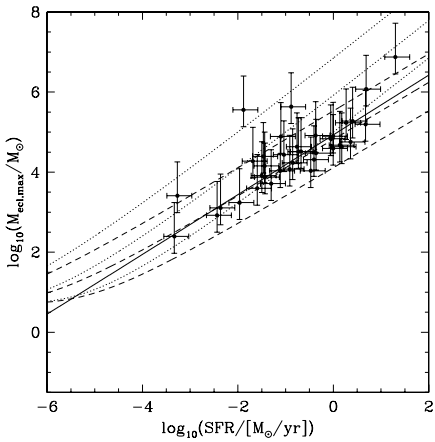

Figure 6. Maximum cluster mass versus global star-formation rate (SFR), both in logarithmic units. Filled dots are observations by Larsen (2001; 2002) with error estimates and the linear regression fit is the solid line (eq. 8). The other curves are theoretical relations (eq. 7) which assume the entire young-cluster population forms in $\delta t = 1$, 10 and 100 Myr (bottom to top). The cluster IMF has $\beta = 2$ (dotted curves) or $\beta = 2.4$ (dashed curves).

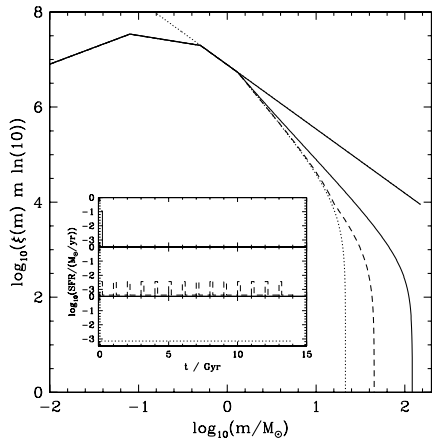

Figure 7. IGIMFs for three dwarf or low-surface brightness galaxies with a final stellar mass of $10^7\,M_\odot$ but different SFHs. The solid curve results from a single initial 100 Myr long burst of star formation. The dashed curve assumes a periodic SFH with 14 peaks each 100 Myr long and 900 Myr quiescent periods in between. The thick dotted curve assumes a constant SFR over 14 Gyr. For all cases the canonical power-law slope above $1\,M_\odot$ ($\alpha = 2.35$) is used and the cluster IMF slope is $\beta = 2.35$. The straight solid line above $0.5\,M_\odot$ shows the canonical input IMF for comparison. The thin dotted line is a Salpeter IMF extended to low masses. Note the downturn of the IGIMFs at high masses. It results from the inclusion of a limiting maximum mass, $m_{\rm max} \leq m_{\rm max*}$, into our formalism.

differently shaded regions are for single burst, episodic and a constant SFR, respectively.

What implications beyond a reduction of the number of SNII do these findings have? The observed diversity of metallicities in different dwarf galaxies of rather similar mass (Mateo 1998; Garnett 2004) may be explained by this effect without invoking individually fitted effective yields as are needed in chemo-dynamical models with 'standard' IMFs (Lanfranchi & Matteucci 2004). On the other hand, our models indicate that massive spirals and ellipticals should show less variations in the IGIMF and thus metallicity due to their

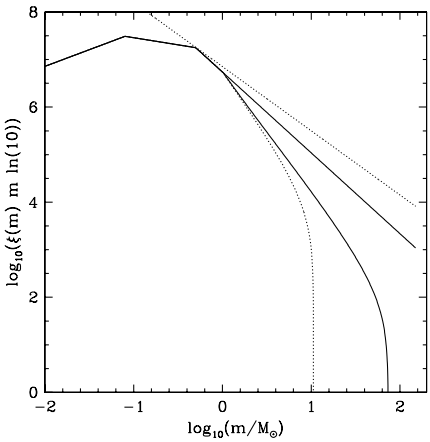

Figure 8. As Fig. 7 but only for two cases of the SFH: the burst case (solid line) and the low continuous case (thick dotted line), assuming $\alpha = 2.70$.

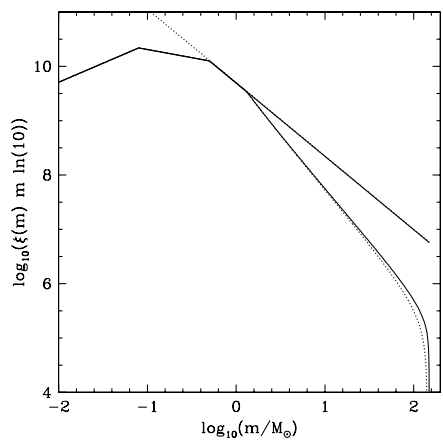

Figure 9. As Fig. 7 but for a galaxy with stellar mass $10^{10}\,M_{\odot}$ and canonical $\alpha = 2.35$. The IGIMF is only shown for a burst SFH (solid curve) and for a continuous SFH (dotted curve).

high average SFR which is actually what is observed in nearby galaxies (fig. 9 in Garnett 2004). Current available models for the chemical evolution of galaxies have difficulties to reproduce the chemical abundances in disc galaxies with a standard galaxial Salpeter IMF, as it produces too many metals (Portinari et al. 2004). This problem may be resolvable by the model presented here but detailed chemo-dynamical calculations incorporating our approach need to be computed. Finally, the mass-to-light ratia of galaxies are too low for models that assume invariant galaxial Salpeter IMFs; the real M/L ratia are larger.

4. Conclusions

• IGIMFs are steeper than the stellar IMF.
• Therefore there are significantly fewer SNII per G-type star per galaxy.
• Chemical enrichment and M/L ratios of galaxies calculated with an invariant Salpeter IMF are wrong.
• The IGIMFs vary from galaxy to galaxy.
• Dwarf galaxies show the largest variations: $3.1 \lesssim \alpha_{\rm IGIMF} \lesssim 3.6$ for $\alpha_{3,\rm true} = 2.35$ (Salpeter) and $\beta = 2.35$.
• The sensitivity of the IGIMF on the SFH increases with α_3. The true value of $\alpha_{3,\rm true}$ for the stellar IMF may actually be significantly larger than 2.35.
• Understanding the corrections for unresolved multiples on the derivation of the high-mass part of the stellar IMF is of fundamental importance!

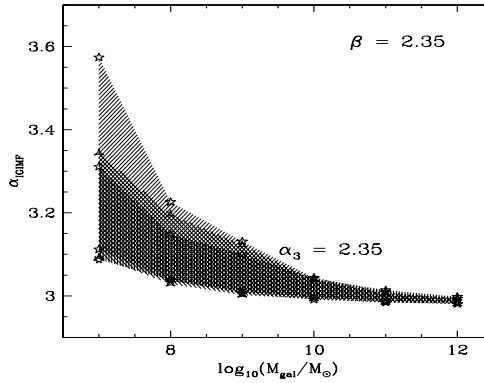

Figure 10. The resulting IGIMF slopes above $1\,M_{\odot}$ are shown in dependence of stellar galaxy mass for different models, as indicated. The lower bounds of the shaded areas are for an initial SF burst forming the entire stellar galaxy while the upper bounds are derived for a continuous SFR. The various symbols correspond to calculated models. Symbols lying within the shaded area correspond to models with an episodic SFH.

Acknowledgement This work is being supported by DFG grant KR1635/3-1.

References

Barrado y Navascués D., et al., 2001, ApJ, 546, 1006
Chabrier G., 2001, ApJ, 554, 1274
Elmegreen B.G., 1999, ApJ, 515, 323
Elmegreen B.G., 2004, MNRAS, 342
Garnett D.R., 2004, In: Cosmochemistry. eds. C. Esteban et al. (CUP), 171
Hambly N.C., et al. , 1999, MNRAS, 303, 835
Hunter D. A., et al., 2003, AJ, 126, 1836
Kroupa P., 2001, MNRAS, 322, 231
Kroupa P., 2002, Science, 295, 82
Kroupa P., Bouvier J., Duchêne G., Moraux E., 2003, MNRAS, 346, 354
Kroupa P., Tout C. A., Gilmore G., 1993, MNRAS, 262, 545
Kroupa P., Weidner C., 2003, ApJ, 598, 1076
Kroupa P., Aarseth S., Hurley J., 2001, MNRAS, 321, 699
Lada C. J., Lada E. A., 2003, ARAA, 41, 57
Lanfranchi G.A., Matteucci F. 2004, MNRAS, 351, 1338
Larsen S.S., 2001, in Extragalactic Star Clusters, IAU Symp. Ser. 207
Larsen S.S., 2002, AJ, 124, 1393
Larson R.B., 1998, MNRAS, 301, 569
Massey P., 1998, in The Stellar Initial Mass Function, eds. G. Gilmore & D. Howell (San Francisco: ASP), 17
Mateo M., 1998, ARA&A, 36, 435

Miller G. E., Scalo J. M., 1979, ApJS, 41, 513
Moraux E., Kroupa P., Bouvier J., 2004, A&A, 426, 75
Portinari L., Sommer-Larsen J., Tantalo R. 2004, MNRAS, 347, 691
Sagar R., Richtler T., 1991, A&A, 250, 324
Salpeter E. E., 1955, ApJ, 121, 161
Scalo J. M., 1986, Fundam. Cosmic Phys., 11, 1
Scalo J.M., 1998, in The Stellar Initial Mass Function, eds. G. Gilmore & D. Howell (San Francisco: ASP), 201
Reid I. N., Gizis J. E., Hawley S. L., 2002, AJ, 124, 2721
Weidner, C., Kroupa, P., 2004, MNRAS, 348, 187
Weidner C., Kroupa P., Larsen S. S., 2004, MNRAS, 350, 1503
Yuan J.W., 1992, A&A, 261, 105
Zhang Q., Fall S. M., 1999, ApJ, 527, L81

Figure 11. A bunch of IMFs: Hollenbach, Scalo, Chabrier, Kroupa.

ON THE FORM OF THE IMF: UPPER-MASS CUTOFF AND SLOPE

M.S. Oey[1,2] and C.J. Clarke[3]
[1]*Lowell Observatory, 1400 W. Mars Hill Rd., Flagstaff, AZ 86001, USA*
[2]*University of Michigan, Dept. of Astronomy, Ann Arbor, MI 48109, USA*
[3]*Institute of Astronomy, Madingley Road, Cambridge CB3 0HA, England, UK*

Abstract We evaluate the existence of an upper-mass cutoff based on statistics of the upper IMF in observed OB associations. We also examine how the relationship between the cluster mass range and stellar mass range affects the observed field star IMF slope.

1. The Upper-mass Limit

The existence and value of an upper-mass limit to the IMF are of fundamental intrinsic interest: how massive can the largest stars be? What physical processes dominate the formation of the highest-mass stars? The upper-mass limit is also of vital importance for interpreting integrated luminosities and feedback processes of stellar populations, galaxies, and star-forming regions. In recent years, studies of super star clusters and conditions in the early Universe have revitalized interest in the upper-mass limit.

Weidner & Kroupa (2004) show that the rich cluster R136a in the 30 Doradus star forming region has an upper-mass cutoff around 150 $M_\odot$. They use statistical arguments to show that, for a Salpeter (1955) IMF slope of –1.35, a value confirmed by Massey & Hunter (1998), stars having masses $\gtrsim 750 M_\odot$ are expected in R136a. In contrast, its most massive stars are only around 150 – 200 $M_\odot$ (Massey & Hunter 1998). Figer et al. (2002) use similar arguments to show that the Arches cluster near the Galactic Center also has an upper-mass cutoff around the same value. While there is a bit of uncertainty in the expected lifetimes of extremely high-mass stars, both R136a and the Arches are young enough that they should retain even the most massive members.

Here, we summarize work (Oey & Clarke 2004) that generalizes analysis of the upper IMF for any OB associations with well-determined star counts and stellar mass estimates. We can write the expectation value for the highest

E. Corbelli et al. (eds.), The Initial Mass Function 50 Years Later, 187–190.

stellar mass in terms of the number of stars in the cluster $N_\star$ and the IMF upper-mass limit $M_{\rm up}$ as:

$$\langle m_{\rm max} \rangle = M_{\rm up} - \int_{m_{\rm lo}}^{M_{\rm up}} \left[\int_{m_{\rm lo}}^{M} \phi(m)\, dm \right]^{N_\star} dM \quad . \tag{1}$$

Massey et al. (1995) compiled a census of stars having $m \geq 10$ M$_\odot$ in OB associations of the Galaxy and Magellanic Clouds. Treating the IMF as a strict probability distribution function, we may consider the total ensemble of these stars for associations younger than 3 Myr (the minimum stellar life expectancy), and compute the expectation value of $m_{\rm max}$. For a total of 263 stars in the associations Berkeley 86, NGC 7380, IC 1805, NGC 1893, NGC 2244, Tr 14/16, LH 10, and LH 117/118, we find $m_{\rm max} \sim 450$ M$_\odot$, for a true $M_{\rm up} = 1000$ M$_\odot$. In contrast, the highest-mass stars seen in any of these clusters are around 120 M$_\odot$. Adding in R136a, which was studied using a consistent analysis by the same group (Massey & Hunter 1998), the grand total of stars having $m \geq 10$ M$_\odot$ in the considered ensemble increases to a lower limit of 913, and corresponding $m_{\rm max} \sim 650$ M$_\odot$ for $M_{\rm up} = 1000$ M$_\odot$. As mentioned above, the observed $m_{\rm max} \sim 150 - 200$ M$_\odot$. Thus, the upper-mass limit is not even close to 1000 M$_\odot$, much less infinity.

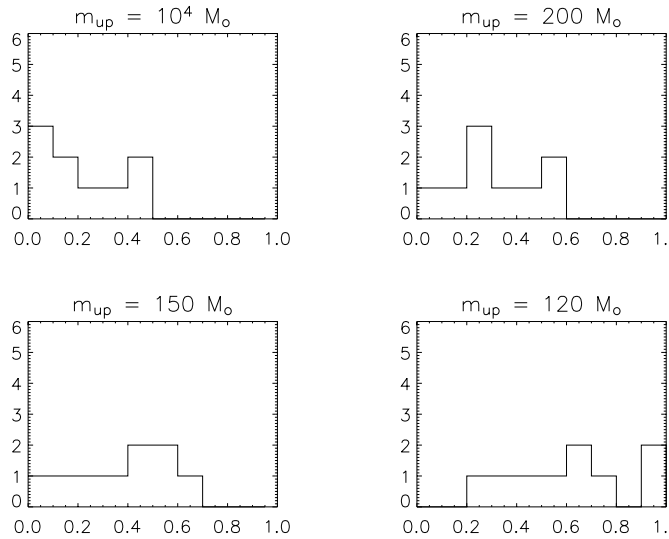

Figure 1. Distribution of probabilities for obtaining the observed $m_{\rm max}$ for the given $M_{\rm up} = 10^4,\ 200, 150,$ and 120 M$_\odot$ in the considered sample of OB associations.

We can also consider the associations individually, and estimate, for a given universal $M_{\rm up}$, the probabilities of the observed values of $m_{\rm max}$ in these clus-

ters. Figure 1 shows the probability distributions for the observed $m_{\rm max}$ for $M_{\rm up} = 10^4$, 200, 150, and 120 $\rm M_\odot$. A uniform distribution is expected for the true $M_{\rm up}$, thus we see that the probabilities of obtaining the observed distributions for the above values of $M_{\rm up}$, respectively, are $P < 0.002$, < 0.02, < 0.12, and < 0.47. This analysis thus also indicates an empirical upper-mass limit $M_{\rm up} \sim 120$ $\rm M_\odot$.

2. Slope of the Field Star IMF

Turning now to the power-law slope of the IMF, Kroupa & Weidner (2003; see also this volume) show that statistical effects can cause the effective IMF of individual field stars to be steeper than the intrinsic, universal value seen in clusters, and that the degree of steepening is a function of the intrinsic cluster IMF slope. Here we demonstrate that the dominant drivers of this effect are the limits in the relative mass ranges for the stars ($m_{\rm lo}$ and $M_{\rm up}$) and the clusters ($M_{\rm lo}$ and $M_{\rm up}$).

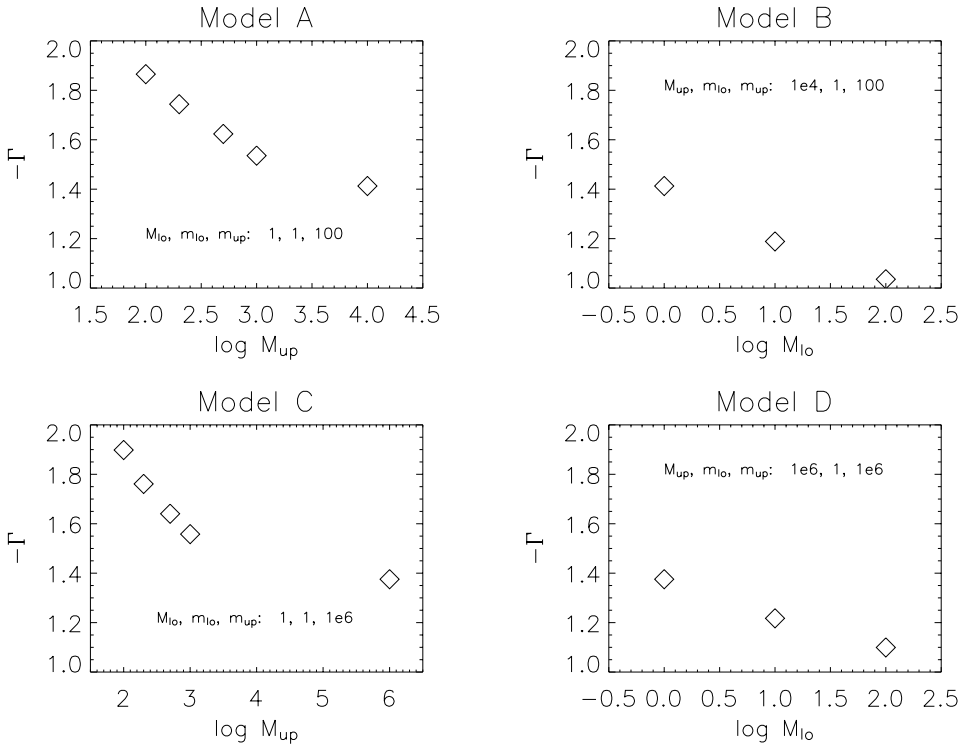

Figure 2. Models for the aggregate field IMF slope, as a function of relative stellar mass range and cluster mass range (see text).

Figure 2 shows the behavior of the effective field star IMF slope as a function of varying the relative mass limits for the stars and clusters. These results are derived from Monte Carlo models that assume a universal input IMF slope of $\Gamma = -1$ for all stars, where

$$N(m)\, dm \propto m^{1+\Gamma}\, dm \quad . \tag{2}$$

Model sets A and B adopt a stellar mass range of 1 to 100 $M_\odot$, and Model sets C and D adopt a stellar mass range of 1 to 10^6 $M_\odot$. Model sets A and C vary the cluster upper-mass limit $M_{\rm up}$ on the abscissa. The circled values show the models for which the cluster mass range is the same as the stellar mass range. Set A shows that for $M_{\rm up} \gg M_{\rm up}$, the effective field star IMF slope approaches the intrinsic, input value of $\Gamma = -1$. However, for $M_{\rm up} \sim M_{\rm up}$, the effective field star slope is steeper, since small clusters have masses below the allowed masses of large stars. This effect is also pronounced in Set C, where the stellar mass range is several decades larger. The steepening slopes approach a value of $\Gamma = -2$, since the effect is that of drawing twice from the $\Gamma = -1$ distribution. Model sets B and D show similar effects by varying the cluster lower-mass limit $M_{\rm lo}$: as the lower limit for the cluster masses increases relative to the stellar mass range, the effective Γ approaches the intrinsic value of –1. This happens as the stellar mass range is less impeded by the given cluster mass range.

Acknowledgments We are pleased to acknowledge discussions with Don Figer and Pavel Kroupa. Many thanks to the organizers for the opportunity to present this work.

References

Figer, D. F., et al. 2002, ApJ, 581, 258
Kroupa, P. & Weidner, C. 2003, ApJ, 598, 1076
Massey, P. & Hunter, D. 1998, ApJ, 493, 180
Massey, P., Johnson, K. E., & DeGioia-Eastwood, K. 1995, ApJ, 454, 151
Oey, M. S. & Clarke, C. J. 2004, in preparation
Salpeter, E. E. 1955, ApJ, 123, 666
Weidner, C. & Kroupa, P. 2004, MNRAS, 348, 187

EVIDENCE FOR A FUNDAMENTAL STELLAR UPPER MASS LIMIT FROM CLUSTERED STAR FORMATION

Carsten Weidner and Pavel Kroupa
Observatory of the University of Bonn, Auf dem Hügel 71, D-53121 Bonn, Germany
cweidner@astro.uni-bonn.de, pavel@astro.uni-bonn.de

Abstract It is shown here that if the stellar initial mass function (IMF) is a power-law with a Salpeter exponent ($\alpha = 2.35$) for massive stars then the richest very young cluster R136 seen in the Large Magellanic Cloud (LMC) should contain stars with masses larger than $750\,M_\odot$. If, however, the IMF is formulated by consistently incorporating a fundamental upper mass limit of about $150\,M_\odot$ then the observed upper mass limit is arrived at readily even if the IMF is invariant. An explicit turn-down or cutoff of the IMF near $150\,M_\odot$ is not required; our formulation of the problem contains this implicitly. We are therefore led to conclude that a fundamental maximum stellar mass near $150\,M_\odot$ exists, unless the true IMF has $\alpha > 2.8$.

1. Results

Using the canonical stellar IMF conveniently written as a multi-power-law, $\xi(m) \propto m^{-\alpha_i}$, with exponents $\alpha_0 = +0.30$ $(0.01 \leq m/\mathrm{M}_\odot < 0.08)$, $\alpha_1 = +1.30$ $(0.08 \leq m/\mathrm{M}_\odot < 0.50)$, $\alpha_2 = +2.35$ $(0.50 \leq m/\mathrm{M}_\odot < 1.00)$ and $\alpha_3 = +2.35$ $(1.00 \leq m/\mathrm{M}_\odot < 150.00)$, together with the assumption of the existence of a fundamental stellar upper mass limit, it is possible to calculate the dependence of maximum mass a star can have in dependence of the mass of the stellar cluster it is born in (see § 1 in Weidner & Kroupa this proceedings). The resulting function of $m_{\max}$ in dependence $M_{\rm ecl}$ is shown in Fig. 1. Here are also two mass estimates for R136 indicated by two vertical lines. It is clearly visible that for exponents α_3 less the 2.8 the upper mass limit for stars in this cluster strongly differs between the limited and the unlimited case.

Fig. 2 visualises the dependencies of $m_{\max}$ on α_3 for the limited and the unlimited case for the two mass estimates for R136. In the overlapping part of the two shaded regions no predictions on the stellar mass limit can be made from our model.

E. Corbelli et al. (eds.), The Initial Mass Function 50 Years Later, 191–192.

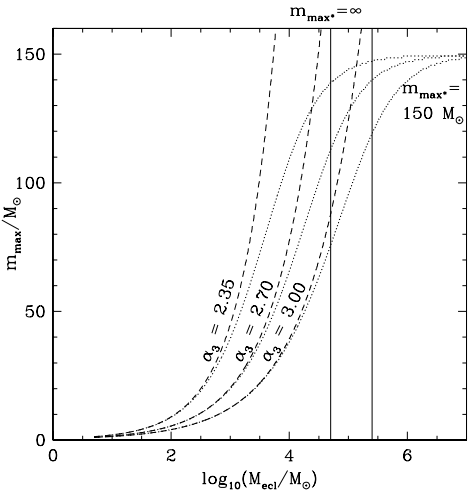

Figure 1. Maximal stellar mass versus cluster mass (logarithmic). Results are shown for different α_3 above $1\,M_\odot$ and for the limited ($m_{\max *} = 150\,M_\odot$) and unlimited case. The vertical lines mark the empirical mass interval for R136 (from Weidner & Kroupa 2004).

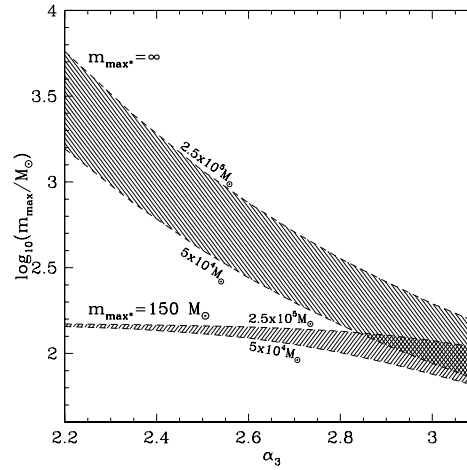

Figure 2. The mass limits ($m_{\max}$) as a function of the IMF exponent α_3 (above $1\,M_\odot$) in the limited case ($m_{\max *} = 150\,M_\odot$) and the unlimited case ($m_{\max *} = \infty$) for the two mass limits of R136.

2. Discussion and Conclusions

Thus, a consistent formulation of a fundamental stellar upper mass limit into the description of the IMF implies the highest mass a star can have in a massive cluster to be different to the case without such a limit. For low-mass clusters ($M_{\rm ecl} < 10^3\,M_\odot$) the differences of the solutions are negligible, but in the regime of the so-called 'stellar super-clusters' ($M_{\rm ecl} > 10^4\,M_\odot$) they become very large. The formulation presented here has the advantage of explaining the observations under the rather simple notion that all stars form in star clusters with the same universal IMF. For further details see Weidner & Kroupa (2004).

References

Weidner, C., Kroupa, P. 2004, MNRAS, 348, 187

MONTE-CARLO EXPERIMENTS ON STAR CLUSTER INDUCED INTEGRATED-GALAXY IMF VARIATIONS

Carsten Weidner and Pavel Kroupa
Observatory of the University of Bonn, Auf dem Hügel 71, D-53121 Bonn, Germany
cweidner@astro.uni-bonn.de, pavel@astro.uni-bonn.de

Abstract As most if not all stars are born in stellar clusters, the shape of the mass function of the field stars is not only determined by the initial mass function of stars (IMF) but also by the cluster mass function (CMF). In order to quantify this, Monte-Carlo simulations were carried out by taking cluster masses randomly from a CMF and then populating these clusters with stars randomly taken from an IMF. Two cases were studied. Firstly, the star masses were added randomly until the cluster mass was reached. Secondly, a number of stars, given by the cluster mass divided by an estimate of the mean stellar mass and sorted by mass, were added until the desired cluster mass was reached. Both experiments verified the analytical results of Kroupa & Weidner (2003) that the resulting integrated stellar initial mass function is a folding of the IMF with the CMF and therefore steeper than the input IMF above 1 $M_\odot$.

1. The Integrated Galactic Initial Mass Function from Clustered Star Formation

Kroupa & Weidner (2003) showed that the integrated galactic stellar initial mass function (IGIMF) is obtained by summing up the stellar IMFs contributed by all the star clusters that formed over the age of a galaxy. In their approach the mass of the most massive star in an embedded cluster with stellar mass $M_{\rm ecl}$ is calculated from by $1 = \int_{m_{\rm max}}^{m_{\rm max*}} \xi(m)\, dm$ and $M_{\rm ecl} = \int_{m_{\rm l}}^{m_{\rm max}} m\, \xi(m)\, dm$. The resulting function $m_{\rm max} = {\rm fn}(M_{\rm ecl})$ is quantified by Weidner & Kroupa (2004) who infer that there exists a fundamental upper stellar mass limit, $m_{\rm max*} \approx 150\, M_\odot$, because otherwise the populous cluster R136 would contain too many stars with m $> 100 M_\odot$.

E. Corbelli et al. (eds.), The Initial Mass Function 50 Years Later, 193–194.

2. Results from the Monte-Carlo simulations

In order to verify the above results we here perform Monte-Carlo simulations of star clusters and the stars within. 50 Million clusters are randomly chosen from a power-law CMF between 5 $M_\odot$ and 10^6 $M_\odot$ and with a Salpeter Index $\beta = 2.35$. These clusters are then filled with stars in two ways. First stars were taken randomly from a canonical Kroupa-IMF and their masses added until the sum equalled the chosen cluster (*long dashed line* in Fig. 1). In the second way, a number of stars given by the mass of the cluster divided by an estimate of the mean stellar mass are randomly chosen, sorted and then added - starting with the least massive star (*short dashed line* in Fig. 1). The addition is terminated as soon as the cluster mass is reached, or the process is repeated if the cluster mass is not reached. The sorted IGIMF agrees very well with the semi-analytical results while the IGIMF from pure random adding shows a somewhat less steeper slope.

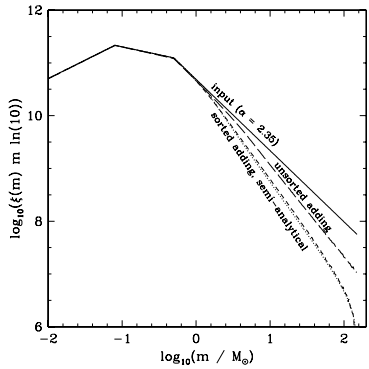

Figure 1: Solid line: Canonical stellar IMF with $\alpha = 2.35$ for $m > 1\,M_\odot$. Dotted line: IGIMF resulting from the semi-analytical approach with $\beta = 2.35$. Short dashed line: IGIMF gained after sorted adding of random stars. Long dashed line: IGIMF produced by unsorted adding of stars.

3. Discussion and Conclusions

- The Monte-Carlo simulations confirm the results of our semi analytical formalism.
- integrated galactic IMFs must always be steeper for $m > 1\,M_\odot$ than the stellar IMF that results from a local star-formation event.

References

Kroupa, P., & Weidner, C. 2003, ApJ, 598, 1076
Weidner, C., & Kroupa, P. 2004, MNRAS, 348, 187

THE INITIAL CONDITIONS TO STAR FORMATION: LOW MASS STARS AT LOW METALLICITY

Martino Romaniello[1], Nino Panagia[2] and Massimo Robberto[2]
[1]*European Southern Observatory, Karl-Schwarzschild-Strasse 2, D-85748 Garching bei München,Germany,*
[2]*Space telescope Science Institute, 3700 San Martin Drive, Baltimore, MD 21218, USA*
mromanie@eso.org,panagia@stsci.edu,robberto@stsci.edu

Abstract We have measured the present accretion rate of roughly 800 low-mass ($\sim 1 - 1.4\ M_{\odot}$) pre-Main Sequence stars in the field of SN 1987A in the Large Magellanic Cloud. The stars with statistically significant excesses are measured to have accretion rates larger than $\sim 1.5 \times 10^{-8} M_{\odot}\ yr^{-1}$ at an age of 12-16 Myrs. For comparison, the time scale for disk dissipation observed in the Galaxy is of the order of 6 Myrs.

1. Introduction

From an observational standpoint, most of the effort to characterize and understand the process of star formation has traditionally been devoted to nearby Galactic star forming regions, such as the Taurus-Auriga complex, Orion, etc. If this, on the one hand, permits one to observe very faint stars at the best possible angular resolution, on the other it is achieved at the expense of probing only a very limited set of initial conditions for star formation (all these clouds have essentially solar metallicity, e.g., Padget 1996). Studying the effects of a lower metallicity on star formation is also essential to understand the evolution of both our own Galaxy, in which a large fraction of stars were formed at metallicities below solar, and what is observed at high redshifts. With a mean metallicity of about a third solar, the Large Magellanic Cloud (LMC) provides an ideal environment for these kinds of studies:

- with a distance modulus of 18.57 ± 0.05 (see the discussion in Romaniello et al. 2000), the LMC is our closest galactic companion after the Sagittarius dwarf galaxy. At this distance one arcminute corresponds to about 15 pc and, thus, one pointing with a typical imaging instrument comfortably covers almost any star forming region in the LMC (10 pc see, e.g., Hodge 1988);

E. Corbelli et al. (eds.), The Initial Mass Function 50 Years Later, 195–198.

- the depth of the LMC along the line of sight is negligible, at least in the central parts we consider (van der Marel & Cioni 2001). All of the stars can, then, effectively be considered at the same distance, thus eliminating a possible spurious scatter in the Color-Magnitude Diagrams;
- the extinction in its direction due to dust in our Galaxy is low, about $\mathrm{E(B-V)} \simeq 0.05$ (Bessell 1991) and, hence, our view is not severely obstructed.

There is currently a widespread agreement that low-mass stars form by accretion of material until their final masses are reached (e.g., Bonnell et al. 2001 and references therein). As a consequence, the accretion rate is arguably *the* single most important parameter governing the process of low-mass star formation and its final results, including the stellar Initial Mass Function. Ground and HST-based studies show that there may be significant differences between star formation processes in the LMC and in the Galaxy. For example, Lamers et al. (1999) and de Wit et al. (2002) have identified by means of ground-based observations high-mass pre-Main Sequence stars (Herbig AeBe stars) with luminosities systematically higher than observed in our Galaxy, and located well above the "birthline" of Palla & Stahler (1990). They attribute this finding either to a shorter accretion time scale in the LMC or to its smaller dust-to-gas ratio. Whether such differences in the physical conditions under which stars form will generally lead to differences at the low-mass end is an open question, but Panagia et al. (2000) offer tantalizing evidence of a higher accretion also for LMC low-mass stars.

In this contribution we present the first measurement of the accretion rate onto low-mass, pre-Main Sequence stars outside of our Galaxy. The full details of our analysis are reported in Romaniello et al. (2004).

2. Measuring the accretion rate

The field of SN 1987A in the LMC was repeatedly imaged over the years with the WFPC2 on-board the HST to monitor the evolution of its Supernova remnant. We have taken advantage of this wealth of data and selected from the HST archive a uniform dataset providing broad-band coverage from the ultraviolet to the near infrared, as well as imaging in the $\mathrm{H}\alpha$ line.

The idea that the strong excess emission observed in some Galactic low-mass, pre-Main Sequence stars (T Tauri stars) is produced by accretion of material from a circumstellar disk dates back to the pioneering work of Lynden-Bell & Pringle (1974). The excess luminosity is, then, related to the mass accretion rate. In particular, the Balmer continuum radiation produced by the material from the disk as it hits the stellar surface has been used as an estimator of the mass infall activity (see, for example, Gullbring et al 1998 and references therein).

First, we have identified candidate pre-Main Sequence stars in the field of SN 1987A in the LMC through their Balmer continuum and Hα excesses. We have, then, derived the accretion rate onto the central star with the following equations:

$$\begin{cases} L_{acc} \simeq \frac{GM_*\dot{M}}{R_*}\left(1-\frac{R_*}{R_{in}}\right) \\ \log\left(\frac{L_{acc}}{L_\odot}\right) = 1.16\ \log\left(\frac{L_{\rm F336W,}exc}{L_\odot}\right) + 1.24 \end{cases} \quad (1)$$

The second equation is the Gullbring et al. (1998) empirical relation between the accretion luminosity L_{acc} and the Balmer excess luminosity, as transformed by Robberto et al. (2004) to the WFPC2 F336W filter. The reader is referred to Romaniello et al. (2004) for a thorough description of the derivation of $\dot{M}$.

When interpreted as pre-Main Sequence stars, the comparison of the objects' location in the HR diagram with theoretical evolutionary tracks allows one to derive their masses ($\sim 1-1.4\ M_\odot$) and ages ($\sim 12-16$ Myrs). At such an age and with an accretion rate in excess of $\sim 1.5\times10^{-8} M_\odot\ yr^{-1}$, these candidate pre-Main Sequence stars in the field of SN 1987A are both older and more active than their Galactic counterparts known to date. In fact, the overwhelming majority of T Tauri stars in Galactic associations seem to dissipate their accretion disks before reaching an age of about 6 Myrs (Haisch et al. 2001; Armitage et al. 2003). Moreover, the oldest Classical T Tauri star known in the Galaxy, TW Hydræ, at an age of 10 Myrs, *i.e.* comparable to that of our sample stars, has a measured accretion rate some 30 times lower than the stars in the neighborhood of SN 1987A Muzerolle et al. (2000).

The situation is summarized in Figure 1, where we compare the position in the age-$\dot{M}$ plane of the stars described here with that of members of Galactic star forming regions. An obvious selection bias that affects our census is that we only detect those stars with the largest Balmer continuum excesses, *i.e.* highest accretion rates. There might be stars in the field with smaller accretion rates, either intrinsically or because they were observed when the accretion activity was at a minimum, which fall below our detection threshold. This selection effect is rather hard to quantify, but it is clear that the locus of the accreting stars that we do detect in the neighborhood of SN 1987A is significantly displaced from the one defined by local pre-Main Sequence stars.

References

Armitage, P.J., Clarke, C.J., and Palla, F. 2003, MNRAS, 342, 1139
Bessell, M.S. 1991, A&A, 242, L17
Bonnell, I.A., Clarke, C.J., Bate, M.R., and Pringle, J. E. 2001, MNRAS, 324, 573
de Wit, W. J., Beaulieu, J. P., and Lamers, H.J.G.L.M. 2002, A&A, 395, 829
Gullbring, E., Hartmann, L., Briceño, C., and Calvet, N. 1998, ApJ, 492, 323
Lamers, H.J.G.L.M., Beaulieu, J. P., and de Wit, W. J. 1999, A&A, 341, 827

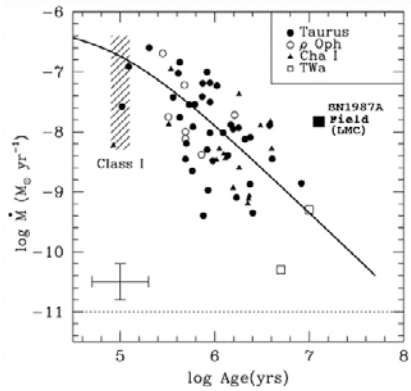

Figure 1 Mass accretion rate as a function of age for Classical T Tauri stars in dif ferent star forming regions (adapted from Muzerolle et al. 2000). Our result for the field of SN 1987A is mark ed with a black square.

Lynden-Bell, D., and Pringle, J.E. 1974, MNRAS, 168, 603

Haisch, K.E., Jr., Lada, E.A, and Lada, C.J. 2001, ApJ, 553, L153

Hartmann, L., Calvet, N., Gullbring, E., and D'Alessio, P. 1998, ApJ, 494, 385

Hodge, P.W. 1988, PASP, 100, 1051

Muzerolle, J., Calvet, N., Briceño, C., Hartmann, L., and Hillenbrand, L. 2000, ApJ, 535, L47

Padgett, D.L. 1996, AJ, 471, 874.

Palla, F., and Stahler, S. 1990, ApJ, 360, L47

Panagia, N., Romaniello, M., Scuderi, S., and Kirschner, R.P. 2000, ApJ, 539, 197

Robberto, M., Song, J., Mora Carillo, G. Beckwith, S.V.W., Makidon, R.B., and Panagia, N. 2004, ApJ, 606, 952

Romaniello, M., Salaris, M., Cassisi, S., and Panagia, N. 2000, APJ, 530, 738

Romaniello, M., Robberto, M., and Panagia, N. 2004, ApJ, 608, 220

van der Marel, R.P., and Cioni, M.R.L. 2001, AJ, 122, 1807

Figure 2 Martino Romaniello and Manuela Zoccali.

STELLAR ASSOCIATIONS IN THE LMC

Best tracers of the Initial Mass Function?

Dimitrios Gouliermis, Wolfgang Brandner and Thomas Henning
Max-Planck-Institut für Astronomie, Königstuhl 17, D-69117 Heidelberg, Germany
dgoulier@mpia-hd.mpg.de, brandner@mpia-hd.mpg.de, henning@mpia-hd.mpg.de

1. Description of the Data

We use archived HST/WFPC2 imaging data on an area, which covers the southwestern part of the large association LH 52 (Lucke & Hodge 1970) in the Large Magellanic Cloud (LMC). The photometry has been performed using the package HSTphot. The data quality parameters returned from this package for each detected source were used for the selection of the stars with the best photometry. The exposures performed in the WFPC2 filters *F555W* (V) and *F814W* (I) were used for the construction of the color-magnitude diagram (CMD) of the area (Fig. 1) and the mass function of the stars in this region (Fig. 2).

2. Results

The mass function (MF) of the detected stars is constructed by counting them between evolutionary tracks (Girardi et al. 2000) according to their positions in the HR Diagram. The transformation of the observed CMD (our measured $V-I$ colors and V magnitudes) into the theoretical HRD (effective temperatures and luminosities) was made through interpolation into a grid of synthetically derived colors and bolometric corrections. In these models the LMC metallicity was taken into account.

We constructed the MF of the stars in the whole WFPC2 field of view (FoV) on the association LH 52 (Fig. 2). Stellar masses down to ~ 0.6 M$_\odot$ with 50% completeness, were revealed. The MF of this area seems to follow different slopes for small (M $\lesssim 3$ M$_\odot$) and intermediate ($3 \lesssim$ M/M$_\odot \lesssim 9$) stellar masses. The MF slope was found to be much steeper than Salpeter's (1955) IMF. However, the MF of the stars of intermediate masses actually follows a typical IMF. The red giant clump shown in the CMD of Fig. 1 represents the population of the LMC field, which surely is observed within the FoV, and which also includes late-type main-sequence stars. The western part of the FoV was se-

E. Corbelli et al. (eds.), The Initial Mass Function 50 Years Later, 199–200.

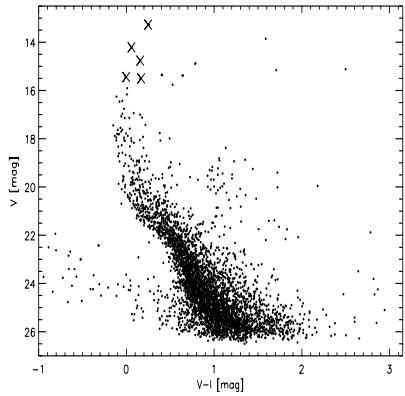

Figure 1. The CMD of all the stars found in the WFPC2 FoV on LH 52. The five bright main-sequence stars marked with crosses are early type OB stars, found earlier from ground-based photometry to have high UV emission (Hill et al. 1995). These stars, saturated in our photometry, indicate that the area is very young.

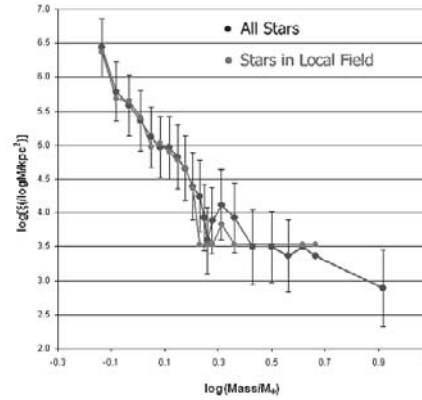

Figure 2. MF of the stars in the WFPC2 FoV on LH 52 for the whole stellar sample (black dots), and for those located in the area selected as the local field (grey dots). It is shown that the MF slope for small masses up to $\simeq 2\ M_{\odot}$ does not differ significantly from one sample to the other.

lected to represent the local background field, due to its emptiness, in order to be used for the field subtraction of the MF of the association. The MF of this local field was found to have the same slope as the MF of the whole stellar sample for masses $M \lesssim 2\ M_{\odot}$. This implies that a more careful treatment for the LMC field should be considered in order to construct the IMF of the stellar association. We have also reduced HST data on an empty nearby area, which is considered as general LMC field. They are currently being used with the technique of synthetic CMDs for disentangling the stellar contamination of the LMC field (Gouliermis, Brandner & Henning 2004). This will lead to the construction, for the first time, of the IMF of an extra-galactic stellar association down to sub-solar masses.

References

Hill, R. S., Cheng, K.-P., Bohlin, R. C., et al. 1995, ApJ, 446, 622
Girardi, L., Bressan, A., Bertelli, G., Chiosi, C. 2000, A&AS, 141, 37
Gouliermis, D., Brandner, W., & Henning, Th. 2004, in preparation
Lucke, P., & Hodge, P. W. 1970, AJ, 75, 171
Salpeter, E. E. 1955, ApJ, 121, 161

THE IMF LONG AGO AND FAR AWAY:

Faint Stars in the UMi Dwarf Spheroidal Galaxy

Rosemary F.G. Wyse
Johns Hopkins University, Department of Physics & Astronomy, Baltimore, USA
wyse@pha.jhu.edu

Abstract The dwarf spheroidal galaxy in Ursa Minor is apparently dark-matter dominated, and is of very low surface brightness, with total luminosity only equal to that of a globular cluster. Indeed its dominant stellar population is old and metal-poor, very similar to that of a classical halo globular cluster in the Milky Way Galaxy. However, the environment in which its stars formed was clearly different from that in the globular clusters in the Milky Way Galaxy – what was the stellar IMF in this external galaxy a long time ago? The fossil record of long-lived, low-mass stars contains the luminosity function, derivable from simple star counts. This is presented here. The mass function requires a robust mass-luminosity relation, and we describe the initial results to determine this, from our survey for eclipsing low-mass binaries in old open clusters. The massive star IMF at early times is constrained by elemental abundances in low-mass stars, and we discuss the available data. All data are consistent with an invariant IMF, most probably of Salpeter slope at the massive end, with a turnover at lower masses.

1. Introduction

The stellar IMF at high redshift is of great importance for a wide range of astrophysical problems, such as the ionization and enrichment of the intergalactic medium, the extragalactic background light, the visibility of galaxies and the rate at which baryons are locked-up into stars and stellar remnants. There are two complementary approaches to the determination of the IMF long ago and far away: one is to observe directly high redshift objects, and attempt inferences on the stellar IMF from the integrated spectrum and photometry, while the second approach analyses the fossil record in old stars at low redshift. The characterization of the stellar IMF in external galaxies, compared to that in the Milky Way, is a crucial step in deciphering the important physical processes that determine the distribution of stellar masses under a range of different physical conditions. The low-mass stellar IMF at the high redshifts

E. Corbelli et al. (eds.), The Initial Mass Function 50 Years Later, 201–208.

at which these stars formed is directly accessible through star counts, plus a mass-luminosity relation. The high-mass IMF at these high redshifts is constrained by the chemical signatures in the low-mass stars that were enriched by the supernovae from the high-mass stars. I will discuss both ends of the IMF at high redshift, in an external galaxy.

2. Extremely Old Stars

Simulations of galaxy formation within the framework of the 'concordance' (Λ)CDM cosmology agree that the first stars form within structures that are less massive than a typical L_* galaxy today (e.g. Kauffmann, White & Guiderdoni 1993; Cole et al. 2000). Large galaxies form hierarchically, through the merging and assimilation of such smaller systems. Satellite galaxies of the Milky Way are survivors of this merging (e.g. Bullock, Kravtsov & Weinberg 2000). The stars that formed at early times are found, at the present day, throughout large galaxies, and also in satellite galaxies. Environments with little subsequent star formation are the best places to find and study old stars – the stellar halo of the Milky Way, and a few of the dwarf spheroidal satellite galaxies.

2.1 The Ursa Minor Dwarf Spheroidal Galaxy

The dwarf spheroidal galaxy in Ursa Minor (UMi dSph), like all members of its morphological class (Gallagher & Wyse 1994), has extremely low surface brightness, with a central value of only $\sim$25.5 V mag/(sq.arcsec), or $\sim$2.5 $L_\odot$/pc^{-2}. The total luminosity is in the range $2 - 4 \times 10^5 L_{V,\odot}$ (Kleyna et al. 1998; Palma et al. 2003), equal to that of a luminous Galactic globular cluster. Again similar to a globular cluster, the Ursa Minor dSph contains little or no gas and has apparently not formed a significant number of stars for $\sim$ 12 Gyr (e.g. Hernandez et al. 2000; Carrera et al. 2002), or since a redshift $z \gtrsim 2$. The metallicity distribution of the stars is narrow, with a mean of [Fe/H] ~ -1.9 dex and a dispersion of ~ 0.1 dex (e.g. Bellazzini et al. 2002). The stellar line-of-sight velocity dispersion is $\sim$ 10 km/s (e.g. Wilkinson et al. 2004), sufficiently large that, unlike globular clusters, equilibrium models have a large mass-to-light ratio, $(\mathcal{M}/L)_V \gtrsim 50\ (\mathcal{M}/L)_{V,\odot}$, perhaps as high as several hundred in solar units if the mass is $\gtrsim 10^8\ \mathcal{M}_\odot$ (Wilkinson et al. 2004), indicating a non-baryonic dark halo. Non-equilibrium models are rather contrived and themselves fail to explain the data (e.g. Wilkinson et al. 2004). Models of the evolution of dwarf spheroidals are by no means well developed, but very likely the stars formed in an environment rather different than that of globular cluster stars, or of current star-forming regions in the disk of the Milky Way.

The distance of the Ursa Minor dSph is only $\sim$ 70 kpc, close enough that a determination of the luminosity function of low-mass main sequence stars

through star counts is feasible, particularly using the Hubble Space Telescope. The (unusually) simple stellar population of this dwarf spheroidal – essentially of single age, single metallicity – makes the derivation of the luminosity function from star counts a robust procedure. This determines the low-mass stellar IMF at redshifts of $\gtrsim 2$. High-resolution spectroscopy of the luminous evolved stars is also possible, yielding elemental abundances which constrain the high-mass stellar IMF that enriched the low-mass stars we observe.

3. The Faint Stellar Luminosity Function and Mass Function at Redshift $\gtrsim 2$

The (very) dominant stellar population in the UMi dSph is very similar to that of a classical Galactic halo globular cluster. The most robust constraint on the low-mass stellar IMF is then obtained by a direct comparison between the faint stellar luminosity functions of the UMi dSph and of representative globular clusters of the same age and metallicity, such as M15 and M92, observed in the same bandpasses, same telescope and detector. With the same stellar populations, this is a comparison between *mass* functions, and differences may be ascribed to variations in the low-mass IMF.

We therefore obtained deep images with the Hubble Space Telescope in a field close to the center of the UMi dSph, using STIS as the primary instrument (optical Long Pass filter), with WFPC2 (V_{606} and I_{814} filters) and NICMOS (NIC2/H-band) in parallel. The WFPC2 filters matched those of extant data for M15 and M92; we obtained our own STIS/LP and NIC2/H-band data for M15. Similarly exposed data for an 'off' field, at 2–3 tidal radii from the centre of UMi dSph, were also acquired. The detailed paper presenting the results from the full dataset is Wyse et al. (2002); preliminary results from a partial WFPC2 dataset were presented in Feltzing, Wyse & Gilmore (1999).

The images are not crowded and standard photometric techniques were used to derive the luminosity functions. For the WFPC2 data, the luminosity functions were based only upon stars (unresolved objects) that lie close to the well-defined UMi dSph main sequence locus in the colour-magnitude diagram (CMD; see Figure 1). The 'off' field CMD confirmed little contamination from Galactic stars. The STIS luminosity function was based on one band only, and we employed various approaches to background subtraction. The NICMOS data served only to exclude a hypothetical population of very red stars and will not be discussed further here. The extant WFPC2 data for the globular clusters (Piotto et al. 1997) are from fields at intermediate radii within the clusters, where effects of dynamical evolution on the mass function should be minimal.

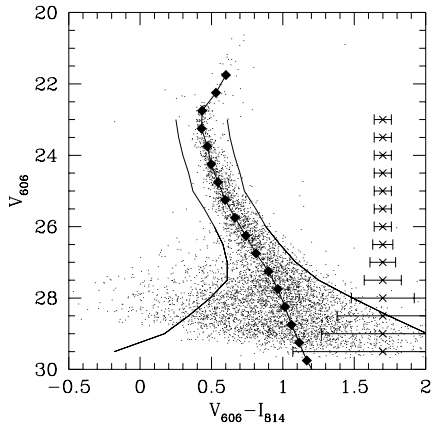

Figure 1

From Wyse et al. (2002). Colour-magnitude diagram for all UMi dSph stars from the three wide-field cameras on WFPC2. The full curves delineate the selection criteria for stars to be included in the luminosity function. The errorbars in each magnitude bin are shown at the right. The well-defined narrow main sequence is the main feature. The few blue stars close to the turn-off are probably blue stragglers, rather than younger stars. The distribution of stars across the main sequence is asymmetric, to the red, and is consistent with a normal population of binary stars.

3.1 Comparisons with Globular Clusters

The comparisons with the WFPC2 colour-magnitude based V-band and I-band luminosity functions are shown in Figure 2. We adopted 0.5 mag bins to have reasonable numbers in each bin, and to minimize effects of e.g. reddening and distance moduli uncertainties. The 50% completeness limits for the UMi dSph data are equivalent to absolute magnitudes of $M_{606} = +9.1$ and $M_{814} = +8.1$, which using the Baraffe et al. (1997) models *both* correspond to masses of $\mathcal{M} \sim 0.3\mathcal{M}_{\odot}$. The STIS/LP data provide an independent check, by both a direct LP-luminosity function comparison between M15 and UMi dSph, and a derived STIS-based I-band luminosity function. All show that the globular cluster stars and the UMi stars have indistinguishable faint luminosity functions, down to an equivalent mass limit of $\sim 0.3\mathcal{M}_{\odot}$ (see Wyse et al. 2002 for details).

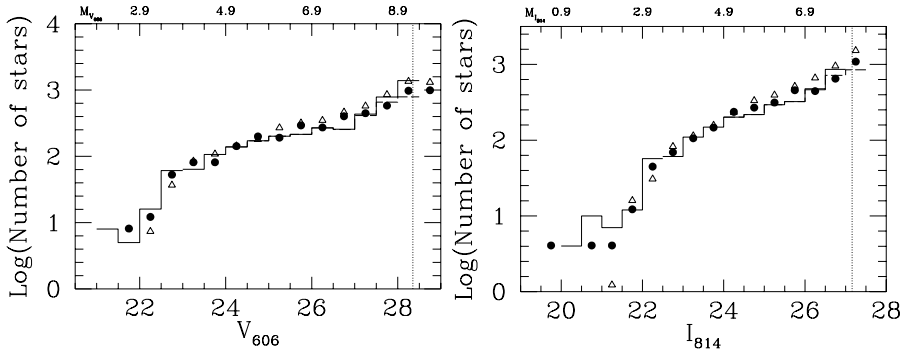

Figure 2. Based on figures in Wyse et al. (2002). Comparisons between the completeness-corrected Ursa Minor luminosity functions (histograms; 50% completeness indicated by the vertical dotted line) in the V-band (left panel) and the I-band (right panel) and the same for M92 (filled circles) and M15 (open triangles) (both taken from Piotto et al. 1997, renormalized and shifted to the same distance as the Ursa Minor dSph). The luminosity functions for the globular clusters and the dwarf spheroidal galaxy are indistinguishable.

We employed various statistical tests to quantify the agreement of the various datasets – e.g. STIS-derived I-band *vs.* WFPC2 I-band etc:

♡ Linear, least-square fits to the (log) counts as a function of apparent magnitude, using various ranges of magnitude and differing bin choices, consistently found agreement to better than 2σ.

♡ Kolmogorov-Smirnov tests on the unbinned data for a variety of magnitude ranges; the results depend on systematics such as the relative distance moduli, but again there is general agreement to better than 5% significance level.

♡ $\chi-$square tests were carried out on the binned data, using a variety of bin centers (maintaining 0.5 mag bin widths) and magnitude ranges and again agreement to better than 5% significance level.

The main result is that the underlying mass functions of low-mass stars in Galactic halo globular clusters and in the external galaxy the UMi dSph are indistinguishable. This is a comparison between two different galaxies, and systems of very different baryonic densities and dark matter content.

4. Low-Mass Stellar Mass Functions

Adopting the Baraffe et al. (1997) models, the 50% completeness limits for the luminosity functions of the stars in the UMi dSph correspond to $\sim 0.3\mathcal{M}_{\odot}$, and the mass function may be fit by a power law, with slope somewhat flatter than the Salpeter (1955) value, over the range we test, of $0.3 \lesssim \mathcal{M}/\mathcal{M}_{\odot} \lesssim 0.8$. This is consistent with the solar neighbourhood mass function over this mass range, and indeed the universal mass function that appears to be the conclusion of this meeting.

However, the light-to-mass transformation is not robustly defined for K/M dwarfs, especially as a function of age and metallicity. Calibration of this is best achieved by analysis of low-mass stars in detached eclipsing binary systems, and we have recently undertaken a photometric survey of open clusters to identify candidate low-mass binary systems to be followed up with spectroscopy for radial velocity curves; this forms the PhD thesis of Leslie Hebb at Johns Hopkins University.

Our sample consists of six open clusters of known age and metallicity (from the brighter turn-off stars), old enough to have low-mass stars on the main sequence, age $\gtrsim 2 \times 10^8$ yr, with the oldest being ~ 4 Gyr. We used both the Wide Field Camera on the 2.5m Isaac Newton Telescope and the Mosaic Camera on the Kitt Peak 4m telescope, each of which provide a field of view of $\sim 35' \times 35'$. The observing strategy we adopted was designed to enable the detection of a 0.05 mag amplitude eclipse in a target 0.3 $\mathcal{M}_{\odot}$ star, monitored on time scales of fraction of an hour, hours and days. The low probability of eclipse means that populous clusters must be observed for many days. We

expect our survey to find 3–5 low-mass eclipsing systems. The details of the survey are presented in Hebb, Wyse & Gilmore (2004).

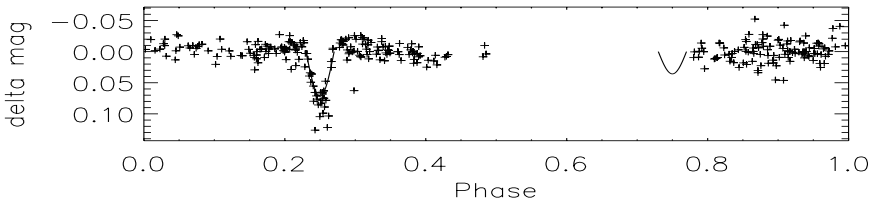

Figure 3. The phase-folded lightcurve for a candidate M-dwarf eclipsing system in the open cluster M35, with a period of just over 1 day. The crosses show all differential photometry measurements for this object collected in January 2002, January 2003 and February 2003. The solid line is a simple sine-wave fit to the measurements taken during the primary eclipse. The phase of the secondary eclipse is marked by the same sine function fit to the primary eclipse, but with half the amplitude.

The imaging data has all been acquired, differential photometry obtained and we are now analyzing the derived light curves. An example of the light curve of a candidate eclipsing low-mass system is shown in Figure 3; the candidate was identified by applying a box-fitting algorithm to the photometric time series. Our photometry, plus infrared data from 2MASS, is consistent with this being an M-dwarf system. We have applied for follow-up spectroscopic data, together with higher time-sampling photometric data, for this system and for our other candidates.

5. High-Mass Stellar Mass Functions

The high-mass stellar mass function long ago can be constrained by the elemental abundances in the long-lived low-mass stars that formed from gas that was enriched by the Type II supernovae from the massive stars of a previous generation (see e.g. review of Wyse 1998). Interpretation of the pattern of elemental abundances is easiest for low-mass stars that formed early in a star-formation event, and were enriched by *only* massive stars. Most of the dwarf spheroidal companions to the Milky Way have had extended star formation, and so are expected to show evidence in the elemental abundances for the incorporation of iron from long-lived Type Ia supernovae. The Ursa Minor dSph is the best candidate for having had a sufficiently short duration of star formation that a significant fraction of its low-mass stars formed prior to the onset of Type Ia supernovae in sufficient numbers to be noticed in the chemical elemental abundances; this time scale is uncertain, but likely to be of the order of 1–2 Gyr.

The elemental mix produced by a generation of massive stars depends on the massive-star mass function, because the yields of a given Type II supernova

depends on its mass. In particular, the α-element yields (nuclei formed by successive addition of a helium nucleus) vary more strongly with progenitor mass than does the iron yield (e.g. Figure 1 of Gibson 1998). There appears to have been surprisingly good mixing at early times, at least in the stellar halo of the Milky Way (see the remarkably low scatter in the ratio of [α/Fe] at [Fe/H] $\lesssim -2.5$ in the sample analysed by Cayrel et al. 2004), so that a well-defined value of [α/Fe] is produced by a generation of massive stars of given IMF. This is seen as the 'Type II plateau' in [α/Fe] for metal-poor Galactic stars.

The available elemental abundance data for a handful of individual stars in the UMi dSph are consistent with the same value for the Type II plateau as seen in stars of the Milky Way (Shetrone et al. 2001), with some downturn for more metal-rich stars, as expected if there is an age spread of 1–2 Gyr and an age-metallicity relationship. The simplest interpretation is that the high-mass IMF was the same in the UMi dSph as in the Galaxy – and that IMF is a power-law with Salpeter (1955) slope.

Most of the stars in the other dwarf spheroidals have low values of [α/Fe], consistent with a standard – Salpeter – IMF for massive stars and an extended star formation history, as implied by their colour-magnitude diagram (see e.g. Venn et al. 2004).

6. Conclusions

The fossil record in low-mass stars at the present time allows the derivation of the stellar IMF at high redshift. The low-mass luminosity function is accessible through star counts, most robustly in a system with a simple stellar population. We have found that the low-mass IMF is invariant between globular clusters in the halo of the Milky Way and an external galaxy, the dwarf spheroidal in Ursa Minor. The underlying mass function is apparently the same as that for present-day star formation in the local disk of the Milky Way. The low-mass IMF is remarkably invariant, over a broad range of metallicities, age, star-formation rate, baryonic density, dark matter content – indeed most of the parameters that *a priori* one might have expected to be important in determining the masses of stars. The high-mass IMF is also apparently independent of these parameters. This invariance is particularly surprising if the Jeans mass plays an important role.

Acknowledgments I thank my colleagues and collaborators Sofia Feltzing, Jay Gallagher, Gerry Gilmore, Leslie Hebb, Mark Houdashelt and Tammy Smecker-Hane for their contributions to the results described here. I would also like to thank the tireless organizers of this stimulating meeting for inviting me.

References

Baraffe, I., Chabrier, G., Allard, F. & Hauschildt, P. 1997, A&A, 327, 1054
Bullock, J., Kravtsov, A. & Weinberg, D. 2000, ApJ, 539, 517
Bellazzini, M., Ferraro, F., Origlia, L., Pancino, E. et al. 2002, AJ, 124, 3222
Carrera, R., et al. 2002, AJ, 123, 3199
Cayrel, R. et al. 2004, A&A, 416, 1117
Cole, S., Lacey, C., Baugh, C. & Frenk, C. 2000, MNRAS, 319, 168
Feltzing, S., Wyse, R.F.G. & Gilmore, G. 1999, ApJL, 516, 17
Gallagher, J.S. & Wyse, R.F.G. 1994, PASP, 106, 1225
Gibson, B. 1998, ApJ, 501, 675
Hebb, L., Wyse, R.F.G. & Gilmore, G. 2004, AJ, December issue (astro-ph/0409289)
Hernandez, X., Gilmore, G. & Valls-Gabaud, D. 2000, MNRAS, 317, 831
Kauffmann, G., White, S.D.M. & Guiderdoni, B. 1993, MNRAS, 264, 201
Kleyna, J., Geller, M., Kenyon, S., Kurtz, M. & Thorstensen, J. 1998, AJ, 115, 2359
Palma, C., Majewski, S., et al. 2003, AJ, 125, 1352
Piotto, G., Cool, A. & King, I. 1997, AJ, 113, 1345
Salpeter, E.E. 1955, ApJ, 121, 161
Shetrone, M., Côté, P. & Sargent, W. 2001, ApJ, 548, 592
Venn, K. et al. 2004, AJ, 128, 1177
Wilkinson, M. et al. 2004, ApJ, 611, L21
Wyse, R.F.G. 1998, in The Stellar IMF, ASP Conf Ser 142, 89
Wyse, R.F.G. et al. 2002, New Ast, 7, 395

Figure 4. Rosy Wyse, Timo Prusti and Francesco at Brunello tasting in the Montalcino's fortress.

THE MASSIVE STAR IMF AT HIGH METALLICITY

Fabio Bresolin
Institute for Astronomy, 2680 Woodlawn Drive, Honolulu, USA
bresolin@ifa.hawaii.edu

Abstract The question of the variation of the upper IMF at high metallicity is briefly reviewed. I show recent results suggesting a revision in the definition of 'high metallicity' in extragalactic H II regions. I present preliminary results concerning constraints on the upper mass limit in metal-rich spiral galaxies derived from the detection of Wolf-Rayet stars in the spectra of their H II regions. The current evidence is in support of an IMF extending up to at least 60–70 $M_{\odot}$ at an oxygen abundance 1–1.5 times the solar value.

1. Questions asked

After roughly three decades since the pioneering work on the massive stellar content of extragalactic H II regions by Searle (1971) and Shields & Tinsley (1976), there is still space for discussions regarding the possible variation of the Initial Mass Function (IMF) properties at high metallicity. This question has been commonly investigated spectroscopically via the analysis of the nebular excitation produced by unresolved populations of stars, embedded in giant H II regions located within spiral galaxies. This method is prone to uncertainties, due to the model-dependent conclusions one can draw on the shape of the IMF. Despite the known presence of massive stars in the metal-rich Galactic center (see, for example, Figer in this volume) and the lack of evidence for variations of the IMF between the Milky Way and the comparatively metal-deficient Magellanic Clouds (Massey et al. 1995), we still need to investigate the possible dependence of the massive star IMF on additional factors, such as the star formation history, the stellar density, and the galactic Hubble type. Moreover, quantifying the chemical abundances in metal-rich star forming regions of spiral galaxies remains, perhaps somewhat surprisingly, an open issue.

In a recent review Schaerer (2003) covered several aspects of the massive star IMF, including the topic discussed in the current contribution. I therefore

E. Corbelli et al. (eds.), The Initial Mass Function 50 Years Later, 209–214.

concentrate on the most recent results and on some of the current work being done on the subject.

2. A different IMF needed?

The upper end of the mass function is loosely defined here as that tail composed by stars more massive than $20\,M_{\odot}$, i.e. O and B stars with effective temperatures above 25,000 K. Although rare, these stars have an important feedback effect on galactic evolution, via the energy and momentum transferred to the interstellar medium by stellar winds, as well as its chemical enrichment, during their whole lifetime up to the supernova deflagration finale. The rarity and the short lifetimes (only a few Myr) of massive stars imply that we must account for statistical effects in the random sampling of the upper IMF, and that the stellar ensemble under consideration needs to be very young.

The notion that stars more massive than a certain threshold do not form at high metallicity (approximately solar and above) derives from early observational trends in samples of extragalactic H II regions, combined with the accretion theory of Kahn (1974). The radial gradients in excitation, measured from the intensity of forbidden metal lines, and in the equivalent width of the nebular Hβ emission line in spiral galaxies led to the suggestion that the upper mass limit is lowered (Shields & Tinsley 1976) and that the slope of the IMF becomes steeper (Terlevich & Melnick 1981) at large metallicity. This idea has received support even recently from further optical and infrared spectroscopy of extragalactic H II regions (among others: Goldader et al. 1997, Bresolin et al. 1999, Thornley et al. 2000). This interpretation relies on the observed softening of the radiation field at high metallicity, seen, for example, from the decreasing He I λ5876/Hβ line ratio in the optical (Bresolin et al. 1999, 2004) and from small fine-structure line ratios (e.g. [Ne III]/Ne [II]) in the mid-IR (Rigby & Rieke 2004; see Leitherer in this volume).

By contrast, the UV spectral properties of regions of active star formation do not support the idea of a varying IMF with metallicity. In particular, the strengths and P Cygni profiles of wind resonance lines, such as C IV λ1550 and Si IV λ1400, in supposedly metal-rich starbursts can be modeled with a 'normal' Salpeter-slope IMF extending up to 100 $M_{\odot}$ (González Delgado et al. 2002). An additional direct probe for the presence of massive stars, the Wolf-Rayet (W-R) emission feature at 4660 Å, has been used to infer the extension of the IMF to large masses ($>$ 30–40 $M_{\odot}$) even at the highest metallicities sampled (Schaerer et al. 2000, Bresolin & Kennicutt 2002, Pindao et al. 2002).

The dichotomy in the IMF properties derived from *indirect* (analysis of nebular lines) and *direct* (UV lines, W-R features) investigation methods seems now to be, at least in part, the result of the inadequacy of the stellar atmosphere

models used in the past for the calculation of the ionizing flux output by hot and massive stars. As shown by González Delgado et al. (2002) and Rigby & Rieke (2004), the adoption of recent non-LTE stellar atmospheres, which include the effects of line-driven winds and line blocking from metals, into the evolutionary population synthesis models used for the interpretation of the spectra, leads to more standard conclusions regarding the upper IMF at high metallicity. In addition, complications arising from the effects of the nebular geometry and density structure of H II regions conjure to make the determination of IMF parameters from nebular lines alone uncertain at best.

3. What *is* metal-rich?

The determination of chemical compositions is a topic where nebular lines *do* provide an essential insight into the physical and evolutionary status of star-forming galaxies. Most of our knowledge of radial abundance gradients in spiral galaxies derives, in fact, from the analysis of forbidden lines in H II regions.

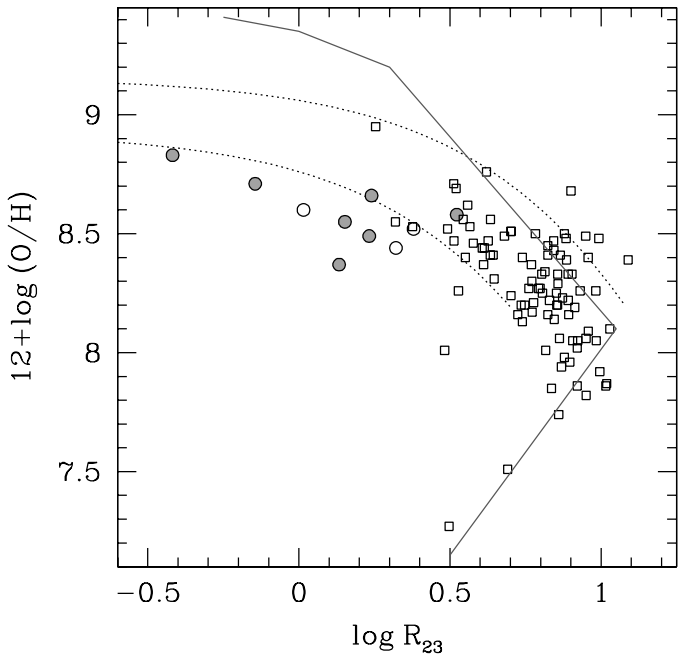

Figure 1. Comparison between extragalactic H II region O/H abundances measured from electron temperatures (dots) and from the semi-empirical abundance indicator R_{23}. The M51 data by Bresolin et al. (2004) are shown as solid circles. Two different calibrations are used for R_{23}: Edmunds & Pagel 1984 (full line) and Pilyugin 2001 (dotted lines), the latter for two representative values of the excitation parameter.

The presence of chemical abundance gradients in spiral galaxies is well-established, but recent extragalactic nebular abundance work is questioning the high end of the metallicity scale of previous investigations. Only recently the faint auroral lines used to determine direct electron temperatures of the nebular gas have become observable at high metallicity, where such lines become extremely faint, requiring large-aperture telescopes for their detection. In the case of M101, arguably the spiral galaxy with the best determination of an abundance gradient, Kennicutt et al. (2003) found a reduction of the central abundance by up to a factor of two with respect to indirect methods relying on strong emission lines (the R_{23} indicator of Pagel et al. 1979). In the metal-rich spiral M51, the measurement of the auroral lines [N II] λ5755 and [S III] λ6312 from Keck LRIS spectra by Bresolin et al. (2004) in a significant number of H II regions led to the determination of an extrapolated central abundance $\log(\mathrm{O/H}) = -3.28$, a roughly solar value, and a factor up to 2-3 times lower than indicated by previous investigations. Figure 1 shows how different calibrations of the R_{23} indicator exceed the abundance inferred from the electron temperatures, believed to represent the correct value.

This and similar results indicate that the term 'high metallicity' needs to be somewhat revisited when referring to extragalactic H II regions. Nebulae that in the past were considered to be of highly supersolar abundance, are very likely to be in the solar abundance regime, perhaps up to 50% higher in the most extreme cases. The results mentioned earlier concerning the massive IMF in our own Galaxy and the lack of evidence for observable differences in the metallicity range bracketed by the Small Magellanic Cloud and the Milky Way might then imply that no variation in the upper mass limit is to be expected in the majority of putative metal-rich star forming galaxies. We might still have to find an H II region with 2–3 times the solar oxygen abundance.

4. Usefulness of W-R features

The detection and measurement of W-R features (e.g. the 4660 Å 'bump') in the spectra of extragalactic H II regions at high metallicity, such as in the nucleus of the spiral galaxy M83 (Bresolin & Kennicutt 2002), offers a powerful method to constrain the upper mass cutoff of star-forming regions. This was elegantly shown by Pindao et al. (2002), who estimated the *minimum* mass of the most massive stars from model predictions of the equivalent width of the Hβ emission line, an evolutionary chronometer for the ionizing stellar clusters, at the beginning of the W-R phase.

We have recently obtained VLT spectra with the purpose of analyzing the nebular properties, as well as the massive stellar (W-R) content, of a sample of extragalactic H II regions contained in metal-rich galaxies (Schaerer, Bresolin, González Delgado & Stasińska, in preparation). Some preliminary results are

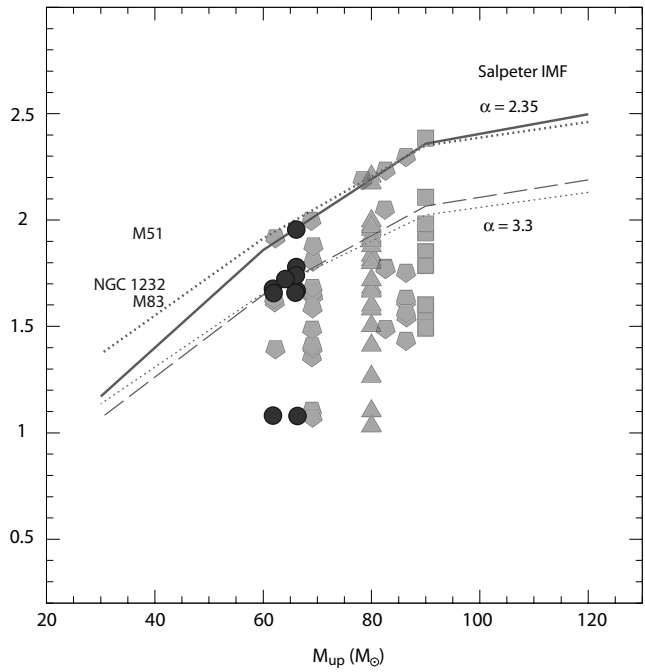

Figure 2. Observational data for H II regions at high metallicity with W-R features in their spectra are compared to the model predictions by Schaerer & Vacca (1998) for two different IMF slopes, and continuous and burst modes of star formation. By equating the observed Hβ emission line equivalent width to its predicted maximum at the onset of the W-R phase, one obtains a lower limit for the upper mass limit of the IMF, $M_{\rm up}$. The dark-grey symbols represent those H II regions for which we have reliably determined a solar oxygen abundance or above (in M51, M83 and NGC 1232) from measurements of their auroral lines. The light-grey symbols represent supposedly metal-rich objects from the compilation of Pindao et al. (2002, squares and triangles), and remaining H II regions from our VLT data.

displayed in Fig. 2, where I consider some of our new observational data about H II regions containing W-R features in NGC 1232, M83 and M51 (dark-grey circles), where the metallicity is confirmed from electron temperature measurements to be about solar, or slightly above that, together with the data compiled by Pindao et al. (2002, squares and triangles), and the other VLT targets for which our analysis is still incomplete (remaining light-grey symbols). Under the minimal assumption that in these objects the W-R phase just started (which corresponds to a maximum Hβ equivalent width), the evolutionary models of Schaerer & Vacca (1998) tell us that the IMF in these H II regions extends up to at least 60–70 $M_{\odot}$, for a Salpeter-slope IMF. If the abundance analysis of the remaining objects will confirm their high metallicity, which is currently just inferred from strong-line methods, we could push the minimum mass of

the upper mass limit to even higher values, in agreement with the findings at lower metallicities.

References

Bresolin, F., Kennicutt, R.C., & Garnett, D.R. 1999, ApJ, 510, 104
Bresolin, F. & Kennicutt, R.C. 2002, ApJ, 572, 838
Bresolin, F., Garnett, D.R., & Kennicutt, R.C. 2004, ApJ, 615, 228
Goldader, J.D., Joseph, R.D., Doyon, R., & Sanders, D.B. 1997, ApJ, 474, 104
González Delgado, R.M., Leitherer, C., Stasińska, G., & Heckman, T.M. 2002, ApJ, 580, 824
Kahn, F.D. 1974, A&A, 37, 149
Kennicutt, R.C., Bresolin, F., & Garnett, D.R. 2003, ApJ, 591, 801
Massey, P., Johnson, K.E., & DeGioia-Eastwood, K. 1995, ApJ, 454, 151
Pagel, B.E.J., Edmunds, M.G., Blackwell, D.E., Chun, M.S., & Smith, G. 1979, MNRAS, 189, 95
Pindao, M., Schaerer, D., González Delgado, R.M., & Stasińska, G. 2002, A&A, 394, 443
Rigby, J.R. & Rieke, G.H. 2004, ApJ, 606, 237
Searle, L. 1971, ApJ, 168, 327
Schaerer, D. 2003, in A Massive Star Odyssey: From Main Sequence to Supernova, ed. K. A. van der Hucht, A. Herrero & C. Esteban (San Francisco: ASP), p. 642
Schaerer, D., Guseva, N., Izotov, Y.I, & Thuan, T.X. 2000, A& A, 362, 53
Schaerer, D. & Vacca, W.D. 1998, ApJ, 497, 618
Shields, G.A. & Tinsley, B.M. 1976, ApJ, 203, 66
Terlevich, R. & Melnick, J. 1981, MNRAS, 195, 839
Thornley, M.D. et al. 2000, ApJ, 539, 641

Figure 3. Fabio Bresolin and Daniel Schaerer.

THE INITIAL MASS FUNCTION IN DISC GALAXIES AND IN GALAXY CLUSTERS: THE CHEMO-PHOTOMETRIC PICTURE

Laura Portinari
Tuorla Observatory, University of Turku, Väisälantie 20, FIN-21500 Pikkiö, Finland
lporti@utu.fi

Abstract The observed brightness of the Tully-Fisher relation suggests a low stellar M/L ratio and a "bottom-light" IMF in disc galaxies, but the corresponding efficiency of chemical enrichment tends to exceed the observational estimates. Either suitable tuning of the IMF slope and mass limits or metal outflows from disc galaxies must then be invoked.

A standard Solar Neighbourhood IMF cannot explain the high metallicity of the hot intra-cluster medium: a different IMF must be at work in clusters of galaxies. Alternatively, if the IMF is universal and chemical enrichment is everywhere as efficient as observed in clusters, substantial loss of metals must occur from the Solar Neighbourhood and from disc galaxies in general; a "non-standard" scenario challenging our understanding of disc galaxy formation.

1. The M_*/L ratio and the IMF in disc galaxies

Cosmological simulations of disc galaxy formation show good agreement with the observed Tully-Fisher relation, provided the mass–to–light ratio of the stellar component is as low as M_*/L_I=0.7–1; a low M_*/L is as well derived when locating onto the Tully–Fisher relation *real* disc galaxies of known stellar mass, such as the Milky Way or NGC 2841 (Fig. 1; Sommer-Larsen et al. 2003; Portinari et al. 2004a, hereinafter PST). Several other arguments support a low M_*/L in spiral galaxies:

Based on bar instability arguments, Efstathiou et al. (1982) suggest an upper limit of $M/L_B \leq 1.5\,h$ for discs, i.e. $M/L_B \leq 1$ for h=0.7 (h indicates the Hubble constant H_0 in units of 100 km sec^{-1} Mpc^{-1}).

The stellar M_*/L is also related to the "maximality" of discs, i.e. to whether they dominate or not the dynamics and rotation curves in the inner galactic regions. For his favoured sub–maximal disc model, Bottema (2002) finds $M_*/L_I \sim 0.82$; and even assuming maximal stellar discs, lower M_*/L ratios

E. Corbelli et al. (eds.), The Initial Mass Function 50 Years Later, 215–220.

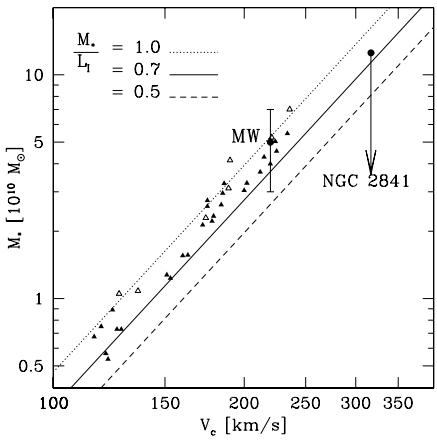

Figure 1. Observed Tully–Fisher relation for Sbc–Sc spirals (Dale et al. 1999; h=0.7), assuming different M_*/L_I. *Triangles*: simulated galaxies; *full dots*: Milky Way and NGC 2841.

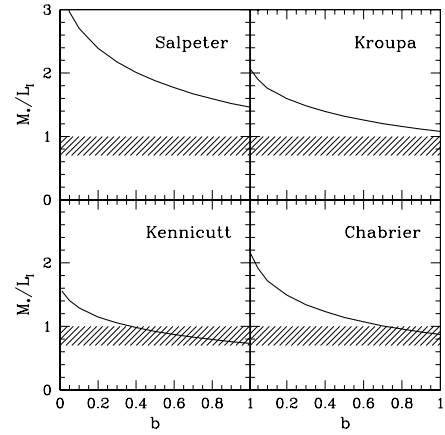

Figure 2. I–band M/L ratio at varying b–parameter of the SFH, for different IMFs. The red shaded area marks the range M_*/L_I=0.7–1 observed for Sbc–Sc discs (b=0.8–1).

are required than those predicted by the Salpeter Initial Mass Function (IMF)[1] (Bell & de Jong 2001).

Finally, recent dynamical studies of individual galaxies yield $M_*/L \sim 1$ in B, V, I for the Sc NGC 4414 (Vallejo et al. 2002) and M_*/L_I=1.1 for the disc of the Sab 2237+0305 (Huchra's lens, Trott & Webster 2002).

The M_*/L ratio of the stellar component of a galaxy, including both living stars and remnants, depends on the stellar IMF and on the star formation history (SFH) of the system.

IMF. Ample observational evidence in the Solar Neighbourhood, in globular and open clusters, and in the Galactic bulge show that the IMF presents a bend-over below $\sim 1 M_\odot$, and is "bottom–light" with respect to a single–slope Salpeter IMF (see the reviews by Scalo, Chabrier, Zoccali and De Marchi in this conference). A bend–over is expected as well from theory (see Session III in this conference).

In this paper, we consider the following IMFs: the "**Salpeter**" IMF (in the sense of footnote 1); the **Kroupa** (1998) IMF, derived for field stars in the Solar Vicinity; the **Kennicutt** IMF, derived from the global properties of spiral

[1]Criticisms to the Salpeter IMF is quite inappropriate at a conference in honour of Ed Salpeter himself. Let me thus underline that criticized in this paper is not the original result by Salpeter (1955), who derived the IMF slope between [0.4–10] $M_\odot$, but rather what has become in the literature the default meaning of "Salpeter IMF": a power law with Salpeter slope extending over [0.1–100] $M_\odot$.

galaxies (Kennicutt et al. 1994); the **Chabrier** (2001, 2002) IMF, derived from observations of local low-mass stars and brown dwarfs. (Further cases are discussed in PST.) With respect to Salpeter, the other IMFs are "bottom–light"; at the high-mass end, slopes range between the Salpeter ($x = 1.35$) and the Scalo one ($x = 1.7$).

SFH. The sequence of Hubble spiral types is a sequence of different SFHs in the discs, traced by the birthrate parameter $b = SFR/ < SFR >$ i.e. the ratio between the present and the past average star formation rate (SFR). The observational Tully–Fisher relation in Fig. 1, indicating M_*/L_I=0.7–1, refers to Sbc–Sc spirals whose "typical" SFH corresponds to b=0.8–1 (Kennicutt et al. 1994; Sommer–Larsen et al. 2003).

In PST we computed chemo–photometric models for disc galaxies predicting the M_*/L_I ratio for different IMFs, as a function of b. Fig. 2 shows that, while the Salpeter IMF yields far too high M_*/L, the other "bottom–light" IMFs do yield the observed M_*/L_I=0.7–1 for late–type spirals ($b = 0.8 - 1$), which agrees very well with our present understanding of the shape of the IMF at the low–mass end.

As to the implications for chemical evolution, some "bottom–light" IMFs (e.g. Kennicutt and Chabrier) are too efficient in metal production, as is evident from the gas fractions predicted by the models, far larger than observed (Fig. 3b): metal enrichment is so efficient that the models reach the typical metallicities of spirals without much gas processing.

This excessive metal production is readily understood since the enrichment efficiency of a stellar population, or its "net yield":

$$y \; = \; \frac{1}{1-R} \int_{M_i}^{M_s} p_Z(M)\, \Phi(M)\, dM \qquad (1)$$

is inversely proportional to the mass fraction 1–R that remains forever locked in low–mass stars and remnants: for bottom–light IMFs the locked–up fraction tends to be small. The yield can be reduced by reducing the number of the massive stars responsible for the bulk of the metal production, i.e. by tuning the upper mass limit (triangles in Fig. 3) or by a steep slope at the high-mass end: for example, the Kroupa IMF is bottom-light but it does not overproduce metals due to the steep Scalo slope above $M = 1\, M_\odot$ (see PST). A steep slope for the integrated field stars IMF is expected, in fact, if stars form in clusters of finite size from an intrinsically shallower IMF (Kroupa & Weidner 2003).

Alternatively, we need to invoke substantial outflows of metals from disc galaxies into the intergalactic medium, to reconcile the high enrichment efficiency with the observed metallicities and low gas fractions. This behaviour would be reminiscent of that of elliptical galaxies, responsible for the enrichment of the hot gas in clusters of galaxies.

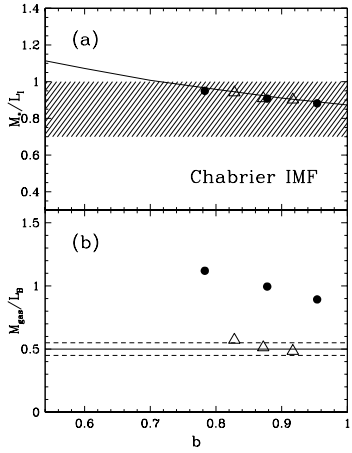

Figure 3. **(a)** M_*/L_I ratio for models with the Chabrier IMF. **(b)** Model gas fractions compared to the observed range (dashed lines). *Dots*: models with IMF mass range [0.1–100] $M_\odot$; *triangles*: models with IMF upper mass limit tuned at 32–33 $M_\odot$ to match the observed gas fraction; note that the effect on M_*/L is negligible.

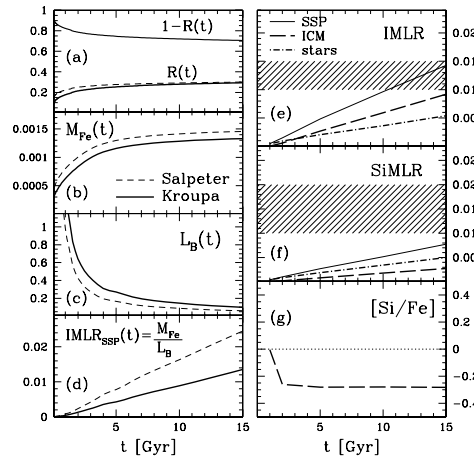

Figure 4. **(a–d)** Locked–up fraction, iron production, luminosity evolution and $IMLR_{SSP}$ for Salpeter and Kroupa IMFs. **(e–f)** Kroupa IMF: partition of metals into stars and ICM, compared to observations (shaded area, Finoguenov et al. 2000). **(g)** Predicted [Si/Fe] in the ICM with the Kroupa IMF.

2. The IMF in clusters of galaxies

Can a "standard" Solar Neighbourhood (SN) IMF account for the observed level of metal enrichment in clusters of galaxies? We can qualitatively address this question by comparing the respective "effective" yield y_{eff}, obtained as the ratio between the metals globally contained in the system and the mass in living stars and remnants; this is the observational counterpart of the theoretical yield y in Eq. 1:

$$y_{eff,SN} = \frac{Z_* \times M_* + Z_{gas} \times M_{gas}}{M_*} \sim \frac{Z_\odot \times M_* + Z_\odot \times (0.2\, M_*)}{M_*} = 1.2\, Z_\odot$$

$$y_{eff,\,cl} = \frac{Z_* \times M_* + Z_{ICM} \times M_{ICM}}{M_*} \sim \frac{Z_\odot \times M_* + 0.3\, Z_\odot \times (5 - 10\, M_*)}{M_*} = 2.5{-}4\, Z_\odot$$

The estimated metal enrichment efficiency in clusters is thus about 3 times larger than in the SN, and the chemical evolution of clusters is often modelled with non–standard IMFs (Portinari et al. 2004b, hereinafter PMCS; and references therein). On the other hand, the following arguments are often given in favour of a universal standard IMF: the Iron Mass–to–Light Ratio (IMLR) in clusters agrees with the predictions of the Salpeter IMF, and the observed [α/Fe] ratios in the ICM are compatible with those in the SN (Renzini et al. 1993; Renzini 1997, 2004; Ishimaru & Arimoto 1997; Wyse 1997).

In PMCS we demonstrated that a "standard" IMF (e.g. the Kroupa IMF) which reproduces the chemical properties of the SN, is unable to enrich the ICM to the observed levels. For a Single Stellar Population (SSP) we computed the rate of supernovæ of type II and type Ia, and the corresponding production of metals in time (Fig. 4b); the ratio between these and the evolving luminosity (Fig. 4c) gives the global IMLR$_{SSP}$, SiMLR$_{SSP}$ etc. relevant to the chosen IMF (Fig. 4d). Not all of the metals produced contribute to the ICM enrichment: a non–negligible fraction must be locked-up by subsequent stellar generations to build up the observed stellar metallicities Z_* of cluster galaxies. The amount of metals locked in the stellar component must be $M_{Z,*} = Z_* \times (1 - R)$, where $1 - R$ is the locked–up fraction consistent with the adopted IMF (Fig. 4a). Once the metals produced are properly partitioned between the stars and the ICM, it is evident that a standard IMF such as the Kroupa IMF cannot possibly reproduce the observed IMLR and SiMLR in the ICM (Fig. 4e,f): it does not match the *global* amount of metals observed in the ICM and it predicts significantly sub–solar [α/Fe] ratios, at odds with observations (Fig. 4g). Henceforth, observing solar [α/Fe] ratios in the ICM *per se* does not suffice to conclude that the same IMF is at play in both environments.

In Fig. 4d we also compare the global IMLR$_{SSP}$ for the Kroupa and the Salpeter IMF. The latter is about twice more efficient in metal production, and is known to be too efficienct to reproduce the SN (PST, PMCS and references therein; Romano, this conference); henceforth, though matching the IMLR in the ICM, it is not the same IMF as in the Milky Way. Besides, the Salpeter IMF (in the sense of footnote 1) fails at reproducing the observed αMLR in the ICM, also predicting significantly subsolar [α/Fe] ratios in the ICM (Matteucci & Vettolani 1988; Renzini et al. 1993; Pipino et al. 2002; PMCS).

3. Conclusions

A "standard" IMF suited to model the chemical evolution of the Solar Neighbourhood cannot account for the observed metal enrichment in clusters: either the IMF differs between the two environments, or the local IMF has a much higher yield than usually assumed. The latter option is in line with some of the "bottom–light" IMFs advocated in §1 to reproduce low disc M$_*$/L ratios. In this case, disc galaxies must disperse much of the metals they produce into the intergalactic medium, just like early type galaxies in clusters. However, substantial outflows would challenge our understanding of disc galaxy formation: disc star formation proceeds at a smooth, non burst–like pace and the observed "fountains" and "chimneys" do not have enough energy to escape the galactic potential; winds are far less plausible than from spheroids. Moreover, strong ongoing stellar feedback and outflows could significantly hamper the dynamical formation of galactic discs from the cool–out of halo gas.

The alternative scenario is a variable IMF with a higher yield in clusters than in disc galaxies. The IMF may vary after Jeans–mass dependence on redshift, and its variation should be more significant than expected from the increasing temperature of the cosmic background (e.g. Chabrier, this conference; Finoguenov et al. 2003; Moretti et al. 2003 and references therein); or, the IMF may be a universal function within star clusters, but generating statistically more high–mass stars in larger star clusters and in regimes of intense star formation like in massive ellipticals (Kroupa & Weidner 2003).

References

Bell E.F. & de Jong R.S., 2001, ApJ 550, 212
Bottema R., 2002, A&A 388, 809
Chabrier G., 2001, ApJ 554, 1274
Chabrier G., 2002, ApJ 567, 304
Dale D.A., Giovanelli R., Haynes M.P., et al., 1999, AJ 118, 1489
Efstathiou G., Lake G. & Negroponte J., 1982, MNRAS 199, 1069
Finoguenov A., David L.P. & Ponman T.J., 2000, ApJ 544, 188
Finoguenov A., Burkert A. & Böhringer H., 2003, ApJ 564, 136
Ishimaru Y., Arimoto N., 1997, PASJ 49, 1
Kennicutt R.C., Tamblyn P. & Congdon C.W., 1994, ApJ 435, 22 (KTC94)
Kroupa P., 1998, ASP Conf. Series vol. 134, p. 483
Kroupa P. & Weidner C., 2003, ApJ 598, 1076
Matteucci F., Vettolani P., 1988, A&A 202, 21
Moretti A., Portinari L. & Chiosi C., 2003, A&A 408, 431
Pipino A., Matteucci F., Borgani S. & Biviano A., 2002, NewA 7, 227
Portinari L., Sommer–Larsen J. & Tantalo R., 2004a, MNRAS 347, 691 (PST)
Portinari L., Moretti A., Chiosi C. & Sommer–Larsen J., 2004b, ApJ 604, 579 (PMCS)
Renzini A., 1997, ApJ 488, 35
Renzini A., 2004, in Clusters of galaxies: probes of cosmological structure and galaxy evolution, ed. J. Mulchaey et al. (Cambridge University Press), p. 261
Renzini A., Ciotti L., D'Ercole A. & Pellegrini S., 1993, ApJ 419, 52
Salpeter E.E., 1955, ApJ 121, 161
Sommer–Larsen J., Götz M. & Portinari L., 2003, ApJ 596, 47
Trott C.M. & Webster R.L., 2002, MNRAS 334, 621
Vallejo O., Braine J. & Baudry A., 2002, A&A 387, 429
Wyse R.F.G., 1997, ApJ 490, L69

STEEPER, FLATTER, OR JUST SALPETER? EVIDENCE FROM GALAXY EVOLUTION AND GALAXY CLUSTERS

Alvio Renzini
ESO, Garching, Germany
arenzini@eso.org

Abstract A single-slope *Salpeter* IMF overpredicts the stellar $M_*/L_{\rm B}$ ratio by about a factor of 2, which requires the IMF to be flatter below $\sim 1\,M_\odot$. On the other hand a Salpeter IMF for $M \gtrsim M_\odot$ predicts an evolution with redshift of the fundamental plane of ellipticals in clusters which is in agreement with the observations and a formation at $z \gtrsim 3$ for these galaxies. A *Salpeter* IMF for $1 \lesssim M \lesssim 40\,M_\odot$ also predicts the observed amount of heavy elements (oxygen and silicon) in clusters of galaxies.

1. Introduction

The most direct way of measuring the IMF is by stellar counts, a technique that can be applied only within a limited distance from us. On the other hand, much of galaxy properties – at low as well as at high redshift – depend on the IMF, including mass-to-light ratios, derived star-formation rates, feedback, metal enrichment, etc. Considering these properties enables us to gather strong constraints on the IMF for stellar systems and astrophysical situations that cannot be probed by stellar counts, and provides *sanity checks* for assumptions and theories of the IMF. In this talk I present the constraints on the IMF slope below $\sim 0.5M_\odot$, between ~ 1 and $\sim 1.4\,M_\odot$, and between ~ 1 and $\sim 25\,M_\odot$ that come respectively from the observed values of the $M_*/L_{\rm B}$ ratio of local elliptical galaxies, from the redshift evolution of the fundamental plane, and from the observed mass of heavy elements in clusters of galaxies. I will also emphasize the role played by the IMF in our attempts at mapping the cosmic history of star formation, and the build up of the overall stellar mass content of the universe. The parameters of the *concordance cosmology* are adopted throughout this paper, i.e., $\Omega_{\rm m} = 0.3$; $\Omega_\Lambda = 0.7$, and $H_\circ = 70$.

E. Corbelli et al. (eds.), The Initial Mass Function 50 Years Later, 221–230.

2. The Mass-to-Light Ratio of Ellipticals and the IMF Slope Below $\sim 1\,M_\odot$

Fig. 1 shows as a function of age the $M_*/L_{\rm B}$ ratio for simple stellar populations (SSP), i.e., assembly of coeaval stars all of the same (solar) chemical composition. SSP models are from Maraston (1998), while the use of other models would give essentially the same result. The mass-to-light ratio varies wildly depending on the assumed IMF, which in this case is described by a single slope power law $\phi(M) \propto M^{-s}$ for $0.1 < M < 100\,M_\odot$, where $s = 2.35$ corresponds to the *Salpeter* IMF (Salpeter 1955). Note that very large mass-to-light ratios are obtained for either very steep ($s = 3.35$) or very flat ($s = 1.35$) IMFs. In the former case the total stellar mass is dominated by the huge number of low mass stars, i.e., the IMF is **dwarf dominated**. In the latter case instead (at late times) most stellar mass is locked into remnants: black holes, neutron stars and white dwarfs, while low mass stars contribute very little to the mass budget, i.e., the top-heavy IMF leads to a **remnant dominated** mass. Of the three choices, the *Salpeter* slope gives the lowest values of $M_*/L_{\rm B}$. Yet, at an age of ~ 12 Gyr, appropriate for the the bulk stellar population of elliptical galaxies[1], the $M_*/L_{\rm B}$ ratio is a factor ~ 2 too high compared to the stellar mass of ellipticals as derived dynamically (e.g. van der Marel 1991). This excludes any single-slope IMF, hence the IMF must flatten with respect to the *Salpeter* value below $\sim 0.5 - 0.7\,M_\odot$, as indeed indicated by all direct stellar count in Disk and Bulge fields and in stellar clusters alike, and extensively reported at this meeting. For example, assuming $s = 2.35$ for $M > 0.6\,M_\odot$ and $s = 1.35$ for $M < 0.6\,M_\odot$ the $M_*/L_{\rm B}$ ratio is reduced by about a factor of 2, thus bringing SSP models in agreement with the observed values.

3. The Redshift Evolution of the Fundamental Plane, and the IMF Slope for $1 \lesssim M \lesssim 1.4\,M_\odot$

As is well known, elliptical galaxies tightly cluster around a plane in the space having for coordinates the central velocity dispersion (σ), the effective radius ($R_{\rm e}$) and the effective surface brightness ($\mu_{\rm e}$) (Djorgovski & Davis 1987; Dressler et al. 1987). This *fundamental plane* (FP) combines two structural/dynamical quantities (σ and $R_{\rm e}$) with the third ($\mu_{\rm e}$) which instead depends on luminosity, hence on the stellar population content of the galaxy and in particular on its age.

The slope of the IMF controls the rate of luminosity evolution of a SSP. The flatter the IMF the faster the luminosity decline past a burst of star formation.

[1]Compelling evidence has accumulated over the years indicating that the star-formation process in elliptical galaxies was virtually complete by $z \simeq 3$, corresponding to an age of ~ 12 Gyr (for an extensive review see Renzini 1999).

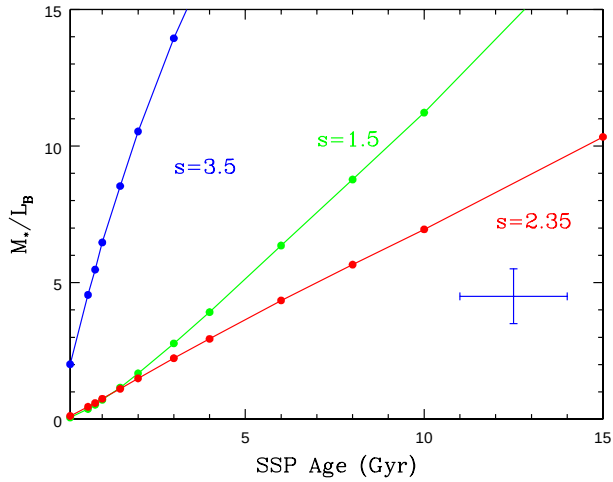

Figure 1. The time evolution of the stellar $M_*/L_{\rm B}$ ratio for solar metallicity simple stellar populations with various slopes (s) of the IMF (synthetic models from Maraston 1998). The cross on the right side of the figure gives the typical ranges for the $M_*/L_{\rm B}$ ratio of local elliptical galaxies and for the ages of their dominant stellar populations.

On the contrary, the steeper the IMF the slower such decline, as the light from the larger number of low-mass stars compensates for the progressive death of the more massive stars. As we look to higher and higher redshift ellipticals, we therefore expect them to depart from the local FP by an amount that depends on the slope of the IMF. Thus, if small ellipticals were to have a different IMF slope w.r.t. large ellipticals, with increasing redshift one would expect the small ellipticals to depart from the local FP by a different amount w.r.t. large ellipticals: the FP would **rotate** with increasing redshift (Renzini & Ciotti 1993). Fig. 2 shows that ellipticals in a cluster at $z = 0.58$ and another at $z = 0.83$ (corresponding to a lookback time of ~ 7 Gyr, or $\sim 1/2$ the age of the universe) align parallel to the FP defined by ellipticals in the COMA cluster (Wuyts et al. 2003): **the FP does not rotate**, hence there is no appreciable trend of the IMF with galaxy size, mass, or luminosity.

The shift in the FP shown in Fig. 2 actually corresponds to a change in the $M/L_{\rm B}$ ratio of the observed galaxies, and Fig. 3 shows such a change for the two mentioned clusters, plus a few others at various redshifts, including one at $z = 1.27$ (van Dokkum & Stanford 2003).[2] Overplotted is also shown the evolution with redshift of the $M_*/L_{\rm B}$ ratio of SSP models (from Maraston 1998) having assumed the SSPs formed at $z_{\rm F} = 5$. The various $M_*/L_{\rm B}$ ratios

[2]In the $z = 1.27$ cluster σ was measured for only two galaxies, and given the errors the slope of the FP could not be reliably measured, so only the zero-point shift is shown here.

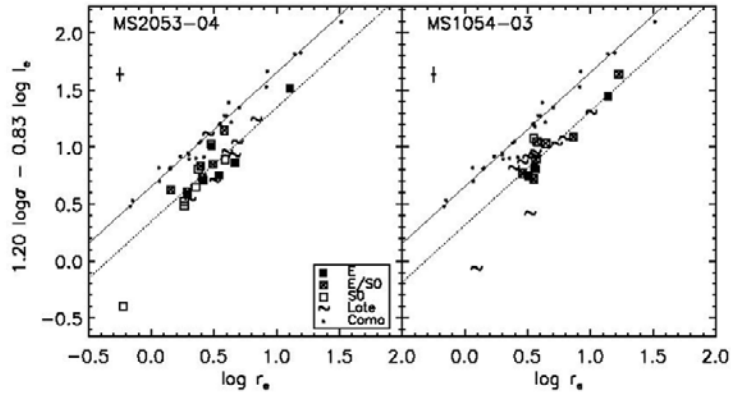

Figure 2. The fundamental plane of clusters MS2053-04 ($z = 0.58$) and MS1054-03 ($z = 0.83$) compared to the FP of Coma (Wuyts et al. 2003). Note that the slope of the FP appears to remain the same with increasing redshift, indicating that the slope of the IMF is independent of elliptical galaxy size, mass, or luminosity.

have been normalized to their value at $z = 0$, so as to emphasize their relative change with redshift.

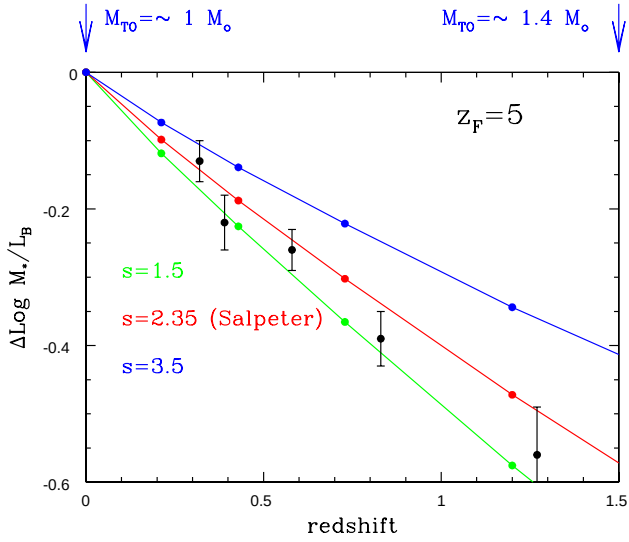

Figure 3. The evolution with redshift of the $M_*/L_{\rm B}$ ratio of simple stellar populations (SSP) of solar metallicity and various IMF slopes, normalized to its value at $z = 0$. A formation redshift $z_{\rm F} = 5$ is assumed for the SSPs. The lines refer to $s = 1.5$ (top), 2.35 (middle) and 3.5 (bottom). The data points refer to the shifts in the fundamental plane locations for clusters of galaxies at various redshifts (from van Dokkum & Stanford 2003). Note that for this assumed redshift of formation the stellar mass at the main sequence turnoff is $\sim 1.4\,M_\odot$ at $z = 1.5$ and $\sim M_\odot$ at $z = 0$, as indicated by the arrows.

At $z = 0$ elliptical galaxies ~ 12 Gyr old harbour stellar populations with $\sim 1\,M_\odot$ stars at the main sequence turnoff (MSTO). By $z = 1.5$ the precursors of such populations have an age of only ~ 3 Gyr, and correspondingly a higher mass at the MSTO, but not by much so. Specifically, the MSTO mass at an age of ~ 3 Gyr is $\sim 1.4 - 1.5\,M_\odot$, and therefore by following the evolution of the FP with redshift up to $z \sim 1.5$ (or equivalently of the mass-to-light ratio) we explore the IMF slope within the rather narrow mass interval $1 \lesssim M \lesssim 1.4\,M_\odot$. In practice, we measure the slope of the IMF near $M = M_\odot$.

Note that in Fig. 3 a *Salpeter* IMF provides a decent, yet not perfect fit to the data. On the other hand, at each redshift the $M_*/L_{\rm B}$ ratio depends on the assumed age of the SSP, hence on the assumed redshift of formation $z_{\rm F}$. This means that to some extent the IMF slope and the formation redshift are degenerate. Indeed, the *Salpeter* IMF provides a better fit to the FP shifts if one assumes a lower formation redshift, e.g. $z_{\rm F} = 3$, as illustrated in Fig. 4.

Of course, the higher the redshift, the larger the difference between the $M_*/L_{\rm B}$ ratios predicted by SSPs with different IMF slopes. Therefore, measuring the FP shift at the highest possible redshift would be of great interest. For quite many years the highest redshift elliptical galaxy known was LBDS 53w091 at $z = 1.55$ (Dunlop et al. 1996; Spinrad et al. 1997), not much beyond the highest redshift ellipticals in the study by van Dokkum & Stanford (2003), which are at $z = 1.27$. However, passively evolving elliptical galaxies have now been identified all the way to $z = 1.9$ (Cimatti et al. 2004), for which it would be very interesting to measure the central velocity dispersion, thus getting the FP parameters, although this may require extremely long integrations.

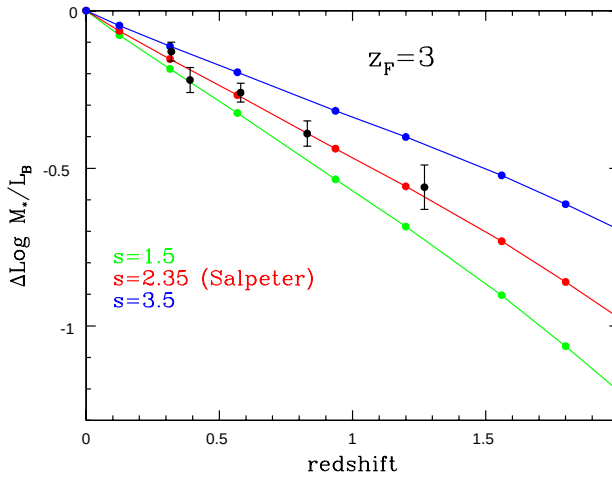

Figure 4. The same as in Fig. 3 but assuming a formation redshift $z_{\rm F} = 3$.

To further illustrate the case of the IMF slope/$z_{\rm F}$ degeneracy, Fig. 5 shows the FP ($M_*/L_{\rm B}$) shift with redshift for SSPs with a *Salpeter* IMF, solar metallicity, and various formation redshifts $z_{\rm F}$. One can conclude that the degeneracy is strong if the formation redshift of ellipticals were to be relatively low (e.g., ~ 2), but for $z_{\rm F} \gtrsim 3$ the degeneracy is quite mild and the data favor an IMF slope for $1 \lesssim M \lesssim 1.4\,M_\odot$ very close to the *Salpeter* value.

4. The Metal Content of Galaxy Clusters, and the IMF Slope for $1 \lesssim M \lesssim 25\,M_\odot$

In clusters of galaxies most of the light comes from early-type galaxies dominated by old stellar populations, i.e., from $\sim 1\,M_\odot$ stars. Meanwhile, one can also measure the amount (mass) of metals contained in the intracluster medium and in the stars. As most metals are produced by Type II supernovae, the total metal mass in a cluster of galaxies is proportional to the number of massive stars ($M \gtrsim 8\,M_\odot$) that have exploded in the far past, therefore dispersing the metals we see today[3]. It follows that the *metal-mass-to-light ratio* of galaxy clusters (e.g., Renzini 2003) provides a measure of the number ratio of massive to $\sim M_\odot$ stars, i.e., of the IMF slope between ~ 1 and $\sim 25\,M_\odot$ (or more)[4] for the stellar populations that – when young – have produced the metals and now – that are old – produce the light we see today.

The IMF of a passively evolving SSP can be written as:

$$\phi(M) = a(t,Z) L_{\rm B} M^{-s}, \tag{1}$$

where $L_{\rm B}$ is its B-band luminosity and $a(t,Z)$ is a (slow) function of the SSP age and metallicity. For example, for $Z = Z_\odot = 0.02$ one has $a(t) = 1.67$ and 2.51, respectively for $t = 10$ and 15 Gyr (Maraston 1998) (with M and $L_{\rm B}$ in solar units). More recent models (Maraston 2004, in preparation) give $a(t) = 1.68$ and 2.8 for the same (t,Z) and $a(t) = 2.50$ and 3.94 for $Z = 2Z_\odot$. For $t = 12$ Gyr (the minimum age for $z_{\rm F} \gtrsim 3$) the new Maraston models give $a(Z) = 2.22$ and 3.12, respectively for $Z = Z_\odot$ and $Z = 2Z_\odot$.

Therefore, the metal-mass-to-light ratio for the "X" element can be calculated in a straightforward manner from:

$$\frac{M_{\rm X}}{L_{\rm B}} = a(t,Z) \int_8^{40} m_{\rm X}(M) M^{-s} dM, \tag{2}$$

[3]Iron is the element whose abundance is most reliably measured both in the ICM and in galaxies. However, its production may be dominated by Type Ia supernovae, whose progenitors are binary stars. Given the complexities introduced by the binary nature of the iron producers, this element is less useful for the determination of the IMF slope.

[4]With a Salpeter IMF the *typical* stellar mass for nucleosynthesis yields is $\sim 25\,M_\odot$, i.e., the overall yield can be approximated by the total number of Type II supernovae times the nucleosynthesis products of a $25\,M_\odot$ star.

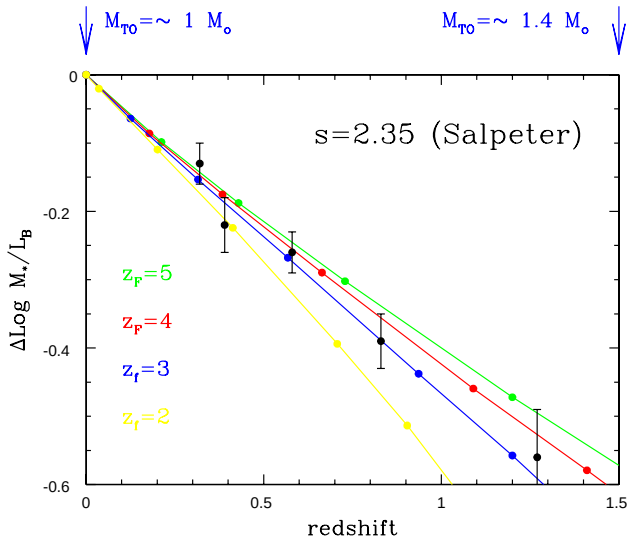

Figure 5. The same as in Fig. 3 for the Salpeter IMF and various values of the formation redshift $z_{\rm F}$, from $z_{\rm F} = 5$ (top) to $z_{\rm F} = 2$ (bottom).

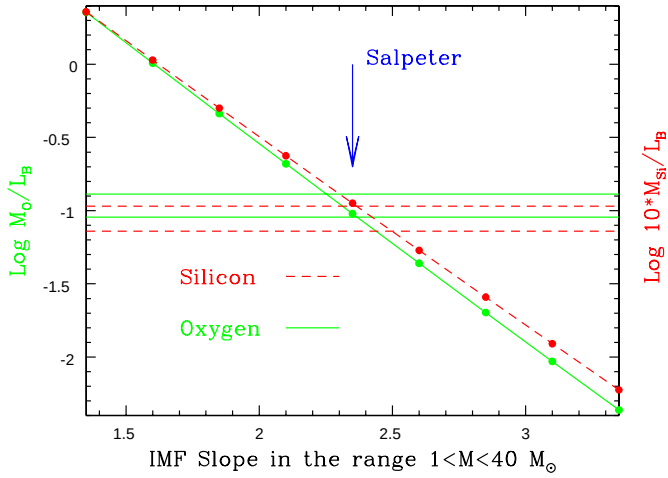

Figure 6. The Oxygen- and the Silicon-Mass-to-Light Ratios as a function of the IMF slope as calculated from Eq. (2) with $a(t, Z) = 3$ and using the nucleosynthesis prescription of Woosley & Weaver (1995). The horizontal lines show the observed average values of this ratios in clusters of galaxies, and their uncertainty range.

where $m_{\rm X}(M)$ is the mass of the element "X" which is produced by a star of mass M. Adopting $a(t, Z) = 3$ and $m_{\rm X}(M)$ for oxygen and silicon from Woosley and Weaver (1995) and integrating Eq. (2) one obtains the *oxygen-* and the *silicon-mass-to-light ratios*, which are shown in Fig. 6 as a function

of the IMF slope. As expected, the $M_{\rm O}/L_{\rm B}$ and $M_{\rm Si}/L_{\rm B}$ ratios are extremely sensitve to the IMF slope. The values observed in clusters of galaxies (ICM plus galaxies) are ~ 0.1 and $\sim 0.01\,M_\odot/L_\odot$, respectively for oxygen and silicon[5] (e.g., Finoguenov et al. 2003; Portinari et al. 2004, and references therein). These empirical values are reported in Fig. 6, which at the meeting was presented to Ed Salpeter as a Happy-Birthday postcard. Indeed, with the *Salpeter* IMF slope ($s = 2.35$) the standard explosive nucleosynthesis from Type II supernovae produces just the right amount of oxygen and silicon to account for the observed $M_{\rm O}/L_{\rm B}$ and $M_{\rm Si}/L_{\rm B}$ ratios in cluster of galaxies, having assumed that most of the cluster B-band light comes from $\gtrsim 12$ Gyr stellar populations.

Fig. 6 also shows that with $s = 1.35$ such a *top heavy* IMF (in various circumstances invoked to ease discrepancies between theories and observations) would overproduce metals by more than a factor of 20. This is indeed the change one expects in $M_{\rm O}/L_{\rm B}$, $M_{\rm Si}/L_{\rm B}$, etc. for a $\Delta s = 1$ when considering that the light $L_{\rm B}$ is provided by $\sim M_\odot$ stars and the metals by $\sim 25\,M_\odot$ stars.

5. Masses and Star Formation Rates of High Redshift Galaxies

As is well known, all SFR indicators (UV continuum, Hα, sub-mm, etc.) measure the formation rate of massive stars. To derive the total SFR an IMF (slope and shape) has to be assumed. Similarly, an IMF must be assumed to derive the total stellar mass of a galaxy from its spectral energy distribution (SED) and luminosity. These are indeed determined by the number of stars producing the bulk of the light (which are typically in a quite narrow range of masses), while remnants and dwarfs produce little light but may contribute a major fraction of the mass. It follows that the time integral of the measured cosmic SFR(z) (in $M_\odot$ yr^{-1} Mpc^{-1}) should agree with the measured stellar mass density $\rho_*(z)$ (in $M_\odot$ Mpc^{-1}), and in turn at $z = 0$ this should agree with its dynamical estimate. Clearly, such a general agreement needs to be achieved with the *right* value of the IMF. Fig. 7 shows a recent attempt in this direction (adopting a Salpeter IMF, Fontana et al. 2004) but error bars are still too large to allow a definitive answer. However, several galaxy surveys (with HST, SST, VLT, etc. etc.) are now well under way, and extremely rapid progress is expected in this field.

[5]These values result from averaging over the reported values for individual clusters with different ICM temperature, and take into account that $\sim 10-30\%$ of the stellar mass in clusters is not bound to individual galaxies (Arnaboldi et al. 2003; Gal-Yam et al. 2003).

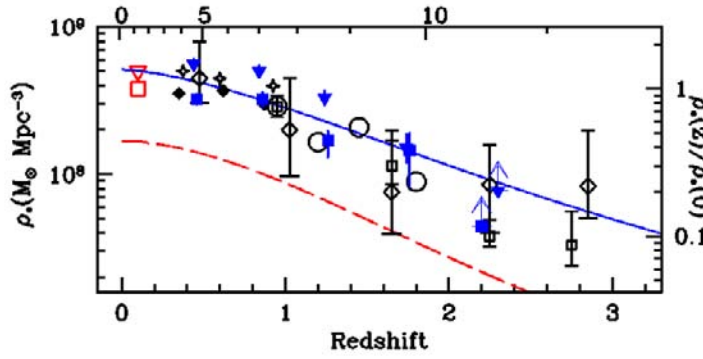

Figure 7. The cosmic evolution of the comoving density of the overall mass in stars from various current surveys, compared with the time integral of the cosmic star-formation rate density, uncorrected (dashed line) and corrected for dust attenuation effects (solid line) (from Fontana et al. 2004).

6. Summary

⋆The IMF of elliptical galaxies is close to *Salpeter* except below $\sim 0.6\,M_\odot$, where it flattens.

⋆The fundamental plane (FP) of ellipticals does not rotate with redshift, implying that the IMF is independent of galaxy luminosity (mass).

⋆The FP shift with redshift is consistent with a *Salpeter* IMF near $M \sim M_\odot$ and a formation at $z \gtrsim 3$ for the bulk of stars in ellipticals.

⋆The overall metal content of galaxy clusters (ICM+galaxies) is well reproduced by a *Salpeter* IMF and classical nucleosynthesis.

⋆Very rapid progress is expected in determining the cosmic history of star formation along with the cosmic build-up of stellar mass and a consistent IMF.

⋆The IMF may not be universal (who knows??) but the one of which this meeting celebrates the 50th anniversary doesn't quite show its age (!).

Acknowledgments I would like to thank Claudia Maraston for having provided her most recent models in advance of publication, and the staff of the Carnegie Observatories (Pasadena) for their kind hospitality during the time when this paper was written and set up.

References

Arnaboldi, M. et al. 2003, AJ, 125, 514

Cimatti, A., et al. 2004, Nature, 430, 184
Djorgovski, S., & Davis, M. 1987, ApJ, 313, 59
Dressler, A. et al. 1987, ApJ, 313, 42
Dunlop, J.S., et al. 1996, Nature, 381, 581
Finoguenov, A., Burkert, A., & Böhringer, H. 2003, ApJ, 594, 136
Fontana, A., et al. 2004, A&A, 424, 23
Gal-Yam, A., et al. 2003, AJ, 125, 1087
Maraston, C. 1998, MNRAS, 300, 872
Portinari, L., et al. 2004, ApJ, 604, 579
Renzini, A., & Ciotti, L. 1993, ApJ, 416, L49
Renzini, A. 1998, AJ, 115, 2459
Renzini, A. 1999, in The Formation of Galactic Bulges, ed. M. Carollo, H. Ferguson, & R. Wise (Cambridge, CUP), p. 9 (astro-ph/9902108)
Renzini, A. 2004, in Clusters of galaxies: Probes of Cosmological Structure and Galaxy Evolution, ed. J.S. Mulchaey, A. Dressler, & A. Oemler (Cambridge, CUP) (astro-ph/0307146)
Salpeter, E. E. 1955, ApJ, 123, 666
Spinrad, H., et al. 1997, ApJ, 484, 581
van der Marel, R. 1991, MNRAS, 253, 710
van Dokkum, P.G., & Stanford, S.S. 2003, ApJ, 585, 78
Woosley, S.E., & Weaver, T.A. 1995, ApJS, 101, 181
Wuyts, S., et al. 2003, ApJ, 605, 677

Figure 8 Alvio Renzini in Hawaiian style.

INITIAL MASS FUNCTION AND GALACTIC CHEMICAL EVOLUTION MODELS

D. Romano[1], C. Chiappini[2], F. Matteucci[3] and M. Tosi[1]
[1]*INAF–Osservatorio Astronomico di Bologna, Via Ranzani 1, I-40127 Bologna, Italy*
[2]*INAF–Osservatorio Astronomico di Trieste, Via G. B. Tiepolo 11, I-34131 Trieste, Italy*
[3]*Dipartimento di Astronomia, Università di Trieste, Via G. B. Tiepolo 11, I-34131 Trieste, Italy*
donatella.romano@bo.astro.it,chiappini@ts.astro.it,matteucci@ts.astro.it,monica.tosi@bo.astro.it

Abstract In this contribution we focus on results from chemical evolution models for the solar neighbourhood obtained by varying the IMF. Results for galaxies of different morphological type are discussed as well. They argue against a universal IMF independent of star forming conditions.

1. Introduction

Galactic chemical evolution (GCE) models are useful tools to understand how galaxies form and evolve. In particular, abundance and abundance ratio trends can be read as records of different evolutionary histories and interpreted in terms of the different time scales on which different objects evolve (Matteucci and François 1989; Wheeler et al. 1989). Unfortunately, dealing with very complex and poorly known mechanisms such as mass accretion, star formation and stellar feedback, brings with it the need for many assumptions and parameters. As a consequence, GCE models are by no means unique (Tosi 1988). Therefore, it is worthwhile quantifying the uncertainties of GCE predictions arising from different treatments of the physical processes involved with structure formation and evolution. Here we concentrate on uncertainties due to different assumptions on the stellar IMF. By comparing the model predictions with the available data, we show that particular IMF slopes can be ruled out in the Galaxy, whilst a "standard" solar neighbourhood IMF is not suitable to describe the high metallicities observed in ellipticals.

2. The IMF in the solar neighbourhood

The most widely used functional form for the IMF is an extension of the "original mass function" proposed by Salpeter (1955) to the whole stellar mass

E. Corbelli et al. (eds.), The Initial Mass Function 50 Years Later, 231–234.

range, $\varphi(m) \propto m^{-1.35}$ for $0.1 \leq m/M_{\odot} \leq 100$. Besides this, multi-slope expressions (Tinsley 1980; Scalo 1986; Kroupa et al. 1993; Scalo 1998) and a lognormal form for the low-mass part of the IMF ($m \leq 1\ M_{\odot}$; Chabrier 2003) are considered here. In the latter case, for the 1–100 $M_{\odot}$ stellar mass range we adopt a power-law form with an exponent x = 1.7.

In Fig. 1 we show the fractional masses falling in specific mass ranges according to different IMF choices, for one single stellar generation. An example of what one gets when integrating over the Galactic lifetime, i.e. over many stellar generations, is given in Fig. 2, where we display the predicted behaviour of [O/Fe] vs [Fe/H] for all the IMFs listed above. We choose oxygen because of its well understood nucleosynthetic origin (François et al. 2004) and because the very high-quality data available for solar neighbourhood stars (Meléndez and Barbuy 2002) allow for a very meaningful comparison between model predictions and observations. Although theoretical errors of the order of 0.2–0.3 dex can be associated to model predictions owing to the uncertainties in the actual IMF form, it is apparent that both Salpeter's and Scalo's (1998) IMFs overproduce oxygen for most of the Galactic lifetime. Generally, models assuming Salpeter's, Tinsley's or Scalo's (1998) IMFs are found to predict far too high global metal abundances ($Z_{\odot} \sim 0.024$–0.033), especially if the most recent measurement of this quantity in the Sun is taken into account ($Z_{\odot}$ = 0.0126; Asplund et al. 2004). The Scalo (1998) IMF also leads to overproduce ^{3}He from the time of solar birth up to now, due to its high percentage of 1–2 $M_{\odot}$ stars (see Fig. 1). On the contrary, the remaining IMFs all guarantee a

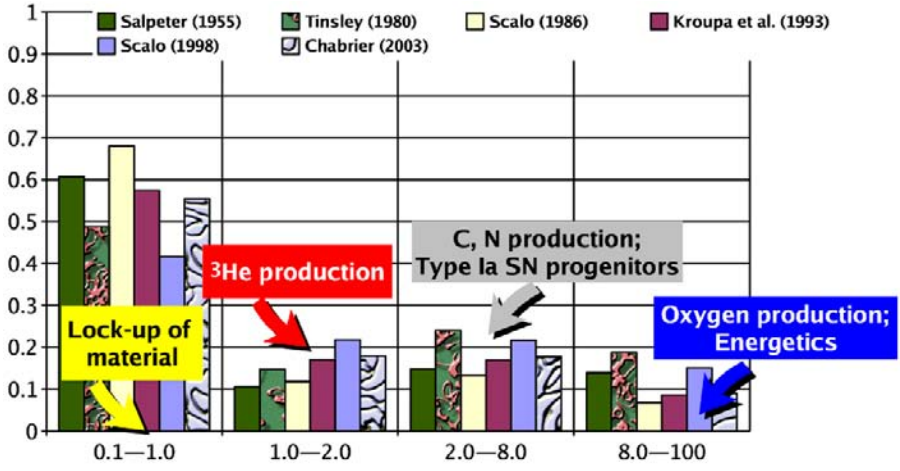

Figure 1. Fractional mass (y axis) falling in each given mass range (x axis) according to different IMF choices, for one single stellar generation.

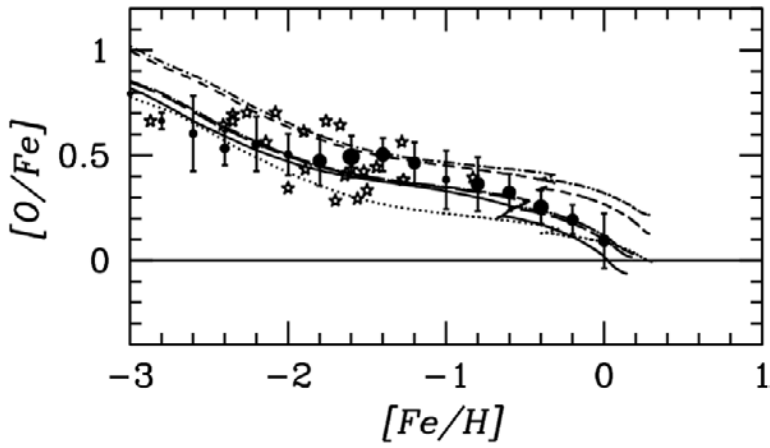

Figure 2. [O/Fe] vs [Fe/H] in the solar neighbourhood as predicted by models adopting different IMFs (short-dashed line: Salpeter 1955; dotted line: Tinsley 1980; solid line: Scalo 1986; long-dashed line: Kroupa et al. 1993; dot-short-dashed line: Scalo 1998; dot-long-dashed line: Chabrier 2003). Data are mean [O/Fe] from [O I] lines in 0.2 dex metallicity bins (circles) and [O/Fe] values from infrared OH lines (stars; Meléndez and Barbuy 2002).

good agreement between the model predictions and the data (see Romano et al. 2004 for details).

Therefore, from simple GCE arguments we conclude that the IMF of field stars in the solar neighbourhood must contain less massive stars than the Salpeter one. An extrapolation of the Salpeter law to the high-mass domain is not suitable to explain the solar neighbourhood properties. This is not surprising; *indeed, the Salpeter slope of x = 1.35 was originally derived for stars less massive than 10 $M_{\odot}$.*

3. The IMF in external galaxies

The observational properties of dwarf galaxies are better explained by assuming a Salpeter-like stellar mass spectrum. This is true for both dwarf spheroidals (Lanfranchi and Matteucci 2003) and late-type dwarf galaxies (Romano, Tosi and Matteucci in preparation). On the other hand, the chemo-photometric properties of massive ellipticals at both low and high redshifts are better explained with an IMF slightly flatter than Salpeter's. In their pioneering work, Arimoto and Yoshii (1987) showed that an IMF with a power index smaller than Salpeter, $\varphi(m) \propto m^{-0.95}$ for $0.05 \leq m/M_{\odot} \leq 60$, gives an excellent fit to the observed colors of giant elliptical galaxies. We find that the chemo-photometric properties of local and high-redshift massive spheroids are well

reproduced with an IMF slope even more similar to Salpeter's, i.e. $\varphi(m) \propto m^{-1.25}$ for $m > 1\ M_{\odot}$ (Romano et al. 2002).

In conclusions, our GCE models give us hints for (small) IMF variations with star forming conditions. Further studies have been presented at this workshop which seem to confirm our findings, from both a theoretical (e.g. C. Chiosi; P. Kroupa; L. Portinari, these proceedings) and an observational (e.g. S. Lucatello, these proceedings) point of view.

Acknowledgments DR and MT wish to thank the organizers for the pleasant and interesting meeting.

References

Arimoto, N., and Yoshii, Y. 1987, A&A, 173, 23

Asplund, M., Grevesse, N., Sauval, A. J., Allende Prieto, C., and Kiselman, D. 2004, A&A, 417, 751

Chabrier, G. 2003, PASP, 115, 763

Francois, P., Matteucci, F., Cayrel, R., Spite, M., Spite, F., and Chiappini, C. 2004, A&A, 421, 613

Kroupa, P., Tout, C. A., and Gilmore, G. 1993, MNRAS, 262, 545

Lanfranchi, G. A., and Matteucci, F. 2003, MNRAS, 345, 71

Matteucci, F., and François, P. 1989, MNRAS, 239, 885

Meléndez, J., and Barbuy, B. 2002, ApJ, 575, 474

Romano, D., Chiappini, C., Matteucci, F., and Tosi, M. 2004, A&A, submitted

Romano, D., Silva, L., Matteucci, F., and Danese, L. 2002, MNRAS, 334, 444

Salpeter, E. E. 1955, ApJ, 121, 161

Scalo, J. M. 1986, Fund. Cosm. Phys., 11, 1

Scalo, J. M. 1998, in The Stellar Initial Mass Function, ed. G. Gilmore & D. Howell (San Francisco: ASP), ASP Conf. Ser., Vol.142, p.201

Tinsley, B. M. 1980, Fund. Cosm. Phys., 5, 287

Tosi, M. 1988, A&A, 197, 33

Wheeler, J. C., Sneden, C., and Truran, J. W., Jr. 1989, ARA&A, 27, 279

NEW DATABASE OF SSP_S WITH DIFFERENT IMF_S

Rosaria Tantalo
Department of Astronomy, University of Padova, Italy
tantalo@pd.astro.it

Abstract In this poster we present a new large database of SSPs calculated by the Padova Galaxy Group using the Stellar Models by Girardi (2003, private communication) for three *Power-law IMFs* and three *exponential IMFs*.

1. The SSPs DataBase: stellar models and spectral library

The New SSPs are based on the New Padova Library of stellar models and companion isochrones according to the version by Girardi et al. (2000) and Girardi (2003, private communication). This particular set of stellar models/isochrones differs from the classical one by Bertelli et al. (1994) for the efficiency of convective overshooting and prescription for the mass-loss rate along the AGB phase. No details on the stellar models are given here; they can be found in Girardi et al. (2000,2002).

The DataBase has been calculated adopting the same composition of the stellar models and to obtain the integrated flux along an isochrone we have adopted the library of synthetic spectra amalgamated by Girardi et al. (2000).

2. The SSPs DataBase: different IMF

Six different laws for the IMFs have been adopted. In particular, we have considered three *power-law IMFs* and three *exponential IMFs* as shown in Fig. 1. The parameters characterizing each IMF are given in detail by Portinari et al. (2004). The evolution of M_V magnitude and M/L_V ratio as a function of age are shown in top and bottom panel of Fig. 2.

3. The SSPs DataBase

At fixed metallicity and for each IMF we will provide:

• The flux as a function of the age: wavelength are in *nm* and fluxes in *ergs* cm^{-2} sec^{-1} Hz^{-1} str^{-1};

• Colors, magnitudes and mass-to-light ratio are given in different photometric-

E. Corbelli et al. (eds.), The Initial Mass Function 50 Years Later, 235–236.

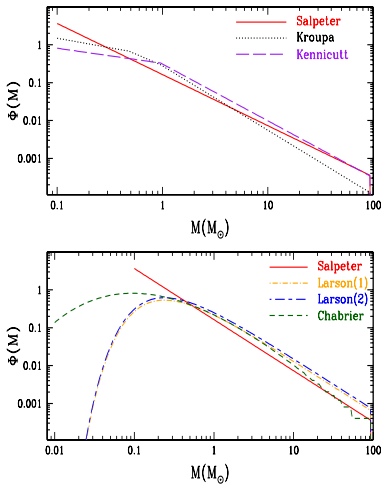

Figure 1. Comparison among six IMFs. Top-panel: three power-law IMFs; Bottom-panel: three exponential IMFs.

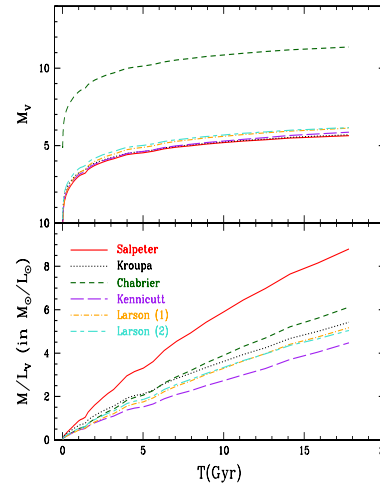

Figure 2. The V magnitude (top panel) and mass-to-light ratios (bottom panel) as a function of age for Z=0.019 and different IMFs.

system (Johnson-Cousins, GAIA, SDSS, HST-NICMOS, HST-WFPC2) and also in VEGAmag, STmag and ABmag system upon request.
In addition, we present a companion grid of 25 absorption line indices on the Lick-System (Worthey et al. 1994) and λ4000 break (Gorgas et al. 1999).
All the data will be made available at: *http://dipastro.pd.astro.it/galadriel*

References

Bertelli, G., Bressan, A., Chiosi, C., Fagotto, F., Nasi, E., 1994, A&AS, 106, 275
Girardi, L., Bertelli, G., Bressan, A., Chiosi, C., Groenewegen, M., Marigo, P., Salasnich, B., Weiss, A., 2002, A&A, 391, 195
Girardi, L., Bressan, A., Bertelli, G., Chiosi, C., 2000, A&AS, 141, 371
Gorgas, J., Cardiel, N., Pedraz, S., González, J.J., 1999, A&AS, 139,29
Worthey, G., Faber, S.M., González, J.J., Burstein, D., 1994, ApJS, 94, 687

THE STARBURST IMF – AN IMPOSSIBLE MEASUREMENT?

Bernhard R. Brandl[1] and Morten Andersen[2]
[1]*Leiden Observatory, P.O. Box 9513, 2300 RA Leiden, The Netherlands*
[2]*Steward Observatory, 933 N Cherry Ave., Tucson AZ 85721, USA*
brandl@strw.leidenuniv.nl,mandersen@as.arizona.edu

Abstract The starburst IMF is probably as much of theoretical interest and practical relevance as it is a subject of observational controversy. In this conference paper, we review the most common methods (star counts, dynamical masses, and line ratios) to derive or constrain the IMF, and discuss potential problems and shortcomings that often lead to claims of anomalous IMF slopes and mass cut-offs.

1. Introduction

The IMF in regions of violent star formation activity, so-called starbursts, is still a rather controversial issue. For instance, the ultra-luminous infrared galaxy Arp 220 with a total gas mass of $1.6 \times 10^{10} M_{\odot}$ Arp 220 has about five times the amount of gas available in the Milky Way. However, its star formation rate of $300 M_{\odot}/yr$ is about 200 times higher than in our Galaxy, and – in addition – the regions of star formation are rather concentrated near the center(s) of the galaxy.

It may seem plausible that in such regions, where the physical boundary conditions for star formation differ so substantially from the solar neighborhood, the IMF may be different as well. Such a difference may be indicated by either a different IMF slope ("top heavy"), a significantly higher low-mass cut-off ("$2 - 5 M_{\odot}$") or a different high-mass cut-off.

The observational verification of these differences is all but trivial: there are few regions that can serve as starburst templates, most of which are at large distances, have unknown morphologies, and are often heavily extincted. For closer regions, which can be resolved into individual stars, the dynamical range of typically more than 10 magnitudes in flux differences between low- and high-mass stars is a significant limitation. Not surprisingly, the strongest support for anomalous IMFs to date comes from the observations of distant

E. Corbelli et al. (eds.), The Initial Mass Function 50 Years Later, 237–244.

starburst galaxies or individual super star clusters. While those environments are indeed rather different from the local ones it should also be kept in mind how little we know about these distant system as the uncertainties in both observations and models are fairly large. In this conference paper we discuss the general difficulties in the IMF determination.

2. Method I: star counts

The most common method, which has also be shown to work well in nearby regions of quiescent star formation, is the direct detection of stars. After photometric extraction of the sources and subtraction of foreground and background field stars, the correction for incompleteness (see below) takes care of instrumental limitations and possibly of the extra contribution from unresolved binary systems. Finally, the conversion from magnitudes to masses leads to a *present-day* mass function, which is often, and not very precisely, called the *initial* mass function as dynamical effects in young clusters are (incorrectly) considered to be of little importance.

The results from a recent study of the IMF in R136, the ionizing cluster in the 30 Doradus nebula, are shown in Figure 1 as a function of radial distance (Andersen, Brandl & Zinnecker 2004). The errors for the innermost 1 pc ($4''$) are very large and the derived slopes not very meaningful. However, outside the core region the slope agrees, within the uncertainties, well with a Salpeter (1954) slope and shows no significant steepening with distance to the cluster center.

However, each step from the observed image to an IMF slope involves potential difficulties, of which we can here address only a few:

2.1 Problem: the high-mass stars

At no time within a massive, coeval cluster's lifetime will it be possible to observe all its members on the main sequence. Many of the most massive stars will have collapsed or exploded before the lower mass stars reach the main sequence. High-mass stars show strong luminosity evolution and mass loss during their short lifetimes. In particular the luminosity evolution of a given spectral subtype within its lifetime can be larger than the initial difference between different spectral subtypes. It is therefore almost impossible to accurately determine masses of O-stars from photometry alone (and individual spectra are usually not available).

There is also mounting evidence that the evolution of massive stars in the core of a dense stellar cluster is significantly influenced by the other cluster members. Portegies Zwart et al. (1999) have shown in N-body simulations that due to the high stellar densities mergers of massive stars occur frequently, and by doing so increase their cross-section while the cluster is becoming denser

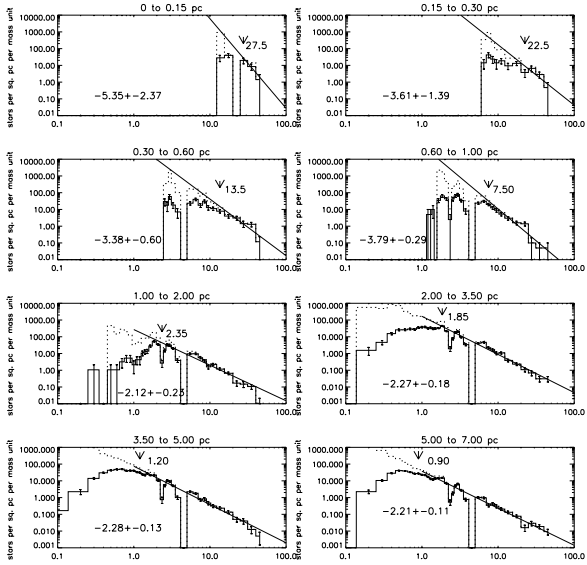

Figure 1. The derived IMFs for R136 in radial bins using a Siess et. al. (2000) 3 Myr isochrone with half-solar metallicity, a distance modulus of 18.5 and an extinction of $A_V = 2$ (Andersen, Brandl & Zinnecker 2004).

due to mass segregation, in some kind of "runaway merger" process. In other words, a central massive star grows steadily in mass through mergers with other stars in less than $3 - 4$ Myr, and the observed properties are not representative of the initial mass distributions.

2.2 Problem: the low-mass stars

Besides the obvious difficulty of detecting relatively faint, low-mass stars a significant uncertainty will be introduced by the fact that in most young clusters they are still in their pre-main sequence (PMS) phase. (The fact that PMS stars are brighter than their main sequence counterparts at infrared wavelengths, improves the situation slightly). However, the models for converting magnitudes to masses depend critically on the cluster age which has typical uncertainties in the order of 0.5 Myr. Usually all stars within a cluster are assumed to be co-eval. Furthermore, the conversion also depends on the wavebands that were used and on the specific PMS model. This situation is illustrated in Table 1.

The effects of heating, outflows and stellar winds (Lamers, Snow & Lindholm 1995), and in particular the strong winds from O stars (Churchwell 1997), will cause the residual gas to be removed from the cluster on rather short time scales of 1 Myr. If the gas cloud was originally virialized, and the star formation efficiency is about 30%, the cluster will loose about 2/3 of its mass.

Table 1. Comparison of IMF slopes derived from the same data but with different PMS models, age assumptions, distance moduli or based on different filter bands. The differences in the resulting slopes are striking! Table from Andersen (2004).

Model[a]	*Age [Myr]*	*DM*[b]	*color*	*slope*
SDF	1	13.9	$J_s - K_s$	-2.20 ± 0.13
SDF	1	13.9	$H - K_s$	-1.46 ± 0.23
SDF	1	14.3	$J_s - K_s$	-2.41 ± 0.14
SDF	2	13.9	$H - K_s$	-1.46 ± 0.34
PS	1	13.9	$J_s - K_s$	-1.70 ± 0.19

[a] SDF – Siess et. al. (2000); PS – Palla & Stahler (1999). [b] DM – distance modulus

As a result, a significant fraction of its young members will get lost, preferentially low-mass stars at the high tail of the velocity dispersion and/or at large distances (Kroupa & Boily 2002).

This has important observational consequences: even for a rather distant Galactic cluster like NGC 3603 at 7 kpc with an assumed velocity dispersion of 5 km/s the radial distances of initial cluster stars can be as large as $100''$ after 1 Myr (including a $\cos(45^o)$ projection factor). If the reference field taken to estimate the field star population is closer than this radius there are two problems: *(i)* stars that were born in the center are now missing there, and *(ii)* those stars may now be mistaken as field stars and subtracted from the cluster sample. Both effects work in the same direction and introduce an artificial flattening of the IMF.

2.3 Problem: differential extinction

Sirianni et al. (2000) reported a "definitive flattening below $\approx 2M_\odot$" of the IMF slope at $r \geq 1.5$ pc around R136. This finding was based on optical data from HST/WFPC2 and the numbers were corrected for incompleteness. Unfortunately, the standard Monte-Carlo technique for incompleteness correction – adding artificial stars to the "real" image and computing their detection probability as a function of distance from the cluster center and source brightness – corrects only for statistical (crowding, blending) and instrumental (noise, flatfield) effects. In contrast, strong variations in the more localized *differential* extinction are caused either by the evolution of the PMS object or by rather compact and patchy foreground extinction, and can vary by several magnitudes at optical wavelengths. These variations cannot be easily corrected with Monte-Carlo techniques (see Figure 2). Since the reddening distribution is very uncertain, the best work-around are observations at near-IR wavelength where the extinction is reduced by about an order of magitude.

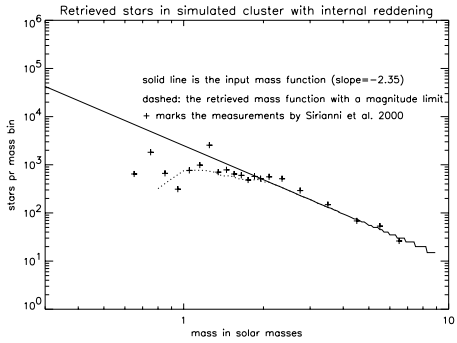

Figure 2. The influence of differential extinction on the observed IMF slope. For a constant detection limit (dashed line) variable reddening can cause an artificial "flattening". Figure from Andersen (2004).

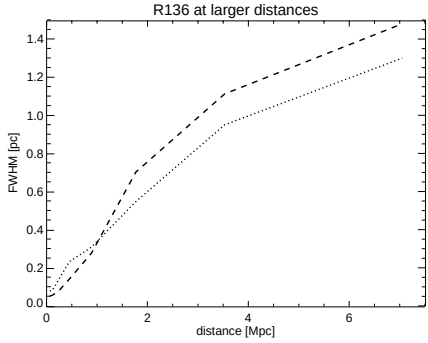

Figure 3. The effect of spatial resolution on the derived half-light radius r_{hl}, measured for R136 locally, and remeasured at larger distances (Brandl et al. 2005).

3. Method II: cluster mass-to-light ratios

Most starburst systems are located well beyond the Local Group and are not resolvable into their individual stellar members (except for the very brightest stars) with current techniques. However, so-called super star clusters (SSCs) may be the result of a recent starburst, and their integrated properties can be observationally studied.

3.1 The basic principle

For a given set of assumptions (see below) the dynamical mass M_{dyn} of a cluster is related to its velocity dispersion σ via

$$M_{dyn} = \eta \frac{\sigma^2 r_{hl}}{G} \tag{1}$$

where $\eta \approx 10$. The velocity dispersion σ can be determined from high resolution spectroscopy and the half-light radius r_{hl} from high resolution imaging. Photometry will yield the total luminosity L and the mass-to-light ratio M/L will provide an estimate of the underlying IMF.

Using this technique Mengel et. al. (2002) found that the IMF in selected SSCs in the Antennae galaxies is approximately consistent with Salpeter for a mass range of $0.1 - 100 M_{\odot}$. On the other hand, Smith & Gallagher (2001) found that in M82-F a lower mass cut-off of $2 - 3 M_{\odot}$ is required for a MF with a Salpeter slope, i.e., *M/L* is $5\times$ lower than normal.

3.2 The problematic assumptions

The approach described above depends on the validity of several assumptions:

• *The correct half-light radius* r_{hl}. Even gravitationally-bound, young clusters often deviate from radially symmetric, King-like cluster profile. A perfect example is R136, which has several bright cluster members at larger distance from the center. While those stars can be easily excluded from the light profile at the distance of the LMC, they blend with the core at larger distances (lower spatial sampling) and increase the measured r_{hl}. This effect is illustrated in Figure 3.

• *A gravitationally bound cluster.* While the two most massive HII regions in the Local Group, 30 Doradus in the LMC and NGC 604 in M 33, have about the same luminosity they have completely different morphological structures. The core of 30 Dor, R136, is a massive compact cluster and presumably gravitationally bound, while NGC 604 consists of a several smaller, less luminous HII regions, which are not gravitationally bound together. However, at the distance of e.g., the Antennae galaxies, where the scale of one WFPC2 pixel corresponds to about 9 parsecs, 30 Dor and NGC 604 would be indistinguishable.

• *A constant M/L*. Massive stars appear to be more concentrated toward the cluster center, see e.g., figure 16 in Brandl et al. (1996). We cannot distinguish here whether this is related to the star formation process (i.e., massive stars form in the densest regions), or the result of mass segregation. At any rate, the most massive stars dominate the light profile, and their concentration around the cluster center produces a gradient in *M/L*.

While the above method certainly allows for rough estimates of dynamical cluster masses, the combined uncertainties make it very difficult to provide sufficient evidence for anomalous IMFs in galaxies beyond the Local Group.

4. Method III: mid-IR fine-structure line ratios

Luminous starbursts are often significantly extincted and require observations at longer wavelengths. The mid-IR spectral range covered by ISO-SWS and Spitzer-IRS provides a wealth of spectral diagnostic features, although the spectra contain only spatially integrated information.

4.1 The basic principle

One of the most common diagnostics are the forbidden fine structure lines [Ne III]15.56μm and [Ne II]12.81μm. With an ionization potential of 63.45 eV, [Ne III] indicates the presence of early-type O-stars, while [Ne II] with only 40.96 eV can be excited by less massive OB stars. Thus, the ratio

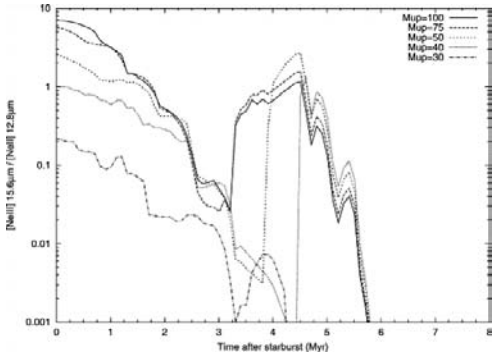

Figure 4. Model ratios of the mid-IR [Ne III]/[Ne II] finestructure lines as a function of time and upper mass cut-offs. Figure from Rigby & Rieke (2004).

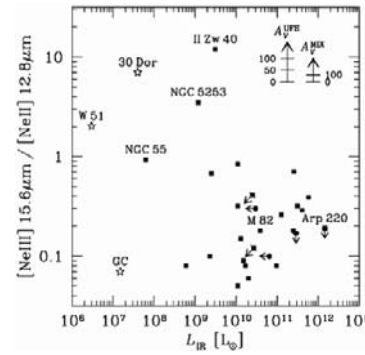

Figure 5. Observed [Ne III]/[Ne II] ratios from ISO-SWS for a variety of Galactic and extragalactic sources. The majority of luminous starburst galaxies fall below a ratio of one. Figure from Thornley et al. (2000).

of [Ne III]/[Ne II] is a very sensitive measure of the strength of the radiation field, which depends on the presence of the most massive stars and on the age of the starburst, as illustrated in Figure 4.

4.2 Problem: the model-observation discrepancy

The observed line ratios (Figure 5) differ significantly from the values predicted by the models such as STARBURST99/CLOUDY (Leitherer et al. 1999). While there seems to be a better agreement for low-metallicity galaxies and dwarf systems, the observed ratios of more luminous starburst galaxies are often more than an order of magnitude lower than the theoretical predictions.

Among the possible explanations being discussed is strong dependency on metallicity, a general lack of the most massive stars in intense bursts, or a larger age spread with complicated morphology of the starburst region. Higher extinction can be ruled out as it would even increase the discrepancy (Figure 5). Rigby & Rieke (2004) proposed that very massive stars in dense and metal-rich starbursts spend a significant fraction of their lifetime embedded in ultra-compact HII regions that prevent the formation of classical HII regions. Hence, the finestructure lines expected from those embedded massive stars cannot even form, and the spectra would be dominated by the lower excitation [Ne II] line produced by the surrounding, less massive stars.

In summary, mid-IR finestructure line diagnostics are an elegant and intriguing method to infer the relative amount of massive stars in a starburst. However, given the complexity of a real starburst region and the model un-

certainties claims of anomalous IMFs, just based on line ratios, need to be taken with care. This is clearly an area where significant improvements can be expected from Spitzer-IRS observations.

References

Andersen, M. 2004, PhD thesis, Potsdam
Andersen, M., Brandl, B.R. & Zinnecker, H. 2004, in preparation
Brandl, B.R. et al. 1996, ApJ, 466, 254
Brandl, B.R. et al. 2005, in "Starbursts – from 30 Doradus to Lyman break galaxies", Cambridge
Churchwell, E. 1997, ApJ, 479, 59
Kroupa, P. & Boily, C.M. 2002, MNRAS, 336, 1188
Lamers, H.J.G.L.M., Snow, Th.P. & Lindholm, D.M. 1995, ApJ, 455, 269
Leitherer, C. et al. 1999, ApJS, 123, 3
Mengel, S. et al. 2002, A&A, 383, 137
Palla, F. & Stahler, S.W. 1999, ApJ, 525, 772
Portegies Zwart, S.F. et al. 1999, A&A, 348, 117
Rigby, J.R. & Rieke, G.H. 2004, ApJ, 606, 237
Salpeter, E.E. 1955, ApJ, 123, 666
Siess, L., Dufour, E. & Forestini, M. 2000, A&A, 358, 593
Sirianni, M. et al. 2000, ApJ, 533, 203
Smith, L.J. & Gallagher, J.S. 2001, MNRAS, 326, 1027
Thornley, M.D. et al. 2000, ApJ, 539, 641

Figure 6. Bernhard Brandl and Don Figer.

GOULD'S BELT TO STARBURST GALAXIES: THE IMF OF EXTREME STAR FORMATION

M.R. Meyer, J. Greissl, M. Kenworthy and D. McCarthy
Steward Observatory, The University of Arizona, Tucson, AZ 85721–0065, USA
mmeyer@as.arizona.edu

Abstract Recent results indicate the stellar initial mass function is not a strong function of star–forming environment or "initial conditions" (e.g. Meyer et al. 2000). Some studies suggest that a universal IMF may extend to sub–stellar masses (see however Briceno et al. 2002). Yet most of this work is confined to star–forming environments within 1 kpc of the Sun. In order to probe the universality of the IMF over a wider range of parameter space (metalicity, ambient pressure, magnetic field strength) new techniques are required. We begin by summarizing our approach to deriving the sub–stellar IMF down to the opacity–limit for fragmentation using NGC 1333 as an example. Next, we describe results from simulations using the observed point–spread function of the new 6.5m MMT adaptive optics system and examine the confusion–limited sensitivity to low-mass stars in rich star–forming clusters out to 0.5 Mpc. We also present preliminary results from observations with this system of the W51 star–forming complex. Finally, we outline a new technique to estimate the ratio of high to low-mass stars in unresolved stellar populations, such as the massive star clusters observed in interacting galaxies (e.g. Mengel et al. 2002). While evidence for variations in the IMF remains inconclusive, new studies are required to rule them out and determine whether or not the IMF is universal over the range of parameter space relevant to star–forming galaxies over cosmic time.

1. Introduction

Any predictive theory of star formation must explain the observed shape of the field star IMF (e.g. Chabrier, 2003) and any deviations from it (e.g. Figer et al. 1999) as a function of physical properties. There are a few critical scales in star formation that one might expect *should* depend on local conditions such as super–critical mass to overwhelm magnetic support (e.g. Shu et al., this volume), or the Jean's mass (e.g. Larson, this volume). Curiously, the stellar IMFs observed toward a number of star–forming regions within 1 kpc of the Sun diplay no evidence for a strong dependence on "initial conditions" and are consistent with having been drawn from the same IMF that characterizes the

E. Corbelli et al. (eds.), The Initial Mass Function 50 Years Later, 245–254.

field (Meyer et al. 2000). For this reason, we are forced to expand the range of parameter space in which we search for variations in the IMF. There are two obvious avenues for further exploration: 1) probing the sub–stellar IMF in nearby regions down to and below the expected minimum mass for opacity–limited fragmentation (e.g. 0.01 $M_{\odot}$ Spitzer, 1978); and 2) more *extreme* star formation over a broader span of physical conditions such as metalicity, stellar density, galactic environment.

2. Probing to the End of the IMF

Advances in optical and infrared instrumentation on large ground–based telescope, as well as the Hubble Space Telescope have led to a number of IMF determinations that probe well into the brown dwarf regime. Several groups have derived sub–stellar IMF slopes in clusters that are flat, or falling, in log–mass units $dN/dlogm = m^{-\Gamma}$ with $\Gamma = 0$ to 1 (e.g. Bouvier et al. 1998; Hillenbrand and Carpenter 2000; Najita et al. 2000). While most regions appear to be consistent with each other, the Taurus dark cloud appears to have a statistically significant dirth of brown dwarfs compared to the Trapezium cluster (Briceno et al. 2002). Whether this is due to Taurus being deficient in brown dwarfs or the Trapezium being overabundant, is still not clear (Luhman, this volume).

A standard approach applied to the study of many young embedded clusters involves deep infrared imaging surveys along with follow-up infrared spectroscopy for as many cluster members as is practical (e.g. Greene and Meyer 1995; Luhman & Rieke 1998). More recently, it has been possible to obtain IR spectra for low luminosity sources enabling astronomers to identify young brown dwarf candidates in large numbers (e.g. Luhman 1999; Wilking et al. 1999). One concern of these early studies was the use of photospheric absorption features to derive spectral types which might also be effected by surface gravity (lower in pre–main sequence "sub–giants" compared to high gravity dwarf standards). In a recent study of brown dwarf candidates in NGC 1333, Wilking et al. (2004) test whether their spectrophotometric reddening–independent H_2O K–band index is effected by gravity. They find that any potential bias introduced by comparing PMS brown dwarf candidate spectra to dwarf star standards is of order the error inherent in the classification scheme. This is consistent with the work of Gorlova et al. (2003) who also find that H_2O in the J–band depends weakly on surface gravity, making it a good temperature indicator for young late–type stars. However, Gorlova et al. did find that the 1.25 μm KI feature, along with the 2.2 μm NaI feature, is sensitive to surface gravity providing a possible tool to distinguish foreground and background stars from "sub–giant" PMS cluster members. We are currently following up this work with an approved Cycle # 13 program on HST using NICMOS

in slitless grism mode to obtain 1.1–1.9 μm spectra of brown dwarf candidates in NGC 1333. Our goal is to probe the IMF down below 10 M_{JUP} (0.01 $M_{\odot}$) in this intermediate density cluster (between Taurus and the Trapezium) to see if there is a correlation with the slope of the sub–stellar IMF.

Another curiosity observed in mass distributions that result from star formation processes, is the brown dwarf desert in the companion mass ratio distribution (CMRD). It is fairly well established from radial velocity surveys as well as seeing–limited common proper motion surveys (Udry et al. 2001; Hinz et al. 2001) that there is a dirth of brown dwarf companions compared to extrapolation of the CMRD of stellar or planetary companions. In fact, the CMRD from 0.1–1.0 $M_{\odot}$ surrounding solar–type stars (Duquennoy & Mayor 1991; DM91) is consistent with having been drawn from a field star IMF, in stark contrast to the frequency of brown dwarf companions to sun–like stars compared to the sub–stellar IMF in the field (Ried et al. 1999). What about the companion mass ratio distribution surrounding young PMS stars? It has been known for some time that the binary frequency of T Tauri stars is high, particularly in low density star–forming regions such as Taurus–Auriga (Ghez et al. 1993; Leinert et al. 1993). However, it is only recently that researchers have begun to obtain multi–color infrared photometry and spatially–resolved IR spectra needed to derive mass estimates for faint companions to T Tauri stars. In fact, detailed comparisons of the CMRD between young clusters and the field are lacking.

In a NICMOS HST study of NGC 2024, Liu et al. (2003) describe how one must carefully consider completeness limits for faint companions as a function of angular separation and then compare the observations to results for field stars only over the appropriate mass ratios as a function of radius from the primary. They also consider what one might expect as a function of cluster age if soft–binaries are preferentially disrupted faster in higher density regions. Taking these effects into account, and combining their data with published results, they find a significant inverse correlation between binary frequency and stellar density. Fundamental survey work still needs to be done on the field star population as well as young star–forming regions, particular with the recent advances in adaptive optics on large telescopes. It will be important to know in this inherently three–dimensional observational problem whether: 1) the CMRD is a function of separation; and 2) whether the CMRD or the integrated period distribution is a function of primary mass. Although strong observational evidence to support the ejection hypothesis (e.g. Reipurth and Clarke 2001) for the formation of free–floating brown dwarfs is lacking (e.g. Muench et al. 2002) it is curious to note that the one region deficient in brown dwarfs in the system IMF (Taurus) is also the lowest density star–forming region with the highest observed binary fraction.

What does the future hold in studying the sub–stellar IMF in star–forming regions? Efforts continue to push down below the minimum mass for opacity–

limited fragmentation in nearby young clusters. If there is a lack of objects below some cutoff mass, it will be hard to miss observationally, and particularly exciting if it depends on local conditions. Peale (1999) points out that if there are significant numbers of brown dwarfs below 0.01 $M_\odot$ in young clusters, it may suggest an IMF that varies over cosmic time as recent MACHO results rule out significant mass in the halo in objects < 0.01 $M_\odot$. One must be cautious in identifying extremely low-mass objects in young clusters from photometry alone as there can be significant contamination in color–magnitude diagrams in deep surveys. We believe that spectroscopic follow–up is essential and spectroscopic diagnostics of surface gravity may be required in order to remove old cool field dwarfs from young cluster samples (Burgasser et al. 2004). We are working to identify a set of surface gravity diagnostics which could be used in filter–photometric imaging surveys to rapidly identify large samples of young late–type objects in star–forming regions. This effort complements recent work developing filter–photometric temperature diagnostics for very cool photospheres (e.g. Mainzer et al. 2003).

3. Star Formation Extreme

How does star formation in the solar neighborhood compare to global star formation in the Milky Way or even other galaxies? If one adds up the total number of high-mass stars along the Gould's Belt within 1 kpc of the Sun (de Zeeuw et al. 1999) and assumes a field star IMF, then the integrated total mass of the system is about 3×10^5 $M_\odot$, comparable to a single "event" such as the R 136 cluster region in the LMC. Is the IMF in extreme star–forming regions such as R 136 (low metalicity, disturbed galactic morphology, high stellar density), or the galactic center (high metalicity, ambient pressure, and magnetic flux density) and comparable to that observed in the solar neighborhood? Can we probe further claims of unusual IMFs indirectly inferred from observations of starburst galaxies? While we may not be able to derive detailed distributions of the numbers of individual objects as a function of mass in these distant stellar systems, we can apply similar techniques to those described above to place limits on the ratio of high to low-mass stars in these unusual regions that represent accessible extreme star–forming environments.

3.1 The Limits of Confusion

In principle, one would like to conduct observational "experiments" where one could compare differentially results from observations of star–forming regions varying one parameter at a time in a controlled way. However, such studies are thwarted by the limits one can achieve in sensitivity and spatial resolution for rare targets which tend to lie at the greatest distances. In particular, studies of the IMF in rich stellar fields are often *confusion–limited* rather

than sensitivity–limited. For example, Andersen et al. (in preparation) find that NICMOS HST observations of the IMF toward R 136 in the LMC are confusion–limited at > 0.5 M$_\odot$. In this case, the spatial resolution afforded by large–ground based telescopes can help, but only if the point–spread function (PSF) is smooth and stable (Stolte et al. 2003).

In order to see how well one can do with currently operating adaptive optics (AO) systems on 6–10 meter telescopes, we performed a series of simulations using the observed PSF of the 6.5m MMT with the new adaptive secondary mirror (Close et al. 2003). We considered the Trapezium cluster observations of Hillenbrand and Carpenter (2000) as input, and simulated what the Trapezium would look like at 5 kpc, 25 kpc, 50 kpc, and 0.5 Mpc. As the cluster gets farther away, the residual uncorrected halo of the bright Trapezium stars dominates the background at progressively larger radii. At 5 kpc, one still reaches the sky background limit at 0.2 parsecs enabling one to easily detect objects at the sub–stellar boundary in reasonable integration times of a few hours. At 25 kpc (Figure 2), one reaches the sky background limit $\times$ 5 farther out still enabling one to measure a significant number of stars at 2.5 R$_{core}$ over the entire stellar mass range. At the core radius of the cluster inside of which most of the stellar population is located, one loses $\Delta H = 6^m$ of sensitivity due to the background of uncorrected halo light from the bright stars. At 50 kpc, one does not hit the sky background limit until 4 R$_{core}$ and the sensitivity at the core radius is almost nine magnitudes worse than the natural background. At 0.5 Mpc, the cluster is competely unresolved. We conclude that while it will be relatively straightforward to characterize the IMF down to the hydrogen burning limit for any Trapezium in the Milky Way galaxy with existing AO systems on 6–10 meter telescopes, achieving similar results in nearby galaxies will require higher spatial resolution afforded by the next generation of large telescopes (e.g. the Large Binocular Telescope).

Figer et al. (1999, this volume) have presented intriguing observations that suggest the IMF in the inner galaxy Arches cluster is flatter than the field star IMF over the mass range observed (2–20 M$_\odot$). In order to test whether or not the ratio of high to low-mass stars in the Milky Way depends on metalicity, ambient ISM pressure, and/or magnetic field strength, we have begun a program using the ARIES camera in tandem with the MMT–AO system to image massive star forming clusters at high spatial resolution and sensitivity. Our first target is the distant luminous UCHII region W51 which contains over 130 stars $>$ 10 M$_\odot$ (Okumura et al. 2000). Preliminary analysis of observations obtained in May, 2004 (Figure 2), indicate that we can reach the hydrogen burning limit in this cluster through A$_v = 30^m$ of extinction (K $< 21^m$) in one hour of on–source integration time. We are currently exploring whether narrow–band IR imaging at R=100 in 6–8 filters can provide the necessary spectrophotometric information to estimate rough temperatures and surface gravities needed to

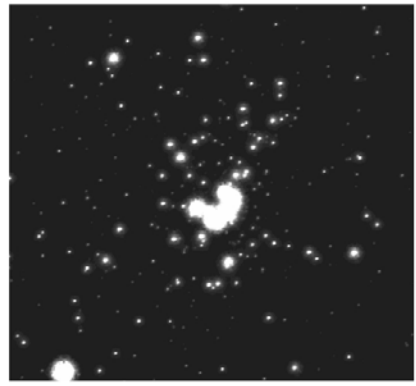

Figure 1. Simulations of the Trapezium cluster projected to a distance of 25 kpc as it would appear observed with the MMT adaptive optics system. These observations would reach the natural background limit outside of 2.5 core radii enabling determination of the IMF over the full range of stellar masses.

distinguish foreground and background stars along this complex line of sight (Meyer et al. 1998).

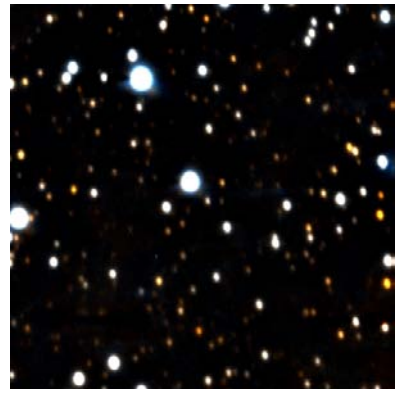

Figure 2. Observations of W51 in the H- and K-bands using the ARIES IR Camera and the MMT-AO system. Coadding 20 minutes of data resulted in images with 0.1" FWHM in the K–band. Preliminary results suggest that we will be able to reach the hydrogen–burning limit in the cluster in one hour of on–source integration time in the K–band.

3.2 Unresolved Super–Star Clusters

Some of the longest lasting claims of unusual IMFs come from observations of starburst galaxies with star–formation rates orders of magnitude higher than normal galaxies. Super–star clusters, recognized as globular cluster analogues in the early stages of formation (O'Connell et al. 1994) have been found fre-

quently within interacting starbursting galaxies. Mengel et al. (2002) used dynamical mass estimates from velocity dispersions to find significant variations in inferred mass–to–light ratios which they interpret as evidence for IMF variations from cluster to cluster in NGC 4038/39. Is there any way we could directly detect the low-mass stars in these super–star clusters and constrain the ratio of high to low-mass stars?

We have explored the contribution to the integrated K–band light from very young low-mass stars in super–star clusters < 10 Myr old (Meyer and Greissl 2004). While a main sequence population is dominated by the light from the highest mass stars because of the steepness of the main sequence mass–luminosity relation, in the PMS this M–L relation is much flatter perhaps rendering the low-mass stars visible for a short time in a forming super–star cluster. Combining an assumed IMF (Salpeter 1955 or Chabrier 2003) with PMS evolutionary models (Siess et al. 2000) and predictions of Starburst99 for the main sequence, post–main sequence, and nebular contributions to the integrated light, we find that between 7–12% of the K–band flux comes from young late–type stars depending on which IMF is assumed. Coupling these luminosity estimates with spectra appropriate for each object in the synthetic luminosity function, we have created model integrated spectra for the combined stellar population (Figure 3). Because these late–type stars are overluminous in the PMS, and because their spectra are dramatically different, with strong broad absorption bands from CO and other molecules, we predict that in a super–star cluster < 10 Myr (before the formation of the first red super–giants dominate the K–band light of the cluster) one might detect directly the integrated light of the low-mass stars as a 2–4 % absorption feature against the continuum. If one could use observations at centimeter and other wavelengths to models the contribution of nebular free–free emission to the 2 μm continuum, the strength of the CO feature from late–type stars could provide a direct constraint on the ratio of high to low-mass stars in these super–star clusters. The high signal to noise spectra (> 100) needed can be obtained at R=2000 with NIRSpec on the Keck telescope in approximately five hours of integration time for the brightest candidate SSCs in NGC 4038/39 that are thought to be < 10 Myr (Frogel et al. 2003).

It must be cautioned that we have ignored some aspects of the problem in these simulations. Near–IR excess emission from disks surrounding the young low-mass stars might *dilute* the expected absorption strength of the photospheric features in the IR (Meyer et al. 1997). However, because PMS stars have sub–giant surface gravities, we are also *underestimating* the strength of CO feature which is surface gravity sensitive (Kleinmann and Hall 1986). We do not argue that these simulations are a perfect representation of what one should expect from the integrated light of super–star clusters. Nevertheless, we draw inspiration from Salpeter (2002), who, while musing about the longevity

of his 1955 paper, suggested that it is not important for all the assumptions in a calculation be correct, but that the largest uncertainties should tend to cancel!

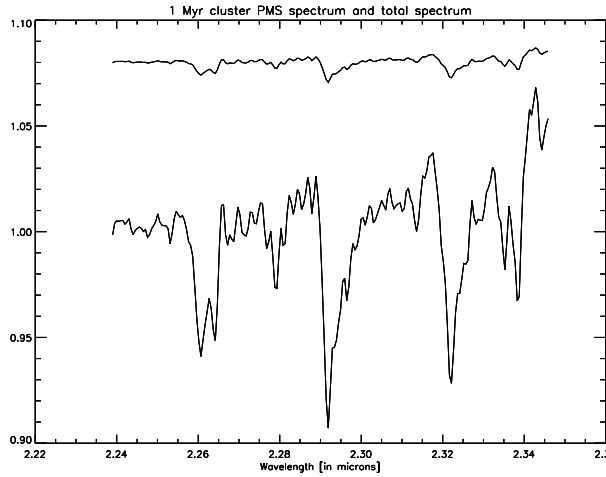

Figure 3. The total integrated K–band spectrum of a 1 Myr old 10^6 $M_\odot$ unresolved super–star cluster (top) and the associated spectrum of the PMS stars only (bottom). In a few hours of integration time on a 6–10 meter telescope, we should be able to detect the signature of the late–type low-mass stars (2–4% absorption features against the continuum) in candidate super–star clusters in NGC 4038/39.

4. Conclusions

Our conclusions can be briefly summarized at follows: 1) the stellar IMF observed in nearby star–forming regions is broadly consistent with the field star IMF and does not vary strongly with local conditions (Meyer et al. 2000); 2) sub–stellar objects contribute less than 10 % of the dynamical mass of young stellar populations (Wilking et al. 2004) and this fraction might vary from region to region (Briceno et al. 2002); 3) there may be a connection between the binary fraction in a young cluster, its stellar density, and the observed system IMF (Liu et al. 2003); 4) spectroscopic estimates of temperature and surface gravity are needed in order to survey down below the expected minimum mass for fragmentation in nearby molecular clouds (Gorlova et al. 2004); 5) while existing AO systems on 6–10m telescopes should enable us to probe down to the hydrogen burning limit throughout the Milky Way galaxy (e.g. W51), it will be extremely difficult to reach this limit even in the local group without higher spatial resolution afforded by the next generation of very large telescopes such as the LBT; and 6) it may be possible to detect directly the low-mass stellar component in the high SNR spectrum of an integrated super–

cluster in nearby interacting galaxies placing constraints on the ratio of high to low-mass stars (Meyer and Greissl 2004).

Acknowledgments We would like to thank the meeting organizers for providing such a stimulating get–together in such a lovely place where we could share ideas on this work with such generous and talented colleagues. We congratulate Prof. Salpeter on his lifetime of important achievements in astrophysics and wish him many more years of good health and happiness. This work was generously supported by a Cottrell Scholar's Award to MRM from the Research Corporation and NASA grant HST13-9846.

References

Bouvier, J., Stauffer, J.R., Martin, E.L., Barrado y Navascues, D., Wallace, B., Bejar, V.J.S. 1998, A&A, 336, 490

Briceno, C. Luhman, K.L., Hartmann, L., Stauffer, J.R., Kirkpatrick, J.D. 2002, ApJ, 580, 317

Burgasser, A.J, Kirkpatrick, J.D, McGovern, M.R., McLean, I.S., Prato, L., Reid, I.N. 2004, ApJ, 604, 827

Chabrier, G. 2003, ApJL, 585, 133

Close, L.M. et. al. 2003, ApJ, 599, 537

Duquennoy, A., Mayor, M. 1991, A&A, 248, 485

Figer, D., Kim, S., Morris, M., Serabyn, E., Rich, R., McLean, I. 1999, ApJ, 118, 2327

Ghez, A.M., Neugebauer, G., Matthews, K. 1993, AJ, 106, 2005

Gorlova, N.I., Meyer, M.R., Rieke, G.H., Liebert, J. 2003, 593, 1074

Greene, T.P., Meyer, M.R. 1995, ApJ, 450, 233

Hillenbrand, L.A., Carpenter, J.M. 2000, ApJ, 540, 236

Hinz, P.M., Hoffmann, W.F., Hora, J.L. 2001, ApJL, 561, 131

Kassin, S.A., Frogel, J.A., Pogge, R.W., Tiede, G.P., Sellgren, K. 2003, AJ, 126, 1276

Kleinmann, S.G., Hall, D.N.B. 1986, ApJS, 62, 501

Leinert, Ch., Zinnecker, H., Weitzel, N., Christou, J., Ridgway, S.T., Jameson, R., Haas, M., Lenzen, R. 1993 A&A, 278, 129

Liu, W.M., Meyer, M.R, Cotera, A.S., Young, E.T. 2003, AJ, 126, 1665

Luhman, K.L. 1999, ApJ, 525, 466

Luhman, K.L., Rieke, G.H. 1998, ApJ, 497, 354

Mainzer, A.K., McLean, I.S. 2003, ApJ, 597, 555

Mengel, S., Lehnert, M.D., Drob, D.P., Porter, H.S. 2002, A&A, 383, 137

Meyer, M.R., Calvet, N., and Hillenbrand, L. 1997, AJ, 114, 198

Meyer, M.R., Edwards, S., Hinkle, K.H., Strom, S.E. 1998, ApJ, 508, 397

Meyer, M.R. et. al. 2000, in Protostars and Planets IV, ed. Mannings, V., Boss, A.P., Russell, S.S. (Tucson: University of Arizona Press), p. 121

Meyer, M.R., and Greissl, J. 2004, ApJ, submitted.

Muench, A.A., Lada, E.A., Lada, C.J., Alves, J. 2002, ApJ, 573, 366

Najita, J.R., Tiede, G.P., Carr, J.S. 2000, ApJ, 541, 977

O'Connell, R.W, Gallagher, J.S., Hunter, D.A. 1994, AJ, 108, 1350

Okumura et. al. 2000, ApJ, 543, 799

Peale, S.J. 1999, ApJL, 524, 67

Reid, I.N., et al. 1999, ApJ, 521, 613
Reipurth, B., Clarke, C. 2001, AJ, 122, 1508
Salpeter, E.E. 2002, ARA&A, 40, 1
Salpeter, E.E. 1955, ApJ, 121, 161
Siess, L., Dufour, E., Forestinin, M. 2000, A&A, 358, 593
Spitzer, L. 1978, *Physical Processes in the Interstellar Medium*, (Wiley: New York).
Stolte, A., Brandner, W., Grebel, E.K., Figer, D.F., Eisenhauer, F., Lenzen, R., Harayama, Y. 2003, Msngr, 111, 9
Udry, S. et al. 2000, A&A, 356, 590
Wilking, B.A., Greene, T.P., Meyer, M.R. 1999, AJ, 117, 469
Wilking, B., Meyer, M., Greene, T., Mikhail, A., Carlson, G. 2004, AJ, 127, 1131
de Zeeuw, P.T., Hoogerwerf, R., de Bruijne, J.H.J., Brown, A.G.A., Blaauw, A. 1999, AJ, 117, 354

Figure 4. Mike Meyer and wife: a happy couple!

MID-IR OBSERVATIONS AT HIGH SPATIAL RESOLUTION: CONSTRAINTS ON THE IMF IN VERY YOUNG EMBEDDED SUPER STAR CLUSTERS

N. Leticia Martín-Hernández[1], Daniel Schaerer[1,2] and Marc Sauvage[3]
[1]*Observatoire de Genève, 51 Chemin des Maillettes, CH-1290 Sauverny, Switzerland,*
[2]*Laboratoire Astrophysique de Toulouse-Tarbes (UMR 5572), Observatoire Midi-Pyrénées, 14 Avenue E. Belin, F-31400 Toulouse, France,*
[3]*CEA/DSM/DAPNIA/SAp, CE Saclay, 91191 Gif sur Yvette Cedex, France*
leticia.martin@aobs.unige.ch, daniel.schaerer@obs.unige.ch, msauvage@cea.fr

Abstract In order to determine reliable constraints on the upper part of the IMF in very young embedded super-star clusters we have undertaken high spatial resolution mid-IR imaging and spectroscopy of young starburst galaxies with TIMMI2 on the ESO 3.6 m. Results on the prototypical starburst NGC 5253 are presented here using detailed photoionisation models to reproduce a large number of observables including mid-IR to radio observations at various spatial resolutions.

1. The N-band spectrum of the embedded SSC in NGC 5253

The embedded super-star cluster (SSC) in NGC 5253, denominated C2 by Alonso-Herrero et al. (2004), is one of the most massive SSCs observed so far. The N-band (8–13 μm) spectrum of this hidden SSC, obtained with TIMMI2, is characterised by a rising continuum due to warm dust, a silicate absorption and a strong [S IV] line at 10.5 μm. Weaker lines of [Ar III] at 9.0 μm and [Ne II] at 12.8 μm are also present. The spatial scale of the observations greatly determine the mid-IR appearance of NGC 5253, with important implications on the interpretation of line fluxes in terms of the properties (age, IMF, etc.) of the embedded cluster. In particular, a comparison with the fluxes measured by the large ISO aperture shows that most of the high-excitation [S IV] line flux is emitted by C2, while only $\sim$20% of the total [Ne II] line flux comes from it.

E. Corbelli et al. (eds.), The Initial Mass Function 50 Years Later, 255–256.

2. Constraints on the age and upper mass cutoff

We have computed sets of nebular models with the photoionisation code CLOUDY using the evolutionary synthesis code STARBURST99 to model the integrated properties of the stellar cluster. The interpretation of the nebular lines in terms of properties of the ionising cluster depends largely on the local abundance and the ionisation parameter U. The detailed dependence of the mid-IR lines on other parameters such as the cluster age, upper mass cutoff and power law index of the IMF, as well as the presence of internal dust and the density structure is discussed in Martín-Hernández et al. (2004). In the case of the SSC C2, high spatial resolution observations at different wavelengths – near-IR with HST (Alonso-Herrero et al. 2004) and Keck (Turner et al. 2003), mid-IR with TIMMI2 and radio with VLA (e.g. Turner & Beck 2004) – have allowed us to strongly constrain the geometry of the region (i.e. Lyman photon rate, density, filling factor and inner/outer radius), leading to an ionisation parameter $\log U \geq -0.5$ dex. This constraint on U leads to two possible solutions for the age and upper mass cutoff of C2 when comparing the observed line fluxes with the predicted ones: *1)* a young (< 4 Myr) cluster with a "non-standard" IMF with a low upper mass cutoff $M_{\rm up} < 50\,{\rm M}_{\odot}$, and *2)* a cluster of $\sim 5-6$ Myr with a standard high upper mass cutoff ($M_{\rm up} \sim 100\,{\rm M}_{\odot}$). The photoionisation models allow higher values of $M_{\rm up}$ for ages < 4 Myr only in the case of an H II region much larger than what the radio continuum imply or when a solar metallicity, for which there is no indication, is considered for the cluster. A young age ($<$ 4 Myr) would agree with the lack of supernovae signatures in C2 and in case of being confirmed, would be the first indication for a “non-standard”, low upper mass cutoff of the IMF for an individual massive cluster. An older age of $\sim$ 5–6 Myr would imply that it is possible to “contain” and hide such a compact cluster for a longer time that what it is generally thought. Based on the available information, we are not able to favour one solution over the other. Observations of massive stellar clusters with similar characteristics will be essential to see if the same result is found.

References

Alonso-Herrero, A., Takagi, T., Baker, A. J., et al. 2004, ApJ, 612, 222
Martín-Hernández, N. L., Schaerer, D., Sauvage, M. 2004, A&A, submitted
Turner, J. L. & Beck, S. C. 2004, ApJ, 602, L85
Turner, J. L., Beck, S. C., Crosthwaite, L. P., et al. 2003, Nature, 423, 621

WOLF-RAYET STARS AS IMF PROBES

Claus Leitherer
Space Telescope Science Institute, 3700 San Martin Drive, Baltimore, MD 21218, USA
leitherer@stsci.edu

Abstract Wolf-Rayet stars are the evolved descendents of massive stars. Their extraordinary properties make them useful tracers of the stellar initial mass function (IMF) in a young stellar population. I discuss how the interpretation of spectral diagnostics are complicated by the interplay of stellar, nebular, and dust properties. There is mounting observational evidence for spatial inhomogeneities in the gas and dust distribution. The interplay of these inhomogeneities can significantly alter frequently used star-formation and IMF indicators. Specific examples presented in this contribution are the starburst galaxies NGC 1614, NGC 2798, and NGC 3125.

1. Background

Star formation in powerful starbursts is an ubiquitous phenomenon both locally and at the highest observable redshifts. A prominent subset of the starburst class are the so-called Wolf-Rayet (W-R) galaxies, whose observational characteristic is the broad emission bump around 4640 – 4690 Å (Conti 1991). The compilation by Schaerer et al. (1999) lists 139 members.

W-R galaxies are important because they permit a study of the star-formation properties via *stellar* spectral features, as opposed to indirect tracers based on gas and/or dust emission. Hot stars are notoriously elusive even in the strongest starbursts because their spectral signatures are too weak, coincide with nebular emission lines, or are in the satellite-ultraviolet (UV). W-R stars are the only hot, massive stellar species detectable at optical wavelengths. This is because they have the strongest stellar winds, which in combination with their high temperatures produce broad ($\sim$1000 km s^{-1}) emission lines not coinciding with emission from H II regions. Examples are N III λ4640, C III λ4650, He II λ1640 and λ4686, C III λ5696, and C IV λ5808. The mere detection of such features proves the presence of stars with masses above 40 – 60 M$_\odot$ (depending on chemical composition) since only stars this massive can evolve into the W-R phase. This powerful diagnostic can be used for, e.g., inferring a massive star population when the space-UV is inaccessible due to dust (in-

E. Corbelli et al. (eds.), The Initial Mass Function 50 Years Later, 257–262.

frared [IR]-luminous galaxies), or when broad nebular lines veil the O stars (Seyfert2 galaxies). Vice versa, the relative strength of the various W-R features gives clues on the distribution of W-R subtypes, which in turn provides much sought constraints on stellar evolution theory.

2. W-R stars as proxies for ionizing O stars

We are currently involved in an optical+near-IR survey of luminous starburst galaxies (Leão, Leitherer, & Bresolin, in prep.). Our goals are (i) to establish an unbiased sample of metal-rich W-R galaxies, (ii) to investigate the stellar content from purely stellar tracers, (iii) to cross-calibrate stellar and nebular diagnostics in metal-rich galaxies, (iv) to correlate the derived stellar initial mass function with host galaxy parameters, and (v) to test stellar evolution theory in high-metallicity environments. Our new survey of starburst galaxies is drawn from an IRAS sample of Lehnert & Heckman (1995). The galaxies have $10 < \log L_{\rm IR}/{\rm L}_\odot < 11.5$, warm IR colors, and are not AGN dominated. Detection of the W-R features, together with other standard diagnostics allows us to probe the stellar content with a suite of models we have developed (Leitherer et al. 1999). In particular, we can search for or against evidence of a peculiar IMF at high metallicity, as indicated, e.g., by IR observations.

Thornley et al. (2000) carried out an ISO spectroscopic survey of 27 starburst galaxies with a range of luminosities from 10^8 to 10^{12} L$_\odot$. The [Ne III] 15.6 μm and [Ne II] 12.8 μm lines are particularly useful. The ionization potentials of neutral and ionized Ne are 22 and 41 eV, respectively, the two lines are very close in wavelength (12.8 and 15.6 μm), and they have similar critical densities. This makes the line ratio a sensitive probe for various star formation parameters, in particular the upper mass cutoff of the IMF ($M_{\rm up}$) and the age and duration of the starburst. Photoionization models of Thornley et al. and Rigby & Rieke (2004) suggest that stars more massive than about 35 to 40 M$_\odot$ are deficient in the observed sample. Either they never formed because of a peculiar IMF, or they have already disappeared due to aging effects. This result echos that obtained from ground-based near-IR spectroscopy: the strategic recombination lines are powered by a soft radiation field originating from stars less massive than $\sim$40 M$_\odot$ (Doyon et al. 1992). An upper-mass cutoff as low as 40 M$_\odot$, however, is difficult to reconcile with the ubiquitous evidence of very massive stars with masses of up to 100 M$_\odot$ in many starburst regions (e.g., Leitherer et al. 1996; Massey & Hunter 1998; González Delgado et al. 2002). Therefore the alternative explanation, an aged starburst seems more plausible. Under this assumption, stars of masses 50 – 100 M$_\odot$ are initially formed in most galaxies, but the starbursts are observed at an epoch when these stars are no longer present. This implies that the inferred burst durations must be less than a few Myr. Such short burst time scales are surprising, in particular for

luminous, starburst galaxies whose dynamical time scales can exceed tens of Myr. Both the peculiar IMF or the short starburst time scales in dusty, IR-bright starbursts are quite unexpected and pose a challenge to conventional models in which the starburst is fed by gas inflow to the nucleus over tens of Myr as a result of angular momentum loss.

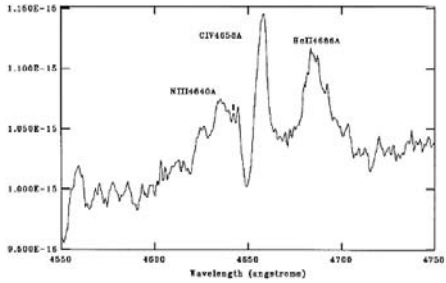

Figure 1. Close-up view of the spectral region around 4650 Å in the starburst galaxy NGC 1614.

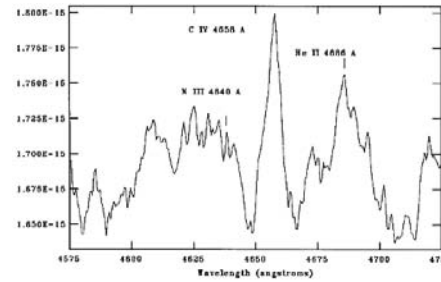

Figure 2. Same as Fig. 1, but for NGC 2798. Note the broad emission-line features from W-R stars.

Early results from our W-R survey urge caution when relating nebular IMF tracers to the actual stellar content. Several metal-rich starburst galaxies exhibiting a soft radiation field do in fact have a substantial W-R population. As an example, we reproduce in Figs. 1 and 2 portions of Keck LRIS spectra around 4650 Å of NGC 1614 and NGC 2798, two archetypal starburst galaxies with low nebular excitation. We clearly detect the tell-tale signatures of W-R stars in these galaxies. Unless stellar evolution proceeds differently than in our Galaxy, massive O stars must be present as well. The fact that we do not *directly* observe these O stars is no contradiction: their spectral lines will be hidden by coinciding nebular emission lines. We should, however, detect their ionizing radiation in a proportion predicted by the measured number of W-R stars and the expected ratio of W-R/O stars. The deficit of radiation suggests that indirect star-formation tracers, like nebular lines, still require careful calibration, in particular when applied to dusty, metal-rich starbursts.

After advocating the use of W-R stars to constrain the IMF, we will present a cautionary view point in the next section. Interpretation of the stellar W-R feature may sometimes be complicated by the inhomogeneous structure of the surrounding interstellar medium (ISM).

3. The extraordinary W-R cluster in NGC 3125

As part of a larger project to quantify the stellar and interstellar properties of local galaxies undergoing active star formation (Chandar et al., in prep.), we have obtained HST Space Telescope Imaging Spectrograph (STIS) long-slit

far- and near-UV spectra for 15 local starburst galaxies. The target galaxies were selected to cover a broad range of morphologies, chemical composition, and luminosity. Most importantly, target selection was not based on W-R content.

The UV counterpart of the optical He II λ4686 line is the $3 \rightarrow 2$ transition of He^+ at 1640 Å. Broad He II λ1640 emission is seen in the UV spectra of individual Galactic and Magellanic Cloud W-R *stars* (e.g., Conti & Morris 1990) but is not prevalent in the integrated spectra of *galaxies* because of the overwhelming light contribution from OB stars in the UV. We observe two different line morphologies of He II λ1640 emission in local starburst galaxies. Some galaxies show narrow, nebular He II emission, while others have a broader profile. If massive stars are forming, He II λ1640 can sometimes appear as a nebular recombination emission line (e.g., Garnett et al. 1991), which has a characteristic narrow-line morphology. In the following we will focus on one outstanding starburst region in our sample: NGC 3125-1. The measured He II FWHM of 5.9 ± 0.4 Å is clearly broader than the estimated instrumental profile of 2.6 Å. The corrected width of the He II λ1640 line is 1000 km s^{-1}. Similar line widths are typically found in the latest subtypes of individual WN stars.

NGC 3125-1 has by far the largest He II λ1640 equivalent width in our sample. In Fig. 3 we show the UV spectrum of this object. The 1640 Å emission is quite prominent and appears significantly stronger than the C IV emission at 1550 Å. In addition to this feature, we also see N IV λ1488 and N IV λ1720 emission typically found in W-R stars, consistent with our interpretation that the strong He II λ1640 emission arises in the winds of massive stars. We estimate that 6100 WNL stars reside in this starburst region, making it the most W-R-rich known example of an individual starburst cluster in the local universe. What makes this region extraordinary is the number of W-R stars relative to other massive stars. The W-R features in Fig. 3 are almost undiluted compared with those seen in single W-R stars. Therefore, most of the continuum light must be emitted by the very same W-R stars. Quantitative modeling leads to approximately equal W-R and O-star numbers. Such an extreme ratio is excluded by stellar evolution models, even for a most unusual IMF.

How can we reconcile these observations with our current understanding of W-R stars? The UV continuum slope is normally dominated by OB stars; however, in this case the large number of W-R stars also makes a significant contribution. One possible explanation is that we are seeing the W-R stars through a "hole" where their energetic winds have blown out the natal cocoon earlier than have the OB stars. The often large reddening derived in starburst regions is consistent with the generally accepted scenario in which very young

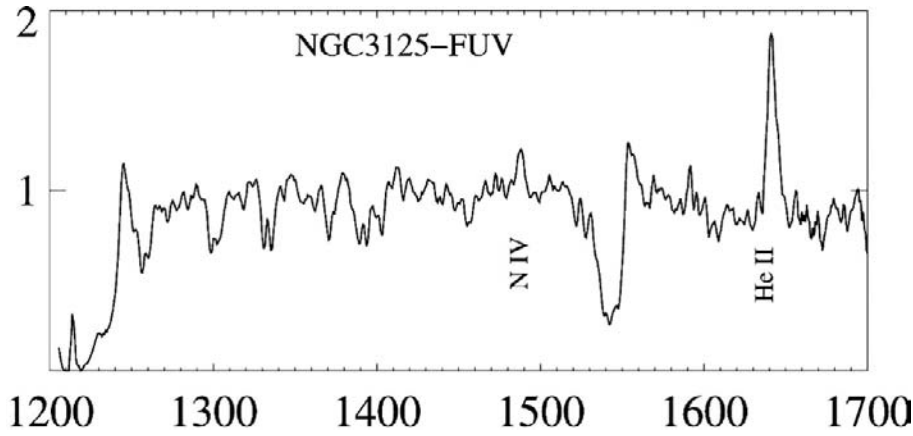

Figure 3. Far-UV spectral region of the starburst region NGC 3125-1. Strong, broad He II at 1640 Å indicates several thousand W-R stars. The W-R stars provide a substantial fraction of the continuum light as well (Chandar et al. 2004).

clusters remain embedded in their natal material until energetic stellar winds from evolving massive stars blow out the surrounding gas and dust.

If W-R stars are preferentially less attenuated than OB stars in NGC 3125-1, the *equivalent width* of He II λ1640 and other W-R lines is skewed towards artificially large values because for a standard stellar population surrounded by a homogeneous ISM, the continuum is emitted by the less massive OB stars. If the ISM is inhomogeneous, a textbook property of a spectral line associated with a single star changes: the equivalent width becomes reddening dependent.

4. Conclusions

Determining the massive-star IMF in starburst regions often relies on indirect methods, such as the recombination luminosity of the ionized gas. While this technique has been demonstrated to be quite reliable in normal galaxies (Kewley et al. 2002), it may break down in extreme cases. The conditions prevailing in dusty, metal-rich starbursts may lead to a decoupling of the emitted ionizing and the observed recombination luminosity. The reasons are still not fully understood but may be related to a combination of the destruction of photons by dust and the spatial morphology of the dust. The latter effect is particularly relevant in powerful starbursts where supernovae and stellar winds can have large effects on the ISM. Starburst models as well as observations of galactic superwinds indicate that 1% to 2% of the bolometric luminosity of starbursts is converted into mechanical luminosity. This mechanical energy input can remove interstellar gas from the star-formation site on a time scale much shorter than the gas consumption time scale, which can be hundreds of

Myr. The resulting ISM structure invalidates the often made assumption of isotropy and homogeneity. As a result, IMF indicators can mimic anomalous stellar populations. In some cases, even purely stellar indicators may change. If different stellar phases are associated with different dust columns, the stellar equivalent widths in the integrated population spectrum may probe dust morphologies, rather than the IMF.

Acknowledgments I am grateful to Rupali Chandar and João Leão for several comments which improved the manuscript.

References

Chandar, R., Leitherer, C., & Tremonti, C. A. 2004, ApJ, 604, 153
Conti, P. 1991, ApJ, 377, 115
Conti, P., & Morris, P. W. 1990, AJ, 99, 898
Doyon, R., Puxley, P. J., & Joseph, R. D. 1992, ApJ, 397, 117
Garnett, D. R., Kennicutt, R. C., Jr., Chu, Y.-H., & Skillman, E. D. 1991, PASP, 103, 850
González Delgado, R. M., Leitherer, C., Stasińska, G., & Heckman, T. M. 2002, ApJ, 580, 824
Kewley, L. J., Geller, M. J., Jansen, R. A., & Dopita, M. A. 2002, AJ, 124, 3135
Lehnert, M. D., & Heckman, T. M. 1995, ApJS, 97, 89
Leitherer, C., et al. 1999, ApJS, 123, 3
Leitherer, C., Vacca, W. D., Conti, P. S., Filippenko, A. V., Robert, C., & Sargent, W. L. W. 1996, ApJ, 465, 717
Massey, P., & Hunter, D. A. 1998, ApJ, 493, 180
Rigby, J. R., & Rieke, G. H. 2004, ApJ, 606, 237
Schaerer, D., Contini, T., & Pindao, M. 1999, A&AS, 136, 35
Thornley, M. D., Schreiber, N. M. F., Lutz, D., Genzel, R., Spoon, H. W. W., Kunze, D., & Sternberg, A. 2000, ApJ, 539, 641

Figure 4. A focused Claus Leitherer with Leonardo Testi in the courtyard.

V

THE ORIGIN OF THE IMF: ATOMIC AND MOLECULAR GAS TRACERS

Figure 5. Visit to the Abbey of Sant'Antimo.

Figure 6. Mrs. Marilisa Cuccia and the Beuthers.

Figure 7. Cooking spaghetti at La Bandita: a busy Alvio.

SMIDGENS OF FUEL FOR STAR FORMATION

Lyle Hoffman[1] and Edwin E. Salpeter[2]
[1]*Lafayette College, Easton, PA, USA*
[2]*Cornell University, Ithaca, NY, USA*
hoffmang@lafayette.edu, ees12@cornell.edu

1. Compact High Velocity Clouds and Mini-HVC

Compact High Velocity Clouds (CHVC) are relatively isolated gas clouds, detected in HI, with velocities typical of our Local Group of galaxies (LG), with angular diameters $\sim 1^o$ or slightly less, and with low metal abundances. CHVC may be good candidates for infall of (almost) primordial material into disk galaxies (Blitz et al. 1999; Braun & Burton 1999), which would replenish hydrogen and provide some dynamical stirring to encourage star formation. This could be of interest for large and small disk galaxies, but more-so for small dwarf irregular galaxies (dIrr) because of their larger ratio of surface area to volume. A possible example of such a CHVC/dIrr merger is shown in Hoffman et al. (2003).

There are at least three controversies about CHVC: (a) Their distances from the Milky Way are unknown, although opinions appear to be converging on 50-200 kpc (Burton, Braun & de Heij 2002; Maloney & Putman 2003). (b) Since even the central column densities of neutral hydrogen (N_{HI}) are not far above $10^{19}\ \mathrm{cm}^{-2}$, the outer layers with smaller N_{HI} may have considerable amounts of ionized hydrogen (see below). (c) The systematic detection surveys for CHVC are not complete for N_{HI} below $10^{19}\ \mathrm{cm}^{-2}$, so we do not know if there are many more clouds with smaller N_{HI}.

In the course of Arecibo mapping with much better N_{HI} sensitivity of two small HVC and of low column density emission around four of the large number of quasars surveyed in HI by Lockman et al. (2002), we have found a total of 15 very small clouds, all well removed spatially or in velocity from any catalogued HVC. Typically, diameters of these mini-HVC are about 15', and central column densities are below $10^{19}\ \mathrm{cm}^{-2}$. Peak column density N_{HI} and diameter D_{HI} for our 15 mini-HVC are both mostly smaller than for CHVC, but the distributions overlap, and the mini-HVC might be an extension of CHVC. If we ignore all possible selection effects, we are led to conclude that low column density CHVC have been undercounted by the surveys and that there are

E. Corbelli et al. (eds.), The Initial Mass Function 50 Years Later, 265–266.

many more in total. If mini-HVC have distances around 200 kpc, as suggested for CHVC, their HI masses would be only $\sim 10^3$ to a few $\times 10^4$ $M_\odot$. However, since N_{HI} is smaller than for CHVC, the ratio of ionized to neutral hydrogen is likely to be large.

2. Discussion

For hydrogen gas with volume density n_H and ionization rate I, due to extragalactic UV plus collisions, there is a critical HI column density $N_{crit} \propto I/n_H$ where the hydrogen is 50% ionized. For $N_{HI} > N_{crit}$ there is little HII (Corbelli & Bandiera 2002; Corbelli, Salpeter & Bandiera 2001; Sternberg, McKee & Wolfire 2002). Below N_{crit} the neutral component decreases very rapidly with decreasing $N_{H,tot}$, so the HI scalelength is a few times smaller than that for total hydrogen. If $N_{crit} << 10^{19}$ cm^{-2} for a CHVC, the ionized hydrogen contributes little and the total gas mass (at 200 kpc) would be about 10^6 $M_\odot$. If $N_{crit} \sim (1 \text{ or } 2) \times 10^{19}$ cm^{-2} as for spiral galaxies, the true total hydrogen scalelength would be much larger and $M_{H,tot}$ could be $> 10^7$ $M_\odot$.

Hα recently detected in several CHVC by Tufte et al. (2002) exceeds that produced solely by extragalactic UV photoionization, and collisional ionization by a hot intragroup medium (Burstein & Blumenthal 2002) is a possibility. For mini-HVCs we have the additional uncertainty that their spatial distribution may differ from that of CHVC. Mapping of additional Lockman et al. sources, or blind mapping of large regions of sky to much higher sensitivity than planned for the ALFA consortium surveys at Arecibo, would be helpful.

References

Blitz, L., et al. 1999, ApJ, 514, 818
Braun, R., & Burton, W. B. 1999, A&A, 341, 437
Burstein, D., & Blumenthal, G. 2002, ApJ, 574, L17
Burton, W. B., Braun, R., & de Heij, V. 2002, in *High-Velocity Clouds*, eds. van Woerden H., Wakker B.P., Schwarz U.J., & de Boer, K (Dordrecht:Kluwer)
Corbelli, E., & Bandiera, R. 2002, ApJ, 567, 712
Corbelli, E., Salpeter, E. E., & Bandiera, R. 2001, ApJ, 550, 26
Hoffman, G. L., Brosch, N., Salpeter, E. E., & Carle, N. J. 2003, AJ, 126, 2774
Lockman, F. J., et al. 2002, ApJS, 140, 331
Maloney, P. R., & Putman, M. E. 2003, ApJ, 589, 270
Sternberg, A., McKee, C. F., & Wolfire, M. G. 2002, ApJS, 143, 419
Tufte, S. L., et al. 2002, ApJ, 572, L153

THE INITIAL MASS FUNCTION IN THE CONTEXT OF WARM IONIZED GAS IN DISK GALAXIES

René A.M. Walterbos
New Mexico State University, Astronomy Department, Las Cruces, NM 88003, USA
rwalterb@nmsu.edu

Abstract Massive stars, through their ionizing radiation and mechanical energy input, play a crucial role in establishing the physical conditions in the interstellar medium in disk galaxies. The ionizing luminosity from these stars is strongly dependent on their mass, and hence on the IMF for an ensemble of stars. A census of the massive stars present in particular environments can be used to infer the IMF. A separate test is to verify that the massive stars present can account for the observed ionization of the interstellar medium present in both HII regions and in the diffuse ionized medium. We summarize the progress that has been made in measuring the ionization requirements of both of these media, and describe recent tests of this ionization energy balance.

1. Introduction

The ionizing radiative output from massive stars is critically dependent on the stellar IMF. Estimates of the star formation rates in galaxies, based on measurements of Hα fluxes or other recombination lines can easily differ by factors of 3 depending on the assumed IMF (e.g. Kennicutt 1983). Since the ionizing UV flux of the stars can never be directly observed, the photo-ionized interstellar medium provides important, if indirect, information on the massive stars present in galactic disks.

HII regions, though most prominent, do not make up the bulk of the ionized ISM. The Warm Ionized Medium (WIM), also referred to as Diffuse Ionized Gas (DIG), is the most massive component of the interstellar medium in disk galaxies (Reynolds 1991). It contains far more mass than either HII regions or the Hot Interstellar Medium, and the column densities can begin to approach those of neutral atomic hydrogen. The medium is diffusely distributed, filling 20% or more of the disk volume. A beautiful view of the Galactic WIM is obtained in the recent WHAM survey (Haffner et al. 2003). In edge-on systems,

E. Corbelli et al. (eds.), The Initial Mass Function 50 Years Later, 267–272.

the gas is seen to extend to many kpc above the disk in galaxies with vigorous rates of star formation (e.g. Rand 1997, Hoopes et al. 1999).

One of the major challenges has been to understand the source of ionization of this gas. In the Milky Way, it is estimated that the ionization requirement is about 15% of that for HII regions (Reynolds 1991). This is too large to account for the ionization by supernova shocks, cosmic rays, or old hot stars. In external galaxies, detailed measurements of the Hα emission from galactic disks shows that the WIM can contribute as much of 40 to 50% of the total Hα luminosity. Based solely on these energy requirements, ionizing photons from massive stars must account for the bulk of the ionization, though not necessarily all of it. There are three critical tests of the photo-ionization picture. One is to compare the inferred ionizing luminosities, derived from the Hα observations assuming Case B recombination with the predicted ionizing luminosities from the massive stars present in and outside HII regions. The second is to measure forbidden line rations in the WIM and compare them against photo-ionization models. The third is to look for helium recombination lines in the WIM; if He is fully ionized, this places severe constraints on the spectral types of the stars that contribute to the ionization of the WIM. We will focus here on the first of these tests.

2. Ionization Tests in the LMC and M33

Our first test of the photo-ionization of the DIG by massive stars centered on a study of HII regions and DIG regions in M33, using data from HST (Hoopes & Walterbos 2000). The second test is a more recent study of HII regions in the LMC (Voges et al. 2004a, Voges et al. 2004b, see also Oey & Kennicutt 1997). The latter is based on data from Massey 2002 on the stellar spectral types and photometry. The two studies use similar analyses. Hα fluxes of HII regions, corrected for average reddening, are translated into Lyman continuum photon requirements. In the case of M33, the HST FUV-optical photometry provided colors and magnitudes for massive stars inside and outside HII regions, from which spectral types were estimated. In the case of the LMC HII regions, the spectral types of embedded stars were either taken from spectral classification whenever available, else estimated from UBV colors and absolute magnitude estimates. It should be noted that UBV colors in themselves are poor discriminants of the spectral type of massive stars. Adding the absolute magnitude helps in at least estimating a luminosity class. But spectroscopic classification is preferred, or, in the absence of that, Far-UV to optical colors. Unfortunately, our intent to use UIT data for the LMC regions did not succeed, due to insufficient accuracy of the UIT photometry. Atmospheric models Smith et al. 2002 for the appropriate spectral types then provide estimated ionizing luminosities

for the stars. In total, we tested about 30 regions in M33 (both HII regions and DIG regions) and 39 HII regions in the LMC.

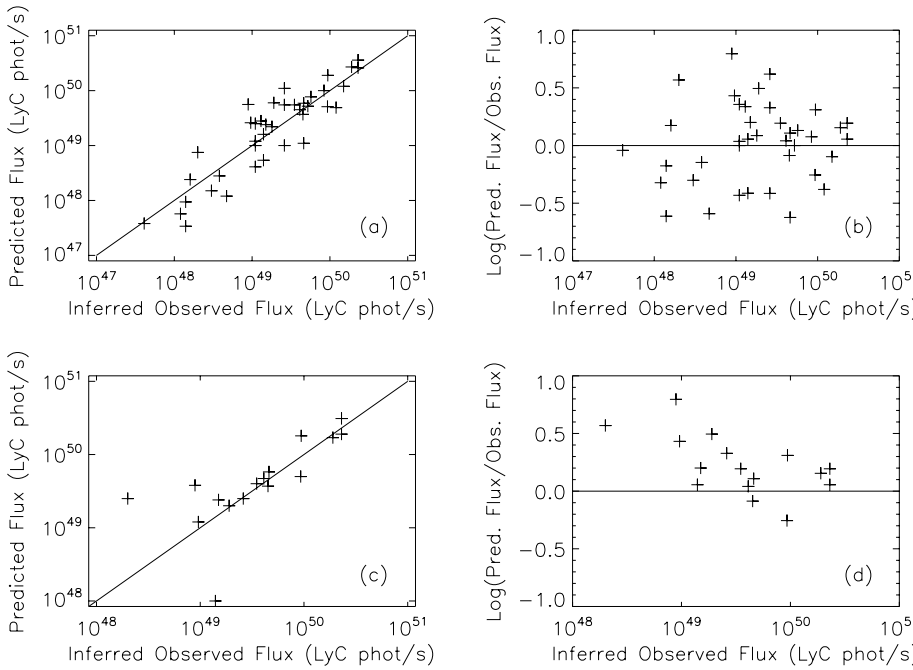

Figure 1. Comparison of predicted and inferred ionizing luminosities for several HII regions in the LMC. The predicted luminosities are based on knowledge of the massive stars observed in the HII regions, while the inferred luminosities come from reddening corrected Hα fluxes of the HI regions. See text for details.

The results can be summarized as follows. First, the agreement between predicted and inferred ionizing luminosities was perhaps better than one might expect from these admittedly rough methods. Our hope was to have a large enough sample to derive conclusions based on the ensemble of regions, not for any one region in particular. This seems to be possible. For M33, the study indicated that about half of the ionization of the DIG could be accounted for by the field O stars observed to be present outside HII regions. The remaining part could just be met by leakage of ionizing photons from massive stars inside HII regions: we derived an average ratio of predicted to inferred Lyman continuum photon rates of 1.07 ± 0.26 for stars inside HII regions. That means that 20 to 30% of ionizing photons might be leaking from HII regions, which is enough to ionize the remaining half of the DIG.

For the LMC we only looked at HII regions so far, not yet at field star populations. The results are shown in Figure 1. It is seen that the massive

stars can comfortably account for the ionization of the HII regions, and that some photons seem to be available to ionize the DIG. On average, we find a ratio of predicted to inferred ionizing photon rates of 1.4 with a slight trend of a higher ratio (i.e. more ionizing photons available) for the lower luminosity HII regions, but the significance of this needs to be verified. Interestingly, we concluded the same for M33. The notion that smaller HII regions would be more "leaky" is somewhat counterintuitive, perhaps.

3. Discussion

If our determinations of the Lyman continuum photon rates are correct, we seem to have just about enough ionizing photons to account for the ionization of the bulk of the DIG in the two galaxies we studied. That doesn't prove how or if photons actually escape from HII regions, but it is reassuring that the numbers are reasonable. Our results also seem to imply that not many ionizing photons actually escape into intergalactic space, a conclusion which is consistent with estimates of escape in the solar neighborhood (Dove et al. 2000) and with the lack of evidence of escaping ionizing photons from nearby starburst galaxies (e.g. Deharveng et al. 2001, Malkan et al. 2003).

Note that we have not attempted to construct a present day mass function or initial mass function from the data on the massive stars. Massey has done this in various studies of the LMC stars, deriving a very steep field IMF and a more normal IMF for the stars in associations. We cannot comment on that result, since we did not study field stars and since we directly go to an empirical estimate of a particular star's spectral type and luminosity class. Still, our results show consistency between the UV flux estimated from the spectral types and the ionization observed in the ISM. In at least this sense, the inferred knowledge of the massive stellar population passes an independent test. There are many uncertainties in our estimates, and it is remarkable the agreement is as good as it is. To improve on this type of work, one needs more actual spectroscopically determined spectral types for stars and a more detailed study of the reddening for individual regions. One has to also close the loop by testing whether He is ionized in the DIG or not. Photo ionization of He requires stars of spectral type O7 or earlier. Are the spectral types derived for field and HII region stars consistent with the presence or absence of He ionization in the DIG? So far, ionized helium in external galaxies has been detected in the bright DIG in M33 (Hoopes & Walterbos 2003, Voges et al. 2004a) and above the disk of the edge-on galaxy NGC 891 (Rand 1997). We hope to answer this question in more detail for the fainter DIG in the near future.

Acknowledgments It was an honor to be invited to a meeting to celebrate the many contributions and continuing challenges offered by Ed Salpeter. Many thanks to the organizers for a thoroughly planned meeting where the en-

vironment, food, and entertainment could not have been better. The LMC research described here is a joint project with Erica Voges and Sally Oey. Funding support for the LMC research was provided by NASA through the ADP Program, grant number NAG5-10768.

References

Deharveng, J.-M., Buat, V., Le Brun, V., Milliard, B., Kunth, D., Shull, J.M., & Gry, C. 2001, A&A 375, 805

Dove, J.B., Shull, J.M., & Ferrara, A. 2000, ApJ 531, 846

Haffner, L.M., Reynolds, R.J., Tufte, S.L., Madsen, G.J., Jaehnig, K.P., & Percival, J.W. 2003, ApJS 149, 405

Hoopes, C.G., & Walterbos, R.A.M. 2000, ApJ 541, 597

Hoopes, C.G., & Walterbos, R.A.M. 2003, ApJ 586, 902

Hoopes, C.G., Walterbos, R.A.M., & Rand, R.J. 1999, ApJ 522, 669

Kennicutt, R.C. 1983, ApJ, 272, 54

Malkan, M., Webb, W., Konopacky, Q. 2003, ApJ 598, 878

Massey, P., 2002, ApJS 141, 81

Oey, M.S., & Kennicutt, R.C. 1997, MNRAS 291, 827

Rand, R.J. 1997, ApJ 474, 129

Reynolds, R. 1991, in The Interstellar Disk-Halo Connection in Galaxies, Ed. H. Bloemen, (Kluwer) p.67

Smith, L.J., Norris, R.P.F., & Crowther, P.A. 2002, MNRAS 337, 1309

Voges, E., Walterbos, R.A.M., & Oey, S.M. 2004a, in Extraplanar Gas, Ed. R. Braun, in press

Voges, E., Walterbos, R.A.M., & Oey, S.M. 2004b, to be submitted to ApJ

Figure 2. Robert Braun, Giora Shaviv and René Walterbos.

Figure 3. A smiling toast: René Walterbos, Giora Shaviv, Edvige and Steve Beckwith.

Figure 4. Shantanu Basu, Al Glassgold, Sally Oey and René Walterbos.

TRACING THE STAR FORMATION CYCLE THROUGH THE DIFFUSE INTERSTELLAR MEDIUM

John M. Dickey
University of Tasmania, School of Maths and Physics, Hobart, TAS 7001, Australia
John.Dickey@utas.edu.au

Abstract The Initial Mass Function is the foundation of the cycle of chemical evolution of the Galaxy; to understand this cycle fully requires a paradigm for how gas propagates through the interstellar phases from hot to cold. Turbulence in the interstellar medium appears to be common to all the phases. The magnetic field also shows a hierarchy of structure that may be associated with turbulence in the gas. Observational tracers of the small scale structure of the diffuse interstellar gas are rare, but recent surveys have provided much new data in this area. This paper presents some recent results as background for driving the turbulence that may ultimately influence cloud collapse and star formation.

1. Background

The past 50 years have shown great advances in all areas of astronomy, many of which Ed Salpeter was behind in one way or another; an extreme case is the study of the Interstellar Medium, which grew in this period from almost nothing into a mature and diverse science. Ed led many of the theoretical developments in this field, but in this one area he also played a significant role in the observations. From the 1960's through the 1980's, Ed took a close interest in the Arecibo Observatory; he played a "friend of the telescope" role for more than 25 years, organizing in particular the scientific justifications for the two major upgrades to the antenna that were completed in the early 1970's and the late 1990's. The former enabled the telescope to study the λ21-cm HI line, and so Ed took a keen interest in this transition and the many things it tells us about physical conditions in the interstellar medium (ISM). Ed guided a whole generation of Ph.D. students and postdocs who worked on Galactic and extra-galactic neutral hydrogen observations from Arecibo and later from the VLA as well. In my own experience, Ed was always glad for a chance to stand a shift in the control room, and he formulated the most innovative and

E. Corbelli et al. (eds.), The Initial Mass Function 50 Years Later, 273–280.

clever data reduction strategies. This was particularly true for studies of the spatial fluctuations of the 21-cm emission discussed below.

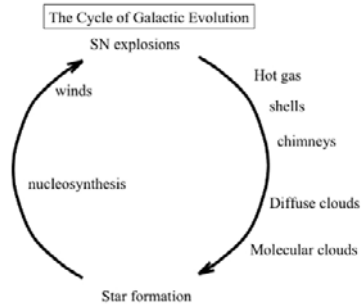

Figure 1. The cycle of nucleosynthesis and enrichment of the Interstellar Medium with heavy elements. This is a well-accepted paradigm for galaxy chemical evolution, but at the time of Ed Salpeter's study of the Initial Mass Function it was a very new idea.

The initial mass function of stars is a subject that incorporates both stellar and interstellar medium science, theoretical and observational, so a conference on this subject constitutes a great synthesis of diverse fields of astronomy. My own representation of this synthesis is sketched in figure 1, which shows the cycle of chemical evolution of galaxies. Stellar nucleosynthesis is on the left, with star formation at the bottom and the late stages of stellar evolution leading to mass loss from red giants and supernova explosions at the top. On the right is the interstellar medium, with the hot phase blown by supernova remnants at the top, and molecular clouds approaching Jeans instability at the bottom. Chemical evolution of a galaxy occurs as matter cycles clockwise around this circle. Ed Salpeter is the only person I know of who has contributed fundamental insight to all quadrants of the circle. But what I did not know until Ed's talk on the first day of this conference is that this entire synthesis was formulated by him even before his 1954 paper on the IMF. Ed told us that part of his motivation for taking up the IMF question was to dispel the misconception that the heavy elements were made in the big bang. So it must have been clear to him, if to no one else at the time, that a cycle like this was at work in the Galaxy. Today in every textbook for university classes in Introductory Astronomy this fact is one of the highlights. So it should be, for the origin of the atoms that make up our bodies and all else in the world around us is one of the few questions whose significance transcends our science to speak to the human condition.

The right hand side of figure 1 is the weak link, in spite of all our advances over the last 50 years. How the interstellar gas makes its way from the interiors

of the hot cavities blown by supernova remnants and stellar winds back to the dense, cold clouds is a process we understand qualitatively, but there are many gaps in our quantitative knowledge. A fundamental concept is that the ISM has phases, specific combinations of density and temperature that can coexist in stable equilibrium. This idea grew out of the work of Spitzer (e.g. 1956) and Field (e.g. 1958); by the 1970's it was a hot topic in theoretical astrophysics. Ed Salpeter realized that a critical issue in establishing this equilibrium is how supernova remnants evolve and cool, his work with Mansfield in the early 70's (Mansfield and Salpeter 1974) was one of the first computational projects to study this. By the early 1970's it was clear that static equilibrium among the phases was too simple, this paradigm did not incorporate the constant flux of energy and matter from one phase to another that completes our cycle. Ed's discussion in his 1975 Russell Lecture (Salpeter 1976) set out the problem and outlined the solution. Shortly afterward McKee and Ostriker (1977) showed in detail how such a dynamic theory could work. Bruce Draine's formulation of the heating of the diffuse medium by the dust grains completed the paradigm that has guided a generation of further work (Draine 1978, Draine and Salpeter 1979).

2. Turbulence in the Different Phases of the Interstellar Medium

To understand how hot gas ejected from stars makes its way down the ladder of interstellar phases to the cold clouds we need to consider not only the densities and temperatures of the phases but also the velocity field that drives thermal instabilities in the gas. This velocity field is described by a turbulence spectrum. In the ionized medium we know quite a bit about this turbulence, as shown on figure 2 (from Armstrong, Rickett, and Spangler 1995), which is the structure function or spatial autocorrelation function of the density field (reviewed recently by Elmegreen and Scalo, 2004). Scintillation and other effects in the propagation of pulsar signals probe this small scale structure in the ionized medium at a variety of scales, from roughly the radius of the earth up to about 0.01 pc. Extending a power law fit to the pulsar data to larger scales (the top left on figure 2), the amplitude of the structure function seems to match the fluctuations found by mapping the distribution of the gas. Interpreting this spectrum as a turbulent cascade fits our conception that the fluctuations in velocity and density should ultimately lead to star formation, but this is still rather wishful thinking if all we have is a tracer of structure in the **ionized** medium.

The neutral atomic medium shows a similar power law structure function on large scales, though for aperture synthesis observations of 21-cm emission it is simpler to study the spatial power spectrum of the density, which is the Fourier Transform of the structure function (Crovisier and Dickey 1983, Kalberla and

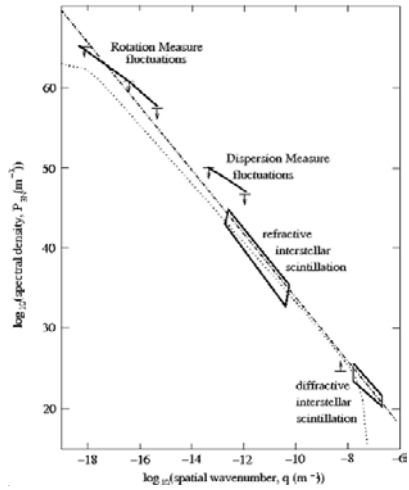

Figure 2. The structure function of the ionized phase of the interstellar medium, after Armstrong et al. (1995). Ranges over which this function is measurable with different techniques are indicated. A power law with index -3.7 fits the data well; this is close to the prediction of the Kolmogorov theory of turbulence.

Stenholm 1983, Green 1993). We can extend the spatial power spectrum analysis to smaller scales by studying fluctuations in the 21-cm absorption in front of extended continuum sources (Deshpande 2000). In a few cases these observations show fluctuations as small as $\sim$100 AU (Faison and Goss 2001); with the planned Square Kilometer Array telescope these studies can be extended much further, perhaps making the connection at last between the turbulence in the atomic medium and that of the molecular clouds (Dickey 2004). An interesting recent advance is the realization that the logarithmic slope of the 21-cm spatial power spectrum changes with the velocity averaging window width (Dickey et al. 2001, Stanimirovic and Lazarian 2001). This is evidence that our interpretation of the power law as reflecting a turbulent cascade of kinetic energy from large scales to small scales is valid.

3. Driving the Turbulence

How the ISM turbulence begins is a fundamental question. In recent 21-cm surveys of the Galactic plane we find large structures morphologically described as bubbles or chimneys (McClure-Griffiths et al. 2000, 2002; Normandeau 1995). The smaller ones could have been blown by one or a few supernova explosions, but the largest require some 10^{53} ergs of kinetic energy, suggesting that 100 or more supernova remnants contribute. The chimney in the third quadrant of the Milky Way shown on figure 3 (GSH 277+00+36 from McClure-Griffiths et al. 2003) has diameter of some 600 pc, swept up mass

about 4×10^6 $M_\odot$, expansion velocity 20 km s^{-1}, and dynamical age of 15 to 20 Myr. The structures in the walls of the chimney are intriguing (e.g. figure 4). Some can be interpreted as Rayleigh-Taylor fingers or "drips" with size scales of $\sim$ 10 pc, caused by the classic instability arising when a dense gas, here the walls of the shell, is accelerated by the hot, low density gas of the interior. The sizes of these drips match the prediction for the fastest growing mode of such instabilities assuming reasonable physical conditions for the shell. We can imagine that this instability will progress in the future, ultimately converting the kinetic energy of expansion of the shell into random motions that drive the turbulence on the outer scale of a few parsecs.

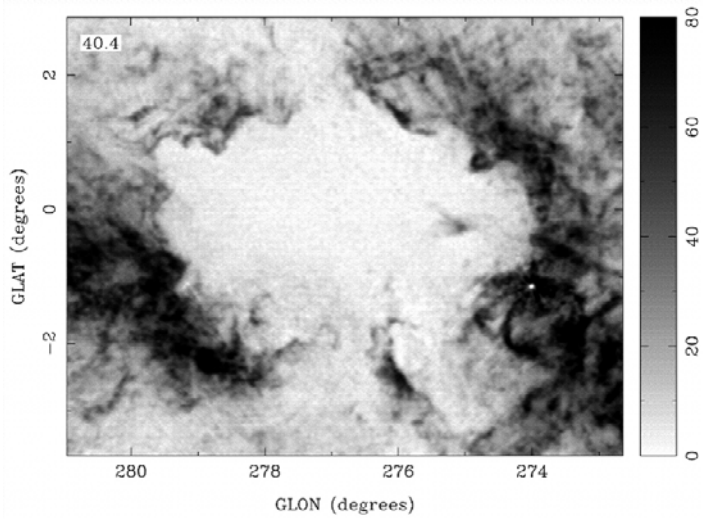

Figure 3. The large interstellar chimney, GSH277+00+36, from McClure-Griffiths et al. (2003). This large bubble is open into the halo above and below the disk. Features in the wall of the chimney are apparently Rayleigh-Taylor instabilities in the swept-up gas.

The magnetic field is another ingredient in the interstellar turbulence recipe that may have dynamical importance, particularly at the smaller scales. A new means of tracing the magnetic component of the turbulence has been developed recently by studying the structure in the linear polarization of the diffuse Galactic background emission at centimeter-waves (figure 4). This widespread synchrotron emission from cosmic ray electrons provides a background for Faraday rotation studies of the diffuse ionized medium (Gaensler et al. 2001). Looking at the structure function of the Rotation Measure deduced from this gives a broken power law, whose slope on the larger scales is typically a function of azimuthal angle (figure 5, from Haverkorn et al. 2004), suggesting that the large scale magnetic field direction is a modulating factor. Comparing with the diffuse Hα emission we can hope to deconvolve the effects of fluctuations

in the density of the ionized gas, leaving the magnetic field structure function alone.

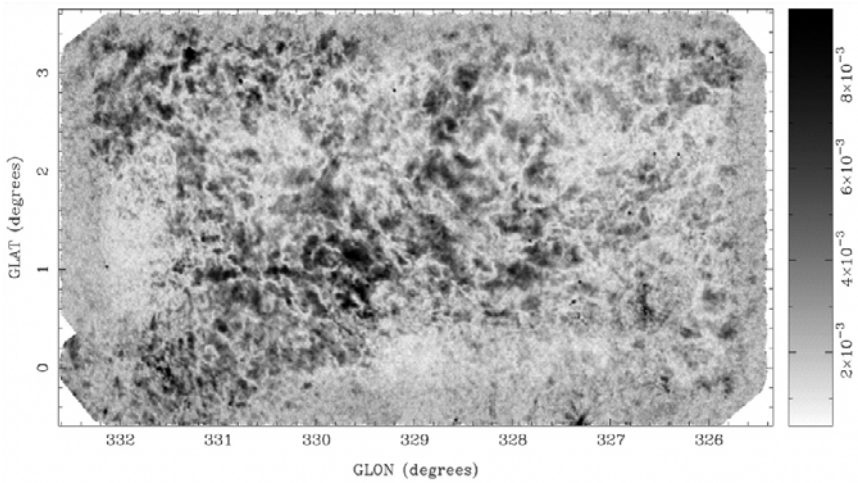

Figure 4. The linear polarized Galactic synchrotron background, as mapped in the Southern Galactic Plane Survey (Gaensler et al. 2001). The Faraday rotation of this background allows us to map the rotation measure due to the intervening magnetized plasma in the interstellar medium

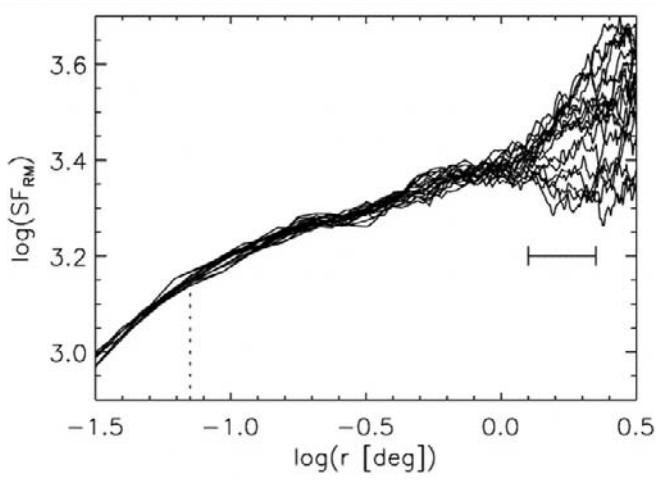

Figure 5. The structure function of the rotation measure derived from the data shown in figure 4, see Haverkorn et al. (2004). The structure function shows a strong azimuthal variation on the larger scales, that may reflect the large scale magnetic field direction.

4. Is the Turbulence Linked Between the Phases?

Tracing separately the structure functions of the magnetic field and of the velocity field in the ionized gas will allow us to determine which dominates the dynamics on various scales. It may be that magnetohydrodynamics controls the cascade of energy in the turbulence spectrum, as Ferrière et al. (1991) propose. If the magnetic field dominates then it may link the turbulence in the ionized and neutral atomic media, and possibly in the molecular clouds as well. This raises the issue of how disjoint the thermal phases are. The diffuse ionized gas and the warm neutral medium may blend, with the ionization fraction, $x = \frac{n(H\,\textsc{ii})}{n(H\,\textsc{ii})+n(H\,\textsc{i})}$, varying smoothly with position, as suggested by Spitzer and Fitzpatrick (1993). Some lines of sight show abrupt changes between neutral ($x \sim 0$) and fully ionized ($x \sim 1$) regions (Hausen et al. 2002), as might be expected if the ionization is due to uv photons near the Lyman edge. On the other hand, pulsar dispersion measures are easier to understand if a significant fraction of the electrons on most lines of sight reside in regions of partial ionization ($x \sim 0.5$).

Spatial mixing between the warm neutral and cool neutral media may be even more common than mixing between the neutral and ionized phases. Recent 21-cm observations by Heiles and Troland (2002) suggest that these phases are mixed on scales much smaller than a few parsecs, if we are to avoid large numbers of clouds with temperatures in the unstable range, 300$<$T$_{spin}$ $<$3000 K. Mixing between the cool neutral (atomic) and molecular phases is also apparently a common phenomenon, as indicated by widespread detections of HI self-absorption in recent years (Kavars et al. 2003, Li and Goldsmith 2003, Gibson et al. 2000). Thus it may be that turbulence in the velocity field of the gas, coupled to a corresponding hierarchy of irregularities in the gas density and the magnetic field strength and direction, is a single process that crosses all the boundaries between the phases of the ISM. Studying the turbulence on a variety of scales using many different tracers may thus illuminate the right hand side of figure 1, connecting the large structures like GSH277 that drive the cascade to the smallest scales where the velocity and magnetic field irregularities are dissipated. Along the way this same turbulence may drive the fragmentation of star formation regions that leads to the initial mass function.

References

Armstrong, J.W., Rickett, J.V., and Spangler, S.R. 1995, ApJ 443, 209
Crovisier, J. and Dickey, J.M. 1983, A&A 122, 282
Deshpande, A.A. 2000, MNRAS 317, 199
Dickey, J.M., McClure-Griffiths, N.M. et al. 2001, ApJ 561, 264
Dickey, J.M. 2004 in Science with the Square Kilometer Array, eds C. Carilli and S. Rawlings, in press
Draine, B.T. 1978, ApJS 36, 595

Draine, B.T. and Salpeter, E.E. 1979, ApJ 231, 77
Elmegreen, B.G. and Scalo, J. 2004, ARAA 42, 211
Faison, M.D., Goss, W.M. 2001, AJ 121, 2706
Ferrière, K.M., Zweibel, E.G., and Shull, J.M. 1988, ApJ 332, 984
Field, G.B. 1958, Proceedings of the IRE, 46, 240
Gibson, S.J., Taylor, A.R., Higgs, L.A., and Dewdney, P.E. 2000, ApJ 540, 851
Gaensler, B.M. et al. 2001, ApJ 549, 959
Green, D.A. 1993, MNRAS 262, 327
Hausen, N.R., Reynolds, R.J., Haffner, L.M., Tufte, S.L. 2002, ApJ 565, 1060
Haverkorn, M. et al. 2004, ApJ 609, 776
Heiles, C. and Troland, T.H. 2003, ApJ 586, 1067
Kalberla, P.M.W., and Stenholm, L.G. 1983, Mitteil. Astron. Gesellschaft 60, 397
Kavars, D. et al. 2002, ApJ 598, 1048
Li, D., and Goldsmith, P.F. 2002, ApJ 585, 823
Normandeau, M., Taylor, A.R., and Dewdney, P.E. 1997, ApJS 108, 279
Mansfield, V.N. and Salpeter, E.E. 1974, ApJ 190, 305
McClure-Griffiths, N.M., Dickey, J.M. et al. 2000, AJ 119, 2828
McClure-Griffiths, N.M., Dickey, J.M. et al. 2002, ApJ 578, 176
McClure-Griffiths, N.M., Dickey, J.M. et al. 2003, ApJ 594, 833
McKee, C.F. and Ostriker, J.P. 1977, ApJ 218, 148
Salpeter, E.E. 1976, ApJ 206, 673
Spitzer, L. Jr. 1956, ApJ 124, 20
Spitzer, L. Jr. and Fitzpatrick, E.L. 1993, ApJ 409, 299
Stanimirovic, S. and Lazarian, A. 2001, ApJ 551, 53

Figure 6. John Dickey, Lyle Hoffman and the Houck's.

EXAMINING THE RELATIONSHIP BETWEEN INTERSTELLAR TURBULENCE AND STAR FORMATION

Mark H. Heyer and Christopher M. Brunt
Department of Astronomy, University of Massachusetts, Amherst, MA 01003, USA
heyer@astro.umass.edu,brunt@astro.umass.edu

Abstract We assess the role of interstellar turbulence in regulating the rate and efficiency of star formation within the interstellar medium using millimeter wave and far infrared observations of 25 molecular clouds. The velocity structure functions, $\delta v = v_\circ L^\gamma$, derived for this sample of clouds are described by a narrow range of scaling exponents, γ, and coefficients, $v_\circ$, that demonstrate the near universality of turbulence within the molecular interstellar medium. In contrast to predictions of turbulent fragmentation models, no relationship is identified between turbulent gas properties and the star formation rate and efficiency.

1. Introduction

The Initial Mass Function (IMF), initially conceptualized by Salpeter (1954), implicitly poses one of the outstanding questions that prevail in astronomical research today. What are the processes that regulate the formation and properties of stars in galaxies? Recent descriptions of interstellar cloud dynamics have suggested that the star formation rate, efficiency and mode (isolated or clustered) are determined by the properties of compressible, turbulent gas flows that characterize the motions within giant molecular clouds (GMCs) (see Mac Low & Klessen 2004). Density fluctuations occur within super-Alfvenic flows as converging gas streams shock and dissipate kinetic energy. Whether an initial compression develops into a self-gravitating, pre-protostellar core from which a newborn star or cluster may condense or is re-subsumed into the general gas flow depends on various turbulent properties. The turbulent driving scale, λ_D, sets the time interval between the initial shock that compresses the gas and a successive shock that may destroy the density perturbation. Larger driving scales correspond to longer intervals that allow a compression to develop into a gravitationally bound configuration decoupled from the overlying flow. Klessen, Heitsch, & Mac Low (2002) suggest that star formation would

E. Corbelli et al. (eds.), The Initial Mass Function 50 Years Later, 281–286.

be more efficient in molecular clouds that are driven on large scales. The Mach number, M_s, of velocity fluctuations sets the amplitude of the density compression for an isothermal medium. Stronger compressions more readily develop into self-gravitating objects so one might expect enhanced star formation efficiencies for deeper compressions. The sonic scale, λ_S, is the spatial scale at which turbulent velocity fluctuations are equal to the local sound speed and therefore, sets the regime at which shocks can occur. A GMC with a larger sonic scale would generate larger, more massive cores and an elevated rate of star formation (Vazquez-Semadeni, Ballesteros-Paredes, & Klessen 2003). Finally, the scaling exponent, γ, of the velocity structure functions sets the degree of spatial coherence of velocity fluctuations and therefore, regulates the spectrum of core sizes and masses generated by turbulent fragmentation. Padoan & Nordlund (2002) relate the scaling exponent to the Salpeter slope of the mass function of newborn stars, $\alpha_{IMF} = 3/(3 - 2\gamma)$.

These processes provide elegant, simple descriptions of how turbulence may regulate star formation in the interstellar medium. In this contribution, we scrutinize these concepts with observations of molecular clouds.

2. Sample of Molecular Clouds

To gauge the relationship between star formation and turbulent properties, we have compiled far infrared and ^{12}CO J=1-0 imaging observations of 25 molecular clouds. The millimeter wave spectroscopic imaging observations are taken from wide field imaging surveys of the Galaxy (Heyer *et al.* 1998; Brunt & Mac Low 2004) and recent targeted observations with the FCRAO 14m telescope. The far infrared data are from the *IRAS All Sky Survey Atlas*. The sample of molecular clouds span a large range in mass, size, and star formation activity. It includes nearby dark clouds (B18, Heiles' Cloud 2, L1228) and giant molecular clouds that contain HII regions and OB associations (Rosette, W5). All clouds are within 3.6 kpc of the Sun.

2.1 Star Formation Rate

Far infrared emission from molecular clouds is due to thermal emission from dust grains heated by the local radiation field of newborn stars. It provides an important gauge of star formation activity within a cloud that is unaffected by extinction. The star formation rate per unit area, Σ_{SFR} for a cloud is calculated from the 60μm and 100μm intensities averaged over the solid angle subtended by the cloud,

$$\Sigma_{SFR} = 3.8 \times 10^{-16}(2.58 < I_{60} > + < I_{100} >) \quad \mathrm{M_\odot yr^{-1} pc^{-2}} \qquad (1)$$

where $< I_\lambda >= \int I_\lambda d\Omega / \int d\Omega$ (Thronson & Telesco 1986). This calculation includes flux from both point sources embedded within the cloud and

extended emission from grains heated by strong, UV fields of massive stars. Consequently, it provides an upper limit to the star formation rate for low mass star forming regions where the diffuse far-infrared dust component is heated by the ambient interstellar radiation field and not by newborn stars. Values for Σ_{SFR} span 2 orders of magnitude from $5.4{\times}10^{-9}$ $M_\odot$ yr^{-1} pc^{-2} (L1228) to $5.6{\times}10^{-7}$ $M_\odot$ yr^{-1} pc^{-2} (W5) that reflect the differences in star forming capacities of low mass dark clouds and infrared luminous giant molecular clouds.

2.2 Turbulent Flow Properties

Several of the turbulent properties described in §1 can be determined from the functional form of the velocity field structure function as this provides a concise, statistical description of the spatial distribution of velocity fluctuations that arise from the dynamics of a fluid volume. Brunt & Heyer (2002) have shown that the decomposition of spectroscopic data cubes using Principal Component Analysis (PCA) can recover the 3-dimensional velocity field statistics over a wide range of resolutions and opacities. From the set of PCA-generated eigenvectors and eigenimages, a relationship is constructed that describes the magnitude of velocity differences as a function of the scale over which those differences occur,

$$\delta v = v_\circ l^{\alpha_{PCA}} \tag{2}$$

where $v_\circ$ is the scaling coefficient. An example of this relationship for the Rosette Molecular Cloud is shown in Figure 1a. Based on empirical calibration of the method against models, the PCA scaling exponent, α_{PCA}, can be related to the scaling exponent of the velocity field structure function, γ (Brunt & Heyer 2002; Brunt *et al.* 2003).

PCA is applied to the set of molecular cloud observations to derive the scaling exponent, γ, and the scaling coefficient, $v_\circ$. Remarkably, the scaling coefficients and scaling exponents do not vary significantly between clouds. The mean value and standard deviation for γ are 0.49 and 0.15 respectively. The mean scaling coefficient is 0.90 $km\,s^{-1}$ with a standard deviation of 0.19 $km\,s^{-1}$. This result is emphasized in Figure 1b that shows the $\delta v, l$ relationship for all clouds overlayed onto a single plot. The narrow distributions of γ and $v_\circ$ imply that turbulence within the molecular interstellar medium is universal as originally posed by Larson (1981). Indeed, the cloud-to-cloud size line width relationship is a direct consequence of near-identical structure functions *within* interstellar cloud volumes. This is demonstrated in Figure 1b. The global values of size and line width sample the velocity fluctuations measured at the scale of the cloud. These correspond to the first points in the measured $\delta v, l$ relationship for each cloud that are highlighted by the filled circles in Figure 1b. This subset of points has the same functional form as the individual structure functions. If there were significant differences between clouds, then

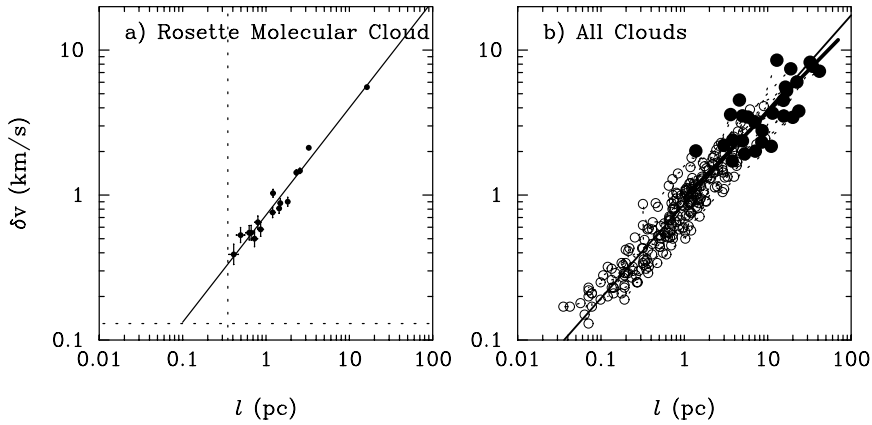

Figure 1. a) The $\delta v, l$ relationship derived from PCA decompositions of ^{13}CO J=1-0 imaging observations of the Rosette Molecular Cloud complex. The solid line is a bisector fit of a power law with the parameters $v_\circ = 0.73 \pm 0.02$ km s^{-1} and $\alpha_{PCA} = 0.74 \pm 0.03$. The vertical and horizontal dotted lines show the spatial and spectral resolution limits respectively. b) The composite $\delta v, l$ relationship from PCA decompositions for all 25 molecular clouds. The small scatter of points demonstrate the near invariance of velocity field structure functions within molecular clouds.

the measured scatter on the cloud-to-cloud size line width relationship would be much larger. Monte Carlo models that replicate the observed scatter in this relationship place *upper limits* on the cloud-to-cloud variation of the scaling exponent and scaling coefficient to be less than 10-20% (Heyer & Brunt 2004).

3. The Variation Σ_{SFR} with Turbulent Properties

We now examine whether star formation activity within the sample of clouds has any dependence on the turbulent flow properties. The role of turbulent driving scale is not considered here as there is no accurate gauge of λ_D but only coarse estimates that λ_D is comparable to or larger than the size of the cloud (Brunt 2003). The Mach number of a cloud is conventionally determined from the global velocity dispersion. We also consider the scaling coefficient, $v_\circ$, as this measures the amplitude of velocity fluctuations at a common reference scale length of 1 pc that is independent of the cloud size, and therefore, a more useful metric to globally characterize and compare turbulent fluctuations within a sample of clouds. The sonic scale, λ_s can be derived from the $\delta v, l$ relationship,

$$\delta v(\lambda_s) = v_\circ {\lambda_s}^{\alpha_{PCA}} = c_s \tag{3}$$

where c_s is the local 1D, isothermal sound speed for H_2 inclusive of He abundance. Given the limited range of $v_\circ$ and α_{PCA} for our sample of clouds, the dynamic range of λ_s is similarly small (0.13 pc $< \lambda_s <$ 0.47 pc).

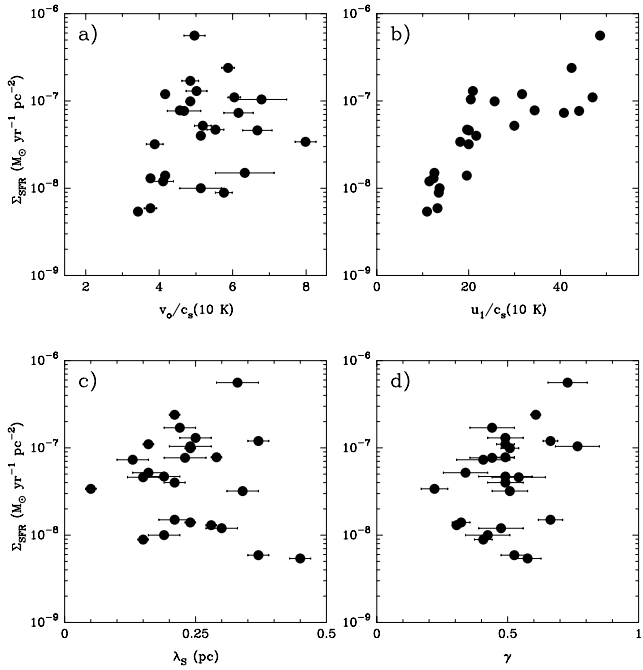

Figure 2. The variation of star formation rate per unit area as a function of turbulent flow properties: a) scaling coefficient,$v_\circ$, b) global velocity dispersion, u_1, c) sonic scale, λ_s, and d) structure function scaling coefficient, γ. The absence of significant correlation suggests that turbulence plays a limited role in regulating star formation within molecular clouds.

The variation of the Σ_{SFR} with the tabulated turbulent flow properties is shown in Figure 2. No significant correlations are identified between the star formation rate per unit area and the values of $v_\circ$, γ, and λ_s. The positive correlation observed between Σ_{SFR} and the global velocity dispersion, u_1, more likely reflects the well known result that massive stars form in large giant molecular clouds.

The absence of the predicted relationships suggests that turbulent fragmentation does not play an exclusive role in regulating star formation within this sample of interstellar clouds. It may be responsible for the generation of initial density fluctuations within a cloud, but apparently must operate in conjunction with other processes such as ambipolar diffusion to create the necessary conditions for newborn stars.

The functional form of the structure functions are similiar despite the large range of Σ_{SFR}. Such invariance could be attributed to a common external source of energy that drives the turbulent motions. Indeed, most of the kinetic energy of a cloud resides within the largest scales as would be expected from large scale driving. These chracteristics may indicate that star formation pro-

vides minimal feedback upon the turbulent flow properties when averaged over the projected area of the cloud.

Acknowledgments This work was supported by NSF grant AST 02-28993 to the Five College Radio Astronomy Observatory.

References

Brunt, C.M. 2003, ApJ, 583, 280
Brunt, C.M. & Mac Low, M. 2004, ApJ, 604, 196
Brunt, C.M. & Heyer, M.H. 2002, ApJ, 566, 276
Brunt, C.M., Heyer, M.H., Vazquez-Semadeni, E., & Pichardo, B. 2003, ApJ, 595, 824
Heyer, M.H., Brunt, C., Snell, R.L., Howe, J.E., Schloerb, F.P., & Carpenter, J.M. 1998, ApJS, 115, 241
Heyer, M.H. & Brunt, C.M. 2004, ApJL, 615, 45
Klessen, R.S., Heitsch, F., & Mac Low, M. 2000, ApJ, 535, 887
Larson, R.B. 1981, MNRAS, 194, 809
Mac Low, M. & Klessen, R.S. 2004, Reviews of Modern Physics, 76, 125
Padoan, P. & Nordlund, A. 2002, ApJ, 2002, 576, 870
Salpeter, E. E. 1955, ApJ, 123, 666
Thronson, H.A. & Telesco, C.M. 1986, ApJ, 311, 98
Vazquez-Semadeni, E., Ballesteros-Paredes, J., & Klessen, R.S. 2003, ApJ, 585, L131

Figure 3. Christopher Brunt and Mark Heyer.

THE IMF OF GIANT MOLECULAR CLOUDS

Leo Blitz and Erik Rosolowsky
Astronomy Department, University of California, Berkeley, CA, USA
blitz@astro.berkeley.edu, eros@astro.berkeley.edu

Abstract The properties of GMCs in several Local Group galaxies are quantified and compared. It is found that the mass spectrum of GMCs varies from galaxy to galaxy. The variations are significant and do not appear to be the result of sytematic uncertainties. Nevertheless, it appears that all of the GMCs follow the same size–linewidth and mass–linewidth relations with little scatter. The power law indices of these relations imply that the GMCs are self-gravitating, and that the mean surface density of Local Group GMCs is approximately constant. This, in turn, implies that the mean internal pressure of GMCs is also constant. If the IMF of stars is determined by a Jeans instability, this constant internal pressure suggests that the distribution of stellar masses does not vary significantly in galactic disks when averaged over suitably large areas. Thus, although the distribution of GMC masses produced by various Local Group galaxies is quite variable, the large-scale properties of the GMCs is not.

1. Introduction

The IMF in galaxies is not directly measurable except in rare cases (see Wyse this volume), but is often taken to be the same as that determined locally (Salpeter 1955) without much justification. Because the evolution of disk masses depends sensitively on the shape of the IMF at the low-mass end, knowledge about the variation of the IMF from galaxy to galaxy is an important parameter for understanding galaxy evolution.

One approach is to look at the GMCs from which the stars form. If the clouds have similar properties within and between galaxies, it would suggest that the stars that form from the GMCs might have similar properties and distributions. It is only within the last few years, however, that unbiased surveys of Local Group GMCs have been performed at sufficient angular resolution and sensitivity to determine the properties of GMCs in external galaxies (e.g., Mizuno et al. 2001a,b; Rosolowsky et al. 2003). These surveys are large enough that comparisons can be made with GMCs in the Milky Way (Solomon et al. 1987; Heyer, Carpenter & Snell 2001). In this paper, we look at the GMC

E. Corbelli et al. (eds.), The Initial Mass Function 50 Years Later, 287–296.

mass functions in the Milky Way, the LMC and M33, as well as the linewidth–size and linewidth–mass relations for these same galaxies to see what might be inferred from the current state of the observations.

2. The mass function of GMCs

Determination of the mass function of GMCs requires a large, unbiased survey of the molecular gas in a galaxy at sufficient angular resolution to separate the individual clouds from one another. It is not necessary to resolve the clouds in external galaxies, since the mass is proportional to the CO flux if the CO-to-H_2 conversion factor (X) is constant within a galaxy and from one galaxy to another. For the Milky Way, sufficient angular resolution has been available since the discovery of the CO line. The problem rather had been the large areas subtended by the CO emission from individual clouds compared to the telescope beams and the velocity blending produced by our edge-on view of the disk. Large surveys of the CO emission were required to obtain reliable GMC catalogues (Dame et al. 1986; Solomon et al. 1987). Nevertheless, attempts to obtain an unbiased catalogue of a sufficiently large sample of clouds suggest that the mass function $dN/dM \propto M^{-1.6}$ (Williams & McKee 1997).

More recently, Heyer et al. (2001) have completed a survey of the outer portions of the Milky Way visible from northern latitudes, and catalogued about 10^4 molecular clouds. Again, resolution was not an issue; sky coverage required more than 1.6×10^6 spectra to complete the survey. Heyer et al. (2001) concluded that $dN/dM \propto M^{-1.9}$, but suggest without detailed analysis that the power law index is not significantly different from that found by Solomon et al. (1987).

Only a few galaxies beyond the Milky Way have had complete surveys of molecular gas done at high enough angular resolution to resolve the emission into GMCs: M33 (Engargiola et al. 2003), the LMC (Mizuno et al. 2001a), the SMC (Mizuno et al. 2001b), and IC 10 (Leroy et al. in preparation). The LMC and the SMC are close enough to be mapped with a filled aperture telescope, but each covers a large enough fraction of the sky that a dedicated program requiring many months has been necessary to map all of the molecular gas. In the SMC there are too few GMCs to obtain a reliable mass spectrum.

Beyond the Magellanic Clouds, aperture synthesis is required to separate and resolve individual GMCs. For a galaxy such as M33, however, a great deal of observing time is needed to make a mosaic large enough to cover the $0.^\circ5$ extent of the molecular emission. Wilson and Scoville (1990) mapped 17 fields in M33 with a $1'$ primary beam to obtain the first maps of individual molecular clouds in M33. Engargiola et al. (2003) required almost 800 fields with a $2'$ beam to get a nearly complete map of the galaxy. A catalogue of GMCs generated from this map, superimposed on an Hα map of the galaxy, is

shown in Figure 1. Figure 2 shows the GMCs superimposed on the HI map of Deul & van der Hulst (1987).

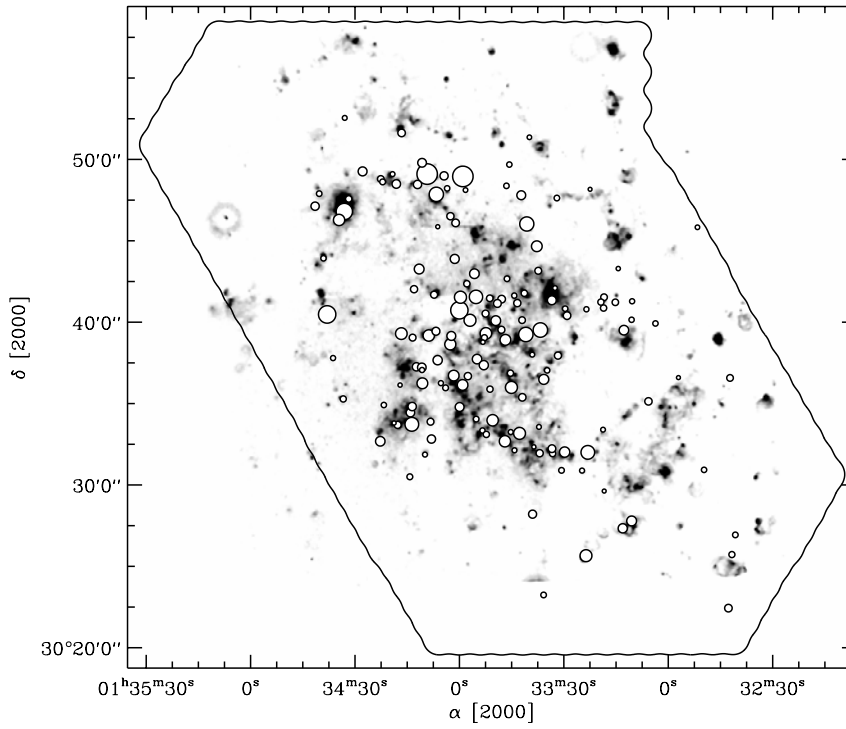

Figure 1. The molecular clouds catalogued by Engargiola et al. (2003), shown at black dots enclosed by white circles, superimposed on a continuum subtracted Hα map from Massey et al. (2002). The diameter of each dot is proportional to the H_2 mass of each GMC. Note the good correspondence between the HII regions and the location of the GMCs.

The mass spectra for M33, the LMC and the Milky Way are derived from the GMC catalogues of Engariola et al. (2003), Mizuno et al. (2001a), Heyer et al. (2001) and Solomon et al. (1987) under the assumption of a single value of $X = N(\mathrm{H_2})/I_{\mathrm{CO}} = 2 \times 10^{20} \mathrm{cm}^{-2}\ (\mathrm{K\ km\ s}^{-1})^{-1}$. The total molecular mass varies greatly among the three galaxies. Thus, to compare the mass spectrum of each galaxy on an equal footing, we make a plot of the cumulative mass distributions normalized to the most massive cloud in each galaxy. A plot comparing the mass spectra of the the three galaxies (showing the inner and outer Milky Way separately) is shown in Figure 3. It can be clearly seen that the mass spectra of all three galaxies can be well described by a power law: $dN/dM \propto M^{-\alpha}$. The index α of 2.3 for M33 is significantly steeper than that of the inner Milky Way.

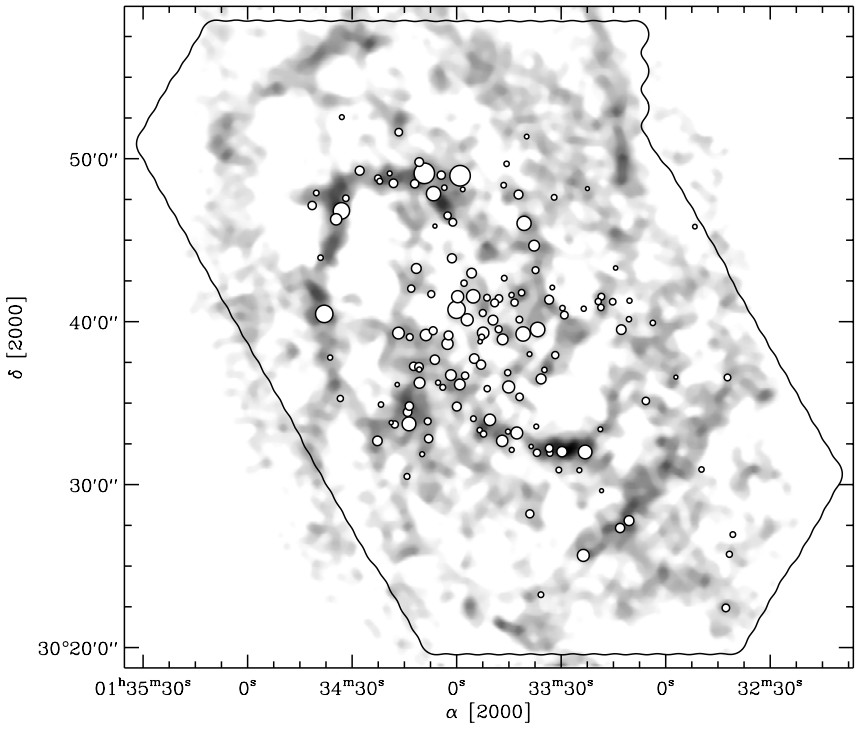

Figure 2. The molecular clouds catalogued by Engargiola et al. (2003) superimposed on a map of HI surface density from the data of Deul & van der Hulst (1987). Note how the HI is arranged along filaments and how the GMCs are located almost exclusively on the filaments.

As a check, we ask the following question: Scaling the H_2 mass of the Milky Way to that of M33, how many GMCs would one expect with a mass greater than that of $7 \times 10^5\ M_\odot$, the largest GMC mass in M33? From the observations of Dame et al. (1986) for the largest GMCs in the Milky Way to M33, we would expect to find 15 clouds with masses larger than the largest mass GMC in M33; these 15 clouds would have a large fraction of the the total mass in GMCs in M33. It is very unlikely that these would have been produced by the same parent population; the difference in the mass spectra between the inner Milky Way and M33 is apparently real. It is unclear why these differences occur, and it is also useful to know whether the clouds themselves have different gross properties.

The particular differences in power law index also imply fundamental differences in the way molecular gas is distributed in the Milky Way and in M33. In the Milky Way, a power law index < 2 implies that most of the mass in molecular gas is in the highest mass clouds. In M33, the power law index is $>$

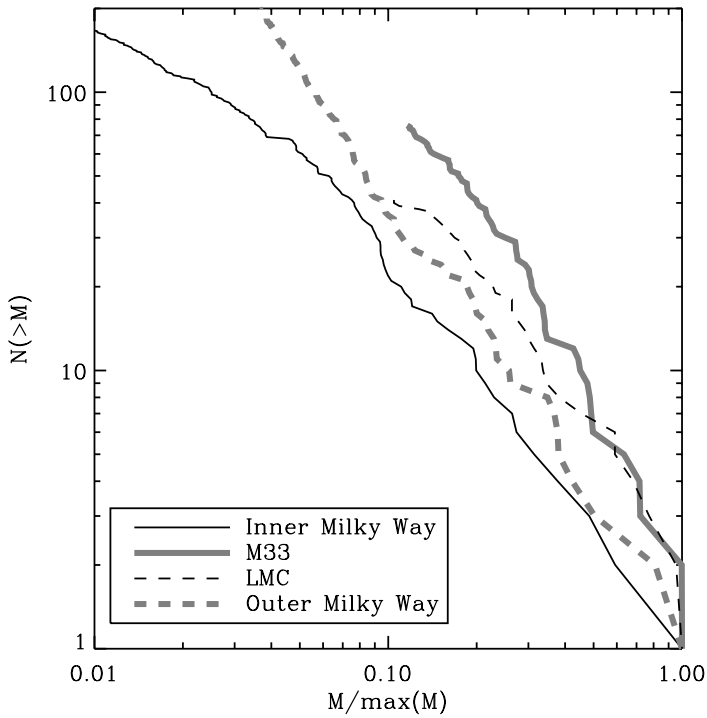

Figure 3. The cumulative mass spectrum for the inner and outer Milky Way, the LMC and M33. Each mass spectrum is normalized to the most massive cloud observed. Note that the mass spectra for the LMC is identical to that for M33 for the 7 most massive clouds, consistent with the results of Mizuno (2001a). There seems to be little question that the mass spectrum of M33 is very different from that of the inner Milky Way.

2, which implies that most of the mass is in the lowest mass clouds. However, to avoid an infinite mass when integrating the mass distribution requires either a mass cutoff or a change in index of the mass distribution. From a knowledge of the total molecular mass in M33, Engargiola et al. (2003) estimate that this change occurs at about 4–6 $\times 10^4$ $M_\odot$. There is thus a knee in the mass distribution and most of the GMC mass in the galaxy occurs near the knee. This implies that there is a characteristic mass of the molecular clouds in M33; for some reason, M33 primarily produces GMCs with masses of about 5×10^4 $M_\odot$.

3. The Properties of GMCs

One way to compare the gross properties of individual GMCs in various galaxies is to look at the size–linewidth relation, a comparison of the radius

of a cloud with its linewidth for many clouds. That such a relation exists was first suggested by Larson (1981). In the Milky Way, several investigators obtain a size–linewidth relation for GMCs with a power law index close to 0.5 with little scatter among the various determinations (e.g. Blitz 1993). This value is to be compared with that determined in other galaxies. Comparisons are complicated by several factors, however. First, most extragalactic GMCs are only marginally resolved and it becomes necessary to deconvolve the beam from the measurements. Second, it is important to correct the data for observations made with different sensitivities. These would likely leave the linewidths unchanged, but can give differing results for the diameters of the clouds. A comparison of the size–linewidth relation is shown in Figure 4 for the Milky Way, the LMC and M33. For the LMC, we take the catalogue of Mizuno et al. (2001a) and apply a correction for the beamsize of the telescope they used. We have only included clouds from the outer Galaxy study of Heyer et al. (2001) that have reliable kinematic distances and show no signs of blending. The GMCs in M33 and the LMC fall nicely on the relationship found for the Milky Way.

One way to get around the problem of observing clouds with only a few resolution elements across them is to look at the mass–linewidth relation. In this case, we plot the CO luminosity ($L_{\rm CO}$) against linewidth (ΔV) and assume that assume that $L_{\rm CO}$ faithfully traces H_2 mass. If GMCs are self-gravitating, we have

$$\Delta V^2 = \alpha G M/R \tag{1}$$

where α is a constant near unity that depends on the mass distribution. If the clouds obey a size–linewidth relation with a power law index of 0.5, then $\Delta V \propto R^{0.5}$. Together, this implies that

$$M/R^2 = \text{constant}; \quad M \propto \Delta V^4 \tag{2}$$

The first condition implies that the surface density of GMCs is constant, the second, that a relation for molecular clouds exists similar to the Faber-Jackson relation for elliptical galaxies (Faber & Jackson 1976). The assumption of self-gravity seems fairly safe; The best argument for Milky Way GMCs comes from comparisons of their internal pressures with the external pressures in the disk that come from the hydrostatic equilibrium of the gas in the disk. In the solar vicinity, internal pressures are generally an order of magnitude greater than the external pressure and the clouds must therefore be self-gravitating if they are older than a crossing time. Since the properties of the catalogued extragalactic GMCs are not grossly different from those in the Milky Way, nor are the values of hydrostatic pressure expected to be very different, this assumption seems reasonable.

Figure 4 shows a plot of $L_{\rm CO}$ vs. ΔV for the catalogued GMCs in the Milky Way, M33 and the LMC. The solid line is not a fit to the data, but a line with

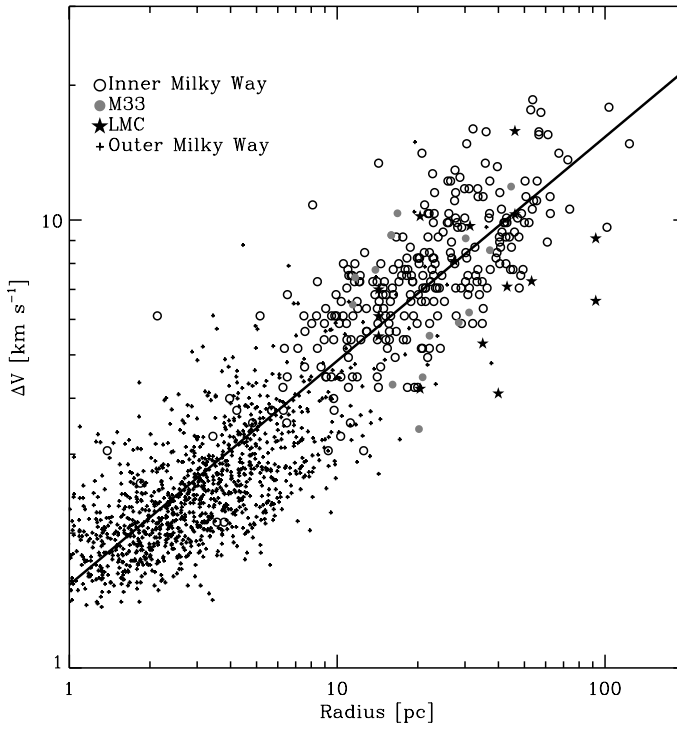

Figure 4. The size–linewidth relation for GMCs in the galaxies indicated. The solid line is not a fit but rather has a power law index of 0.5 showing that such a slope is a good fit to the data.

a power law index of 4. Clearly, this index represents the GMCs quite well; a single power law seems to describe all of the Local Group GMCs with no offset and with a scatter of only about a factor of two.

Thus, the two relations suggest that the GMCs in M33 and the LMC are similar to those in the Milky Way in that they are self-gravitating, that they obey the same size–linewidth relation and they have the same mean surface density with a relatively small scatter about the mean ($\sim 100\ M_\odot$ pc^{-2}). That is, even though the GMCs in the three galaxies under consideration here produce GMCs with different distributions of mass, the GMCs themselves have rather similar properties.

Recall, though, that the mean internal pressure P in a self-gravitating gas cloud is proportional to the square of the surface density Σ_{gas} only.

$$P = \beta \frac{\pi}{2} \Sigma_{gas}^2 \tag{3}$$

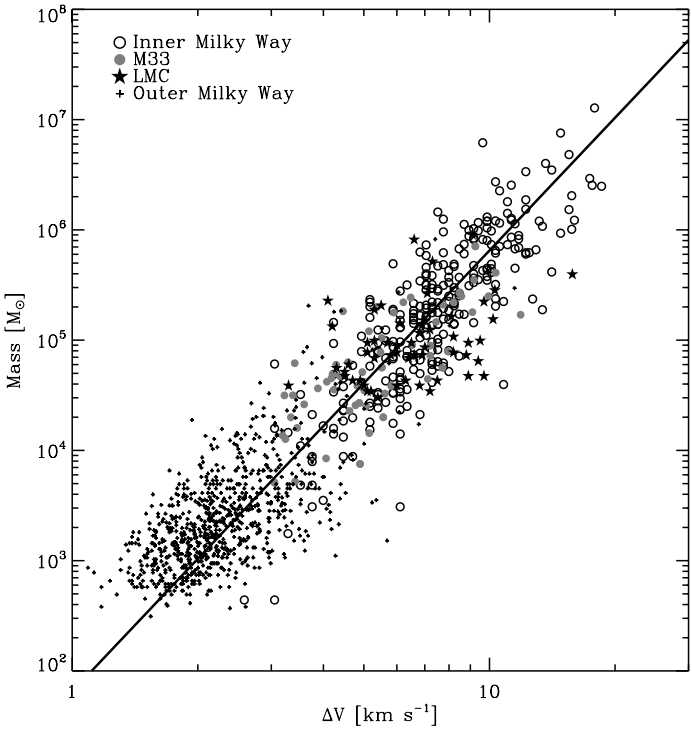

Figure 5. The mass–linewidth relation for GMCs in the galaxies indicated. The solid line is not a fit, but rather has a power law index of 4 showing that it is a good fit to the data. A slope of 4 suggests that the clouds have a size–linewidth relation such that $M \propto \Delta V^4$ and that the clouds are self gravitating.

where β is a constant near unity depending on the geometry of the cloud. Thus, the internal pressure of the GMCs in these galaxies show little variation because their measured surface densities show little variation. If star formation is the result of a Jeans instability, as many astronomers believe, then the constancy of the mean internal pressure suggests that the range of physical conditions among star-forming GMC is quite small. This, in turn, suggests that the ability to form stars with mass distributions different from those found in the Milky Way is also small. The IMF, therefore may show little change from galaxy to galaxy within the Local Group, and very likely, in galactic disks with properties similar to three galaxies discussed here.

References

Blitz, L. 1993, Protostars and Planets III, 125
Dame, T. M., Elmegreen, B. G., Cohen, R. S., & Thaddeus, P. 1986, ApJ, 305, 892

Deul, E. R. & van der Hulst, J. M. 1987, A&AS, 67, 509
Engargiola, G., Plambeck, R. L., Rosolowsky, E., & Blitz, L. 2003, ApJS, 149, 343
Faber, S. M. & Jackson, R. E. 1976, ApJ, 204, 668
Heyer, M. H., Carpenter, J. M., & Snell, R. L. 2001, ApJ, 551, 852
Larson, R. B. 1981, MNRAS, 194, 809
Massey, P., Hodge, P. W., Holmes, S., Jacoby, J., King, N. L., Olsen, K., Smith, C., & Saha, A. 2002, Bulletin of the American Astronomical Society, 34, 1272
Mizuno, N., et al. 2001, PASJ, 53, 971
Mizuno, N., Rubio, M., Mizuno, A., Yamaguchi, R., Onishi, T., & Fukui, Y. 2001, PASJ, 53, L45
Rosolowsky, E., Engargiola, G., Plambeck, R., & Blitz, L. 2003, ApJ, 599, 258
Salpeter, E. E. 1955, ApJ, 121, 161
Solomon, P. M., Rivolo, A. R., Barrett, J., & Yahil, A. 1987, ApJ, 319, 730
Williams, J. P. & McKee, C. F. 1997, ApJ, 476, 166
Wilson, C. D. & Scoville, N. 1990, ApJ, 363, 435

Figure 6. Leo Blitz with the Glassgold's.

Figure 7. Brindisi of Berkeley network at large: Prusti, Adams, Lada, Blitz and Shu.

Figure 8. Cluster network: Bate, Bonnell, Clarke, Monin, Bouvier, Andersen, Whitworth and McCaughrean (back).

MULTIPHASE MOLECULAR GAS AND STAR FORMING SITES IN M33

Edvige Corbelli[1] and Mark H. Heyer[2]
[1]*INAF-Osservatorio Astrofisico di Arcetri, Largo E. Fermi 5, 50125 Firenze, Italy*
[2]*Department of Astronomy, University of Massachusetts, Amherst, MA 01003, USA*
edvige@arcetri.astro.it,heyer@astro.umass.edu

Abstract Complete imaging of molecular clouds complexes in the nearby galaxy M33 have recently been completed using the BIMA interferometer and the FCRAO-14m telescope. Molecular gas is only 10% of the total gas mass but apparently only a much smaller fraction is concentrated around massive star formation sites. There are different molecular phases and different mechanisms which regulate the molecular fraction in this galaxy and operates at different scales. These will be briefly outlined here and linked to the star formation properties of the disk.

A large scale map of the ^{12}CO J=1-0 in M33, made with the FCRAO-14m telescope at a spatial resolution of $\sim$200 pc, has revealed a population of cloud complexes of several hundreds of pcs (Heyer, Corbelli, Schneider, & Young 2004). The estimated total mass in molecular form is of 2×10^8 solar masses. This is only 10% of the ISM mass of this galaxy, but is a much larger fraction than any other previous estimate. Recent imaging of the whole star forming disk of M33 with the BIMA interferometer has in fact revealed a population of massive GMCs with macroscopic properties similar to our Milky Way, which however make up only 10% of the estimated FCRAO molecular gas mass (Engargiola, Plambeck, Rosolowsky, & Blitz 2003). BIMA whole disk survey has been carried out with a spatial resolution of $\sim$50 pc, down to a completeness limit of 10^5 $M_\odot$. More than half of the FCRAO-14m detected gas mass resides in large complexes localized near the BIMA GMCs, in the nucleus, close to the northern spiral arm and over the southern spiral arm. The rest of the molecular mass in M33 is visible only when we average CO spectra in concentric tilted rings, which match the 3-D HI gas surface and kinematics in this galaxy. This is a very pervasive and diffuse molecular component which might be present throughout the SF disk of M33. It can be responsible for the birth of the numerous field OB stars which Hoopes & Walterbos (2000) invoke to explain the diffuse Hα emission in the M33 disk. The FCRAO-14m telescope detects a radial scalelength of about 2.5 kpc for the ^{12}CO 1-0 line intensity (Corbelli

E. Corbelli et al. (eds.), The Initial Mass Function 50 Years Later, 297–298.

2003) which declines with no visible abrupt radial cut-off. After computing the disk stellar mass from the best fit to the M33 rotation curve, we use the 21-cm Arecibo data and the FCRAO-CO data to evaluate the pressure and the molecular fraction f_{H_2} throughout the M33 disk. Assuming a radiation field proportional to the stellar surface density we find a good correlation between P and f_{H_2} with index $n = 2.3 \pm 0.05$, in excellent agreement with Elmegreen's prediction for a pressure regulated molecular fraction (Elmegreen 1993). The stellar disk mass is also an important ingredient for the Toomre criterion to predict correctly the outer star formation threshold radius in this galaxy (Corbelli 2003). Therefore the origin of the global disk properties of this galaxy, like the average radial star formation rate and molecular fraction, are now well understood. Large scale instabilities, like spiral arms, enhance the molecular gas distribution in special disk locations and originates the large molecular complexes which are visible in the FCRAO-14m map (Heyer et al. 2004). These must be still unfragmented or made of small mass clouds to explain the difference in mass with BIMA detections. Only parts of these complexes will further collapse and form gravitationally bound GMCs. These more compact clouds, detected by BIMA, are a necessary step towards the birth of massive star complexes. They are strongly linked to bright star formation sites, localized from the peaks of Hα and IR flux intensity of point sources in the disk. The radial scalelength of this third molecular phase is much shorter than that of the other two and indicates that a process, different from the average disk pressure, is regulating the onset of this phase. The rest of the molecular gas in the large complexes shows no evident signs of SF. If future observations confirm the above picture, taking into account also LMC and SMC data (Fukui et al. 1999), we can conjecture that molecular clouds with little or no massive SF become more numerous as we move along the Hubble sequence, towards late type galaxies.

References

Corbelli, E. 2003, MNRAS, 342, 199
Elmegreen, B. G. 1993, ApJ, 411, 170
Engargiola, G. Plambeck, R. L., Rosolowsky, E., & Blitz, L. 2003, ApJS, 149, 343
Fukui, Y. et al. 1999, PASJ, 51, 745
Heyer, M. H., Corbelli, E., Schneider, S. E., & Young, J. S. 2004, ApJ, 602, 723
Hoopes, C. G. & Walterbos, R. A. M. 2000, ApJ, 541, 597

HOW DOES STAR FORMATION BUILD A GALACTIC DISK?

Tony Wong[1,2] and Leo Blitz[3]
[1]*Australia Telescope National Facility, PO Box 76, Epping NSW 1710, Australia*
[2]*School of Physics, University of New South Wales, Sydney NSW 2052, Australia*
[3]*Department of Astronomy, University of California, Berkeley CA 94720, USA*
Tony.Wong@csiro.au

Abstract The combination of near-infrared and Hα photometry with CO and H I imaging allows us to probe past, ongoing, and future star formation in galaxies. Such a comparison for our Galaxy has yielded a puzzling contradiction between the derived star formation history and the assumed star formation law, but the uncertainties in the gas and stellar radial profiles are large. Recent data for seven nearby galaxies are presented and reveal no such contradiction: star formation has roughly declined in accordance with the consumption of gas assuming a standard Schmidt star formation law, arguing against strong temporal variations in the IMF. Furthermore, the effective oxygen yield shows no strong radial gradient, arguing against strong radial variations in the IMF.

The star formation history of a galaxy can be crudely described by the ratio of the present to average past star formation rate, a quantity often referred to as the b parameter (Scalo 1986):

$$b = \frac{\mathrm{SFR}}{\langle \mathrm{SFR} \rangle_{\tau_G}} \approx \frac{\mathrm{SFR}}{M_*} \tau_G (1 - \epsilon_*) \quad (1)$$

Here τ_G is the age of the Galaxy (taken to be 10 Gyr), M_* is the mass in stars, and $\epsilon_* \approx 0.3$ is a recycling factor (Kennicutt et al. 1994).

The difficulty in deriving radial profiles for the Galaxy complicates estimation of $b(R)$, but commonly used parameters lead to $b \sim 1$ over a large range in radius. This would suggest a fairly long time scale τ_{gas} for gas consumption by star formation. Surprisingly, however, τ_{gas} is observed to be much less than a Hubble time, especially in the inner Galaxy. Figure 1 (*left*) compares the observed values of τ_{gas} and b against two closed-box models with star formation laws of the form $\Sigma_{\mathrm{SFR}} \propto (\Sigma_{\mathrm{gas}})^n$, with n=1, 2. The present SFR in the inner Galaxy is more than a factor of 2 larger than allowed by such models.

In order to assess the severity of this problem in external galaxies, we have compared b and τ_{gas} for the sample of seven nearby galaxies which was stud-

E. Corbelli et al. (eds.), The Initial Mass Function 50 Years Later, 299–300.

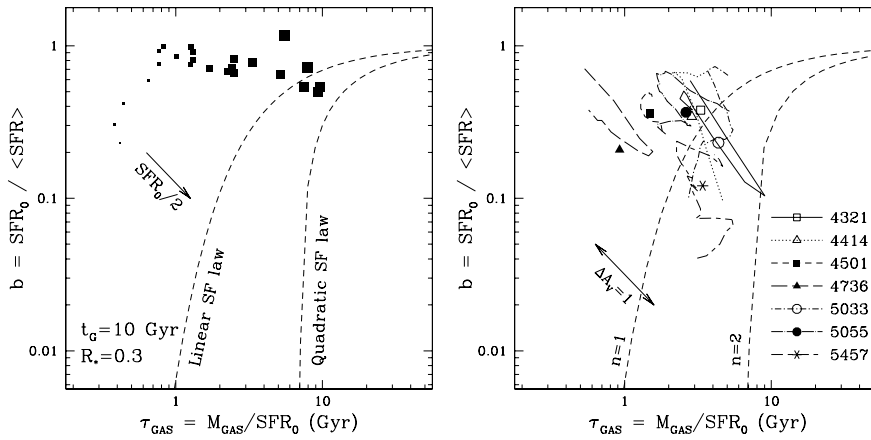

Figure 1. The birthrate parameter vs. the gas consumption time for separate annuli within galaxies: (Left) Milky Way data, with plot symbol size indicating galactocentric radius. The effect of halving the current SFR is shown. (Right) Data for annuli within seven nearby galaxies, with plot symbols indicating disk averages.

ied by Wong & Blitz (2002). For each galaxy the radial profiles of stars, gas, and current SFR were obtained from near-infrared 2MASS images, fully sampled CO and H I images, and Hα images respectively. Although the conversion factors used are still quite uncertain, the radial profiles are themselves straightforward to obtain, unlike the case for our Galaxy. On average, we find that the $\tau_{\rm gas}$ values are generally consistent with a linear star formation law, with only NGC 4736 showing an unsustainably high SFR associated with its starburst ring (Figure 1, *right*). There is no clear indication that inflows of material or variations in the IMF or star formation history are required to match the data.

For six of the galaxies with measured O/H abundances, we also find that the radial gradients in gas fractions and abundances are consistent with closed-box evolution models, with no apparent gradient in the effective oxygen yield. This suggests the IMF is not dependent on radius or metallicity. However, the average yield does seem to differ among galaxies, possibly indicating a failure of the closed-box assumption.

References

Kennicutt, R. C., Tamblyn, P., and Congdon, C. W. 1994, ApJ, 435, 22
Scalo, J. M. 1986, Fund. Cosmic Phys., 11, 1
Wong, T. and Blitz, L. 2002, ApJ, 569, 157

MAPPING EXTRAGALACTIC MOLECULAR CLOUDS: CENTAURUS A (NGC 5128)

Yuri Beletsky and João Alves
European Southern Observatory, Garching 85748, Germany
ybialets@eso.org, jalves@eso.org

Abstract We propose a novel albeit proven technique that uses dust extinction as a tracer of H_2 to study the physical structure of a large sample of extragalactic GMCs. We present results for the nearby galaxy NGC 5128 where we were able to construct an extinction map at subarcsec resolution (≈10 pc)

1. Introduction

The physics of the formation of GMCs is one of the major unsolved problems of the interstellar medium. Although many papers have been written on the subject (Elmegreen, 1993 and references therein) it is not yet known what the dominant formation mechanism is. One avenue for testing these theories is to study molecular clouds in a wide range of environments, ideally from a view point outside the galaxy's plane, and to determine which aspects of the environment set the cloud properties.

2. Observations

The observations were made in March 2001 using the SOFI infrared camera ($JHKs$) on the 3.5m NTT telescope in La Silla, Chile. We took 60 images per band with a total integration time of 1000 s. The field of view was approximately 5×5 arc min, with a pixel scale of 0.29 arc sec pixel^{-1}.

3. The technique

We are extending the successful idea of mapping dust column density through a molecular cloud (NICE method) proposed by Lada et al. 1994 to extragalactic GMCs. Instead of measuring the color of thousands of background stars to molecular clouds, we measure the average color of the unresolved thousand stars that fall on a pixel of a NIR detector. We measure the NIR diffuse galaxy light seen through GMCs, in a simple analogy to our Galactic work. The tech-

E. Corbelli et al. (eds.), The Initial Mass Function 50 Years Later, 301–302.

nique allows one to derive the basic characteristics (morphology, mass, statistics) for this population and compare the dust extinction results with published molecular line data, in particular with CO interferometric data having almost the sub-arcsec resolution that is achievable in the extinction maps.

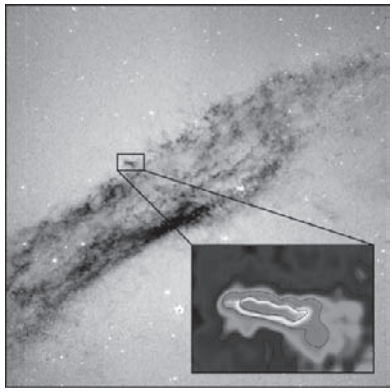

Figure 1. Centaurus A extinction map derived from the NIR observations. Inset: a $\sim 10^6$ $M_\odot$ GMC

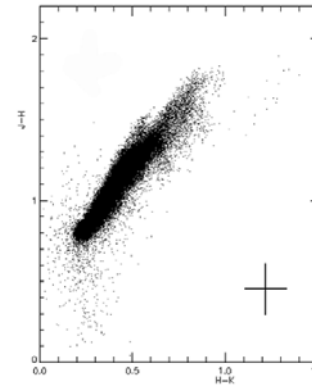

Figure 2. $(H-K)$ vs. $(J-H)$ colour-colour diagram for the pixels of NGC 5128 image. Photometric errors are illustrated at the lower right.

4. Conclusions

- The proposed technique is sensitive to dust and allows us to probe the extinction up to 10^m in this galaxy.
- The reddening law of Centaurus A is similar to the Milky Way reddening law.
- We can determine precise masses of giant molecular clouds in Centaurus A.
- The subarcsecond resolution achieved by our method (0.6 arc sec or 10 pc at the distance to Centaurus A) opens a new window on extragalactic molecular clouds research.

References

Elmegreen, B.G. 1993, ApJ, 419, 29
Lada, C.J., Lada, E.A., Clemens, D.P. & Bally, J. 1994, ApJ, 429,694

TINY HI CLOUDS IN THE LOCAL ISM

Robert Braun[1] and Nissim Kanekar[2]
[1]*ASTRON, Postbox 2, 7990 AA Dwingeloo, The Netherlands,*
[2]*Kapteyn Inst., Postbox 800, 9700 AV Groningen, The Netherlands*
rbraun@astron.nl,nissim@astro.rug.nl

Abstract Very sensitive HI absorption spectra ($\Delta\tau \sim 10^{-4}$ over 1 km/s) toward high latitude QSOs have revealed a population of tiny discrete features in the diffuse ISM with peak τ of 0.1 – 2% and core line-widths corresponding to temperatures as low as 20 K. Imaging detections confirm linear dimensions of a few 1000 AU. We suggest these structures may be formed by the stellar winds of intermediate mass stars. A more speculative origin might involve molecular "dark matter".

1. Introduction

Over the past decades there have been several lines of evidence suggesting a surprising degree of small-scale structure in the atomic interstellar medium. One of the first of these was the observation of spatially variable HI absorption seen toward compact radio sources (e.g. Dieter et al. 1976, Davis et al. 1996, Faison et al. 1998, Faison & Goss 2001). In the most extreme cases, for example toward 3C138, there is good evidence for a variation in the HI opacity, $\tau = 1.7(n \cdot s)/(T\Delta V)$[cm^{-3}pc/K-km/s], of as much as $\Delta\tau$ = 0.1 on 20 AU transverse scales (Faison et al. 1998). The "simplest" interpretation of these observations are very large variations in the volume density, $\Delta n_{HI} \sim 10^5$ cm^{-3}, assuming that all of the other relevant variables (specifically pathlength, s, and temperature, T) are kept fixed. However, as argued by Deshpande (2000), realistic ISM structure functions can lead to large variations of τ with small angular offsets simply from the statistical fluctuations in the effective pathlength with position. Another line of evidence for small-scale atomic structure came from searches for time variability in the HI absorption seen toward pulsars (e.g. Frail et al. 1994, Johnston et al. 2003, Stanimirovic et al. 2003). However, the early claims for ubiquitous and significant time variations in τ have not been confirmed in the recent careful studies. A third line of evidence has come from observations of Na I observation toward nearby pairs of stars (Watson & Meyer 1996, Lauroesch et al. 1998). These observations

E. Corbelli et al. (eds.), The Initial Mass Function 50 Years Later, 303–308.

have revealed strong evidence for discrete absorption features in the local ISM which have highly variable properties on 100's of AU scales. Since discrete features are being probed by these observations, rather than simply the projection along a long line-of-sight, the structure function arguments of Deshpande do not seem to apply.

2. Observations

We have undertaken a series of extremely sensitive HI absorption observations toward bright background QSOs near the North Galactic Pole (NGP) utilizing the Westerbork Synthesis Radio Telescope (WSRT). The initial motivation for these observations was detection of HI absorption from a Warm Neutral Medium (WNM), even if it's temperature was as high as 10^4 K. Such an experiment was prompted by the detection of HI absorption by Kanekar et al. (2003) at velocity widths extending at least as high as an equivalent temperature of 3500 K, which corresponded to the sensitivity limit of those data. The NGP region was chosen since it was expected that the lines-of-sight through our Galaxy disk might be as short as possible and therefore relatively simple. Sensitive data were acquired toward 3C286 (14.7 Jy), 3C287 (7 Jy), 4C+32.44 (5 Jy) and B2 1325+32 (1.4 Jy) by observing in an in-band frequency-switching mode utilizing a 1 MHz throw every 5 minutes inside a 2.5 MHz total bandwidth with 0.5 km/s channel width. The in-band frequency switching allowed exceptionally good band-pass calibration while providing 100% of the observing time on-source. For the brightest sources we achieve an RMS $\Delta\tau \ < \ 2 \times 10^{-4}$ over only 1 km/s, making these the most sensitive HI (21cm) absorption measurements of which we are aware.

3. Results

Rather than detecting only the simple, broad and shallow absorption profile of the WNM toward these high latitude lines-of-sight, we were surprised to find instead that multiple narrow absorption features were detected at discrete line-of-sight velocities with peak opacities in the range 0.1 to 2%. The detection of discrete absorption features was particularly surprising since the peak emission brightness seen in these directions (with the 35 arcmin total power beam) was only between about 2 and 5 K. The four observed lines-of-sight are compared in Figure 1. Since many of the absorption lines are detected with high signal-to-noise it is possible to say with confidence that the profiles of individual features are non-Gaussian, and instead appear to be semi-Lorentzian with very narrow line-cores that merge smoothly into broader wings. Of course it is always possible to represent each feature with a sum of coincident Gaussians, but such a procedure appears to be quite arbitrary and it is far from clear what physical interpretation might be attached to such an arbitrary decomposition.

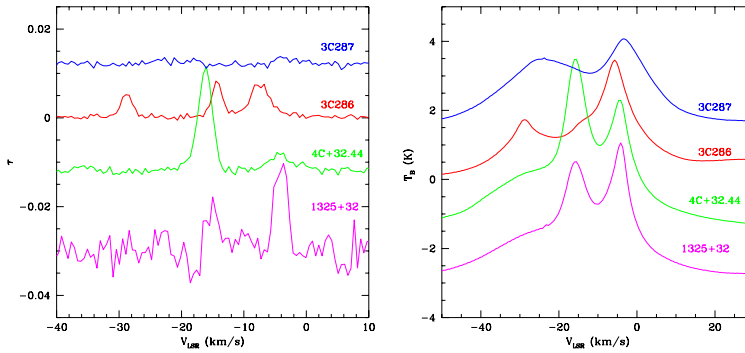

Figure 1. HI absorption (left) and total power emission (right) spectra.

Moderately near-by lines-of-sight show essentially uncorrelated absorption features and only weakly correlated total power emission features. Only in the case of 4C+32.44 and B2 1325+32 which have an angular separation of only 15 arcmin is there some possibility of similar velocity components having been detected.

4. Analysis

Motivated by the non-Gaussian line profiles we have explored some simple spherically symmetric, iso-baric cloud models of the form:

$$n_H(r) = n_o exp[-(r/s)^{\alpha_1}] \qquad \text{for } T < 4000 \text{ K} \tag{1}$$

$$n_H(r) = n_o exp[-(r/s)^{\alpha_2}] \qquad \text{for } T > 4000 \text{ K} \tag{2}$$

where we further relate volume density to temperature using the thermal pressure which was assumed to be constant at $P/k_B = n_H T$ = 1500 cm^{-3}K. The temperature was allowed to vary between $T_{min} = 20\ K$ and $T_{max} = 15000$ K, yielding an assumed thermal velocity dispersion of $\sigma^2 = 0.0086T$. The predicted HI absorption and total power emission spectra were calculated for a "cloud" placed at the central velocity of each observed feature in an attempt to simultaneously reproduce the observed spectra shown in Fig. 1. The most important free parameters in this process were the cloud scale-length, s, the cloud distance, d (which most strongly influences the predicted total power emission) and an impact parameter, b. This last parameter was used to allow for the likely circumstance that each spherical model cloud may not be penetrated exactly on-axis by the background absorber. The two power-law indices of the scaled distance, α_1 and α_2 determine the characteristic line-shape in the cold core and warm halo respectively. Although these were in principle also

free parameters, it was found that only minor variations from "standard" values of about α_1=1/4 and α_2=1/8 were needed.

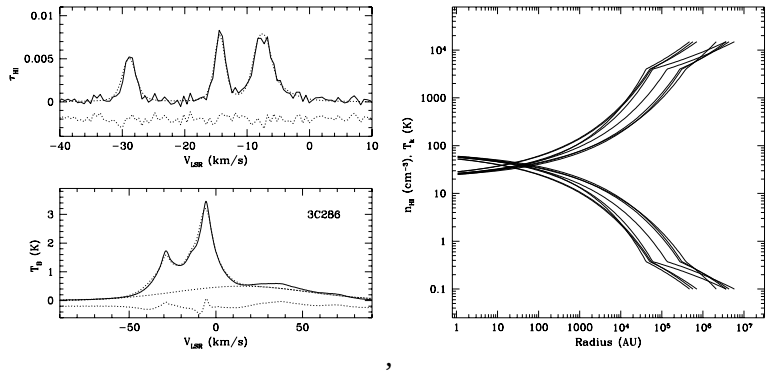

Figure 2. Overlay of observed and modeled spectra for the 3C286 l-o-s (left). Density and temperature profiles of all modeled "clouds" (right).

An illustration of the simultaneous emission and absorption line fitting is shown in Fig. 2 for the 3C286 line-of-sight. No χ^2 fitting has actually been carried out, but merely a χ-by-eye to illustrate the possibilities of this approach. The entire set of density and temperature profiles for the required clouds along all four lines-of-sight is also shown in the Figure. This illustrates the basic similarities of the modeled features, although the apparent scale-lengths do vary by about an order of magnitude. The apparent distances used in reproducing the spectra was about 10 pc, and the typical half-density radius was 100 AU, although these were not very well-constrained given the very low angular resolution of our total power data (35 arcmin). These modeling results can be easily scaled to other assumed thermal pressures by a linear scaling of n_H together with an inverse linear scaling of both s and d. For example, with a typical thermal pressure of only 150 cm^{-3}K, comparable fits would be obtained at apparent distances of 100 pc and typical half-density radii of 1000 AU. Variations from the idealized spherical cloud symmetry would have a similar impact on apparent distances and sizes.

We also have more concrete information regarding the nature of these features, since the same WSRT observations that provided the absorption spectra also allow an imaging search for emission counterparts. Cubes of HI line emission were produced at a range of angular resolutions (15, 30, 60 and 120 arcsec). Obtaining sufficient brightness sensitivity to achieve detections in emission typically required smoothing to 60 arcsec. At those velocities where total power emission exceeding about 1 K is seen in Fig. 1 compact emission clumps of 2–3 K brightness are detected at apparently random locations in the field superposed on the poorly-sampled diffuse background emission. One such emis-

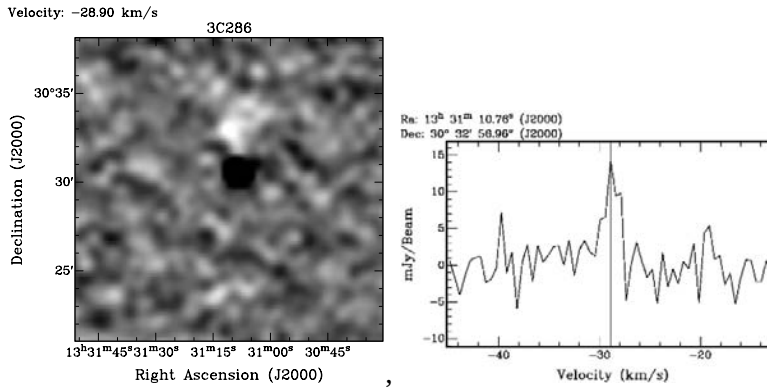

Figure 3. HI emission clump adjacent to 3C286 in map (left) and spectrum (right).

sion clump, immediately adjacent to the 3C286 line-of-sight is shown in Fig. 3. The intrinsic angular size of these clumps appears to be about 30 arcsec, while their FWHM line-widths are 1–2 km/s, corresponding to the thermal linewidths of 20–80 K HI. A representative detected column density for the clumps in the 3C286 field is $N_{HI} \sim 5 \times 10^{18}$cm^{-2}. At an assumed distance of say, 100 pc, the clump size would correspond to 3000 AU and the central volume density would be about 100 cm^{-3}.

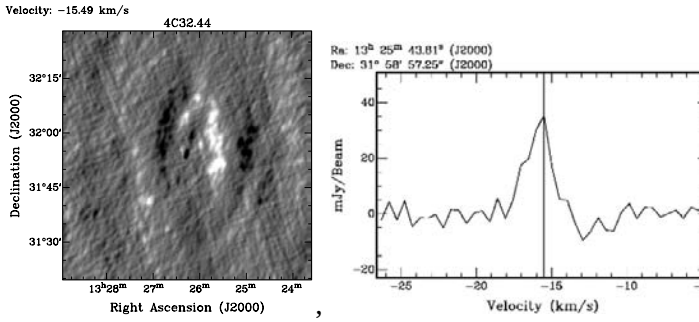

Figure 4. HI emission shell toward 4C+32.44 in map (left) and spectrum (right).

A more interesting emission structure is detected in the 4C+32.44 field. The line-of-sight toward this background source appears to intersect a 15 arcmin diameter shell of HI emission as shown in Fig.4. Although it may be a chance super-position, this apparent shell includes the G0III star HD 116856 at $(\alpha, \delta)_{2000}$ = (13:25:55.835,+31:51:40.629). The measured parallax of this star places it at 105±11 pc, where the shell would have a 0.45 pc diameter. The stellar proper motion $(\Delta\alpha, \Delta\delta)$ = (+14.73,−43.40) mas/yr is directed pre-

dominantly toward the South. Peak column densities in this structure reach $N_{HI} > 10^{19}$cm^{-2} with FWHM line-widths of 2–3 km/s.

5. Discussion

Although more work needs to be done to fully characterize the type and quantity of sub-structure in the "diffuse" ISM, it is already becoming clear that even the most diffuse regions are populated by tiny distinct structures of very high density- and temperature-contrast. For example, the low scale-size end of the turbulent power spectrum is predicted (Deshpande 2000) to have HI opacity fluctuations of only 10^{-5} on spatial scales of 1000 AU. In fact, we measure more than two orders of magnitude larger opacity fluctuations of $> 10^{-3}$ on these scales. There appears to be substantial injection of fluctuation power on very small scales. The physical origin of these tiny structures is not yet clear, but it seems conceivable that the stellar winds of intermediate mass stars may play an important role in their formation, whenever such stars find themselves within a diffuse atomic structure. A more speculative origin might be some relation to molecular "dark matter" (e.g. Pfenniger & Combes 1994). New observations should test various scenarios.

References

Davis, R. J., Diamond, P. J., Goss, W. M. 1996, MNRAS, 283, 1105
Deshpande, A. A. 2000, MNRAS, 543, 227
Dieter, N. H., Welch, W. J., Romney, J. D. 1976, ApJ, 206, L113
Faison, M., Goss, W. M., Diamond, P. J., Taylor, G. B. 1998, AJ, 116, 2916
Faison, M., Goss, W. M. 2001, AJ, 121, 2706
Frail, D. A., Weisberg, J. M., Cordes, J. M., Mathers, C. 1994, ApJ, 436, 144
Johnston, S., Koribalski, B., Wison, W., Walker, M.,2003, MNRAS, 341, 941
Kanekar, N., Subrahmanyan, R., Chengalur, C., Safouris, V. 2003, MNRAS, 346, L57
Lauroesch, J. T., Meyer, D. M., Watson, J. K., Blades, J. C. 1998, ApJ, 507, L89
Pfenniger, D., Combes, F. 1994, A&A, 285, 94
Stanimirovic, S., Weisberg, J. M., Hedden, A. et al. 2003, ApJ, 598, 23
Watson, J. K., Meyer, D. M. 1996, ApJ, 473, L127

SUBMM OBSERVATIONS OF PRESTELLAR CONDENSATIONS: PROBING THE INITIAL CONDITIONS FOR THE IMF

Philippe André
CEA Saclay, Service d'Astrophysique, F-91191 Gif-sur-Yvette Cedex, France
pandre@cea.fr

Abstract Several (sub)millimeter continuum surveys of nearby protoclusters have revealed prestellar condensations that seem to be the direct progenitors of individual stars and whose mass distribution resembles the IMF. In a number of cases, small internal and relative motions are measured for these protocluster condensations, indicating they are much less turbulent than their ambient cloud and do not have time to interact before collapsing to (proto)stars. These findings suggest that the IMF is at least partly determined by pre-collapse cloud fragmentation and that the main key to understanding the origin of stellar masses lies in the physical mechanisms responsible for the formation and decoupling of prestellar condensations within molecular clouds.

1. Introduction

One of the main limitations in our present understanding of the star formation process is that we do not know well the initial conditions for protostellar collapse. In particular, there is a major ongoing controversy between two schools of thought for the formation and evolution of dense cores within molecular clouds: The classical picture based on magnetic support and ambipolar diffusion (e.g. Shu et al. 1987, 2004; Mouschovias & Ciolek 1999) has been seriously challenged by a new, more dynamic picture, which emphasizes the role of supersonic turbulence in supporting clouds on large scales and generating density fluctuations on small scales (e.g. Klessen et al. 2000; Padoan & Nordlund 2002).

Improving our knowledge of the initial stages of star formation is especially important since there is now good evidence that these stages control the origin of the stellar IMF. In particular, recent studies strongly suggest that the effective reservoirs of mass required for the formation of individual stars are already selected at the prestellar core stage. First, detailed (sub)-millimeter

E. Corbelli et al. (eds.), The Initial Mass Function 50 Years Later, 309–318.

emission and infrared absorption mapping of a few nearby sources indicates that the density profiles of prestellar cores typically feature flat inner regions and sharp outer edges, hence are reminiscent of the density structure expected for *finite-size/mass*, self-gravitating isothermal spheroids (such as 'Bonnor-Ebert' spheres) (e.g. Ward-Thompson et al. 1994; Bacmann et al. 2000; Alves et al. 2001). Second, several ground-based (sub)-millimeter continuum surveys of nearby, compact cluster-forming clouds have uncovered 'complete' (but small) samples of prestellar condensations whose mass distributions resemble the stellar IMF (see § 2).

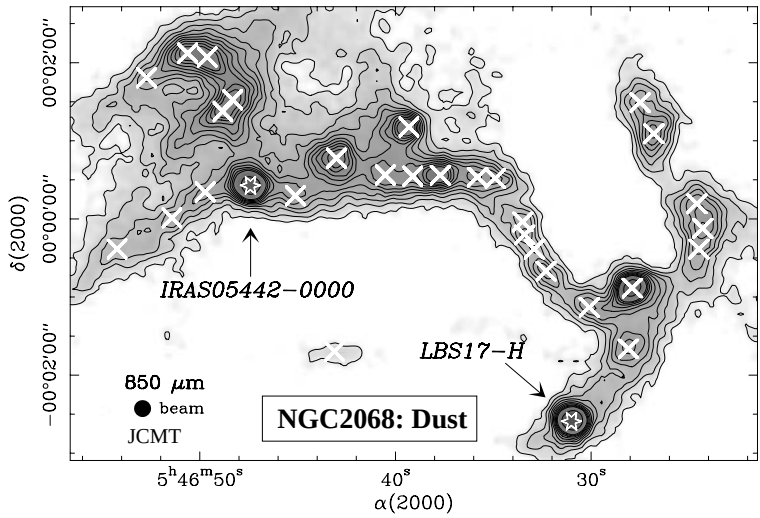

Figure 1. SCUBA $850\,\mu$m dust continuum map of the NGC 2068 protocluster extracted from the mosaic of NGC 2068/2071 by Motte et al. (2001). A total of 30 compact starless condensations (marked by crosses), with masses between $\sim 0.4\,M_{\odot}$ and $\sim 4.5\,M_{\odot}$, are detected in this ~ 1 pc $\times$ 0.7 pc field.

2. Submillimeter Continuum Surveys for Prestellar Condensations

Wide-field (sub)mm dust continuum mapping is a powerful tool to take a census of dense cores within star-forming clouds. The recent advent of large-format bolometer arrays on (sub)millimeter radiotelescopes such as the IRAM 30m and the JCMT has led to the identification of numerous cold, self-gravitating condensations that do not obey the Larson (1981) self-similar scaling laws of molecular clouds and are intermediate in their properties between

diffuse CO clumps and infrared young stellar objects (cf. André et al. 2000 for a review). As an example, Fig. 1 shows the condensations found by Motte et al. (2001) at 850 μm in the NGC 2068 protocluster (Orion B). A small fraction of such centrally-peaked submillimeter continuum condensations lie at the base of powerful jet-like outflows and correspond to very young protostars which have not yet accreted the majority of their final masses (Class 0 objects – cf. André et al. 2000). However, the majority of them are starless/jetless and appear to be the immediate prestellar progenitors of individual protostars or protostellar systems.

In particular, the mass distribution of these prestellar condensations is remarkably similar to the stellar IMF (e.g. Motte, André, Neri 1998 – MAN98; Testi & Sargent 1998; Johnstone et al. 2000; Motte et al. 2001). This is illustrated in Fig. 2a which shows the cumulative mass spectrum of the 57 starless condensations found by MAN98 in their 1.3 mm continuum survey of the ρ Oph main cloud. These condensations, which were identified using a multi-resolution wavelet analysis (cf. Starck et al. 1998), are seen *on the same spatial scales as protostellar envelopes* (i.e., $\sim$ 2500–5000 AU or $\sim 15'' - 30''$ in ρ Oph). Their mass spectrum is consistent with the Salpeter (1955) power-law IMF at the high-mass end and shows a tentative break at $\sim 0.4\,M_{\odot}$ (see Fig. 2a). The latter is reminiscent of the flattening observed in the IMF of field stars below $0.5\,M_{\odot}$ (e.g. Kroupa et al. 1993, Chabrier 2003), also present in the mass function of ρ Oph pre-main sequence objects (Luhman et al. 2000, Bontemps et al. 2001). If real, the break occurs at a mass comparable to the typical Jeans mass in the dense ($n_{H_2} \sim 10^5$ cm^{-3}) DCO$^+$ cores of the ρ Oph cloud (cf. Loren et al. 1990).

Such a close resemblance to the IMF suggests that *the starless condensations identified in the (sub)millimeter dust continuum are about to form stars on a one-to-one basis, with a high ($\gtrsim 50\%$) local efficiency*. This strongly supports scenarios according to which the bulk of the IMF is at least partly determined by pre-collapse cloud fragmentation (e.g. Larson 1985, Padoan & Nordlund 2002).

The results of MAN98 in ρ Oph have been essentially confirmed by an independent 850 μm SCUBA study of the same region with JCMT (Johnstone et al. 2000), using a different algorithm for analyzing cloud structure (*Clumpfind* – cf. Williams et al. 1994).

Present determinations of the prestellar core mass distribution are limited by small-number statistics and have to rely on rather strong assumptions about the *dust (temperature and emissivity) properties*. Both T_{dust} and κ_{dust} are uncertain (by a factor $\gtrsim 2$) and may possibly vary from object to object. Radiative transfer calculations show that the dust temperature at the center of a starless condensation depends primarily on the degree of shielding from the external interstellar radiation field (e.g. Evans et al. 2001, Stamatellos & Whitworth

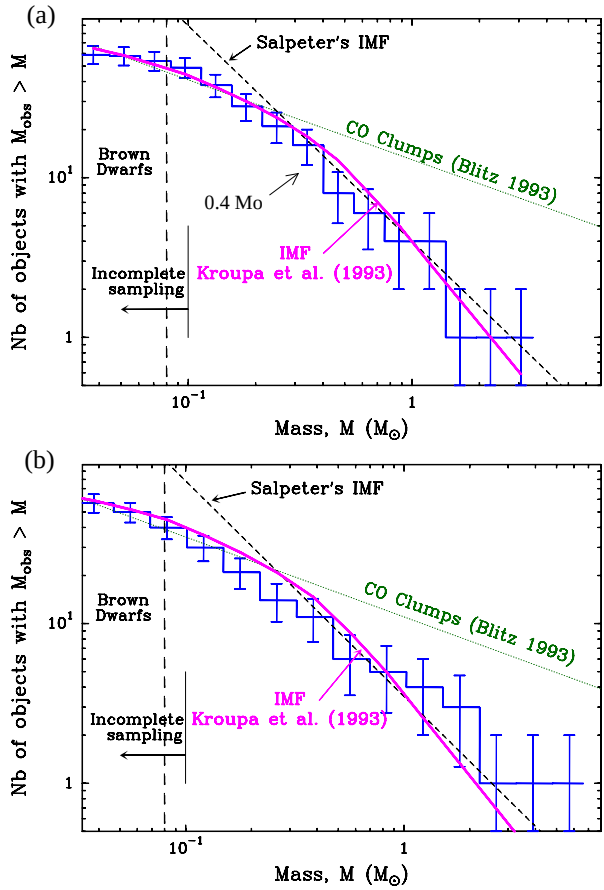

Figure 2. **(a)** Cumulative mass distribution of a sample of 57 prestellar condensations, complete down to $\sim 0.1\,M_\odot$, in the ρ Oph protocluster (histogram with error bars – from MAN98). (Here, the condensation masses were derived assuming the same dust properties for all condensations: $T_d = 15$ K, $\kappa_d(1.3\mathrm{mm}) = 0.005\,\mathrm{cm^2\,g^{-1}}$.) For comparison, the dotted and dashed lines show power-laws of the form $N(>M) \propto M^{-0.6}$ (typical mass distribution of CO clumps – see Blitz 1993) and $N(>M) \propto M^{-1.35}$ [Salpeter (1955)'s IMF], respectively. The solid curve shows the shape of the field star IMF (e.g. Kroupa et al. 1993). Note the flattening of these mass distributions below $\sim 0.4\,M_\odot$. **(b)** Same as (a) but assuming a distribution of dust temperatures for the ρ Oph condensations, in agreement with radiative transfer calculations which suggest that more massive, higher column-density condensations may be colder (e.g. Bouwman et al. 2004). Note that the flattening of the prestellar mass distribution near $\sim 0.4\,M_\odot$ essentially goes away. Direct temperature measurements, which will be possible with the future submillimeter space telescope *Herschel*, are needed to eliminate this uncertainty.

2003, Bouwman et al. 2004). Since more massive condensations tend to have higher column densities (cf. MAN98) and to be more shielded, one may ex-

pect them to be colder on average than low-mass condensations, which may lead to a differential distortion of the derived mass distribution if uniform dust properties are assumed. Figure 2b displays the mass distribution of ρ Oph prestellar condensations obtained after correcting for this effect based on the results of radiative transfer models. Comparison with Fig. 2a shows that the steep, Salpeter-like slope of the prestellar mass spectrum at the high-mass end is robust, but that the presence of a break at $\sim 0.4\,M_{\odot}$ is much less robust. (Note, however, that Fig. 2b is likely to overestimate the effect of changes in dust properties since it assumes a fixed dust opacity, while in actual fact κ_d may be larger in denser condensations due to dust coagulation – e.g. Ossenkopf & Henning 1994.)

With $Herschel$, the future submillimeter space telescope to be launched by ESA in 2007, it will be possible to dramatically improve on the statistics and to essentially eliminate the mass uncertainties through direct measurements of the dust temperatures (see André 2001).

3. Kinematics of Protocluster Condensations

Investigating the dynamics of the prestellar condensations identified in submillimeter dust continuum surveys is of great interest to discriminate between possible theoretical scenarios for their formation and evolution. Interesting results have emerged from recent spectroscopic studies using molecules such as NH_3, N_2H^+, N_2D^+, and DCO^+, which do not deplete onto dust grains until fairly high densities (e.g. Bergin & Langer 1997, Tafalla et al. 2002). As an example, Figure 3 shows an N_2H^+(1–0) map of the NGC 2068 protocluster obtained at the IRAM 30 m telescope (Belloche, André, Motte, in prep.). Such observations set valuable constraints on the kinematics of protocluster condensations which we discuss below (§ 3.1 and § 3.2).

3.1 Internal Motions

First, it appears that the small-scale (~ 0.03 pc) prestellar condensations observed in the Ophiuchus, Serpens, Perseus, and Orion cluster-forming regions are characterized by fairly narrow ($\Delta V_{FWHM} \lesssim 0.5$ km s^{-1}) N_2H^+(1-0) line widths (see, e.g., Fig. 4 and Belloche et al. 2001). For instance, the nonthermal velocity dispersion toward the starless condensations of the ρ Oph protocluster is about half the thermal velocity dispersion of H_2 ($\sigma_{NT}/\sigma_T \sim 0.7$ – Belloche et al. 2001). This indicates that the initial conditions of individual protostellar collapse are 'coherent' (cf. Goodman et al. 1998) and essentially free of turbulence ($\sigma_{NT} < \sigma_T \sim 0.2$ km s^{-1}), even when the parent cluster-forming clouds/cores have relatively high levels of turbulence ($\sigma_{NT} \gtrsim 0.4$ km s^{-1} – cf. Loren et al. 1990; Jijina et al. 1999). In some cases, the condensations are observed to have significantly narrower lines (by a factor ~ 2) than their

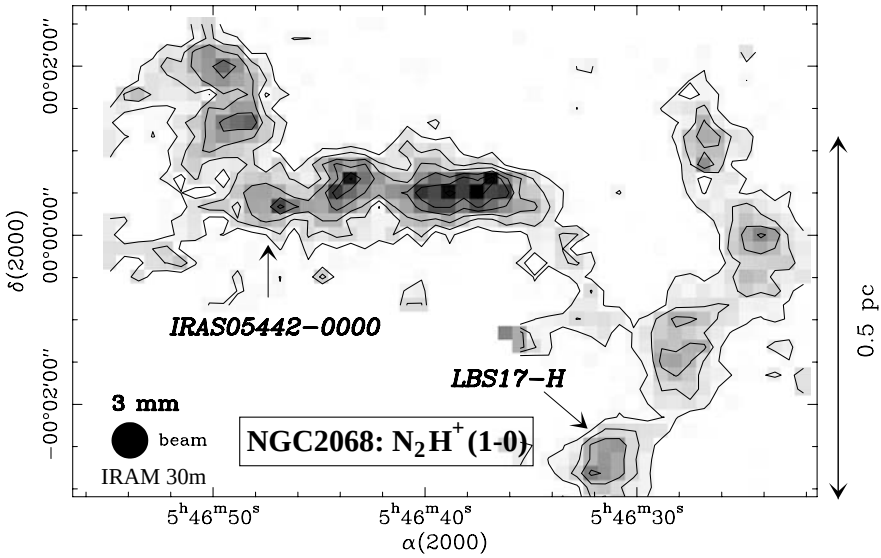

Figure 3. N_2H^+(1–0) integrated intensity map of the NGC2068 protocluster taken at the IRAM 30m telescope in the on-the-fly scanning mode (Belloche, André, Motte, in prep.). Most of the protocluster condensations identified in the 850 μm map (Fig. 1) show up in N_2H^+(1–0), despite a factor of ~ 2 lower angular resolution.

parent cores. These findings are in qualitative agreement with the 'kernel' picture proposed by Myers (1998), according to which protocluster condensations correspond to zones of minimum turbulence, of size comparable to the cutoff wavelength for MHD waves, developing in turbulent cloud cores. At variance with this picture, however, some cluster-forming cores such as Oph-E also exhibit narrow linewidths, similar to those of their own condensations, suggesting the dissipation of MHD turbulence is not the only mechanism responsible for core fragmentation.

As an aside, the narrow N_2H^+ linewidths of the condensations imply virial masses which generally agree well with the mass estimates derived from the dust continuum. This confirms that most of the starless submm continuum condensations are gravitationally bound and very likely *prestellar* in nature.

Second, some starless condensations show *evidence of collapse motions* in optically thick line tracers such as HCO^+(3–2). As an example, toward OphE-MM2 in the ρ Oph protocluster, the HCO^+(3–2) line exhibits a self-absorbed, double-peaked profile with a blue peak stronger than the red peak, while small optical depth lines such as N_2H^+(101–012) are single-peaked and peak in the absorption dip of HCO^+(3–2) (see Fig. 4). This type of blue asymmetry is now accepted as a classical spectral signature of collapse (cf. Evans 1999). The infall speeds derived from radiative transfer modeling are $\sim 0.1 - 0.3$ km s^{-1}

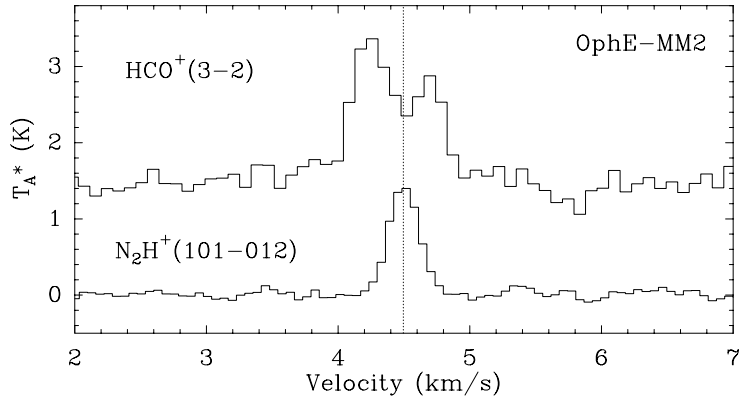

Figure 4. HCO^+(3–2) and N_2H^+(101-012) spectra observed at the IRAM 30 m telescope toward the starless 1.3 mm continuum condensation E-MM2 identified by MAN98 in the ρ Oph protocluster. The optically thick HCO^+ line is self-absorbed and skewed to the blue, which is the classical signature of collapse (e.g. Evans 1999), while the optically thin N_2H^+ line is narrow ($\Delta V \lesssim 0.3$ km s^{-1}) indicating small levels of turbulence. (From Belloche et al. 2001.)

(e.g. Belloche et al. 2001), consistent with a typical condensation lifetime $\sim 10^5$ yr. The detection of infall motions further supports the idea that *the protocluster condensations identified in the submm dust continuum are on the verge of forming protostars.*

3.2 Overall Protocluster Kinematics

Line observations can also provide information on the relative motions between condensations, as well as on possible global, large-scale motions in the parent protoclusters.

For instance, Belloche et al. (2001) have analyzed the distribution of line-of-sight velocities among 45 condensations of the ρ Oph protocluster, based on Gaussian fits to the observed N_2H^+(1–0) lines. The results indicate a global, one-dimensional velocity dispersion $\sigma_{1D} \sim 0.37$ km s^{-1} about the ρ Oph mean systemic velocity. Assuming isotropic relative motions, this corresponds to a three-dimensional velocity dispersion $\sigma_{3D} \sim 0.64$ km s^{-1}. With a ρ Oph central cloud diameter of ~ 1.1 pc, such a small velocity dispersion implies a typical crossing time $D/\sigma_{3D} \sim 1.7\times10^6$ yr. The crossing times determined for the individual DCO^+ cores or subclusters of ρ Oph are only slightly shorter ($\sim 0.6 \times 10^6$ yr). Since neither the age of the embedded IR cluster nor the lifetime

of the 1.3 mm condensations can be much larger than 10^6 yr (cf. Bontemps et al. 2001 and § 3.1 above), it appears that *the pre-stellar condensations do not have time to orbit through the protocluster gas and collide with one another* (even inside individual cores) before evolving into young stars. (This would require several crossing times – cf. Elmegreen 2001.) Similar results have been obtained for 25 condensations in the NGC 2068 protocluster (Belloche et al. in prep.). As the estimated tidal-lobe radius of the ρ Oph condensations is comparable to their observed radius $\lesssim 5000$ AU (cf. MAN98), competitive accretion may nevertheless play a role in limiting the condensation masses (see Bonnell et al. 2001).

4. Conclusions and Future Prospects

The mass distribution of prestellar condensations in star forming clouds appears to be consistent with the stellar IMF between $\sim 0.1\,M_\odot$ and $\sim 3 - 5\,M_\odot$, although large uncertainties remain especially at the low- and high-mass ends (cf. § 2). Small internal and relative motions are measured for these prestellar condensations, implying they are much less turbulent than their ambient cloud and do not have time to interact before collapsing to (proto)stars (cf. § 3). Taken at face value, these results are at variance with models in which dynamical interactions play a key role in shaping the distribution of stellar masses (e.g. Klessen & Burkert 2000, Bate et al. 2003). They rather support a picture of star formation in which individual protostellar collapse is initiated in decoupled condensations resulting from turbulent (e.g. Padoan & Nordlund 2002) and/or magnetic (e.g. Mouschovias & Ciolek 1999, Shu et al. 2004) cloud fragmentation. In cluster-forming clouds such as ρ Oph, the star formation efficiency within each condensation is high (cf. § 2): most ($> 50\%$) of the initial mass at the onset of collapse seems to end up in a star (or a stellar system). In regions of more distributed star formation like the Taurus cloud, the size of individual condensations is larger (e.g. MAN98), the local star formation efficiency is lower ($\sim 15\%$ – Onishi et al. 2002), and the feedback of protostellar outflows may be more important in limiting accretion and defining stellar masses (e.g. Adams & Fatuzzo 1996, Shu et al. 2004).

To fully understand how the IMF comes about, it is crucial to further investigate the processes by which prestellar condensations form and evolve in molecular clouds. With present submillimeter instrumentation, observational studies are limited by small-number statistics and restricted to the nearest regions. The advent of major new facilities at the end of the present decade should yield several breakthroughs in this area. With an angular resolution at 75–300 μm comparable to (or better than) the largest ground-based millimeter radiotelescopes, $Herschel$, the Far InfraRed and Submillimeter Telescope to be launched by ESA in 2007 (cf. Pilbratt et al. 2001 and references therein), will make pos-

sible complete surveys for prestellar condensations down to the proto-brown dwarf regime in the cloud complexes of the Gould Belt ($d \lesssim 0.5$ kpc).
High-resolution ($0.01'' - 0.1''$) imaging with the 'Atacama Large Millimeter Array' (ALMA, first available around 2008, fully operational in 2013 – cf. Wootten 2001) at $\sim$ 450 μm–3 mm will will beat source confusion and allow us to probe individual condensations in distant, massive protoclusters, all the way to the Galactic center and the Magellanic clouds.
Complementing each other nicely, *Herschel* and ALMA will tremendously improve our global understanding of the initial stages of star formation in the Galaxy.

References

Adams F.C., & Fatuzzo, M. 1996, ApJ, 464, 256

Alves, J.F., Lada, C.J., & Lada, E.A. 2001, Nature, 409, 159

André, P., Ward-Thompson, D., & Barsony, M. 2000, in Protostars and Planets IV, Eds. V. Mannings, A.P. Boss, & S.S. Russell (Univ. of Arizona Press, Tucson), p. 59

André, P. 2001, in The Promise of the *Herschel* Space Observatory, Eds. G.L. Pilbratt et al., ESA SP-460, p. 169

Bacmann, A., André, P., Puget, J.-L., Abergel, A., Bontemps, S., & Ward-Thompson, D. 2000, A&A, 361, 555

Bate, M.R., Bonnell, I.A., & Bromm, V. 2003, MNRAS, 339, 577

Belloche, A., André, P., & Motte, F. 2001, in From Darkness to Light, Eds. T. Montmerle & P. André, ASP Conf. Ser., 243, p. 313

Bergin, E.A., & Langer, W.D. 1997, ApJ, 486, 316

Blitz, L. 1993, in Protostars & Planets III, Eds. E.H. Levy & J.I. Lunine (Tucson: Univ. of Arizona Press), p. 125

Bonnell, I.A., Bate, M. R., Clarke, C. J. & Pringle, J.E. 2001, MNRAS, 323, 785

Bontemps, S., André, P., & Kaas, A.A. 2001, A&A, 372, 173

Bouwman, J., André, P., & Galli, D. 2004, in preparation

Chabrier, G. 2003, ApJ, 586, L133

Elmegreen, B. 2001, in From Darkness to Light, Eds. T. Montmerle & P. André, ASP Conf. Ser., 243, p. 255

Evans, N.J. 1999, ARA&A, 37, 311

Evans, N.J. II, Rawlings, J.M.C., Shirley, Y.L., & Mundy, L.G. 2001, ApJ, 557, 193

Goodman, A.A., Barranco, J.A., Wilner, D.J., & Heyer, M.H. 1998, ApJ, 504, 223

Jijina, J., Myers, P.C., & Adams, F.C. 1999, ApJS, 125, 161

Johnstone, D., Wilson, C. D., Moriarty-Schieven, G., et al. 2000, ApJ, 545, 327

Klessen, R.S., & Burkert, A. 2000, ApJS, 128, 287

Klessen, R.S., Heitsch, F., & Mac Low, M.-M. 2000, ApJ, 535, 887

Kroupa, P., Tout, C. A., & Gilmore, G. 1993, MNRAS, 262, 545

Larson, R.B., 1981, MNRAS, 194, 809

Larson, R.B. 1985, MNRAS, 214, 379

Loren, R.B., Wootten, A., & Wilking, B.A. 1990, ApJ, 365, 229

Luhman, K., Rieke, G.H., Young, E.T. et al. 2000, ApJ, 540, 1016
Motte, F., André, P.,& Neri, R. 1998, A&A, 336, 150 (MAN98)
Motte, F., André, P., Ward-Thompson, D., & Bontemps, S. 2001, A&A, 372, L41
Mouschovias, T.M., & Ciolek, G.E. 1999, in The Origin of Stars and Planetary Systems, Eds. C.J. Lada & N.D. Kylafis, p. 305
Myers, P.C. 1998, ApJL, 496, L109
Nakano, T. 1998, ApJ, 494, 587
Onishi, T., Mizuno, A., Kawamura, A., Tachihara, K. & Fukui, Y. 2002, ApJ, 575, 950
Ossenkopf, V., & Henning, Th. 1994, A&A, 291, 943
Padoan, P., & Nordlund, A. 2002, ApJ, 576, 870
Pilbratt, G., Cernicharo, J., Heras, A.M., Prusti, T., & Harris, R. 2001, The Promise of the Herschel Space Observatory (ESA, Noordwijk), ESA SP-460
Salpeter, E.E. 1955, ApJ, 121, 161
Shu, F.H., Adams, F.C., & Lizano, S. 1987, ARA&A 25, 23
Shu, F.H., Li, Z.-Y., & Allen, A. 2004, ApJ, 601, 930
Stamatellos, D., & Whitworth, A.P. 2003, A&A, 407, 941
Starck, J.L., Murtagh, F., & Bijaoui, A. 1998, Image Processing and Data Analysis: The Multi-scale Approach, Cambridge University Press (Cambridge, UK)
Tafalla, M., Myers, P.C., Caselli, P., Walmsley, C.M., & Comito, C. 2002, ApJ, 569, 815
Testi, L., & Sargent, A.I. 1998, ApJL, 508, L91 Troland, T.H., Crutcher, R.M., Goodman, A.A., Heiles, C., Kazès, I., & Myers, P.C. 1996, ApJ, 471, 302
Ward-Thompson, D., Scott, P.F., & Hills, R.E., & André, P. 1994, MNRAS, 268, 276
Williams, J.P., de Geus, E.J., & Blitz, L. 1994, ApJ, 428, 693
Wootten, A. 2001, Science with the Atacama Large Millimeter Array, ASP Conf. Ser., vol. 235

Figure 5 A lively discussion between Philippe André and Ian Bonnell.

HOW WELL DETERMINED IS THE CORE MASS FUNCTION OF ρ OPH?

D. Stamatellos and A. Whitworth
School of Physics & Astronomy, Cardiff University, Wales, UK
D.Stamatellos@astro.cf.ac.uk, A.Whitworth@astro.cf.ac.uk

Abstract Modeling of ρ Oph A indicates that the heating of the clump is mainly due to radiation from HD147889, a nearby star, which heats the clump to temperatures between 7 and 27 K. However, most of the clump volume is colder than 15 K. This low temperature means that previous mass estimates of the prestellar cores in ρ Oph A based mm observations may have underestimated core masses by up to a factor of 3. This affects the core mass function by moving the "knee" to a higher mass.

1. Introduction

The core mass function (CMF) of ρ Oph is similar to the stellar IMF, which suggests that the masses of stars are determined by fragmentation at a very early phase (Motte et al. 1998). Core masses in ρ Oph have been estimated from submm and mm observations, with the main uncertainties coming from our limited knowledge of the properties of the dust in cores and the dust temperature.

2. The model

We represent ρ Oph A by a Plummer-like density profile (see Fig. 1a), and assume standard MRN dust that has coagulated and accreted thin ice mantles. We also assume a thin layer ($A_{\rm V}=0.17$) around the clump with constant density and standard MRN dust. The system is heated (i) by an isotropic interstellar radiation field, and (ii) by HD147889, a B2V star at distance 0.5 pc from the clump (with parameters from Liseau et al. 1999). The radiative transfer calculations are performed using PHAETHON, a 3D Monte Carlo radiative transfer code (see Stamatellos & Whitworth 2003).

E. Corbelli et al. (eds.), The Initial Mass Function 50 Years Later, 319–320.

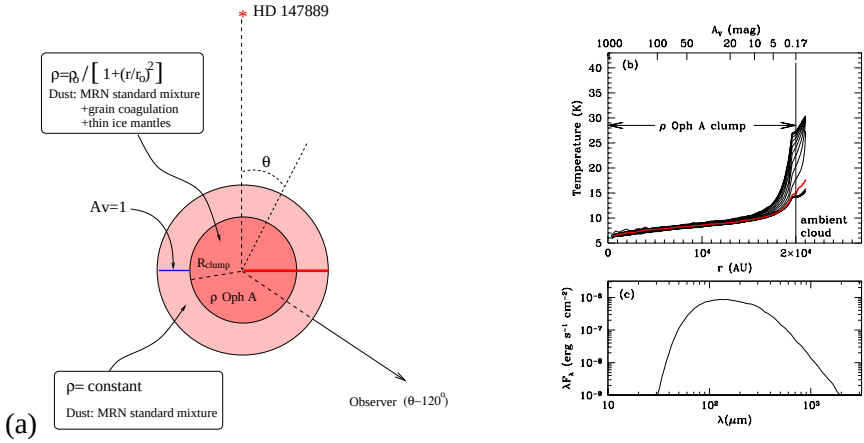

Figure 1. **(a)** ρ Oph A model **(b)** Dust temperature versus radius (lower axis), and visual extinction from the surface of the core (upper axis). We plot the radial profile from $\theta = 0^\circ$ to 180° every 9°. **(c)** The SED of the clump.

3. Results and Conclusions

The radiation from the star dominates, and heats the clump to temperatures 7-27 K (Fig. 1b). However, 80% of the clump volume has temperature less than 15 K. The ambient cloud dust has temperature $25 - 30$ K on the side closer to the star, which is consistent with previous estimations (Liseau et al. 1999). The SED of the model of ρ Oph A (Fig. 1c) peaks at around 130 μm, suggestive of a temperature around ~ 19 K (cf. André et al. 1993). The model suggests that most of the cores in the clump have temperature $T_{\rm dust} \lesssim 15$ K. This result has important implications about the masses obtained using mm observations. If a temperature of e.g. $T_{\rm dust} = 20$ K is assumed then the core mass is underestimated by a factor of 1.5 (if the correct temperature is $T_{\rm dust} = 15$ K) and by a factor of 2.7 (if $T_{\rm dust} = 10$ K). Since most of the core radiation comes from the denser but colder central core region, $T_{\rm dust} = 10$ K is a more appropriate temperature to be used, which suggests that the masses of many of the cores in ρ Oph A may have been underestimated by a factor of up to ~ 3. This should affect the CMF by moving the "knee" to a higher mass (also see André this volume).

References

André, P., Ward-Thompson, D., & Barsony, M. 1993, ApJ, 406, 122
Liseau, R. et al. 1999, A&A, 344, 342
Motte, F., André, P., & Neri, R. 1998, A&A, 336, 150
Stamatellos, D. & Whitworth, A. P. 2003, A&A, 407, 941

FROM DENSE CORES TO PROTOSTARS IN LOW-MASS STAR FORMING REGIONS

Toshikazu Onishi
Department of Astrophysics, Nagoya University, Chikusa-ku, Nagoya 464-8602, Japan
ohnishi@a.phys.nagoya-u.ac.jp

Abstract We present the results of a survey for dense molecular condensations in nearby low-mass star forming regions and the succeeding detection of a high-density condensation that is very close to the moment of the formation of a protostellar core within a time scale of $\sim 10^4$ yr.

1. Introduction

A study of star formation has been largely progressed by detections of protostars accompanying outflow phenomenon. Fairly young protostars have been observed as molecular outflows and are sometimes designated as Class I or Class 0 objects whose evolutionary time scale is in the order of 10^5 yr (e.g., Lada 1987; Fukui et al. 1989; André et al. 1993). However, there still remain a number of unresolved problems in a study of dense molecular cores before protostar formation. This is mainly because surveys of dense cores have been biased toward known optical and/or infrared features. We thus have carried out a molecular-line survey for starless condensations in an unbiased way toward $\sim$10 low-mass star forming regions in the lines of $C^{18}O$ and $H^{13}CO^+(J = 1 - 0)$. The observed regions include Taurus, Ophiuchus, Chamaeleon, Lupus, and so on. All the data were taken purely based on molecular data; all the observations have been made based on ^{13}CO observations that reveal entire distribution of gas of an intermediate density.

2. Summary of our Survey for Dense Cores

With these observations, we have obtained a uniform and almost complete sample of dense cores with a density $n(H_2)$ from 10^4 to $10^6 cm^{-3}$ in the observed star forming regions. This enables us to study the evolution of dense cores to protostars statistically for the first time. It is to be noted that a big advantage of the molecular line observations over continuum observations is that

E. Corbelli et al. (eds.), The Initial Mass Function 50 Years Later, 321–322.

the velocity dispersion of a core can be measured to determine the dynamical status. This information is crucial to find gravitationally bound structures that directly lead to a star formation.

We identified 179 $C^{18}O$ cores in total, and found that the intensity of $C^{18}O$ emission is a good tracer of the star formation activity. In particular, the column density of the $C^{18}O$ has a good positive correlation with the probability of star formation and has a threshold value for star formation. We also found that turbulent decay is indicated by diminishing line-width from the starless to the star-forming cores. The mass spectrum of the $C^{18}O$ cores can not be fitted by a single power-law function, and the index of the high-mass end resembles the stellar IMF (Tachihara et al. 2002, and see also Onishi et al. 1996, 1998).

Based on the $C^{18}O$ data above, we have carried out $H^{13}CO^{+}$(J=1 − 0) observations by using the NRO 45m telescope and the SEST. These starless condensations are compact (R $\lesssim$ 0.1 pc) and of high density ($\gtrsim 10^5$ cm^{-3}) and thus are highly probable candidates for protostellar condensations just before star formation. The time scale of the starless condensations is estimated to be $\sim 4 \times 10^5$ yr from the statistical analysis, and is several times larger than the free-fall time scale of gas with 10^5 cm^{-3}, $\sim 10^5$ yr. A comparison of masses between starless condensations and those with stars indicates that most of the starless condensations will not experience fragmentation except for binary formation, i.e, these condensations are a fundamental unit of star formation. The mass spectrum of the condensations is very steep and similar to that of the stellar IMF (Onishi et al. 2002).

Subsequent higher transition-line studies found the densest starless condensation, which is only less than 10^4 years away from the moment of protostar formation(Onishi et al. 1999).

References

André P., Ward-Thompson D., & Barsony M. 1993, ApJ 406, 122

Fukui Y., Iwata T., Takaba H., Mizuno A., Ogawa H., Kawabata K.,& Sugitani K. 1989, Nature 342, 161

Lada C.J. 1987, in IAU Symp. 115, Star forming regions , ed. M. Peimbert, J. Jugaku (D. Reidel:Dordrecht) p1

Onishi, T., Mizuno, A., Kawamura, A., Ogawa, H., & Fukui, Y. 1996, ApJ, 465, 815

Onishi, T., Mizuno, A., Kawamura, A., Ogawa, H., & Fukui, Y. 1998, ApJ, 502, 296

Onishi, T., Mizuno, A., & Fukui, Y. 1999, PASJ, 51, 257

Onishi, T., Mizuno, A., Kawamura, A., Tachihara, K., & Fukui, Y. 2002, ApJ, 575, 815

Tachihara, K., Onishi, T., Mizuno, A., & Fukui, Y. 2002, A&A, 385, 909

FRAGMENTATION OF A HIGH-MASS STAR FORMING CORE

Henrik Beuther
Harvard-Smithsonian Center for Astrophysics, 60 Garden Street, Cambridge MA 02138, USA
hbeuther@cfa.harvard.edu

Abstract At the earliest evolutionary stages, massive star forming regions are deeply embedded within their natal cores and not observable at optical and near-infrared wavelengths. Interferometric high-spatial resolution mm dust continuum observations of one very young high-mass star forming region disentangle its cluster-like nature already at the very beginning of the star formation process. The derived protocluster mass function is consistent with the stellar IMF. Hence, fragmentation of the initial massive cores may determine the IMF and the masses of the final stars. This implies that stars of all masses can form via accretion, and coalescence of protostars appears not to be necessary.

1. Introduction

One mystery in star formation is at what evolutionary stage in the cluster formation process the shape of the IMF gets established. For low-mass clusters, Motte et al. (1998) have shown that the protocluster mass function of ρ Oph resembles already the final IMF, but so far no comparable study exists for very young high-mass star forming regions. Additionally, I like to address how studying the earliest fragmentation processes of massive star forming regions helps to differentiate between the two proposed scenarios for massive star formation: accretion versus coalescence (e.g., McKee & Tan 2002, Bonnell et al. 1998). Employing the Plateau de Bure Interferometer (PdBI), we studied the dust continuum emission at 1.3 and 3 mm toward the massive star forming region IRAS 19410+2336. This region of 10^4 L$_\odot$ at a distance of ~ 2 kpc is at an early evolutionary stage prior to forming a hot core. The results of this study have recently been reported by Beuther & Schilke (2004).

2. Results

The large scale continuum emission observed at 1.2 mm with the IRAM 30 m telescope (Fig. 1a) shows two massive gas cores. Based on the intensity

E. Corbelli et al. (eds.), The Initial Mass Function 50 Years Later, 323–326.

profiles, we predicted that the cores should split up into sub-structures at scales between $3''$ and $5''$ (Beuther et al. 2002a). The PdBI 3 mm data at more than twice the spatial resolution show that both sources split up into sub-structures at the predicted scales, about four sources in the southern core and four in the northern core (Fig. 1b). At the highest spatial resolution (Figs. 1c & d), we observe that the gas clumps resolve into even more sub-sources. We find small clusters of gas and dust condensations with 12 sources per protocluster over the 3σ limit of 9 mJy/beam. Both protoclusters are dominated by one central massive source and surrounded by a cluster of less massive sources. This provides evidence for the fragmentation of a high-mass protocluster down to scales of 2000 AU at the earliest evolutionary stages.

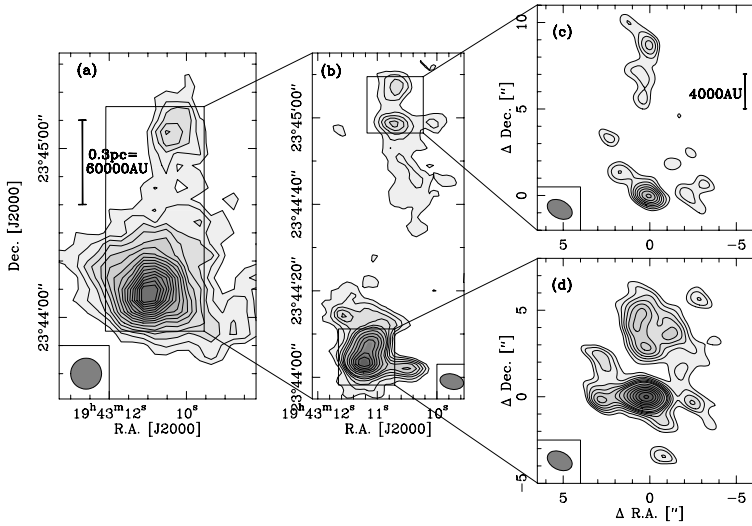

Figure 1. Dust continuum images of IRAS 19410+2336. Left: 1.2 mm single-dish data obtained with the IRAM 30 m at $11''$ (Beuther et al. 2002a). Middle and right: 3 mm and 1.3 mm PdBI data obtained with spatial resolutions nearly an order of magnitude better ($5.5'' \times 3.5''$ and $1.5'' \times 1''$, respectively).

Assuming the mm continuum flux to be due to optically thin thermal dust emission, one can calculate the masses following the method outlined in Hildebrand (1983). Based on IRAS far-infrared observations we estimate the average dust temperature to be around 46 K (Sridharan et al. 2002), the dust opacity index β is set to 2 (Beuther et al. 2002a). At the given temperature, the 9 mJy/beam sensitivity corresponds to a mass sensitivity limit of 1.7 $M_\odot$. The range of clump masses is 1.7 to 25 $M_\odot$. Combining the data from both clusters, we can derive a protocluster mass spectrum $\Delta N/\Delta M$, with the number of clumps ΔN per mass bin ΔM (Fig. 2). The best fit to the data results in

a mass spectrum $\Delta N/\Delta M \propto M^{-a}$ with the power law index $a = 2.5$ and a mean deviation $da = 0.3$.

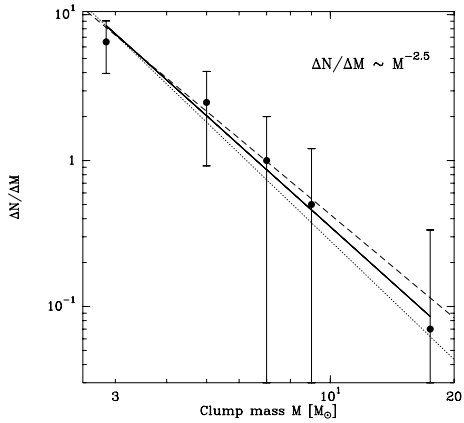

Fig. 2: The mass spectrum of IRAS 19410+2336. The clump-mass bins are [1.7(3σ),4], [4,6], [6,8], [8,10] and [10,25] $M_\odot$. The best fit to the data $\Delta N/\Delta M \sim M^{-a}$ is $a = 2.5$, the dashed and dotted lines show the IMFs derived from Salpeter (1955) with $a = 2.35$ and Kroupa et al. (1993) with $a = 2.7$, respectively.

Caveats: One uncertainty is the assumption of a uniform dust temperature because higher temperatures for the massive clumps would decrease their masses whereas lower temperatures for the less massive clumps would increase those. These effects could result in a somewhat flattened slope a. However, the protocluster is at an early evolutionary stage prior to forming a significant hot core, and the temperature variations in the protocluster should still be small. Hence, it is plausible to assume a similar dust temperature for all sub-sources, and the relative accuracy between the clumps masses – and thus the slope of the mass spectrum – is high. An additional caveat is that we are dealing with low-number statistics and just five mass bins. Only future more sensitive observations of a statistical significant number of massive protoclusters will allow to handle the statistics better. In contrast to this, we do not believe that the spatial filtering properties of the interferometer affect our results because the size of all clumps is far smaller than the spatial structures filtered out (of sizes $> 20''$). Consequently, only a large-scale halo common to all sources is affected by the filtering, whereas the sources we are interested in are not. Another uncertainty is whether all mm continuum emission is really due to protostellar condensations, because Gueth et al. (2003) have shown that such emission can also be caused by molecular outflows. Since at least seven outflows are observed toward IRAS 19410+2336 (Beuther et al. 2003), one or the other emission feature could be due an outflow as well. However, outflow associated emission features are expected to be rather weak. As a consistency check, we increased the lower mass limit slightly including less clumps in the power spectrum. The resulting values of the power-law index a varied only within the error margins. Therefore, we conclude that outflow contributions should not alter the derived slope a significantly.

3. Discussion

The derived power-law spectrum can be compared with the IMFs of more evolved clusters. Although open issues remain, this conference has confirmed the general consensus that the IMF for stars $> 1\,M_\odot$ can be approximated by $a = 2.5 \pm 0.2$ (e.g., Salpeter 1955, Miller & Scalo 1979, Scalo 1998, Kroupa et al. 1993). Furthermore, Motte et al. (1998) have shown that a similar slope is found between 0.5 and $3\,M_\odot$ toward the young low-mass protocluster ρ Oph. While the observations of ρ Oph already suggested that the IMF of low-mass stars is determined at early evolutionary stages, this was not obvious for more massive clusters because competitive accretion and merging of intermediate-mass protostars could establish the IMF at later stages as well (e.g., Bonnell et al. 2004). The new data now indicate that the upper end of the IMF is also determined at the earliest evolutionary stages. This supports the disk-accretion scenario for stars of all masses. However, the observations do not rule out that coalescence might occur within the dense centers of individual sub-cores.

References

Beuther, H. & Schilke, P. 2004, Science, 303, 1167
Beuther, H., Schilke, P., Menten, K. M., et al. 2002a, ApJ, 566, 945
Beuther, H., Schilke, P., & Stanke, T. 2003, A&A, 408, 601
Bonnell, I. A., Bate, M. R., & Zinnecker, H. 1998, MNRAS, 298, 93
Bonnell, I. A., Vine, S. G., & Bate, M. R. 2004, MNRAS, 349, 735
Gueth, F., Bachiller, R., & Tafalla, M. 2003, A&A, 401, L5
Hildebrand, R. H. 1983, QJRAS, 24, 267
Kroupa, P., Tout, C. A., & Gilmore, G. 1993, MNRAS, 262, 545
McKee, C. F. & Tan, J. C. 2002, Nature, 416, 59
Miller, G. E. & Scalo, J. M. 1979, ApJS, 41, 513
Motte, F., Andre, P., & Neri, R. 1998, A&A, 336, 150
Salpeter, E. E. 1955, ApJ, 121, 161
Scalo, J. 1998, in The Stellar Initial Mass Function, ASP Conf. Ser. 142, eds. Gilmore G. & Howell D., p.201
Sridharan, T. K., Beuther, H., Schilke, P., et al., 2002, ApJ, 566, 931

VI

THE ORIGIN OF THE IMF: CLOUD FRAGMENTATION AND COLLAPSE

Figure 1. Ed puzzled by Gouliermis' insight.

Figure 2. Relaxing in the hot springs of Bagno Vignoni.

UNDERSTANDING THE IMF

Richard B. Larson
Department of Astronomy, Yale University, New Haven, CT 06520-8101, USA
larson@astro.yale.edu

Abstract It is suggested that the thermal physics of star-forming clouds may play a more important role than has usually been recognized in the origin of the stellar IMF and in determining a characteristic mass scale. The importance of the thermal physics has been clearly demonstrated for the formation of the first stars in the universe, where it is well understood and results in cooling to a characteristic minimum temperature at a preferred density, and hence in a characteristic scale for fragmentation. In present-day star-forming clouds, an analogous situation may exist in that at low densities the temperature is expected to decrease with increasing density, reaching a minimum when the gas becomes thermally coupled to the dust and then rising slowly at higher densities. A minimum temperature of about 5 K is predicted to occur at a density of the order of $10^{-18}\,\mathrm{g\,cm^{-3}}$, and at this point the Jeans mass is about 0.3 solar masses, similar to the mass at which the IMF peaks. If most of the fragmentation in star-forming clouds occurs in filaments, as is suggested by many simulations as well as by observations, fragmentation seems likely to occur preferentially at the density where the temperature reaches a minimum, and the Jeans mass at this point may then determine a characteristic scale for fragmentation and hence a preferred stellar mass.

1. Introduction

As we have seen at this meeting, much evidence now supports a general form for the stellar IMF which is similar to the original Salpeter power law at masses above one solar mass, but which flattens at lower masses and peaks at a few tenths of a solar mass when expressed in terms of the number of stars per unit logarithmic mass interval (Scalo 1986, 1998; Kroupa 2002; Larson 2003a). Nearly all studies of the lower end of the IMF have shown that the IMF declines in the brown-dwarf regime, making it clear that the IMF is a peaked function. Nature thus makes stars with a preferred mass that is between one-tenth and one solar mass. The amount of mass that goes into stars in each logarithmic mass interval is also a broadly peaked function that has a maximum at about 0.5 solar masses, according to the approximation suggested by Kroupa

E. Corbelli et al. (eds.), The Initial Mass Function 50 Years Later, 329–340.

(2002). Thus, in terms of where most of the mass goes, there is a characteristic stellar mass that is of the order of half of a solar mass. This is probably the most fundamental fact about star formation that needs to be explained by any theory of how stars form: some feature of the physics of star formation must result in a characteristic stellar mass a little below one solar mass.

A further remarkable fact for which we have seen much evidence here is that the IMF shows a considerable degree of universality: very similar, and often indistinguishable, results for the IMF are found in many different star-forming environments in our Galaxy and other nearby galaxies, and no clear dependence has been found on any plausibly relevant astrophysical parameters such as metallicity. Thus, not only must some aspect of the fundamental physics of star formation lead to a preferred mass scale, but it must operate in a relatively universal way that is only weakly dependent on the environment and on most astrophysical parameters. This fact poses a clear challenge to the theory of star formation.

2. The Role of Cloud Fragmentation and the Jeans Mass

Recent millimeter-wavelength surveys of star-forming clouds have revealed the existence of many small dense clumps that have masses extending well down into the brown-dwarf regime, and that appear likely to be direct stellar progenitors (e.g., Motte et al 1998; Motte & André 2001a,b). Part of the evidence that these small dense clumps or 'cloud cores' may be direct stellar progenitors is the fact that their mass spectrum is similar to the stellar IMF at masses below a few solar masses (Luhman & Rieke 1999; Motte & André 2001a,b), suggesting that stars in this mass range may gain their masses directly from those of the cloud cores in which they form. Other authors have found similar results, but with core masses that are systematically somewhat larger (Johnstone et al 2000, 2001); these results could still be consistent with the direct collapse of these cores into stars but with a somewhat lower efficiency of star formation. If low-mass stars gain their masses from those of the prestellar cloud cores in which they form, the problem of understanding stellar masses then becomes, to a large extent, the problem of understanding cloud fragmentation processes, i.e. of understanding how the material in a star-forming cloud becomes divided up into individual star-forming units.

Perhaps even more direct evidence that low-mass stars owe their characteristic mass to cloud fragmentation processes is provided by the fact that stars typically form in small clusters of a few hundred stars in which the efficiency of star formation is moderately high, of the order of 25 to 30 percent (Lada & Lada 2003). This means that the average stellar mass is determined to within a factor of 3 or 4 just by the number of stars that form in each cluster-forming region, since the average mass is equal to the total stellar mass divided by the

number of stars, and this is equal within a factor of 3 or 4 to the total mass of the cluster-forming region divided by the number of stars formed in it. The problem of understanding the preferred stellar mass is then basically one of understanding the number of star-forming cloud cores that form in such a region. That is, the problem is one of understanding the typical scale of fragmentation – does most of the mass go into a few large objects or many small ones?

The most classical type of fragmentation scale is the well-known Jeans scale based on balancing gravity against thermal pressure, which has been known for more than 100 years (Jeans 1902, 1929). Although the original derivation by Jeans of a minimum length scale for fragmentation in an infinite uniform medium was not self-consistent, rigorous stability analyses have yielded dimensionally equivalent results for a variety of equilibrium configurations, including sheets, filaments, and spheres (Larson 1985, 2003b). Many simulations of cloud collapse and fragmentation that include gravity and thermal pressure have also shown a clear imprint of the Jeans scale on the results: the number of star-forming cloud cores formed is always comparable to the number of Jeans masses present initially (e.g., Larson 1978; Monaghan & Lattanzio 1991; Klessen 2001; Bate, Bonnell, & Bromm 2003). As long as gravity is strong enough to cause collapse to occur, the scale of fragmentation is not expected to be greatly altered by the presence of rotation or magnetic fields (Larson 1985, 2003b). Simulations of turbulent fragmenting clouds have also shown that the amount of fragmentation that occurs is not strongly dependent on the way in which turbulence is introduced, or even on whether turbulence is initially present at all; the number of fragments formed always remains similar to the number of Jeans masses present initially, although fragment masses may be somewhat reduced by compression occurring during the collapse (Klessen 2001; Bonnell & Bate 2002; Bate et al 2003). The effect of a magnetic field is less clear, but simulations of MHD turbulence typically show that that the nature of the turbulence is not qualitatively altered by the presence of a magnetic field; similar filamentary and clumpy structures are still seen (Mac Low & Klessen 2004).

Thus, while the relevance of the Jeans scale has not been established in all circumstances, many theoretical and numerical results have suggested that it has wide applicability. Its relevance to star formation might not at first seem obvious, given that during the early stages of the process gravity is opposed mainly by magnetic fields and turbulence, while the Jeans criterion involves only gravity and thermal pressure (Mac Low & Klessen 2004). However, the early evolution of star-forming clouds is expected to be characterized, to a considerable extent, by the loss of magnetic flux and the dissipation of turbulence in the densest contracting core regions, leaving thermal pressure eventually as the main force opposing gravity in the small dense prestellar cores that form. Thus star formation in effect gets rid of most of the initial magnetic field and

turbulence, as well as angular momentum, at a relatively early stage. As would be expected on this basis, observed prestellar cores show a rough balance between gravity and thermal pressure, with a minor contribution from turbulence and a contribution from magnetic fields that may be comparable to thermal pressure but probably is not dominant. The thermal physics must then play an important role in the later stages of the star formation process and in the processes that determine stellar masses and the IMF.

3. Importance of the Thermal Physics of Star-Forming Clouds

If the Jeans criterion indeed plays a significant role in determining stellar masses, it is important to understand the thermal behavior of star-forming clouds because the Jeans mass depends strongly on the temperature, varying either as $T^{3/2}\rho^{-1/2}$ or as $T^2P^{-1/2}$, depending on whether the density or the pressure of the medium is specified. Most of the simulations of cloud collapse and fragmentation that have been made in the past few decades have adopted a simple isothermal equation of state, and the results show, as was noted above, that fragmentation during isothermal collapse is limited to producing a number of fragments that is typically comparable to the number of Jeans masses present in the initial cloud. This means that the scale of fragmentation during isothermal collapse is largely determined by the initial conditions, or by the conditions existing when isothermal collapse begins. In the simulations the initial conditions can be chosen arbitrarily, but how does nature choose the initial conditions? Why should nature prefer initial conditions for isothermal collapse that yield a Jeans mass of the order of one solar mass?

One way of explaining a universal mass scale might be in terms of some universality in the properties of star-forming molecular clouds or their internal turbulence, for example a characteristic turbulent ram pressure that translates into a preferred Jeans mass (Larson 1996). The turbulent pressures in nearby star-forming clouds have about the right order of magnitude for such an explanation to seem feasible (Larson 2003a). However, beyond the local region, star-forming clouds and environments in our Galaxy and others vary so widely in their properties, and turbulence is such a variable and poorly defined phenomenon, that this view does not clearly offer an appealing explanation for a quasi-universal IMF.

Another possibility, not widely explored until now, is that there is some universality in the internal physics of star-forming clouds, for example in their thermal physics, that results in a preferred mass scale for fragmentation. This might be the case if the gas does not remain isothermal during the collapse, since variations in the temperature could then have an important effect on fragmentation, given the strong sensitivity of the Jeans mass to temperature.

For example, if significant cooling occurs during the early stages of collapse, this can greatly increase the amount of fragmentation that occurs during these stages (Monaghan & Lattanzio 1991). The temperatures of star-forming clouds are controlled by processes of atomic and molecular physics that should operate in much the same way everywhere, and this might result in a mass scale for fragmentation that depends only on atomic-scale physics and therefore is relatively universal.

One problem of star formation in which the thermal physics is well understood and has a clear impact on the scale of fragmentation is the problem of the formation of the first stars in the universe, before any heavy elements had been produced. This topic is reviewed briefly in the next section as an example of the possible importance of the thermal physics for stellar masses and the IMF.

4. An Example: The Masses of the First Stars

In contrast to present-day star formation where the thermal physics is complicated and involves many types of processes and particles, the thermal physics of the first star-forming clouds is relatively simple; because of the absence of any heavy elements, it involves only hydrogen molecules that control the temperature by their infrared line emission. As reviewed by Bromm & Larson (2004), calculations by several groups made with varying assumptions have converged on a consistent picture of the thermal behavior of the first star forming clouds that is largely independent of many of the details, including the cosmological initial conditions, and is determined basically by the physics of the H_2 molecule. A parameter exploration by Bromm, Coppi, & Larson (2002) also showed a robust thermal behavior that was largely independent of the parameters varied.

The first star-forming systems or primitive 'protogalaxies' are predicted to form at redshifts of the order of 20 to 30, and because of the absence at first of any significant coolants, the gas collapses adiabatically in each small dark halo and forms a rotating, flattened, possibly disk-like configuration. Compressional heating during this collapse raises the gas temperature to above 1000 K, and this increases the rate of formation of H_2 molecules by ion chemistry, producing a molecular abundance fraction of about 10^{-3}. The hydrogen molecules then become an important coolant via their infrared line emission, and this causes the temperature of the denser gas to fall again to a minimum value of about 200 K that is determined by the level spacing of the H_2 molecules. At about the same time, as the gas density approaches $10^4\,\mathrm{cm}^{-3}$, the upper levels of the H_2 molecules become thermalized, and this reduces the density dependence of the cooling rate so that the cooling time no longer decreases with increasing density. The cooling time then becomes longer than the free-fall time, and the densest clumps approach a rough balance between

pressure and gravity. They then nearly satisfy the Bonnor-Ebert criterion for a marginally stable isothermal sphere, which is dimensionally equivalent to the Jeans criterion. The masses of these slowly contracting clumps therefore become essentially equal to the Jeans or 'Bonnor-Ebert' mass at a characteristic temperature and density of about 200 K and $10^4\,\mathrm{cm}^{-3}$. Calculations by several groups (Abel, Bryan, & Norman 2000, 2002; Bromm, Coppi, & Larson 1999, 2002; Nakamura & Umemura 2001, 2002) have all shown convergence into a similar regime of temperature and density. In this preferred regime, the Bonnor-Ebert mass is several hundred solar masses, and as might be expected, all of the simulations have yielded clump masses of this order, that is, between a few hundred and a thousand solar masses.

The final evolution of these clumps has not yet been determined, but none of the simulations has yet shown any tendency for them to fragment further when the calculations are followed with high resolution to much higher densities. This is perhaps not too surprising, given that the temperature rises slowly with increasing density and the contraction of the clumps is slowed by inefficient cooling, making it seem unlikely that further fragmentation will occur, except possibly for the formation of binaries. Therefore it seems likely that a star with a mass of at least a hundred solar masses will form, unless feedback effects strongly inhibit accretion during the later stages. Omukai & Palla (2003) have studied the accretion problem with spherical symmetry, including all of the relevant radiative effects, and they have found that if the accretion rate is not too high, accretion can continue up to a mass of at least 300 solar masses. High-resolution calculations of the accretion phase by Bromm & Loeb (2004) have yielded accretion rates that according to Omukai & Palla (2003) are in the range that can allow accretion to continue up to a maximum mass that could be as large as 500 solar masses (Bromm 2005). While this is not yet a final answer because radiative effects have not yet been included in a realistic three-dimensional calculation, it seems very likely that the first stars were indeed massive objects, quite possibly more massive than 100 solar masses. If this conclusion is correct, this large mass scale can be attributed basically to the physics of the H_2 molecule, and it depends only secondarily on other factors such as the details of the cosmological initial conditions.

5. Thermal Physics of Present-Day Star-Forming Clouds

As was noted above, the thermal behavior of the first collapsing clouds is expected to be characterized by an early phase of rapid cooling by H_2 line emission to a minimum temperature of $\sim 200\,\mathrm{K}$, followed by a phase of slower contraction during which temperature slowly rises again. A qualitatively similar situation is expected to occur in present-day star-forming clouds: as can be seen in Figure 2 of Larson (1985), observations and theory both show that

at low densities the temperature decreases with increasing density, in this case because of cooling by line emission from C^+ ions and O atoms, while at high densities, the temperature is predicted to rise slowly with increasing density; this occurs when the gas becomes thermally coupled to the dust grains, which then control the temperature by their far-infrared thermal emission. Between these two thermal regimes, the temperature reaches a predicted minimum value of about 5 K at a density of the order of 10^{-18} g cm^{-3}, at which point the Jeans mass is a few tenths of a solar mass. Does this expected thermal behavior play a role in determining the resulting stellar IMF?

The variation of temperature with density described above can be approximated at low densities by a polytropic equation of state $P \propto \rho^{\gamma}$ with an exponent of $\gamma \sim 0.7$, and at high densities by a polytropic equation of state with an exponent of $\gamma \sim 1.1$. The collapse and fragmentation of turbulent clouds with various assumed values of γ has been simulated by Li, Klessen, & Mac Low (2003), and they found that such a variation in γ can make a large difference to the amount of fragmentation that occurs: in particular, they found that, for the same initial conditions and the same treatment of turbulence, a simulation with $\gamma = 0.7$ produced about 380 bound condensations, while one with $\gamma = 1.1$ produced only about 20 bound objects, a factor of 20 fewer. This dramatic reduction in the amount of fragmentation that occurs when γ is increased from 0.7 to 1.1 suggests that in real star-forming clouds, much more fragmentation will occur during the low-density phase of collapse when the effective value of γ is close to 0.7 than during the high-density phase when γ is closer to 1.1. Fragmentation may then almost come to a halt at the transition density where the temperature reaches a minimum and the Jeans mass is a few tenths of a solar mass. If this is indeed the case, and if fragmentation and the resulting mass spectrum are really so sensitive to the thermal physics, it is important to understand as accurately as possible the detailed thermal behavior of collapsing and fragmenting clouds.

The observational and theoretical results reviewed by Larson (1985) were taken from early work that included predictions by Larson (1973) of the temperature-density relation at the higher densities, but more recent work has mostly yielded similar results. In the low-density regime, the work of Koyama & Inutsuka (2000), which assumes that heating is due to the photoelectric effect rather than cosmic rays, as had been assumed in earlier work, yields a similar predicted decrease of temperature with increasing density. The observations compiled by Myers (1978) and plotted in Figure 2 of Larson (1985) had suggested temperatures rising again toward the high end of this regime, but these observations referred mostly to relatively warm and massive cloud cores and not to the small, dense, cold cores in which low-mass stars form; as reviewed by Evans (1999), these low-mass cores have much lower temperatures that are typically only about 8.5 K at a typical density of 10^{-19} g cm^{-3},

and this value is consistent with a continuation of the decreasing trend seen at lower densities, and with the continuing validity of a polytropic equation of state with $\gamma \sim 0.7$ up to a density of at least $10^{-19}\,\mathrm{g\,cm^{-3}}$.

At much higher densities, where the gas becomes thermally coupled to the dust grains, few temperature measurements exist because most of the molecules freeze out onto the grains, but most of the available theoretical predictions (Larson 1973; Low & Lynden-Bell 1976; Masunaga & Inutsuka 2000) agree well concerning the expected temperature-density relation, and they are consistent with an approximate power-law dependence with an equivalent γ of about 1.1. All of the theoretical predictions mentioned in this section can be fitted to within about ± 0.1 dex by the following approximation consisting of two power laws:

$$T = 4.4\,\rho_{-18}^{-0.275} \ \ \mathrm{K}, \quad \rho < 10^{-18}\,\mathrm{g\,cm^{-3}}$$

$$T = 4.4\,\rho_{-18}^{+0.075} \ \ \mathrm{K}, \quad \rho > 10^{-18}\,\mathrm{g\,cm^{-3}}$$

where ρ_{-18} is the density in units of $10^{-18}\,\mathrm{g\,cm^{-3}}$. This approximation to the equation of state, in which the value of γ changes from 0.725 to 1.075 at a density of $10^{-18}\,\mathrm{g\,cm^{-3}}$, is valid for densities between about $10^{-22}\,\mathrm{g\,cm^{-3}}$ and $10^{-13}\,\mathrm{g\,cm^{-3}}$. The actual predicted temperature minimum is somewhat smoothed out compared with this simple two-part approximation, and the predicted minimum temperature is actually about 5 K at a density of about $2 \times 10^{-18}\,\mathrm{g\,cm^{-3}}$. The minimum temperature attained in real clouds is somewhat uncertain because observations have not yet confirmed the predicted very low values; such cold gas would be very difficult to observe, but various efforts to model the observations have suggested central temperatures between 6 K and 10 K for the densest observed prestellar cores, whose peak densities may approach $10^{-17}\,\mathrm{g\,cm^{-3}}$. (e.g., Zucconi et al 2001; Evans et al 2001; Tafalla et al 2004). The temperature minimum may therefore in reality be shallower and more smoothed out than the predicted one, but the above approximation should still be valid for densities below $10^{-19}\,\mathrm{g\,cm^{-3}}$ or well above $10^{-17}\,\mathrm{g\,cm^{-3}}$.

6. The Fragmentation of Filaments

To explore the effect of an equation of state in which γ changes from about 0.7 at low densities to about 1.1 at high densities, Jappsen et al (2003, 2005) have made calculations of the collapse and fragmentation of turbulent clouds, which are similar to the those of Li et al (2003) except that γ is assumed to change from 0.7 to 1.1 at some critical density ρ_{crit} (see also Klessen 2005, this conference). The value of ρ_{crit} is then varied to test the effect of this parameter

on the mass spectrum of the star-forming condensations that form. The results show a clear dependence of the mass spectrum on $\rho_{\rm crit}$ in the expected sense that as $\rho_{\rm crit}$ is increased and the Jeans mass at the point of minimum temperature is thereby decreased, the number of bound condensations increases and their median mass decreases. This result shows that the detailed temperature-density relation in a collapsing cloud can play an important role in determining the mass spectrum of the fragments that form. These results also show that the number of fragments increases with increasing numerical resolution, which indicates that very high resolution is needed to obtain reliable results for the higher values of $\rho_{\rm crit}$.

A striking feature of these results is the prominence of filamentary structure in the simulated collapsing clouds, and the fact that nearly all of the bound condensations form in filaments. Filamentary structure is, in fact, a very common feature of simulations of collapse and fragmentation (Monaghan & Lattanzio 1991; Klessen & Burkert 2001; Bonnell & Bate 2002; Bate et al 2003). Many observed star-forming clouds also exhibit filamentary structure, and together with the evidence that much of the star formation in these clouds occurs in filaments (Schneider & Elmegreen 1979; Larson 1985; Curry 2002; Hartmann 2002), this suggests that the formation and fragmentation of filaments may be an important mode of star formation quite generally. If most of the fragmentation that leads to star formation occurs in filaments, this may offer an explanation for the fact that the amount of fragmentation that was found by Li et al (2003) depends so strongly on the assumed value of γ, especially for values of γ near unity. This sensitivity may result from the fact that $\gamma = 1$ is a critical value for the collapse of cylinders: for $\gamma < 1$, a cylinder can collapse indefinitely toward its axis and fragment indefinitely into many very small objects, while for $\gamma > 1$, this is not possible because pressure then increases faster than gravity and stops the collapse at a finite maximum density, where the Jeans mass has a finite minimum value. More fragmentation would then be expected to occur when $\gamma < 1$, as was indeed found by Li et al (2003).

The evolution of collapsing configurations can often be approximated by similarity solutions (Larson 2003b), and further insight into the collapse and fragmentation of filaments can be obtained from the similarity solutions derived by Kawachi & Hanawa (1998) for the collapse of cylinders with a polytropic equation of state. These authors found that the existence of such solutions depends on the value of γ: similarity solutions exist for $\gamma < 1$ but not for $\gamma > 1$. For the solutions with $\gamma < 1$, the collapse becomes slower and slower as γ approaches unity from below, asymptotically coming to a halt when $\gamma = 1$. This result shows in a particularly clear way that $\gamma = 1$ is a critical value for the collapse of filaments. Kawachi & Hanawa (1998) suggested that the slow collapse predicted to occur for values of γ approaching unity will in reality cause a filament to fragment into clumps, because the timescale for

fragmentation then becomes shorter than the timescale for collapse toward the axis. If in real clouds the effective value of γ increases with increasing density as the collapse proceeds, as is expected from the thermal behavior discussed above, fragmentation might then be favored to occur at the density where γ reaches unity, i.e. at the density where the temperature reaches a minimum. As was noted earlier, the Jeans mass at the density where the temperature attains its minimum value is predicted to be about 0.3 solar masses, coincidentally close to the mass at which the stellar IMF peaks. This similarity suggests that filament fragmentation with an increasing polytropic exponent may play an important role in the origin of the stellar IMF and its characteristic mass scale. Further calculations to test this hypothesis are currently under way, and some first results have been reported at this conference by Klessen (2005).

7. Summary

The problem of understanding the origin of the stellar IMF and its seeming universality remains unsolved, but recent work suggests that the mass scale for cloud fragmentation may depend importantly on the thermal physics of collapsing and fragmenting clouds. Nearly all numerical work has used a simple isothermal equation of state, but if collapsing clouds develop filamentary structures and if most of the star formation occurs in filaments, then the collapse and fragmentation of such configurations can be quite sensitive to variations in temperature. If, as expected, there is a low-density regime of decreasing temperature and a high-density regime of slowly rising temperature, fragmentation seems likely to be favored at the transition density where the temperature reaches a minimum. Existing simple treatments of the thermal physics predict that a minimum temperature of about 5 K is attained at a density of about $2 \times 10^{-18}\,\mathrm{g\,cm^{-3}}$, at which point the Jeans mass is about 0.3 solar masses, close to the mass at which the IMF peaks. Establishing more clearly the nature of any connection between these quantities will be an important goal of continuing research.

References

Abel, T., Bryan, G., & Norman, M. L. 2000, ApJ, 540, 39
Abel, T., Bryan, G., & Norman, M. L. 2002, Science, 295, 93
Bate, M. R., Bonnell, I. A., & Bromm, V. 2003, MNRAS, 339, 577
Bonnell, I. A., & Bate, M. R., 2002, MNRAS, 336, 659
Bromm, V. 2005, in The Initial Mass Function, ed. E. Corbelli, F. Palla, & H. Zinnecker (Dordrecht: Kluwer Acad. Publ.), in press (this volume)
Bromm, V., & Larson, R. B. 2004, ARA&A, 42, 79
Bromm, V., & Loeb, A. 2004, New Astron, 9, 353
Bromm, V., Coppi, P. S., & Larson, R. B. 1999, ApJ, 527, L5
Bromm, V., Coppi, P. S., & Larson, R. B. 2002, ApJ, 564, 23
Curry, C. L. 2002, ApJ, 576, 849

Evans, N. J. 1999, ARA&A, 37, 311
Evans, N. J., Rawlings, J. M. C., Shirley, Y. L., & Mundy, L. G. 2001, ApJ, 557, 193
Hartmann, L. 2002, ApJ, 578, 914
Jappsen, A.-K., Li, Y., Mac Low, M.-M., & Klessen, R. S. 2003, BAAS, 35, 1214
Jappsen, A-K., Klessen, R. S., Larson, R. B., Li, Y., & Mac Low, M.-M. 2005, A&A, in press.
Jeans, J. H. 1902, Phil Trans Roy Soc, 199, 49
Jeans, J. H. 1929, Astronomy and Cosmogony (Cambridge: Cambridge Univ. Press; reprinted by Dover, New York, 1961).
Johnstone, D., Wilson, C. D., Moriarty-Schieven, G., Joncas, G., Smith, G., Gregersen, E., & Fich, M. 2000, ApJ, 545, 327
Johnstone, D., Fich, M., Mitchell, G. F., & Moriarty-Schieven, G. 2001, ApJ, 559, 307
Kawachi, T., & Hanawa, T. 1998, PASJ, 50, 577
Klessen, R. S. 2001, ApJ, 556 837
Klessen, R. S. 2005, in The Initial Mass Function, ed. E. Corbelli, F. Palla, & H. Zinnecker (Dordrecht: Kluwer Acad. Publ.), in press (this volume)
Klessen, R. S., & Burkert, A. 2001, ApJ, 549, 386
Koyama, H., & Inutsuka, S.-I. 2000, ApJ, 532, 980
Kroupa, P. 2002, Science, 295, 82
Lada, C. J., & Lada, E. A. 2003, ARA&A, 41, 57
Larson, R. B. 1973, Fundam Cosmic Phys, 1, 1
Larson, R. B. 1978, MNRAS, 184, 69
Larson, R. B. 1985, MNRAS, 214, 379
Larson, R. B. 1996, in The Interplay Between Massive Star Formation, the ISM, and Galaxy Evolution, ed. D. Kunth, B. Guiderdoni, M. Heydari-Malayeri, & T. X. Thuan (Gif sur Yvette: Editions Frontières), p. 3
Larson, R. B. 2003a, in Galactic Star Formation Across the Stellar Mass Spectrum, ASP Conf. Ser. Vol. 287, ed. J. M. De Buizer & N. S. van der Bliek (San Francisco: Astron. Soc. Pacific), p. 65
Larson, R. B. 2003b, Rep Prog Phys, 66, 1651
Li, Y., Klessen, R. S., & Mac Low, M.-M. 2003, ApJ, 592, 975
Low, C., & Lynden-Bell, D. 1976, MNRAS, 176, 367
Luhman, K. L., & Rieke, G. H. 1999, ApJ, 525, 440
Mac Low, M.-M., & Klessen, R. S. 2004, Rev Mod Phys, 76, 125
Masunaga, H., & Inutsuka, S.-I. 2000, ApJ, 531, 350
Monaghan, J. J., & Lattanzio, J. C. 1991, ApJ, 375, 177
Motte, F., & André, P. 2001a, in From Darkness to Light: Origin and Evolution of Young Stellar Clusters, ASP Conf. Ser. Vol. 243, ed. T. Montmerle & P. André (San Francisco: Astron. Soc. Pacific), p. 310
Motte, F., & André, P. 2001b, A&A, 365, 440
Motte, F., André, P., & Neri, R. 1998, A&A, 336, 150
Myers, P. C. 1978, ApJ, 225, 389
Nakamura, F., & Umemura, M. 2001, ApJ, 548, 19
Nakamura, F., & Umemura, M. 2002. Prog Theor Phys Suppl, 147, 99
Omukai, K., & Palla, F. 2003, ApJ, 589 677
Scalo, J. M. 1986, Fundam Cosmic Phys, 11, 1
Scalo, J. M. 1998, in The Stellar Initial Mass Function, ASP Conf. Ser. Vol. 142, ed. G. Gilmore & D. Howell (San Francisco: Astron. Soc. Pacific), p. 201
Schneider, S., & Elmegreen, B. G. 1979, ApJ Suppl, 41, 87
Tafalla, M., Myers, P. C., Caselli, P., & Walmsley, C. M. 2004, A&A, 416, 191
Zucconi, A., Walmsley, C. M., & Galli, D. 2001, A&A, 376, 650

Figure 1. Eric Feigelson, Richard Larson and Kevin Luhman.

Figure 2. Gilles Chabrier to Richard Larson: you better explain it!

FLOWS, FILAMENTS AND FRAGMENTATION

Lee Hartmann
Smithsonian Astrophysical Observatory, 60 Garden St., Cambridge, MA 02138, USA
hartmann@cfa.harvard.edu

Abstract The location and extension of protostellar cloud cores in Taurus suggests that gravitational fragmentation in filaments is responsible for making those cores. To understand the basic mechanisms of this kind of fragmentation, we conducted simple simulations of finite self-gravitating sheets, envisioning these sheets as an approximation to molecular clouds formed by large scale flows. These simulations show that overall equilibrium is difficult if not impossible to maintain; that filaments are a general result of gravitational collapse in non-circular sheets; and that the structure of cloud edges are amplified by gravity to make focal points which can be the trigger for low-mass core fragmentation on small scales as well as likely sites for large mass concentrations needed to make high-mass stars and clusters. The effects of gravity suggest a possible link between cloud edges and mass spectra.

1. Introduction

It seems probable that several different physical mechanisms are at work in producing the form of the stellar IMF, given its form and the wide range of masses spanned. Here I wish to focus on one particular aspect which must be included in any theory of the IMF: the fragmentation of molecular clouds into cores and protocluster gas clouds.

2. Fragmentation in Taurus

Current theories of this core formation tend to focus on the role of turbulent motions in forming mass concentrations, which are then subject to gravitational contraction (e.g., Padoan & Nordlund 2002; Klessen 2001; see the contributions by Padoan, Klessen, and Vazquez-Semadeni in this volume). However, some of these simulations have certain difficulties in explaining the molecular cloud cores in the Taurus star-forming region. In particular, many calculations impose driven turbulence on small scales, with the result that the cores thus formed are distributed in a kind of "frothy" structure. In contrast, the Taurus cloud exhibits three large-scale bands or filaments of dense gas which

E. Corbelli et al. (eds.), The Initial Mass Function 50 Years Later, 341–346.

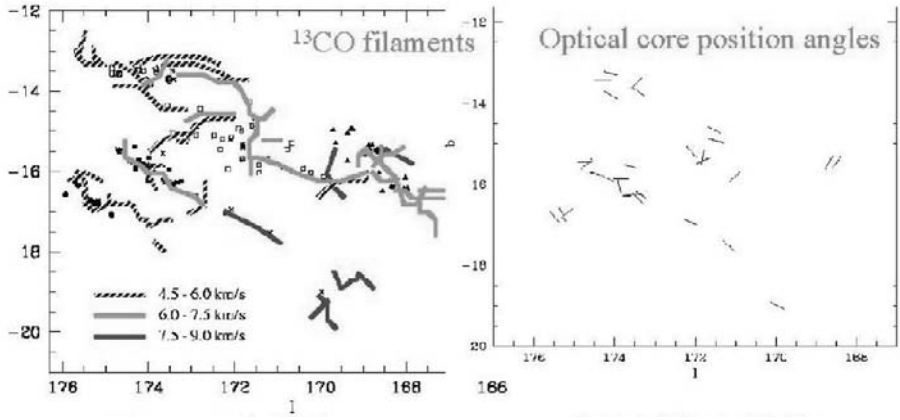

Figure 1. Structure in Taurus. Left panel: ^{13}CO filament structure indicated schematically with radial velocity ranges, from Mizuno et al. (1995). Right panel: positions of optical cores in Taurus, with position angles of elongation indicated, from Lee & Myers (1999). The cores are found in filaments and are generally elongated along their filament (see text).

span large distances roughly parallel to each other (Figure 1, left). As Klessen (2001) showed, this kind of structure requires turbulence with a large-scale component, not dominated by small-scale driving. The recent simulations by Bate, Bonnell, & Bromm (2003, and references therein) are not driven, and have gravity on from the beginning, and thus seem more realistic. However, the initial small-scale turbulence imposed produces a much more complex and frothy structure than observed at least in Taurus.

The location of cores in such extended and narrow filaments in Taurus suggests that cores are not simply formed by the action of flows in concentrating material. Instead, I suggested that gravitational fragmentation within flow-formed filaments is the operative mechanism (Hartmann 2002). As I noted, the linear theory of gravitational fragmentation in a filament, as developed by Larson (1985), suggests that the fastest-growing modes should be a few times the filament width, and this could explain the observation that the Taurus cores are generally elongated in the direction of their parent filament (Figure 1, right). One problem with this idea is that it is not clear how applicable linear theory is to the situation of these filaments, which are not likely to be static (that is, they exhibit supersonic line widths). However, numerical time-dependent simulations suggest that, under certain circumstances, gravitational fragmentation can occur in a manner that is roughly consistent with the linear theory, as mentioned by Monaghan (1994; also Klessen & Ballesteros-Paredes, personal communication).

Taurus is not a typical star-forming region in our galaxy, and its IMF may be somewhat anomalous (Briceno et al. 2002; Luhman et al. 2003; Luhman, this volume). Nevertheless, a complete theory of the IMF should also explain Taurus. Moreover, filamentary substructure may be present in denser, more complicated, and more distant regions than Taurus, substructure which may not have been recognized at present.

3. Filament and cluster formation

It is clear from the preceding considerations that the process of filament formation could have important implications for subsequent fragmentation into cores. Several studies have shown that filaments can form in gas layers with some preferred direction, possibly given by a magnetic field (Miyama et al. 1987; Nagai, Inutsuka, & Miyama 1998) or by some flow field (Klessen 2001). Here I focus on the formation of filaments and fragmentation in a finite medium, rather than infinite layers or boxes with periodic boundary conditions. Previously, Monaghan (1994) showed that an elongated spheroidal cloud can collapse to a filament, and Burkert & Bodenheimer (1993) showed filament formation from a spherical cloud with a significant initial low-order non-axisymmetric perturbation; here I wish to describe a particularly simple situation which is advantageous to understanding what is going on.

In a recent paper (Hartmann, Ballesteros-Paredes, & Bergin 2001), we argued that molecular clouds in the solar neighborhood are generally produced by large-scale flows (e.g., supernova-driven) sweeping up diffuse gas. This mechanism naturally produces clouds that are portions of "bubble walls". Andi Burkert and I were thus led to begin an analysis of fragmentation of such walls. To do this in the simplest possible situation, we approximated bubble walls as two-dimensional, isothermal, self-gravitating sheets. What we found (Burkert & Hartmann 2004) was surprising, at least to us (perhaps it shouldn't have been).

We found that, if one starts with sheets of uniform surface density, material immediately piles up at their edges due to the non-linear variation of gravitational acceleration as a function of spatial position. (This effect was found by Bastien (1983) in the context of cylindrical clouds.) Furthermore, if there are regions where the sheet edge initially has a non-uniform radius of curvature, enhanced concentrations of material build up at these flow "focal points". For example, Figures 2 and 3 show the evolution of an initially elliptical, uniform density sheet – in this case, with a modest amount of initial solid-body rotation. The immediate increase of density at the sheet edge is apparent in the left panel of Figure 2, along with the already-prominent buildup of mass at the ends of the (collapsing) ellipse. As collapse proceeds (right panel), the end focal points continue to attract matter, making large lumps of mass ("protocluster

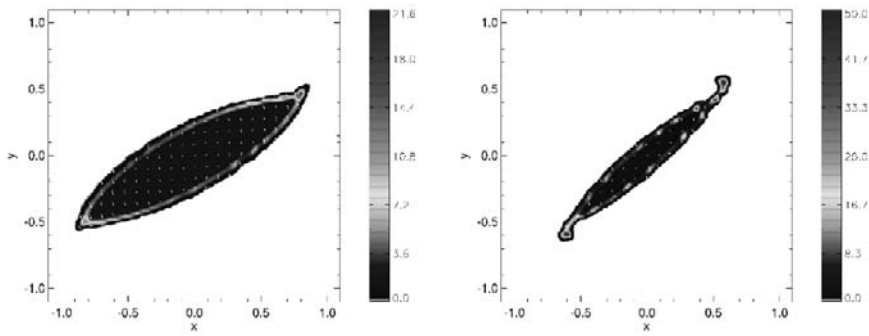

Figure 2. Collapse of the rigidly rotating elliptical uniform sheet. Focal points form and an eventual filament results (see also following figure) which has significant rotational support against gravity (see text)

clouds"). Fragmentation starts to occur in the "filaments" formed by the piled-up edge material; these fragments develop from small inhomogeneities in the initial conditions (basically, representing an ellipse on a rectangular grid). As the collapse proceeds further (Figure 3, left panel), the cloud collapses toward a single, rotating filament with large perturbations (the resolution of our simulations is insufficient to follow this fragmentation further).

Because of non-linear behavior of the gravitational acceleration in a finite (uniform density) sheet as a function of spatial position implies that it is very difficult to stabilize a cold sheet (negligible gas pressure support) everywhere. Rotation or expansion of the sheet can prevent collapse in the inner regions, but pileup still occurs at the sheet edge unless the sheet is violently flying apart. The modest rotation of the simulation in Figures 2 and 3 was insufficient to stabilize the sheet; faster rotation simply expels material. A limited linear expansion of the sheet does not prevent collapse to an edge, but simply results in an expanding (and fragmenting) ring. Modest decreases of surface density toward the edge just displace the position of the "edge" where material piles up. A variation of surface density with position, carefully calibrated to avoid pileup, seems unreasonable. Moreover, any small radius of curvature in the edge will result in a focal point, independent of edge effects.

We did not see evidence for fragmentation in the interior of our sheets; global collapse motions tended to overtake any growth of fragments, except in the edge regions, emphasizing the importance of the long-range nature of gravity. Thus, gravity combined with finite cloud dimensions can produce qualitatively different behavior from that seen in simulations with implicit infinite extent,

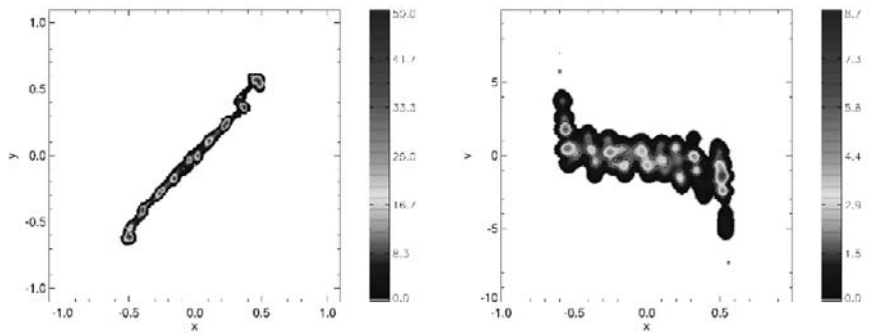

Figure 3. Left panel: formation of a filament from the rotating ellipse simulation (Figure 2). The size and number of subfragments are not quantitatively reliable. Right panel: contours of constant surface density integrated in the y-direction as a function of velocity in the x-direction. The overall rotation of the filament is evident, as well as infall toward the massive concentrations at the ends of the filament, and "turbulent" motions internal to the filament generated by the gravitational attraction between individual fragments (see text)

such as periodic boundary conditions, as well as the results from calculations in which gravity is only turned on at the last moment.

The right-hand panel of Figure 3 shows an "optically-thin" calculation of the x-direction velocity of the filament shown in the left-hand panel. One observes structure and substantial dispersion in the motions on small scales, in addition to the overall rotation. Thus, the attraction of clumps to diffuse gas and toward each other result in "turbulence" (e.g., Bonnell & Bastien 1993). Many simulations assume that a turbulent velocity field is imposed from the initial conditions of cloud formation in the ISM, or by a driven component (winds? jets?), but one should not forget the possibility of gravitationally-driven turbulence naturally resulting from self-gravity and density structure. Indeed, if self-gravitating clumps are present in clouds – as many molecular cloud cores are thought to be – one cannot avoid this turbulence.

We speculate that individual cores might have their origin in initial "edge" curvatures of clouds that subsequently collapse into filaments; this might represent a physical mechanism for translating quasi-fractal structure of clouds into a mass spectrum (e.g., Larson 1995). On larger scales, focal points appear to be a very attractive mechanism for channeling large amounts of mass at potentially high infall rates into small regions, necessary to the formation of protocluster gas clouds and/or high-mass stars. Much more investigation of these possibilities is necessary before we can fully understand the role of gravity in forming filaments, cores, and clusters.

Acknowledgments This work has been supported in part by NASA grants NAG5-9670 and NAG5-13210.

References

Bastien, P. 1983, A&A, 119, 109

Bate, M. R., Bonnell, I. A., & Bromm, V. 2003, MNRAS, 339, 577

Bonnell, I. & Bastien, P. 1993, ApJ, 406, 614

Briceño, C., Luhman, K. L., Hartmann, L., Stauffer, J. R., & Kirkpatrick, J. D. 2002, ApJ, 580, 317

Burkert, A. & Bodenheimer, P. 1993, MNRAS, 264, 798

Burkert, A. & Hartmann, L. 2004, ApJ, in press

Hartmann, L. 2002, ApJ, 578, 914

Hartmann, L., Ballesteros-Paredes, J., & Bergin, E. A. 2001, ApJ, 562, 852

Klessen, R. S. 2001, ApJ, 556, 837

Larson, R. B. 1985, MNRAS, 214, 379

Larson, R. B. 1995, MNRAS, 272, 213

Lee, C. W. & Myers, P. C. 1999, ApJS, 123, 233

Luhman, K. L., Briceño, C., Stauffer, J. R., Hartmann, L., Barrado y Navascués, D., & Caldwell, N. 2003, ApJ, 590, 348

Miyama, S. M., Narita, S., & Hayashi, C. 1987a, Prog. Theoretical Physics, 78, 1051

Mizuno, A., Onishi, T., Yonekura, Y., Nagahama, T., Ogawa, H., & Fukui, Y. 1995, ApJL, 445, L161

Monaghan, J. J. 1994, ApJ, 420, 692

Nagai, T., Inutsuka, S., & Miyama, S. M. 1998, ApJ, 506, 306

Padoan, P. & Nordlund, Å. 2002, ApJ, 576, 870

Figure 4. A dubious Lee Hartmann with Hans and Francesco.

MINIMUM MASS FOR OPACITY-LIMITED FRAGMENTATION IN DYNAMICALLY TRIGGERED STAR FORMATION

Anthony Whitworth and Douglas Boyd
School of Physics & Astronomy, Cardiff University, Wales, UK
ant@astro.cf.ac.uk,Douglas.Boyd@astro.cf.ac.uk

Abstract We present a new analysis of the minimum mass for star formation, based on opacity-limited fragmentation. Our analysis differs from the standard one, which considers hierarchical fragmentation of a three-dimensional medium, and yields $M_{\rm MIN} \sim 0.010$ to $0.015 M_\odot$, for Population I star formation. Instead, we consider the more dynamic – and we would argue, more realistic – scenario in which there is one-shot fragmentation of a shock-compressed layer, of the sort which arises when star formation is triggered impulsively. Our analysis includes both the competition with other fragmentation mass-scales, and the continuing growth of a fragment by accretion during its condensation. We find that $M_{\rm MIN}$ can be as small as $0.003 M_\odot$.

Consider two streams of gas having the same uniform density ρ, which collide at relative velocity $2\,v$. A shock-compressed layer forms on either side of the contact discontinuity. Suppose that the post-shock gas in the layer has isothermal sound speed a (a could be an effective isothermal sound speed incorporating contributions from turbulence, magnetic fields, etc.). As long as it is not perturbed, the layer is in equilibrium. In the direction *perpendicular* to the contact discontinuity, it is held together by the ram pressure of the inflowing gas, and not by self-gravity.

However, the layer is unstable against gravitational fragmentation. In the first instance, fragmentation entails motions driven by self-gravity *parallel* to the contact discontinuity. From linear perturbation analysis, the time of fragmentation, and the mass of the fastest growing condensation are

$$t_{\rm FRAG} \simeq \left(\frac{a}{G\,\rho\,v}\right)^{1/2}, \qquad M_{\rm FRAG} \simeq \left(\frac{a^7}{G^3\,\rho\,v}\right)^{1/2}. \tag{1}$$

We note (i) that the layer can fragment whilst it is still accumulating mass from the colliding streams; (ii) that at their inception the fragments are more extended parallel to the contact discontinuity than perpendicular to it, i.e. they

E. Corbelli et al. (eds.), The Initial Mass Function 50 Years Later, 347–348.

are like oblate spheroids; (iii) that $M_{\rm FRAG}$ is not the standard Jeans mass corresponding to the post-shock density and sound speed (which would be $(a^8/G^3\rho v^2)^{1/2}$).

In order to treat the non-linear fragmentation of the layer, we model a proto-fragment as a self-gravitating spheroid. The extent in the dimension perpendicular to the contact discontinuity is z and the extent in the two dimensions parallel to the contact discontinuity is r. Our model takes account of (i) self-gravity; (ii) internal pressure, (iii) external pressure, and (iv) the inflowing gas due to the colliding streams. The inflowing gas exerts ram pressure and inertial drag on a proto-fragment, as well as increasing its mass as it tries to condense out.

To survive, a fragment must satisfy three criteria. (A) It must condense out faster than all others. (B) It must still be condensing by the time $r < 0.5\,r_{\rm init}$ and $z < 0.5\,r_{\rm init}$. (C) The heating rate due to compression of the matter already in the fragment,

$$\mathcal{H} \;\equiv\; -\,P\,\frac{dV}{dt} \;=\; -\,M\,a^2\,\left[\frac{2\dot{r}}{r} \,+\, \frac{\dot{z}}{z}\right]\,, \tag{2}$$

plus the rate of dissipation of energy by the matter accreting onto the fragment from the continuing inflow,

$$\mathcal{D} \;=\; \frac{\dot{M}\,(v+\dot{z})^2}{2} \;-\; \frac{\dot{M}\dot{r}^2}{5}\,, \tag{3}$$

must be less than the maximum possible radiative cooling rate,

$$\mathcal{C} \;=\; 2\,\pi\,r^2\,\sigma_{\rm SB}\,T^4\,. \tag{4}$$

For the purpose of illustration, we adopt $a = 0.2\,{\rm km\,s^{-1}}$ (corresponding to H_2 at $T = 10\,{\rm K}$). Fragments with mass $< 5M_{\rm JUPITER}$ condense out for a wide range of pre-shock density ρ between 10^{-17} and $10^{-15}\,{\rm g\,cm^{-3}}$ and collision velocity v between 3 and $30\,{\rm km\,s^{-1}}$. The minimum mass, $2.6\,M_{\rm JUPITER}$, is produced by $\rho \sim 10^{-15}\,{\rm g\,cm^{-3}}$ and $v \sim 4\,{\rm km\,s^{-1}}$; it starts off with mass $1.1M_{\rm JUPITER}$, but grows by accretion during the early stages of condensation. We stress that all these fragments condense out faster than larger or smaller ones; and that their final masses include the mass acquired by accretion during condensation.

ORIGIN OF THE CORE MASS FUNCTION

Anthony Whitworth
School of Physics & Astronomy, Cardiff University, Wales, UK
ant@astro.cf.ac.uk

Abstract We show that if the core mass function is determined by a self-similar statistical equilibrium involving gravitational fragmentation and merging, it has a knee at $\sim M_\odot$: for lower masses the mass function has slope ~ -1, and for higher masses the slope is ~ -1.75 (*cf.* Salpeter's -2.35). We argue that efficient star formation requires the pressure to exceed $\sim k_{\rm B} 10^5\,{\rm cm}^{-3}\,{\rm K}$, since this ensures that the gas can cool efficiently by coupling thermally to the dust and thereby radiating in the continuum.

1. Introduction

In this contribution I shall adopt the viewpoint that star formation is triggered dynamically (i.e. 'in a crossing time' – as opposed to proceeding more quasistatically, via ambipolar diffusion). A fundamental process in dynamical star formation is the gravitational fragmentation of a shock-compressed layer formed by the collision of two converging streams of gas. In Section 2, I review the physics of the fragmentation of a shock-compressed layer, and give an expression for the mass $M_{\rm FRAG}$ of the fastest condensing fragment, as a function of the collision speed v, the pre-shock density ρ, and the post-shock velocity dispersion σ. In Section 3, I introduce Larson's scaling relations between the mass M, radius R and internal velocity dispersion σ of a core ($R \propto M^\alpha$, $\sigma \propto M^\beta$), and the core mass function (i.e. the number of cores per unit mass interval, $d\mathcal{N}/dM|_{\rm CORE} \propto M^{-\gamma}$). In Section 4, I use the assumption of scale-free statistical equilibrium to derive a relationship between α, β and γ. In Section 5, I consider cores whose support is dominated by turbulence, and show that, if the process whereby large cores fragment to produce smaller ones is self-similar, then these cores must have $R \propto M^{1/2}$, $\sigma \propto M^{1/4}$, and $d\mathcal{N}/dM|_{\rm CORE} \propto M^{-7/4}$. In Section 6, I consider cores whose support is dominated by thermal pressure, and show that these cores must have $R \propto M^1$, $\sigma \propto M^0$ and $d\mathcal{N}/dM|_{\rm CORE} \propto M^{-1}$. Thus, given the assumptions of statistical equilibrium and self-similarity, the core mass function has a knee. For

E. Corbelli et al. (eds.), The Initial Mass Function 50 Years Later, 349–354.

typical parameters in star forming gas, the knee is at $\sim M_\odot$; for higher masses the core mass function is steeper, and for lower masses it is shallower. In Section 7, I suggest that what determines whether a core collapses to form a star, or disperses and merges with other cores, is whether the gas is able to couple thermally to the dust (and thereby cool efficiently) or not. This gives a critical pressure $\sim k_{\rm B}\,10^5\,{\rm cm}^{-3}\,{\rm K}$, above which cores are likely to collapse to form stars, and below which they are not.

2. Fragmentation of a shock-compressed layer

We consider the simplest case, in which two streams of gas, both having uniform density ρ, collide head-on at relative velocity $2v$. Each stream therefore approaches the contact discontinuity with speed v, and if v is much greater than the velocity dispersion σ in the decelerated gas, a shock-compressed layer is formed. The layer grows steadily in mass until its column-density is high enough to promote non-linear gravitational fragmentation. Before it fragments, the layer is contained, in the direction *perpendicular* to the contact discontinuity, by the ram pressure of the inflowing gas, $P_{\rm RAM}$, and not by self-gravity; the layer is close to equilibrium and has approximately uniform density $\sim \rho(v/\sigma)^2$. The layer can fragment whilst it is still accumulating, and its fragmentaion is driven by self-gravity acting in directions *parallel* to the contact discontinuity. The fastest condensing fragment has finite extent, and at its inception its extent $R_{\rm FRAG}$ in directions parallel to the contact discontinuity is much greater than its extent $Z_{\rm FRAG}$ in directions perpendicular to the contact discontinuity, i.e. it is like an oblate spheroid. Specifically, $t_{\rm FRAG}$ (the time of non-linear fragmentation), $R_{\rm FRAG}$, $Z_{\rm FRAG}$ and $M_{\rm FRAG}$ (the mass of the fastest growing fragment) are given by

$$t_{\rm FRAG} \simeq \left(\frac{\sigma}{G\,\rho\,v}\right)^{1/2}, \qquad R_{\rm FRAG} \simeq \left(\frac{\sigma^3}{G\,\rho\,v}\right)^{1/2}, \tag{1}$$

$$Z_{\rm FRAG} \simeq \left(\frac{\sigma^5}{G\,\rho\,v^3}\right)^{1/2}, \qquad M_{\rm FRAG} \simeq \left(\frac{\sigma^7}{G^3\,\rho\,v}\right)^{1/2}. \tag{2}$$

The initial aspect ratio of a fragment is therefore

$$\frac{R_{\rm FRAG}}{Z_{\rm FRAG}} \simeq \frac{v}{\sigma}\,. \tag{3}$$

Because initially fragmentation of a shock compressed layer is essentially a two-dimensional process, $M_{\rm FRAG}$ is not the same as the Jeans mass corresponding to the shocked density, which is $M_{\rm JEANS} \simeq (\sigma^8/G^3\rho v^2)^{1/2}$.

3. Scaling relations and the core mass function

We shall assume that cores subscribe to Larson-type scaling relations, i.e. the radius R of a core, and the internal velocity dispersion σ within a core are related to its mass M by

$$R(M) \simeq R_{\rm O}\,(M/M_{\rm O})^{\alpha}\,, \tag{4}$$

$$\sigma(M) \simeq \sigma_{\rm O}\,(M/M_{\rm O})^{\beta}\,. \tag{5}$$

From this it follows that the density ρ in a core, and the dynamical time-scale t of a core, are given by

$$\rho(M) \simeq \rho_{\rm O}\,(M/M_{\rm O})^{(1-3\alpha)}\,, \tag{6}$$

$$t(M) \simeq t_{\rm O}\,(M/M_{\rm O})^{(\alpha-\beta)}\,. \tag{7}$$

Here $M_{\rm O}$, $R_{\rm O}$, $\sigma_{\rm O}$, $\rho_{\rm O} = 3M_{\rm O}/4\pi R_{\rm O}^3$ and $t_{\rm O} = R_{\rm O}/\sigma_{\rm O}$ are reference values. We shall return later to the question of how these reference values are normalized. In the meantime, we note that typical values in local star forming regions are $M_{\rm O} \simeq M_{\odot}$, $R_{\rm O} \simeq 0.1\,{\rm pc}$, $\sigma_{\rm O} \simeq 0.2\,{\rm km\,s^{-1}}$, $\rho_{\rm O} \simeq 2 \times 10^{-20}\,g\,{\rm cm^{-3}}$ (equivalently $n_{\rm H_2} \simeq 5 \times 10^3\,{\rm cm^{-3}}$) and $t_{\rm O} \simeq 5 \times 10^5\,{\rm yrs}$. We also note that in star forming gas there are many structures, including 'sheets' (like the shock-compressed layer we have invoked in Section 2) and 'filaments' (the fragmentation of a shock-compressed layer entails the formation of filaments). However, the 'cores' in a dust-continuum or molecular-line map are identified and quantified in such a way that aspect ratios greater than two are rare, and therefore it is appropriate to consider approximately spherical entities when deriving a core mass function for comparison with observation.

We shall also assume that the core mass function is a power law, so that the number of cores in unit mass interval is

$$\left.\frac{d\mathcal{N}}{dM}\right|_{\rm CORE} \simeq K\,M^{-\gamma}\,. \tag{8}$$

It follows that the total mass of cores in unit mass interval is

$$\left.\frac{d\mathcal{M}}{dM}\right|_{\rm CORE} \simeq K\,M^{(1-\gamma)}\,; \tag{9}$$

and the total mass of cores in unit logarithmic mass interval is

$$\left.\frac{d\mathcal{M}}{d\ell n[M]}\right|_{\rm CORE} \simeq K\,M^{(2-\gamma)}\,. \tag{10}$$

4. Scale-free statistical equilibrium

By adopting Larson's power-law scaling relations, and a power-law core mass function, we are implying that there is a range of core masses over which the ensemble of cores evolves in a scale-free, self-similar manner. Eventually we will need to review this assumption, but for the time being we simply pursue its consequences.

In addition, we know that – if we average over a sufficiently large volume – star formation is very inefficient, in the sense that there is not wholesale conversion of interstellar matter into new stars on a dynamical timescale. Therefore matter must migrate up and down the range of core masses (*up* by merging, and *down* by fragmentation) in an approximately statistical equilibrium, perturbed only by a slow leakage to star formation at the low-mass end. We will return to what controls the rate of leakage (i.e. the rate at which matter is lost from the ensemble of cores to star formation) in Section 7.

Fragmentation and merging proceed on a dynamical timescale. Consequently, statistical equilibrium requires that the mass in equal logarithmic mass intervals must be proportional to the dynamical timescale. Combining Eqns. (10) and (7) this gives

$$2 - \gamma = \alpha - \beta \qquad \Longrightarrow \qquad \gamma = 2 - \alpha + \beta \,. \tag{11}$$

We shall refer to this relation as the statistical equilibrium condition.

5. Cores supported mainly by turbulence

Observations with different resolution and/or in different molecular lines (with different critical densities) indicate that cores are hierarchical, i.e. a core at one level of the hierarchy breaks up into smaller cores if observed more closely. Thus, if we focus on a core of mass M having internal velocity dispersion $\sigma(M)$ and mean internal density $\rho(M)$, this *child* core is part of a larger *parent* core having mass FM ($F > 1$), internal velocity dispersion $\sigma(FM) \simeq F^{\beta}\sigma(M)$ and mean internal density $\rho(FM) \simeq F^{(1-3\alpha)}\rho(M)$. Similarly the parent core is part of an even larger *grandparent* core having mass F^2M, internal velocity dispersion $\sigma(F^2M) \simeq F^{2\beta}\sigma(M)$ and mean internal density $\rho(F^2M) \simeq F^{(2-6\alpha)}\rho(M)$. We presume that the child core is formed by gravitational fragmentation of the parent core when it collides with another core of comparable mass, and therefore we can substitute in Eqn. (2): $M_{\rm FRAG} \rightarrow M$ and $\sigma \rightarrow \sigma(M) \simeq \sigma_{\rm O}(M/M_{\rm O})^{\beta}$. On the other hand, the preshock density must be the mean internal density of the two colliding parent clouds, so we must substitute $\rho \rightarrow \rho(FM) \simeq F^{(1-3\alpha)}\rho(M) \simeq F^{(1-3\alpha)}\rho_{\rm O}(M/M_{\rm O})^{(1-3\alpha)}$, and the speed with which the two parent cores collide must be the intenal velocity dispersion of the grandparent core, so $v \rightarrow \sigma(F^2M) \simeq F^{2\beta}\sigma(M) \simeq F^{2\beta}\sigma_{\rm O}(M/M_{\rm O})^{\beta}$. Making all these sub-

stitutions in Eqn. (2), we obtain

$$F^{(-3\alpha+2\beta+1)} \left(\frac{M}{M_{\rm O}} \right)^{(3\alpha+6\beta-3)} \quad = \quad \frac{G^3 \, \rho_{\rm O} \, M_{\rm O}^2}{\sigma_{\rm O}^6} \, . \tag{12}$$

Since the righthand side of Eqn. (12) is a constant, the lefthand side must also be a constant. Therefore both the exponents on the lefthand side must be zero, and the constant on the righthand side must be unity. This gives $\alpha = 1/2$, $\beta = 1/4$, and hence, using Eqn. (11), $\gamma = 7/4$. Thus, for cores supported mainly by turbulence we have

$$R \simeq R_{\rm O} \left(\frac{M}{M_{\rm O}} \right)^{1/2} , \;\; \sigma \simeq \sigma_{\rm O} \left(\frac{M}{M_{\rm O}} \right)^{1/4} , \;\; \left. \frac{d\mathcal{N}}{dM} \right|_{\rm CORE} \simeq K \left(\frac{M}{M_{\rm O}} \right)^{-7/4} . \tag{13}$$

We note that this corresponds to the cores in the hierarchy having the same surface-density, and hence the same ambient dynamical pressure,

$$P_{\rm AMB} \quad \equiv \quad \rho \sigma^2 \, . \tag{14}$$

6. Cores supported mainly by thermal pressure

For cores of sufficiently low mass, the turbulent velocity dispersion is less than the thermal velocity dispersion. In this limit we have

$$\sigma(M) \quad \simeq \quad a_{\rm O} \;\simeq\; 0.2 \, {\rm km \, s^{-1}} \, , \tag{15}$$

where we have assumed that the gas is molecular with mean gas-particle mass $\bar{m} \simeq 4 \times 10^{-24} \, {\rm g}$, temperature $T \simeq 10 \, {\rm K}$, and hence isothermal sound speed $a_{\rm O} = (k_{\rm B} T / \bar{m})^{1/2} \simeq 0.2 \, {\rm km \, s^{-1}}$. It follows that $\sigma(M) \propto M^0$ and so $\beta \simeq 0$. Hydrostatic equilibrium requires

$$\frac{G \, M}{R(M)} \quad \simeq \quad \sigma^2(M) \;\simeq\; a_{\rm O}^2 \, , \tag{16}$$

and hence $R(M) \propto M^1$ or $\alpha \simeq 1$. Thus for cores supported mainly by thermal pressure we have $\alpha \simeq 1$, $\beta \simeq 0$, and $\gamma \simeq 1$, or

$$R(M) \simeq \frac{G \, M}{a_{\rm O}^2}, \;\; \sigma(M) \simeq a_{\rm O}, \;\; \left. \frac{d\mathcal{N}}{dM} \right|_{\rm CORE} \simeq K \left(\frac{M}{M_{\rm O}} \right)^{-1} . \tag{17}$$

It follows that there should be a 'knee' in the core mass function separating the low-mass regime, where support is dominated by thermal pressure, from the high-mass regime, where it is dominated by turbulence. If we choose to put $\sigma_{\rm O} = a_{\rm O}$ in Eqn. (13) (we are free to make this choice arbitrarily), then

the knee falls at $M = M_{\rm O}$. In addition, we require that the righthand side of Eqn. (12) is equal to unity; if we substitute $\rho_{\rm O} = P_{\rm AMB}/\sigma_{\rm O}^2$ and $\sigma_{\rm O} = a_{\rm O}$, we obtain

$$M_{\rm O} \simeq \frac{a_{\rm O}^8}{G^3\,P_{\rm AMB}} \simeq M_\odot \left(\frac{P_{\rm AMB}}{k_{\rm B}\,10^5\,{\rm cm^{-3}\,K}}\right)^{-1/2}. \quad (18)$$

Thus, for typical pressures found in star formation regions, $M_{\rm O} \simeq M_\odot$.

7. The critical pressure for star formation

We now hypothesize that cores collapse to form new stars if they are sufficiently dense for the gas to couple thermally to the dust. This is because once the gas couples thermally to the dust it becomes able to radiate in the continuum, as opposed to just at the discrete wavelengths of molecular lines. Consequently it is able to lose the internal energy it gains from PdV work during gravitational contraction. Specifically, this requires that

$$t_{\rm COUPLE} \lesssim t_{\rm FF}\,, \quad (19)$$

where

$$t_{\rm FF} \simeq \left(\frac{3\,\pi}{32\,G\,\rho}\right)^{1/2} \quad (20)$$

is the freefall time, and

$$t_{\rm COUPLE} \simeq \frac{(2\pi)^{1/2}\,r_{\rm DUST}\,\rho_{\rm DUST}}{Z_{\rm DUST}\,\rho\,a\,\alpha_{\rm THERM}} \quad (21)$$

is the timescale on which the gas couples thermally with the dust. Here $r_{\rm DUST}$ and $\rho_{\rm DUST}$ are – respectively – the radius and the internal density of a representative dust grain, $Z_{\rm DUST}$ is the fraction by mass of dust in a core, ρ and a are – respectively – the density and sound speed in the gas, and $\alpha_{\rm THERM}$ is the thermal accommodation coefficient. Substituting from Eqns. (20) and (21) in Eqn. (19), we obtain

$$P \equiv \rho a^2 \gtrsim P_{\rm COUPLE} \equiv \frac{64G}{3\alpha_{\rm THERM}} \left(\frac{r_{\rm DUST}\rho_{\rm DUST}}{Z_{\rm DUST}}\right)^2 \simeq k_{\rm B}10^5{\rm cm^{-3}K}, \quad (22)$$

where we have evaluated the righthand side of the inequality by substituting $\alpha_{\rm THERM} \simeq 1$ (appropriate for temperatures $T \lesssim 100\,{\rm K}$), $r_{\rm DUST} \simeq 10^{-5}\,{\rm cm}$, $\rho_{\rm DUST} \simeq 3\,{\rm g\,cm^{-3}}$ and $Z_{\rm DUST} \simeq 10^{-2}$.

THE CONNECTION BETWEEN THE CORE MASS FUNCTION AND THE IMF IN TAURUS

S.P. Goodwin, A. Whitworth and D. Ward-Thompson
Dept. Physics & Astronomy, Cardiff University, 5 The Parade, Cardiff, CF24 3YB, UK
Simon.Goodwin@astro.cf.ac.uk

Abstract The Taurus star forming region has an unusual core mass function (CMF) and an unusual initial mass function (IMF). We show that the unusual IMF of Taurus may well be a direct result of all of the stars only forming in cores of a few $M_\odot$. This produces a two-component IMF consisting of $\sim 1M_\odot$ stars that remain in cores, and low-mass stars and brown dwarfs that are ejected from cores.

Observations show that the CMF usually has a form similar to the IMF (Motte et al. 1998; Testi & Sergent 1998; Motte et al. 2001). This has lead to the suggestion that the IMF is directly related to the CMF.

Taurus has a peculiar IMF with a significant peak at $\sim 1M_\odot$ (Luhman et al. 2003) as illustrated in Fig. 1 (open histogram with errors). Taurus also has an unusual CMF in which most cores have masses of a few $M_\odot$ (Onishi et al. 2002), rather than the usual Salpeter-type power-law form.

We have conducted ensembles of simulations of slightly turbulent (turbulent virial ratios of $\alpha_{\rm turb} = E_{\rm turb}/|\Omega| = 0.05 - 0.25$) $5.4M_\odot$ molecular cores with realistic initial conditions (see Goodwin et al. 2004a,b,c). Most of these cores fragment into several objects (stars and brown dwarfs).

Figure 1 shows the combined mass function of 50 simulations (hashed histogram) compared to the IMF of Taurus (open histogram). The agreement between the two IMFs is striking.

Each core forms an average of about 4 or 5 objects. Dynamical interactions eject low-mass objects on a short timescale (< 0.1 Myr) until a stable low-N multiple remains (cf. Riepurth & Clarke 2001). The IMF in the simulations has a peak at $\sim 1M_\odot$ of stars which remain bound in cores and so are able to accrete significant amounts of gas. It also comprises a tail of low-mass stars and brown dwarfs that are ejected from cores by dynamical interactions before they can grow to high masses.

E. Corbelli et al. (eds.), The Initial Mass Function 50 Years Later, 355–356.

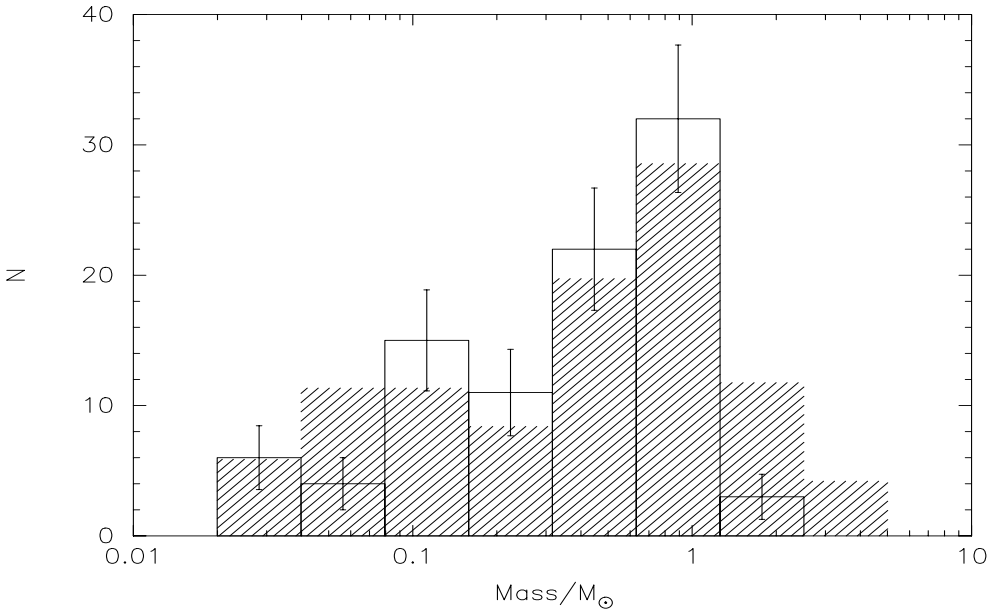

Figure 1. A comparison of the observed IMF in Taurus (open histogram, from Luhman et al. 2003) and the IMF from an ensemble of 50 simulations (hashed histogram, from Goodwin et al. 2004c).

Taurus is different to most other star forming regions in both its CMF and IMF, and it is probable that these differences are connected. These results are presented in more detail in Goodwin et al. (2004c).

References

Goodwin, S. P., Whitworth, A. P. & Ward-Thompson, D. 2004a, A&A, 414, 633

Goodwin, S. P., Whitworth, A. P. & Ward-Thompson, D. 2004b, A&A, 423, 169

Goodwin, S. P., Whitworth, A. P. & Ward-Thompson, D. 2004c, A&A, 419, 543

Luhman, K. L., Briceño, C., Stauffer, J. R., Hartmann, L., Barrado y Navascués, D. & Nelson, C. 2003, ApJ, 590, 348

Motte, F., André, P. & Neri, R. 1998, A&A, 336, 150

Motte, F., André, P., Ward-Thompson, D. & Bontemps, S. 2001, A&A, 372, L41

Onishi, T., Mizuno, A., Kawamura, A., Tachihara, K. & Fukui, Y. 2002, ApJ, 575, 950

Reipurth, B. & Clarke, C. J. 2001, AJ, 122, 432

Testi, L. & Sargent, A. 1998, ApJ, 508, L91

THE STELLAR IMF AS A PROPERTY OF TURBULENCE

Paolo Padoan[1] and Åke Nordlund[2]
[1]*Department of Physics, University of California, San Diego, La Jolla, CA, USA*
[2]*Astronomical Observatory / NBIfAFG, Copenhagen, Denmark*
ppadoan@ucsd.edu,aake@astro.ku.dk

Abstract We propose to interpret the stellar IMF as a property of the turbulence in the star–forming gas. Gravitationally unstable density enhancements in the turbulent flow collapse and form stars. Their mass distribution can be derived analytically from the power spectrum of the turbulent flow and the isothermal shock jump conditions in the magnetized gas. For a power spectrum index $\beta = 1.74$, consistent with Larson's velocity dispersion–size relation as well as with new numerical and analytic results on supersonic turbulence, we obtain a power law mass distribution of dense cores with a slope equal to $3/(4-\beta) = 1.33$, consistent with the slope of Salpeter's stellar IMF. Below one solar mass, the mass distribution flattens and turns around at a fraction of a solar mass, as observed for the stellar IMF in a number of stellar clusters, because only the densest cores are gravitationally unstable. The mass distribution at low masses is determined by the Log–Normal distribution of the gas density. The intermittent nature of this distribution is responsible for the generation of a significant number of collapsing cores of brown dwarf mass.

1. Introduction

The origin of the stellar initial mass function (IMF) is a fundamental problem in astrophysics because the stellar IMF determines photometric properties of galaxies and the dynamical and chemical evolutions of their interstellar medium. In this contribution we address the relation between statistical properties of turbulence and the origin of the stellar IMF as discussed in Padoan & Nordlund (2002, 2004). The main result of these works is that the power law slope, s, of the stellar IMF measured by Salpeter (1955) is the consequence of the turbulent nature of the star–forming gas and is directly related to the turbulent power spectrum slope, β, $s = 3/(4-\beta)$. From this point of view it is not surprising that the origin of Salpeter's result has remained mysterious for half a century, as our understanding of turbulence has not improved much since the seminal work by Kolmogorov (1941). The situation has changed during the

E. Corbelli et al. (eds.), The Initial Mass Function 50 Years Later, 357–362.

last decade, because ever increasing computer resources have recently allowed significant progress in both fields of turbulence and star formation.

Since Salpeter's work, the stellar IMF has been measured successfully in many systems. We now know that the IMF in young clusters (e.g. Chabrier 2003) reaches a maximum at a fraction of a solar mass, and then turns around with a relative abundance of brown dwarfs (BDs) that may vary from cluster to cluster (e.g. Luhman et al. 2000). The work we present here explains also this feature of the IMF as a consequence of the supersonic turbulence in the star–forming gas.

Using the properties of supersonic turbulence we have derived from recent numerical simulations, we predict the stellar IMF essentially without free parameters. This predicted IMF is shown to depend on the rms Mach number, mean density and temperature of the turbulent flow. It is also shown to agree well with Salpeter's IMF for large stellar masses and with the low mass IMF derived for young stellar clusters. Our view of the IMF as a natural property of supersonic turbulence in the magnetized and isothermal star–forming gas provides an explanation for the origin of BDs as well. According to this picture, BDs may be formed in the same way as hydrogen–burning stars.

2. Statistics of Supersonic MHD Turbulence

The velocity power spectrum in the inertial range of turbulence (between the scales of energy injection and viscous dissipation) is a power law, $E_v(k) \propto k^{-\beta}$, where k is the wave–number. The spectral index is $\beta \approx 5/3$ for incompressible turbulence (Kolmogorov 1941), and $\beta \approx 2$ for pressureless turbulence (Burgers 1974; Gotoh & Kraichnan1993). In recent numerical simulations of isothermal, super–Alfvénic and highly supersonic MHD turbulence we have obtained a power spectrum intermediate between the Burgers and the Kolmogorov power spectra (Boldyrev, Nordlund & Padoan 2002) and consistent with the prediction by Boldyrev (2002), $E(k) \propto k^{-1.74}$.

The probability density function (PDF) of gas density in isothermal turbulent flows is well approximated by a Log–Normal distribution with moments depending on the rms Mach number of the flow (Nordlund & Padoan 1999; Ostriker, Gammie & Stone 1999). The density structure is characterized by a complex system of interacting shocks resulting in a fractal network of dense cores, filaments, sheets and low density "voids", with a large density contrast. Most of the mass concentrates in a small volume fraction (according to the Log–Normal PDF), a manifestation of the intermittent nature of the turbulence. An example of a projected turbulent density field is shown in Figure 1.

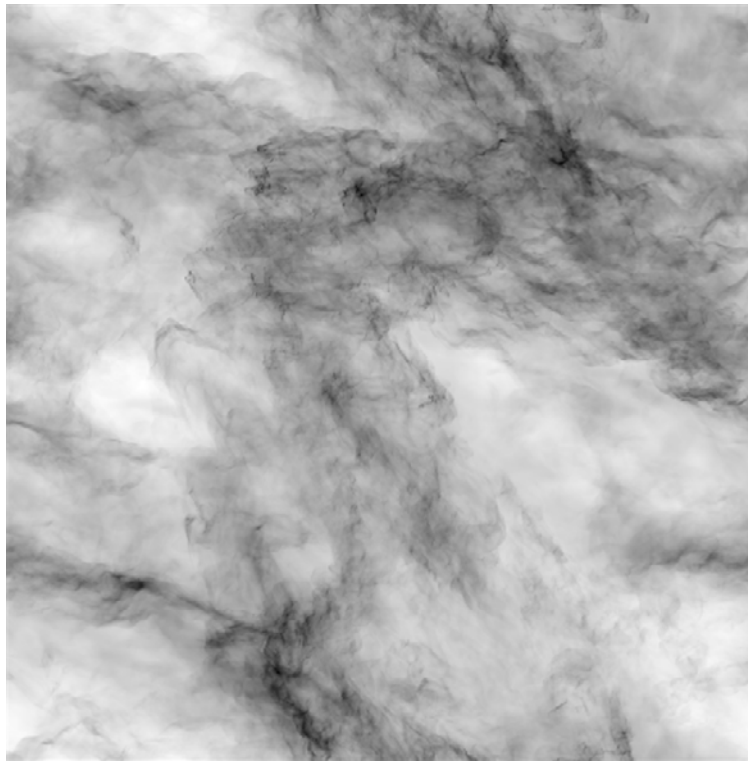

Figure 1. Projected density field from a numerical simulation of isothermal, supersonic hydrodynamic turbulence with an effective resolution of 1024^3 computational zones (Kritsuk, Padoan & Norman, in preparation). The contrast has been reduced in order to show details of the low density regions.

3. From Kolmogorov to Salpeter: The Mass Distribution of Collapsing Cores

A simple model of the expected mass distribution of dense cores generated by supersonic turbulence has been proposed in Padoan & Nordlund (2002). The model is based on two assumptions: i) The power spectrum of the turbulence is a power law; ii) the typical size of a dense core scales as the thickness of the postshock gas. The first assumption is a basic result for turbulent flows and holds also in the supersonic regime (Boldyrev et al. 2002). The second assumption is suggested by the fact that postshock condensations are assembled by the turbulent flow in a dynamical time. Condensations of virtually any size can therefore be formed, independent of their Jeans' mass.

With these assumptions, together with the jump conditions for MHD shocks, the mass distribution of dense cores can be related to the power spectrum of

turbulent velocity, $E_v(k) \propto k^{-\beta}$:

$$N(m)\,\mathrm{d}\ln m \propto m^{-3/(4-\beta)}\mathrm{d}\ln m\,. \qquad (1)$$

If the turbulence spectral index β is taken from the analytical prediction by Boldyrev (2002), which is consistent with the observed velocity dispersion–size Larson relation (Larson 1979, 1981) and with our numerical results (Boldyrev et al. 2002), then $\beta \approx 1.74$ and the mass distribution is $N(m)\,\mathrm{d}\ln m \propto m^{-1.33}\mathrm{d}\ln m$, almost identical to Salpeter's stellar IMF. The exponent of the mass distribution is rather well constrained, because the value of β for supersonic turbulence cannot be smaller than the incompressible value, $\beta = 1.67$ (slightly larger with intermittency corrections), and the Burgers case, $\beta = 2.0$. As a result, the exponent of the mass distribution is predicted to be within the range of values of 1.3 and 1.5.

While massive cores are usually larger than their critical Bonnor–Ebert mass, $m_{\rm BE}$, the probability that small cores are dense enough to collapse is determined by the statistical distribution of core density. In order to compute this collapse probability for small cores, we assume i) the distribution of core density can be approximated by the Log–Normal PDF of gas density and ii) the

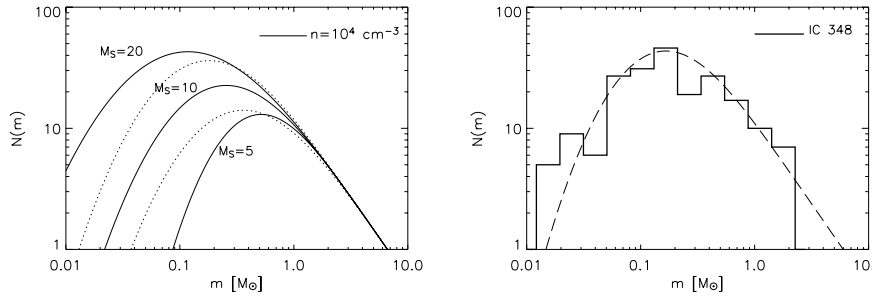

Figure 2. Left panel: Analytical mass distributions computed for $\langle n\rangle = 10^4$ cm^{-3}, $T = 10$ K and for three values of the sonic rms Mach number, $M_{\rm S} = 5$, 10 and 20 (solid lines). The dotted lines show the mass distribution for $T = 10$ K, $M_{\rm S} = 10$ and $\langle n\rangle = 5 \times 10^3$ cm^{-3} (lower plot) and $\langle n\rangle = 2 \times 10^4$ cm^{-3} (upper plot). Right panel: IMF of the cluster IC 348 in Perseus obtained by Luhman et al. (2003) (solid line histogram) and theoretical IMF computed for $\langle n\rangle = 5 \times 10^4$ cm^{-3}, $T = 10$ K and $M_{\rm S} = 7$ (dashed line).

core density and mass are statistically independent. Because of the intermittent nature of the Log-Normal PDF, even very small (sub–stellar) cores have a finite chance to be dense enough to collapse. Based on the first assumption, we can compute the distribution of the critical mass, $p(m_{\rm BE})\,dm_{\rm BE}$, from the Log–Normal PDF of gas density assuming constant temperature (Padoan, Nordlund & Jones 1997). The fraction of cores of mass m larger than their critical mass is given by the integral of $p(m_{\rm BE})$ from 0 to m. Using the second assumption

of statistical independence of core density and mass, the mass distribution of collapsing cores is

$$N(m)\,\mathrm{d}\ln m \propto m^{-3/(4-\beta)}\left[\int_0^m p(m_{\rm BE})\mathrm{d}m_{\rm BE}\right]\,\mathrm{d}\ln m\,. \qquad (2)$$

This mass distribution is a function of the rms Mach number, mean density and temperature of the turbulent flow, as these parameters enter the PDF of gas density and thus $p(m_{\rm BE})$. Figure 1 (left panel) shows five mass distributions computed from equation (2) with three different values of the sonic rms Mach number and two different values of density. Padoan & Nordlund (2004) have suggested that BDs may originate from the process of turbulent fragmentation like hydrogen–burning stars. This is illustrated by the analytical IMF in the left panel of Figure 1, which shows a relatively large abundance of BDs is predicted for sufficiently large values of the mean density or rms Mach number.

The IMF of the cluster IC 348 in Perseus, obtained by Luhman et al. (2003), is plotted in the right panel of Figure 1 (solid line histogram). The IMF of this cluster has been chosen for the comparison with the theoretical model because it is probably the most reliable observational IMF including both BDs and hydrogen burning stars. In Figure 1 we have also plotted the theoretical mass distribution computed for $\langle n\rangle = 5\times10^4$ cm^{-3}, $T = 10$ K and $M_{\rm S} = 7$. These parameters are appropriate for the central 5×5 arcmin of the cluster (0.35×0.35 pc), where the stellar density corresponds to approximately 2×10^4 cm^{-3}. The figure shows that the theoretical distribution of collapsing cores, computed with parameters inferred from the observational data, is roughly consistent with the observed stellar IMF in the cluster IC 348. Similar IMFs have been obtained for several other young clusters (Chabrier 2003).

4. Conclusions

We have proposed to explain the stellar IMF as a property of supersonic turbulence. This scenario is very different from previous theories of star formation (see Shu, Adams & Lizano 1987), where it is assumed that stars of small and intermediate mass are formed from sub–critical cores evolving quasi–statically, on the time–scale of ambipolar drift. These theories do not account for the ubiquity of turbulence in star–forming clouds and therefore ignore the effect of turbulence in the fragmentation process.

A naive interpretation of our results may lead to the conclusion that the stellar IMF at large masses should be a universal power law, with a slope very close to Salpeter's value. The statistics of turbulence controlling the origin of the stellar IMF are indeed universal (they depend on *flow* properties such as the rms Mach number, not *fluid* properties, and are insensitive to initial conditions that are soon "forgotten" due to the chaotic nature of the turbulence). However, such statistics are derived from ensemble averages. According to

our derivation, massive stars originate from shocks on relatively large scales. In any given system (for example a molecular cloud) the number of large scale compressions (thus the number of massive stars) is relatively small. Because of the small size of the statistical sample and because of the intermittent nature of the turbulence, large deviations from Salpeter's IMF are possible in individual systems. Salpeter's IMF is therefore a universal property of supersonic turbulence, but it is not necessarily reproduced precisely in every star–forming region.

References

Boldyrev, S. 2002, ApJ, 569, 841
Boldyrev, S., Nordlund, Å., & Padoan, P. 2002, ApJ, 573, 678
Burgers, J. M. 1974, in The Nonlinear Diffusion Equation (Reidel, Dordrecht)
Chabrier, G. 2003, PASP, 115, 763
Gotoh, T. & Kraichnan, R. H. 1993, Phys. Fluids, A, 5, 445
Kolmogorov, A. N. 1941, Dokl. Akad. Nauk. SSSR, 30, 301
Larson, R. B. 1979, MNRAS, 186, 479
—. 1981, MNRAS, 194, 809
Luhman, K. L., Rieke, G. H., Young, E. T., Cotera, A. S., Chen, H., Rieke, M. J., Schneider, G., & Thompson, R. I. 2000, ApJ, 540, 1016
Luhman, K. L., Stauffer, J. R., Muench, A. A., Rieke, G. H., Lada, E. A., Bouvier, J., & Lada, C. J. 2003, ApJ, 593, 1093
Nordlund, Å. K. & Padoan, P. 1999, in Interstellar Turbulence, 218
Ostriker, E. C., Gammie, C. F., & Stone, J. M. 1999, ApJ, 513, 259
Padoan, P. & Nordlund, Å. 2002, ApJ, 576, 870
—. 2004, ApJ, in press (astro-ph/0205019)
Padoan, P., Nordlund, Å., & Jones, B. 1997, MNRAS, 288, 145
Salpeter, E. E. 1955, ApJ, 121, 161
Shu, F. H., Adams, F. C. & Lizano, S., 1987, ARA&A, 25, 23

THE STELLAR MASS SPECTRUM FROM NON-ISOTHERMAL GRAVOTURBULENT FRAGMENTATION

Ralf Klessen[1], Katharina Jappsen[1], Richard Larson[2], Yuexing Li[3,4] and Mordecai-Mark Mac Low[3,4]
[1] *Astrophysikalisches Institut Potsdam, 14482 Potsdam, Germany*
[2] *Department of Astronomy, Yale University, New Haven, CT 06520-8101, USA*
[3] *Department of Astrophysics, AMNH, New York, NY 10024-5192, USA*
[4] *Department of Astronomy, Columbia University, New York, NY 10027, USA*
rklessen@aip.de, akjappsen@aip.de, larson@astro.yale.edu, yuexing@amnh.org, mordecai@amnh.org

Abstract Identifying the processes that determine the initial mass function of stars (IMF) is a fundamental problem in star formation theory. One of the major uncertainties is the exact chemical state of the star forming gas and its influence on the dynamical evolution. Most simulations of star forming clusters use an isothermal equation of state (EOS). We address these issues and study the effect of a piecewise polytropic EOS on the formation of stellar clusters in turbulent, self-gravitating molecular clouds using three-dimensional, smoothed particle hydrodynamics simulations. In these simulations stars form via a process we call gravoturbulent fragmentation, i.e., gravitational fragmentation of turbulent gas. To approximate the results of published predictions of the thermal behavior of collapsing clouds, we increase the polytropic exponent γ from 0.7 to 1.1 at some chosen density $n_{\rm c}$, which we vary from from $4.3\times10^4\,{\rm cm}^{-3}$ to $4.3\times10^7\,{\rm cm}^{-3}$. The change of thermodynamic state at $n_{\rm c}$ selects a characteristic mass scale for fragmentation $M_{\rm ch}$, which we relate to the peak of the observed IMF. We find a relation $M_{\rm ch}\propto n_{\rm c}^{-0.5\pm0.1}$. Our investigation supports the idea that the distribution of stellar masses largely depends on the thermodynamic state of the star-forming gas. The thermodynamic state of interstellar gas is a result of the balance between heating and cooling processes, which in turn are determined by fundamental atomic and molecular physics and by chemical abundances. Given the abundances, the derivation of a characteristic stellar mass may thus be based on universal quantities and constants.

E. Corbelli et al. (eds.), The Initial Mass Function 50 Years Later, 363–370.

1. Introduction

Although the IMF has been derived from vastly different regions, from the solar vicinity to dense clusters of newly formed stars, the basic features seem to be strikingly universal to all determinations Kroupa (2001). Initial conditions in star forming regions can vary considerably. If the IMF depends on the initial conditions, there would thus be no reason for it to be universal. Therefore a derivation of the characteristic stellar mass that is based on fundamental atomic and molecular physics would be more consistent.

There are many ways to approach the formation of stars and star clusters from a theoretical point of view. In particular models that connect stellar birth to the turbulent motions ubiquiteously observed in Galactic molecular clouds have become increasingly popular in recent years. See, e.g., the reviews by Larson (2003) and MacLow & Klessen (2004). The interplay between turbulent motion and self-gravity of the cloud leads to a process we call gravoturbulent fragmentation: Supersonic turbulence generates strong density fluctuations with gravity taking over in the densest and most massive regions (Larson 1981, Fleck 1982, Padoan 1995, Padoan et al. 1997, Klessen et al. 1998, 2000, Klessen 2001, Padoan & Nordlund 2002). Once gas clumps become gravitationally unstable, collapse sets in. The central density increases and soon individual or whole clusters of protostellar objects form and grow in mass via accretion from their infalling envelopes.

However, most current results are based on models that do not treat thermal physics in detail. Typically, a simple isothermal equation of state (EOS) is used. The true nature of the EOS, thus, remains a major theoretical problem in understanding the fragmentation properties of molecular clouds.

Recently Li et al. (2003) conducted a systematic study of the effects of a varying polytropic exponent γ on gravoturbulent fragmentation. Their results showed that γ determines how strongly self-gravitating gas fragments. They found that the degree of fragmentation decreases with increasing polytropic exponent γ in the range $0.2 < \gamma < 1.4$ although the total amount of mass in collapsed cores appears to remain roughly consistent through this range. These findings suggest that the IMF might be quite sensitive to the thermal physics. However in their computations, γ was left strictly constant in each case. Here we study the effects of using a piecewise polytropic equation of state and investigate if a change in γ determines the characteristic mass of the gas clump spectrum and thus, possibly, the turn-over mass of the IMF.

2. Thermal Properties of Star-Forming Clouds

Observational evidence predicts that dense prestellar cloud cores show rough balance between gravity and thermal pressure Benson & Myers (1989), Myers et al. (1991). Thus, the thermodynamical properties of the gas play an

important role in determining how dense star-forming regions in molecular clouds collapse and fragment. Observational and theoretical studies of the thermal properties of collapsing clouds both indicate that at densities below $10^{-18}\,\mathrm{g\,cm^{-3}}$, roughly corresponding to a number density of $n = 2.5 \times 10^5\,\mathrm{cm^{-3}}$, the temperature decreases with increasing density. This is due to the strong dependence of molecular cooling rates on density (Koyama & Inutsuka 2000). Therefore, the polytropic exponent γ is below unity in this density regime. At densities above $10^{-18}\,\mathrm{g\,cm^{-3}}$, the gas becomes thermally coupled to the dust grains, which then control the temperature by far-infrared thermal emission. The balance between compressional heating and thermal cooling by dust causes the temperature to increase again slowly with increasing density. Thus the temperature-density relation can be approximated with γ above unity in this regime (Larson this volume; see also Larson 1985, Spaans & Silk 2000). Changing γ from a value below unity to a value above unity results in a minimum temperature at the critical density. As shown by Li et al. (2003), gas fragments efficiently for $\gamma < 1.0$ and less efficiently for higher γ. Thus, the Jeans mass at the critical density defines a characteristic mass for fragmentation, which may be related to the peak of the IMF.

3. Numerical Approach

To gain insight into how molecular cloud fragmentation the characteristic stellar mass may depend on the critical density we perform a series of smoothed particle hydrodynamics calculations of the gravitational fragmentation of supersonically turbulent molecular clouds using the parallel code GADGET designed by Springel et al. (2001). SPH is a Lagrangian method, where the fluid is represented by an ensemble of particles, and flow quantities are obtained by averaging over an appropriate subset of SPH particles, see Benz (1990) and Monaghan (1992). The method is able to resolve large density contrasts as particles are free to move, and so naturally the particle concentration increases in high-density regions. We use the Bate & Burkert (1997) criterion the resolution limit of our calculations. It is adequate for the problem considered here, where we follow the evolution of highly nonlinear density fluctuations created by supersonic turbulence. We replace the central high-density regions of collapsing gas cores by sink particles Bate et al. (1995). These particles have the ability to accrete gas from their surroundings while keeping track of mass and momentum. This enables us to follow the dynamical evolution of the system over many local free-fall timescales.

We compute models where the polytropic exponent changes from $\gamma = 0.7$ to $\gamma = 1.1$ for critical densities in the range $4.3 \times 10^4\,\mathrm{cm^{-3}} \leq n_\mathrm{c} \leq 4.3 \times 10^7\,\mathrm{cm^{-3}}$. Each simulation starts with a uniform density distribution, and turbulence is driven on large scales, with wave numbers k in the range $1 \leq k < 2$.

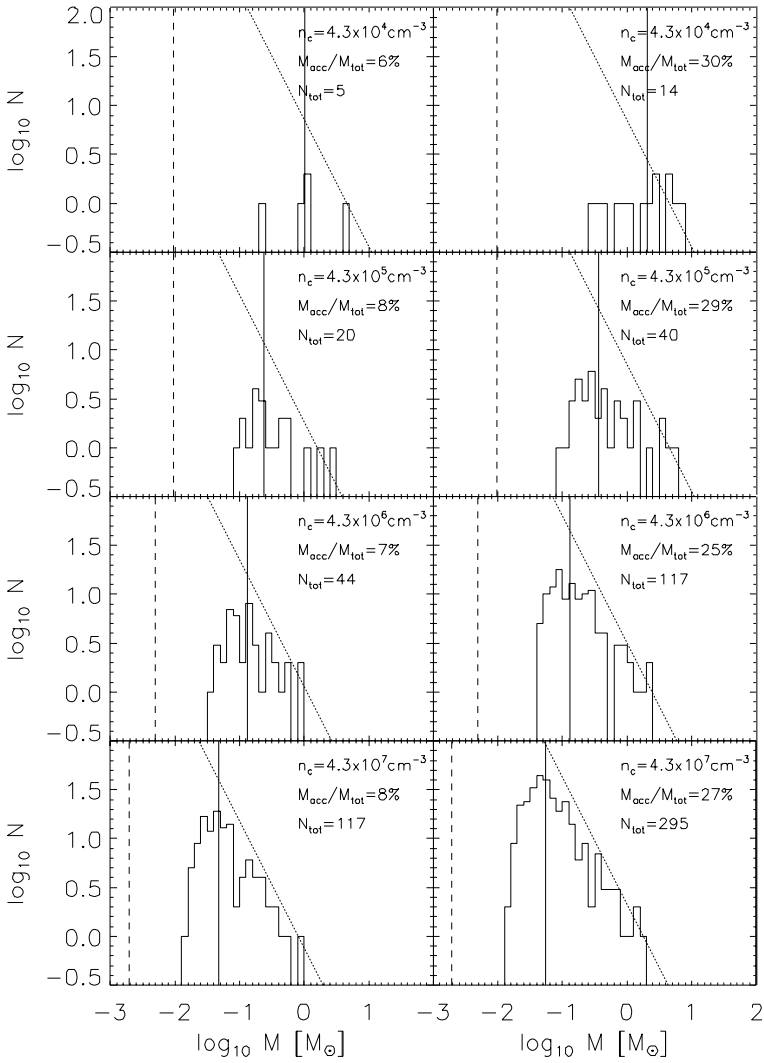

Figure 1. Mass spectra of protostellar cores for four models with critical densities in the range $4.3 \times 10^4\ \mathrm{cm}^{-3} \leq n_\mathrm{c} \leq 4.3 \times 10^7\ \mathrm{cm}^{-3}$. We show two phases of evolution, when about 10% and 30% of the mass has been accreted onto protostars. The *vertical solid line* shows the median mass of the distribution. The *dotted line* serves as a reference to the Salpeter (1955) slope of the observed IMF at high masses. The *dashed line* indicates our mass resolution limit.

We use the same driving field in all four models. The global free-fall timescale is $\tau_\mathrm{ff} \approx 10^5\,\mathrm{yr}$. For further details see Jappsen et al. (2004).

4. Dependency of the Characteristic Mass

To illustrate the effects of varying the critical density, we plot in Fig. 1 the resulting mass spectra at different times when the fraction of of mass accumulated in protostellar objects has reached approximately 10% and 30%. This range of efficiencies corresponds roughly to the one expected for regions of clustered star formation Lada & Lada (2003). In the top-row model, the change in γ occurs below the initial mean density. It shows a flat distribution with only few, but massive cores. These reach masses up to $10\,M_\odot$ and the minimum mass is about $0.3\,M_\odot$. The mass spectrum becomes more peaked for higher $n_{\rm c}$ and shifts to lower masses.

We find closest correspondence with the observed IMF Scalo (1998), Kroupa (2002), Chabrier (2003) for a critical density $n_{\rm c}$ of $4.3 \times 10^6\,{\rm cm}^{-3}$ and for stages of accretion around 30%. For high masses, the distribution exhibits a Salpeter (1955) power-law behavior. For masses about the median mass the distribution has a small plateau and then falls off towards smaller masses.

The change of median mass $M_{\rm median}$ with critical density $n_{\rm c}$ is quantified in Fig. 2. As $n_{\rm c}$ increases $M_{\rm median}$ decreases. We fit our data with straight lines. The slopes take values between -0.4 and -0.6.

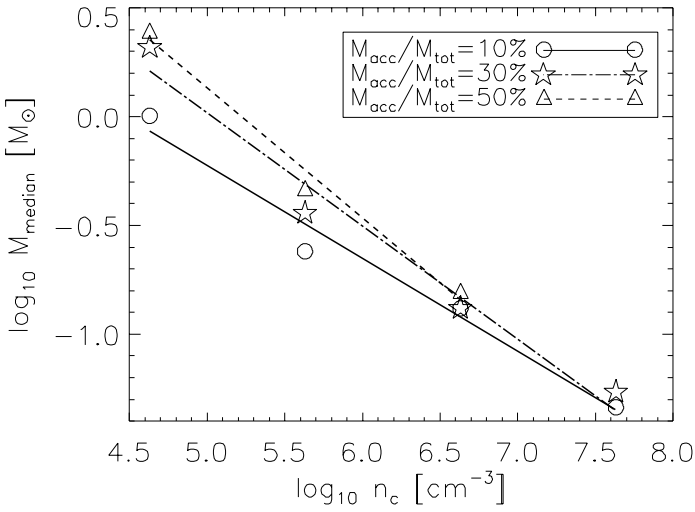

Figure 2. Plot of the median mass of the protostellar cores $M_{\rm median}$ versus critical density $n_{\rm c}$. We display results for different ratios of accreted gas mass to total gas mass $M_{\rm acc}/M_{\rm tot}$, and fit the data with straight lines. Their slopes take the values -0.43 ± 0.05 (*solid line*), -0.52 ± 0.06 (*dashed-dotted line*), and -0.60 ± 0.07 (*dashed line*), respectively.

5. Discussion and Summary

Using SPH simulations we investigate the influence of a piecewise polytropic EOS on the gravoturbulent fragmentation of molecular clouds. We study the case where the polytropic index γ changes from 0.7 to 1.1 at a critical density $n_{\rm c}$, and consider the range $4.3 \times 10^4\,{\rm cm}^{-3} \leq n_{\rm c} \leq 4.3 \times 10^7\,{\rm cm}^{-3}$.

A simple scaling argument based on the Jeans mass $M_{\rm J}$ at the critical density $n_{\rm c}$ leads to $M_{\rm J} \propto n_{\rm c}^{-0.95}$ (see Jappsen et al. 2004). If there is a close relation between the average Jeans mass and the gravoturbulent fragmentation spectrum, a similar relation should hold for the characteristic mass $M_{\rm ch}$ of protostellar cores. Our simulations qualitatively support this hypothesis, however, with the weaker density dependency $M_{\rm ch} \propto n_{\rm c}^{-0.5\pm0.1}$. So indeed, the density at which γ changes from below unity to above unity defines a preferred mass scale. Consequently, the peak of the resulting mass spectrum decreases with increasing critical density. The distribution not only shows a pronounced maximum but also a power-law tail towards higher masses, similar to the observed IMF.

Altogether, supersonic turbulence in self-gravitating molecular gas generates a complex network of interacting filaments. The overall density distribution is highly inhomogeneous. Turbulent compression sweeps up gas in some parts of the cloud, but other regions become rarefied. The fragmentation behavior of the cloud and its ability to form stars depend on the EOS. However, once collapse sets in, the final mass of a fragment depends not only on the local Jeans criterion, but also on additional processes. For example, protostars grow in mass by accretion from their surrounding material. In turbulent clouds the properties of the gas reservoir are continuously changing. And in addition protostars may interact with each other, leading to ejection or mass exchange. These dynamical factors modify the resulting mass spectrum, and may explain why the characteristic stellar mass depends on the EOS more weakly than expected from simple Jeans-mass scaling arguments.

Our investigation supports the idea that the distribution of stellar masses depends, at least in part, on the thermodynamic state of the star-forming gas. If there is a low-density regime in molecular clouds where the temperature T sinks with increasing density ρ, followed by a higher-density phase where T increases with ρ, fragmentation seems likely to be favored at the transition density where the temperature reaches a minimum. This defines a characteristic mass scale. The thermodynamic state of interstellar gas is a result of the balance between heating and cooling processes, which in turn are determined by fundamental atomic and molecular physics and by chemical abundances. The theoretical derivation of a characteristic stellar mass may thus be based on quantities and constants that depend mostly on the chemical abundances in the star forming cloud.

References

Bate, M. R., Bonnell, I. A., & Price, N. M. 1995, MNRAS, 277, 362
Bate, M. R. & Burkert, A. 1997, MNRAS, 288, 1060
Benson, P. J. & Myers, P. C. 1989, ApJS, 71, 89
Benz, W. 1990, in *Numerical Modelling of Nonlinear Stellar Pulsations Problems and Prospects*, ed. J. R. Buchler (Dordrecht: Kluwer), 269
Chabrier, G. 2003, PASP, 115, 763
Fleck, R. C. 1982, PASP, 201, 551
Jappsen, A.-K., Klessen, R. S., et al. 2004, A&A, submitted (astro-ph/0410351)
Klessen, R. S. 2001, ApJ, 556, 837
Klessen, R. S., Burkert, A., & Bate, M. R. 1998, ApJ, 501, L205
Klessen, R. S., Heitsch, F., & Mac Low, M.-M. 2000, ApJ, 535, 887
Koyama, H. & Inutsuka, S. 2000, ApJ, 532, 980
Kroupa, P. 2001, MNRAS, 322, 231
—. 2002, Science, 295, 82
Lada, C. J. & Lada, E. A. 2003, ARAA, 41, 57
Larson, R. B. 1981, MNRAS, 194, 809
—. 1985, MNRAS, 214, 379
—. 2003, Rep. Prog. Phys., 66, 1651
Li, Y., Klessen, R. S., & Mac Low, M.-M. 2003, ApJ, 592, 975
Mac Low, M.-M. & Klessen, R. S. 2004, Rev. Mod. Phys., 76, 125
Monaghan, J. J. 1992, ARAA, 30, 543
Myers, P. C. et al. 1991, ApJ, 376, 561
Padoan, P. 1995, MNRAS, 277, 377
Padoan, P. & Nordlund, Å. 2002, ApJ, 576, 870
Padoan, P., Nordlund, A., & Jones, B. J. T. 1997, MNRAS, 288, 145
Salpeter, E. E. 1955, ApJ, 121, 161
Scalo, J. 1998, in *The Stellar Initial Mass Function*, ed. G. Gilmore & D. Howell (San Francisco: ASP), 201
Spaans, M. & Silk, J. 2000, ApJ, 538, 115
Springel, V., Yoshida, N., & White, S. D. M. 2001, New Astronomy, 6, 79

Figure 3. Celebrating Brunello at Moltalcino's fortress: Shang, Petr-Gotzens, Klessen, Chernoff, Shaviv, Barrado.

Figure 4. Reasoning after some glass of wine: Chernoff, Prusti and Adams.

TURBULENT CONTROL OF THE STAR FORMATION EFFICIENCY

Enrique Vázquez-Semadeni
Centro de Radioastronomía y Astrosfísica, UNAM, Morelia, México.
e.vazquez@astrosmo.unam.mx

Abstract Supersonic turbulence plays a dual role in molecular clouds: On one hand, it contributes to the global support of the clouds, while on the other it promotes the formation of small-scale density fluctuations, identifiable with clumps and cores. Within these, the local Jeans length $L_{\rm J,c}$ is reduced, and collapse ensues if $L_{\rm J,c}$ becomes smaller than the clump size and the magnetic support is insufficient (i.e., the core is "magnetically supercritical"); otherwise, the clumps do not collapse and are expected to re-expand and disperse on a few free-fall times. This case may correspond to a fraction of the observed starless cores. The star formation efficiency (SFE, the fraction of the cloud's mass that ends up in collapsed objects) is smaller than unity because the mass contained in collapsing clumps is smaller than the total cloud mass. However, in non-magnetic numerical simulations with realistic Mach numbers and turbulence driving scales, the SFE is still larger than observational estimates. The presence of a magnetic field, even if magnetically supercritical, appears to further reduce the SFE, but by reducing the probability of core formation rather than by delaying the collapse of individual cores, as was formerly thought. Precise quantification of these effects as a function of global cloud parameters is still needed.

1. Introduction

The observed efficiency of star formation (SFE, the fraction of a cloud's mass deposited in stars during its lifetime) is low, on the order of a few percent (e.g., Evans 1991). For over two decades, the accepted explanation (Mouschovias 1976a,b; Shu, Adams & Lizano 1987) to this low observed SFE was that low-mass stars form in so-called "magnetically subcritical" molecular clouds, which, under ideal MHD conditions (perfect flux freezing), would be absolutely supported by magnetic forces against their own self-gravity, regardless of the external pressure. In practice, however, in dense clumps within the clouds, the ionization fraction drops to sufficiently low values that the process known as "ambipolar diffusion" (AD; Mestel & Spitzer 1956) allows quasi-static con-

E. Corbelli et al. (eds.), The Initial Mass Function 50 Years Later, 371–378.

traction of the clumps into denser structures ("cores"), and ultimately collapse. The low SFE then arises from the fact that only the material in the densest regions could proceed to gravitational collapse, and on the AD time scale, which is in general much larger than the free-fall time scale. High-mass stars, on the other hand, were proposed to form from either supercritical clouds assembled by agglomeration of smaller clouds into large complexes (Shu, Adams & Lizano 1987), or by super-Alfvénic shock compression of sub- or nearly critical clouds (Mouschovias 1991). In this scenario, which we refer to as the "standard model" of star formation, *gravitational* fragmentation along flux tubes containing many Jeans masses (e.g., Shu et al. 1987; Mouschovias 1991), was considered to be the mechanism responsible for clump formation.

However, molecular clouds are known to be supersonically turbulent (e.g., Zuckerman & Evans 1974; Larson 1981; Blitz 1993), and this is bound to produce large density fluctuations, even if the turbulence is sub-Alfvénic.[1] In this case, the clumps and cores within molecular clouds, as well as the clouds themselves, are likely to be themselves the turbulent density fluctuations within the larger-scale turbulence of their embedding medium (von Weizsäcker 1951; Sasao 1973; Elmegreen 1993; Ballesteros-Paredes, Vázquez-Semadeni & Scalo 1999), being transient, time-dependent, out-of-equilibrium objects in which the kinetic compressive energy of the large-scale turbulent motions is being transformed into the internal, gravitational and perhaps smaller-scale turbulent kinetic energies of the density enhancements. The typical formation time scales of the density fluctuations should be of the order of the rms turbulent crossing time across them.

If clumps and cores within molecular clouds are indeed formed through this rapid, dynamic process, such an origin and out-of-equilibrium nature appear difficult to reconcile with the quasi-magnetostatic nature of the AD contraction proposed to occur in the standard model. Moreover, a number of additional problems with the standard model have been identified (see the review by Mac Low & Klessen 2004), among which a particularly important one is that molecular clouds are generally observed to be magnetically supercritical or nearly critical (e.g., Crutcher 1999, 2003; Bourke et al. 2001), in agreement with expectations from the cloud formation mechanism (Hartmann, Ballesteros-Paredes & Bergin 2001).

In this paper we review how the SFE can be maintained at low levels within the context of what has become known as the "turbulent model" of molecular cloud formation, without having to necessarily resort to quasi-static, AD-mediated slow contraction.

[1] In fact, numerical simulations suggest that strongly magnetized cases develop larger density contrasts than weakly magnetized ones (e.g., Passot, Vázquez-Semadeni & Pouquet 1995; Ostriker, Gammie & Stone 1999; Ballesteros-Paredes & Mac Low 2002).

2. Turbulent control of gravitational collapse

In this section we consider the role of turbulence neglecting the magnetic field.

In most early treatments of self-gravitating clouds, turbulence had been considered only as a source of support (e.g., Chandrasekhar 1951; Bonazzola et al. 1987; Lizano & Shu 1989). However, one of the main features of turbulence is that it is a multi-scale process, with most of its energy at large scales. Thus, it is expected to have a *dual* role in the dynamics of molecular clouds (Vázquez-Semadeni & Passot 1999): over all scales on which turbulence is supersonic, it is the dominant form of support, while simultaneously it induces the formation of small-scale density peaks ("clumps"). If the latter are still supersonic inside, further, smaller-scale peak formation is expected in a hierarchical manner (Vázquez-Semadeni 1994; Passot & Vázquez-Semadeni 1998), until small enough scales are reached that the typical velocity differences across them are subsonic, at which point turbulent energy ceases to be dominant over thermal energy for support, and also further turbulent subfragmentation cannot occur (Padoan 1995; Vázquez-Semadeni, Ballesteros-Paredes & Klessen 2003). These can be identified (Klessen et al. 2005) with "quiescent" (Myers 1983), "coherent" (Goodman et al. 1998) cores. We refer to the scale at which the typical turbulent velocity difference equals the sound speed as the "sonic scale", denoted $\lambda_{\rm s}$. It depends on both the slope and the intercept of the turbulent energy spectrum.

For a molecular cloud of mean density $n \sim 10^3$ cm^{-3} and temperature 10 K, the thermal Jeans length is $L_{\rm J} \sim 0.7$ pc, and so sub-parsec clumps will generally be smaller than the cloud's *global* Jeans length $L_{\rm J,g}$. However, in the clumps, the *local* Jeans length $L_{\rm J,c}$ is reduced, and in some cases it may become smaller than the clump's size, at which point the clump can proceed to collapse. If the clump is internally subsonic, then $L_{\rm J,c}$ is given by the thermal Jeans length; otherwise, $L_{\rm J,c}$ should include the turbulent support (Chandrasekhar 1951). Moreover, in the latter case, the clump can still fragment due to the turbulence, with the fragments collapsing earlier than the whole clump (because they have shorter free-fall times), probably producing a bound cluster. On the other hand, if $L_{\rm J,c}$ never becomes smaller than clump's size during the compression, then the clump is expected to re-expand after the turbulent compression ends, on times a few times larger than the free-fall time (Vázquez-Semadeni et al. 2005). This is because in the absence of a magnetic field, *stable* equilibria of self-gravitating isothermal spheres require the presence of an external, confining pressure. In the case of clumps formed as turbulent fluctuations, the external pressure includes the fluctuating turbulent ram pressure, and is therefore time variable, being at a maximum when the

clump is being formed, and later returning to the mean value of the ambient thermal pressure.

The formation of collapsing objects is a highly nonlinear and time dependent process, which is most easily investigated numerically. Early studies in two dimensions suggested that gravitational collapse could be almost completely suppressed by turbulence driving if the driving was applied at scales smaller than the global Jeans length (Léorat, Passot & Pouquet 1990). This was later supported by the 3D studies of Klessen, Heitsch & Mac Low (2000), who investigated the evolution of the collapsed mass fraction as a function of the rms Mach number and the driving scale of the turbulence in numerical simulations of isothermal, non-magnetic, self-gravitating driven turbulence. However, for driving scales larger than $L_{\rm J,g}$, Klessen et al. (2000) still found collapsed fractions well below unity, showing that the SFE is reduced even if the driving scale is larger than $L_{\rm J,g}$. This is important because it is likely that the turbulence in molecular clouds is driven from large scales (Ossenkopf & Mac Low 2002), the clouds actually being part of the general turbulent cascade in the ISM (Vázquez-Semadeni et al. 2003). In this case, the driving scale is not a free parameter, and the ability to reduce the SFE even with large-scale driving is essential.

Vázquez-Semadeni et al. (2003) later showed that, for the simulations they considered, all of which had the same number of Jeans lengths in the box (J, equal to 4 there), the SFE correlates better with the sonic scale than with either the rms Mach number or the driving scale, substantiating the relevance of the sonic scale. The correlation was empirically fit to a function of the form SFE $\propto \exp\left(-\lambda_0/\lambda_{\rm s}\right)$, with $\lambda_0 \sim 0.11$ pc in the simulations studied. If the driving scale is kept constant (say, at its largest possible value), then the dependence of the SFE on the sonic scale translates directly into a dependence on the Mach number. Indeed, the data of Klessen et al. (2001) and of Vázquez-Semadeni et al. (2003) show that the SFE in simulations driven at a fixed scale is systematically reduced as the Mach number is increased. For example, in simulations driven at $2L_{\rm J,g}$, efficiencies $\sim 40\%$ were observed for rms Mach numbers ~ 10 (Vázquez-Semadeni et al. 2003). A theory explaining this functional dependence is lacking. Moreover, the experiments so far remain incomplete, since they have not tested the dependence of the SFE on the Jeans number of the flow J.

In summary, in the non-magnetic case, the numerical experiments show that the SFE can be reduced by turbulence alone, without the need for magnetic fields. However, for realistic rms Mach numbers, the efficiencies observed are still larger than observed if one admits that clouds are likely to be driven at large scales.

3. The role of the magnetic field

The magnetic field may provide the necessary further reduction of the SFE to reach the observed levels, even in supercritical clouds. Early numerical studies showed that global collapse in a magnetic simulation can only be completely suppressed if the box is magnetically subcritical and AD is neglected (Ostriker et al. 1999; Heitsch, Mac Low & Klessen 2001). Supercritical boxes readily collapse, although on time scales up to twice the global free-fall time $\tau_{\rm f,g}$. Heitsch et al. (2001) and Li et al. (2004) additionally have shown that MHD waves within supercritical clumps are apparently insufficient to prevent their collapse. Heitsch et al. (2001) also investigated the collapsed mass fraction as a function of magnetization in supercritical boxes, but were not able to find any clear trends, because the effect of the magnetic field was obscured by stochastic variations between different realizations of flows with the same global parameters.

Recently, Li & Nakamura (2004) have considered the same issue in two-dimensional, decaying (rather than driven) simulations, in both sub- and supercritical regimes, including a prescription for AD. They found that stronger magnetic fields delay the initial formation of collapsed objects, although all their simulations at a fixed Mach number achieved comparable final collapsed mass fractions at long times. They also concluded that higher levels of initial turbulence speed up the collapse in subcritical clouds by producing high-density clumps in which the AD time scale is short, and thus avoiding the problem that AD by itself gives collapse times that are too long compared to observational evidence (e.g., Jijina, Myers & Adams 1999; Lee & Myers 1999; Hartmann 2003).

The above studies have focused on the global collapsed mass fraction in simulations, but further insight can be obtained by focusing on the evolution of individual clumps. Vázquez-Semadeni et al. (2005) have investigated the evolution of individual clumps in three-dimensional, driven MHD simulations neglecting AD. These showed that the typical times for clumps to go from mean densities $\sim 10^4$ cm^{-3} (the level of the densest fluctuations produced by the turbulence in their Mach-10 simulations) to full collapse differ by less than a factor of 2 between supercritical and non-magnetic simulations, being $\lesssim 2\tau_{\rm f,c} \sim 1$ Myr in the former, and $\sim 1\tau_{\rm f,c} \sim 0.5$ Myr in the latter, where $\tau_{\rm f,c} \equiv L_{\rm J,c}/c$ is the *local* free-fall time in the clumps, and c is the isothermal sound speed. Furthermore, these authors showed that in subcritical simulations without AD, in which collapse cannot occur, the clumps only reached mean densities $\sim$ 10–20 $\times\, 10^4$ cm^{-3}, to then rapidly become dispersed again in times ~ 1 Myr. An estimate of the AD time scale $\tau_{\rm AD}$ in one such clump taking into account its closeness to the critical mass-to-flux ratio (Ciolek & Basu 2001) gave $\tau_{\rm AD} \gtrsim 1.3$ Myr, suggesting that in the presence of AD the

clump might possibly increase its mass-to-flux ratio and proceed to collapse by the effect of AD, although on time scales not significantly longer than the dynamical ones observed in the supercritical and non-magnetic simulations. If AD acts on significantly longer time scales, then it cannot bind the clumps before they are dispersed by the turbulence.

Vázquez-Semadeni et al. (2005) also noticed that the appearance of the first collapsing cores in the supercritical simulations was delayed with respect with the non-magnetic simulation, and that fewer cores formed in the magnetic cases than in the non-magnetic one. These findings are consistent with previous results that the presence of the magnetic field delays the collapse (Ostriker et al. 1999; Heitsch et al. 2001), but suggests that the delay at the global scale occurs by reducing the probability of forming collapsing cores, rather than by delaying the collapse of individual clumps. This may be the consequence of the magnetic field reducing the effective dimensionality of turbulent compressions, which become nearly one-dimensional in the limit of very strong fields, in which case the compressions cannot produce collapsing objects (e.g., Shu, Adams & Lizano 1987; Vázquez-Semadeni, Passot & Pouquet 1996).

4. Conclusions

The results summarized here show that the SFE in supersonically turbulent molecular clouds is naturally reduced because the turbulence opposes global cloud collapse while inducing the formation of local density peaks that contain small fractions of the total mass, and which may collapse if they become locally gravitationally unstable. However, not all density peaks ("clumps") manage to do so, and a number of them are expected to instead re-expand and merge with their environment. This mechanism operates even in the absence of magnetic fields, although for realistic parameters of the turbulence, the efficiencies in numerical simulations are higher than observed. Including the magnetic field further reduces the efficiency of collapse, even in supercritical cases, but apparently not by delaying the formation and collapse of individual clumps, which occurs on comparable time scales in both the magnetic and non-magnetic cases, but by reducing the probability of collapsing-core formation by the turbulence. Further work is now needed to quantify the SFE and the fraction of collapsing versus non-collapsing peaks as a function of the global parameters, and to eventually produce a collective theory that describes the process in a statistical fashion.

Acknowledgments The author has benefited from a critical reading of the manuscript by Javier Ballesteros-Paredes, and from financial support from CONACYT through grant 36571-E.

References

Ballesteros-Paredes, J., Vázquez-Semadeni, E., & Scalo, J. 1999a, ApJ, 515, 286
Ballesteros-Paredes, J. & Mac Low, M. 2002, ApJ, 570, 734
Blitz, L., 1993, in Protostars and Planets III, eds. E. H. Levy and J. I. Lunine (Tucson: Univ. of Arizona Press), 125
Bonazzola, S., Heyvaerts, J., Falgarone, E., Pérault, M. & Puget, J. L., A&A 172, 293
Bourke, T. L., Myers, P. C., Robinson, G., Hyland, A. R. 2001, ApJ 554, 916
Ciolek, G. E. & Basu, S. 2001, ApJ 547, 272
Chandrasekhar, S. 1951, Proc. R. Soc. London A, 210, 26
Crutcher, R. M. 1999, ApJ 520, 706
Crutcher, R. 2004, in Magnetic Fields and Star Formation: Theory versus Observations, eds. Ana I. Gomez de Castro et al, (Dordrecht: Kluwer Academic Press), in press
Elmegreen, B. G. 1993, ApJL, 419, 29
Evans, N. J., II 1991, in Frontiers of Stellar Evolution, ed. D. L. Lambert (San Francisco: ASP), 45
Goodman, A. A., Barranco, J. A., Wilner, D. J., & Heyer, M. H. 1998, ApJ 504, 223
Hartmann, L. 2003, ApJ 585, 398
Hartmann, L., Ballesteros-Paredes, J., & Bergin, E. A. 2001, ApJ, 562, 852
Heitsch, F., Mac Low, M. M., & Klessen, R. S. 2001, ApJ, 547, 280
Jijina, J., Myers, P. C., & Adams, F. C. 1999, ApJS 125, 161
Klessen, R. S., Heitsch, F., & MacLow, M. M. 2000, ApJ, 535, 887
Klessen, R. S., Ballesteros-Paredes, J., Vázquez-Semadeni, E. C. & Durán, C. 2004, ApJ, submitted (astro-ph/0306055)
Larson, R. B. 1981, MNRAS, 194, 809
Lee, C. W. & Myers, P. C. 1999, ApJS 123, 233
Léorat, J., Passot, T. & Pouquet, A. 1990, MNRAS 243, 293
Li, Z.-Y. & Nakamura, F. 2004, ApJL, 609, 83
Lizano, S. & Shu, F. H. 1989, ApJ, 342, 834
Mac Low, M.-M. & Klessen, R. S. 2004, Rev. Mod. Phys. 76, 125
Mestel, L. & Spitzer, L., Jr. 1956, MNRAS 116, 503
Mouschovias, T. C. 1976a, ApJ 207, 141
Mouschovias, T. C. 1976b, ApJ 206, 753
Mouschovias, T. C. 1991, in The Physics of Star Formation and Early Stellar Evolution, eds. C. J. Lada & N. D. Kylafis (Dordrecht: Kluwer), 449
Myers, P. C. 1983, ApJ 270, 105
Ossenkopf, V. & Mac Low, M.-M. 2002, A&A 390, 307
Ostriker, E. C., Gammie, C. F. & Stone, J. M. 1999, ApJ 513, 259
Padoan, P. 1995, MNRAS, 277, 377
Passot, T., Vázquez-Semadeni, E. & Pouquet, A. 1995, ApJ 455, 536
Passot, T. & Vázquez-Semadeni, E. 1998, Phys. Rev. E 58, 4501
Sasao, T. 1973, PASJ 25, 1
Shu, F. H., Adams, F. C., & Lizano, S. 1987, ARAA, 25, 23
Vázquez-Semadeni, E. 1994, ApJ 423, 681
Vázquez-Semadeni, E., Passot, T. & Pouquet, A. 1996, ApJ 473, 881

Vázquez-Semadeni, E. & Passot, T. 1999, in Interstellar Turbulence, ed. J. Franco & A. Carramiñana (Cambridge: Univ. Press), 223

Vázquez-Semadeni, E., Ballesteros-Paredes, J. & Klessen, R. S. 2003, ApJL 585, 131

Vázquez-Semadeni, E., Kim, J., Shadmehri, M. & Ballesteros-Paredes, J. 2005, ApJ, in press (astro-ph/0409247)

von Weizsäcker, C.F. 1951, ApJ 114, 165

Zuckerman, B. & Evans, N. J. II 1974, ApJL 192, 149

Zuckerman, B. & Palmer, P. 1974, ARAA 12, 279

Figure 1. Getting ready for the bus ride: Hollenbach and Vazquez in the foreground.

THERMAL CONDENSATION IN A TURBULENT ATOMIC HYDROGEN FLOW

Patrick Hennebelle[1] and Edouard Audit[2]
[1] *Ecole normale supérieure and Observatoire de Paris, 24 rue Lhomond 75005 Paris, France,*
[2] *Service d'Astrophysique, CEA/DSM/DAPNIA/SAp, C. E. Saclay F-91191 Gif-sur-Yvette, France*
patrick.hennebelle@ens.fr,eaudit@cea.fr

Abstract The interstellar neutral hydrogen is a thermally bistable medium. The dynamical processes with two coexisting phases involve a large range of spatial (and temporal) scales, that need to be adequately represented in numerical simulations. Here we present 2-d simulations of a turbulent HI hydrogen flow.

We present 2D numerical simulations of the thermally bistable interstellar atomic hydrogen with a numerical resolution of 0.02 pc and 1000^2 pixels. The numerical scheme is a 2nd order Rieman solver. In order to mimic a large scale converging flow of WNM, we impose a converging velocity field on 2 sides of the box. Perturbations on the incoming flow of various amplitude are superimposed. For small amplitudes the flow is almost laminar whereas large amplitudes lead to a very turbulent flow in the box.

In the case of a weakly turbulent flow (not displayed here for conciseness), a layer of dense gas forms because of the converging flow. It fragments into several structures having a typical size of about 0.1 pc and a velocity dispersion of few km/s. Only a small fraction of the gas is in the thermally unstable regime. Fig.1 displays the density and the velocity fields in the case of a very turbulent flow. Several structures of cold gas embedded into the warm phase form. In spite of the high turbulence, stiff thermal fronts separating the warm and the cold phase are clearly seen. A significant fraction of the gas is in the thermally unstable domain.

Fig.2 displays the fraction of thermally unstable plus cold gas and the fraction of cold gas alone as a function of the mean value of the eigenvalue of the shear tensor ($\Sigma = d_x V_x - d_y V_y$ in the eigenframe). This parameter describes straining motions which are generated by turbulence. The reason of choosing it is that it appears as the key parameter in a semi-analytical model developped in Audit & Hennebelle (2004, in press) to explain the origin of the unstable gas. It is seen that the fraction of cold and thermally unstable gas is almost in-

E. Corbelli et al. (eds.), The Initial Mass Function 50 Years Later, 379–380.

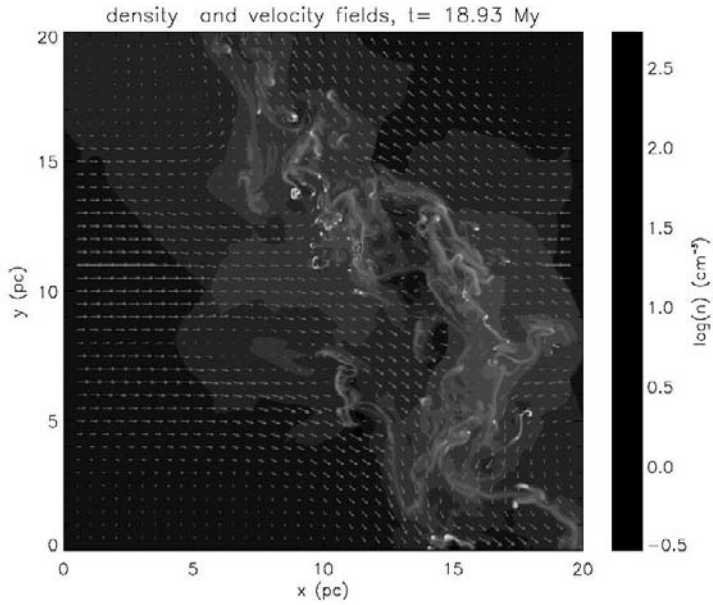

Figure 1. Density and velocity field for a very turbulent flow

dependent of Σ whereas the fraction of cold gas decreases with it. This shows that turbulence is able to transiently stabilize the thermally unstable gas.

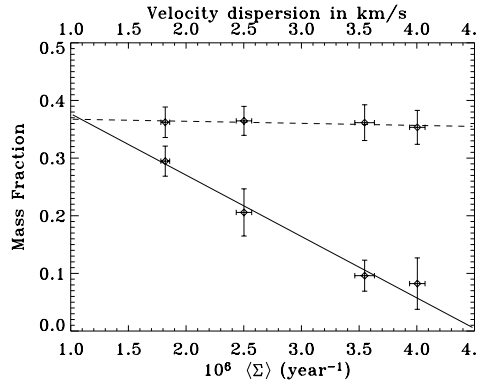

Figure 2. Fraction of cold gas and fraction of thermally unstable plus cold gas as a function of $\Sigma =< d_x V_x - d_y V_y >$.

THE FORMATION OF MOLECULAR CLOUDS

Shu-ichiro Inutsuka[1] and Hiroshi Koyama[2]
[1]*Department of Physics, Kyoto University Kyoto, 606-8502, Japan*
[2]*Department of Earth and Planetary Sys. Sci., Kobe University, Nada, Kobe 657-8501, Japan*
inutsuka@tap.scphys.kyoto-u.ac.jp,hkoyama@kobe-u.ac.jp

Abstract The propagation of a shock wave into atomic interstellar medium is analyzed by taking into account radiative heating/cooling, thermal conduction, and physical viscosity, in three-dimensional magnetohydrodynamical simulations. The results show that the thermal instability in the post-shock gas in the interstellar medium produces high-density molecular cloudlets embedded in warm neutral medium. The molecular cloudlets have velocity dispersion which is supersonic with respect to the sound speed of the cold medium but is subsonic with respect to the warm medium. The dynamical evolution driven by thermal instability in the post-shock layer is an important basic process for the transition from warm gases to cold molecular gases, because the shock waves are frequently generated by supernovae in the Galaxy.

Observations show that stars are formed in molecular clouds. Molecular clouds are characterized by *supersonic* line-widths of the emission lines from various molecules, which can be related to the supersonic internal motion of gas, or *turbulence*, in molecular clouds. Obviously this "turbulence" should be very different from well-studied incompressible turbulence in laboratory physics. The maintenance and dissipation processes of the turbulence in molecular clouds are supposed to be important in the theory of star formation (see, e.g., Mac Low & Klessen 2004). The understanding of the origin of the turbulence and the internal substructure of molecular clouds has fundamental importance for a consistent theory of star formation and ISM. Recent numerical simulations show that supersonic turbulence in isothermal or adiabatic medium quickly decays within a crossing time, unless the driving energy is continuously supplied. In contrast, Koyama & Inutsuka (1999, 2000, 2002a) proposed that the propagation of a strong shock wave into warm neutral medium (WNM) inevitably produce turbulent post-shocked cold layer as a result of thermal instability. Their result predict that the molecular clouds are born with turbulent velocity dispersion, and the cold cloudlets are embedded in warm medium of which sound speed is larger than the velocity dispersion of these cloudlets. Their continued study is now including the study on the effects of viscosity,

E. Corbelli et al. (eds.), The Initial Mass Function 50 Years Later, 381–382.

thermal conduction, and magnetic field (Inutsuka & Koyama 1999, 2002a,b; Koyama & Inutsuka 2002b, 2004). The importance of thermal instability is pointed out also by Hennebelle & Pérault (1999,2000) who demonstrated that cold clouds are generated by convergent flows in warm turbulent medium.

The role of thermal instability is studied also by Kritsuk & Norman (2002), and Vazquez-Semadeni, Gazol, & Scalo (2000). However, we should be careful in interpreting the results of numerical simulations without thermal conduction because it is essential to resolve the "Field length", a critical length scale for the evolution driven by thermal instability (for details, see Koyama & Inutsuka 2004).

Once the total column density of the ensemble of clouds becomes larger than the critical value ($\sim 10^{21}\mathrm{cm}^{-2}$), the two-phase medium is expected to become one phase medium with the timescale of cooling. Further evolution driven by gravitational force is outlined in Inutsuka & Tsuribe (2001) which includes simple explanations for the results by Nagai, Inutsuka, & Miyama (1998) and Inutsuka & Miyama (1992, 1997).

References

Hennebelle, P., & Pérault, M. 1999, A&A, 351, 309
Hennebelle, P., & Pérault, M. 2000, A&A, 359, 1124
Inutsuka,S. & Koyama, H. 1999, in Star Formation 1999, ed. T. Nakamoto, (Nobeyama Radio Observatory), 112
Inutsuka,S. & Koyama, H. 2002a, Ap&SS, 281, 67, 2002
Inutsuka,S. & Koyama, H. 2002b, in IAU 8th Asian Pacific Regional Meeting (Vol. I), ed. S. Ikeuchi, J. Hearnshaw, & T. Hanawa, 195
Inutsuka, S. & Tsuribe, T. 2001, in IAU Symp. 200, The Formation of Binary Stars, eds. Zinnecker, H. & Mathieu, R. (San Francisco: ASP 2001), 391
Inutsuka, S. & Miyama, S. M. 1992, ApJ, 388, 392
Inutsuka, S. & Miyama, S. M. 1997, ApJ, 480, 681
Koyama, H., & Inutsuka, S. 1999, in Star Formation 1999, ed. T. Nakamoto, (Nobeyama Radio Observatory), 114
Koyama, H., & Inutsuka, S. 2000, ApJ, 532, 980
Koyama, H., & Inutsuka, S. 2002a, ApJ, 564, L97
Koyama, H., & Inutsuka, S. 2002b, in IAU 8th Asian Pacific Regional Meeting (Vol. II), ed. S. Ikeuchi, J. Hearnshaw, & T. Hanawa, 159
Koyama, H., & Inutsuka, S. 2004, ApJ, 602, L25
Kritsuk, A. G., & Norman, M. L. 2002, ApJ, 569, L127
Mac Low, M.-M., & Klessen, R. S. 2004, Rev. Mod. Phys., 76, 125
Nagai, T., Inutsuka, S. & Miyama, S. M. 1998, ApJ, 506, 306
Vazquez-Semadeni, E., Gazol, A., & Scalo, J. 2000, ApJ, 540, 271

TURBULENCE-ACCELERATED STAR FORMATION IN MAGNETIZED CLOUDS

Fumitaka Nakamura[1] and Zhi-Yun Li[2]
[1]*Niigata University, 8050 Ikarashi-2, Niigata 950-2181, Japan*
[2]*University of Virginia, P.O. Box 3818, Charlottesville,VA22903, USA*
fnakamur@ed.niigata-u.ac.jp, zl4h@virginia.edu

1. Introduction

The standard scenario of low-mass star formation envisions quasi-static condensation of dense cores out of magnetically subcritical clouds and inside-out core collapse leading to star formation. In this scenario, how such quasi-static cores are formed was not addressed in details. It is unlikely for them to condense directly from a background of average density ($\sim 10^2$ cm^{-2}) through ambipolar diffusion, because in such a low density region the diffusion timescale is longer than the cloud lifetime. An alternative is the turbulence-controlled star formation, with magnetic fields playing a minor role if any. In this picture, dense cores arise from compression in the supersonic turbulence ubiquitously observed in molecular clouds. However, the cores so formed tend to have dynamic internal motions, which are difficult to reconcile with the subsonic internal motions inferred in low-mass starless cores. A more serious difficulty with the turbulence-controlled picture is that the efficiency of star formation is too high without additional support if not regulated by magnetic fields. Here, we study the evolution of turbulent, magnetized clouds with MHD simulation taking into account the ambipolar diffusion. We demonstrate that in strongly magnetized clouds, turbulent compression creates overdense regions in a (short) turbulent crossing time, sidestepping the relatively long process of ambipolar diffusion in the low density background medium, which leads to relatively rapid star formation with a low efficiency.

2. Results and Conclusion

The figure shows the evolution of two turbulent clouds magnetized to different degrees. Panels (a) through (e) are for an initially magnetically subcritical cloud with $\Gamma_0 = 1.2$, and (f) through (h) for a supercritical cloud with $\Gamma_0 = 0.8$. The clouds are stirred at $t = 0$ by the same random velocity field

E. Corbelli et al. (eds.), The Initial Mass Function 50 Years Later, 383–384.

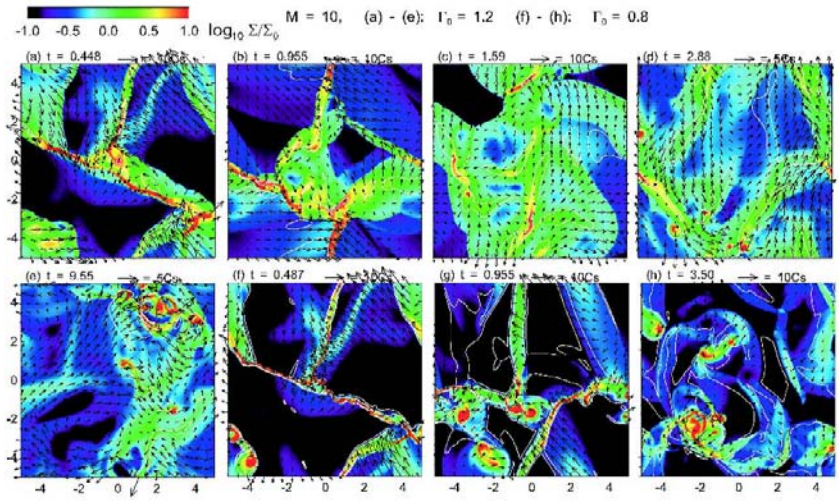

Figure 1. Evolution of turbulent clouds magnetized to different degrees. The color bar is for column density (in units of the initial value Σ_0). Γ_0 is the flux-to-mass ratio measured to the critical value. The time labeled above each panel is in units of the gravitational collapse time t_g, and the length unit is the Jeans length L_J. See Li & Nakamura (2004, ApJL, 609, L83) in more details.

of Mach number $\mathcal{M} = 10$. In clouds that are initially magnetically subcritical, supersonic turbulence can speed up star formation, through enhanced ambipolar diffusion in shocks. The formation of dense supercritical cores accelerated by supersonic turbulence begins in $1 - 2\ t_g$ and continues over an extended period of time. In contrast, in the initially supercritical cloud, dense cores form more rapidly with a higher efficiency. In both cases, the envelopes of the dense cores become magnetically subcritical due to ambipolar diffusion, which are likely to prevent rapid dynamic collapse of the entire cores. The speedup due to turbulent compression overcomes a major objection to the standard scenario of low-mass star formation involving ambipolar diffusion, since the diffusion time scale at the average density of a molecular cloud is typically longer than the cloud life time. At the same time, the strong magnetic field can prevent the large-scale supersonic turbulence from converting most of the cloud mass into stars in one (short) turbulence crossing time, and thus alleviate the high efficiency problem associated with the turbulence-controlled picture for low-mass star formation. Thus, we propose that relatively rapid but inefficient star formation results from supersonic collisions of somewhat subcritical gas in strongly magnetized, turbulent clouds.

CLUSTER DENSITY AND THE IMF

Bruce G. Elmegreen
IBM T.J. Watson Research Center, PO Box 218 Yorktown Hts., NY 10598, USA
bge@watson.ibm.com

Abstract Observed variations in the IMF are reviewed with an emphasis on environmental density. The local field IMF is not a dependable representation of star-forming regions because of uncertain assumptions about the star formation history. The remote field IMF studied in the LMC by several authors is clearly steeper than most cluster IMFs, which have slopes close to the Salpeter value. Local field regions of star formation, like Taurus, may have relatively steep IMFs too. Very dense and massive clusters, like super star clusters, could have flatter IMFs, or inner-truncated IMFs. We propose that these variations are the result of three distinct processes during star formation that affect the mass function in different ways depending on mass range. At solar to intermediate stellar masses, gas processes involving thermal pressure and supersonic turbulence determine the basic scale for stellar mass, starting with the observed pre-stellar condensations, and they define the mass function from several tenths to several solar masses. Brown dwarfs require extraordinarily high pressures for fragmentation from the gas, and presumably form inside the pre-stellar condensations during mutual collisions, secondary fragmentations, or in disks. High mass stars form in excess of the numbers expected from pure turbulent fragmentation as pre-stellar condensations coalesce and accrete with an enhanced gravitational cross section. Variations in the interaction rate, interaction strength, and accretion rate among the primary fragments formed by turbulence lead to variations in the relative proportions of brown dwarfs, solar to intermediate mass stars, and high mass stars. The observed IMF variations may be explained in this way.

1. Introduction

The initial stellar mass function proposed by Edwin Salpeter in 1955 followed remarkably soon after the discovery of star formation itself. Only several years earlier, Ambartsumian (1947) noted that the clusters h and χ Persei and NGC 6231 were too rarefied to resist galactic tidal forces. He said they should be elongated by galactic shear, and because they were not, they had to be young, expanding, and dispersing. Soon after, Blaauw (1952) found the predicted 10 km s^{-1} proper motions in the ζ Perseus association, and Zwicky (1953) proposed that stellar expansion followed gas expulsion from bound

E. Corbelli et al. (eds.), The Initial Mass Function 50 Years Later, 385–398.

newborn clusters. This was the beginning of the recognition that stars had to form and evolve continuously (Spitzer 1948; Hoyle 1953).

Salpeter (1955) reasoned that if stars form continuously, and if their lifetimes depend on mass because of nuclear burning with a steep mass-luminosity relation, then many more remnants from massive stars than from low mass stars should populate the Milky Way disk. Consequently, the stellar birth rate is a shallower function of mass than the present day mass distribution.

The local field initial stellar mass function (IMF) derived by Salpeter (1955) was based on the available population studies, some of which were old even then, and on simple assumptions about stellar lifetimes and galactic star formation history. The result was a power law initial mass function with a slope of $\Gamma \sim -1.35$ (when plotted with equal intervals of $\log M$). Considering the improvements in modern stellar data, there is no reason to expect the mass function derived in 1955 would be the same as today's. Indeed, subsequent studies almost always got steeper field IMFs for the solar neighborhood: Scalo (1986) got $\Gamma \sim -1.7$ at intermediate to high mass, and Rana (1987) got $\Gamma \sim -1.8$ for $M > 1.6$ M$_\odot$. The Salpeter value of $\Gamma \sim -1.35$ predicts three times more massive stars ($10 - 100$ M$_\odot$) than intermediate mass stars ($1 - 10$ M$_\odot$) compared to the Scalo or Rana functions. Such an excess can be ruled out for the local field today.

The steep slope of field IMFs becomes even more certain in recent studies. Parker et al. (1998) derived $\Gamma = -1.80 \pm 0.09$ for the LMC field that was far away from the HII regions catalogued by Davies, Elliot & Meaburn (1976). Note the small statistical error in this study. Massey et al. (1995, 2002) also surveyed the remote field in the LMC and SMC: at distances greater than 30 pc from Lucke & Hodge (1970) or Hodge (1986) OB associations, in a survey complete to 25 M$_\odot$, $\Gamma \sim -3.6$ to -4 for a constant star formation rate during the last 10 My. There were 450 stars in the most recent Massey et al. LMC sample, which would give a statistical uncertainty in the slope of only ± 0.15 (Elmegreen 1999).

These steep field IMF slopes are reminiscent of that found by Garmany et al. (1982). In a survey of the solar neighborhood out to 2.5 kpc, and complete for $M > 20$ M$_\odot$, Garmany et al. found $\Gamma = -1.6$ overall, $\Gamma \sim -1.3$ inside the Solar circle, and $\Gamma \sim -2.1$ outside the Solar circle. They proposed that the difference between these values arose because of an excess of massive stars in the associations of the Carina and Cygnus spiral arms, which are inside the Solar circle. That is, the low density regions have steep IMF slopes and the high density regions have shallow IMF slopes. This observation led to the concept of bimodal star formation: Güsten & Mezger (1983) proposed that metallicity gradients in the Galaxy arose from an interarm IMF that was steeper than the spiral arm IMF. Larson (1986) proposed that a sub-population formed with a shallow IMF would have more remnants contributing to dark matter.

Such extreme bimodality was never confirmed, although the steep field IMF slope persisted. Also, in contrast to Garmany et al., a recent study of the Milky Way disk by Casassus et al. (2000) got the same IMF inside and outside the Solar circle using IR sources in ultra-compact HII regions. They got the steep value in both places, however, $\Gamma \sim -2$.

The problem with most of the field IMFs is that they are subject to systematic uncertainties in the essential assumptions: the star formation history, the mass dependence of the galactic scale height, galactic radial migration, etc.. Fits to a constant historical star formation rate in the Milky Way are inconsistent with the Madau et al. (1996) result, for example, which suggests that cosmological star formation was significantly higher 10 Gy ago, the likely age of the Milky Way disk (this excess could be from different galaxies, however). Also uncertain is the disk formation history, considering the possibility of gaseous accretion and minor mergers. Similar uncertainties arise for recent times: a burst of star formation from the most recent passage of a spiral density wave would give a decaying star formation rate locally, changing the history corrections in the IMF and making the slope shallower for $M > 5$ M$_\odot$. In fact it is likely that local star formation varies on a 100 My time scale. These uncertainties translate into unknown corrections for the IMF during the conversion from present day star counts to relative fractions at birth. For this reason, moderately steep field IMFs at intermediate to high mass may not be representative of the average IMF in field regions of star formation.

The extreme fields in the Large and Small Magellanic Clouds seem different, however. The steep slope differs from the Salpeter value by a statistically significant margin, there is no scale height uncertainty because the line of sight integrates through the entire disk, massive stars are easily detected, and their 10 My lifetimes minimize uncertainties in the star formation history. The resulting IMF seems trustworthy. In addition, small-scale local star formation, as in Taurus, could be unusually steep too for $M > 1$ M$_\odot$ (Luhman 2000).

Cluster IMFs are difficult to measure because of the small number of stars in most clusters (Scalo 1998) and because of mass segregation (de Grijs et al. 2002). Some clusters have the same steep IMF as the field (e.g., the upper Sco OB association – Preibisch et al. 2002), but other clusters have what appears to be an excess of high mass stars in certain subgroups, making their overall slopes shallower. W51 (Okumura et al. 2000) is an example where the intermediate mass IMF has a slope of ~ -1.8, but sub-regions 2 and 3 have a statistically significant excess of stars at $M \sim 60$ M$_\odot$ (a 2 to 3 σ deviation).

After uncertain corrections for mass segregation, field contamination, and completeness, most clusters have IMF slopes that are significantly shallower than $\Gamma = -1.8$, and more like the original Salpeter value of $\Gamma = -1.35$. R136 in the 30 Dor region of the LMC is a good example (Massey & Hunter 1998). Other examples are h and χ Persei (Slesnick, Hillenbrand & Massey 2002),

NGC 604 in M33 (González Delgado & Perez 2000), NGC 1960 and NGC 2194 (Sanner et al. 2000), and NGC 6611 (Belikov et al. 2000). Massey & Hunter (1998) proposed that the Salpeter IMF spans a factor of 200 in cluster density. If this is the case, then clustered star formation produces a shallower IMF than extreme field star formation.

The most extreme cases of clustered star formation are in starburst regions (Rieke et al. 1993), particularly in super star clusters. Sternberg (1998) derived a high L/M for the super star cluster NGC 1705-1, and inferred that either $|\Gamma| < 1$ or there is an inner-mass cutoff greater than the local value of 0.5 $M_\odot$ (Kroupa 2001). Smith & Gallagher (2001) got a high L/M in M82F and proposed an inner cutoff of 2 to 3 $M_\odot$ for $\Gamma = -1.3$. They also confirmed the Sternberg result for NGC 1705-1. Alonso-Herrero et al. (2001) got a high L/M in the starburst galaxy NGC 1614. Förster Schreiber et al. (2003) found the same for M82, proposing an inner IMF cutoff of 2 to 3 $M_\odot$ for $\Gamma = -1.35$. Similarly, McCrady et al. (2003) found a deficit in low mass stars in the cluster MGG-11 of M82. Not all super star clusters require an inner IMF cutoff: N1569-A (Sternberg 1998), NGC 6946 (Larsen et al. 2001), and M82: MGG-9 (McCrady et al. 2003) do not.

We might summarize these results as follows: The field IMF is systematically steeper than the cluster IMFs, but both are uncertain. Nevertheless, in the field and in low-density clustered regions, the IMF slope is fairly steep, perhaps $\Gamma = -1.8$ or steeper, while in clusters it is more shallow, $\Gamma = -1.3$ or shallower, with even more of a high mass bias for the most extreme clusters in starburst regions. This IMF difference suggests a difference in star formation mechanisms, and is reminiscent of Motte & André's (2001) suggestion that accretion processes and pre-stellar condensation sizes are different in the low density regions of Taurus compared to the higher density associations in Perseus and Ophiuchus. Significantly steep IMFs in some dispersed associations, and very steep IMFs in remote fields contribute to this picture. In the disks of low surface brightness galaxies, a high mass-to-light ratio suggests the entire IMF is steep with $\Gamma = -2.85$ (Lee et al. 2004); star formation in the low-density "field" mode could be pervasive.

In addition to these observations, the segregation of stellar mass in many clusters, apparently at birth (Bonnell & Davies 1998), also suggests high mass stars prefer dense environments (Pandey, Mahra & Sagar 1992; Subramaniam, Sagar & Bhatt 1993; Malumuth & Heap 1994; Brandl et al. 1996; Fischer et al. 1998; Hillenbrand & Hartmann 1998; Figer, McLean, & Morris 1999; Le Duigou & Knödlseder 2002; Stolte et al. 2002; Sirianni et al. 2002; Muench et al. 2003; Gouliermis et al. 2004; Lyo et al. 2004).

We conclude that dense regions favor massive star formation. A more comprehensive survey of the observations is in Elmegreen (2004).

2. Theoretical expectations

There has long been a notion that massive star formation should be more likely in dense environments. It takes ultra-high pressures to confine the winds and radiation from massive stars (Garay & Lizano 1999; Yorke & Sonnhalter 2002; Churchwell 2002; McKee & Tan 2003), and these pressures require high density cloud cores. Massive stars could also form by enhanced accretion from high density gas reservoirs (Zinnecker 1982; Larson 1999, 2002; Myers 2000; Bonnell et al. 1997, 2001, 2004), by the coalescence of pre-stellar condensations (Zinnecker 1986; Larson 1990; Price & Podsiadlowski 1995; Stahler, Palla & Ho 2000), coalescence after accretion drag (Bonnell, Bate, & Zinnecker 1998), or coalescence after accretion-induced cloud-core contraction (Bonnell, Bate & Zinnecker 1998; Bonnell & Bate 2002). Indeed, numerical simulations in Gammie et al. (2003) showed that the high-mass part of the IMF gets shallower with time as a result of coalescence and enhanced accretion. Li, et al. (2004) also found enhanced accretion and coalescence played a role in massive star formation.

Nearly every attempt to confirm these ideas has been incomplete or fraught with selection effects. The observation of larger most-massive stars in denser clusters would support this picture (Testi, Palla, & Natta 1999), but it appears instead to be the result of sampling statistics: all of the clusters in their survey were about the same size and so the cluster density correlated with total cluster mass (Bonnell & Clarke 1999; Elmegreen 2000). More massive clusters usually give more massive most-massive stars by sampling further out in the IMF. Earlier observations of cloud-mass versus star-mass correlations (Larson 1982) apparently had the same size of sample effect (Elmegreen 1983).

We are concerned with a more subtle effect here however, and one dependent on both density and mass rather than just mass. The observations suggest all clusters are more or less the same, i.e., having a fairly shallow IMF, so differences between clusters will be dominated by sampling, selection, and mass segregation. However, star formation at very low density, in the extreme field or in low surface brightness galaxies, is apparently different, producing steep IMFs. We choose to emphasize here the difference between clusters as a whole and the remote field, rather than a density dependence for the IMF among the clustered population alone. With this more extreme comparison, it seems reasonable to think that the relatively isolated star formation of remote field regions will not produce much coalescence of pre-stellar condensations, and will therefore lack the "cluster-mode" of competitive accretion and dense core interactions that are illustrated by numerical simulations (e.g., Bonnell, Bate, & Vine 2003). In this limited sense, we believe the massive-star IMF should vary with density (Elmegreen 2004; Shadmehri 2004).

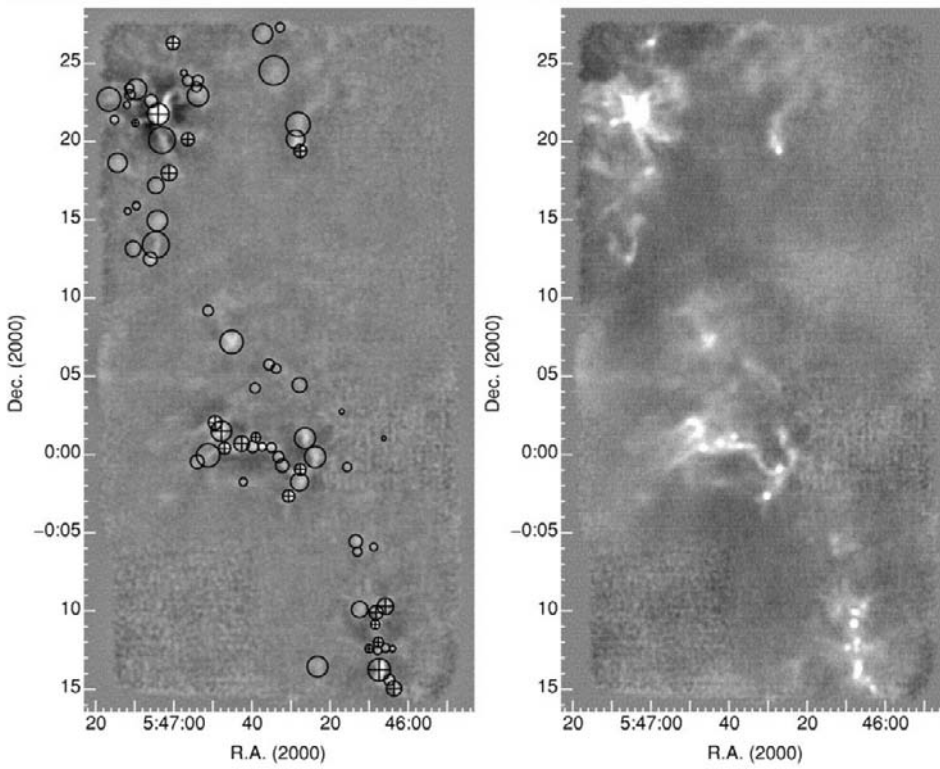

Figure 1. 850 μm continuum observations of Orion from Johnstone et al. (2001). The left panel shows identifications of pre-stellar condensations made by a clump-finding algorithm, and the right panel shows the emission. These condensations are typical for dense pre-stellar objects. In this cluster-forming environment, they are often close together, suggesting that some will coalescence in the future. Reproduced by permission of the AAS.

Figure 1 shows the mm-wave continuum emission in the Orion B region, from Johnstone et al. (2001). The tiny knots of emission are examples of pre-stellar condensations, similar to those found in many other regions (Motte et al. 1998). The figure shows how closely packed many of these condensations are, giving credence to the idea that some will interact or coalesce with their nearest neighbors. A statistical study of such coalescence, limited to the pre-stellar condensation phase when the objects are fairly large ($\sim 10^4$ AU), suggests that the most massive and dense clusters should have the most coalescence (Elmegreen & Shadmehri 2003). That is, the ratio of the coalescence time to the collapse time of pre-stellar condensations decreases for more massive clusters or for denser clusters. The mass dependence arises because more massive clusters have more massive stars, which are more strongly attracting to other pre-stellar condensations. The pre-stellar condensations are more widely sepa-

rated in Taurus (Motte & André 2001) than in Orion B. This supports our view that interactions at this phase are relatively less important in the low-density field environment.

Theoretical considerations in Elmegreen (2004) and Shadmehri (2004) suggest there are three distinct regimes of physical processes in the IMF:

- For solar to intermediate mass stars, cloud or gas processes connected with turbulence and the thermal Jeans mass, M_{J0}, are important for the formation of pre-stellar condensations (e.g., see review in Mac Low & Klessen 2004, and see Gammie et al. 2003; Li, et al. 2004).

- Brown dwarfs differ because gravitational instabilities at such low mass require ultra-high pressures. These naturally occur inside the M_{J0} pieces formed by cloud processes; i.e., in disk instabilities surrounding M_{J0} protostars, in the ejecta from collisions between M_{J0} objects, in the early ejection of accreting protostars from tight clusters, and so on, as in the usual models (Padoan & Nordlund 2002; Reipurth & Clarke 2001; Bate, Bonnell & Bromm 2002; Preibisch et al. 2003; Kroupa & Bouvier 2003). In addition, collisions between M_{J0} objects should induced gravitational instabilities in the shocked gas. Because the pre-stellar condensation density is higher than the ambient cloud density by a factor of ~ 100, the Jeans mass for these shock instabilities will be lower than M_{J0} by a factor of ~ 10, placing them in the brown dwarf range.

- High mass stars form by cloud processes too, but their formation rate can be greatly enhanced by the coalescence of M_{J0} pieces and by gas accretion. These are runaway processes considering gravitationally enhanced cross sections, and so become more prominent when the condensation mass exceeds M_{J0} by a factor of ~ 10.

We consider that these three regimes of star formation produce three separate IMFs that usually combine into one in a way that gives the seemingly universal power law with a low mass turnover at about M_{J0}. However, variations in the importance of these three processes, particularly with variations in the ambient cloud density, produce variations in the relative amplitudes of the three IMFs, and these variations have the effect of changing the slope of the power-law fit at intermediate to high mass.

Such variations can also change the proportion of brown dwarfs and normal stars. IC 348 (Preibisch, Stanke & Zinnecker 2003; Muench et al. 2003; Luhman et al. 2003) and Taurus (Luhman 2000; Briceño et al. 2002) have brown dwarf-to-star ratios that are ~ 2 times lower than in many other local clusters, including the Orion trapezium cluster (Hillenbrand & Carpenter 2000; Luhman et al. 2000; Muench et al. 2002), the Pleiades (Bouvier et al. 1998; Luhman et al. 2000), M35 (Barrado y Navascués et al. 2001) and the galactic field (Reid

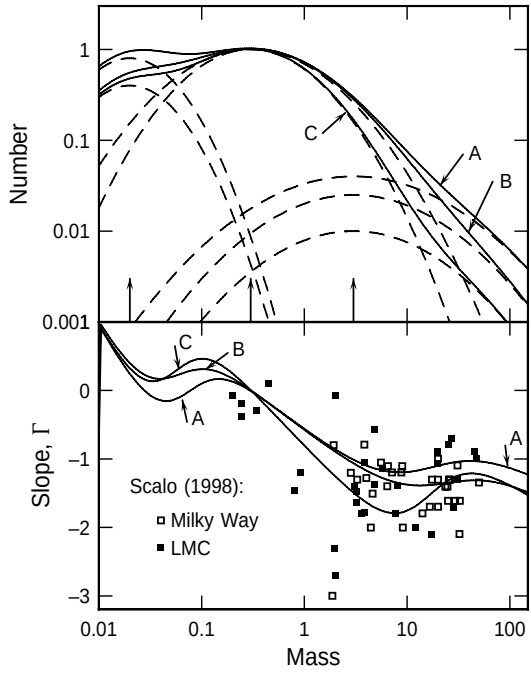

Figure 2. Three component models of the IMF with the distinct components indicated by dashed lines. The top panel shows the IMFs and the bottom panel shows the slopes along with observations from Scalo (1998). Each component is a log-normal with a characteristic amplitude, central mass (indicated by arrows along the abscissa of the top panel), and dispersion. Curves A, B, and C correspond in the top and bottom panels. The combined IMFs have pseudo-power laws at intermediate to high mass. Based on a figure in Elmegreen (2004).

et al. 1999). IC 348 and Taurus differ even in the subsolar range (Luhman et al. 2003).

Figure 2 shows an example of how variability in three distinct mass intervals, separated by factors of 10, can produce variability in the summed IMF that is similar to what is observed (from Elmegreen 2004). Three distinct log-normals, one for each physical process, are shown to sum to a near power law between 1 and 100 $M_\odot$. The intermediate-to-high mass slope gets shallower as the high-mass contribution increases. The brown dwarf range can be made to vary too.

Figure 3 shows IMF models where a cloud forms stars with a locally log-normal mass distribution that has a central mass and dispersion increasing with cloud density (from Elmegreen 2004). The cloud density has the form $\rho_c(r) = \left(1 + [r/r_0]^2\right)^{-1}$ for core radius is r_0. The local IMF is taken to

be $f(M) = A \exp\left(-B\left[\log\{M/M_0\}\right]^2\right)$ for exponential factor $B = B_1 - B_2\rho_c(r)$ and central mass $M_0 = M_1 + M_2\rho_c(r)$. With these expressions, the local log-normal is broader and shifted toward higher mass in the cloud core. The Miller-Scalo (1979) IMF has $B_1 = 1.08$ and $M_1 = 0.1$ $M_\odot$ with no density dependence. The total mass function in the cloud is determined by integrating over radius out to r_{max} with a weighting factor equal to the $3/2$ power of density; this accounts for the available mass and a star formation rate locally proportional to the dynamical rate. The figure shows the Miller-Scalo IMF ($B_2 = M_2 = 0$) as a dotted line and sample IMFs with $B_2 = B_1$, $M_2 = 1$, and $r_{max} = 2r_0$ (solid line), $5r_0$ (dashed), and $10r_0$ (dot-dashed). The IMF slope is shallower for smaller r_{max}, indicating mass segregation. The bottom panel plots mean separation between the logs of the masses in the IMF along with observations of R136 from Massey & Hunter (1998). The slope of the distribution of points is the negative power, $-\Gamma$, of a power-law IMF. The R136 points have $\Gamma \sim -1.1$. Clearly a variable IMF can be made to fit this observation using only local IMFs that are log-normal in form.

3. Summary

There is apparently no "Universal IMF." Low-pressure star formation in remote field regions is characterized by widely-separated, pre-stellar condensations with masses centered on the thermal Jeans mass, (M_{J0}). These condensations rarely interact, so they produce a "gas-only" IMF with no high-mass component and a steep slope at intermediate to high stellar mass. High-pressure star formation in clusters produces the same gas-only IMF for pre-stellar condensations, but these condensations collapse and collide to make ultra-high pressure regions (disks, shocks, etc.), leading to brown dwarfs. The same high-pressure cluster environment also promotes coalescence of pre-stellar condensations to build up more massive stars. Thus at least one process of brown dwarf formation correlates with the enhanced formation of massive stars.

Stellar IMFs for galaxies and clusters are about the same because most stars form in clusters. There is apparently little correlation (aside from sampling effects) between stellar mass and cluster mass for these stars. At very low densities and pressures, as in the field, or in low surface brightness galaxies, or in some dwarf galaxies, the IMF should be relatively steep ($\Gamma \leq -1.7$), with few massive stars because of a lack of significant pre-main-sequence coalescences, and relatively few brown dwarfs because of a lack of collision remnants. At very high densities, as in dense clusters, the IMF should be shallow, like the Salpeter IMF or perhaps shallower, because of the coalescence of pre-stellar condensations and because of enhanced gas accretion. Brown dwarfs should be relatively common in these regions too because of the high pressures formed by interactions.

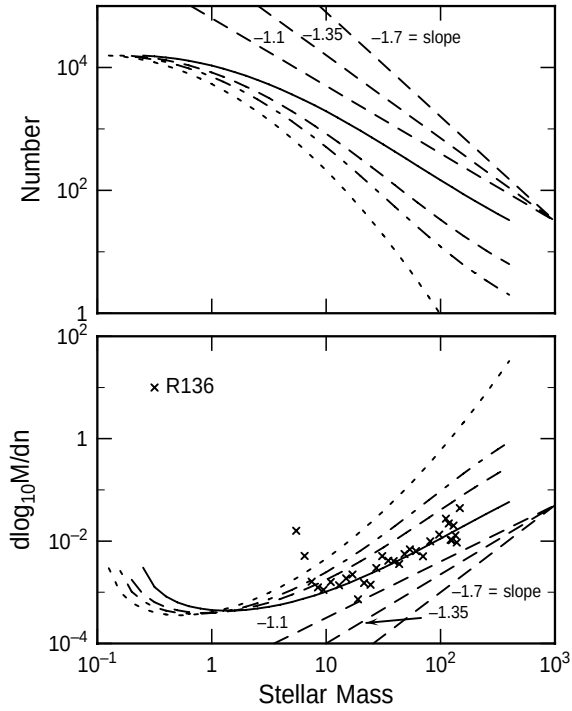

Figure 3. (top) IMF model based on a log-normal mass distribution in which the dispersion increases with density. The IMF is integrated over a cloud density profile out to 2, 5, and 10 cloud core radii for solid, dashed, and dot-dashed lines. The dotted line is the Miller-Scalo (1979) IMF. (bottom) The mean separation between the log of the masses for the model IMFs shown in the top and for the R136 cluster in the LMC.

References

Alonso-Herrero, A., Engelbracht, C.W., Rieke, M.J., Rieke, G.H., & Quillen, A.C. 2001, ApJ, 546, 952

Ambartsumian, V.A. 1947, 1949 AZh, 26, 3

Barrado y Navascués, D., Stauffer, J.R., Bouvier, J., & Martín, E.L. 2001, ApJ, 546, 1006

Bate, M.R., Bonnell, I.A. & Bromm, V. 2002, MNRAS, 332, L65

Belikov, A.N., Kharchenko, N.V., Piskunov, A.E., & Schilbach, E. 2000, A&A, 358, 886

Blaauw, A. 1952, BAN, 11, 405

Bonnell, I.A., Bate, M.R., Clarke, C.J., & Pringle, J. E., 1997, MNRAS, 285, 201

Bonnell, I.A., & Davies, M.B. 1998, MNRAS, 295, 691

Bonnell, I.A., Bate, M.R., & Zinnecker, H. 1998, MNRAS, 298, 93

Bonnell, I.A., & Clarke, C.J. 1999, MNRAS, 309, 461

Bonnell, I.A., Clarke, C.J., Bate, M.R. & Pringle, J.E. 2001, MNRAS, 324, 573

Bonnell, I.A., & Bate, M.R. 2002, MNRAS, 336, 659

Bonnell, I.A., Bate, M.R., & Vine, S.G. 2003, MNRAS, 343, 413

Bonnell, I.A., Vine, S.G., & Bate, M.R. 2004, MNRAS, 349, 735
Bouvier, J., Stauffer, J.R., Martin, E.L., Barrado y Navascues, D., Wallace, B., & Bejar, V.J.S. 1998, A&A, 336, 490
Brandl, B., Sams, B. J., Bertoldi, F., Eckart, A., Genzel, R., Drapatz, S., Hofmann, R., Loewe, M. & Quirrenbach, A. 1996, ApJ, 466, 254
Briceño, C., Luhman, K.L., Hartmann, L., Stauffer, J.R., & Kirkpatrick, J.D. 2002, ApJ, 580, 317
Casassus, S., Bronfman, L., May, J., Nyman, L.-Å 2000, A&A, 358, 514
Churchwell, E. 2002, ARAA, 40, 27
Davies, R.D., Elliott, K.H., Meaburn, J. 1976, Memoirs RAS, 81, 89
de Grijs, R., Gilmore, G.F., Johnson, R.A., & Mackey, A. D. 2002, MNRAS, 331, 245
Elmegreen, B.G. 1983, MNRAS, 203, 1011
Elmegreen, B.G. 1999, ApJ, 515, 323
Elmegreen, B.G. 2000, ApJ, 539, 342
Elmegreen, B.G. 2004, MNRAS, 354, 367 astroph/0408231
Elmegreen, B.G., & Shadmehri, M. 2003, MNRAS, 338, 817
Figer, D.F., McLean, I.S., & Morris, M. 1999, ApJ, 514, 202
Fischer, P., Pryor, C., Murray, S., Mateo, M., & Richtler, T. 1998, AJ, 115, 592
Förster Schreiber, N.M., Genzel, R., Lutz, D., & Sternberg, A. Th. 2003, ApJ, 599, 193
Garay, G., & Lizano, S. 1999, PASP, 111, 1049
Gammie, C.F., Lin, Y.-T., Stone, J.M., & Ostriker, E.C. 2003, ApJ, 592, 203
Garmany, C.D., Conti, P. S., & Chiosi, C. 1982, ApJ, 263, 77
González Delgado, R.M., & Pérez, E. 2000, MNRAS, 317, 64
Gouliermis, D., Keller, S.C., Kontizas, M., Kontizas, E., & Bellas-Velidis, I. 2004, A&A, 416, 137
Güsten, R., & Mezger, P.G. 1983, Vistas. Astron., 26, 159
Hillenbrand, L.A., & Hartmann, L.W. 1998, ApJ, 492, 540
Hillenbrand, L.A., & Carpenter, J.M. 2000, ApJ, 540, 236
Hodge, P.W. 1986, PASP, 98, 1113
Hoyle, F. 1953, ApJ, 118, 513
Johnstone, D., Fich, M., Mitchell, G.F., & Moriarty-Schieven, G. 2001, ApJ, 559, 307
Kroupa, P. 2001, MNRAS, 322, 231
Kroupa, P. & Bouvier, J. 2003, MNRAS, 346, 369
Larsen, S.S., Brodie, J.P., Elmegreen, B.G., Efremov, Y.N., Hodge, P.W., & Richtler, T. 2001, ApJ, 556, 801
Larson, R.B. 1982, MNRAS, 200, 159
Larson, R.B. 1986, MNRAS, 218, 409
Larson, R.B. 1990, in Physical processes in fragmentation and star formation, eds. R. Capuzzo-Dolcetta, C. Chiosi & A. Di Fazio, Dordrecht: Kluwer, p. 389
Larson, R.B. 1999, in Star Formation 1999, ed. T. Nakamoto, Nobeyama: Nobeyama Radio Observatory, p.336
Larson, R.B. 2002, MNRAS, 332, 155
Le Duigou, J.-M., & Knödlseder, J. 2002, A&A, 392, 869
Lee, H.-C., Gibson, B.K., Flynn, C., Kawata, D., & Beasley, M.A. 2004, MNRAS, 353, 113
Li, P.S., Norman, M.L., Mac Low, M.-M., & Heitsch, F. 2004, ApJ, 605, 800
Lucke, P.B. & Hodge, P.W. 1970, AJ, 75, 171

Luhman, K.L. 2000, ApJ, 544, 1044
Luhman, K.L., Rieke, G.H., Young, E.T., Cotera, A.S., Chen, H., Rieke, M.J., Schneider, G., & Thompson, R. I. 2000, ApJ, 540, 1016
Luhman, K.L., Stauffer, J.R., Muench, A.A., Rieke, G.H., Lada, E.A., Bouvier, J., & Lada, C.J. 2003, ApJ, 593, 1093
Lyo, A.-R., Lawson, W.A., Feigelson, E.D., & Crause, L. A. 2004, MNRAS, 347, 246
Mac Low, M.-M., & Klessen, R.S. 2004, Rev. Mod. Phys., 76, 125
Madau, P., Ferguson, H.C., Dickinson, M.E., Giavalisco, M., Steidel, C.C., & Fruchter, A. 1996, MNRAS, 283, 1388
Malumuth, E.M., & Heap, S.R. 1994, AJ, 107, 1054
Massey, P. 2002, ApJS, 141, 81
Massey, P., Lang, C.C., DeGioia-Eastwood, K., & Garmany, C.D. 1995, ApJ, 438, 188
Massey, P., & Hunter, D.A. 1998, ApJ, 493, 180
McCrady, N., Gilbert, A., & Graham, J.R. 2003, ApJ, 596, 240
McKee, C.F., & Tan, J.C. 2003, ApJ, 585, 850
Miller G.E., & Scalo J.M., 1979, ApJS, 41, 513
Motte, F., André, P., & Neri, R. 1998, A&A, 336, 150
Motte F., & André P. 2001, A&A, 365, 440
Muench, A.A., Lada, E.A., Lada, C.J., & Alves, J. 2002, ApJ, 573, 366
Muench, A.A., Lada, E.A., Lada, C.J., Elston, R.J., Alves, J.F., Horrobin, M., Huard, T.H., Levine, J.L., Raines, S.N., & Román-Zíñiga, C. 2003, AJ, 125, 2029
Myers, P.C. 2000, ApJ, 530, L119
Okumura, S., Mori, A., Nishihara, E., Watanabe, E., & Yamashita, T. 2000, ApJ, 543, 799
Padoan, P., & Nordlund, A. 2002, ApJ, 576, 870
Pandey, A.K., Mahra, H.S., & Sagar, R. 1992, Astr.Soc.India, 20, 287
Parker, J.W., Hill, J.K., Cornett, R.H., Hollis, J., Zamkoff, E., Bohlin, R. C., O'Connell, R.W., Neff, S.G., Roberts, M.S., Smith, A.M., & Stecher, T.P. 1998, AJ, 116, 180
Preibisch, T., Brown, A.G.A., Bridges, T., Guenther, E., & Zinnecker, H. 2002, AJ, 124, 404
Preibisch, T., Stanke, T., & Zinnecker, H. 2003, A&A, 409, 147
Price, N.M., & Podsiadlowski, Ph. 1995, MNRAS, 273, 1041
Rana, N.C. 1987, A&A, 184, 104
Reid, I.N., Kirkpatrick, J.D., Liebert, J., Burrows, A., Gizis, J.E., Burgasser, A., Dahn, C.C., Monet, D., Cutri, R., Beichman, C.A., & Skrutskie, M. L 1999, ApJ, 521, 613
Reipurth, B., & Clarke, C. 2001, AJ, 122, 432
Rieke, G.H., Loken, K., Rieke, M.J., & Tamblyn, P. 1993, ApJ, 412, 99
Salpeter, E. 1955, ApJ, 121, 161
Sanner, J., Altmann, M., Brunzendorf, J., & Geffert, M. 2000, A&A, 357, 471
Scalo, J.M. 1986, Fund.Cos.Phys, 11, 1
Scalo, J.M. 1998, in The Stellar Initial Mass Function, ed. G. Gilmore, I. Parry, & S. Ryan, Cambridge: Cambridge University Press, p. 201
Shadmehri, M. 2004, MNRAS, 354, 375
Sirianni, M., Nota, A., De Marchi, G., Leitherer, C., & Clampin, M. 2002, ApJ, 579, 275
Slesnick, C.L., Hillenbrand, L.A., & Massey, P. 2002, ApJ, 576, 880
Smith, L.J., & Gallagher, J.S. 2001, MNRAS, 326, 1027
Spitzer, L., Jr. 1948, Phys. Today, 1, 6

Stahler, S.W., Palla, F., & Ho., P.T.P. 2000, in Protostars and Planets IV, eds. V.Mannings, A. P. Boss & S. S. Russell, Tucson: Univ. Arizona Press, p. 327

Sternberg, A. 1998, ApJ, 506, 721

Stolte, A., Grebel, E.K., Brandner, W., & Figer, D.F. 2002, A&A, 394, 459

Subramaniam, A., Sagar, R., & Bhatt, H.C. 1993, A&A, 273, 100

Testi, L., Palla, F., & Natta, A. 1999, A&A, 342, 515

Yorke, H.W., & Sonnhalter, C. 2002, ApJ, 569, 846

Zinnecker, H. 1982, in Symposium on the Orion Nebula to Honor Henry Draper, eds. A. E. Glassgold, P. J. Huggins, & E. L. Schucking, New York: New York Academy of Science, p. 226

Zinnecker, H. 1986, in Luminous Stars and Associations in Galaxies, IAU Symposium 116, eds. C.W.H. de Loore, A.J. Willis, P. Laskarides, Dordrecht: Reidel, p. 271

Zwicky, F. 1953, PASP, 65, 205

Figure 4. Bruce and Berhard entartaining the Scalo's at dinner.

Figure 5. Elemgreen, Walterbos, Wyse, Oey, and Schneider.

Figure 6. A typical breakfast at Ocaiolo.

VII

THE ORIGIN OF THE IMF: FROM GAS TO STARS

Figure 7. Explaining the IMF: Shu vs. Padoan.

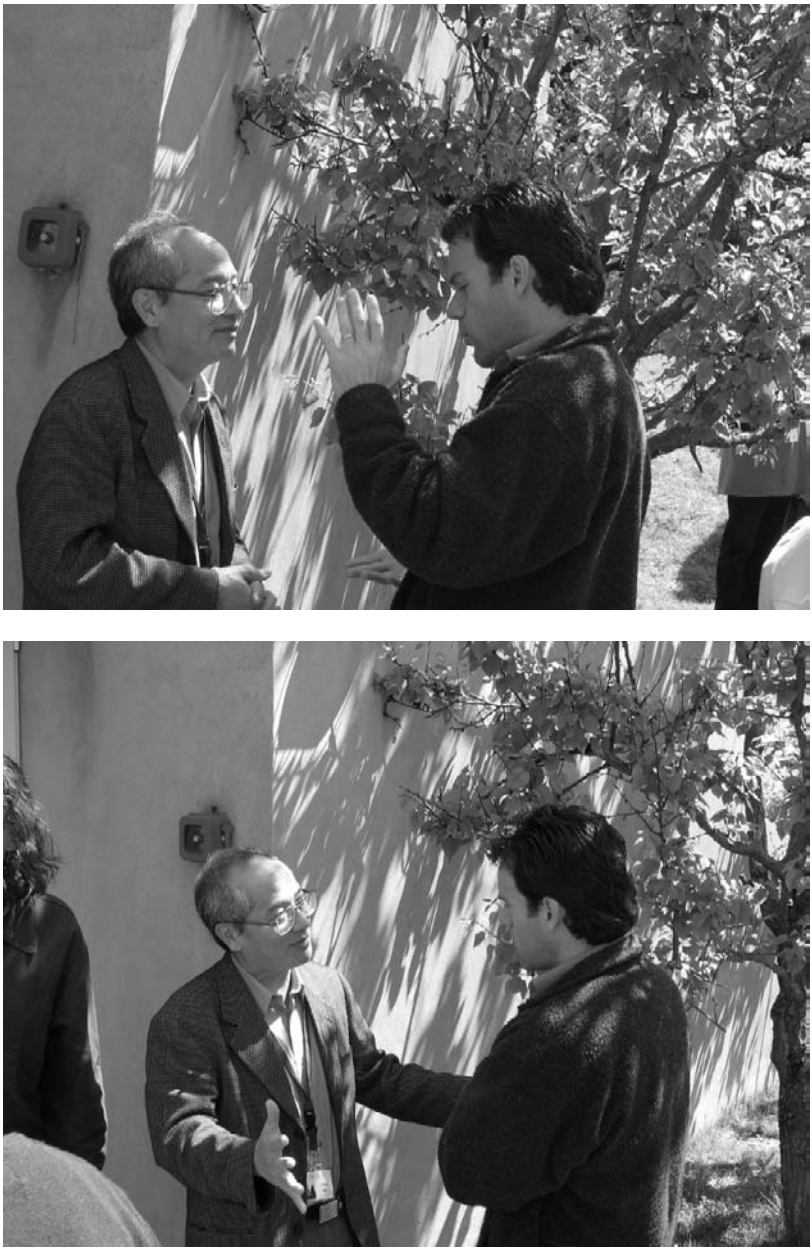

Figure 8. "...perhaps we do agree!"

A THEORY OF THE IMF

Frank H. Shu[1], Zhi-Yun Li[2] and Anthony Allen[3]
[1]*National Tsing Hua University, Hsinchu 30013, Taiwan, R.O.C.*
[2]*Department of Astronomy, University of Virginia, Charlottesville, VA 22903, USA,*
[3]*Institute of Astronomy and Astrophysics, Academia Sinica, Taipei 106, Taiwan, R.O.C.*
shu@mx.nthu.edu.tw,zl4h@virginia.edu,allen@asiaa.sinica.edu.tw

Abstract Magnetic fields play a prominent role in the formation of stars in giant molecular clouds (GMCs). They explain the low efficiency of star formation in the Galaxy. They yield the mechanism underlying jets from young stellar objects and bipolar outflows. Joining these topics together allows a theoretical derivation of the Salpeter initial mass function.

1. Introduction

Molecular clouds have masses typically 10^5 times larger than the stars that they form. Why then are sunlike stars the usual outcome of gravitational collapse in interstellar clouds? Answers to this fundamental question range from opacity-limited thermal fragmentation (Hoyle 1953, Lynden-Bell 1973, Rees 1976, Silk 1977), to magnetically-limited fragmentation (Mestel 1965, 1985), to turbulence-induced fragmentation (Scalo 1985,1990; Larson 1995; Elmegreen & Efremov 1997; Truelove et al. 1998; Falgarone 2002; Padoan & Nordlund 2002; Klein et al. 2003), to wind-limited mass infall (Shu & Terebey 1984, Shu et al. 2000).

Under local Galactic conditions, star formation occurs at an overall rate that is more than two orders of magnitude lower than the natural rate of free-fall collapse (Zuckerman & Evans 1974). Moreover, stars condense only in the densest, darkest regions known as molecular cloud cores (Evans 1999; Lada & Lada 2003). The general inefficiency of star formation suggests a broad framework in which interstellar magnetic fields play a crucial role (Mestel 1965, 1985; Spitzer 1968; Mouschovias 1976; Shu, Adams, & Lizano 1987).

The discriminant is the projected mass per unit area Σ loaded on field lines of strength B. We define a dimensionless mass-to-flux ratio (Nakano & Naka-

E. Corbelli et al. (eds.), The Initial Mass Function 50 Years Later, 401–410.

mura 1978; Basu & Mouschovias 1994; Shu & Li 1997):

$$\lambda \equiv \frac{2\pi G^{1/2}\Sigma}{B}. \tag{1}$$

A region is supercritical, capable of continued gravitational collapse, if $\lambda > 1$; it is subcritical, incapable of continued gravitational collapse, if $\lambda < 1$. The overall inefficiency of star formation can then be understood if the bulk of molecular clouds (i.e., their envelopes) are subcritical. The alternative suggestion – that molecular clouds are sustained against gravitational collapse by supersonic turbulence alone (e.g., Boldyrev, Nordlund, & Padoan 2002) – is undercut by numerical simulations that show supersonic turbulence, magnetized or not, is highly dissipative and cannot support molecular clouds for many free-fall times without continuous local driving (Heitsch,MacLow, & Klessen 2001; Ostriker, Stone, & Gammie 2001; Li & Nakamura 2004).

Zeeman measurements show that modern-day GMCs have near-critical levels of magnetization (Crutcher, Heiles, & Troland 2003). Shu et al. (1999) argued that this is probably no coincidence. Highly subcritical clouds are too non-self-gravitating to become molecular clouds; they are present in galaxies as H I clouds. On the other hand, highly supercritical clouds are too vulnerable to gravitational collapse; they have long since disappeared to become the interiors of stars. McKee (1989) made the important point that the ultraviolet photons associated with the interstellar radiation field suffice to keep regions with less than 4 mag of visual extinction, i.e., the envelopes of molecular cloud cores, too highly ionized to permit appreciable ambipolar diffusion. Evolution to star-forming capability can occur only in dense cores with visual extinction greater than this level (Johnstone, DiFrancesco, & Kirk 2004).

Lizano & Shu (1989, see also Shu et al. 1999) outlined a bimodal process to obtain supercritical cores. In the distributed mode of star formation, ambipolar diffusion produces small, well-separated, quiescent, cores. In the cluster mode, cloud-cloud collisions along field lines produces large, turbulent, cores and crowded conditions of star formation. Molecular-cloud turbulence can accelerate the rate of star formation in the distributed mode, both in concentrating matter during the dissipation of turbulence (Myers & Lazarian 1998, Myers 1999) and in enhancing the effective speed of ambipolar diffusion by the effects of fluctuations (Fatuzzo & Adams 2002, Zweibel 2002).

Mouschovias (1976) made the intriguing suggestion that magnetic tension in a magnetized cloud might be able to hold up the envelope, preventing it from joining the mass of the cloud core that collapses to the center to form the central star. Despite initial enthusiasm for this idea to define stellar masses (e.g., Shu 1977), subsequent collapse calculations of supercritical clouds (or the parts of them that are supercritical) showed that the original proposal based on curvature arguments was not well-founded (Galli & Shu 1993a,b; Li &

Shu 1997; Allen et al. 2003a,b). Shu, Li, & Allen (2004; hereafter SLA) considered a modified form of the question for models where the cloud cores are supercritical but the envelopes are subcritical.

By a final-state analysis, SLA found that magnetic levitation can stop cloud infall only if the star traps essentially all its original interstellar magnetic flux. The resulting stellar magnetic fields are then of order 10 megagauss. Mestel & Spitzer (1956) recognized long ago that field freezing would predict stars at birth with surface magnetic fields much larger than observationally plausible. They also pointed out (Mestel 1965, 1985; Spitzer 1968) that conservation of angular momentum in the gravitational collapse of stars from interstellar clouds would lead to absurd rotational velocities of the final objects, again contrary to the observational evidence. They proposed that a solution be found to link these two problems via magnetic braking and field slippage. We believe that magnetic reconnection of the type contemplated by Galli & Shu (1993b, see also Mestel & Strittmatter 1967) is the actual agent which eliminates the implied split monopole trapped by the central object.

2. Infall and Outflow

In addition to the final-state analysis, SLA performed time-dependent, axisymmetric, simulations for a singular isothermal sphere (SIS) with isothermal sound speed a, threaded initially for a uniform magnetic field B_0 in the z direction (see also Allen et al. [2003a,b]). The initial state thus has an equatorial radius dividing core and envelope:

$$r_0 = \frac{\pi a^2}{G^{1/2} B_0}, \tag{2}$$

and core mass linked on the corresponding flux tube:

$$M_0 = \frac{\pi^2 a^4}{G^{3/2} B_0}. \tag{3}$$

SLA initiated an inside-out collapse at $t = 0$ by adding a small seed mass in the central cell of the calculation.

The mass infall rate at small $\tau \equiv at/r_0$ is close to the unmagnetized SIS value. For $\tau > 1$, as the wave of expanding infall engulfs ever more subcritical envelope material, the infall rate declines steadily. Figure 1 depicts the flow in the meridional plane at $\tau = 1.0$ and 2.5. For each frame, a split monopole emerges from the central cell, which pushes out the field lines threading an inflowing pseudodisk before the split monopole fields straighten to attach to the imposed background fields. The fields threading the midplane of the configuration, in turn, progressively push on their neighbors radially farther out to give the magnetic tension forces that suspend the outer envelope against the part of

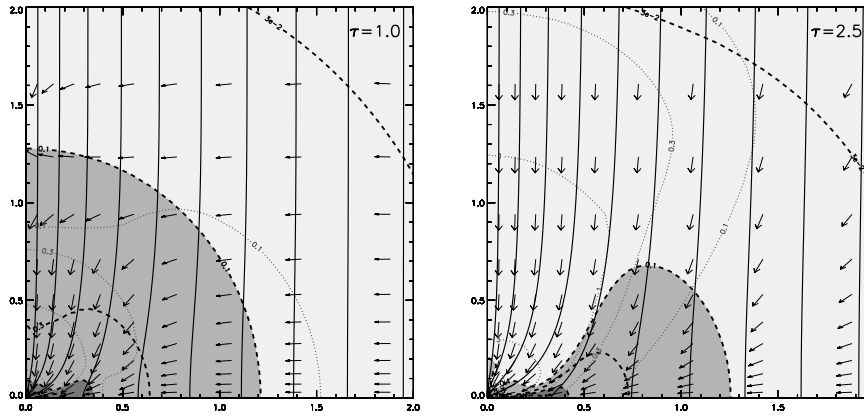

Figure 1. The infall flow direction (unit arrows) and magnetic field lines (solid curves) in the meridional plane at a dimensionless times $\tau \equiv at/r_0 = 1.0$ and 2.5. Distances (axes), isodensity contours (heavy dashed curves), and isovelociy contours (light dotted curves) are plotted with r_0, M_0/r_0^3, and a as the units of time, density, and speed. At $\tau = 1$, an infalling pseudodisk is apparent at small radii along the midplane. At large distances from the origin, a motion occurs primarily toward the magnetic axis, which carries field lines almost cylindrically to replace those that have been pinched inward by the point source at the center. At $\tau = 2.5$, the inward bunching of field lines has grown sufficiently to prevent much further cylindrical concentration of field lines, and the gas flow becomes more nearly along field lines. As a consequence, a near-vacuum region forms close to the magnetic axis as most of the material above the midplane drains onto the pseudodisk. An X-wind finally cutting off infall at $\tau = 2.5$, which would be consistent with the observed shapes of bipolar outflow cavities, would result in a stellar mass equal to 1/3 of the core mass M_0 (from SLA).

the gravity of the central mass point and the pseudodisk that is not resisted by the gas-pressure gradient.

The strong sheet current driven by the reversal of field lines across the midplane of a split monopole will dissipate in the presence of finite resistivity, which was not included in SLA's simulations. Once the long lever arms associated with the trapped interstellar flux have been destroyed, Keplerian disks can form because of the centrifugal barrier encountered by infalling rotating matter. The elimination of direct infall onto the surface of a star with its accompanying accretion shock will cease to pile up material of ever higher specific entropy onto the surface of the protostar (see Stahler, Shu, & Taam 1980), and a surface convection zone may result. This surface convection zone should combine with stellar rotation to operate a stellar dynamo (Parker 1979). Off the surface of the star, the dynamo-generated stellar fields will generally have a dipole or higher multipole structure (Mohanty & Shu 2004). The interaction of these dynamo-driven fields with the surrounding accretion disk, and the subsequent opening of the stellar field lines (or the simple pressing of the remnant

interstellar field lines against the magnetopause) can then create an X-wind (Shu et al. 1988, 1994, 2000). In summary, newly formed stars do not need 10 megagauss fields to halt the inflow of gravitational collapse. Surface fields of a few kilogauss, when combined with the rapid rotation from an adjoining accretion disk, suffice to provide dynamic levitation (a physical blowing away) of cloud envelopes.

Putting everything together, therefore, we suppose that 1/2 of the core mass M_0 will have dropped into the central regions before an X-wind can effectively halt the infall (see caption to Fig. 1). Of this 1/2, only 2/3 has ended up on the star (1/3 has come out as an X-wind); thus, $M_* = (2/3)(1/2)M_0 = M_0/3$. The entire description would then lend physical content to the observational definition that the transition from Class 0 to Class I marks the end of the phase of major infall in protostellar evolution (André, Ward-Thompson, & Barsony 1993).

2.1 Distribution of Core Masses

Recently, Motte, André & Neri (1998), Testi & Sargent (1998), and Motte et al. (2001) have found that the mass distributions of cloud cores as mapped by dust emission in turbulent molecular clouds resemble the empirical initial mass function (IMF) of newly formed stars (Salpeter 1955, Scalo 1986). The weighting of cloud cores toward small (typically solarlike) masses instead of toward large masses (typically thousands of $M_\odot$) as in cloud clumps is particularly striking.

Lada & Lada (2003; see also Lefloch et al. 1998, and Sandell & Knee 2001) make the interesting suggestion that outflows may transform the mass-spectrum of cloud clumps, which resembles the mass distribution of embedded clusters, to the mass-spectrum of cloud cores, which resembles the mass distribution of stars. In what follows, we suggest a mechanistic process for performing such a task in a statistically invariant way, particularly in the clustered mode of star formation, if ambipolar diffusion plus turbulent decay form cloud cores and outflows provide the rejuvenating source of the turbulence present in star-forming clouds.

2.2 Initial Mass Function

The processes described in this paper allow us to compute the stellar IMF (see also Silk 1995 and Adams & Fatuzzo 1996). First, we consider the contribution lent by turbulent velocities v to the support of molecular clouds. At a heuristic level, we imagine that v can be added in quadrature to the isothermal sound speed a in formulae that involve the gravitational constant G (e.g., Stahler, Shu, & Taam 1980; Shu et al. 1987). For even greater simplicity, we

use v below to mean the turbulent velocity when the turbulence is supersonic, and we substitute a for v when that turbulence is subsonic.

We further assume that the mass of magnetized molecular-cloud material with turbulent velocity between v and $v + dv$ in 1-D is given by the power-law distribution suggested by the swept-up mass in bipolar outflows (Masson & Chernin 1992, Li & Shu 1996, Lada & Fich 1996),

$$\mathcal{M}(v)\,dv \propto v^{-2}\,dv. \tag{4}$$

To avoid divergence of the integrated mass at very small v, we cut off the distribution (4) when v becomes smaller than the thermal line-width a, noting that the important applications occur at $v < 1$ km s^{-1}.

We also suppose that the core mass M_0 can be approximated as (see eq. [3]):

$$M_0 = \frac{m_0 v^4}{G^{3/2} B_0}, \tag{5}$$

where the coefficient m_0 has a probabilistic distribution centered about π^2 with a variance of a factor of perhaps a few. Finally, we suppose that the final stellar mass is a fraction 1/3 of M_0:

$$M_* \sim \frac{1}{3} M_0 \sim \frac{m_0 v^4}{3 G^{3/2} B_0}. \tag{6}$$

With a stellar mass-accumulation rate behaving as (2/3 times the infall rate) $\dot{M}_* \sim 2v^3/3G$ (cf. Shu et al. 1987), we get a characteristic formation time,

$$t_{\rm sf} \equiv \frac{M_*}{\dot{M}_*} \sim \frac{m_0 v}{2 G^{1/2} B_0} = \frac{m_0^{1/2} r_0}{2v}, \tag{7}$$

where we have adopted equation (2) with a and π replaced, respectively by v and $\sqrt{m_0}$ to estimate the core radius r_0.

According to Myers & Fuller (1993), stars of all masses take the same time, $\sim$ a few times 10^5 yr, to form once gravitational collapse starts. Applied to equation (7), this observation implies that B_0 scales directly as v. With $B_0 \propto v$, equation (6) becomes $M_* \propto v^3$, and the mass of stars formed from a cumulative fraction F of molecular cloud cores with stellar masses between M_* and $M_* + dM_*$ is now given by

$$M_* \mathcal{N}(M_*)\,dM_* = \frac{F}{3} \mathcal{M}(v)\,dv \propto M_*^{-4/3}\,dM_*. \tag{8}$$

Eq. (8) corresponds to Salpeter's (1955) IMF for low- and intermediate-mass stars if we take the liberty of approximating 1.35 by $4/3$.

Departures from a $-4/3$ power law in the observed IMF may appear at the highest stellar masses. An exponent for $M_* \mathcal{N}(M_*)$ steeper than $-4/3$ can

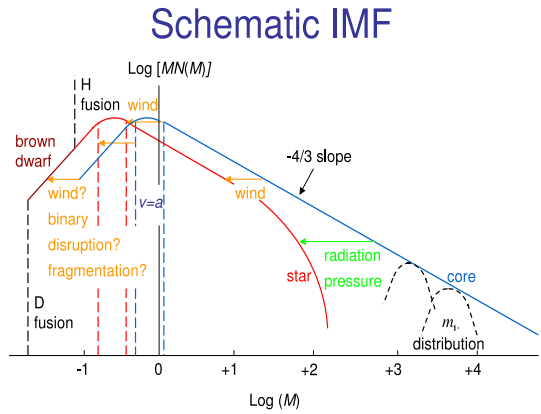

Figure 2. The distribution $M\mathcal{N}(M)$ plotted schematically for cloud cores and young stars against mass M in a log-log format. The unit of mass is solar masses, and the vertical scale is arbitrary. Cloud cores of given $v^4/G^{3/2}B_0$ have a statistical distribution of masses as indicated by the two bell-functions at large core masses, because of the variation of the coefficient m_0. The convolution of a bell distribution with a $-4/3$ power-law distribution of $v^4/G^{3/2}B_0$ produces the solid curve labeled by "core." This distribution reaches a natural peak when v equals the thermal sound speed a, which itself has a range of values indicated schematically by the two vertical dashed lines.

arise at large stellar masses because radiation pressure acting on dust grains aids YSO winds to reduce M_* as a fraction of the initial core mass M_0 (Wolfire & Cassinelli 1987, Jijina & Adams 1996). If this interpretation is correct, the non-power-law features in the stellar IMF contain clues on how stars help to limit their own masses by blowing away cloud material that might have otherwise fallen gravitationally into the stars (cf. Adams & Fatuzzo 1996). Figure 2 gives a schematic depiction of the ideas of this section.

2.3 Embedded Cluster Formation

The above derivation of the IMF formally seems to hold only for the distributed mode of starbirth, where competitive accretion does not occur. But outflows have a better chance of being the dominant source of turbulence in embedded clusters. Moreover, the sometimes evoked picture of protostars growing by Bondi-Hoyle accretion as they move freely in a background of more-or-less smooth clump gas may be flawed. Stars have to grow by gravitational collapse of small dense cores that are themselves self-gravitating substructures in the cloud clump. The cores' gravitational potential form local minima that are sharper than the large bowl representing the smoothed potential of the clump and associated embedded cluster. The tidal forces of the latter

will not rip asunder the small cores if their mean densities are appreciably larger than the mean density of the background clump/cluster gas (which is the so-called Roche criterion).

The mean density inside a *sphere* of radius r_0 of a uniformly magnetized SIS is given by

$$\bar{\rho}_{\rm core} = \frac{2a^2 r_0/G}{4\pi r_0^3/3} = \frac{3B_0^2}{2\pi^3 a^2}. \quad (9)$$

For $a = 0.2$ km s^{-1} and $B_0 = 30$ μG, $\bar{\rho}_{\rm core}$ has a numerical value 1.1×10^{-19} g cm^{-3} $\approx 1.6 \times 10^3$ M$_\odot$ pc^{-3}. The actual part of the core that forms a star is several times denser yet, which is larger than the mean density of any observed clump forming an embedded cluster in the local GMCs of our Galaxy, except perhaps for the central regions of the very densest clumps (Lada & Lada 2003, Table 1). In the turbulent central regions of very dense clumps, individual small cores may merge, yielding the large cores that give rise to massive stars.

As long as the growing protostar is trapped by the local potential minimum of its parent core, the situation will resemble the case of isolated star formation. Sooner or later, such a protostar will develop an X-wind and begin to blow away its placental core. As an extreme, we may think of a turbulent clump which is supercritical everywhere as *completely* packed with cores, $F = 1$, with no surrounding "common envelope." In that case, the efficiency of wind-limited star formation for the clump is the same as the average efficiency for a typical core, which we have taken to be 1/3 (see eq. [6]). It is then interesting to note that the maximum star-formation efficiency deduced by Lada & Lada (2003, Table 2) for embedded star clusters is indeed 33%.

References

Adams, F. C., & Fatuzzo, M. 1996, ApJ, 464, 256

Allen, A., Shu, F. H., & Li, Z.-Y. 2003a, b, ApJ, 599, 352, 363

André, P., Ward-Thompson, D., & Barsony, M. 1993, ApJ, 406, 122

Basu, S., & Mouschovias, T. 1994, ApJ, 432, 720

Boldyrev, S., Nordlund, A., & Padoan, P. 2002, ApJ, 573, 678

Crutcher, R. M., Heiles, C., & Troland, T. H. 2003, in Turbulence and Magnetic Fields in Astrophysics, Lecture Notes in Physics, 614, 155

Elmegreen, B. G., & Efremov, Y. N. 1997, ApJ, 480, 235

Evans, N. J. 1999, ARAA, 37, 311

Falgarone, E. 2002, in Infrared and Submillimeter Space Astronomy, ed. M. Giard, J. P. Bernard, A. Klotz, & I. Ristorcelli (EDP Sciences), 87

Fatuzzo, M., & Adams, F. C. 2002, ApJ, 570, 210

Galli, D., & Shu, F. H. 1993a, b, ApJ, 417, 220, 243

Heitsch, F., MacLow, M., & Klessen, R. S. 2001, ApJ, 547, 280

Hoyle, F. 1953, ApJ, 118, 513

Jijina, J. & Adams, F. C. 1996, ApJ, 462, 874

Johnstone, D., DiFrancesco, J, & Kirk, H. 2004, ApJ, 611, L45

Klein, R. I. et al. 2003, Rev. Mex. de Astron., 15, 92
Lada, C. J., & Fich, M. 1996, ApJ, 459, 638
Lada, C. J., & Lada, E. A. 2003, ARAA, 41, in press
Larson, R. B. 1995, MNRAS, 272, 213
Lefloch, B. et al. 1998, A&A, 334, 269
Li, Z. Y., & Nakamura, F. 2004, ApJ, 609, L83
Li, Z. Y., & Shu, F. H. 1996, ApJ 472, 211
Li, Z. Y., & Shu, F. H. 1997, ApJ, 475, 237
Lizano, S., & Shu, F. H. 1989, ApJ, 342, 834
Lynden-Bell. D. 1973, in Dynamical Structure and Evolution of Stellar Systems, ed. G. Contopoulos et al. (Geneva Observatory), 131
Masson, C. R., & Chernin, L. M. 1992, ApJ, 387, L47
McKee, C. F. 1989, ApJ, 345, 782
Mestel, L. 1965, QJRAS, 6, 161
Mestel, L. 1985, in Protostars and Planets II, eds. D. C. Black & M. S. Matthews (Tucson: University of Arizona Press), 320
Mestel, L., & Spitzer, L. 1956, MNRAS, 116, 503
Mestel, L., & Strittmatter, P. A. 1967, MNRAS, 137, 95
Mohanty, S., & Shu, F. H. 2004, ApJ, in preparation
Motte, F., André, P., & Neri 1998, A&A, 336, 150
Motte, F., André, P., Ward-Thompson, D., & Bontemps, S. 2001, A&A, 372, 41
Mouschovias, T. Ch. 1976, ApJ, 207, 141
Myers, P. C., & Fuller, G. A. 1993, ApJ, 402, 635
Myers, P. C., & Lazarian, A. 1998, ApJ, 507, L157
Nakano, T. 1979, PASJ, 31, 697
Nakano, T., & Nakamura, T. 1978, PASJ, 30, 671
Ostriker, E. C., Stone, J. M., & Gammie, C. F. 2001, ApJ, 546, 980
Padoan, P., & Nordlund, A. 2002, ApJ, 576, 870
Parker, E. N. 1989, Cosmical Magnetic Fields (Oxford University Press)
Rees, M. J. 1976, MNRAS, 176, 483
Salpeter, E. E. 1955, ApJ, 121, 161
Sandell, G., & Knee, L. 2001, ApJ, 546, L49
Scalo, J. M. 1986, in Fund. Cosmic Phys., 11, 1
Scalo, J. M. 1985, in Protostars & Planets II, ed. D. C. Black & M. S. Matthews (Tucson: University of Arizona Press), 201
Scalo, J. M. 1990, in Physical Processes in Fragmentation and Star Formation, ed. R. Capuzzo-Dolcetta, C. Chiosi, & A. Di Fazio (Dordrecht: Kluwer), 151
Shu, F. H. 1977, ApJ, 214, 488
Shu, F. H., Adams, F. C., & Lizano, S. 1987, ARAA, 25, 23
Shu, F. H. et al. 1999, in The Origin of Stars and Planetary Systems, ed. C. Lada & N. Kylafis (Dordrecht: Kluwer), 193
Shu, F. H., Lizano, S., Ruden, S. P., & Najita, J. 1988, ApJ, 328, L19
Shu, F. H., & Li, Z. Y. 1997, ApJ, 475, 251
Shu, F. H., Li, Z. Y., & Allen, A. 2004, ApJ, 601, 930 (SLA)
Shu, F. H. et al. 1994, ApJ, 429, 781

Shu, F. H. et al. 2000, in Protostars & Planets IV, ed. Mannings, V., Boss, A. P., & Russell, S. S. (Tucson: University of Arizona Press), 789
Silk, J. 1977, ApJ, 214, 152
Silk, J. 1995, ApJ, 438, L41
Spitzer, L. 1968, in Nebulae and Interstellar Matter, ed. B. M. Middlehurst & L. H. Aller (Chicago: University of Chicago Press), 1
Stahler, S. W., Shu, F. H., & Taam, R. E. 1980, ApJ, 241, 637
Testi, L., & Sargent, A. I. 1998, ApJ, 508, L91
Truelove, J. K. et al. 1998, ApJ, 495, 821
Wolfire, M. G., & Cassinelli, J. P. 1987, ApJ, 319, 850
Zuckerman, B., & Evans, N. J. 1974, ApJ, 192, L149
Zweibel, E. G. 2002, ApJ, 567, 962

Figure 3. Frank Shu lighting the 80th candle.

A CLASS OF IMF THEORIES

Fred C. Adams
Physics Department, University of Michigan, Ann Arbor, MI 48109, USA
fca@umich.edu

Abstract This paper discusses a class of models for the initial mass function (IMF) for stars forming within molecular clouds. In simplest version of this theory, stars help determine their masses through the action of stellar outflows. Using this concept, we calculate a transformation between the initial conditions in molecular clouds and final stellar masses. Other transformations can be derived and treated similarly. For a given transformation, each set of distributions of initial conditions predicts a corresponding IMF. In the limit in which many independent physical variables determine stellar masses, the central limit theorem implies that the IMF approaches a log-normal form. In general, this extreme limit is not fully realized and the IMF retains tails at both the high and low mass ends of the distribution. This formulation shows that the current paradigm of star formation produces an IMF that is roughly consistent with observations.

1. Introduction

The initial mass function (IMF) is perhaps the most important outcome of the star formation process. A detailed knowledge of the IMF is required to understand galaxy formation, chemical evolution of galaxies, the structure of the interstellar medium, and the nature of baryonic dark matter (brown dwarfs and/or white dwarfs in the galactic halo). Although the current theory of star formation is not complete (Shu et al. 1987a), we can begin building models of the IMF. This contribution presents a class of IMF models (based on Adams & Fatuzzo 1996; hereafter AF96) for which we can conceptually divide the process that determines the IMF into two subprocesses:

[A] The spectrum of initial conditions produced by the star forming environment (molecular clouds).

[B] The transformation between a given set of initial conditions and the mass (and perhaps other properties) of the newly formed star.

The initial mass function in our galaxy has been estimated empirically. The first such determination (Salpeter 1955) showed that the number of stars with

E. Corbelli et al. (eds.), The Initial Mass Function 50 Years Later, 411–416.

masses in the range m to $m + dm$ is given by

$$f(m)\, dm \sim m^{-\mu}\, dm\,, \tag{1}$$

where $m \equiv M_*/(1M_\odot)$ and where the index $\mu \approx 2.35$ for stars in the mass range $0.4 \leq m \leq 10$. More recent work (Miller & Scalo 1979; Scalo 1986; Rana 1991; the rest of this volume) indicates that the IMF deviates from a pure power-law. The distribution becomes flatter and then turns over at the lowest stellar masses, with the turnover at m_C = 0.1 – 0.2. The IMF may become steeper at the highest stellar masses. As a working approximation, the observed IMF can be modeled with a log-normal form

$$\ln f(\ln m) = A - \frac{1}{2\langle\sigma\rangle^2}\Big\{\ln[m/m_C]\Big\}^2\,, \tag{2}$$

where A is a normalization constant, $m_C \approx 0.1 - 0.2$, and $\langle\sigma\rangle \approx 1.6$. The actual IMF has more structure than a simple log-normal form, but equation (2) provides a good reference point and can be used as a benchmark to compare with theoretical models.

2. A General Formulation of IMF Theory

In order to construct a theory of the IMF, we need to find the relationship between the distributions of the initial variables and the resulting distribution of stellar masses. The first step is to determine the transformation between the initial variables and the masses of stars. Here, we consider transformations that can be written in the general form of a product of variables

$$M_* = \prod_{j=1}^{N} \alpha_j\,, \qquad \text{so that} \qquad \ln M_* = \sum_{j=1}^{N} \ln \alpha_j\,, \tag{3}$$

where the α_j represent the variables which determine the masses of forming stars (e.g., the sound speed a, the rotation rate Ω, etc., all taken to the appropriate powers). Each variable has a distribution $f_j(\alpha_j)$ with a mean value given by

$$\ln \bar{\alpha}_j = \langle \ln \alpha_j \rangle = \int_{-\infty}^{\infty} \ln \alpha_j\, f_j(\ln \alpha_j)\, d \ln \alpha_j\,, \tag{4}$$

and a corresponding variance given by

$$\sigma_j^2 = \int_{-\infty}^{\infty} \xi_j^2 f_j(\xi_j) d\xi_j\,. \tag{5}$$

In the limit of a large number N of variables, the composite distribution (the IMF) approaches a log-normal form. This behavior is a direct consequence

of the central limit theorem (Richtmyer 1978). As long as a large number of independent physical variables are involved in the star formation process, the resulting IMF must be approximately described by a log-normal form. The departure of the IMF from a purely log-normal form depends on the shapes of the individual distributions f_j. For example, when the individual f_j have power-law tails, the composite distribution (the IMF) is described by a *gamma distribution* (see AF96) which retains power-law tails at both high and low masses. In the limit where the IMF is described to leading order by a log-normal form, however, there are simple relationships between the distributions of the initial variables and the shape parameters m_C and $\langle\sigma\rangle$ that determine the IMF. The mass scale m_C is determined by the mean values of the logarithms of the original variables α_j, i.e.,

$$m_C \equiv \prod_{j=1}^{N} \exp[\langle \ln \alpha_j \rangle] \,. \tag{6}$$

The dimensionless parameter $\langle\sigma\rangle$ determines the width of the stellar mass distribution and is given by the sum

$$\langle\sigma\rangle^2 = \sum_{j=1}^{N} \sigma_j^2 \,. \tag{7}$$

3. A Particular Theory of the IMF

This section uses the general formulation described above to construct an IMF theory based on the idea that stars, in part, determine their masses through the action of stellar outflows (Shu et al. 1987b; Lada & Shu 1990; see Arce & Sargent 2004 for recent observational evidence). Star formation takes place in molecular clouds, which are not collapsing as a whole (Zuckerman & Palmer 1974), so it makes sense to divide IMF theory into the two steps given above. The initial conditions for the star formation process are provided by smaller condensations called molecular cloud cores, which ultimately experience a phase of dynamic collapse. The flow is characterized by a well-defined mass infall rate $\dot{M} \approx a^3/G$ (Shu 1977), where a is the effective sound speed and includes contributions from turbulence and magnetic fields, i.e.,

$$a^2 = a_{\rm therm}^2 + a_{\rm mag}^2 + a_{\rm turb}^2 \,. \tag{8}$$

Notice that no mass scale appears in the problem, only a mass infall *rate* $\dot{M}$. In general, the total amount of mass available to a forming star is much larger than the final stellar mass. This feature is consistent with the finding that star formation is an inefficient process.

The cores are rotating and contain magnetic fields (see Shu, this volume). Due to conservation of angular momentum, a large portion of the infalling material fails to reach the stellar surface and collects in a circumstellar disk. An important aspect of this rotating flow is that the ram pressure is weakest along the rotational poles of the system. In this paradigm, the central star/disk system gains mass and becomes more luminous until it can generate a powerful stellar wind which breaks through the infall at the rotational poles and leads to a bipolar outflow; the star then separates itself from the surrounding molecular environment. The mechanism that generates these winds is under intense study (Shu et al. 1994) and outflows have been well studied observationally (Lada 1985). The basic working hypothesis of this IMF theory is that these outflows help separate nearly formed stars from their infalling envelopes and thereby determine, in part, the final stellar masses.

Using the idea that the stellar mass is determined when the outflow strength exceeds the infall strength, we write the transformation between the initial conditions (e.g., sound speed a and rotation rate Ω) and the final stellar properties (luminosity L_* and mass M_*) in the form

$$L_* M_*^2 = 8 m_0 \gamma^3 \delta \frac{\beta}{\alpha \epsilon} \frac{a^{11}}{G^3 \Omega^2} \, . \tag{9}$$

The parameters α, β, γ, δ, and ϵ are efficiency factors (AF96; Shu et al. 1987b). For young stellar objects, the luminosity L_* has many contributions (Stahler et al. 1980; Palla & Stahler 1990). For most the of stellar mass range, infall (material falling through the gravitational potential well of the star) provides the most important source of luminosity; the star also generates internal luminosity which becomes important at higher stellar masses. We parameterize these contributions to obtain a luminosity versus mass relation of the form

$$\widetilde{L} = L_*/(1 L_\odot) = 70 \, \eta \, a_{35}^2 \, m \, + m^4 \, , \tag{10}$$

where the first term arises from infall and the second term arises from internal luminosity. The efficiency parameter η is the fraction of the total available energy that is converted into photons and the dimensionless sound speed $a_{35} \equiv a/(0.35 \, \mathrm{km \ s^{-1}})$.

All of the input variables appearing in equation (9) have distributions of values and these individual distributions ultimately determine the composite distribution of stellar masses. As a result, if these distributions were measured precisely, equation (9) would predict the IMF. As discussed above, however, the mass distribution approaches a log-normal form to leading order. Since the individual distributions are not well measured, we can use their mean values and dimensionless widths, in conjunction with equations (6) and (7), to estimate the shape parameters in the log-normal form of the IMF. The observed distributions indicate that $m_C \approx 0.25$ and $\langle \sigma \rangle \approx 1.8$ (AF96). These values are

in reasonable agreement with those of the observed IMF (m_C = 0.1 – 0.2 and $\langle\sigma\rangle$ = 1.6) and hence this theory is consistent with observations.

4. Summary and Discussion

In this contribution, we have presented a basic working theory for the initial mass function for stars forming in molecular clouds. Although the formulation is general (§2), we have constructed a specific theory (§3) in which the transformation between initial conditions and stellar masses is accomplished through the action of stellar outflows which separate newly formed stars from their background environment. To leading order, the IMF is expected to have nearly a log-normal form; to next order, the IMF will retain power-law tails at both the high and low mass ends of the distribution. The log-normal limiting form is specified by only two shape parameters: the width $\langle\sigma\rangle$ and the mass scale m_C. In observed stellar populations, the IMF does not vary appreciably and the shape parameters have nearly the same values ($m_C \approx 0.1 - 0.2$ and $\langle\sigma\rangle \approx 1.6$). In this theory, the values of these shape parameters are specified by the distributions of the physical variables that determine stellar masses. The observed distributions of these variables, in conjunction with this theoretical formulation, imply values for the shape parameters ($m_C \approx 0.25$ and $\langle\sigma\rangle \approx 1.8$) that are in good agreement with the observed values.

A vital test of any theory is to examine its predictions, especially those that the theory was not explicitly constructed to explain. This theory makes two such predictions: **[1]** The formation of large numbers of brown dwarfs is difficult within this paradigm and hence brown dwarfs cannot provide a substantial contribution to the galactic supply of dark matter. In the limit where many physical variables conspire to produce a nearly log-normal IMF, the mass scale and width must have specific values ($m_C \approx 0.1 - 0.2$ and $\langle\sigma\rangle \approx 1.6$) to be consistent with the observed IMF. As a result, the number of stars with masses less than m_C (objects below the brown dwarf limit) is suppressed. This claim is stronger than a blind extrapolation of the observed IMF into the unknown: In the large N limit, the distribution approaches a log-normal form and there are no additional parameters to specify (other than m_C and $\langle\sigma\rangle$). Specifically, only $\sim 45\%$ of the objects and $\sim 5\%$ of the total mass resides in the brown dwarf portion of the population. Brown dwarfs do not dominate the mass budget and are not a significant constituent of the galactic dark matter. (If brown dwarfs contribute to the mass of the galactic halo, they must arise from a population with an IMF markedly different from that of field stars.) Note that recent observational surveys (e.g., Liebert et al. 1999; Tej et al. 2002) indicate that the brown dwarf population (by number) is roughly comparable to that of ordinary stars (in agreement with this prediction). **[2]** This theory also makes a prediction for the time scale for star formation. The infall collapse time is

about 10^5 yr (and varies by only a factor of 2) over the entire range of stellar masses. Although this prediction remains to be definitively confirmed or falsified, observations show some indication for a collapse time of order 10^5 yr (e.g., Visser et al. 2002; Myers & Fuller 1992).

Finally, we note that the formulation presented here (§2) can be applied to any proposed transformation between initial conditions and final stellar masses (not just the outflow model used in §3). For any such formula (e.g., see the chapter by Shu in this volume), the theoretical values of the mass scale m_C and total width $\langle\sigma\rangle$ can be determined from the observed distributions through equations (6) and (7), and must be consistent with the mass scale and width of the observed IMF.

References

Adams, F.C., & Fatuzzo, M. 1996, ApJ, 464, 256 (AF96)
Arce, H.G., & Sargent, A.I. 2004, ApJ, in press
Lada, C.J. 1985, ARA&A, 23, 267
Lada, C.J., & Shu, F.H. 1990, Science, 1111, 1222
Liebert, J. et al., 1999, in From Extrasolar Planets to Cosmology: The VLT Opening Symposium, ed. J. Bergeron & A. Renzini (Berlin: Springer Verlag), p. 505
Miller, G.E., & Scalo, J.M. 1979, ApJ Suppl., 41, 513
Myers, P.C., & Fuller, G.A. 1992, ApJ, 396, 631
Palla, F., & Stahler, S.W. 1990 ApJ, 360, L47
Rana, N.C. 1991, ARA&A, 29, 129
Richtmyer, R.D. 1978, Principles of Advanced Mathematical Physics (New York: Springer-Verlag)
Salpeter, E.E. 1955, ApJ, 121, 161
Scalo, J.M. 1986, Fund. Cos. Phys., 11, 1
Shu, F.H. 1977, ApJ, 214, 488
Shu, F.H., Adams, F.C., & Lizano, S. 1987a, ARA&A, 25, 23
Shu, F. H., Lizano, S., & Adams, F.C. 1987b, in Star Forming Regions, IAU Symp. No. 115, ed. M. Peimbert & J. Jugaku (Dordrecht: Reidel), p. 417
Shu, F.H. et al., 1994, ApJ, 429, 781
Stahler, S.W., Shu, F.H., & Taam, R. 1980, ApJ, 241, 63
Tej, A., et al., 2002, ApJ, 578, 523
Visser, A.E., Richer, J.S., & Chandler, C.J. 2002, AJ, 124, 2756
Zuckerman, B., & Palmer, P. 1974, ARA&A, 12, 279

AN EFFECTIVE INITIAL MASS FUNCTION FOR GALACTIC DISKS

David Hollenbach[1], Antonio Parravano[2] and Christopher F. McKee[3]
[1]*NASA Ames Research Center, MS 245-3, Moffett Field, CA, 94035-1000, USA*
[2]*Universidad de Los Andes, Centro De Física Fundamental, Mérida 5101a, Venezuela*
[3]*University of California, Physics and Astronomy Dept., Berkeley, CA, 94720, USA*
hollenbach@ism.arc.nasa.gov, parravan@ula.ve, cmckee@astro.berkeley.edu

Abstract We propose a simple analytic form for the effective galactic initial mass function (IMF), $\psi(m)$, which represents the IMF averaged over the age of the galactic disk. The shape of $\psi(m)$ is determined by only three parameters set by observational constraints: the slope γ of the IMF at low mass, the slope $-\Gamma$ of the IMF at high mass, and a characteristic mass $m_{\rm ch}$ where the IMF turns over. We assume that the star formation rate in a galaxy can be expressed as the product of $\psi(m)$ and a time and space dependent rate $\dot{\varsigma}_{*T}$. We determine $\langle\dot{\varsigma}_{*T}\rangle$, the time-averaged value of the star formation rate, from the observed surface density of M dwarfs. We determine $\dot{\varsigma}_{*T}$, the current rate, from the current high-mass star formation rate, which is inferred from the rate of galactic ionizing photon production. From the effective IMF and the star formation rates we derive a number of interesting parameters at the solar circle, such as the fractional number of brown dwarfs and high-mass stars, the average mass of a star, the mass of stars formed per high-mass star, the fraction of the initial stellar mass that is returned to the ISM during the age of the Galaxy, and the ratio of current star formation rate to the rate averaged over the life of the Galaxy.

1. Introduction

It is impressive that after half a century, the Salpeter (1955) Initial Mass Function (IMF) is still the accepted IMF for intermediate and high-mass stars and his global statements derived from his IMF are still basically correct. In that paper, Salpeter fit a power law to what he called the "original mass function" from about 0.3 $M_\odot$ to high-mass stars, and then integrated that mass function over the low mass stars that live longer than the current Galaxy age as well as the high-mass stars that die in times shorter than the galactic age to arrive at the following conclusions. (i) "The total mass which has been in the form of main sequence stars but has taken on different form by now is of the

E. Corbelli et al. (eds.), The Initial Mass Function 50 Years Later, 417–424.

same order of magnitude as the total mass of present stars." (ii) If the dead stars generally lead to white dwarfs, then roughly 10% of existing stars should be white dwarfs. (iii). "An appreciable fraction of the interstellar gas present has at some time passed through the interior of stars" (he then pointed out that if this were true, then it supported Hoyle's (1946) theory that suggested that the chemical elements were formed in the interior of stars).

Since the pioneering work by Salpeter (1955), the IMF has been derived in a variety of systems such as clusters of different ages, field stars, the galactic bulge, globular clusters, and nearby galaxies. Scalo (1998) and Chabrier (2003) have provided recent reviews of the IMF (see also their contributions in this volume). The major new discovery concerning the IMF in recent years is that it turns over at about 0.3 $M_\odot$. Therefore, the pure power law suggested by Salpeter must be modified at low mass.

A number of workers have suggested analytic fits to the empirically-derived IMF including this low mass turnover (e.g., Miller & Scalo 1979, Larson 1986, Scalo 1986, Adams & Fatuzzo 1996, Kroupa 2001, Chabrier 2001, Elmegreen 2004). In general, these fits involve either power law or log-normal forms, motivated by theoretical considerations of what forms nature may produce. A single pure log normal can be constructed that fits quite well at low mass (e.g., Miller & Scalo 1979, Scalo 1986, Chabrier 2001), but the fit fails at high mass, where a power law is preferred (as discussed by these authors). The recent Kroupa (2001) fits involve 3 or 4 power law segments.

We propose a simple single analytic form that becomes a power law with characteristic slope γ and $-\Gamma$ in the limits of low mass and high mass respectively, and that smoothly transitions from one to the other around a characteristic mass $m_{\rm ch} \sim 0.24$ (we use lower case m to denote stellar masses in solar units). These are the fundamental three parameters of our IMF; the other two parameters, the lower and upper mass cutoffs, are common to all IMFs. On theoretical grounds, one expects that there will be a lower limit to the mass of a star set by opacity effects; Low & Lynden-Bell (1976) estimate that this occurs at about 0.075 $M_\odot$. This lower cutoff has no appreciable effect on quantities integrated over our effective IMF.

We use the term "effective IMF" to mean the Initial Mass Function of stars uncorrected for unresolved binaries (so that these systems are treated as a single star with an effective mass) averaged over the Galactic disk. We make three important assumptions: The first assumption is the weak form of the hypothesis of a universal IMF. The strong form of this hypothesis is that all newly formed stars are drawn from the same IMF. However, it is possible that the IMF is affected by the physical conditions in the star-forming region. The weak form of the universal IMF hypothesis is that the IMF approaches a universal form when averaged over a significant volume or period of time. Our second assumption is that IMF has not changed significantly over the lifetime

of the disk of the Galaxy (although the *rate of star formation* may have), and that the time-averaged IMF at the solar circle is about the same as that spatially averaged over the Galactic disk. Finally, we assume that the IMF is a smooth function of stellar mass that is characterized by a relatively small number of parameters. There are no known physical processes that would make the IMF complex, particularly after averaging over the disparate physical conditions in Galactic star-forming regions.

Our approach is different from the classical approach of inferring the IMF at each mass directly from the data (e.g., Scalo 1986). In particular, we infer the IMF of intermediate-mass stars by interpolation between the PDMF of low-mass stars and the IMF of massive stars, thereby avoiding distortions of the Present Day Mass Function (PDMF) due to time variations in the star formation rate over the lifetime of the intermediate mass stars. Our approach is similar to that of Kroupa (2001), who introduced a three power-law fit to his "universal" IMF; our form is simpler in that it has one less characteristic mass and is more amenable to analytic computation. Details of our methods can be found in Parravano, McKee, & Hollenbach (2004, hereafter PMH04).

2. The Proposed Effective IMF of the Galactic Disk

We propose the following simple analytic form for the effective IMF $\psi(m)$ (the probability that the initial mass of a star lies between m and $m + d\ln m$) of the galactic disk:

$$\psi(m) = k\, m^{-\Gamma} \left\{1 - \exp\left[-(m/m_{\rm ch})^{\gamma+\Gamma}\right]\right\} \qquad (m_\ell \le m \le m_u), \qquad (1)$$

with $\gamma = 0.8$, $\Gamma = 1.35$, and $m_{\rm ch} = 0.24$ for the case where we do not correct for unresolved binaries. Each of the five parameters ($m_\ell,\ m_u,\ m_{\rm ch},\ \gamma$, and Γ) has a direct physical significance. We assume that star formation is suppressed below a mass $m_\ell \simeq 0.075$ and above a mass $m_u \simeq 120$. The parameter $m_{\rm ch}$ approximately determines the position of the IMF maximum. The form of Eq. (1) is such that $\psi(m) \propto m^\gamma$ for $m << m_{\rm ch}$, and $\psi(m) \propto m^{-\Gamma}$ for $m >> m_{\rm ch}$ (the Salpeter IMF). The normalization factor k ensures that $\int_{m_\ell}^{m_u} \psi(m)\, d\ln m = 1$. Numerical evaluation for our standard effective IMF gives $1/k \simeq 11.7$ for the whole mass range (i.e. $0.075 < m < 120$). If only main sequence stars are considered (i.e. $0.075 < m < 120$), the normalization factor is $1/k_{\rm ms} \simeq 8.8$. Keep in mind that the effective IMF $\psi(m)$ represents the birth probability per logarithmic mass interval of single stellar objects plus unresolved binaries. PMH04 discuss the correction for unresolved binaries. The individual-star IMF $\psi^{\rm ind}$, which includes a correction for a binary fraction of 0.44 among main sequence stars, has $\gamma = 0.4$, $\Gamma = 1.35$, $m_{\rm ch} = 0.18$, and $1/k \simeq 23$ or $1/k_{\rm ms} \simeq 12.4$. As described below, the chosen values for the slopes γ and $-\Gamma$ are their average values inferred from the mass distributions in clusters and the local field population. The value of the cutoff mass m_u is

the maximum stellar mass inferred from observations of large clusters in the Galaxy. The parameter $m_{\rm ch}$ is derived from the surface mass distribution of field M dwarfs.

At the solar circle the average star formation rate per unit area of galactic disk per unit logarithmic mass interval is given by

$$\langle \dot{\varsigma}_*(m) \rangle \equiv \left\langle \frac{d^2 \dot{\mathcal{N}}_*(m)}{dA\, d\ln m} \right\rangle \equiv \langle \dot{\varsigma}_{*T} \rangle \psi(m), \tag{2}$$

with $\dot{\mathcal{N}}_*(m)$ the total rate of the formation of stars more massive than m, and $\langle \dot{\varsigma}_{*T} \rangle$ the average value of the star formation rate per unit area at the solar circle. For a disk age of $t_0 = 11$ Gyr, the average rate of main sequence (i.e., $m > 0.075$) stars per unit area is given by $\langle \dot{\varsigma}_{*T} \rangle_{\rm ms} \simeq 5530$ kpc^{-2} Myr^{-1}. Corrected for unresolved binaries, it is $\simeq 7760$ kpc^{-2} Myr^{-1}. The corresponding total values are $\langle \dot{\varsigma}_{*T} \rangle = (k_{\rm ms}/k) \langle \dot{\varsigma}_{*T} \rangle_{\rm ms}$, and $\langle \dot{\varsigma}_{*T} \rangle_{\rm bd} = \langle \dot{\varsigma}_{*T} \rangle - \langle \dot{\varsigma}_{*T} \rangle_{\rm ms}$. We discuss the observational constraints that led to our choices of γ, Γ, $m_{\rm ch}$, m_u, and $\langle \dot{\varsigma}_{*T} \rangle$ in the next section.

3. Observational Constraints to the IMF

Measured Slope of the IMF Versus Stellar Mass. Kroupa (2001) and Hillenbrand (2004) present summaries of observational constraints on the measured slope of the IMF versus stellar mass. Figure 1 reproduces the figure from Hillenbrand with the slope of our proposed effective IMF (heavy curve) superimposed. The dashed diagonal line corresponds to the Miller-Scalo (1979) log-normal relation while labeled lines represent other field star results in the solar neighborhood from Reid et al. (1999) and Kroupa (2001). The horizontal lines indicate the mass range over which the slope was determined, and the dots plot the slope in the middle of that range. One sees definite evidence for a power law slope close to the Salpeter value of $-\Gamma = -1.35$ at high mass ($m \gtrsim 1$), where log-normal fits fail.

Constraints from M Dwarfs and the Trapezium Cluster. Figure 2 summarizes constraints derived from the work of Zheng et al. (2001, hereafter ZFGBS01) on the PDMF of disk M dwarfs in the solar vicinity. The crosses correspond to the ZFGBS01 CMR1 data, which assumes a color magnitude relation for solar metallicity, and the filled squares correspond to the ZFGBS01 CMR2 data, which assumes a color magnitude relation that considers a vertical metallicity gradient above the plane. The error bars for the CMR1 data are not plotted but are similar to the plotted error bars for the CMR2 data. The dashed area represents the range of cluster IMFs permitted by Muench et al. (2002) models of the Trapezium K-band luminosity function.

Upper Limit of Stellar Mass. The existence of an upper limit to the mass function has been controversial; for example, Massey & Hunter (1998) suggest

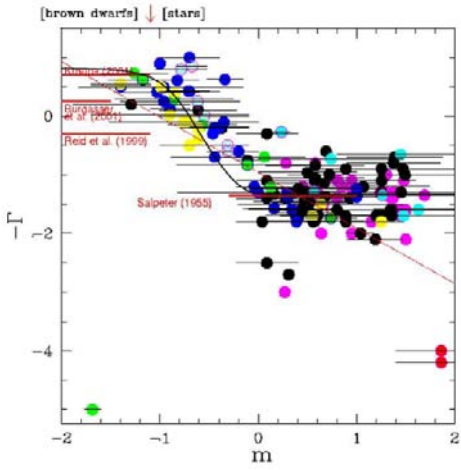

Figure 1. Hillenbrand (2004) compilation of several studies providing the IMF slope as function of the mass covered by the study. The heavy curve is the average slope (over a factor 5 in mass) of the IMF proposed in this paper [i.e. eq. (1)], which provides a good description of the composite data at all masses.

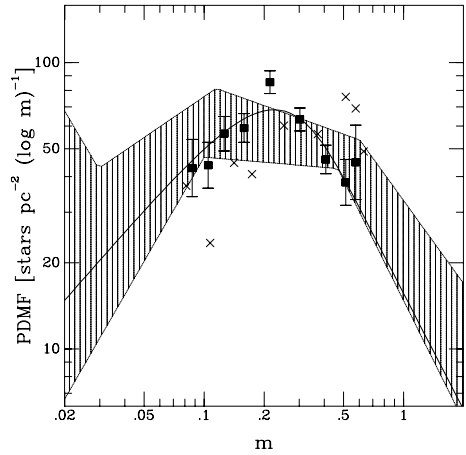

Figure 2. Mass distribution of field M dwarfs from ZFGBS01 (see text). The dashed area represents the range of cluster IMFs permitted by Muench et al. (2002) models of the Trapezium K-band luminosity function. The curve is the best-fit of equation (1) to ZFGBS01 data with assumed metallicity gradient (boxes).

that the apparent cutoff is due to the scarcity of very massive stars. This issue was addressed in a general way by McKee & Williams (1997) and Parravano et al. (2003), who showed that the cutoff is physically significant for various samples of stars in the Galaxy. Recently, Elmegreen (2000) proposed a model that shows a high-mass turndown in the IMF. For our standard model we adopt $m_u = 120$.

Rates of Star Formation. For $\gamma = 0.8$ and $\Gamma = 1.35$, the PMH04 fit (Eq. 1) to the PDMF shown in Figure 2 was made by varying $m_{\rm ch}$ and $\langle \dot{\varsigma}_{*T} \rangle_{\rm ms}\, t_0$. For a Galactic age of $t_0 = 11$ Gyr, the resulting average star formation rate over that age is $\langle \dot{\varsigma}_{*T} \rangle_{\rm ms} \simeq 5530$ kpc^{-2} Myr^{-1}. Here we use the fact that for M stars, PDMF$= \psi(m)\, t_0\, \langle \dot{\varsigma}_{*T} \rangle$.

The value of $\dot{\varsigma}_{*T}$ at present at the solar circle is derived from the star formation rate of high-mass stars, which in turn is inferred from the galactic ionizing photon production. Radio surveys of the Galaxy provide an estimate for the total ionizing photon production rate, $S_T = 2.6 \times 10^{53}$ photons s^{-1}, good to a factor of about 1.35 (McKee & Williams 1997) and in good agreement with observations of the rate of emission of ionizing photons per unit area at the Solar circle. PMH04 provide the details on how this observed rate is translated to a current (averaged over the last $\sim$ 10 Myr, the lifetime of O stars) star

formation rate of $\dot{\varsigma}_{*,\,\mathrm{ms}} \simeq 6028$ kpc^{-2} Myr^{-1}. Therefore, the ratio $b(t_0)$ of the current star formation rate in the solar neighborhood to the rate averaged over the life t_0 of the Galaxy is $b = 1.09$ for $t_0 = 11$ Gyr.

TABLE 1
Parameters Derived for the Effective IMF

Parameter	PMH04	Salpeter
number fraction of brown dwarfs[1]	0.24	
number fraction of high-mass stars[1]	0.0037	
number fraction of high-mass stars[2]	0.0049	0.0026
ratio of brown dwarfs to ms stars	0.32	
average mass (star and brown dwarfs)	0.41 $M_\odot$	
average mass of main sequence stars	0.53 $M_\odot$	0.35$M_\odot$
mass of stars formed per core collapse SN	109 $M_\odot$	135 $M_\odot$
local surface density of M stars[3]	12.2 $M_\odot$pc^{-2}	23.1 $M_\odot$pc^{-2}
local surface density of ms stars	17.9 $M_\odot$pc^{-2}	28.9 $M_\odot$pc^{-2}
surface density of white dwarfs	2.3 $M_\odot$pc^{-2}	2.5 $M_\odot$pc^{-2}
surface density of neutron stars+black holes	0.42 $M_\odot$pc^{-2}	0.45 $M_\odot$pc^{-2}
surface density of brown dwarfs	0.76 $M_\odot$pc^{-2}	
average ms star formation rate in Galaxy	1.6 $M_\odot$yr^{-1}	2.1 $M_\odot$yr^{-1}
years between Type II SN in Galaxy	69 yr	64 yr
fraction of initial stellar mass that is returned to ISM during age of Galaxy	0.36	0.28
current star formation rate/ rate averaged over age of Galaxy[3]	1.09	1

[1] This fraction is to main sequence stars and brown dwarfs. We note that the effective IMF does not count brown dwarf companions to main sequence stars. High mass stars have $m > 8$.
[2] This fraction is to just main sequence stars.
[3] Salpeter IMF normalized to produce observed rate of ionizing photons.

4. Application of the Effective IMF

Table 1 summarizes a comparison of parameters derived with our effective IMF with the predictions of the IMF that Salpeter proposed in 1955. The last 50 years have improved these numbers primarily because of better understanding of the IMF of low mass stars. In making the necessary integrations in Table 1, we have assumed that our PMH04 effective IMF (Eq. 1) is valid from $m_\ell = 0.075$ to $m_u = 120$, whereas we take the Salpeter IMF from $m_\ell = 0.1$ to $m_u = 120$. It must be emphasized that the data on brown dwarfs are not sufficiently accurate to confidently extrapolate our IMF to small brown dwarf masses. The Salpeter IMF certainly does not extrapolate, so we have omitted these numbers. However, an extrapolation of our proposed IMF does give a rough idea of the brown dwarf quantities presented in Table 1.

5. Conclusions and Summary

We derive a semi-empirical effective galactic initial mass function (IMF), which represents the IMF uncorrected for unresolved binaries and averaged over the age of the galactic disk, from observational constraints. We assume that the star formation rate in a galaxy can be expressed as the product of the IMF, $\psi(m)$, which is a smooth function of mass m (in units of $M_\odot$), and a time and space dependent rate $\dot{\varsigma}_{*T}$. The mass dependence of the proposed IMF is determined by five parameters: the low-mass slope γ, the high-mass slope $-\Gamma$, the characteristic mass $m_{\rm ch}$ at which the IMF turns over, and the lower and upper limits on the mass, m_ℓ and m_u. The chosen values for γ and Γ are their average values inferred from the mass distributions in clusters and local field stars. The value of the cutoff mass m_u is the maximum stellar mass inferred from observations of large clusters in the Galaxy. The parameters $m_{\rm ch}$ and $\langle\dot{\varsigma}_{*T}\rangle$ (the time-averaged value of the star formation rate) are derived by the best fit of $\langle\dot{\varsigma}_{*T}\rangle \times t_0 \times \psi(m)$ to the surface mass distribution of field M dwarfs. For a disk age of $t_0 = 11$ Gyr, the average value of the effective star formation rate at the solar circle is $\langle\dot{\varsigma}_{*T}\rangle_{\rm ms} \simeq 5530$ kpc^{-2} Myr^{-1}. Corrected for unresolved binaries, it is $\simeq 7760$ kpc^{-2} Myr^{-1}. The corresponding surface mass density rate for star formation is $\langle\Sigma_{*T}\rangle_{\rm ms} \simeq 2930$ $M_\odot$ kpc^{-2} Myr^{-1} for the effective IMF; it is about 10% higher after the binary correction. The value of $\dot{\varsigma}_{*T}$ at present at the solar circle is derived from the star formation rate of high-mass stars, which in turn is inferred from the galactic ionizing photon production. The corresponding star formation rate for the whole Galaxy can be obtained by multiplying these surface rates by the effective area of the galactic disk, (~ 530 kpc^2; McKee & Williams 1997 and Parravano et al. 2003). For a disk age of 11 Gyr, the ratio of the present to the mean SFR is $b(t_0) = \dot{\varsigma}_{*T}/\langle\dot{\varsigma}_{*T}\rangle = 1.09$. From the effective IMF and the average star formation rate we derive a number of interesting parameters at the solar circle such as the fractional number of brown dwarfs and high-mass stars, the average mass of a star, the mass of stars formed per high-mass star, and the fraction of the initial stellar mass that is returned to the ISM during the age of the Galaxy. The details of our derivation of the effective IMF are provided in PMH04, as is a discussion of possible small modifications to take into account the observed mass distribution of nearby ($\lesssim 20$ pc) individual stars (Reid et al. 1997, 2002; Reid 2004, this volume).

Acknowledgments The research of DH is supported in part by the Spitzer Legacy project "SINGS", that of AP by the University of Los Andes (CDCHT project C-1275-04-05-B), and that of CFM by NSF grant AST00-98365.

References

Adams, F.C. & Fatuzzo, M. 1996, ApJ, 464, 256

Chabrier, G. 2001, ApJ, 554, 1274
Chabrier, G. 2003, PASP, 115, 763
Elmegreen, B.G. 2000, ApJ, 539, 342
Elmegreen, B.G. 2004, MNRAS, 354, 367
Hillenbrand L.A. 2004, in The Dense Interstellar Medium in Galaxies, eds. S. Pfalzner, C. Kramer, C. Straubmeier & A. Heithausen (Berlin: Springer-Verlag), in press
Hoyle, F. 1946, MNRAS, 106, 343
Kroupa, P. 2001, MNRAS, 322, 231
Larson, R.B. 1986, MNRAS, 218, 409
Low, C., & Lynden-Bell, D. 1976, MNRAS, 176, 367
Massey, P., & Hunter, D.A. 1998, ApJ, 493, 180
McKee, C.F., & Williams, J.P. 1997, ApJ, 476, 114
Miller, G.E. & Scalo, J.M. 1979, ApJS, 41, 513
Muench, A.A., Lada, E.A., & Lada, C.J. 2000, ApJ 533, 358
Muench, A.A., Lada, E.A., & Lada, C.J. & Alves, J. 2002, ApJ, 573, 366
Parravano, A., Hollenbach, D.J., & McKee, C.F. 2003, ApJ, 584, 797
Parravano, A., McKee, C.F., & Hollenbach, D. 2004, in preparation (PMH04)
Reid, I.N. & Gizis, J.E. 1997, AJ, 113, 2246
Reid, I.N., Kirkpatrick, J.D., Liebert, J., et al. 1999, ApJ, 521, 613
Reid, I.N., Gizis, J.E., Hawley, S.L. 2002, AJ, 124, 2721
Salpeter, E.E. 1955, ApJ, 121, 161
Scalo, J.M. 1986, Fundamentals of Cosmic Physics, 11, 1
Scalo, J.M. 1998, in The Stellar Initial Mass Function, Proceedings of the 38th Herstmonceux Conference, ed. G. Gilmore & D. Howell. ASP Conference Series, Vol. 142, p.201
Zheng, Z., Flynn, C., Gould, A., Bahcall, J.N., & Salim, S., 2001, ApJ, 555, 393 (ZFGBS01)

Figure 3. Yervant Terzian and David Hollenbach (Cesare Chiosi smoking in the background).

COMPETITIVE ACCRETION AND THE IMF

Ian A. Bonnell
School of Physics and Astronomy, University of St Andrews, St Andrews, KY16 9SS, UK
iab1@st-and.ac.uk

Abstract Competitive accretion occurs when stars in a cluster accrete from a shared reservoir of gas. The competition arises due to the relative attraction of stars as a function of their mass and location in the cluster. The low relative motions of the stars and gas in young, gas dominated clusters results in a tidal limit to the accretion whereas in the stellar dominated cluster cores, the high relative velocities results in Bondi-Hoyle accretion. The combination of these two accretion processes produces a two power-law IMF with $\gamma \approx -1.5$, for low-mass stars which accrue their mass in the gas dominated regime, and a steeper, $\gamma \approx -2.5$, IMF for higher-mass stars that form in the core of a cluster. Simulations of the fragmentation and formation of a stellar cluster show that the final stellar masses, and IMF, are due to competitive accretion. Competitive accretion also naturally results in a mass segregated cluster and in a direct correlation between the richness of a cluster and the mass of the most massive star therein. The *knee* where the IMF slope changes occurs near the Jeans mass of the system.

1. Introduction

Star formation is a dynamical process where most stars form in a clustered environment (Lada & Lada 2003; Clarke, Bonnell & Hillenbrand 2000). In such an environment, stars and gas move in their combined potential on timescales comparable to the formation time of individual stars. Furthermore, the initial fragmentation of a molecular cloud is very inefficient (eg., Motte *et al.* 1998), such that the youngest clusters are dominated by their gas content. In such an environment, gas accretion can contribute significantly to the final mass of a star.

Stellar clusters are found to be mass segregated even from the youngest ages. The location of massive stars in the cores of clusters cannot be explained by dynamical mass segregation as the systems are too young (Bonnell & Davies 1998). A Jeans mass argument also fails as the Jeans mass in the core should be lower then elsewhere in the cluster. Mass segregation is a natural outcome of competitive accretion due to the gas inflow to the centre of the cluster potential.

E. Corbelli et al. (eds.), The Initial Mass Function 50 Years Later, 425–430.

2. Accretion in stellar clusters: two regimes

In a series of numerical experiments , we investigated the dynamics of accretion in gas-dominated stellar clusters (Bonnell *et al.* 1997, 2001a). In the initial studies of accretion in small stellar clusters, we found that the gas accretion was highly non-uniform with a few stars accreting significantly more than the rest. This occurred as the gas flowed down to the core of the cluster and was there accreted by the increasingly most-massive star. Other, less massive stars were ejected from the cluster and had their accretion halted (see also Bate, Bonnell & Bromm 2002). In a follow-up study investigating accretion in clusters of 100 stars, we discovered two different physical regimes (Bonnell *et al.* 2001a) resulting in different accretion radii, $R_{\rm acc}$, for the mass accretion rate

$$M_{\rm acc} = \rho v \pi R_{\rm acc}^2, \tag{1}$$

where ρ is the local gas density and v is the relative velocity of the gas. Firstly, in the gas dominated phase of the cluster, tides limit the accretion as the relative velocity between the stars and gas is low. The tidal radius, due to the star's position in cluster potential,

$$R_{\rm tidal} \approx 0.5 \left(\frac{M_*}{M_{\rm enc}} \right)^{\frac{1}{3}} R_*, \tag{2}$$

is then smaller than the traditional Bondi-Hoyle radius and determines the accretion rate. Accretion in this regime naturally results in a mass segregated cluster as the accretion rates are highest in the cluster core.

Once accretion has increased the mass of the stars, and consequently decreased the gas mass present, the stars begin to dominate the stellar potential and thus virialise. This occurs first in the core of the cluster where higher-mass stars form due to the higher accretion rates there.The relative velocity between the gas and stars is then large and thus the Bondi-Hoyle radius,

$$R_{\rm BH} = 2GM_*/(v^2 + c_s^2), \tag{3}$$

becomes smaller than the tidal radius and determines the accretion rates.

3. Resultant IMFs

We can use the above formulation of the accretion rates, with a simple model for the stellar cluster in the two physical regimes, in order to derive the resultant mass functions (Bonnell *et al.* 2001b). The primary difference is the power of the stellar mass in the accretion rate equation, $M_*^{2/3}$ for tidal-accretion and M_*^2 for Bondi-Hoyle accretion. Starting from a gas rich cluster with equal stellar masses, tidal accretion results in higher accretion rates in the centre of the cluster where the gas density is highest. This results in a spread of stellar mass

and a mass segregated cluster. The lower dependency of the accretion rate on the stellar mass results in a fairly shallow IMF of the form (where Salpeter is $\gamma = -2.35$)

$$dN/dM_* \propto M_*^{-3/2}. \quad (4)$$

Once the cluster core enters the stellar dominated regime where Bondi-Hoyle accretion occurs, the higher dependency of the accretion rate on the stellar mass results in a steeper mass spectrum. Zinnecker (1982) first showed how a Bondi-Hoyle type accretion results in a $\gamma = -2$ IMF. In a more developed model of accretion into the core of a cluster with a pre-existing mass segregation, the resultant IMF is of the form

$$dN/dM_* \propto M_*^{-5/2}. \quad (5)$$

This steeper IMF applies only to those stars that accrete the bulk of their mass in the stellar dominated regime, ie. the high-mass stars in the core of the cluster (see Figure 1).

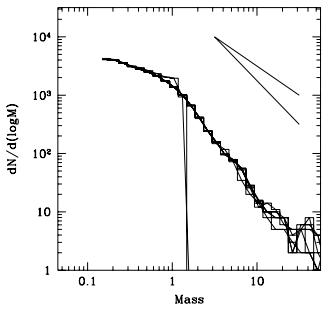

Figure 1. The IMF that results from competitive accretion in a model cluster. the two power-law IMF results from a combination of tidal accretion for low-mass stars and Bondi-Hoyle accretion for high-mass stars (BCBP 2001).

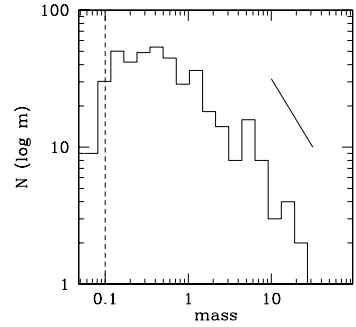

Figure 2. The IMF that results from a numerical simulation of the fragmentation of a turbulent cloud and the formation of a stellar cluster containing 419 stars. The comparison slope is for a $\gamma = -2$ IMF (BBV 2003).

4. The formation of stellar clusters

In order to asses the role of accretion in determining the IMF, we need to consider self-consistent models for the formation of the cluster. We followed the fragmentation of a 1000 $M_\odot$ cloud with a 0.5 pc radius (Bonnell, Bate & Vine 2003). The cloud is initially supported by turbulence which decays on the cloud's crossing time. As the turbulence decays, it generates filamentary

structure which act as the seeds for the subsequent fragmentation. The cluster forms in a hierarchical manner with many subclusters forming before eventually merging into one larger cluster. In all 419 stars form in 5×10^5 years. The simulation produces a field star IMF with a shallow slope for low-mass stars steepening to a Salpeter-like slope for high-mass stars (Figure 2). The stars all form with low masses and accrete up to their final masses. The stars that are in the centres of the subclusters accrete more gas and thus become higher-mass stars.

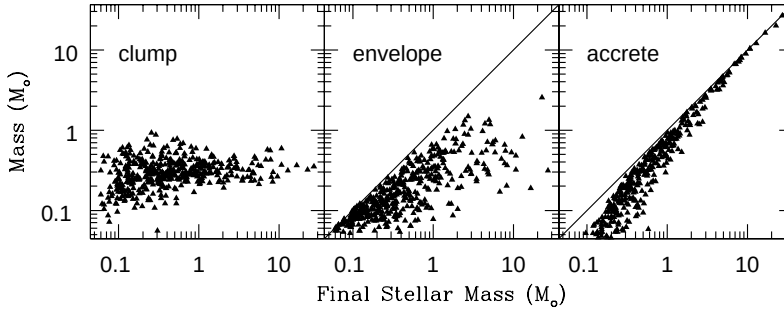

Figure 3. The relation between fragment mass (left) mass in a contiguous envelope (middle) and mass accreted from beyond the cluster (right) is plotted against final stellar mass. High-mass stars attain their mass due to competitive accretion of gas infalling into the stellar cluster (Bonnell, Vine & Bate 2004).

A careful dissection of the origin of the more massive stars reveals the importance of competitive accretion in setting the IMF. the Lagrangian nature of the SPH simulations allows us to trace the mass from which a star forms. We can therefore distribute this mass as being in one of three categories: 1) The original fragment which formed the star; 2) A contiguous envelope around the fragment until we reach the next forming star; and 3) mass which originates beyond the forming group or cluster of stars. Figure 3 shows the three contributions to the final stellar mass of the 419 stars (Bonnell, Vine & Bate 2004). We see that the initial fragment mass is generally around $0.5M_{\odot}$ and fails to account for both high-mass and low-mass stars. The contiguous envelope does a better job as it accounts for subfragmention into lower-mass stars. It still fails to explain the mass of higher-mass stars. We are thus left with accretion from beyond the forming protocluster in order to explain the existence of higher-mass stars. Thus, high-mass stars are formed due to competitive accretion of gas that *infalls* into the stellar cluster.

5. Massive stars and cluster formation

One of the predictions that we can extract from the simulations is that there should be a strong correlation between the mass of the most massive star and the number of stars in the cluster (Figure 4, Bonnell, Vine & Bate 2004). This occurs due to the simultaneous accretion of stars and gas into a forming stellar cluster. Given an effective initial efficiency of fragmentation, for every star that falls into the cluster a certain amount of gas also enters the cluster. This gas joins the common reservoir from which the most massive star takes the largest share in this competitive environment. Thus, the mass of the most massive star increases as the cluster grows in numbers of stars.

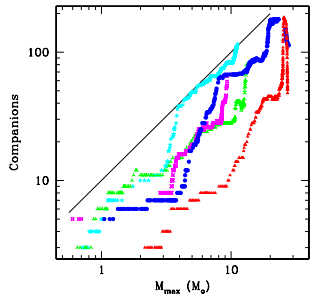

Figure 4. The number of stars in a sub-cluster is plotted against the mass of the most massive star therein(BVB 2004).

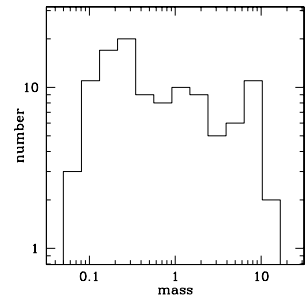

Figure 5. The IMF that results from a fragmentation of a 1000 $M_\odot$ cloud where the Jeans mass is 5 $M_\odot$..

6. What is the role of the Jeans mass?

If competitive accretion is the determining factor in setting the IMF, what role does the Jeans mass play? We saw above that the average fragment mass in which stars form is $\approx$ 0.5 $M_\odot$ while the initial Jeans mass is $= 1M_\odot$. The Jeans mass is therefore important at setting the scale of the initial fragmentation. We have run a simulation identical to the one in Bonnell, Bate & Vine (2003) except with a Jeans mass of $5M_\odot$. The resultant IMF, shown in Figure 5, is fairly shallow up to masses of $\approx 5-10M_\odot$, corresponding roughly to the Jeans mass. In Figure 2 we see that the slope of the IMF becomes steeper at $\approx 1M_\odot$, the Jeans mass in this simulation. We can thus deduce that the Jeans mass helps set the *knee* in the IMF, with lower masses determined by fragmentation and the tidal shearing of nearby stars, while higher-masses are determined by accretion in a clustered environment.

7. Conclusions

Competitive accretion is a simple physical model that can explain the origin of the initial mass function. It relies on gravitational competition for gas in a clustered environment and does not necessarily involve large-scale motions of the accretors. The two physical regimes (gas and stellar dominated potentials) naturally result in a two power-law IMF. It is probably even more important for any model of the IMF to have secondary characteristics that can be compared to observations. For example, competive accretion naturally results in a mass segregated cluster, and predicts that massive star formation is intrinsically linked to the formation of a stellar cluster. Some of the simulations reported here were performed with the UK's Astrophysical Fluid facility, UKAFF.

References

Bate, M. R., Bonnell, I. A., & Bromm, V. 2002, MNRAS, 336, 705

Bonnell, I. A., Bate, M. R., Clarke, C. J., & Pringle, J. E. 1997, MNRAS, 285, 201

Bonnell, I. A., Bate, M. R., Clarke, C. J., & Pringle, J. E. 2001, MNRAS, 323, 785

Bonnell, I. A., Bate, M. R., & Vine, S. G. 2003, MNRAS, 343, 413 (BBV)

Bonnell, I. A., Clarke, C. J., Bate, M. R., & Pringle, J. E., 1997, MNRAS, 324, 573 (BCBP)

Bonnell, I. A., & Davies, M. B. 1998, MNRAS, 295, 691

Bonnell, I. A., Vine, S. G., & Bate, M. R. 2004, MNRAS, 349, 735 (BVB)

Clarke, C. J., Bonnell, I. A., & Hillenbrand, L. A., 2000, in Protostars and Planets IV, eds. Mannings V., Boss A. P., & Russell S. S., p. 151

Lada C. J., & Lada, E. 2003, ARA&A,

Motte, F., Andre, P., & Neri, R. 1998, A&A, 336, 150

Salpeter, E. E. 1955, ApJ, 123, 666

Zinnecker, H. 1982, New York Academy Sciences Annals, 395, 226

THE DEPENDENCE OF THE IMF ON INITIAL CONDITIONS

Matthew R. Bate
School of Physics, University of Exeter, Exeter EX4 4QL, United Kingdom
mbate@astro.ex.ac.uk

Abstract Based on hydrodynamical simulations, we discuss the dependence of the initial mass function (IMF) on the initial conditions in molecular clouds and how the IMF may originate from accretion that is terminated by the dynamical ejection of objects from dense molecular cores.

1. Introduction

Recently, Bate, Bonnell & Bromm (2003) published results from the largest hydrodynamical simulation of star formation to date. The calculation followed the evolution of a 50-$M_\odot$ turbulent molecular cloud as it formed 50 stars and brown dwarfs. The resolution of the calculation was sufficient to resolve the opacity limit for fragmentation, meaning that objects with masses down to the expected cut-off in the initial mass function (IMF) at a few times the mass of Jupiter, $M_{\rm J}$, were resolved. Binaries with separations as small as 1 AU and circumstellar discs with radii $\gtrsim 20$ AU were also resolved.

The calculation produced an IMF in good agreement with the observed IMF (Figure 1, top-left panel), although the most massive star was 0.7 $M_\odot$ so only the low-mass IMF was addressed by the calculation.

2. New calculations

Over the past two years, three further calculations have been performed to test the dependence of the star formation on the initial conditions in the molecular cloud. Compared to the original calculation these calculations began with

- a cloud whose radius had been reduced so the initial cloud density was 9 times greater and, thus, the mean thermal Jeans mass in the cloud was reduced by a factor of 3 from 1 $M_\odot$ to 1/3 $M_\odot$;

E. Corbelli et al. (eds.), The Initial Mass Function 50 Years Later, 431–436.

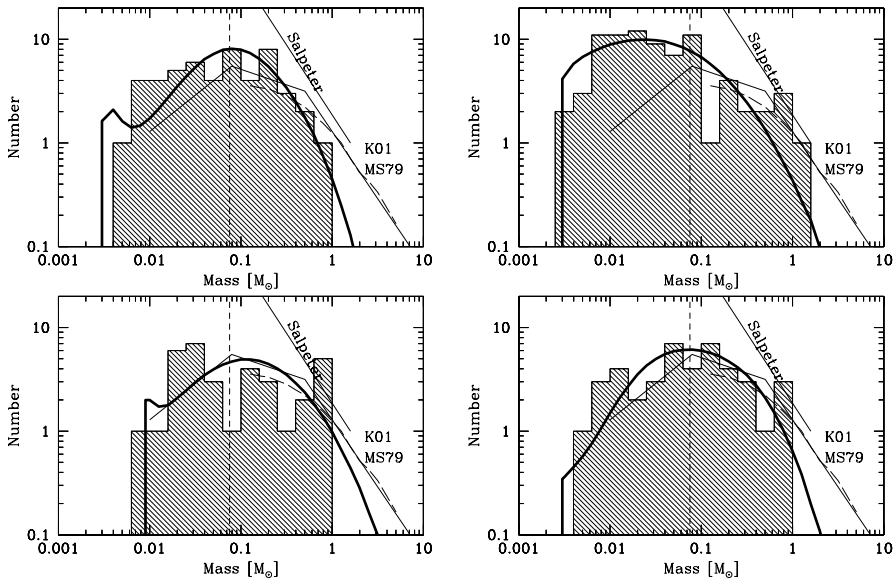

Figure 1. Comparisons of the IMFs produced by the four hydrodynamical calculations (histograms) with fits to the observed IMF (Salpeter 1955; Miller & Scalo 1979; Kroupa 2001) and the simple accretion/ejection model (thick solid lines; Section 5).

- a cloud whose metallicity had been decreased, increasing the cut-off mass associated with the opacity limit for fragmentation by a factor of 3 from $\approx$ 3 M_J to $\approx$ 9 M_J. The calculations did not model radiative transfer or metallicity explicitly. Rather, the reduced metallicity was modelled by allowing gas to depart from an isothermal equation of state at a density 9 times lower than in the original calculation;

- a cloud with a different initial turbulent power spectrum. The original calculation used a power spectrum $P(k) \propto k^{-4}$ in order to reproduce the observed linewidth-size relation of molecular clouds, $\sigma(\lambda) \propto \lambda^{1/2}$. The new calculation began with a turbulent power spectrum $P(k) \propto k^{-6}$, resulting in much more power on large-scales in the initial turbulent velocity field.

Together, these four calculations test the dependence of star formation on the mean thermal Jeans mass in a cloud (i.e., temperature and density), the metallicity of the gas, and the initial turbulent power spectrum. In this proceedings, we concentrate on the effect of these changes on the form of the IMF, although other properties such as binarity and disc properties may also be affected.

3. Results

The IMFs obtained from the four calculations are displayed in Figure 1. It is immediately apparent that the denser cloud produces a greater fraction of brown dwarfs. A Kolmogorov-Smirnov test performed on the cummulative distributions gives only a 1.9% probability of the two IMFs being drawn from the same underlying distribution (i.e., they differ at the $\approx 2.4\sigma$ level). By contrast, the IMFs produced by the lower metallicity cloud and the cloud with the different initial turbulent power spectrum are indistinguishable from the IMF of the original calculation (they have probabilities of 45 and 95%, respectively, of having been drawn from the same underlying distribution as the original calculation). Thus, the IMF seems to depend primarily on the mean thermal Jean mass in molecular clouds and is relatively insensitive to changes in the metallicity and turbulence.

4. The origin of the IMF

As discussed by Bate et al. (2003), in these calculations the IMF originates from a combination of competitive accretion between protostars and dynamical interactions which eject objects from the dense gas, terminating their accretion and setting their final masses. All of the objects in the calculations begin as opacity-limited fragments with masses a few times that of Jupiter. Subsequently, they accrete from the surrounding gas. Those that end up as brown dwarfs are involved in dynamical interactions soon after they form that eject them from the dense gas and, thus, terminate their accretion while they still have substellar masses. Those that become stars are simply those that accrete to a stellar mass before their accretion is terminated (either by dynamical ejection from the cloud or by exhausting the local gas reservoir).

Evidence that this mechanism produces the IMF in these calculations is provided in Figure 2. Here, for each of the calculations, we plot the time between the formation and ejection of each object versus the mass of the object at the end of the calculation. There is a clear correlation between the time an object has spent in the cloud and its final mass.

5. A simple model for the IMF

Based on these hydrodynamical calculations, we propose a simple accretion/ejection model for the origin of the IMF.

- We assume all objects begin with masses set by the opacity limit for fragmentation ($\approx$ 3 or 9 $\mathrm{M_J}$ for the calculations presented here) and then accrete at a fixed rate $\dot{M}$ until they are ejected.
- We assume the accretion rates of individual objects are drawn from a log-normal distribution with a mean accretion rate (in log-space) given

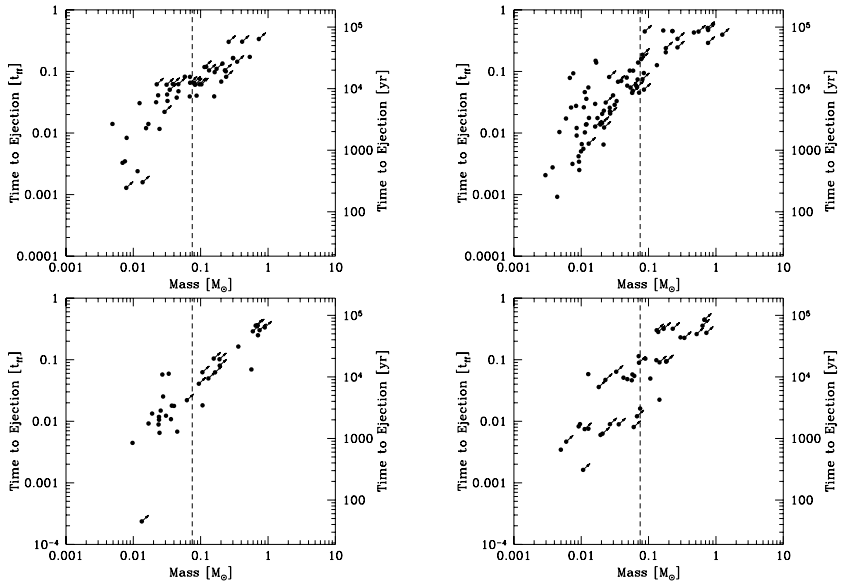

Figure 2. In each calculation, there is a clear correlation between the final mass of each object and the time between its formation and its ejection, indicating that the IMF originates from the termination of accretion by dynamical ejections.

by $\log_{10}(\overline{\dot{M}}) = \overline{\log_{10}(\dot{M})}$ and a dispersion of σ dex (i.e. $\log_{10}(\dot{M}) = \log_{10}(\overline{\dot{M}}) + \sigma G$, where G is a random Gaussian deviate with zero mean and unity variance).

- The ejection of protostars from an N-body system is a stochastic process. We assume that there is a single parameter, $\tau_{\rm eject}$, that is the characteristic timescale between the formation of an object and its ejection from the cloud. The probability of an individual object being ejected is then $\exp(-t/\tau_{\rm eject})$ where t is the time elapsed since its formation.

Clearly, these are assumptions involve gross simplifications. However, over a large number of objects, one might hope that these assumptions give a reasonable description of the behaviour of a typical object (e.g. in Figure 2, the mass of an object seems to depend linearly on the time it spends accreting with only a small dispersion).

Assuming that the cloud forms a large number of objects, N, and that the time it is evolved for is much greater than the characteristic ejection time, $T \gg \tau_{\rm eject}$, then there are essentially only three free parameters in this model. These are the mean accretion rate times the ejection timescale, $\overline{M} = \overline{\dot{M}}\tau_{\rm eject}$, the dispersion in the accretion rates, σ, and the minimum mass provided by

the opacity limit for fragmentation, $M_{\rm min}$. If $\overline{M} >> M_{\rm min}$, then $\overline{M}$ is the characteristic mass of an object.

5.1 Reproduction of the hydrodynamical IMFs

The hydrodynamical calculations are not followed until all the stars and brown dwarfs have finished accreting (i.e., the IMF is not fully formed). It is not the case that $T \gg \tau_{\rm eject}$. This must be taken into account when calculating simple accretion/ejection models for comparison with the results of the hydrodynamical calculations. To do this, we evolve the simple models over the same periods of time that the hydrodynamical simulations took to form their stars and brown dwarfs and the times of formation of each of the objects are taken directly from the hydrodynamical simulations.

We then generate model IMFs for comparison with the results of the two hydrodynamical calculations (Figure 1). Each model IMF is the average of 30000 random realisations of the simple accretion/ejection model, keeping the values of the input parameters fixed. The parameter values $\overline{\dot{M}}$, σ, and $\tau_{\rm eject}$ are measured directly from the simulations.

Figure 1 shows that the simple accretion/ejection models match the hydrodynamical IMFs very well. Kolmogorov-Smirnov tests show that the four hydrodynamical IMFs have probabilities of 92, 27, 7, and 20%, respectively, of being drawn from the corresponding model IMFs (i.e. the simple model is consistent with the hydrodynamical results). Thus, we demonstrate that a simple model of the interplay between accretion and ejection can reproduce the low-mass IMFs produced by the hydrodynamical calculations and give a near-Salpeter slope for high masses ($M \gtrsim 0.5$ M$_\odot$).

5.2 An analytical form for the IMF model

In the limit that the cloud forms a large number of objects, N, and that the time it is evolved for is much greater than the characteristic ejection time, $T \gg \tau_{\rm eject}$ (i.e., all objects have finished accreting and the star formation is complete), the simple accretion/ejection IMF model can be formulated semi-analytically rather than requiring Monte-Carlo simulation (see Bate & Bonnell, submitted).

The analytical form of the mass function is

$$f(M) = \int_0^\infty f(M,t) e(t) {\rm d}t, \qquad (1)$$

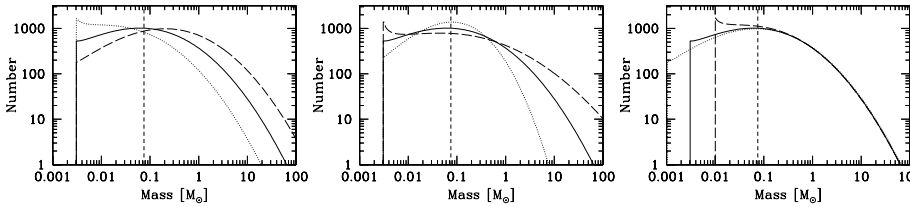

Figure 3. Examples of how the simple accretion/ejection IMF model varies with the characteristic mass, $\overline{M} = \overline{\dot{M}}\tau_{\rm eject}$ (left), dispersion in the accretion rates, σ (centre), and the minimum mass, $M_{\rm min}$ (right)

where

$$f(M,t) = \frac{1}{\sqrt{2\pi}\sigma(M-M_{\rm min})}\exp\left(\frac{-\left(\log\left(\frac{M-M_{\rm min}}{t}\right)-\log\overline{\dot{M}}\right)^2}{2(\log(10)\sigma)^2}\right), \quad (2)$$

for $M > M_{\rm min}$ and the probability an object is ejected at time t is

$$e(t) = \frac{1}{\tau_{\rm eject}}\exp\left(-\frac{t}{\tau_{\rm eject}}\right). \quad (3)$$

Equation 1 cannot be integrated analytically, but it is trivial to integrate numerically. Examples of the resulting mass function are shown in Figure 3. We note that this model has some similarities with the IMF models of Myers (2000) and Basu & Jones (2004) who also propose that the accretion of individual objects is terminated stochastically. However, there are several significant differences between their models and ours, leading to the models giving different forms for the IMF (see Bate & Bonnell, submitted, for further details).

Acknowledgments The computations reported here were performed using the U.K. Astrophysical Fluids Facility (UKAFF).

References

Basu, S. & Jones, C.E. 2004, MNRAS, 347, L47
Bate, M. R., Bonnell, I. A., & Bromm, V. 2003, MNRAS, 339, 577
Kroupa, P. 2001, MNRAS, 322, 231
Miller, G. E. & Scalo, J. M. 1979, ApJS, 41, 513
Myers, P. C. 2000, ApJ, 530, L119
Salpeter, E. E. 1955, ApJ, 123, 666

A MINIMUM HYPOTHESIS EXPLANATION FOR AN IMF WITH A LOGNORMAL BODY AND POWER LAW TAIL

Shantanu Basu and C.E. Jones
Department of Physics and Astronomy, The University of Western Ontario, London, Ontario N6A 3K7, Canada
basu@astro.uwo.ca, cjones@astro.uwo.ca

Abstract We present a minimum hypothesis model for an IMF that resembles a lognormal distribution at low masses but has a distinct power-law tail. Even if the central limit theorem ensures a lognormal distribution of condensation masses at birth, a power-law tail in the distribution arises due to accretion from the ambient cloud, coupled with a non-uniform (exponential) distribution of accretion times.

1. A Model for the Initial Mass Function

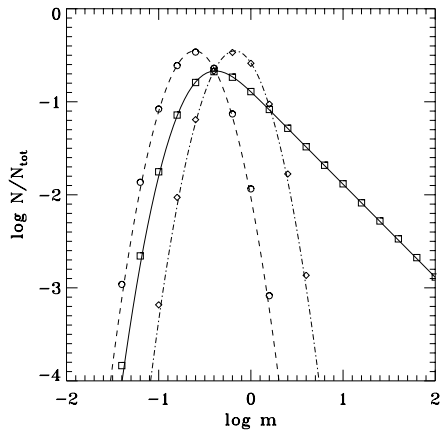

Figure 1. Evolution of a distribution of masses m undergoing accretion growth $dm/dt = \gamma m$. Dashed line and circles: an initial lognormal probability density function (pdf), with $\mu_0 = -1.40, \sigma_0 = 0.52$. Dash-dotted line and diamonds: pdf after accretion growth of all masses for a time $t = \gamma^{-1}$. Solid line and squares: pdf if accretion lifetimes have a pdf $f(t) = \delta e^{-\delta t}$ and $\delta = \gamma$. From Basu & Jones (2004).

E. Corbelli et al. (eds.), The Initial Mass Function 50 Years Later, 437–438.

Observations of the field star IMF have long established the existence of a power-law tail in the intermediate and high mass regime (Salpeter 1955). Recent observations of stars within young embedded clusters (e.g., Muench et al. 2002), have also established the existence of a low mass peak in the stellar mass distribution. Submillimeter observations of dense protostellar condensations (e.g., Motte, André, & Neri 1998) also imply a power-law tail in the intermediate and high mass regime. Given the evidence for a peaked distribution, a natural explanation is to invoke the central limit theorem of statistics and argue that the IMF should be characterized by the lognormal probability density function (pdf)

$$f(m) = \frac{1}{\sqrt{2\pi}\sigma m} \exp\left[-\frac{(\ln m - \mu)^2}{2\sigma^2}\right] \quad (1)$$

for the masses m, where μ and σ^2 are the mean and variance of $\ln m$. Now, assume that condensation masses are initially drawn from the above distribution with mean μ_0 and variance σ_0^2. Furthermore, if they accrete mass at a rate $dm/dt = \gamma m$, (this may be a reasonable assumption at the condensation stage, but not for a protostar accreting from its parent core), and the accretion time t has an exponential distribution with a pdf $f(t) = \delta e^{-\delta t}$, the pdf of final masses is

$$\begin{aligned} f(m) &= \frac{\alpha}{2} \exp\left[\alpha\mu_0 + \alpha^2\sigma_0^2/2\right]\ m^{-1-\alpha} \\ &\quad \times \mathrm{erfc}\left[\frac{1}{\sqrt{2}}\left(\alpha\sigma_0 - \frac{\ln m - \mu_0}{\sigma_0}\right)\right]. \end{aligned} \quad (2)$$

In this equation, $\alpha = \delta/\gamma$ is the dimensionless ratio of 'death' rate to 'growth' rate of condensations, and erfc is the complementary error function. This analytically derivable three-parameter formula has the advantage of being near lognormal at low masses but having an asymptotic dependence $f(m) \propto m^{-1-\alpha}$. If the 'death' and 'growth' rates are both controlled by the parent cloud, we might expect $\alpha \approx 1$, so that the distribution is Salpeter-like. See Basu & Jones (2004) for details, and references to other areas (e.g., distribution of incomes, city sizes, and Internet file sizes) where similar ideas are applicable.

References

Basu, S., & Jones, C. E. 2004, MNRAS, 347, L47
Motte F., André P., & Neri R. 1998, A&A, 336, 150
Muench, A. A., Lada, E. A., Lada, C. J., & Alves, J. 2002, ApJ, 573, 366
Salpeter E. E. 1955, ApJ, 121, 161

FEEDBACK AND THE INITIAL MASS FUNCTION

Joseph Silk
Astrophysics, Department of Physics, University of Oxford, Oxford OX1 3RH, UK
silk@astro.ox.ac.uk

Abstract I describe a turbulence-inspired model for the stellar initial mass function which includes feedback and self-regulation via protostellar outflows. A new aspect of the model provides predictions of the star formation rate in molecular clouds and gas complexes. A similar approach is discussed for self-regulation on kiloparsec scales via supernova input, and an expression is presented for the global star formation rate that depends on the turbulent pressure of the interstellar medium.

1. Introduction

The turbulence paradigm seems to be increasingly accepted in star formation theory. The dissipation time of the observed supersonic turbulence especially in giant molecular clouds (GMCs) is less than the cloud lifetime, demonstrating that cloud support is by turbulent pressure. Implications include the consequences that molecular clouds on all scales are short-lived and hence that large-scale star formation is relatively inefficient. This corresponds to what is observed: about 0.1-1 percent of a GMC is in stars, and the dynamical time-scale of a GMC is $10^6 - 10^7$ yr, giving consistency with the global star formation rate of the Milky Way galaxy, that requires about 10 percent efficiency of conversion of gas to stars over a galactic rotation time. On small scales, such as cloud cores, supersonic turbulence is still present, although less dominant, and one generally observes a much higher efficiency of star formation. The efficiency for star clusters embedded in molecular clouds, which have ages less than 5×10^6 yr, is 10-30 % (Lada & Lada 2003). Presumably an important difference is that self-gravity plays a prominent role on these scales. The turbulence drivers are not well understood. Possible sources include external drivers (galactic rotation, Parker instability, OB wind/SN-driven super-bubbles) as well as internal sources (protostellar jets and outflows, gravi-

E. Corbelli et al. (eds.), The Initial Mass Function 50 Years Later, 439–448.

tational collapse), and the turbulence is likely to be multi-scale, controlled both by cascades and inverse cascades.

I will focus here mostly on protostellar outflows on small scales, although I will also discuss supernova input on larger scales, as sources of interstellar turbulence. The aim will be to demonstrate that outflow-generated turbulence allows self-regulation of star formation via control of the accretion rate. A GMC is viewed as a network of overlapping, interacting protostellar-driven outflows. This leads to simple derivations of the IMF and of the star formation rate.

Similar ideas are implicit in models of competitive accretion by turbulent fragments (Bonnell, Vine and Bate 2004). The idea of a network of interacting wind-driven shells is a manifestation of the fragmentation models developed by Klessen and collaborators, in which colliding, supersonic flows shock, dissipate and produce dense gravitationally unstable cores (Klessen, Heitsch and MacLow 2000; Burkert 2004).

2. Observational issues

Substantial churning of molecular clouds by protostellar outflows is a common phenomenon. Observations of some cloud complexes such as Circinus, Orion and NGC 1333 support the idea that protostellar outflows drive the observed turbulence (Yu, Bally and Devine 1997; Bally et al. 1999; Bally and Reipurth 2001; Sandell & Knee 2001). Quantitatively, such flows seem to be an important source of turbulence. One may estimate the outflow strength as (e.g., Konigl 2003)

$$\dot{M}_{wind} \sim (r_d/r_A)^2 \dot{M}_{acc} \sim 0.1 \dot{M}_{acc} \sim 0.1 v_{amb}^3/G,$$

where the wind velocity is of order 100 km/s, and $v_{amb} \sim 0.3 - 3 \mathrm{km\,s^{-1}}$. In general, one expects that $v_{wind} >> v_{amb}$. Moreover, outflow momenta accumulate since typical outflow durations are $t_{wind} \sim 10^5 \mathrm{yr}$, so that the cloud lifetime $t_{dyn} >> t_{wind}$. Hence one wind outflow event per forming star ejecting 10 percent of its mass can, on the average, balance the accretion momentum in a typical cloud core that forms stars at $\sim 10\%$ efficiency.

An important issue is the extent to which the outflows are localised. Observed jets suggest that some outflows deposit energy far from the dense cores, but this inference cannot easily be generalised since it is likely to be highly biased by extinction. Jets may be ubiquitous, but could still be unstable enough to drive bipolar outflows and mostly deposit their energy in and near dense cores. Protostellar outflows are a possible source of the observed molecular cloud turbulence, and the only one that is actually observed in situ. The relevant driving scales cover a wide range, and may well yield the observed, apparently scale-free cloud turbulence.

The projected density profiles of some dense cores are well fit by a pressure-confined self-gravitating isothermal sphere (Alves, Lada and Lada 2001). Others require supercritical cores undergoing subsonic collapse (Harvey et al. 2003). Magnetic support offers one explanation of the initial conditions, with magnetically supercritical cores surrounded by subcritical envelopes. However the core profiles can also, more debatably, be reproduced as supersonic turbulence-compressed eddies (Ballesteros-Paredes, Klessen and Vazquez-Semadeni 2003).

3. IMF Theory

There are many explanations that yield a power-law IMF, $mdN/dm = Am^{-x}$, with $x \approx 4/3$, the Salpeter value. However it is harder to account for the interesting physics embedded in $A(p, t...)$, which determines the star formation rate and efficiency. It is likely that molecular clouds are controlled by feedback. Protostellar outflows feed the turbulence which controls ambient pressure, which in turn regulates core formation. Pressure support includes magnetic fields. There are different views about the details of self-regulation, depending on the relative roles of magnetic and gravitational support versus turbulent compression. Collapse of the supercritical cores into protostellar disks might drive outflows that levitate the envelopes, thereby limiting core masses (Shu et al. 2004). Ambipolar diffusion and magnetic reconnection would be controlled by the turbulence, thereby setting the mass scale of cores (Basu & Ciolek 2004). The outflows should cumulatively set the ambient pressure that in turn controls both core masses and the accretion rate at which cores can grow (Silk 1995).

Consider a simple model for a spherically symmetric outflow into a uniform medium that drives a shock-compressed shell until either the shell encounters another expanding shell or until pressure balance with the ambient medium is achieved. At this point, the shell breaks up into blobs confined by ram or by turbulent pressure, with the relevent turbulent velocity being that of the shell at break-up.

Now the shell radius is $R = \left(\dot{M}_{wind} v_w / \rho_a\right)^{1/4} t^{1/2} \Rightarrow R \propto v^{-1}, \quad t \propto v^{-2}$. Here $v = dR/dt$ is the shell velocity. The protostellar outflows generate a network of interacting shells that form clumps with a velocity distribution:

$$N(> v) = 4\pi R^3 t \dot{N}_* = \left(\dot{M}_{wind} v_w / \rho_a\right)^2 v^{-5} \dot{N}_*.$$

To convert to a mass function, I combine this expression for the velocity distribution of clumps with the relation between mass m and turbulent velocity (identified with v) for a clump: $m = v^3 G^{-3/2}(v/B)$ for magnetically supercritical cores or $m = v^3 G^{-3/2}(v p^{-1/2})$ for gravitationally supercritical Bonnor-Ebert

cores. Now B scaling suggests $B \overset{\propto}{\sim} v \Rightarrow \epsilon = 3$ (cf. Shu et al. 2004). Alternatively, scaling from Larson's laws yields $\rightarrow \rho \overset{\propto}{\sim} v^{-2} \Rightarrow \epsilon = 4$. If I instead generalise the wind-driven, approximately momentum-conserving, shell evolution to $R \propto t^{\delta}$, the IMF can now be written in the form $\rightarrow mdN/dm \propto m^{-x}$ with $x = \frac{3\delta+1}{\epsilon(1-\delta)}$ where $R \propto t^{\delta}$ and $m \propto v^{\epsilon}$. One finally obtains the following values for x: $x = 5/3$ if $\delta = 1/2$; $x = 4/3$ if $\delta = 3/7$ $(\epsilon = 3)$, and $x = 5/4$ if $\delta = 1/2$; $x = 4/3$ if $\delta = 13/25$ $(\epsilon = 4)$. There seems to be little difficulty in obtaining a Salpeter-like IMF.

However in practice, the IMF is not a simple power-law in mass. It may be described by a combination of three different power-laws: $x = -2/3$ over 0.01 to 0.1 $M_{\odot}$; $x = 1/3$ over 0.1 to 1 $M_{\odot}$; $x = 4/3$ over 1 to 100 $M_{\odot}$ (Kroupa 2002). A scale of around 0.3 $M_{\odot}$ must therefore be built into the theory. One clue may come from the fact that the observed IMF is similar to the mass function of dense clumps in cold clouds, at least on scales above $\sim 0.3 M_{\odot}$ (Motte et al. 2001).

4. Feedback

I now describe an approach that yields the normalisation of the IMF, and in particular its time-dependence. The idea is that the network of interacting shells must self-regulate, in that star formation provides both the source of momentum that drives the shells, and is itself controlled by the cumulative pressure that enhances clump collapse. I introduce porosity as the parameter that controls self-regulation, via the overlap of outflows. I define porosity as $Q = 4\pi R_{max}^3 \dot{N}_* t_{max}$. Now for self-regulation, I expect that $Q \sim 1$. One may rewrite the IMF as

$$mdN/dm = Q(m_a/m)^x$$

where $m_a = v_a^3 G^{-3/2}(v_a/B_a)$ or $m_a = v_a^4 G^{-3/2} p_a^{-1/2}$. Now with $Q \sim 1$, one can expect self-regulation. However in addition, one must require self-gravity to avoid clump disruption. This allows the possibility of either negative or positive feedback.

The predicted IMF is $mdN/dm = Am^{-x}$. The preceding argument yields A. More generally with regard to x, if $R_{wind} \propto t^{\delta}$ and $m_{clump} \propto v^3$, we obtain $\delta = 2/5, 3/7, 1/2 \rightarrow x = 2/3, 4/3, 5/3$. The principal new result is the self-regulation ansatz that yields A. We infer that $A \propto Q$ where porosity Q can be written as $f_{\text{low density phase}} = 1 - e^{-Q}$. The IMF slope is in accordance with observations for plausible choices of parameters. Of course numerical simulations in 3-D are needed to make a more definitive calculation of the IMF in the context of the present model.

Nevertheless, there is one encouraging outcome. Turbulent feedback seems to be significant for stars of mass $\gtrsim 0.3 M_{\odot}$. This is an observed fact, and is attributed to detailed models that generally invoke magnetically driven accre-

tion disk outflows and jets. Of course even sub-stellar objects display outflows but the outflow rates are dynamically unimportant for the parent cloud (e.g., Barrado et al. 2004). Such a hypothesis could help explain why a feedback explanation of the IMF naturally selects a characteristic mass of $\sim 0.3\mathrm{M}_{\odot}$. As the stellar mass increases, negative feedback mediates the numbers of more massive clumps and stars. The numbers of increasingly massive stars fall off according to the power-law derived here.

5. Summary of IMF results

There are 3 crucial components to star formation phenomenology. These are the initial stellar mass function or IMF, the star formation efficiency or SFE, and the star formation rate or SFR. The outflow-driven turbulence model predicts these quantities, provided we can identify the mass of a star with $m = \mu v^3 G^{-3/2} \rho^{-1/2}$, where $\mu = p^{1/2}/B$ or 1, for either magnetically or pressure-supported clouds. One then finds that, above the feedback scale, the IMF is

$$mdN/dm \propto Q(v_a/v)^5 = f\mu\rho_a Q {m_a}^{2/3} m^{-5/3}.$$

Here f is a constant of order unity.

The SFR is

$$\dot{n}_* = \frac{Q}{R_a^3 t_a} = Q v_a^{\frac{3\delta+1}{1-\delta}} \left(\frac{\rho_a}{\dot{M}_{wind} v_w} \right)^{\frac{1}{1-\delta}} \propto \frac{Q\rho_a^2}{v_a}.$$

In the final expression, I set $\delta = 1/2$ and $\dot{M}_{wind} = 0.1 v_a^3/G$. The SFR $\overset{\propto}{\sim} \rho_a^2$. This means that the SFR accelerates as the cloud evolves and contracts. The enhanced dissipation from outflows most likely results in the increase of turbulent density in the cloud, at least until sufficiently massive stars form whose energetic ouflows, winds and eventual explosions blow the cloud apart. Evidence for accelerating star formation in many nearby star-forming regions, based on pre-main-sequence evolutionary tracks, is presented by Palla and Stahler (2000). This suggests that a ministarburst is a common phenomenon.

The SFE is

$$\frac{m^*_{char} \dot{n}_* t_{dyn}}{\rho_a} \sim \frac{m^*_{char} \dot{n}_*}{G^{1/2} \rho_a^{3/2}} \propto \frac{Q\rho_a^{1/2}}{v_a}.$$

This scaling gives an SFE that is $\sim 10 - 100$ times larger in cores than in a GMC, more or less as is observed.

There are a number of unresolved issues. The scale-free nature of the observed turbulence in molecular clouds is suggestive of a cascade. Normally these proceed from large to small scales. With internal protostellar sources, an inverse cascade must be invoked, such as could arise via injection of turbulence associated with jet-driven helical magnetic fields. Alternatively, the wide

range of jet and outflow scales suggests that the driving scale may largely be erased.

Efficient thermal accretion onto low protostellar mass cores coupled with protostellar outflows and turbulent fragmentation, for which $M_J^{turb} \sim \mathcal{M}^2 M_J^{therm}$ (Padoan & Nordlund 2002), will help to imprint the characteristic stellar mass scale. This suggests that magnetic fields, insofar as they regulate and drive outflows, are likely to play an important role in setting the characteristic stellar mass scale. Moreover, regions of enhanced turbulence, such as would be associated with star formation induced by merging galaxies, could plausibly have a increased feedback scale and hence a top-heavy IMF.

6. A theory for kiloparsec-scale outflows

I now show that a porosity formulation of outflows can also lead to a large-scale burst of star formation. Rather than consider molecular cloud regions, where the physics is more complex, I discuss a more global environment where the physics can be simplified but the essential ingredient of interacting outflows remains. Consider a larger-scale version of self-regulated feedback. I model a cubic kiloparsec of the interstellar medium, which contains atomic and molecular gas clouds and ongoing star formation. I assume that the dominant energy and momentum to the multiphase interstellar medium is via supernovae. One expects self-regulation to lead to a situation in which the porosity $Q \sim 1$. The porosity is initially small, but increases as outflows and bubbles develop. If it is too large, I argue that molecular clouds are disrupted and the galaxy blows much of the gas out of the disk, e.g. via fountains into the halo. Star formation is quenched until the gas cools and resupplies the cold gas reservoir in the disk. Whether the gas leaves in a wind is not clear; this may occur for dwarf galaxy starbursts, but cannot happen for Milky-Way type galaxies as long as the supernova rates are those assumed to apply in the recent past. I further speculate that the feedback is initially positive, in a normal galaxy. The outflows drive up the pressure of the ambient gas which enhances the star formation rate by accelerating collapse of molecular clouds. The feedback eventually is negative in dwarf galaxies, once a wind develops. In more massive galaxies, the ensuing starburst is only limited by the gas supply.

To develop a simple model, I make the following ansatz. The porosity may be defined by

$$Q \sim (SN\,bubble\,rate) \times (maximum\,bubble\,4\text{-}volume)$$

$$\propto (star\ formation\ rate) \times \left(turbulent\ pressure^{-1.4}\right).$$

Expansion of a supernova remnant is limited by the ambient pressure, when it can be described as a radiation pressure-driven snowplow with $R_a^3 t_a \propto p_{turb}^{1.4}$ (Cioffi et al. 1988). Hence the star formation rate may be taken to be

$\propto Qp_{turb}^{1.4}$, and by introducing a new parameter ϵ may also be written as $\epsilon \times rotation\,rate \times gas\,density$. What is in effect the global SF efficiency is now given by $\epsilon \equiv \left(\frac{\sigma_{gas}}{\sigma_f}\right)^{2.7}$, where $\sigma_f \approx 20\mathrm{kms}^{-1}\left(\mathrm{E_{SN}}/10^{51}\right)^{1.27}(200\mathrm{M}_\odot/\mathrm{m_{SN}})$. We expect positive feedback at high gas turbulent velocities. High resolution numerical simulations of a multiphase medium demonstrate that a starburst is generated, and that the porosity formalism describes the star formation rate (Slyz et al. 2004). The porosity formulation yields a star formation rate that gives a remarkably good fit to the numerical results. The positive feedback arises from the implementation of the derived star formation law with star formation rate proportional to turbulent gas pressure. Pressure enhancements are mostly due to shocked gas. It is interesting to note that a star formation law which favours shock dissipation can more readily account for the spatial extent of star formation as modelled for interacting galaxies (Barnes 2004) than can an expression in which the star formation rate is only a function of gas density (as in the Schmidt-Kennicutt law).

Porosity may therefore regulate star formation, on the physical grounds that porosity can be neither too large nor too small. If it is too small, the rate of massive star formation (and death) accelerates until the porosity increases. If the porosity is too large the cloud is blown apart via a wind and loses its gas reservoir. To make the concept of a porosity-driven wind more precise, I write the disk outflow rate as the product of the star formation rate, the hot gas volume filling factor, and the cold gas mass loading factor. If the hot gas filling factor $1 - e^{-Q}$ (Q is porosity) is of order 50%, then this suggests that the outflow rate is of order the star formation rate. I emphasize that such a result is plausible but only qualitative: it has yet to be numerically simulated in a sufficiently large box.

One infers that the metal-enriched mass ejected in a wind is generically of order the mass in stars formed. This is similar to what is observed for nearby starbursting dwarf galaxies (e.g. NGC 1569: Martin, Kobulnicky and Heckman 2002). Observations suggest that massive galaxies should have had massive winds in the past, in order both to account for the observed baryonic mass and the galaxy luminosity function (Benson et al. 2003), although theory has difficulty in rising to this challenge. It is clear that, energetically, with conventional supernova rates, one cannot drive winds from massive or even Milky Way-like galaxies (Springel & Hernquist 2003). The situation is very different for dwarfs, where supernova input suffices to drive vigorous winds, although even in these cases geometric considerations are important (MacLow & Ferrara 1999).

Simulations in a multiphase medium currently lack sufficient resolution to adequately treat such instabilities as Rayleigh-Taylor and Kelvin-Helmholtz, that will respectively enhance the porosity and the wind loading. The highest

resolution simulations to date (Slyz et al. 2004) of a multiphase medium already show that SN energy input efficiency is considerably underestimated by failure to have adequate resolution to track the motions of OB stars from their birth sites in dense clouds before they explode.

It is likely therefore that feedback may occur considerably beyond the scales hitherto estimated (Dekel & Silk 1986), possibly extending to the galactic (stellar) mass scale of about $3 \times 10^{10}\mathrm{M}_{\odot}$, only above which the star formation efficiency is inferred to be approximately constant (Kauffmann et al. 2003).

Whether even more refined and detailed hydrodynamical simulations can be consistent with the requirement of substantial early gas loss from massive galaxies is uncertain (Silk 2003). One simply lacks the energy input. Instead, recourse must be made either to an early top-heavy IMF or outflows from a quasar phase that coincided with the epoch of bulge formation, A top-heavy IMF is motivated by the earlier derivation of an IMF driven by turbulent feedback. The case for an early quasar phase during galaxy bulge formation is motivated by the empirical bulge-supermassive black hole correlation, high quasar metallicities and SMBH growth times (Dietrich & Hamann 2004). Yet another option is an enhanced early rate of hypernovae in starbursts, as suggested by the interpretation of the peculiar abundances found in the starburst galaxy M82 (Umeda et al. 2002).

While all of these enhanced sources of energy and momentum are likely to play some role in forming galaxies, it is intriguing to note that early reionisation, in concordance with requirements from CMB measurements by the WMAP satellite, can also be accomplished by the first of these hypotheses which can simultaneously account for chemical evolution of the metal-poor IGM and the abundance ratios observed in extreme metal-poor halo stars (Daigne et al. 2004). Moreover, a top-heavy IMF, if identified with luminous starbursts, can also account for the faint sub-millimetre galaxy counts (Baugh et al. 2004) and the chemical abundances in the enriched intracluster medium (Nagashima et al. 2004).

References

Alves, J., Lada, C. & Lada, E. 2001, Nature, 409, 159
Ballesteros-Paredes, J. Klessen, R. & Vazquez-Semadeni, E. 2003, ApJ, 592, 188
Bally, J. et al. 1999, AJ, 117, 410
Bally, J. & Reipurth, B. 2001, ApJ, 546, 299
Barnes, J. 2004, MNRAS, 350, 798
Barrado y Navascuès, D., Mohanty, S. & Jayawardhana, R. 2004, ApJ, 604, 284
Basu, S. & Ciolek, G. 2004, ApJ, 607, L39
Baugh, C. et al. 2004, astro-ph/0406069
Benson, A. et al. 2003, ApJ, 599, 38
Bonnell, I., Vine, S. & Bate, M. 2004, MNRAS, 349, 735
Burkert, A. 2004, astro-ph/0404015

Cioffi, D., McKee, C. & Bertschinger, E. 1988, ApJ, 334, 252
Daigne, F. et al. 2004, A&A, submitted
Dekel, A. & Silk, J. 1986, ApJ, 303, 39
Dietrich, M. & Hamann, F. 2004, ApJ, 611, 761
Harvey, D. et al. 2003, ApJ, 598,1112
Kauffmann, G. et al. 2003, MNRAS, 341, 54
Klessen, R., Heitsch, F. & MacLow, M. 2000, ApJ, 535, 887.
Konigl, A. 2003, astro-ph/0312287
Kroupa, P. 2002, Science, 295, 82
Lada, C. & Lada, E. 2003, ARA&A, 41, 57
Martin, C., Kobulnicky, H. & Heckman, T. 2002, ApJ, 574, 663
MacLow, M. & Ferrara, A. 1999, ApJ, 513, 142
Motte, F. et al. 2001, A&A, 372, L41
Nagashima, M. et al. 2004, astro-ph/0408529
Padoan, P. & Nordlund, A. 2002, ApJ, 576, 870
Palla, F. & Stahler, S. 2000, ApJ, 540, 255.
Sandell, G. & Knee, L. 2001, ApJ, 546, L49
Shu, F. et al. 2004, ApJ, 601, 930
Silk, J. 1995, ApJ, 438, L41
Silk, J. 2003, MNRAS, 343, 249
Slyz, A. et al. 2004, MNRAS, submitted.
Springel, V. & Hernquist, L. 2003, MNRAS, 339, 289
Umeda, H. et al. 2002, ApJ, 578, 855
Yu, K., Bally, J. & Devine, D. 1997, ApJ, 485, L45

Figure 1. Smiling Joe Silk and Hans.

Figure 2 Ian Bonnell perfoming the last simulation.

Figure 3 Matthew Bate and Jerome Bouvier (Martino Romaniello in the background).

FEEDBACK IN STAR FORMATION SIMULATIONS: IMPLICATIONS FOR THE IMF

C.J. Clarke[1], R.G. Edgar[2] and J.E. Dale[3]
[1]*Institute of Astronomy, Madingley Road, Cambridge U.K.*
[2]*Stockholms Observatorium, AlbaNova Universitetscentrum, Stockholm, Sweden*
[3]*Department of Physics & Astronomy, University of Leicester, Leicester, U.K.*
cclarke@ast.cam.ac.uk, rge21@astro.su.se, jed20@astro.le.ac.uk

Abstract We discuss recent simulations that incorporate radiative feedback from massive star formation and consider their implications for the IMF.

1. Introduction

Recent years have seen several simulations of star formation which have had some success in reproducing the observed IMF (Bate et al.2003, Padoan & Nordlund 2002). Nevertheless, these simulations are inadequate in regions of massive star formation since they do not include feedback from the intense radiation field and winds produced by these objects. Hydrodynamical simulations of star formation that include feedback are in their infancy and require the development of robust algorithms that can treat the highly inhomogeneous and complex gas structures found in star forming regions. Here we report on recent advances in incorporating two forms of feedback from massive stars in numerical simulations of star formation: the inclusion of ionising radiation (which influences the global evolution of a protocluster's gas content) and radiation pressure on dust (which acts more locally so as to control the accretion flow on to individual massive stars).

2. Feedback from photoionising radiation

Recently, Dale et al.(submitted) have developed an algorithm for the inclusion of ionising radiation in SPH simulations. This method is loosely based on that of Kessel-Deynet & Burkert (2000), as it employs the on the spot approximation (valid in high density regions) and uses the lists of neighbour particles in the SPH simulations to build recombination integrals between gas particles and the ionising source. The algorithm thus constructs an instantaneous Strom-

E. Corbelli et al. (eds.), The Initial Mass Function 50 Years Later, 449–454.

gren volume around the source and sets the temperature of the gas according to its ionisation state. Although the effect of ionising radiation on gas dynamics has been well studied in simple geometries (Yorke et al.1989, Franco et al.1990, Garcia-Segura & Franco 1996) and the propagation of ionising radiation in static clumpy media is likewise well studied (Hobson & Padman 1993, Rollig et al.2002), this is the first time that feedback has been included in star formation simulations with realistically inhomogeneous gas.

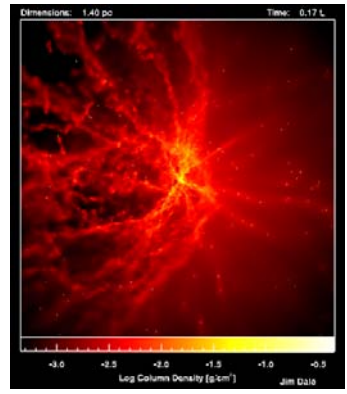

Figure 1. The impact of ionising radiation on a high density proto-cluster. The grey scale denotes gas column density, 1.7×10^5 years after the switch on of an ionising source in the cluster core. The filamentary structures in the left hand side of the image are predominantly neutral gas that has been compressed between adjoining low density channels of outflowing gas. From Dale, Bonnell, Clarke & Bate (submitted).

Figure 1 is a snaphsot of a protocluster subject to ionising radiation from a single OB star that formed at the intersection of a number of nearly radial filaments converging on the cluster core. The radiation field sees a highly inhomogeneous gas distribution and accordingly the escape of ionising radiation is concentrated along the channels between the filaments. Photoheated gas in these channels expands outwards at > 10 km / s, and, together with neutral gas that it sweeps up, drives outflows whose mass and momentum loss rates are comparable with those observed in regions of massive star formation (Churchwell 1997). Note that such outflows are collimated purely by the filamentary gas structure and have a complex and multi-lobed structure. It is unclear what fraction of observed outflows (which are currently interpreted as bipolar structures collimated by an accretion disc) could in fact be in this category (Shepherd et al.1997, Beuther et al.2002).

The simulation demonstrates both positive and negative feedback. Lateral expansion of the ionised channels compresses the intervening walls of neutral gas and induces additional star formation (absent in control simulations without ionising radiation). On the other hand, ionisation feedback reduces the flow

of gas into the central regions and so inhibits the growth of massive stars in the cluster core. It is currently unclear which of these effects is dominant, since the level of induced star formation is underestimated by the finite resolution of the simulations.

The structure and kinematics of the photoionised region in Figure 1 is very different from that of a control simulation using an azimuthally smoothed density profile. In the latter case, the ionisation front is confined to the cluster core, in contrast to Figure 1 where much of the cloud volume is affected by heating and acceleration due to photoionisation. The thermal and kinetic energy that the gas in Figure 1 has absorbed from the stellar radiation field comfortably exceeds the gravitational binding energy of the cluster. However, most of the cluster gas remains bound, since this energy is mainly absorbed by material in the outflows which is accelerated to many times the cluster's escape velocity, but which represents a small fraction of the cluster mass.

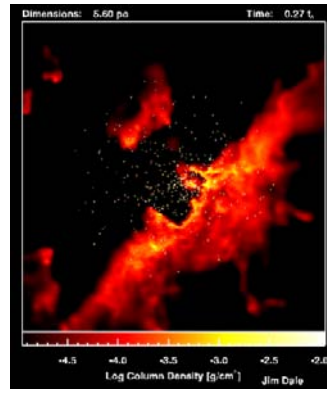

Figure 2. Low density cluster, 5.4×10^5 years after the switch on of an OB star.

In lower density clusters, the effect of photoionisation is much more dramatic. In Figure 2, in which the cluster initial half mass radius (2.8 pc) is twice that in Figure 1, the radiation has cleared the gas from the stellar region of the cluster, producing an image reminiscent of the NGC 3603 region. Note that in both Figures 1 and 2, the initial filamentary gas density distributions (taken from the simulations of Bonnell & Bate (2002)) were fairly symmetric globally, but that the cloud becomes very asymmetric once it has been sculpted by ionising radiation. This is due to the preferential propagation of ionising radiation in low density regions, which exacerbates small differences in the initial gas density.

3. Radiation pressure on dust

Another feedback mechanism for massive stars involves momentum transfer from the stellar ultraviolet radiation field to dust grains. For stellar luminosity L_*, this interaction involves the input of momentum into the dust/gas at a rate $\sim L_*/c$ at the dust sublimation radius, r_d, plus a further distributed input of momentum at radius $> r_d$ of magnitude $\tau_R L_*/c$, where τ_R is the Rosseland mean optical depth of the dusty flow. The former component represents the momentum transfer from the first strike of ultraviolet photons, which are absorbed in a thin layer close to r_d, while the latter results from the interaction between re-emitted (infrared) photons and the dusty flow. Wolfire and Casinelli (1986) showed that hydrodynamic calculations using grey opacities fail to capture the momentum transfer associated with the first strike of radiation and may drastically underestimate the efficacy of feedback. Nevertheless, most subsequent hydrodynamic calculations of massive star formation have used grey opacities for reasons of computational economy. A notable exception is the recent simulations of Yorke & Sonnhalter (2002), which combine hydrodynamic calculations with full frequency dependent radiative transfer. (See also Edgar & Clarke (2003, 2004) (henceforth EC03, EC04) for details of a computationally cheaper algorithm which retains some of the advantages of full frequency dependent radiative transfer calculations).

The early work of Wolfire & Casinelli (1986,1987) on the formation of massive stars by spherical accretion yielded the well known result that radiative feedback prevents the formation of OB stars unless the dust is strongly depleted in small grains. In these steady state calculations, the gas at the outer edge must experience a net inward force if it is to accrete. EC03 however showed that with time dependent calculations it is possible to form OB stars with a normal dust abundance even in spherical symmetry. This is because material starts to fall in before the star has switched on and once the central object produces a significant radiation field, the dusty flow may already be traveling fast enough to reach the star even if subject to a net outward force. EC03 showed that the fraction of the initial cloud mass ending up in the star is very sensitive to the initial thermal content of the gas (Figure 3). This is because cold gas collapses nearly homologously so that most of the core mass has attained high velocities when the central star switches on. In warmer collapses, by contrast, pressure gradients delay the collapse of the outer regions of the core, which may then be expelled by the radiation.

In reality, however, the accretion flow on to massive stars is unlikely to be spherical (see the recent observations of Beltran et al.(2004) and Chini et al.(2004) for evidence of disc like structures around massive stars). Simulations of accretion in disc geometry (Yorke & Sonnhalter 2002) have shown that radiation pressure on dust does *not* in this case prevent the formation of

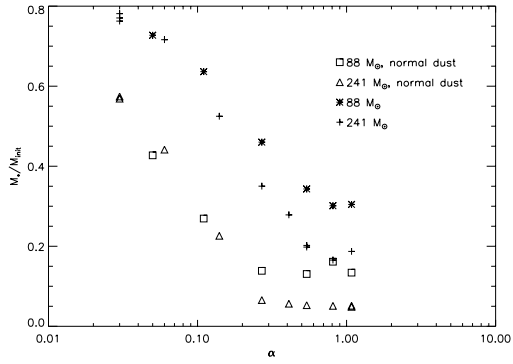

Figure 3. Fraction of cloud mass ending up in star as a function of the initial ratio of thermal energy to gravitational energy. Symbols denote cloud masses and normal or reduced dust opacities. Note the clustering of objects around $10M_{\odot}$ (From EC03).

OB stars, since the radiation field drives a low density circumpolar wind, but not does not impede equatorial accretion.

Alternatively, Bonnell et al.(1998) have argued that the widespread association between OB stars and clustered star formation suggests a role for collective effects in massive star formation. They suggest that cluster cores collapse due to mass loading of stars in the core by accretion of inflowing gas. Massive stars are then formed through stellar collisions, thus by-passing the issue of radiative feedback on dust.

In this collisional scenario, however, stars that are destined to attain high masses first gain mass by Bondi Hoyle accretion and only in the final stages undergo further build up through merging. Although simulations of this process (Bonnell & Bate 2002) have so far omitted feedback , EC04 found that accretion in Bondi Hoyle geometry is highly susceptible to disruption by radiation pressure on dust. In unperturbed Bondi Hoyle flow, streamlines are gravitationally focused and shocked downstream of the star (Bondi & Hoyle 1944, Edgar 2004) so that accretion proceeds via a radial accretion column in the star's wake. Before reaching the shock, however, the flow follows a nearly tangential trajectory and is easily deflected into an outflow by the radial impulse of the radiation field. Consequently, EC04 found that , for normal dust abundances, stars cannot grow by Bondi Hoyle accretion to masses more than $\sim 10M_{\odot}$.

Is this a problem for the collisional scenario? In principle there is no problem in forming stars only from collisions once they attain a mass of $\sim 10M_{\odot}$ if the cluster core is dense enough. However since it is mass loading of the stars that drives the core's shrinkage, it is unclear whether this can be achieved if only the low mass stars can accept mass.

4. Afterword

Recent simulations have shown that massive stars can form by accretion, if one relaxes the assumption of steady state spherical accretion. Nevertheless, although stars may grow to $> 10M_{\odot}$ in certain circumstances, there are many sets of initial conditions which 'fail' to produce massive stars and instead deposit stars near the critical mass of $10M_{\odot}$ where radiation pressure on dust becomes significant (see Figure 3). One therefore expects $10M_{\odot}$ to be an important mass scale in the IMF. There is however little observational evidence for any break in the Salpeter slope at around $10M_{\odot}$, suggesting that massive star formation is considerably less sensitive to radiation pressure on dust than many of the current models. A clear goal for massive star formation theories is thus to ensure that there is no trace of the $10M_{\odot}$ mass scale in the IMF.

References

Bate, M.R., Bonnell, I.A., Bromm, V., 2003. MNRAS 339,577
Beltran, M.T., Cesaroni, R., Neri, R. et al., 2004, ApJL, 601, 187
Beuther, H., Schilke, P., Gueth. F. et al., 2002, A&A, 387, 931
Bondi, H. & Hoyle, F., 1944, MNRAS, 104, 273
Bonnell, I.A., & Bate, M.R., 2002, MNRAS, 336, 659
Bonnell, I.A., Bate, M.R., & Zinnecker, H., 1998, MNRAS, 298, 93
Chini, R., Hoffmeister, V., Kimeswinger, S. et al., 2004, Nature, 429, 155
Churchwell, E., 1997, ApJL, 479, 59
Edgar, R., 2004. New Astr. Reviews, in press
Edgar, R.G., & Clarke, C.J., 2003, MNRAS, 338, 962 (EC03)
Edgar, R.G., & Clarke, C.J., 2004, MNRAS, 349, 678
Franco, J., Tenorio-Tagle, G., Bodenheimer, P., 1990, ApJ, 349, 126
Garcia-Segura, G. & Franco, J., 1996, ApJ, 469, 171
Hobson, M., & Padman, R., 1993, MNRAS, 264, 161
Kessel-Deynet, O. & Burkert, A., 2000, MNRAS, 315, 713
Padoan, P., & Nordlund, A., 2002, ApJ, 576, 870
Rollig, M., Hegmann, M., & Kegel, W., 2002, A&A, 392, 1081
Shepherd, D., Churchwell, E., Wilner, D., 1997, ApJ, 482, 355
Wolfire, M.G., & Cassinelli, J.P., 1986, ApJ, 310, 207
Wolfire, M.G., & Cassinelli, J.P., 1987, ApJ, 319, 850
Yorke, H.W., & Sonnhalter, C., 2002, ApJ, 569, 846

MASSIVE STAR FEEDBACK ON THE IMF

M. Robberto[1,2], J. Song[3], G. Mora Carrillo[4], S.V.W. Beckwith[1], R.B. Makidon[1] and N. Panagia[1,2]
[1]*Space Telescope Science Institute, 3700 San Martin Drive, Baltimore, MD 21218, USA*
[2]*Affiliated with the Space Telescope Division of the European Space Agency, ESTEC, Noordwijk, The Netherlands*
[3]*Departement of Astronomy, University of Illinois at Urbana-Champaign, USA*
[4]*Instituto de Astrofísica de Canarias, La Laguna, Tenerife, Spain*

Abstract We have obtained the first measures of the mass accretion rates on stars of the Trapezium Cluster. They appear systematically lower than those of similar stars in the Taurus-Auriga association. Together with premature disk evaporation, dramatically revealed by the HST images of the Orion proplyds, this result suggests that low mass stars in a rich cluster may be "dwarfed" by the influence of nearby OB stars. This feedback mechanism affects the IMF, producing an excess of low mass stars and brown dwarfs. The observed frequency of low mass objects in Orion vs. Taurus seems to confirm this scenario.

1. Introduction

In a recent paper (Robberto et al. 2004), we have presented the first measures of mass accretion rates on stars in the core of the Orion Nebula Cluster ("Trapezium Cluster"). Using the UV excess in the Balmer continuum, measured through the F336W filter of the *WFPC2* onboard *HST*, and the known correlation between the U-band excess and the total accretion luminosity (Gullbring et al. 1998), we estimate accretion rates in the range 10^{-8}–10^{-12} $M_{\odot}yr^{-1}$. For stars older than 1 Myr there is some evidence of a relation between mass accretion rates and stellar age. Overall, mass accretion rates are significantly lower than those measured by other authors in the Orion flanking fields (Rebull et al. 2000) or in Taurus-Auriga association (Hartmann et al. 1988). In particular, in the Taurus-Auriga association Hartmann et al. find an average accretion rate of 10^{-8} $M_{\odot}yr^{-1}$ for a sample containing a similar number of stars with masses and ages comparable to ours in the Trapezium cluster. It appears that the main accretion phase in the Trapezium cluster has been recently terminated, nearly for all sources and independently on their ages.

E. Corbelli et al. (eds.), The Initial Mass Function 50 Years Later, 455–458.

2. Disk evolution in a young OB cluster

Mass accretion is expected to decrease with time and eventually cease with disk exhaustion. In our case, however, it seems rather artificial to have all disks depleted almost at the same time across such a young cluster ($\sim$ 1 Myr). An attractive possibility is to attribute the drop in mass accretion to a common trigger event caused by an external agent. It is known that disks in Orion are photo-ablated by the UV radiation of OB stars, the "proplyd" phenomenon (O'Dell, Wen, & Hu 1993, O'Dell & Wen 1994), with estimated mass-loss rates $10^{-7} - 10^{-6}$ $M_{\odot}yr^{-1}$ (Churchwell et al. 1987, Henney & O'Dell 1999). When a protostar is exposed to the ionizing flux of a new-born OB star, the disk mass decreases rapidly with time. This may regulate the mass accretion rate through the disk and, therefore, to the star.

3. Consequences for the IMF

Hester et al. (1996) have proposed for M16 a scenario in which O-type stars evaporate the dusty cocoons hosting a nearby forming protostar, suggesting that this process, rather than stellar mass loss, determines the final mass of stars near ionizing sources. In Orion we find evidence that this type of process is active at later phases, when the stars with their circumstellar disks are completely exposed to the environmental radiation. If low-mass stars terminate their pre-main sequence evolution with masses lower than those they would have reached if disk accretion could have proceeded undisturbed until the final disk consumption, the IMF of the cluster should be affected. For isolated star formation, i.e. occurring with negligible influence from the environment, the final stellar mass is fixed in the early stages of protostar formation through competitive collapse/fragmentation phenomena regulated by magnetic fields or supersonic turbulence. Most of the stellar material is then accreted from the circumstellar disks at a rate that decreases with time. There is growing evidence that low mass stars and sub-stellar mass objects share this type of evolution (Muzerolle et al. 2003), possibly on longer time scales. However, if a star is not isolated, envelope and especially disk evaporation will eventually abort the star formation process. Low mass objects, therefore, remain "dwarfed" in a OB cluster, resulting in a relative overabundance of low mass stars and brown dwarfs. Within this scenario, one should expect to find systematic differences between the stellar population in the core of the Orion Nebula and that in other regions, such as the Taurus-Auriga association, or the outskirts of the Orion Nebula itself, where the ionizing flux is negligible. Various authors, in particular Luhman (2000), have recently reported an overabundance by a factor of 2 in brown dwarfs in Orion relative to Taurus. At the same time, the overabundance of low mass stars and brown dwarfs should be compensated for by a depletion of intermediate mass stars, and it is intriguing to note that Hillenbrand (1997)

found a flattening of the IMF in the core of the Trapezium cluster at masses lower than 0.6 $M_{\odot}$, whereas the overall Orion stellar population follows the Salpeter law down to the completeness limit of her survey, $0.1\ M_{\odot}$. This flattening could be the final outcome of the disk depletion, with all low mass stars cascading into lower mass bins. There is, in conclusion, growing observational evidence of a feedback mechanism intrinsic to the IMF, in the sense that the formation and onset of massive stars affects the mass distribution of low mass stars within the same cluster.

References

Churchwell, E., Wood, D. O. S., Felli, M., & Massi, M. 1987, ApJ, 321, 516

Gullbring, E., Hartmann, L., Briceno, C., & Calvet, N. 1998, ApJ, 492, 323

Hartmann, L., Calvet, N., Gullbring, E., & D'Alessio, P. 1998, ApJ, 495, 385

Henney, W. J., & O'Dell, C. R. 1999, AJ, 118, 2350

Hester, J. J. et al. 1997, ApJ, 111, 2349

Hillenbrand, L. A. 1997, AJ, 113, 1733

Luhman, K. L. 2000, ApJ, 544, 1044

Muzerolle, J., Hillenbrand, L., Calvet, N., Briceño, C., Hartmann, L. 2003, ApJ, 592, 266

O'Dell, C. R., & Wen, Z. 1994, AJ, 436, 194

O'Dell, C. R., Wen, Z., & Hu, X. 1993, ApJ, 410, 696

Rebull, L. M., Hillenbrand, L. A., Strom, S. E., Duncan, D. K., Patten, B. M., Pavlovsky, C. M., Makidon, R., & Adams, M. T. 2000, AJ, 119, 3026

Robberto, M., Song, J., Mora Carrillo, G., Beckwith, S. V. W., Makidon, R. B., & Panagia, N. 2004 ApJ, 606, 952

Figure 1. Lizards in the sun, including Massimo Robberto.

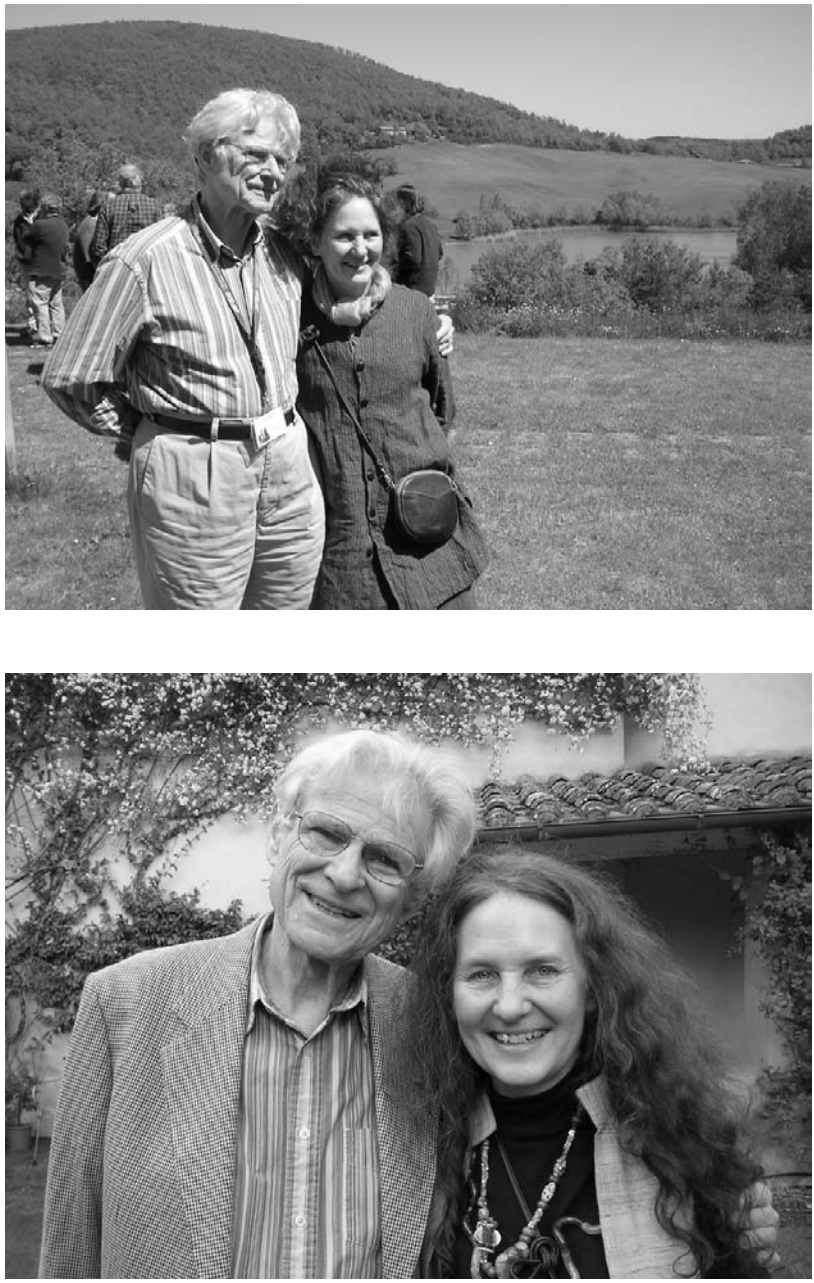

Figure 2. Ed and Lhamo.

TURBULENCE AND MAGNETIC FIELDS IN CLOUDS

Discussion

Shantanu Basu
Department of Physics and Astronomy, The University of Western Ontario, London, Ontario N6A 3K7, Canada
basu@astro.uwo.ca

Abstract We discuss several categories of models which may explain the IMF, including the possible role of turbulence and magnetic fields.

1. Introduction

Given the pervasive presence of non-thermal motions in molecular clouds and evidence for energetically significant magnetic fields, it is tempting to suggest that turbulence and/or magnetic fields play a critical role in determining the stellar initial mass function (IMF). In this discussion, we review several categories of IMF models, and discuss how they are influenced by turbulence and magnetic fields.

On one hand, the IMF can be thought to be determined by a direct mapping from the core (or condensation) mass function (CMF), if the core truly represents a finite mass reservoir for star formation. Alternatively, the IMF may be determined from interactions that happen very close to a forming protostar, as it accretes matter from its parent core. In the latter case, the CMF may not be directly mapped onto the IMF. We review several possibilities in the next two sections.

2. The CMF leads to the IMF

The main difficulty to overcome here is the definition of a core itself. A core boundary is not nearly as well defined as a stellar surface, so the mapping of a CMF to IMF is problematic from the outset.

Cores have often been defined as a region within which emission from a certain molecule is detected. This is hardly a physical demarcation. More recently, near-infrared absorption maps (Bacmann et al. 2000) have captured

E. Corbelli et al. (eds.), The Initial Mass Function 50 Years Later, 459–466.

the merger of a density profile into the background. This may represent a physical boundary. A theoretical definition of a core boundary may rely on the presence of a magnetically subcritical envelope around a supercritical inner region (the core), or it may rely on the (usually larger) gravitational zone of influence of a density peak.

In any case, there are three main candidates for the determination of the CMF: (1) pure gravitational fragmentation; (2) turbulent fragmentation, and (3) magnetically regulated fragmentation. Furthermore, in an extension to these models, the CMF (if clearly definable) may develop a power-law tail due to accretion effects. We treat this as a fourth possibility which is not independent of the first three.

2.1 Gravitational fragmentation

Any non-isotropic medium that is dominated by gravity is expected to fragment into Jeans-mass type fragments, through an initial collapse into a sheet, followed by the break up of the sheet. This is the famous Zeldovich (1970) hypothesis in cosmology. In the interstellar medium, sheet-like initial configurations may be promoted by effectively one-dimensional compressions due to supernova shock waves and expanding HII regions, or by relaxation along magnetic field lines. The preferred fragmentation scale in an isothermal non-magnetic flattened sheet of column density Σ is $\lambda_{\rm m} = 4.4\,c_{\rm s}^2/(G\Sigma)$ (Simon 1965), where $c_{\rm s}$ is the isothermal sound speed and G is the gravitational constant. The formation time for a cluster of stars is effectively the sound crossing time across this distance, typically less than a few Myr for most molecular clouds. Mass that does not accrete to one gravitating center is within the gravitational sphere of influence of a neighboring core. We note that the resulting CMF (by any definition) from this kind of fragmentation will likely be peaked around the Jeans mass $M \sim \Sigma\lambda_{\rm m}^2$, but has not yet been calculated in detail.

The most likely candidates for gravitational fragmentation are the embedded clusters in which multiple stars are forming in close proximity, and which account for a majority of star formation (Lada & Lada 2003). However, the above authors also point out that the star formation efficiency (SFE, defined as the fraction of gas mass converted into stars) in these clusters is still quite low, in the 10% - 30% range. Perhaps the feedback effect of outflows can explain at least the upper values ($\sim$ 30%) of SFE's (e.g., Matzner & McKee 2000). A full numerical simulation of the feedback on a cloud from outflows is still prohibitive. However, pure gravitational fragmentation does seem to be excluded as a possibility for giant molecular clouds (GMC's) as a whole, since their overall SFE is only a few percent (Lada & Lada 2003). This point can be traced back to Zuckerman & Evans (1974).

2.2 Turbulent fragmentation

A way to explain the low SFE is to postulate that turbulent support prevents gravitational fragmentation on large scales, but that cores are also created by turbulent compressions. This is broadly consistent with the observation that turbulent motions dominate on large scales but become sub-thermal on dense core scales, in accordance with the well-known linewidth (σ)-size (R) relation, $\sigma \propto R^{0.5}$ (e.g., Solomon et al. 1987). Strong turbulent driving in clouds can explain the overall low SFE (see Vazquez-Semadeni, this volume), by keeping most material in a disturbed and non-self-gravitating state. It has also been shown that isothermal turbulence leads to a lognormal probability density function (pdf) for the gas density (e.g., Padoan, Nordlund, & Jones 1997; Passot & Vazquez-Semadeni 1998; Scalo et al. 1998; Ostriker, Stone, & Gammie 2001; Klessen 2001). Elmegreen (2002) demonstrates that a lognormal density pdf will lead to power-law clump mass distribution when thresholded at various levels, with different indices for different threshold levels. Padoan & Nordlund (2002, see also Padoan in this volume) also demonstrate that a lognormal density pdf is consistent with a power-law CMF given that the power-spectrum is a power law, and assuming that the cores have sizes comparable to the thickness of post-shock gas layers.

In all models of turbulent fragmentation, an important question arises: is the CMF just a property of how cores are defined, or does it represent the finite reservoirs of mass that may be available for star formation? A further problem is that turbulence tends to decay away in a crossing time if not continually driven, so that turbulent fragmentation may quickly give way to gravitational fragmentation. If the latter leads to runaway peaks and star formation within a crossing time, we are again hard pressed to understand the overall low SFE of GMC's.

2.3 Magnetically regulated fragmentation

Real interstellar clouds are both turbulent and contain magnetic fields which are in approximate equipartition with gravity (e.g., Crutcher 1999). The turbulence itself likely consists of MHD disturbances. Therefore, a realistic scenario is that of turbulent dissipation followed by magnetically regulated fragmentation in dense regions. The unique features of fragmentation of clouds with near-critical mass-to-flux ratio are: (1) a longer timescale for collapse than simply the hydrodynamic crossing time, and (2) the outer envelopes may remain supported against global collapse. Basu & Mouschovias (1995) have demonstrated that a magnetically supercritical fragment within a subcritical envelope evolves very rapidly once it is large enough to also be thermally unstable. The resulting collapse scale is smaller than the the original fragmentation scale of a subcritical cloud. Hence, an inter-core medium exists which is subcritical and

remains in a state of slow evolution. Furthermore, Basu & Ciolek (2004) have demonstrated that even if the background cloud has an exactly critical mass-to-flux ratio, the mass and flux redistribution effected by ambipolar diffusion naturally leads to both supercritical cores and a subcritical envelope.

Magnetic fields may also prevent unstable fragments from becoming extremely elongated, as occurs in models of pure gravitational fragmentation (Miyama, Narita, & Hayashi 1987). Two-dimensional magnetic fragmentation models of Basu & Ciolek (2004) show much milder elongations when magnetic fields are significant, and are in principle more consistent with the inference from observations that cores are overall triaxial but more nearly oblate than prolate (Jones, Basu, & Dubinski 2001). Their results also show that the magnitude of infall motions and the preferred fragmentation scale are dependent on the initial mass-to-flux ratio. Li & Nakamura (2004, also Nakamura this volume) have developed a model of turbulent fragmentation in a subcritical cloud with ambipolar diffusion, also using a two-dimensional simulation. They show that supercritical fragments can be formed in a few Myr, but that the magnetic field helps maintain a relatively low SFE.

A key challenge to this theory is to find the putative subcritical envelopes through highly sensitive Zeeman observations of molecular cloud envelopes. If subcritical envelopes are observed, this will go a long way toward explaining the low inferred SFE. Current magnetic field data is consistent with a near-uniform (and near-critical) mass-to-flux ratio in the column density range $10^{21}\,\mathrm{cm}^{-2} - 10^{23}\,\mathrm{cm}^{-2}$. However, there is an apparent mild bias toward subcritical mass-to-flux ratios at low column densities (Crutcher 2004).

2.4 Accretion modification of the CMF

If any of the above scenarios lead to a lognormal initial distribution of core masses, it is possible that the gravitational influence of the core on the surrounding cloud will lead to accretion that alters the distribution of masses M. An original model of this type is due to Zinnecker (1982), in which Bondi accretion ($dM/dt \propto M^2$) leads to a power-law tail in the number (N) of stars per unit mass interval, i.e., $dN/dM \propto M^{-2}$. This is due to larger initial masses growing at a relatively faster rate. A different model in this category is due to Basu & Jones (2004, see also this volume); they show that an exponential distribution of accretion lifetimes and accretion rate $dM/dt \propto M$ can lead to a power-law tail in dN/dM. This can produce an IMF with a lognormal body and a power-law tail. A similar explanation was offered by Myers (2000).

3. The IMF from star-core interactions

There are two main ideas for how the IMF may be determined by interactions occurring very close to a forming protostar: (1) outflow limited accretion,

and (2) termination of accretion by an ejection process. In an extreme form of this approach, the CMF is irrelevant because infall is terminated before any finiteness of the available mass comes into play.

3.1 Outflow interactions

Strong outflows are present in the earliest observed stages of protostellar accretion (see André, this volume). It has been proposed that winds and/or swept-up outflows can reverse infall (e.g., Shu, Adams, & Lizano 1987). Some IMF models have been developed based on this concept. Adams & Fatuzzo (1996, see also Adams in this volume) have argued that mass accretion will be halted when its rate drops below the mass outflow rate. The presence of a variety of multiplicative input parameters leads them to infer a near-lognormal distribution for the IMF. A similar model has been presented by Silk (1995, see also this volume), which results in a power-law IMF. However, it is still not clear that outflows are sufficiently wide-angled to reverse infall in all directions, so a finite mass reservoir may still be necessary.

The best scenario may be a combination of a nearly finite mass reservoir and the action of outflows to clear residual material. Shu, Li, & Allen (2004) have carried forward the type of model presented by e.g., Basu & Mouschovias (1995) to its logical limit, by studying the accretion onto a protostar from a subcritical envelope. They find that a final equilibrium is possible only if the gravity of the point mass (the protostar) at the core can be offset by unrealistically large amounts of magnetic flux within the protostar. The breakdown of ideal MHD near the protostar will ultimately prevent magnetic levitation of the subcritical envelope, but outflows are invoked as a last line of defense against the low-level infall from the subcritical envelope.

The above scenario may be appropriate to explain isolated star formation as well as cluster formation in which the SFE is quite low. For regions that give rise to bound open clusters (a distinctively rare occurrence according to Lada & Lada 2003) the SFE must be rather high for the cluster to remain bound. In such cases, a simple gravitational (or highly supercritical) fragmentation model may be adequate.

3.2 Competitive accretion

Another process that occurs deep within a core is the interaction between protostars that may have formed in the same core. Multiple protostars come from direct fragmentation during collapse, or from the fragmentation of a circumstellar disk after the first protostar has formed. Bate, Bonnell, & Bromm (2003, see also Bate in this volume) have argued that the IMF can be explained by the evolution of multiple protostars which start out with a mass approximately equal to the Jeans mass for the density $n \sim 10^{10}\,\mathrm{cm}^{-3}$ at which the gas

becomes opaque. Dynamical interactions between the protostars then cause them to be ejected from the parent core at various stages of mass accretion from that core. Their simulations show this effect and the calculated protostar mass distributions resemble a lognormal, but may be interpreted as having a weak power-law tail. In this picture, star formation is very efficient, and the problem of low SFE is pushed back to the unmodeled regions outside the cluster-forming cores. Turbulence and magnetic fields are also not required except to understand the outer unmodeled regions.

4. Conclusions

Both turbulence and magnetic field effects are important physical processes in molecular cloud evolution, and are a great challenge to theorists due to the complexity of the nonlinear equations that describe them. However, for the purpose of this discussion, it is also worth asking the hard question: do these effects fundamentally affect the IMF? Heyer (this volume) has questioned the existence of any linkage between turbulent properties of a cloud and the rate of star formation within them. Large-scale magnetic fields are also invoked as a formidable opponent to gravity, but if most stars form in local cluster-forming regions which are supercritical, then the magnetic field may not be a dominant effect. On the other hand, magnetic fields are necessary for the generation of outflows, which are in turn invoked to explain why observed dense embedded clusters have an SFE no greater than about 30%. A key outstanding question is whether outflows can really limit the SFE to 30% (or less!) in a highly supercritical cloud region. An ultimate model of star formation will likely have to account for the low SFE of GMC envelopes (using turbulent and/or magnetic effects) as well as include the self-consistent feedback effect of outflows upon gravitational collapse.

Acknowledgments I wish to thank the organizing committee for the outstanding concept of IMF@50 and for creating a remarkably stimulating meeting. I also thank Martin Houde, Carol Jones, and Takahiro Kudoh for their comments on the manuscript.

References

Adams, F. C., & Fatuzzo, M. 1996, ApJ, 464, 256
Bacmann, A., André, P., Puget, J. L. et al. 2000, A&A, 314, 625
Basu, S., & Ciolek, G. E. 2004, ApJ, 607, L39
Basu, S., & Jones, C. E. 2004, MNRAS, 347, L47
Basu, S., & Mouschovias, T. Ch. 1995, ApJ, 453, 271
Bate, M. R, Bonnell, I. A., & Bromm, V. 2003, MNRAS, 339, 577
Crutcher, R. M. 1999, ApJ, 520, 706

Crutcher, R. M. 2004, in Magnetic Fields and Star Formation: Theory versus Observations, eds. A. I. Gomez-de Castro et al., in press
Elmegreen, B. G. 2002, ApJ, 564, 773
Jones, C. E., Basu. S., & Dubinski, J. 2001, ApJ, 551, 387
Klessen, R. S. 2001, ApJ, 556, 837
Lada, C. J., & Lada, E. A. 2003, ARA&A, 41, 57
Li, Z.-Y., & Nakamura, F. 2004, ApJ, 609, L83
Matzner, C. D., & McKee, C. F. 2000, ApJ, 545, 364
Miyama, S. M., Narita, S., & Hayashi, C. 1987, Prog. Theor. Phys., 78, 1273
Myers, P. C. 2000, ApJ, 530, L119
Ostriker, E. C., Stone, J. M., & Gammie, C. F. 2001, ApJ, 546, 980
Padoan, P., Nordlund, A., & Jones, B. J. T. 1997, MNRAS, 288, 145
Padoan, P., & Nordlund, A. 2002, ApJ, 576, 870
Passot, T., & Vazquez-Semadeni, E. 1998, Phys. Rev. E, 58, 4501
Silk, J. 1995, ApJ, 438, L41
Scalo, J. M., Vazquez-Semadeni, E., Chappell, D., & Passot, T. 1998, ApJ, 504, 835
Simon, R. 1965, Annales d'Astrophysique, 28, 40
Solomon, P. M., Rivolo, A. R., Barrett, J., & Yahil, A. 1987, ApJ, 319, 730
Shu, F. H., Li, Z.-Y., & Allen, A. 2004, ApJ, 601, 930
Shu, F. H., Adams, F. C., & Lizano, S. 1987, ARA&A, 25, 23
Zeldovich, Y. B. 1970, A&A, 5, 84
Zinnecker H., 1982, in Symposium on the Orion Nebula to Honour Henry Draper, A. E. Glassgold et al., eds, (new York: New York Academy of Sciences), 226
Zuckerman, B., & Evans, N. J. 1974, ApJ, 192, L149

Figure 1. Fumitaka Nakamura and Shantanu Basu.

Figure 2. Richard Larson and Shu-ichiro Inutsuka (Lorenzo Falai in the background).

Figure 3. Volker Bromm and Cathie Clarke in the courtyard.

VIII

THE “INITIAL” IMF

Figure 4. Confinensamble playing the concert in the Abbazia di Spineto.

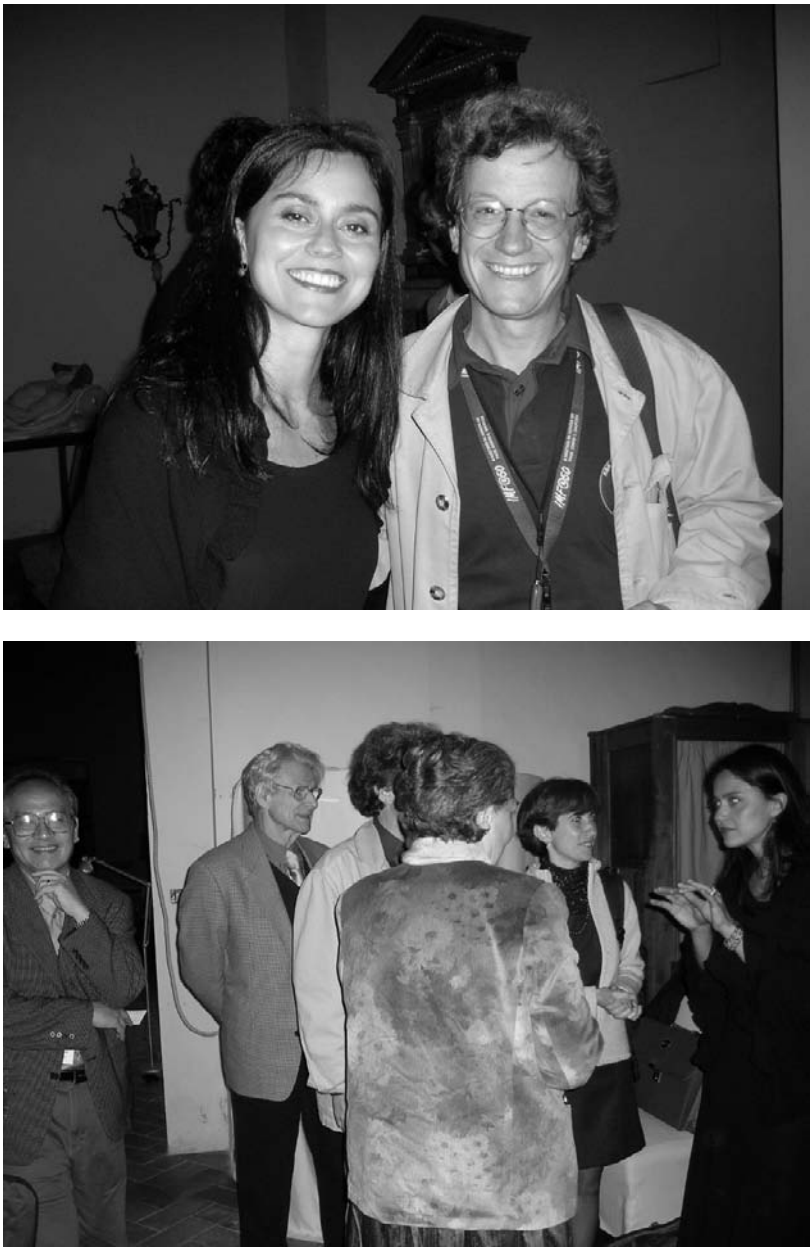

Figure 5. Anna Aurigi, the soprano singer.

THE PRIMORDIAL IMF

Volker Bromm
Department of Astronomy, University of Texas, Austin, TX 78712, USA
vbromm@astro.as.utexas.edu

Abstract I discuss the formation of the first stars in the universe. The results from recent theoretical and numerical work suggest that these so-called Population III stars were typically many times more massive than stars forming today. I speculate that in addition to this overall larger mass scale, primordial star formation was characterized by a very different initial mass function (IMF). Thus, we may have to consider the earliest cosmic times to find significant deviations from the otherwise so robustly universal Salpeter IMF.

1. Introduction

For over five decades, elucidating the physical processes which govern the formation of stars, and which shape the initial mass function (IMF) has been a preeminent challenge in astrophysics. Until quite recently, most of our attention has been directed toward star formation in the local universe, where the metal-rich chemistry, magnetohydrodynamics, and radiative transfer involved is complex, and we still lack a comprehensive theoretical framework that predicts the IMF from first principles (for a recent review, see Larson 2003). Empirically, however, we have learned that the present-day star formation process is surprisingly universal, resulting in an IMF which is close to the Salpeter form at the high mass end (Salpeter 1955).

Star formation in the high redshift universe, on the other hand, poses a theoretically more tractable problem due to a number of simplifying features, such as: (i) the initial absence of heavy elements and therefore of dust; and (ii) the absence of dynamically-significant magnetic fields in the pristine gas left over from the big bang. The cooling of the primordial gas does then only depend on hydrogen in its atomic and molecular form. Whereas the initial state of the star forming cloud is poorly constrained in the present-day interstellar medium, the corresponding initial conditions for primordial star formation are simple, given by the popular ΛCDM model of cosmological structure formation.

E. Corbelli et al. (eds.), The Initial Mass Function 50 Years Later, 469–474.

How did the first stars form, what were their physical properties, and what was their impact on cosmic history (Larson 1998)? The first stars constitute the so-called Population III (e.g., Carr 1987), and formed at the end of the cosmic dark ages. They contributed to the reionization of the universe, produced the first heavy elements, dispersed them into the intergalactic medium (IGM), and consequently had important effects on subsequent galaxy formation and on the large-scale polarization anisotropies of the cosmic microwave background (for recent reviews, see Barkana & Loeb 2001; Bromm & Larson 2004). *When did the cosmic dark ages end?* In the context of popular cold dark matter (CDM) models of hierarchical structure formation, the first stars are predicted to have formed in dark matter halos of mass $\sim 10^6 M_\odot$ that collapsed at redshifts $z \simeq 20 - 30$ (e.g., Yoshida et al. 2003).

Results from recent numerical simulations of the collapse and fragmentation of primordial clouds suggest that the first stars were predominantly very massive, with typical masses $M_* \geq 100 M_\odot$ (Bromm, Coppi, & Larson 1999, 2002; Abel, Bryan, & Norman 2000, 2002; Nakamura & Umemura 2001). Despite the progress already made, many important questions remain unanswered. Among them is the particularly important one: *How does the primordial IMF look like?* Having constrained the characteristic mass scale, still leaves undetermined the overall range of stellar masses and the detailed functional form. In addition, it is presently unknown whether binaries or, more generally, clusters of zero-metallicity stars, can form. *What is the nature of the feedback that the first stars exert on their surroundings?* The first stars are expected to produce copious amounts of UV photons (e.g., Cen 2003; Wyithe & Loeb 2003), and to possibly explode as energetic supernovae (e.g., Mori, Ferrara, & Madau 2002; Bromm, Yoshida, & Hernquist 2003). These negative feedback effects could suppress star formation in neighboring high-density clumps (e.g., Mackey, Bromm, & Hernquist 2003).

Predicting the properties of the first sources of light is important for the design of upcoming instruments, such as the *James Webb Space Telescope* (JWST) [1], or the next generation of large (> 10m) ground-based telescopes. The hope is that over the upcoming decade, it will become possible to confront current theoretical predictions about the properties of the first stars with direct observational data.

2. The Characteristic Mass Scale of Population III Star Formation

How did the first stars form? A complete answer to this question would entail a theoretical prediction for the Population III IMF, which is rather chal-

[1] See http:// ngst.gsfc.nasa.gov.

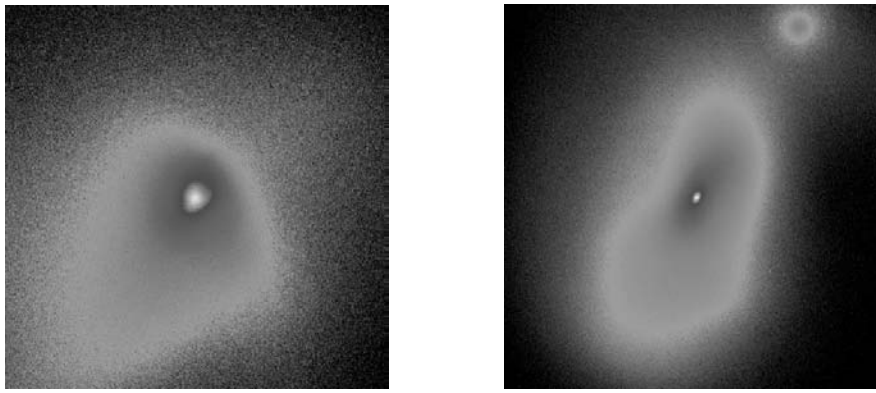

Figure 1. Collapse and fragmentation of a primordial cloud (from Bromm & Loeb 2004). Shown is the projected gas density at a redshift $z \simeq 21.5$, briefly after gravitational runaway collapse has commenced in the center of the cloud. Left panel: The coarse-grained morphology in a box with linear physical size of 23.5 pc. Right panel: The fine-grained morphology in a box with linear physical size of 0.5 pc. The central density peak, vigorously gaining mass by accretion, is accompanied by a secondary clump.

lenging. Let us start by addressing the simpler problem of estimating the characteristic mass scale, M_c, of the first stars. This mass scale is observed to be $M_c \sim 1 M_\odot$ in the present-day universe. To investigate the collapse and fragmentation of primordial gas, Bromm et al. (1999, 2002) have carried out numerical simulations, using the smoothed particle hydrodynamics (SPH) method. This work included the chemistry and cooling physics relevant for the evolution of metal-free gas. Improving on earlier work (Bromm et al. 1999, 2002) by initializing the simulation according to the ΛCDM model, Bromm & Loeb (2004) focused on an isolated overdense region that corresponds to a $3\sigma-$peak: a halo containing a total mass of $10^6 M_\odot$, and collapsing at a redshift $z_{\rm vir} \simeq 20$. Figure 1 (*left panel*) shows the gas density within the central ~ 25 pc, briefly after the first high-density clump has formed as a result of gravitational runaway collapse.

How massive were the first stars? Star formation typically proceeds from the 'inside-out', through the accretion of gas onto a central hydrostatic core. Whereas the initial mass of the hydrostatic core is very similar for primordial and present-day star formation (Omukai & Nishi 1998), the accretion process – ultimately responsible for setting the final stellar mass, is expected to be rather different. On dimensional grounds, the accretion rate is simply related to the sound speed cubed over Newton's constant (or equivalently given by the ratio of the Jeans mass and the free-fall time): $\dot{M}_{\rm acc} \sim c_s^3/G \propto T^{3/2}$. A simple comparison of the temperatures in present-day star forming regions

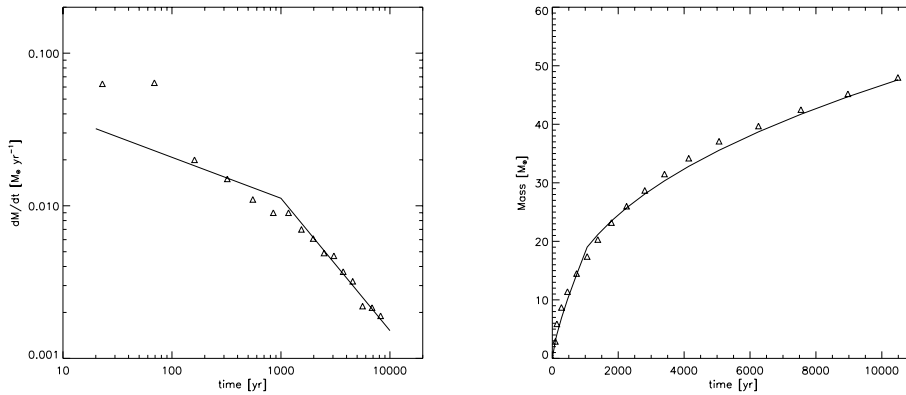

Figure 2. Accretion onto a primordial protostar (from Bromm & Loeb 2004). The morphology of this accretion flow is shown in Fig. 1. Left panel: Accretion rate (in $M_\odot$ yr^{-1}) vs. time (in yr) since molecular core formation. Right panel: Mass of the central core (in $M_\odot$) vs. time. Solid line: Accretion history approximated as: $M_* \propto t^{0.75}$ at $t < 10^3$ yr, and $M_* \propto t^{0.4}$ afterwards. Using this analytical approximation, we extrapolate that the protostellar mass has grown to $\sim 120 M_\odot$ after $\sim 10^5$ yr, and to $\sim 500 M_\odot$ after $\sim 3 \times 10^6$ yr, the total lifetime of a very massive star.

($T \sim 10$ K) with those in primordial ones ($T \sim 200 - 300$ K) already indicates a difference in the accretion rate of more than two orders of magnitude.

Our high-resolution simulation (Bromm & Loeb 2004) enables us to study the three-dimensional accretion flow around the protostar (see also Ripamonti et al. 2002; Omukai & Palla 2003; Tan & McKee 2004). We allow the gas to reach densities of 10^{12} cm^{-3} before being incorporated into a central sink particle. At these high densities, three-body reactions (Palla, Salpeter, & Stahler 1983) have converted the gas into a fully molecular form. Figure 2 shows how the molecular core grows in mass over the first $\sim 10^4$ yr after its formation. The accretion rate (*left panel*) is initially very high, $\dot{M}_{\rm acc} \sim 0.1 M_\odot$ yr^{-1}, and rapidly declines afterwards. The mass of the molecular core (*right panel*), taken as an estimator of the protostellar mass, grows approximately as: $M_* \sim \int \dot{M}_{\rm acc} {\rm d}t \propto t^{0.75}$ at $t < 10^3$ yr, and $M_* \propto t^{0.4}$ subsequently. A rough upper limit for the final mass of the star is then: $M_*(t = 3 \times 10^6 {\rm yr}) \sim 500 M_\odot$. In deriving this upper bound, we have conservatively assumed that accretion cannot go on for longer than the total lifetime of a very massive star (VMS).

Can a Population III star ever reach this asymptotic mass limit? The answer to this question is not yet known with any certainty, and it depends on whether the accretion from a dust-free envelope is eventually terminated by feedback from the star (e.g., Ripamonti et al. 2002; Omukai & Palla 2003; Tan & McKee 2004). The standard mechanism by which accretion may be terminated in metal-rich gas, namely radiation pressure on dust grains (Wolfire &

Cassinelli 1987), is evidently not effective for gas with a primordial composition. Recently, it has been speculated that accretion could instead be turned off through the formation of an H II region (Omukai & Inutsuka 2002), or through the radiation pressure exerted by trapped Lyα photons (Tan & McKee 2004). The termination of the accretion process defines the current unsolved frontier in studies of Population III star formation.

3. The Primordial IMF

Although there is general agreement between different studies on the overall magnitude of the fragmentation scale, it is still not clear whether Population III stars always form in isolation, or sometimes in groups and small clusters. Whether indeed primordial clusters of metal-free stars are able to form in the first galaxies is an important open question. The answer will determine the proper interpretation of the primordial IMF. If Population III star formation were generally clustered, as is the case in the present-day universe, the IMF would simply describe the actual distribution of stellar masses in a given cluster. If, on the other hand, the first stars formed predominantly in isolation, the IMF would have the meaning of a probability distribution in a random process that results in only one stellar mass per 'draw'. The present-day IMF, however, appears to be shaped largely by the chaotic interactions between many accreting protostars in a common reservoir of gas (e.g., Bate, Bonnell, & Bromm 2003; Chabrier 2003). If there were no cluster to begin with, how would the IMF be build up? Would there still be a self-similar extension at masses $M > M_c$? Although progress has to rely on improved simulations in future work, it is interesting to speculate at the outcome.

At one extreme, the mass of a Population III star could be completely set by protostellar feedback effects. Initially, the protostar would have a mass close to the opacity limit, $M_{\rm F} \sim 10^{-3} M_{\odot}$, to subsequently grow by accretion (Omukai & Nishi 1998; Bromm & Loeb 2004). Once the protostar has reached a critical mass, $M_{\rm term}$, the stellar radiation field would have become sufficiently intense to terminate accretion. In this case, the corresponding IMF may be Gaussian, or asymptotically given by a Dirac delta function. The mass of a Population III star would then be a fundamental quantity, somewhat akin to the Chandrasekhar mass: $M_{\rm PopIII} \sim M_{\rm term} \sim {\rm const}$. At the other extreme, feedback effects may be unable to ever terminate the accretion process. Here, the stellar mass would simply be set by the mass of the host clump: $M_{\rm PopIII} \sim M_{\rm clump}$. The appropriate IMF would then reflect the range of conditions in the hydrogen-helium clumps inside of which the Population III star forms, and would possibly be given by a log-normal distribution (e.g., Chabrier 2003). It will be exciting to explore the true nature of the primordial IMF,

through a confluence of observations and ever more sophisticated numerical simulations.

References

Abel, T., Bryan, G. L., & Norman, M. L. 2000, ApJ, 540, 39
Abel, T., Bryan, G. L., & Norman, M. L. 2002, Science, 295, 93
Barkana, R., & Loeb, A. 2001, Physics Reports, 349, 125
Bate, M. R., Bonnell, I. A., & Bromm, V. 2003, MNRAS, 339, 577
Bromm, V., Coppi, P. S., & Larson, R. B. 1999, ApJ, 527, L5
Bromm, V., Coppi, P. S., & Larson, R. B. 2002, ApJ, 564, 23
Bromm, V., & Larson, R. B. 2004, ARAA, 42, 79
Bromm, V., & Loeb, A. 2004, New Astron., 9, 353
Bromm, V., Yoshida, N., & Hernquist, L. 2003, ApJ, 596, L135
Carr, B. J. 1987, Nature, 326, 829
Cen, R. 2003, ApJ, 591, L5
Chabrier, G. 2003, PASP, 115, 763
Larson, R. B. 1998, MNRAS, 301, 569
Larson, R. B. 2003, Rep. Prog. Phys., 66, 1651
Mackey, J., Bromm, V., & Hernquist, L. 2003, ApJ, 586, 1
Mori, M., Ferrara, A., & Madau, P. 2002, ApJ, 571, 40
Nakamura, F., & Umemura, M. 2001, ApJ, 548, 19
Omukai, K., & Inutsuka, S. 2002, MNRAS, 332, 59
Omukai, K., & Nishi, R. 1998, ApJ, 508, 141
Omukai, K., & Palla, F. 2003, ApJ, 589, 677
Palla, F., Salpeter, E. E., & Stahler, S. W. 1983, ApJ, 271, 632
Ripamonti, E., Haardt, F., Ferrara, A., & Colpi, M. 2002, MNRAS, 334, 401
Salpeter, E. E. 1955, ApJ, 121, 161
Tan, J. C., & McKee, C. F. 2004, ApJ, 603, 383
Wolfire, M. G., & Cassinelli, J. P. 1987, ApJ, 319, 850
Wyithe, J. S. B., & Loeb, A. 2003, ApJ, 588, L69
Yoshida, N., Abel, T., Hernquist, L., & Sugiyama, N. 2003, ApJ, 592, 645

COSMIC RELEVANCE OF THE FIRST STARS

Raffaella Schneider
Centro Enrico Fermi, Via Panisperna 89/A 00184 Roma, Italy,
INAF/Osservatorio Astrofisico di Arcetri, Largo Enrico Fermi 5 50125 Firenze, Italy
raffa@arcetri.astro.it

Abstract Theoretical results from cosmological simulations consistently predict that the first (PopIII) stars formed in the universe were very massive ($M \geq 100 M_{\odot}$). The detection of these very early cosmic star formation records represents the central goal of future instrumental facilities. On the other hand, observations in the present-day universe show that PopII/I stars form according to a Salpeter IMF with a characteristic mass of $\sim 1 M_{\odot}$. This situation stimulates a few fundamental questions, such as *Has a transition from the early massive star formation mode occurred? What physical processes caused it? When did it happen? What are its cosmological consequences?*

1. The Chemical Feedback

A number of independent studies yield a consistent result: the collapse of metal-free gas clouds lead to the formation of stars with characteristic mass 100 - 600 $M_{\odot}$ (see the contribution of Volker Bromm in this volume). In spite of this general agreement, very little is known about the shape of the IMF in primordial star forming regions. However, at least a fraction of the first stars must have masses in the range $140 - 260\ M_{\odot}$ to avoid the so-called *star formation conundrum* (Schneider et al. 2002). Indeed, stellar evolution studies have shown that non rotating Z=0 stars with mass below $140\ M_{\odot}$ (but larger than $50\ M_{\odot}$) and above $260\ M_{\odot}$ cannot avoid complete collapse to black holes and are unable to eject their metals (Heger & Woosley 2002). Conversely, stars with mass in the range $140 - 260\ M_{\odot}$ are completely disrupted in pair-instability supernova explosions (PISN) and eject about half of their initial mass in heavy elements. The ashes of these first supernova explosions pollute with metals the gas out of which subsequent generations of low-mass PopII/I stars form, driving a transition from a top-heavy IMF to a 'Salpeter-like' IMF (for a more extensive discussion on the critical metallicity threshold $Z_{\rm cr}$ we refer to Schneider et al. 2002, 2003).

E. Corbelli et al. (eds.), The Initial Mass Function 50 Years Later, 475–476.

Thus, the cosmic relevance of Pop III stars depends on the efficiency of metal enrichment from the first stellar explosions, the so-called *chemical feedback*, which is strictly linked to the number of Pop III stars that explode as PISN, the metal ejection efficiency, diffusion and mixing in the intergalactic medium. If a large fraction of first stars is nucleosynthetically sterile and ends up with the formation of very massive black holes, then the chemical feedback is less efficient and the transition from PopIII star formation epoch to PopII/I star formation epoch (or, equivalently from a top-heavy IMF to a 'Salpeter-like' IMF) can be delayed. This scenario seems to be required to account for the amplitude and anisotropy excess observed in the NIRB (Salvaterra & Ferrara 2003; Magliocchetti, Salvaterra & Ferrara 2003).

It is very likely that the transition occurred rather smoothly because the process of metal enrichment is highly inhomogeneous (Madau, Ferrara & Rees 2001; Scannapieco, Ferrara & Madau 2002). Even at moderate redshifts, $z \approx 3$ the clustering properties of CIV and SiIV QSO absorption systems are consistent with a metal filling factor of 10%, showing that metal enrichment is incomplete and inhomogeneous (Schaye et al. 2003). As a consequence, the use of the critical metallicity as a global criterion is somewhat misleading because chemical feedback is a *local process*, with regions close to star formation sites rapidly becoming metal-polluted and overshooting $Z_{\rm cr}$, and others remaining essentially metal-free. Thus, PopIII and PopII/I star formation modes could have been coeval and detectable signatures from PopIII stars could continue well after the volume-averaged metallicity has become larger than critical (Scannapieco, Schneider & Ferrara 2003).

References

Heger, A. & Woosley, S. 2002, ApJ, 567, 532
Madau, P., Ferrara, A. & Rees, M. J. 2001, ApJ, 555, 9
Magliocchetti M., Salvaterra R. & Ferrara A., 2003, MNRAS, 342, 25
Salvaterra, R. & Ferrara A. 2003, MNRAS, 339, 973
Scannapieco, E., Ferrara, A. & Madau, P. 2002, ApJ, 574, 590
Scannapieco, E., Schneider, R. & Ferrara, A. 2003, ApJ, 589, 1
Schaye, J. et al. 2003, ApJ, 596, 768
Schneider R., Ferrara A., Natarajan P., & Omukai K. 2002, ApJ, 571, 30
Schneider R., Ferrara A., Salvaterra R., Omukai K., & Bromm V. 2003, Nature, 422, 869

STAR FORMATION TRIGGERED BY FIRST SUPERNOVAE

Fumitaka Nakamura
Niigata University, 8050 Ikarashi-2, Niigata 950-2181, Japan
fnakamur@ed.niigata-u.ac.jp

1. Introduction

Recent studies based on multi-dimensional numerical simulations have suggested that the first generation stars are low-mass deficient and their initial mass function is likely to be top-heavy. Massive first stars are expected to affect the evolution of the surrounding medium through their UV radiation and supernova explosions. Both processes should influence subsequent star formation by changing the thermal and dynamic property of the ambient gas. Whether first supernovae can trigger subsequent star formation has already been discussed in order to explain the metal abundance pattern of the extremely metal-poor stars observed in our Galactic halo. In those studies, however, the masses of the progenitor stars (i.e., the first stars) have been a central issue under debate, and the characteristics of the next-generation stars so formed have been directed little attention. In this study, we reexamine the condition that the first supernova can trigger subsequent star formation, taking into account non-equilibrium chemistry, and try to estimate the typical masses of the next-generation stars.

2. Results and Conclusion

As a supernova shell expands and radiative cooling becomes efficient, a cooling shell is formed. The cooling shell is likely to fragment into many dense self-gravitating clumps where next-generation stars are expected to be formed. Here, we follow the expansion of the supernova shell and its subsequent fragmentation separately. First, the evolution of the supernova shell is followed from the free-expansion to the radiative cooling phases by means of a semi-analytic approximation. Non-equilibrium chemical and thermal evolution of the gas shell is solved numerically. We then derive the condition that the gas shell becomes self-gravitating by comparing several characteristic timescales. Next, the fragmenation of the cooling shell is followed numerically with 2D

E. Corbelli et al. (eds.), The Initial Mass Function 50 Years Later, 477–478.

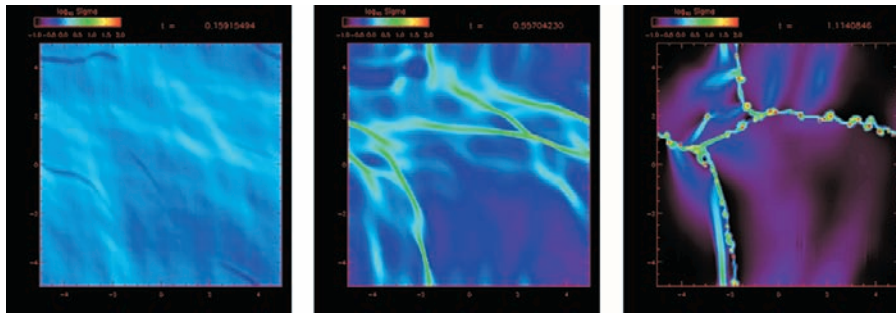

Figure 1. Fragmentation of a self-gravitating SNR shell

hydrodynamic simulations under the assumption that the shell is a geometrically thin sheet if the gas shell becomes self-gravitating. The semi-analytic solutions indicate that the expansion of the self-gravitating shell is very slow compared to the free-fall time. Thus, we neglect the expansion of the gas shell. We also consider the case in which the metalicity is smaller than 10^{-3} $Z_{\odot}$, below which the metal cooling plays a minor role in *low-density* gas. The effects of metal mixing will be considered in future.

Our calculations indicate that the gas shell can become self-gravitating relatively easily and the temperature descends to $\sim 10^2$ K due to HD cooling instead of H_2. The details will be shown elsewhere. In the following, we describe the numerical results on fragmentation of the self-gravitating gas shell. Figure 1 shows the snapshots of the supernova shell at different 3 times. At the initial state, the small velocity fluctuations are added. The shell begins to break up into many clumps whose masses are around $10 - 40$ $M_{\odot}$. The clumps so formed tend to rotate very rapidly. The magnetic braking is not likely to contribute to the efficient angular momentum transfer in the clumps, implying that they tend to have rotation energies larger than dense cores observed in nearby star-forming regions like Taurus and Orion. The clumps are also interacting with themselves, leading to the formation of binaries or small multiple stars. Thus, we conclude that if the metal mixing is inefficient, massive binary and multiple stars are a natural outcome of fragmentation of a gas shell formed by a first supernova. We note that tendency to binary formation would be independent of metallicity, although the masses of clumps would be small for high metallicity.

DETECTING PRIMORDIAL STARS

Nino Panagia
ESA/Space Telescope Science Institute, 3700 San Martin Drive, Baltimore, MD, USA
panagia@stsci.edu

Abstract We discuss the expected properties of the first stellar generations in the Universe. We find that it is possible to discern truly primordial populations from the next generation of stars by measuring the metallicity of high-z star forming objects. The very low background of the future James Webb Space Telescope (*JWST*) will enable it to image and study first-light sources at very high redshifts, whereas its relatively small collecting area limits its capability in obtaining spectra of z$\sim$10–15 first-light sources to either the bright end of their luminosity function or to strongly lensed sources. With a suitable investment of observing time *JWST* will be able to detect *individual* Population III supernovae, thus identifying the very first stars that formed in the Universe.

1. Introduction

One of the primary goals of modern cosmology is to answer the question: "When did galaxies begin to form in the early Universe and how did they form?" Theorists predict that the formation of galaxies is a gradual process in which progressively larger, virialized masses, composed mostly of dark matter, harbor star formation as time elapses. These dark-matter halos, which harbor stellar populations, then undergo a process of hierarchical merging and evolution to become the galaxies that make up the local Universe. In order to understand what are the earliest building blocks of galaxies like our own, one must detect and identify "first light" sources, i.e, the emission from the first objects in the Universe to undergo star formation.

The standard picture is that at zero metallicity the Jeans mass in star forming clouds is much higher than it is in the local Universe, and, therefore, the formation of massive stars, say, 100 $M_\odot$ or higher, is highly favored. The spectral distributions of these massive stars are characterized by effective temperatures on the Main Sequence (MS) around 10^5 K (*e.g.*, Tumlinson & Shull 2000, Bromm *et al.* 2001, Marigo *et al.* 2001). Due to their temperatures these stars are very effective in ionizing hydrogen and helium. It should be noted

E. Corbelli et al. (eds.), The Initial Mass Function 50 Years Later, 479–486.

that zero-metallicity (the so-called population III) stars of all masses have essentially the same MS luminosities as, but are much hotter than their solar metallicity analogues. Note also that only stars hotter than about 90,000 K are capable of ionizing He twice in appreciable quantities, say, more than about 10% of the total He content (*e.g.,* Oliva & Panagia 1983, Tumlinson & Shull 2000). As a consequence even the most massive population III stars can produce HeII lines only for a relatively small fraction of their lifetimes, say, about 1 Myr or about 1/3 of their lifetimes.

The second generation of stars forming out of pre-enriched material will probably have different properties because cooling by metal lines may become a viable mechanism and stars of lower masses may be produced (Bromm *et al.* 2001). On the other hand, if the metallicity is lower than about $5 \times 10^{-4} Z_{\odot}$, build up of H_2 due to self-shielding may occur, thus continuing the formation of very massive stars (Oh & Haiman 2002). Thus, it appears that in the zero-metallicity case one may expect a very top-heavy Initial Mass Function (IMF), whereas it is not clear if the second generation of stars is also top-heavy or follows a normal IMF.

2. Primordial HII Regions

The high effective temperatures of zero-metallicity stars imply not only high ionizing photon fluxes for both hydrogen and helium, but also low optical and UV fluxes. As a result, one should expect the rest-frame optical/UV spectrum of a primordial HII regions to be largely dominated by its nebular emission (both continuum and lines), so that the best strategy to detect the presence of primordial stars is to search for the emission from associated HII regions.

In Panagia *et al.* (2004, in preparation) we report on our calculations of the properties of primordial, zero-metallicity HII regions (*e.g.,* Figure 1). We find that the electron temperatures is in excess of 20,000 K and that 45% of the total luminosity is converted into the Ly-α line, resulting in a Ly-α equivalent width (EW) of 3000 Å (Bromm, Kudritzki & Loeb 2001). The helium lines are also strong, with the HeII λ1640 intensity comparable to that of Hβ (Tumlinson *et al.* 2001, Panagia *et al.* 2004, in preparation). An interesting feature of these models is that the continuum longwards of Ly-α is dominated by the two-photon nebular continuum. The Hα/Hβ ratio for these models is 3.2. Both the red continuum and the high Hα/Hβ ratio could be naively (and *incorrectly*) interpreted as a consequence of dust extinction even though no dust is present in these systems.

From the observational point of view one will generally be unable to measure a zero-metallicity but will usually be able to place an upper limit to it. When would such an upper limit be indicative that one is dealing with a population III object? According to Miralda-Escudé & Rees (1998) a metallic-

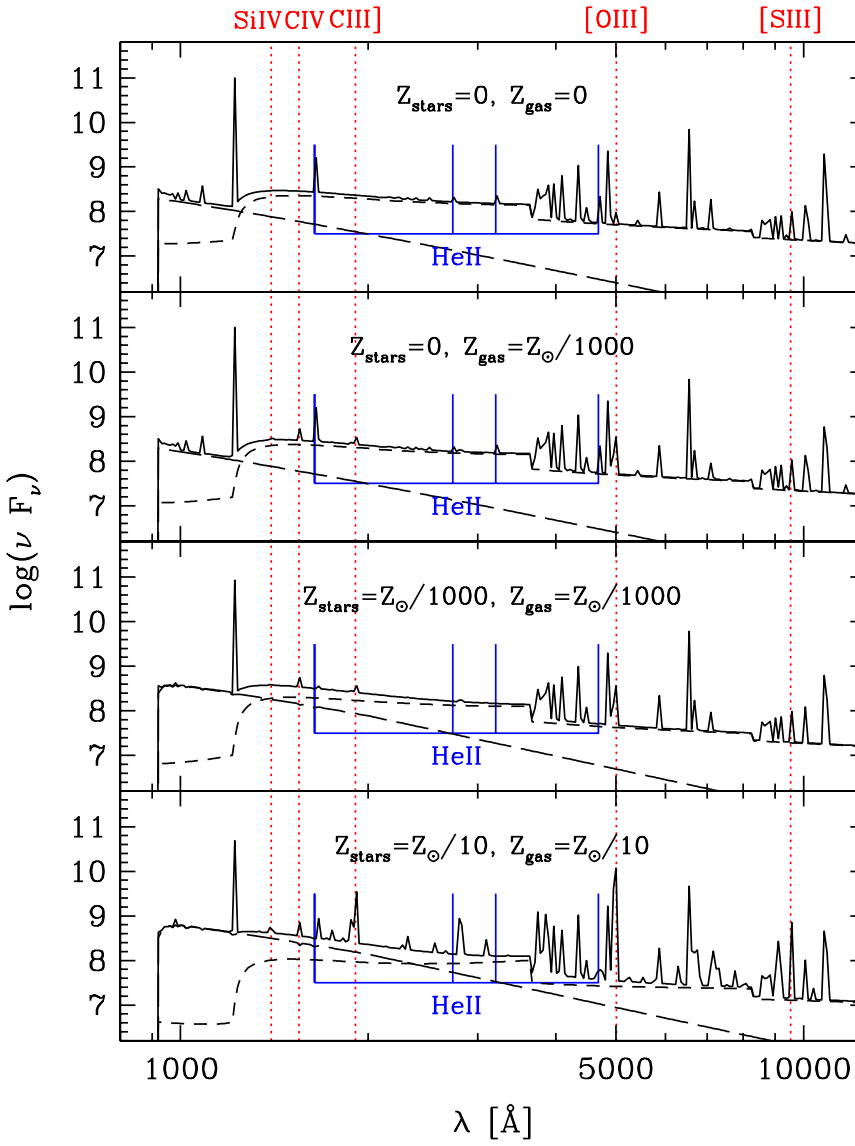

Figure 1. The synthetic spectrum of a zero-metallicity HII region (top panel) is compared to that of HII regions with various combinations of stellar and nebular metallicities (lower panels). The long-dashed and short-dashed lines represent the stellar and nebular continua, respectively.

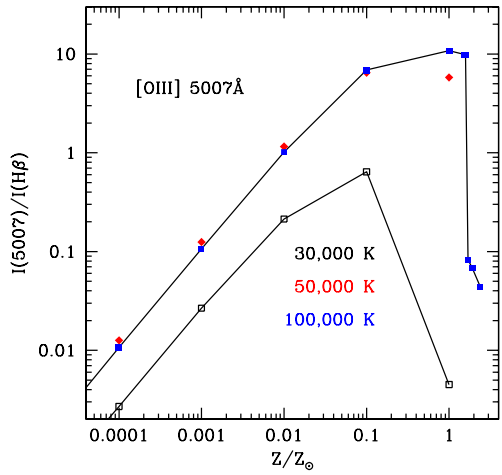

Figure 2. The ratio [OIII]λ5007 / Hβ is plotted as a function of metallicity for three different stellar temperatures: 30,000K (open squares and lower line), 50,000K (solid diamonds), and 100,000K (solid squares and upper line).

ity Z$\simeq 10^{-3} Z_{\odot}$ can be used as a dividing line between the pre- and post-reionization Universe. A similar value is obtained by considering that the first supernova (SN) going off in a primordial cloud will pollute it to a metallicity of $\sim 0.5 \times 10^{-3} Z_{\odot}$ (Panagia *et al.* 2004, in preparation). Thus, any object with a metallicity higher than $\sim 10^{-3} Z_{\odot}$ is not a true first generation object.

3. Low Metallicity HII Regions

We have also computed model HII regions for metallicities from three times solar down to $10^{-6} Z_{\odot}$ (Panagia *et al.* 2004, in preparation). In Figure 1 the synthetic spectrum of an HII region with metallicity $10^{-3} Z_{\odot}$ (third panel from the top) can be compared to that of an object with zero metallicity (top panel). The two are very similar except for a few weak metal lines. It is also apparent that values of EW in excess of 1,000Å are possible already for objects with metallicity $\sim 10^{-3} Z_{\odot}$. This is particularly interesting given that Ly-α emitters with large EW have been identified at z=5.6 (Rhoads & Malhotra 2001).

The metal lines are weak, but some of them can be used as metallicity tracers. In Figure 2 the intensity ratio of the [OIII]λ5007 line to Hβ is plotted for a range of stellar temperatures and metallicities. We notice that for $Z < 10^{-2} Z_{\odot}$ this line ratio traces metallicity linearly. Our reference value $Z = 10^{-3}$ corresponds to a ratio [OIII]/Hβ = 0.1. The weak dependence on stellar temperature makes sure that this ratio remains a good indicator of metallicity also when

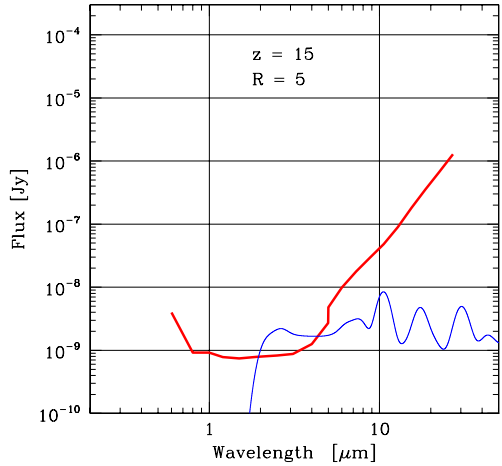

Figure 3. Synthetic spectral energy distribution of a Z=$10^{-3} Z_{\odot}$ starburst object at z=15 containing 10^6 $M_{\odot}$ in massive stars (thin line) compared to the imaging limit of $JWST$ at R=5 (thick line). The $JWST$ sensitivity refers to 4×10^5 s exposures with S/N=10.

one considers the integrated signal from a population with a range of stellar masses.

Another difference between zero-metallicity and low-metallicity HII regions lies in the possibility that the latter may contain dust. For a $Z = 10^{-3} Z_{\odot}$ HII region dust may absorb up to 30 % of the Ly-α line, resulting in roughly 15 % of the energy being emitted in the far IR (Panagia *et al.* 2004, in preparation).

4. How to discover and characterize Primordial HII Regions

It is natural to wonder whether primordial HII regions will be observable with the generation of telescopes currently on the drawing boards. In this section we will focus mostly on the capabilities of the James Webb Space Telescope (*JWST*; *e.g.* Stiavelli *et al.*). Here we consider a starburst with $\sim 10^6$ $M_{\odot}$ in massive stars(which corresponds to a Ly-α luminosity of $\sim 10^{10}$ $L_{\odot}$) as our reference model.

The synthetic spectra, after allowance for IGM HI absorption of the Ly-α radiation (*e.g.* Miralda-Escudé & Rees 1998, Madau & Rees 2001) and convolution with suitable filter responses are compared to the *JWST* imaging sensitivity for 4×10^5s exposures in Figure 3. It is clear that *JWST* will be able to easily detect such objects. Due to the high background from the ground, *JWST* will remain superior even to 30m ground based telescopes for these applications.

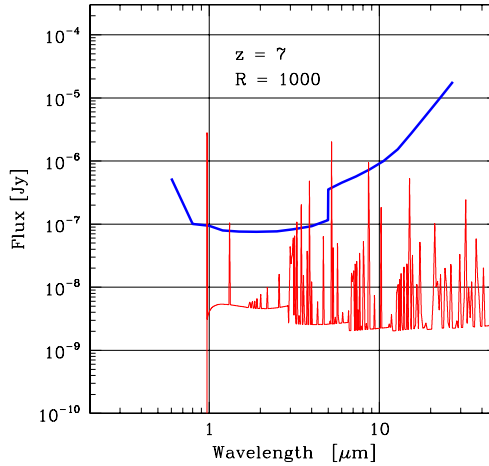

Figure 4. Synthetic spectrum of a Z=$10^{-3} Z_{\odot}$ starburst object at z=7 containing 10^6 $M_{\odot}$ in massive stars (thin line) compared to the spectroscopic limit of $JWST$ at R=1000 (thick line). The $JWST$ sensitivity refers to $4 \times 10^5 s$ exposures with S/N=10.

The synthetic spectra can also be compared to the *JWST* spectroscopic sensitivity for $4 \times 10^5 s$ exposures (see Figure 4). It appears that while the Ly-α line can be detected up to $z \simeq 15 - 20$, for our reference source only at relatively low redshifts (z$\sim$ 7) can *JWST* detect other diagnostics lines lines such as HeII 1640Å, and Balmer lines. Determining metallicities is then limited to lower redshifts or to brighter sources.

We can reverse the argument and ask ourselves what sources can *JWST* detect and characterize with spectroscopic observations. Figure 5 displays, as a function of redshift, the total luminosity of a starburst whose lines can be detected with a S/N=10 for a 4×10^5s exposure time. The loci for Ly-α, HeII 1640Å, Hβ, and [OIII] 5007Å are shown. It appears that Ly-α is readily detectable up to z$\simeq$20, the HeII 1640Å line may also be detected up to high redshifts, whereas "metallicity" information, *i.e.* the intensity ratio I([OIII])/I(Hβ), can be obtained at high z only for sources that are ~ 30 times more massive or that are magnified ~ 30 times by gravitational lensing.

5. Primordial Supernovae

Even if *JWST* cannot detect individual massive Population III stars, supernova explosions may come to the rescue. In the local Universe supernovae (SNe) can be as bright as an entire galaxy (*e.g.*, Type Ia supernovae (SNIa) at maximum light have $M_B(SNIa) \simeq$-19.5) and are detectable up to large distances. However, SNIa, originating from moderate mass stars, are not ex-

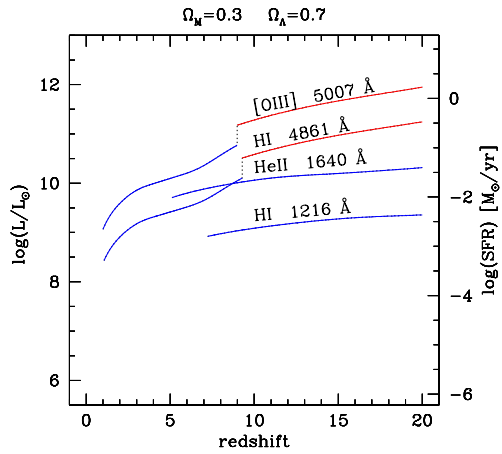

Figure 5. Limiting *total* luminosity of the ionizing stars (left-hand scale) and top-heavy IMF star formation rate (right-hand scale) to detect various emission lines using $JWST$ spectroscopy, with S/N=10 in integrations of 100 hours, as a function of the source redshift.

pected to occur during the first 1 billion years after Big Bang. In addition, SNIa are efficient emitters only at rest frame wavelengths longer than 2600A, which makes them hard to detect at high redshifts (Panagia 2003a,b). Type II supernovae (SNII) are much more efficient UV emitters but only rarely they are as bright as a SNIa. As a consequence, they will barely be detected at redshifts higher than 10, or, if they are exceptionally bright (à la SN 1979C or SN 1998S) they would be rare events (Panagia 2003a,b).

On the other hand, massive population III stars are much more massive than Pop II or Pop I stars, and the resulting supernovae may have properties very different from those of local Universe SNe. Heger et al (2001) have considered the fate of massive stars in conditions of zero metallicity and have found that for stellar progenitors with masses in the range 140-260 $M_\odot$ the SN explosions would be caused by a pair-production instability and would be 3 to 100 times more powerful than core-collapse (Type II and Type Ib/c) SNe, so that a Pop III SN at a redshift of z = 20 could attain a peak flux of about 100 nJy at 5 μm. Such a high flux would be easily detectable with *JWST* observations made with an integration time of a few hours.

Next point to consider is: “Do Pop III SNe occur frequently enough to be found in a systematic search?" For a standard cosmology ($\Omega_\Lambda = 0.7$, $\Omega_m = 0.3$, $H_0 = 65\ km\ s^{-1} Mpc^{-1}$, $\Omega_b = 0.047$), and assuming that at z=20 a fraction 10^{-6} of all baryons goes into stars of 250 $M_\odot$, Heger *et al.* (2001) predict an overall rate of 0.16 events per second over the entire sky, or about 3.9×10^{-6} events per second per square degree. Since for these primor-

dial SNe the first peak of the light curve lasts about a month, about a dozen of these SNe per square degree should be at the peak of their light curves at any time. Therefore, by monitoring about 100 NIRCam fields with integration times of about 10,000 seconds at regular intervals (every few months) for a year should lead to the discovery of three of these primordial supernovae. We conclude that, with a significant investment of observing time (a total of 4,000,000 seconds) and with a little help from Mother Nature (to endorse our theorists views), *JWST* will be able to detect *individually* the very first stars and light sources in the Universe.

References

Baraffe I., Heger A., Woosley S. E., 2001, ApJ, 550, 890

Bromm V., Ferrara A., Coppi P. S., Larson R. B., 2001, MNRAS, 328, 969

Bromm V., Kudritzki R. P., Loeb, A., 2001, ApJ, 552, 464

Heger A., Woosley S. E., Baraffe I., Abel T., 2001, in The Most Celestial Objects and Their Use for Cosmology, Proceedings of the MPA/ESO, p. 369

Madau P., Rees M. J., 2001, ApJ, 551, L27

Marigo P., Girardi L., Chiosi C., Wood P. R. 2001, A&A 371, 252

Miralda-Escudé J., Rees M. J., 1998, ApJ, 497, 21

Oh S. P., Haiman Z., 2002, ApJ, 569, 558

Oliva E., Panagia N., 1983, Ap&SS, 94, 437

Panagia N., 2003a, in Supernovae and Gamma-Ray Bursters, ed. K. W. Weiler (Berlin: Springer-Verlag), p. 113-144

Panagia N., 2003b, STScI Newsletter, Vol. 20, Issue 4, p. 12

Rhoads, J. E., Malhotra S., 2001, ApJ, 563, L5

Stiavelli, M., et al. 2004, JWST Primer, (Baltimore: STScI)

Tumlinson J., Shull J. M., 2000, ApJ, 528, L65

Tumlinson J., Giroux M. L., Shull J. M., 2001, ApJ, 550, L1

Figure 6 Nino Panagia and Cesare Chiosi.

CONSTRAINTS ON THE IMF IN LOW METALLICITY AND POPIII ENVIRONMENTS

Daniel Schaerer
Geneva Observatory, 51, Ch. des Maillettes, CH–1290 Sauverny, Switzerland
daniel.schaerer@obs.unige.ch

Abstract We summarize and discuss various constraints on the IMF at very low or zero metallicity. Taken together the indications from stars, high-z galaxies, and indirect constraints show some possible deviations (favoring massive stars) from a Salpeter like IMF. However, the empirical evidence remains presently arguably weak.

1. Introduction

The importance of the underlying IMF in metal-poor and even zero metallicity (hereafter called PopIII) environments for a variety of astrophysical questions is obvious and discussed in various contributions in these proceedings. E.g. knowing the IMF at low metallicity has important implications for our understanding of the early chemical evolution of the Universe, its reionization and star formation history, to name just few. This concerns obviously in particular the massive stars if one is interested in the distant/early/young Universe. However, no direct "measurement" of the massive star (upper part of the) IMF exists at metallicities below the lowest value observed in massive star forming regions in the local Universe, which is the metallicity of I Zw 18 with $12 + \log(\mathrm{O/H}) \sim 7.2$ i.e. $\sim 1/50$–$1/30$ solar, the latter value applying for the most recent solar O/H determination (Asplund et al. 2004).

In fact, studies of the IMF in extra-galactic H II regions or "small starbursts" down to these metallicities (loosely denoted by Z henceforth) studies of the IMF exist (see e.g. reviews by Leitherer 1998, Schaerer 2002). So far, basically all the data appears consistent with a "normal" Salpeter-like IMF and a "normal", high upper limit of the IMF, $M_{\rm up} \sim$ 100–150 $\mathrm{M}_{\odot}$. However, various hydrodynamical simulations tend to show that the typical mass of stars formed below a certain "critical metallicity" $Z_{\rm crit}$ ($\sim 10^{-5\pm1} Z_{\odot}$, Schneider et al. 2004) would be more massive than their higher metallicity, "normal" counterparts, implying possibly a significantly different IMF in early times

E. Corbelli et al. (eds.), The Initial Mass Function 50 Years Later, 487–492.

(cf. review of Bromm, these proceedings). Taking a conservative approach I will try to review below various observational indicators, direct and indirect ones, which could potentially probe such predictions. I will argue that so far, no strong convincing evidence for a different IMF favoring massive stars at $Z \lesssim Z_{\rm crit}$ has been found.

2. Observables probing the massive stars IMF at low Z

Basically, the most direct probes of the upper part of the IMF at low metallicity reside in 1) peculiar/different stellar or galaxy spectra, and 2) signatures related to the presence or absence of pair instability supernovae (PISN) expected at low Z from very massive ($M_{\rm ini} \sim$ 130–260 $M_\odot$, e.g. Ober et al. 1993) stars.

First, galaxy spectra dominated by a low Z population of stars with a "massive" IMF are expected to show very strong Lyman-α emission, possibly even nebular He II emission at very low Z, and more generally to emit Lyman continuum photons with a high efficiency (e.g. large ionizing photon production per unit stellar mass formed). These observables, sensitive to the fraction of massive stars formed and to metallicity (through stellar and nebular properties), have been discussed by Tumlinson et al. (2001, 2004), Schaerer (2002, 2003) and others.

Concerning spectra I would like to clarify in passing that, in contrast to some popular belief, the shape of the (restframe) UV spectrum (e.g. the often used UV slope β) can in principle not be used to constrain the IMF (and/or metallicity) of an individual galaxy. This is illustrated by Fig. 1, which shows the strong degeneracies between β, Z, age, and SF history (here the limiting cases of a burst or SFR=const). Furthermore, given the increasing dominance of nebular continuous emission even in the UV (Schaerer 2002), the UV slope of a young very metal-poor population ($Z \lesssim 10^{-5}$) is actually expected to be *redder*, not bluer as naively expected. However, this warning does not exclude that, on a statistical basis, the UV slope contains information on e.g. the metallicity or maybe even on the IMF. Such correlations are known to apply for UV selected nearby starbursts (Heckman et al. 1998).

Second, if the IMF at low metallicity forms stars in the mass range of PISN, such objects should leave various fingerprints which should be discernible. E.g. peculiar abundance pattern are expected in such a case: high Si/O, C/O abundance ratios may be detectable in the Lyman-α forest (Schaerer 2002), strong odd/even pattern and low Zn/Fe (e.g. Heger & Woosley 2002) which could be reflected in abundances of "second generation" stars of low Z, particularly luminous SNae (cf. Heger et al. 2003), and peculiar dust production/composition (cf. Omukai 2000, Schneider et al. 2003, 2004).

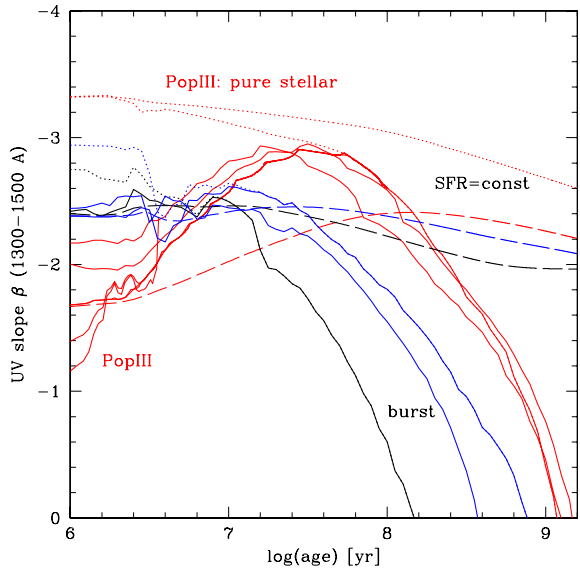

Figure 1. Temporal evolution of the UV slope β from models of different metallicities (PopIII, $Z = 10^{-5}$, to solar) and for instantaneous bursts (solid lines) and constant SF (long dashed lines). The dotted lines show β if nebular continuous emission is neglected, i.e. assuming pure stellar emission. Further discussions in the text

Whether there is any trace of such fingerprints will be examined below in various astrophysical objects.

3. Evidence for a different/“massive” IMF at low metallicity?

3.1 From stars . . .

The mere existence of an old (hence very low mass) halo star could contradict the postulate of a purely massive IMF at very low metallicity. However, the most metal-poor star found so far ([Fe/H] $\sim$ –5.3, Christlieb et al. 2002) is in the transition metallicity range between normal and “massive” SF (Schneider these proceedings, Schneider et al. 2004), thus insufficient to provide a stringent test.

Hernandez & Ferrara (2001) have argued for an increase of the characteristic stellar mass at metallicities $Z \lesssim 10^{-3} Z_{\odot}$ from an analysis of the number of Galactic halo stars. Although probably strongly dependent on complex modeling assumptions (including cosmological modeling) this could provide an interesting indication for an IMF change.

Recent accurate abundance determinations in a sample of very metal-poor halo stars (down to [Fe/H] $\sim$ –4.1) have shown "normal" abundance pattern which can be understood by "regular" type II SN nucleosynthesis. No signature of $Z = 0$ yields and PISN are found; furthermore the observed increase of Zn/Fe towards low Z is in contrast with PISN predictions (Cayrel et al. 2004). From stellar abundance pattern there is so far no sign of PopIII or PISN, which could imply that the IMF did not form stars in the range of 130–260 $M_\odot$, or that this phase was very short. Tumlinson et al. (2004) find similar conclusions.

3.2 From individual galaxies near and far . . .

As already mentioned above, stellar population studies of nearby galaxies, providing access to more or less detailed information on the objects, have not yet produced any convincing case for an "unusual" upper part of the IMF down to $\sim$ 1/30–1/50 $Z_\odot$ (cf. reviews by Leitherer 1998, Schaerer 2003a).

Currently the most puzzling result available in the literature is from the LALA survey at the 4m in Kitt peak, providing a large sample of Lyman-α emitters at redshift z =4.5 and 5.7 (+ few at higher z). Indeed, the Lyman-α equivalent width of these objects, as determined from narrow-band imaging, seem to show a surprisingly large fraction of objects with very high equivalent widths ($W_{\rm rest}$(Lyman-α) > 250), which is difficult if not impossible to explain by stellar photoionization with a normal, Salpeter-like IMF (see Schaerer 2003b). As AGN now seem to be excluded (Wang et al. 2004), metallicities $Z \lesssim 10^{-5}$ and/or a "massive" IMF would need to be invoked as postulated by Malhotra & Rhoads (2002, cf. Rhoads & Malhotra 2001). However, finding such a large number of very metal-poor objects at relatively low redshift could be surprising (cf. Scannapieco et al. 2002). Also, the reliability of the equivalent width determination from the imaging could be questioned; e.g. using similar selection criteria Hu et al. (2004) found 26 $z = 5.7$ Lyman-α emitters, 19 of them being confirmed spectroscopically, but less than 25 % of them showing large Lyman-α equivalent widths (see also samples of Ajiki et al. 2002, 2004). They suggest that the difference with the LALA survey could be due to deeper imaging (narrow- and broad-band) resulting in more accurate W determinations. Indeed, most of the LALA sources are detected in one or few filters and little is presently known about them (cf. the deep spectra of Dawson et al. 2004). Definitely a better understanding of the properties (nature, stellar content etc.) of the LALA sources and related objects could be of great interest in particular to verify if these truly represent objects with a peculiar IMF or extremely low metallicity.

$z \gtrsim$ 6 galaxies: So far, for none of the galaxies found at even higher redshift, there is any information requiring a deviation from a "standard" Salpeter IMF. In the first place, the available observations are few and insufficient or

inappropriate to provide constraints on the IMF. E.g. samples of high-z galaxy candidates from deep surveys (e.g. the Hubble Ultra Deep Field) are generally only detected in few ($\sim$ 2–3) broad-band filters (Stanway et al. 2003, Bouwens et al. 2004ab). In the case of gravitationally lensed objects more/better photometry is available in several cases (e.g. the $z = 6.56$ galaxy of Hu et al. 2002, and the probable $z \sim 7$ galaxy of Kneib et al. 2004, and $z > 7$ candidates of Pelló et al. 2004ab). However, even in these cases it is not possible to constrain the IMF (see Pelló et al. 2004a, Schaerer & Pelló 2004), given the degeneracies of the UV restframe spectrum discussed above. Also, claims for unusual IMFs as e.g. voiced by Ricotti et al. (2004) based on estimates of the star formation rate density or the space density of high-z sources should probably taken with great caution. First these estimate are derived from very small samples, and second the volume probed by the "survey" relying on gravitational lensing cannot be determined accurately without detailed modeling. In short, before more detailed information of high-z galaxies will be available, especially jointly photometric and spectroscopic data allowing e.g. to secure their starburst nature and to measure a very hard ionizing spectrum (e.g. from lines including He II λ1640), it appears difficult to expect direct constraints on the IMF in such objects.

3.3 More indirect . . .

Other observations, could provide interesting, though more indirect, information on the IMF in the early Universe.

Briefly, e.g. observations of the near-IR background radiation at 1–2.3 μm show an apparent "excess", which could be explained by halos with strong Lyman-α emission from PopIII galaxies with a massive IMF if such objects are frequent/dominate at redshift $z \geq 8$ (see Santos et al. 2002, Salvaterra & Ferrara 2003). Also, indications of a high electron scattering optical depth from recent WMAP observations (Kogut et al. 2003) have triggered various papers claiming the need for massive PopIII stars to produce the apparent observed early and strong re-ionization. However, this WMAP measurement may be subject to revision. In any case, various alternate solutions exist (e.g. Haiman & Holder 2003) and a conservative approach does not require a non-standard IMF (Ciardi et al. 2003).

3.4 Summary: . . . really different ?

The exploration of the distant Universe has allowed us over recent years to gain a lot of insight on early star formation, stellar populations, galaxy evolution and related topics discussed elsewhere. Despite the reasonable number of high-z and potentially very metal-poor galaxies known now, it is fair to say that so far little is known about the IMF – in particular the high mass part of interest

here. Adopting a conservative approach I have argued that there is no strong evidence for an IMF differing from the "normal" Salpeter. Among the most intriguing elements possibly in favor of a different, top-heavy IMF, in low or zero metallicity environments are some Lyman-α emitters with very large equivalent widths (LALA sources), or the apparent excess of (unresolved) near-IR background radiation. Firming up these results and attempting additional, new approaches will be required to achieve a firm empirical/observational knowledge of the IMF in the early Universe.

Acknowledgments Its a pleasure to thank the organizers for this wonderful, perfect and stimulating conference.

References

Ajiki, M., et al., 2002, ApJ, 576, L25
Ajiki, M., et al., 2004, PASJ, 56, 597
Asplund, M., et al., 2004, A&A, 417, 751
Bouwens, R.J., et al., 2004a, ApJ, 606, L25
Bouwens, R.J., et al., 2004b, ApJ, in press (astro-ph/0409488)
Cayrel, R., et al., 2004, A&A, 416, 1117
Christlieb, N., et al., 2002, Nature, 419, 904
Ciardi, B., et al., 2003, MNRAS, 344, L7
Dawson, S., et al., 2004, ApJ, in press (astro-ph/0409090)
Haiman, Z., Holder, G.P., 2003, ApJ, 595, 1
Heckman, T.M., et al., 1998, ApJ, 503, 646
Heger, A., Woosley, S., 2002, ApJ, 567, 532
Heger, A., et al., 2002, in Lighthouses of the Universe, MPA/ESO, 369
Hernandez, J., Ferrara, A., 2001, MNRAS, 324, 848
Hu, E., et al., 2004, AJ, 127, 563
Kogut, A., 2003, ApJS, 148, 161
Leitherer , C., 1998, in The Stellar Initial Mass Function, ASP Conf. Series, Vol. 142, 61
Malhotra, S., Rhoads, J.E., 2002, ApJ, 565, L71
Ober, W.W., et al., 1993, A&A, 119, 61
Omukai, K., 2000, ApJ, 534, 809
Pelló, R., et al., 2004, A&A, 416, L35
Pelló, R., et al., 2004, IAU Symp 225, in press (astro-ph/0410132)
Ricotti, M., et al., 2004, MNRAS, 352, L21
Rhoads, J.E., et al., 2003, AJ, 125, 1006
Salvaterra, R., Ferrara, A., 2003, MNRAS, 339, 973
Santos, M.R., et al., 2002, MNRAS, 336, 1082
Scannapieco, E., et al., 2003, ApJ, 589, 35
Schaerer, D., 2002, A&A, 382, 28
Schaerer, D., 2003a, in A massive star odyssey IAU Symp. 212, 642
Schaerer, D., 2003b, A&A, 397, 527
Schneider, R., et al., 2004, MNRAS, submitted
Stanway et al., 2003, MNRAS, 342, 439
Tumlinson, J., Giroux, M.L., Shull, J.M., 2001, ApJ, 550, L1
Tumlinson, J., et al., 2004, ApJ, 612, 602
Wang, J.X., et al., 2004, ApJ, 608, L21

THERMAL EVOLUTION OF STAR FORMING CLOUDS IN LOW METALLICITY ENVIRONMENT

K. Omukai
National Astronomical Observatory of Japan, Mitaka, Tokyo 181-8588, Japan
omukai@th.nao.ac.jp

The thermal and chemical evolution of star-forming clouds is studied for different values of metallicity. The model developed by Omukai (2000) is updated by including deuterium chemistry and the cosmic microwave background (CMB) radiation. The cooling owing to HD-line emission is found to be dominant in thermal balance for clouds in metallicity range of $Z \sim 10^{-5} - 10^{-3} Z_\odot$ for the number density $\sim 10^5 \mathrm{cm}^{-3}$. Hot CMB in high-z universe affects the thermal evolution only in such a way that the temperature below the radiation temperature is prohibited while the evolution in higher temperature regime is hardly altered. From the obtained temperature evolution, the fragmentation properties of the clouds with different metallicities are discussed. By using the linear perturbation theory, growth of elongation $\delta \equiv (b-a)/a$, where a, b are short and long axis lengths of the clouds, is followed. It is assumed that when the clouds become elongated significantly, i.e., when the elongation δ reaches some critical value in the linear theory, fragmentation takes place and the mass of fragments is given by the thermal Jeans mass at that time. With these assumptions and given initial distribution of elongation, the mass distribution of fragments is obtained as a function of metallicity. For metal-free gas, fragmentation is found to occur only at the end of rapid H_2 cooling phase ($\sim 10^4 \mathrm{cm}^{-3}$) and all the fragments are very massive, $> 10^3 M_\odot$, consistently with previous studies. On the other hand, for slightly metal-polluted clouds, some clumps fragment again at higher density $> 10^{10} \mathrm{cm}^{-3}$ owing to the cooling by dust grains after fragmenting at H_2 cooling phase. By this mechanism, sub-solar mass-scale fragments are produced. This dust-induced fragmentation can occur even for metallicity as low as $\sim 10^{-6} Z_\odot$ although those low-mass stars are still rare for such low metallicity. For metallicity $0.001 - 0.01 Z_\odot$, there are two peaks in fragmentation

E. Corbelli et al. (eds.), The Initial Mass Function 50 Years Later, 493–494.

mass distribution corresponding to the two modes of fragmentation. When the metallicity reaches $\sim 0.1 Z_{\odot}$, the two peaks merge and thus the IMF becomes singly peaked. At this epoch, transition to an ordinary Salpeter-like IMF is expected to take place.

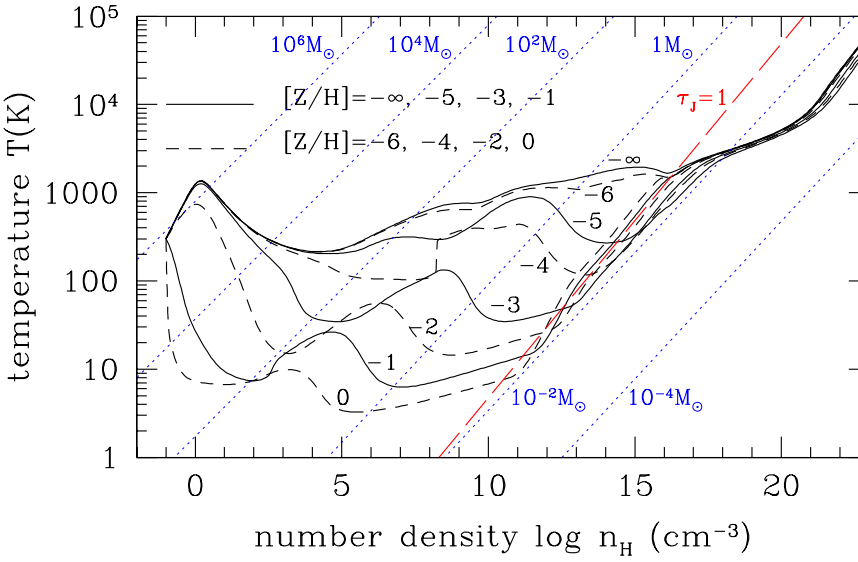

Figure 1. Temperature evolution of pre-stellar clouds with different metallicities. Those with metallicities [Z/H]=-∞ (Z=0), -5, -3, and -1 (-6, -4, -2, and 0) are shown by solid (dashed) lines. Only the present-day CMB is considered as an external radiation field. The lines for constant Jeans mass are indicated by thin dotted lines. The positions where the central part of the clouds becomes optically thick to continuum self-absorption is indicated by the thin solid line. The intersection of thin solid line with each evolutionary trajectory corresponds to the epoch when the cloud becomes optically thick to continuum. To the right of this line, the clouds are optically thick and there is little radiative cooling.

References

Omukai, K. (2000), ApJ, 534, 809
Omukai, K., Tsuribe, T., Schneider, R., and Ferrara, A. (2004), in preparation

OBSERVATIONAL EVIDENCE FOR A DIFFERENT IMF IN THE EARLY GALAXY

Sara Lucatello[1], Raffaele Gratton[1], Timothy Beers[2] and Eugenio Carretta[3]
[1]*INAF-Osservatorio Astronomico di Padova, Vicolo dell'Osservatorio 5 35122, Padova, Italy*
[2] *Department of Physics & Astronomy and JINA, Michigan State University, East Lansing, Michigan 48824-1116, USA*
[3] *INAF-Osservatorio Astronomico di Bologna, via Ranzani 1, 40127, Bologna, Italy*
lucatello@pd.astro.it, gratton@pd.astro.it, beers@pa.msu.edu, carretta@bo.astro.it

Abstract The unexpected high incidence of carbon-enhanced, *s*-process enriched unevolved stars amongst extremely metal-poor stars in the halo provides a significant constraint on the Initial Mass Function (IMF) in the early Galaxy. We argue that these objects are evidence for the past existence of a large population of intermediate-mass stars, and conclude that the IMF in the early Galaxy was different from the present, and shifted toward higher masses.

1. The background

The largest searches aimed at identifying metal poor stars (e.g. HK by Beers *et al.* 1992, HES by Christlieb *et al.* 2003) have consistently been finding that the fraction of C-enriched star among stars that have not reached the AGB yet, which is constant up to a few percent of solar (McConnel, Frye & Upgren 1972), abruptly increases at low metallicity ([Fe/H]< -2.5). C-enhanced metal poor stars (CEMP) are characterized by a variety of abundance patterns. At least five possible classes have been discussed (see e.g. Lucatello et al. 2003), however most are associated with an *s*-process enhancement. *S*-process enriched, CEMP stars (CEMP-s) are all very likely members of binary systems (see Lucatello *et al.* 2004a) and they owe their peculiar composition to the transfer of material processed by an IMS companion during its AGB phase. These IMS stars have ended their nuclear burning phase long ago and are now faint white dwarfs. However, their less massive companions, CEMP-s stars, carry the signature of their past existence, providing an unique opportunity to study a population of long extinct stars .

E. Corbelli et al. (eds.), The Initial Mass Function 50 Years Later, 495–498.

2. The data and the assumptions

The most recent results from the HK survey indicate that 20% of stars at [Fe/H]<-2.5 have [C/Fe]>1.0. It must be kept in mind that this value is strictly a lower limit. In fact there are two effects which act in this sense: **Luminosity effect**: the presence of C bands (CH and C2) lowers the B flux and thus B magnitude limited surveys such the HK and the HES will be biased against CEMP, leading to an underestimate of the CEMP fraction; **C-enhancement selection effect**: in order to be positively identi-fied as CEMP the star must display [C/Fe]>1. Stars which have already undergone the first dredge-up dilute their C content, possibly dropping below the threshold. High luminosity stars, which make up most of the sample in this surveys, are expected to be affected by this effect. We will adopt the value of 20% for the fraction of CEMP and warn the reader that it is *strictly* a lower limit.
In making the calculations a few assumptions are required: **Binary fraction**: Assumed to be the same as at solar metallicity 60% (Jahreiß& Wielen 1996). **Separation range**: in order for the accretion of processed material to take place, the orbital separation (and period) between the two components must lie within the useful range, which has been determined to be (see Lucatello *et al.* 2004a) $-0.65<\log P(\text{days})<5.4$. Adopting the Duquennoy & Mayor (1991) orbital distribution, this range includes 59% of all binaries. **Mass range**: The mass ranges for stars to become C-rich on the AGB is metallicity dependent. We assume the range 1.2 $M_\odot$ (Lattanzio 2003 priv. comm.) to 6 $M_\odot$ (Karakas 2004) for EMP.

3. CEMP-*s* and IMF

Aoki *et al.* (2003) found that CEMP-s stars account for at least 70% of CEMP. Therefore, given the formation scenario for CEMP-s the straightforward interpretation would be that 14% of stars with [Fe/H]< -2.5 had an IMS companion, with an orbital separation in the range useful for the mass transfer to occur. The fraction of IMS in a population can be derived by the simple formula: $f(IMS) = \frac{c(IMS)}{(b \times p_{eff})}$ Where $c(IMS)$ is the fraction of stars which had IMS companions with the appropriate separations to transform them into the presently observed CEMP-s, b is the binary fraction and p_{eff} indicates the percentage of binaries with orbital separation suitable for the mass accretion to take place effectively. Substituted in the formula, we find that 40% of EMP stars were IMS. Assuming for the IMS a range between 1.2 and 6 $M_\odot$, the Miller & Scalo (1979-MS) IMF (with mass-cuts 0.1-125 $M_\odot$) predicts a fraction of 10%. Even the most strict lower limit for the IMS fraction among EMP (derived by assuming 100% binary fraction and 100% period separation effectiveness) i.e. 14% would still be higher than the predicted one. Note that an analogous calculation performed for Solar and slightly more metal poor

stars ([Fe/H]$\sim$-1), on the basis of the frequency of Ba and classical CH-stars, yields a value of $\sim$5%, which is in reasonable agreement with the MS predictions of an $\sim$8% fraction of IMS (1.5-6 $M_{\odot}$ at [Fe/H]$\sim$0). Therefore, it can be concluded that the present data indicate that the early IMF was likely shifted towards more massive stars, producing a large number of IMS.

References

Aoki, W., Ryan, S. G., Tsangarides, S., Norris, J. E., Beers, T. C., & Ando, H. 2003, in Elemental Abundances in Old Stars and Damped Lyman-α Systems, 25th meeting of the IAU, Joint Discussion 15

Beers, T. C., Preston, G. W., & Shectman, S. A. 1992, AJ, 103, 1987

Christlieb, N. 2003, Rewiews in Modern Astronomy, vol 16

Duquennoy, A. & Mayor, M. 1991, A&A, 248, 485

Jahreiß, H. & Wielen, R. 2000, IAU Symposium, 200, 129

Karakas, A. 2003, PhD thesis, Monash University

Lucatello, S., Gratton, R., Cohen, J. G., Beers, T. C., Christlieb, N., Carretta, E., & Ramírez, S. 2003,AJ, 125, 875

Lucatello, S., Gratton, R., Beers, T. C., Carretta, E., Ryan, S. G., & Tsangarides, S. 2004a, ApJ, submitted

Lucatello, S., Gratton, R., Beers, T. C., & Carretta E. 2004b, ApJ, in press

McConnell, D. J., Frye, R. L., & Upgren, A. R. 1972, AJ, 77, 384

Miller, G. E. & Scalo, J. M. 1979, ApJS, 41, 513

Salpeter, E. E. 1955, ApJ, 121, 161

Figure 1 Tha Padova school.

Figure 2. Smiling italians at lunch: Zoccali, Calura, Tantalo, Lucatello, Prisinzano, Flaccomio and Portinari.

Figure 3. Fred Adams and Laura Portinari.

THE ROLE OF THE IMF IN THE COSMIC METAL PRODUCTION

Francesco Calura
Dipartimento di Astronomia, Universitá degli Studi di Trieste, via G.B. Tiepolo 11, 34131 Trieste, Italy
fcalura@ts.astro.it

Abstract By means of detailed chemo-photometric models for elliptical, spiral and irregular galaxies, we evaluate the cosmic history of metal production as well as the metal mass density of the present-day universe for different initial mass functions (IMFs): a Salpeter IMF, a Scalo IMF and a top-heavy IMF only in spheroids. A standard (i.e. Salpeter-like) IMF is sufficient to account for the local metal budget, whereas with a top-heavy IMF we overestimate the total metal density by a factor of ~ 4.

1. The evolution of cosmic metal production

We compute the cosmic metal production by means of detailed chemical evolution models for galaxies of different morphological types, namely ellipticals, spirals and irregular galaxies. All the details concerning these models can be found in Calura & Matteucci (2003, 2004). Elliptical galaxies are assumed to form by means of a rapid collapse of a gas cloud occurring at high redshift (Matteucci 1994). Spirals are formed through a double-infall process (Chiappini et al. 1997). Irregulars galaxies assemble through continuos infall and form stars at a continuous and very low ($\sim 0.01 M_{\odot}/yr$) star formation rate. To calculate galaxy spectra, we use the spectro-photometric code by Jimenez et al. (1998). The number densities of the various morphological types are normalized according to the local B-band luminosity function (Marzke et al. 1998). We assume a scenario of pure-luminosity evolution and no evolution in number. We assume that all galaxies started forming stars at redshift $z_f = 5$, and adopt a flat EdS cosmology with $h = 0.5$, $\Omega_m = 1$, $\Omega_{\Lambda} = 0$. In our models, for the stellar initial mass function (IMF) we investigate different forms (Salpeter, Scalo, Top-Heavy ($x \sim 1$, TH)) and compare our predictions with values derived by other authors in different manners. In Figure 1, we show our predicted values of Ω_Z, i.e. the comoving density of all the metals at the present time

E. Corbelli et al. (eds.), The Initial Mass Function 50 Years Later, 499–500.

in units of the critical density of the universe ($\rho_c = 6.94 \cdot 10^{10} M_\odot / Mpc^3$ for the value of $h = 0.5$ adopted here), along with other estimates performed previously by various authors. We note that the Salpeter IMF allows us to reproduce the amount of metals present in the local universe. On the other hand, a THIMF in ellipticals causes an overestimation of the local metal budget by a factor of ~ 4. In Figure 2, we show the average mass-weighted metallicities of various components of the universe (ISM, stars, IGM, Calura & Matteucci, in prep.). Our results indicate that the average metallicity evolution as observed in Damped-Lyman Alpha (DLA) systems is consistent with a population of spiral and irregular galaxies dominating the neutral gas cross section.

Author	Ω_Z	$\rho_Z (M_\odot / Mpc^3)$
Dunne et al 2003	$9.6 \cdot 10^{-5} - 1.9 \cdot 10^{-4}$	$6.7 - 13.3 \cdot 10^5$
Finoguenov et al 2003	$9.9 \cdot 10^{-5} - 2.00 \cdot 10^{-4}$	$6.9 - 13.8 \cdot 10^5$
present work (Salpeter IMF)	$1.35 \cdot 10^{-4}$	$9.37 \cdot 10^5$
present work (TH IMF in spheroids)	$5.9 \cdot 10^{-4}$	$4.12 \cdot 10^6$

Figure 1. Predicted value of Ω_Z (i.e. the total mass density of all the metals divided by the critical density of the universe) at $z = 0$ for a Salpeter and a Top-Heavy IMF in spheroids and compared with previous determinations.

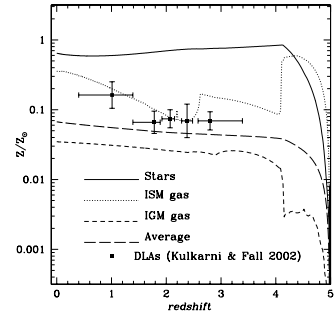

Figure 2. Average mass-weighted metallicities in ISM gas and stars in galaxies and average mass-weighted metallicity of the IGM as functions of redshift. The solid squares are the mass-weighted metallicities observed.

References

Calura, F., Matteucci, F. 2003, ApJ, 596, 734
Calura, F., Matteucci, F. 2004, MNRAS, 350, 351
Chiappini, C., Matteucci, F., Gratton, R. 1997, ApJ, 477, 765
Dunne, L., Eales, S. A., Edmunds, M. G. 2003, MNRAS, 341, 589
Finoguenov, A., Burkert, A., Boehringer, H. 2003, ApJ, 594, 136
Jimenez, R., et al. 1998, MNRAS, 299, 123
Kulkarni, V. P., Fall, S. M. 2002, ApJ, 580, 732
Matteucci, F. 1994, A&A, 288, 57
Marzke, R. O., et al. 1998, ApJ, 503, 617

FROM POPULATION III STARS TO (SUPER)MASSIVE BLACK HOLES

Francesco Haardt
Università dell'Insubria, Como, Italy
haardt@uninsubria.it

Abstract Pregalatic Massive Black Holes (MBHs) formed within minihalos above the cosmological Jeans mass at z=30, as relics of massive POPIII stars. The merger and accretion history of dark halos and MBHs, followed by means of Montecarlo realizations of the merger hierarchy in a ΛCDM cosmology, reveals several interesting aspects. A fraction of MBHs accreted gas during major mergers, shining in the EUV/soft X-rays as an early population of miniquasars. Such population could have been responsible of the early reionization of the IGM implied by the recent WMAP data. On the other hand, long dynamical friction timescales in minor mergers left many MBHs wandering in galaxy halos. Finally, one of the most fascinating prediction of the cosmic history of MBHs is the copious emission of low frequency gravitational waves associated to coalescence of MBH binaries, in principle detectable by the planned LISA interferometer.

1. Introduction

In Volonteri, Haardt & Madau (2003) we have assessed a model for the assembly of massive black holes (MBHs)at the center of galaxies that trace their hierarchical build-up far up in the dark halo 'merger tree'. We have assumed that the first 'seed' black holes (BHs) had intermediate masses, $m_{seed} \approx 150\, m_{\odot}$, and formed in (mini)halos collapsing at $z \sim 20$ from high-σ density fluctuations. These pregalactic holes evolve in a hierarchical fashion, following the merger history of their host halos. During a merger event BHs approach each other owing to dynamical friction, and form a binary system. Stellar dynamical processes drive the binary to harden and eventually coalesce.

The merger history of dark matter halos and associated black holes is followed through Monte Carlo realizations of the merger hierarchy (merger trees) which allow to track the evolution of MBHs along cosmic time, analyze their role in reionizing the Universe, and estimate the contribution of MBH binaries to the *LISA* data stream.

E. Corbelli et al. (eds.), The Initial Mass Function 50 Years Later, 501–506.

Details and all the relevant references can be found in Volonteri et al. (2003), Madau et al. (2004), Sesana et al. (2004a, 2004b).

2. Accretion history

The first stars must have formed out of metal-free gas, with the lack of an efficient cooling mechanism possibly leading to a very top-heavy initial stellar mass function. If stars form above 260 $m_{\odot}$, after 2 Myr they would collapse to MBHs containing at least half of the initial stellar mass. The mass density parameter of our '3.5-σ' pregalactic holes is $\Omega_{seed} \geq 2 \times 10^{-9}\, h$. This is much smaller than the density parameter of the supermassive variety found in the nuclei of most nearby galaxies, $\Omega_{\rm SMBH} \approx 2 \times 10^{-6}$, Clearly, if SMBHs form out of very rare Pop III BHs, the *present-day mass density of SMBHs must have been accumulated during cosmic history via gas accretion, with BH-BH mergers playing a secondary role*. This is increasingly less true, of course, if the seed holes are more numerous and populate the 2- or 3-σ peaks instead, or halos with smaller masses at $z > 20$.

To avoid introducing additional parameters to our model, as well as uncertainties linked to gas cooling, star formation, and supernova feedback, we adopt a simple prescription for the mass accreted by a SMBH during each major merger assuming that in every accretion episode the BH accretes a mass proportional to the observed correlation between stellar velocity dispersion and SMBH mass. The normalization factor is of order unity and is fixed in order to reproduce both the stellar velocity dispersion and SMBH mass relation observed locally and the optical LF of quasars in the redshift range 1<z<5.

3. Reionization from Mini-QSO

Population III IMBHs accreting gas from the surrounding medium will shine as 'miniquasars' at $z \sim 15$ and generate a soft X-ray background that may catalyze the formation of H_2 molecules in dense regions and counteract the destruction by UV Lyman-Werner radiation (Cen 2003b; Glover & Brandt 2003; Haiman, Abel, & Rees 2000). The net effect would be an increase in the cooling rate and star formation efficiency of minihalos (but see Machacek, Bryan, & Abel 2003 who find the positive feedback effect of X-rays to be quite mild). In this paper we point out that miniquasars represent an additional source of Lyman-continuum photons that must be taken into account in models of early reionization by Population III objects. Thin disk accretion onto a Schwarzschild black hole releases about 100 MeV per baryon. If 'seed' IMBHs were able to (say) double their initial mass via gas accretion, and just a few percent of the radiated energy were emitted above and close to the hydrogen Lyman edge, then *miniquasars would be more efficient at photoionizing the universe than their metal-free stellar progenitors.*

To illustrate the implications of these results, consider the following estimate for the number of H-ionizing photons emitted by the initial population of progenitor massive stars. In our model the fraction, f_*, of cosmic baryons incorporated into Population III massive stars – progenitors of seed IMBHs – at $z = 24$ is,

$$f_* = \frac{\langle m_* \rangle}{\langle m_\bullet \rangle} \frac{\Omega_\bullet}{\Omega_b} \approx 5 \times 10^{-7}, \quad (1)$$

where Ω_b is the baryon density parameter. Zero-metallicity stars in the range $40 < m_* < 500\, M_\odot$ emit about 70,000 photons above 1 ryd per stellar baryon (Schaerer 2002). The total number of ionizing photons produced per baryon by progenitor Population III stars is,

$$\frac{n_{\rm ion}}{n_b} \approx 70,000 f_* \approx 0.04, \quad (2)$$

well below what is needed to reionize the universe. Figure 1 shows that, if $f_{\rm UV}/\langle h\nu \rangle$ is greater than $0.1\,{\rm ryd}^{-1}$ and gas is accreted efficiently onto IMBHs, then *miniquasars may be responsible for cosmological reionization at redshift* ~ 15.

4. Dynamical evolution of BH binaries

During the merger of two halo+BH systems of comparable masses, dynamical friction drags in the satellite hole toward the center of the newly merged system, leading to the formation of a bound BH binary in the violently relaxed stellar core. The subsequent evolution of the binary is determined by the initial central stellar distribution. As the binary separation decays, the effectiveness of dynamical friction slowly declines and the BH pair then hardens via three-body interactions, i.e., by capturing and ejecting at much higher velocities the stars passing close to the binary. The hardening of the binary modifies the stellar density profile, removing mass interior to the binary orbit, depleting the galaxy core of stars, and slowing down further hardening. If the hardening continues sufficiently far, gravitational radiation losses finally take over, and the two BHs coalesce in less than a Hubble time. The merger timescale is computed adopting a simple semi-analytical scheme that qualitatively reproduces the evolution observed in N-body simulations.

5. Gravitational waves from MBH binaries

Massive black hole binaries, with masses in the range $10^3 - 10^8 M_\odot$, are one of the primary target for the planned Laser Interferometer Space Antenna (*LISA*). Stellar dynamical processes dominates the orbital evolution of black hole binaries at large separations, while gravitational wave emission takes over

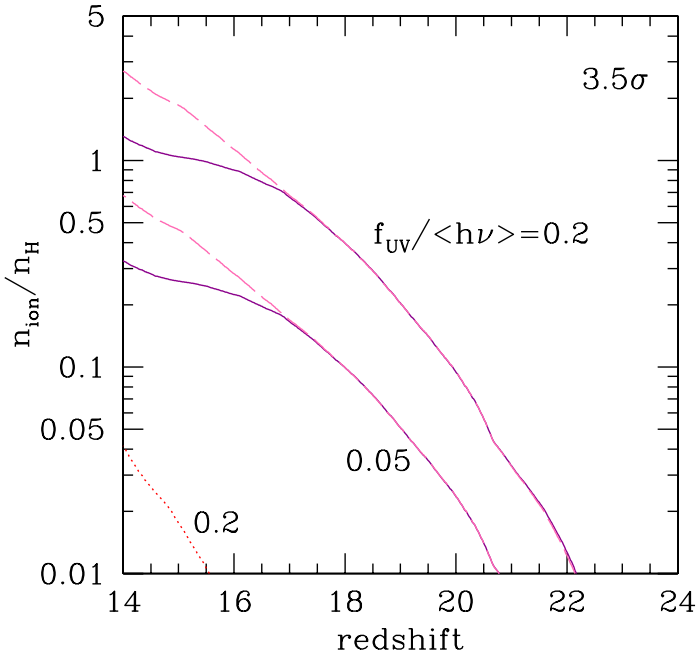

Figure 1. Cumulative number of ionizing photons per hydrogen atom produced by mini-quasars, for different values of the fraction $f_{\rm UV}$ of the bolometric power that is emitted as radiation above 1 ryd with mean energy $< h\nu >$ (in ryd). Solid curves: in each major merger the BH in the main halo accretes a mass $\Delta m_{\rm acc} = 2m_{\rm BH}$. Dashed curves: same with $\Delta m_{\rm acc} = 10^{-3}\, M_h$. Dotted curve: same with $\Delta m_{\rm acc} = 10^{-3}\, M_h$, $f_{\rm UV}/ < h\nu >= 0.2\,{\rm ryd}^{-1}$, but with gas accretion suppressed in minihalos with virial temperature $T_{\rm vir} \lesssim 10^4$ K.

at small radii, causing the final coalescence of the pairs. GW signal from this population, in a 3 year *LISA* observation, will be resolved into $\simeq 88$ discrete events (see figure 2) with $S/N \geq 5$, among which $\simeq 33$ will be observed above threshold until coalescence. These “merging binaries" involve relatively massive binaries, $M \sim 10^5 M_\odot$, in the redshift range $2 \lesssim z \lesssim 6$. The remaining $\simeq 55$ events come from higher redshift, less massive in-spiral binaries ($M \sim 5 \times 10^3 M_\odot$ at $z \gtrsim 6$) and, although their S/N integrated over the duration of the observation can be substantial, the final coalescence phase is at too high frequency to be directly observable by *LISA*. The total number of detected events accounts for a fraction $\gtrsim 90\%$ of all coalescences of massive black hole binaries at $z \lesssim 5$. The residual confusion noise from unresolved massive black hole binaries is expected to be at least an order of magnitude below the estimated stochastic *LISA* noise.

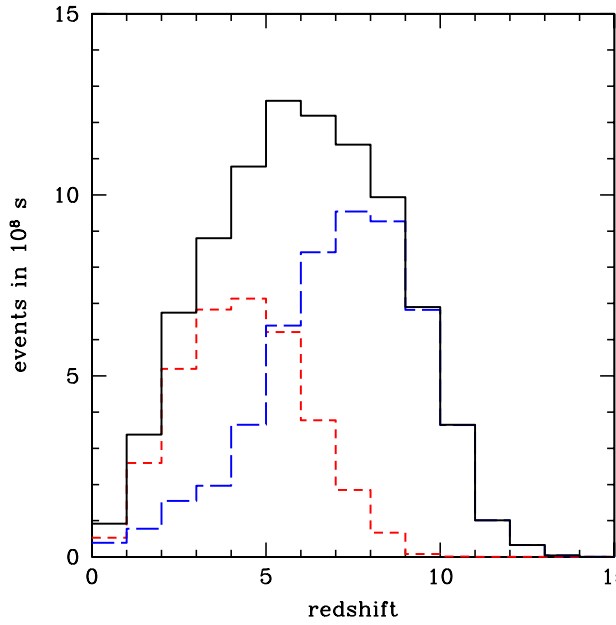

Figure 2. Differential redshift distribution of MBHBs resolved with $S/N > 5$ by LISA in a 3-year mission (solid line). The separate counts for merging (short-dashed line) and in-spiral (long-dashed line) binaries are also shown.

References

Madau P., Rees M.J., Volonteri M., Haardt F., Oh S.P., 2004, ApJ, 604, 484
Sesana A., Haardt F., Madau P., Volonteri M., 2004, ApJ, 611, 623
Sesana A., Haardt F., Madau P., Volonteri M., 2004, ApJ, submitted (astro-ph/0409255)
Volonteri M., Haardt F., Madau P., 2003, ApJ, 582, 559

Figure 3 Francesco Haardt and Gloria Lucchesi (the flutist).

Figure 4. Gary Melnick ignored by Francesco and Edvige.

Figure 5. Francesco and Mark McCaughrean.

GAMMA-RAY BURST AFTERGLOWS AS PROBES OF HIGH-Z STAR FORMATION

P.M. Vreeswijk
European Southern Observatory, Casilla 19001, Santiago 19, Chile
pvreeswi@eso.org

Abstract Gamma-Ray Bursts (GRBs) are bright and distant explosions, caused by the death of a massive star, making them excellent probes of star formation at all redshifts. One application of GRBs is to perform optical spectroscopy of their afterglows, thereby obtaining detailed information about the inter-stellar medium of the host galaxy, even when the latter is not detected. This application is demonstrated through VLT/FORS spectroscopy of the afterglow of GRB 030323.

Gamma-Ray Burst (GRB) afterglows have three characteristics that make them potentially very powerful probes of the high-redshift universe and its star-formation properties: they are distant sources (at least up to z=4.5; Andersen et al., 2000), they can be extremely bright (e.g. GRB 990123 was measured to have V=9 at z=1.6; Akerlof et al., 1999), and their origin is related to the deaths of very massive stars (e.g. Hjorth et al., 2003).

One possible promise of GRB afterglows is that they may be the cleanest probes of the epoch of re-ionization (e.g. Barkana and Loeb, 2004). It is not yet clear if the first generation of stars produces GRBs as well, but if they do, they will allow study of this important transition period in great detail. An important question at somewhat lower redshifts, is the evolution of the star-formation density of the universe above redshifts of z=2-3. GRBs could potentially provide additional insights, but first a large sample of GRB afterglows is needed and possible biases need to be understood, before GRBs can be linked with the global star-formation density. A third application can already put to use now: measuring detailed characteristics of the inter-stellar medium (ISM) in star-forming regions as a function of redshift, through high-resolution optical spectroscopy of GRB afterglows.

The optical spectrum of the afterglow of GRB 030323, shown in Fig. 1, serves as an excellent example of what can be learnt regarding the latter application, even though this spectrum was taken with a rather low resolution grism: R$\sim$2000. From the spectrum we deduce the following properties of GRB 030323 and its environment:

E. Corbelli et al. (eds.), The Initial Mass Function 50 Years Later, 507–510.

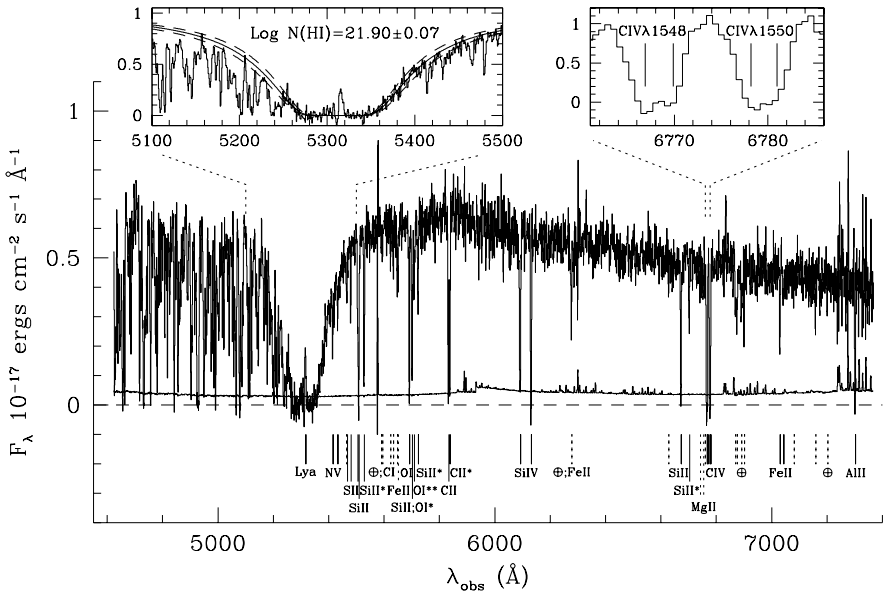

Figure 1. VLT/FORS2 spectrum of GRB 030323 at z=3.372. Damped Lyman-α and several metal-absorption lines are apparent. The value for the H I column density (see inset) is log N(H I)=21.90±0.07, which is larger than any of the previously measured DLA column densities (see Fig. 2). Even though this spectrum was taken with a resolving power of 2,000, we were still able to infer the metallicity, [S/H]=–1.3±0.2, a strong upper limit on the H_2 fraction, f $\lesssim 10^{-6}$, and a star-formation rate of 1 $M_\odot$/year. We also detected the fine-structure lines of Silicon: Si II*, which have never been clearly detected in QSO-DLAs, suggesting an origin close to the GRB. From this line we can make a rough estimate of the H I volume density of 10^2-10^4 cm^{-3}. From Vreeswijk et al. 2004.

- a redshift of z=3.372
- a neutral Hydrogen column density of log N(H I)=21.9±0.07 (see also Fig. 2) at the host galaxy redshift
- Iron and Sulphur abundances: [Fe/H]=–1.5±0.2, [S/H]=–1.3±0.2 (see Fig. 3)
- star-formation rate (from Lyman-α in emission) of $\sim$ 1 $M_\odot$/year
- strong limit on the fraction of molecular hydrogen: $2N(H_2)/(2N(H_2)+N(H\,I))\lesssim 10^{-6}$
- detection of Si II*: H I volume density of 10^2-10^4 cm^{-3}?

All these properties can be inferred irrespective of the brightness of the host galaxy. In the case of GRB 030323, HST imaging performed several

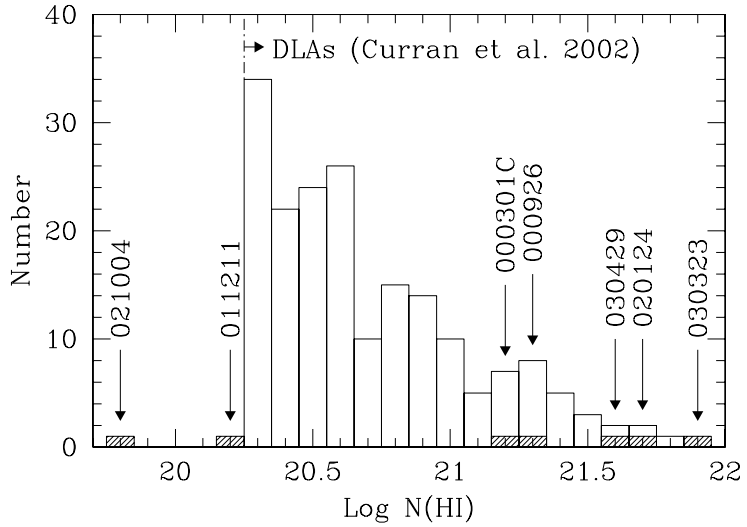

Figure 2. Histogram of the column densities of DLA systems measured through the damping wings of Lyman-α discovered in the spectrum of a background QSO (compilation taken from Curran et al., 2002). The shaded histogram shows measurements in GRBs for which the redshift was large enough to detect Lyman-α. Out of 7 GRBs, 5 show neutral hydrogen column densities above the DLA definition of 2×10^{20} atoms cm^{-2} (log N(H I)=20.3). The host of GRB 030323 contains a column density larger than in any observed (GRB- or QSO-) DLA system (Vreeswijk et al. 2004).

months after the burst show a very faint (V=28) galaxy, $0\farcs14$ away from the early-afterglow position (Vreeswijk et al. 2004). This demonstrates the power of GRB afterglows as probes of detailed characteristics of high-redshift star-forming regions.

Up to now, GRB afterglows in general have R>20 when the spectra are taken (e.g. the spectrum of Fig. 1 was taken when the afterglow had R=21.5), making high-resolution spectroscopy impossible but for exceptional cases. However, the Swift satellite (launch: October 2004; see http://swift.gsfc.nasa.gov) will provide rapid ($\sim$ 3 min) and accurate ($< 1''$) localizations of $\sim$100 GRB afterglows per year. This offers the unique possibility to perform high-resolution spectroscopy of a large sample of afterglows, probing detailed characteristics of the ISM of star-forming regions as a function of redshift.

References

Akerlof, C., et al. 1999, *Nature*, 398, 400
Andersen, M. I., et al. 2000, *A&A*, 364, L54
Barkana, R. and Loeb, A. 2004, *ApJ*, 601, 64

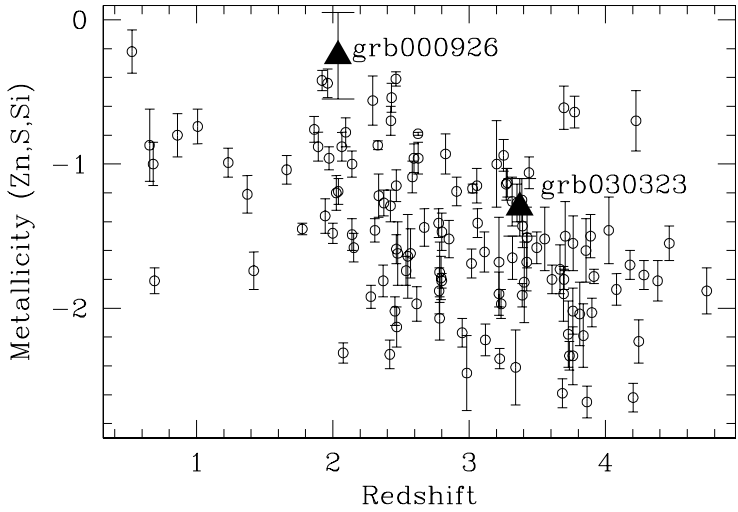

Figure 3. Comparison of the metallicities of a sample of QSO-DLAs, taken from Prochaska et al., 2003 (open circles), with the two GRBs for which a metallicity has been determined (solid triangles): GRB 000926 and GRB 030323 (Vreeswijk et al. 2004). The GRB hosts are located at the metal-rich end of the QSO-DLA distribution.

Curran, S. J., Webb, J. K., Murphy, M. T., Bandiera, R., Corbelli, E., and Flambaum, V. V. 2002, *PASA*, 19, 455

Hjorth, J., et al. 2003, *Nature*, 423, 847

Prochaska, J. X., Gawiser, E., Wolfe, A. M., Castro, S., and Djorgovski, S. G. 2003, *ApJ*, 595, L9

Vreeswijk, P. M., et al. 2004, *A&A*, 419, 927

Figure 4. The Foresteria and Abbey above the Spineto lake.

IX

CHUZPAH TALKS

"To calculate how many massive stars were born and have died over the lifetime of our galaxy required 3 ingredients: the lifetime of a star as a function of its mass, the mass-luminosity relation, and the luminosity function for Population I main sequence stars. Each of these was known only approximately in 1954 bu I have learned my lesson about the importance of **Chutzpah***: I used what little I could find in print on each of these 3 functions...."* (from Ann. Rev. Astron. Astrophys. 2002).

Figure 5. Ed and Edvige during the Chuzpah question time.

"We are ready to start the Chuzpah Lottery with questions for Ed, but let us first ask Ed: what does the word Chuzpah mean ?"

"I use the word **Chuzpa**[1] it in a very positive sense, something like savoir faire, but coupled with taking risks with just a little bit of impudence added on."

[1]Note that there are as many spellings of this word as meanings!

Figure 6. Jerome Bouvier and Andrea Stolte acknowledging the IMF committee with presents from the participants.

ELECTROSTATIC SCREENING OF NUCLEAR REACTIONS 50 YEARS LATER

Giora Shaviv
Department of Physics , Israel Institute of Technology Haifa 32,000 , Israel
gioras@physics.technion.ac.il

Abstract We show that under the conditions prevailing in the Sun, fluctuations dominate the electrostatic screening. We show that Salpeter, in his original 1954 paper, stipulates that his theory is valid when fluctuations are not large. Recent authors ignored Salpeter's assumptions.

1. Introduction

The idea of screening was first invented by Schatzman (1948) in connection with White Dwarfs. It was Salpeter, who in 1954 provided the first full self consistent theory of electrostatic screening of nuclear reactions in stellar plasmas. According to Salpeter, the screening is the enhancement of the nuclear reaction rate via interactions of the two scattering particles with the environment. The fundamental idea of Salpeter is that the binding energy of the particle in the plasma is added to the relative kinetic energy of the colliding particles. In this thermodynamic theory, all particles gain exactly the same energy irrespective of their kinetic energy. The energy gained is the mean potential energy per particle in the plasma (which may depend on the charge of the particle).

The dynamic picture of two particles with two screening clouds colliding and transferring energy from (or to) the plasma is very complicated, yet it is very simple in the thermodynamic limit. How this happens? This simple minded picture leaves many questions, like: What happens to the cloud of the second particle? Do the scattering particles polarize the plasma? How can the light mass electrons transfer energy to the heavy proton in a single collision?

In the Statistical Mechanics approach the reaction rate in plasma is given by:

$$R = n_1 n_2 \int f_2(\vec{x}_1, \vec{x}_2, \vec{v}_1, \vec{v}_2)\sigma(E_{kin-rel})|\vec{v}_2 - \vec{v}_1| d\vec{v}_{12} \qquad (1)$$

E. Corbelli et al. (eds.), The Initial Mass Function 50 Years Later, 513–520.

where $f_2(\vec{x}_1, \vec{x}_2, \vec{v}_1, \vec{v}_2)$ is the two body correlation function. The standard BBGKY expansion starts with the ansatz:

$$f_2(\vec{x}_1, \vec{x}_2, \vec{v}_1, \vec{v}_2) = f_1(\vec{v}_1) f_1(\vec{v}_2)(1 + g(\vec{x}_1, \vec{x}_2, \vec{v}_1, \vec{v}_2)). \quad (2)$$

If the interaction does not depend on momentum, then the statistical limit implies:

$$g(\vec{x}_1, \vec{x}_2, \vec{v}_1, \vec{v}_2) \rightarrow g(\vec{x}_2 - \vec{x}_1). \quad (3)$$

In the thermodynamic limit we define a potential $\phi(x)$ via:

$$1 + g(\vec{x}_2 - \vec{x}_1) = e^{-\frac{\phi(x)}{kT}}; \quad x = |\vec{x}_2 - \vec{x}_1| \quad (4)$$

with $\phi(x)$ being the self consistent mean field. If ϕ is known then the classical Salpeter approximation (in the weak screening limit) is:

$$R = n_1 n_2 e^{-\frac{\phi(0)}{kT}} \int f(v_{12}) \sigma(E_{kin-rel}) v_{12} dv_{12}. \quad (5)$$

The above result, with the assumption that ϕ can be represented by the Debye potential, constitute the basic Salpeter theory of 1954 (though he derived the result differently). The crucial question is how valid is the picture of a smooth central potential ϕ under the conditions prevailing in cores of Main Sequence stars and the Sun.

1.1 The situation in the Sun

Consider a simple hydrogen plasma in the Sun. The standard assumption is that $\phi(r) = \exp(-r/r_D)/r$, namely the Debye mean field with r_D being the Debye radius. The condition for the validity of the Debye mean field is that the number of particles in a Debye sphere be much larger than unity. Or:

$$N_D = (4\pi/3) \left(r_D/\langle r \rangle\right)^3 \gg 1, \quad (6)$$

where $\langle r \rangle$ is the mean inter-particle distance. This is exactly condition (6) in Salpeter (1954).

In the Sun the combination of density and temperature is such that $N_D \approx 3 - 4$ all throughout the Sun and hence the mean field is not expected to be valid and fluctuations should be the rule. Along the main sequence we find that $N_D \sim N_{D\odot}(M/M_\odot)^{1/7}$ and hence to a large extent the same condition as those found in the Sun.

Our basic thesis is that since the number of particles in the Debye sphere is too small for a mean field theory to be a good approximation. Thus, fluctuations dominate and the potential is time dependent and not central. Any theory which relies on a spherically symmetric constant mean field theory is not strictly valid.

2. How to approach the Problem?

In view of the many tacit assumptions (and questions) we find that the best way to attack the problem is to start from first principles and this is carried out by the Molecular Dynamics method. Moreover, while the fundamental problem is the energy exchange between the environment and the pair of scattering particles, most methods do not take into account the recoil of the particles which compose the environment. Because of the peculiarities of the present problem, special attention was paid to near-by particles. We did not assume periodic boundary conditions but rather summed the interaction over all particles within few Debye radii from the interacting pair.

The calculation is based on identifying a scattering pair, following it from the moment of identification through the approach to the classical turning point and then till the pair separates to a distance beyond several Debye radii. Then the energies at the distance of closest approach are compared with those at the separation point. We in particular do not infer from ensemble average the consequences of the energy exchange in the collisions.

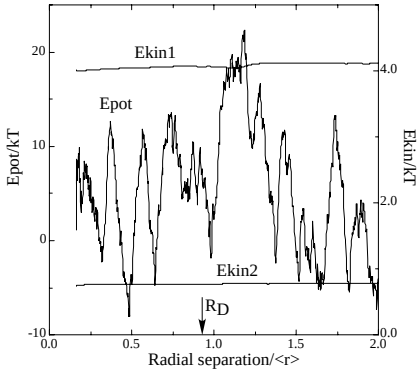

Figure 1. The potential and kinetic energies as a function of radial separation. The R_D is marked by an arrow.

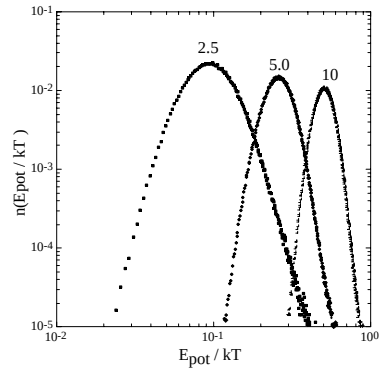

Figure 2. The distribution of potential energy for $R_n >< r >$. The numbers are $R_n/\langle r \rangle$.

In fig.(1) we show a typical case of the potential energy as a function of time in a pair of scattering particles. The conditions are pure Hydrogen plasma at a number density of 10^{26} and a temperature of $1.5 \times 10^7 K$, conditions which are characteristic to the Solar core. The fluctuations in the potential energy are obvious. The kinetic energies change very little and the changes do not follow the fluctuations in the potential energy. The reasons are two (a) the lion share of the fluctuations is due to fast electrons, but these, being so light, hardly exchange energy (in a single collision) with the protons, and (b) a significant part of the energy exchange goes into the energy of the center of mass. There

is no energy conservation for just the two scattering particles. The conclusions are:

- Fluctuations control the p-p scattering in the Sun and Main Sequence stars.
- The protons scatter from a time dependent stochastic potential created by the fluctuations (caused by random passage of few particles).
- The mean field approximation is not expected to be a good description for p-p scattering under such conditions.
- The pair correlation function g(0) is obtained by averaging over many configurations (it is the long time average - thermodynamic average) and hence is relevant to thermodynamic quantities like equation of state but not to the screening under the conditions prevailing in Main Sequence stars.

3. The gedanken numerical experiment

The fundamental interaction in the plasma is a long range Coulomb interaction. However, in the plasma the interaction between positive and negative charges leads to a finite effective range. The existence of positive and negative charges dictates right away an effective finite interaction radius. Many of the difficulties in appreciating the effect of the finite radius and small number of particles in the Debye sphere result from the so dictated *effective* interaction range. To understand the role of a finite effective interaction with a range of the order of the inter-particle distance we decided to carry out a gedanken numerical experiment in which the gedanken potential has a controllable range and strength and is not dictated by the density and temperature in an unchangeable manner. Basic idea therefore is: conduct a numerical experiment with a hypothetical potential in such a way that the parameters of the potential can be varied at will keeping the thermodynamic conditions fixed. In this way we hope to learn how the thermodynamic limit is reached and what happens before this limit becomes a good approximation. Such a potential is for example:

$$\begin{aligned} V(r > R_n) &= 0 \\ V(r < R_n) &= C_f\,(1/r - 1/R_n) \end{aligned} \tag{7}$$

The strength of the interaction C_f and the range R_n are free parameters.

3.1 Results

In fig.(2) we show the distribution of potential energy for $R_n > 1$ the distribution approaches a guassian with a decreasing width. Thus, as the number

of particles in the Debye sphere increases, the distribution narrows. In fig.(3) we see the distribution of the potential energy for $R_n < 1$. We find that the distribution is not narrow nor guassian. The distribution vanishes for $E_{pot} = 0$ then rises very quickly to a maximum value from which it declines slowly.

The ensemble average of the potential energy per particle should be summed over all positions of particles. However, if we bias the averaging, say average over particles only when they are close to each other, a different result may be obtained. In figs.(4,5) we show the two distributions for two values of R_n.

The resulting screening for $R_n = 0.4\langle r\rangle$ is shown in fig.(6). The dependence on the relative kinetic energy is clear as well as the difference between the ensemble average (thermodynamic) and the calculated according to the Molecular Dynamics. In fig.(7) we give the energy distribution of the screening for several ranges. It is evident that as the range increases and the number of particles in the interaction zone increases, the dependence on energy decreases. As one approaches the thermodynamic limit ($N_D >> 1$) the energy dependence disappears, as expected.

The ratio of the present screening calculation to the classical Salpeter value is shown in fig.(8). For $R_n >> 1$ the Salpeter thermodynamic value is recovered, while for R_n where the mean field Debye theory is not expected to be valid, large deviations are found. The actual screening is smaller than the thermodynamic value. The very large fluctuations do not average to the thermodynamic ensemble average in this range.

When $N_D \sim 1$ the energy change by the center of mass due to the non spherically symmetric interaction is not negligible. The average energy change of the center of mass is shown in fig.(9). Again, as $N_D \rightarrow >> 1$ the energy change of the CM diminishes and vice versa, as$N_D \sim 1$ the energy change increases along with the increase in the fluctuations.

The effect is not proportional to the strength of the interaction as can be seen from fig.(10). Only at high energies we find proportionality.

As is well known, $g(r, E) \rightarrow g(r)$ in the thermodynamic limit. In fig.(11) we show that for $R_n = 5$ this is almost the case while for $R_n = 0.4$ the energy dependence is still obvious.

4. Conclusions

- The statistical limit is obtained for $R_n \rightarrow \infty$. In reality, the limit is reached very quickly.

- Fluctuations control the scattering of ions under the condition prevailing in the Sun.

- For Main Sequence stars the statistical limit does not apply.

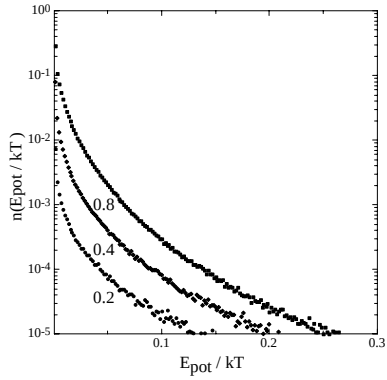

Figure 3. The potential energy distribution for $R_n = 0.8 < r >< 1$.

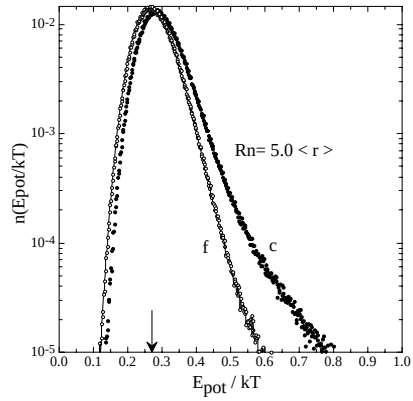

Figure 4. The distribution of potential energy for $R_n = 5 < r >$. c is for close and f for far away.

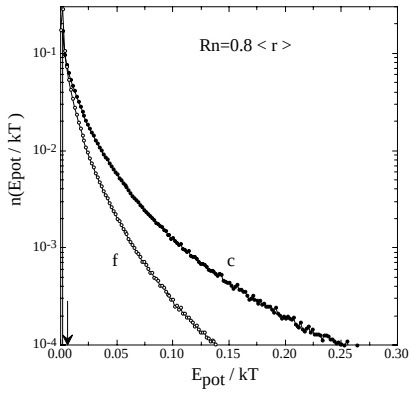

Figure 5. The potential energy distribution for $R_n = 0.8 < r >$. The c is for close and f for far apart. The arrow marks the ensemble average.

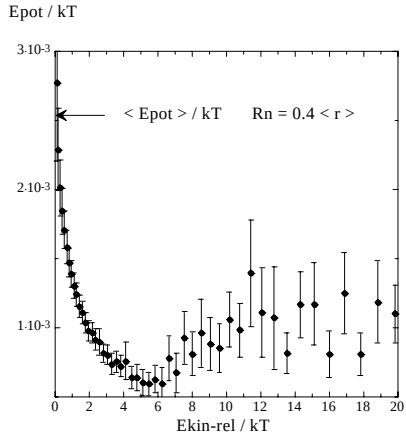

Figure 6. The screening energy as a function of relative kinetic energy for $Rn = 0.4 < r >$.

5. Criticism of Shaviv and Shaviv

Bahcall et al (2002) claim that the Salpeter classical expression is valid in the Sun. The authors ignore the assumptions stated by Salpeter (1954) that a prerequisite for the validity of the theory is $N_D >> 1$. In Salpeter's words: *"For this procedure to be strictly valid many nuclei and electrons should be contained in a volume small enough so that $\rho(r)$ and $U(r)$ do not vary appreciably over this volume ....Hence our procedure is valid as long as $a \ll R$".*

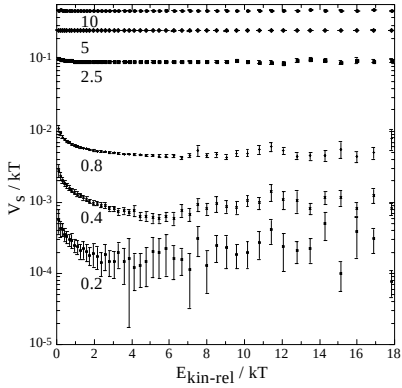

Figure 7. The screening energy as a function of relative kinetic energy for several values of R_n.

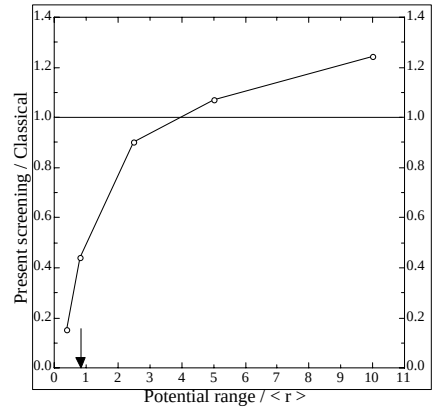

Figure 8. The ratio: new to the classical (Salpeter) screening correction as a function of R_n.

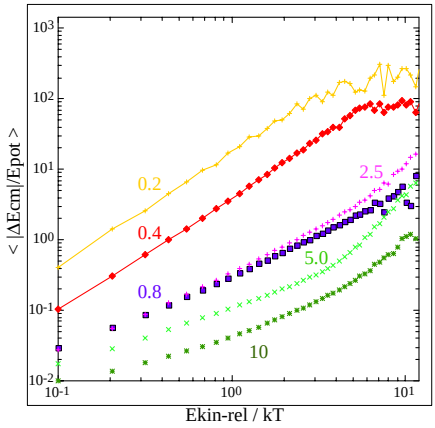

Figure 9. ΔE_{CM} for several values of R_n as a function of relative kinetic energy.

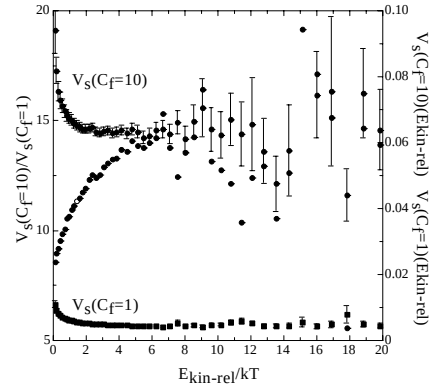

Figure 10. A comparison between two potential strengths. The full points are the ration

Bahcall et al (2002) repeat the text book 'plausible' explanation which is based on thermodynamic arguments which tacitly assume $N_D >> 1$. We note in passing, that the definition of the screening given by Salpeter agrees with the definition given here and is not the one given by the 'plausibility' arguments.

Alastuey & Jancovici formulation of the screening in terms of $g(0)$ is also based on the tacit assumption that $N_D >> 1$. In fig.(11) we show the pair correlation function for several relative kinetic energy bins. We find that for $R_n \leq 1$ $g = g(r, E)$ and not $g = g(r)$.

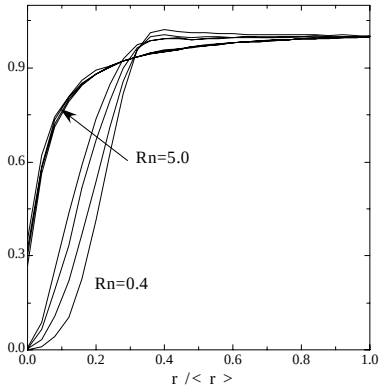

Figure 11. The pair correlation function as a function of the relative kinetic energy. Different curves refer to different relative kinetic energies.

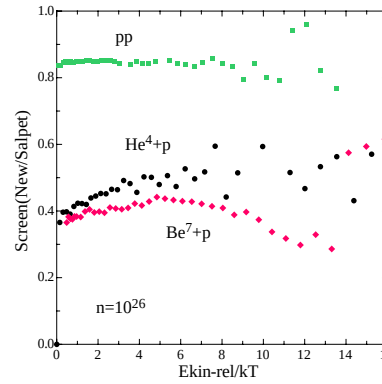

Figure 12. The ratio of the actual screening corrections to the classical Salpeter value for three important reactions in the Solar plasma.

6. The new screening for the Sun

We turn now to actual screening calculations. In fig.(12) we show results for the solar plasma. The conditions are $n = 10^{26}/cc, T = 1.7 \times 10^7 K, X(H) = 0.9, X(He) = 0.08, X(Be^7) = 0.02$. The mass fraction of Be^7 is because of numerical reasons much above the actual one. We find that the screening enhancement of all reactions is less then the classical value. The higher the nuclear charge, the greater is the reduction.

References

Alastuey, A. A. & Jancovici, B. 1973, ApJ, 226, 1034

Bahcall, J. N., Brown, L. S., Gruzinov, A., & Sawyer, R. F. 2002, A&A, 383, 291

Salpeter, E. E. 1954, Australian J. Physics, 7, 373

Schatzman E. 1948, J. Phys. Rad., 9, 46

Shaviv, N. J. & Shaviv, G., 1997, in White dwarfs, eds. I. M. Hernanz & E. Gracia-Berro (Dordrecht: Kluwer, ASSL 214), 43

Shaviv, G. & Shaviv, N. J. 2000, ApJ, 529, 473

Shaviv, G., 2000, astro-ph/0010152

THE LIFE AND DEATH OF PLANETARY NEBULAE

Yervant Terzian and Artin Teymourian
NAIC, Cornell University, U.S.A.
yt28@cornell.edu, apt8@cornell.edu

Abstract Distance measurements to Planetary Nebulae have always been inaccurate and depending on what technique is used to determine the distance, severely conflicting results may emerge. A new technique for determining distances, the Expansion Parallax method, is being used to obtain much more accurate distances. This technique is based upon the relationship between the angular expansion of the PNe in the sky and the velocity of expansion of the PNe.

1. Introduction

Stellar evolution has indicated that most stars in our galaxy will eventually become planetary nebulae, therefore a good estimate for the number and birthrate of these objects is important. If an accurate measurement for the birthrate of PNe is found, then we have a good number for the deathrate of stars, which will help us to better understand the evolution of our galaxy. Up to now there have been $\sim$1500 observed planetary nebulae in the galaxy, although the total number is much higher. These objects range in size from $\sim$0.04 to 0.7 pc and range in mass from $\sim$0.2 to a few $M_{\odot}$. The measured expansion velocity of PNe is between 20 and 30 km/sec (Gurzadyan and Terzian 1991), and the lifetime corresponding to this velocity for a visible nebula is about 20-40$\times 10^3$ years. AGB stars that become PNe have many things in common and undergo many of the same processes. The stars usually have a radius of about 2 AU and an initial mass of $\sim$1-8 $M_{\odot}$. These stars have a mass loss rate which increases from 10^{-8} to 10^{-4} $M_{\odot}$/yr. A slow wind develops, which creates an expanding envelope that includes molecules such as CO, CS, SiO, HCN, and dust particles. The lifetime of AGB stars is about 10^6 years, characterized by a "Helium shell burning phase", and a "Thermal pulse phase". After $\sim 10^6$ years, the core quickly collapses into a White Dwarf that heats and ionizes the inner nebula, and a fast wind compresses the surrounding envelope to a thin radiating shell.

E. Corbelli et al. (eds.), The Initial Mass Function 50 Years Later, 521–526.

2. Distances

Finding distances to PNe has always been a problem (see Terzian 1993). There are many proposed methods for determining distances. However, most of these use statistical methods or assumptions that are not always realistic. Because of these assumptions, the distance derived to a certain PN using different methods can bring about vastly different results. This discrepancy can be seen when considering PNe within 1 kpc. Using distances of 40 PNe derived by various authors that employed different methods, the results show that Zhang and Kwok (1993) found only 1 PN within 1 kpc, whereas Amnuel et al. (1984), for the same group of objects, found 23 within 1 kpc, other authors derived numbers spanning 5 to 20 within 1 kpc. This illustrates the real problem; there has not been a consensus for an accurate measurement of the distance to PNe. The discrepancies in distance measurements also impact estimates of PNe spatial densities in the galaxy. Using different methods for obtaining distances, authors find number densities ranging from 36 kpc^{-3}, estimated by Weidemann (1977), to 430 kpc^{-3}, estimated by Khromov (1979). These numbers can also be affected by the use of different scale heights for the galaxy by different authors. In general, the estimated number densities tend to be closer to $\sim$80 kpc^{-3}. The birthrate of PNe are also affected by differing distance scales. This number tends to range from a low estimate of 1.0 yr^{-1} kpc^{-3} (Drilling and Schönberner 1985) to a high of 8.3 yr^{-1} kpc^{-3} (Ishida and Weinberger 1987), whereas most estimates fall near $\sim$ 3.0 yr^{-1} kpc^{-3}. The expansion parallax distance method, as used in recent years, has shown promising results (Hajian et al. 1995, Reed et al. 1999, Palen et al. 2002). This method uses very few assumptions, most of which being true in most cases. Nebular angular expansions are detactable in the radio (as seen with the VLA), and optical wavelengths (as seen with the HST), thus accurate measurements of the expansion can be made. The angular velocity ($\dot{\theta}$) is measured from these observations, and the velocity of expansion (V_{exp}) is found from ground based spectroscopy. The nebular distances are then derived from:

$$D_{pc} = 21.1 \frac{V_{exp}(\text{km/sec})}{\dot{\theta}(\text{arcsec/century})}$$

$$D_{pc} = 211 \frac{V_{exp}(\text{km/sec})}{\dot{\theta}(\text{mas/yr})}$$

Since angular expansion rates cannot feasibly be observed over a century, minute and accurate measurements must be made of the expansions (in mas) within a few years. Modern technologies allow for accurate measurements of such small angular expansions, namely the Hubble Space Telescope for optical observations and the VLA for radio observations.

3. Distance Scales

In recent years parallax distances for several PNe were measured and these distances have been compared to those found using several other methods, as shown in Table 1 (see Terzian 1993 for a full discussion).

Table 1. Comparative Distances of PNe (in kpc)

PN	C74	D82	A84	G87	MP88	CKS92	ZK92	YT/AT04
NGC246	0.57	0.46	0.45	0.50	-	0.47	-	0.53[1]
NGC1514	1.1	0.67	0.65	0.50	-	0.75	-	0.29[1]
NGC2392	2.0	1.2	0.86	-	2.7	1.3	-	0.67[1]
NGC3132	-	1.0	0.80	0.60	0.54	1.3	-	0.64[1]
NGC3242	1.7	0.73	0.52	0.50	2.0	1.1	1.5	0.42[2]
NGC6572	0.90	0.47	0.43	0.41	0.68	0.66	3.3	1.2[3]
NGC6578	-	1.4	1.2	2.0	2.0	2.3	4.3	1.6[4]
NGC6720	1.3	0.79	0.64	0.65	-	0.87	1.9	0.60[1]
NGC6884	-	1.1	1.4	1.8	1.8	2.1	-	1.6[4]
NGC7009	1.9	0.76	0.59	0.58	2.4	1.2	1.1	0.6[5]
NGC7027	0.51	0.18	0.82	1.1	0.94	0.27	-	0.88[6]
NGC7293	0.21	0.15	0.18	-	0.30	0.16	-	0.21[1]
NGC7662	1.57	0.84	0.67	0.98	-	1.2	1.9	0.79[7]
He 2-138	-	2.2	1.9	-	5.0	3.6	2.3	0.47[1]
IC2448	-	2.5	-	-	3.5	4.0	3.6	1.4[4]

[1]Phillips (2002); [2]Hajian, et al. (1995); [3]Kawamura and Masson (1996); [4] Palen, et al. (2002); [5]Liller, et al. (1966); [6]Masson (1989); [7]Hajian and Terzian (1996). Sources: G87 (Gathier 1987); A84 (Amnuel, et al. 1984); D82 (Daub 1982); C74 (Cudworth 1974); CKS92 (Cahn, et al. 1982); MP88 (Mallik and Peimbert 1988); ZK92 (Zhang and Kwok 1993); YT/AT04 (This Paper)

The last column of Table 1 shows measured distances for different PNe using several different parallax methods. These methods include expansion parallaxes in the radio and optical wavelengths, and also trigonometric parallaxes for closer PNe. The value from Liller, et al. (1966) may have a large uncertainty due to the use of different emulsions in developing the optical images since this may cause discrepancies between the different images resulting in an inaccurate measurement. The above distances from various authors were analyzed statistically and were normalized to obtain a distance scale, giving values between 1.0 and 3.5. Mellema (2004) has pointed out that the pattern velocities and matter velocities are not necessarily the same in PNe where the angular expansion velocity in the sky is compared to the radial velocity of the gas. The pattern velocities are typically 20-30% larger than the matter velocities, and thus the measurements must be corrected to account for this. After correcting for these effects, we obtain the distance scales given in Table 2.

The expansion parallax method has a few limitations in its use. First, one must find the angular expansion and radial expansion of the same volume ele-

Table 2. PNe Distance Scale

Author	Normalized Calibration
Gathier 1987	1.0
Amnuel, et al. 1984	1.5
Daub 1982	1.5
Parallax Distances 2004	2.0
Cudworth 1974	2.5
Cahn, et al. 1992	2.5
Mallik and Peimbert 1988	2.5
Zhang and Kwok 1993	3.5

ment. Also, since the angular expansion rate is so small ($\sim$0.2 arcsec/century), this method can only be used out to a few kpc. One also needs kinematical models to correct for nebular shape and inclination. There is also the assumption made that the ionization front moves much faster than the expansion motion of the gases. There can possibly be unknown changes in ionizing luminosity, which may affect radio flux density changes within small time intervals.

4. PNe Population

Authors who have made estimates of distances to PNe have also estimated their total number in the galaxy to be $\sim$20,000 - 100,000. The distance scale to PNe from the study of expansion parallaxes is $\sim$2.0, corresponding to a total population of $\sim$45,000. Different methods for determining distances result in varying numbers of total PNe in the galaxy. Maciel (1987) has used observations of other galaxies within the local group to estimate the PNe number at 15,000 - 60,000 assuming that the total mass of the galaxy is M =1.5$\times 10^{11}$ $M_{\odot}$. Our new estimate of 45,000 fits well within this estimate. Other estimates from Ford and Jacoby (1977) show that M31 contains about 27,000 - 54,000 PNe. It has been thought that the mass of M31 is approximately twice that of our own galaxy, thus using this data, Cahn and Wyatt (1977) have obtained a total number of 13,500 - 27,000 PNe in our galaxy. Once again, it must be realized that the total mass of the galaxy is still only an approximation; therefore the number of PNe using this method may be inaccurate. Adopting a total population of 45,000 PNe, a spatial density of $\sim$150 kpc^{-3} can be calculated, indicating a birthrate of $\sim 5 \times 10^{-3}$ kpc^{-3} yr^{-1}. This brings the total PNe birthrate in the galaxy to $\sim$1 yr^{-1}. Phillips (2002) had estimated the total PNe birthrate at 1.43 yr^{-1} which is very close to the estimate noted here. Table 3 summarizes these results.

Weidemann (1991) has calculated a total White Dwarf birthrate of $\sim 2.3 \times 10^{-3}$ kpc^{-3} yr^{-1}, which appears to be somewhat low compared to the PNe birthrate indicated above. However, Bond (1987) has pointed out that these

Table 3. PNe Parameters in the Galaxy

Total Number of PNe	$\sim$45,000
Galactic Scale Height	$\sim$200 pc
Number of PNe per Solar Mass	$\sim 2 \times 10^{-7}$
Birthrate	$\sim$1 yr^{-1}
Mass Return to Interstellar Medium	$\sim$20 M$_\odot$/100yr($\sim$SNR Rate)

numbers may represent a lower limit, since many white dwarfs can be concealed in binary systems with main-sequence primaries. The number of white dwarfs and their density in the galaxy has also been investigated by Tat and Terzian (1999) where they have attempted to derive parameters from 'complete' white dwarf samples.

Acknowledgments The authors acknowledge useful discussions with Arsen Hajian and Bruce Balick. One of us (AT) thanks the New York NASA Space Grant Program for a student Research Fellowship.

References

Amnuel, P. R. et al. 1984, Astroph. Sp. Sc., 107, 19
Bond, H. E., 1987, in Planetary Nebulae, ed. S. Torres- Peimbert (Dordrecht: Kluwer), 251
Cahn, J. H., Kaler, J. B., and Stanghellini, L., 1992, A&AS, 94, 399
Cahn, J. H., and Wyatt, S. P., 1977, in Planetary Nebulae, ed. Y. Terzian (Dordrecht: Reidel), 3
Cudworth, K. M., 1974, AJ, 79, 1384
Daub, C. T., 1982, ApJ, 260, 612
Drilling, J. S., and Schönberner, D., 1985, A&A, 146, L23
Gathier, R., 1987, A&AS, 71, 245
Gurzadyan, G.A., and Terzian, Y., 1991, AJ, 101, 1752
Hajian, A. R., and Terzian, Y., 1996, PASP, 108, 419
Hajian, A. R., Terzian, Y., and Bignell, C., 1995, AJ, 109, 2600
Ishida, K., and Weinberger, R., 1987, A&A, 178, 227
Kawamura, J., and Masson, C., 1996, ApJ, 461, 282
Khromov, G. S., 1979, Astrofizika, 15, 445
Liller, M. H., Welther, B. L., and Liller, W., 1966, ApJ, 144, 280
Maciel, W. J., 1987, in Planetary Nebulae, ed. S. Torres- Peimbert (Dordrecht: Kluwer), 73
Mallik, D. C. V., and Peimbert, M., 1988, Rev. Mex. Astron. Astrof., 16, 111
Masson, C. R., 1989, ApJ, 336, 294
Mellema, G., 2004, A&A, 416, 623
Napiwotzki, R., 2001, A&A, 367, 973
Palen, S. et al., 2002, AJ, 123, 2666
Phillips, J. P., 2002, ApJS, 139, 199
Tat, H. H., and Terzian, Y., 1999, PASP, 111, 1258
Terzian, Y., 1993, in Planetary Nebulae, eds. R. Weinberger and A. Acker (Dordrecht: Kluwer), 109
Weidemann, V., 1977, A&A, 61, L27
Weidemann, V., 1991,in White Dwarfs, eds. G. Vaulclair and E. Sion, (Dordrecht: Kluwer), 67
Zhang, C. Y., and Kwok, S., 1993, A&AS, 88, 137

Figure 1. Yervant Terzian and Ed having spaghetti at Ocaiolo.

EARLY RESULTS FROM THE INFRARED SPECTROGRAPH ON THE SPITZER SPACE TELESCOPE

J.R. Houck[1], V. Charmandaris[1] and B.R. Brandl[2]
[1]*Cornell University, Space Sciences, Cornell University, Ithaca, NY 14853, USA*
[2]*Leiden Observatory, Niels Bohrweg 2,#535, P.O. Box 9513, 2300 RA Leiden, Netherlands*
jrh13@cornell.edu,vassilis@astro.cornell.edu,brandl@strw.leidenuniv.nl

Abstract The Infrared spectrograph, IRS, on the Spitzer Space Telescope has greatly improved the sensitivity in the thermal infrared and opened many new avenues in infrared astronomy over the range of 5.5 to 38 microns. With the IRS an object with mid-infrared flux of $\sim$1 mJy can produce a usable low resolution spectrum in an hour of telescope time. The mid-infrared study of star formation at low metallicity has been enabled by this new sensitivity.

1. Introduction

The infrared spectrograph (IRS; Houck et al. 2004a), one of the instruments in the Spitzer Space Telescope (Werner et al. 2004) the fourth and last of NASA's Great Observatories, was launched into orbit about the Sun on August 25, 2003. Routine observations began in December 2003, with all of the instruments performing extremely well. The IRS consists of four individual spectrographs that are identified by their wavelength range and spectral resolution: Short-Low (SL, 5.5–14.5 μm; $R = \lambda/\delta\lambda$ $\sim$90), Short-High(SH, 9.9–19.6; $R = 600$), Long-Low (LL,14.0–38; $R = 90$), and Long-High (LH, 18.7–37; $R = 600$). The widths of the entrance slits are set to $\lambda_{\rm max}/D$ where $\lambda_{\rm max}$ is the longest usable wavelength for each module and $D = 85$ cm, the telescope aperture. The slits lengths vary from 11.8 to 151.3 arcsec. The slit widths are imaged onto two detector pixels. The low resolution slits are as long as possible given the limited space available. The high resolution modules are crossed echelle spectrographs with slit lengths of 6 pixels. In addition the IRS SL module has two imaging apertures ($\sim$60$\times$90 arcsec) with bandpass centers at 16 μm and 22 μm. These are used for direct imaging and target acquisition. The detectors are 128$\times$128 arrays of Si:As (SL and SH) and Si:Sb (LL and LH) with pixel sizes of 75$\times$75 μm. There are no moving parts in the IRS.

E. Corbelli et al. (eds.), The Initial Mass Function 50 Years Later, 527–532.

Additional information on the design and operation of the IRS can be found in Chapter 7 of the Spitzer Observers Manual and at the IRS Science Center [1].

Nearly 100 science papers based on the early observations from Spitzer have been published in a special issue of the Astrophysical Journal Supplements (vol.154, 1 Sep 2004). In this paper we discuss the early results on the study of star formation in a very low metallicity blue compact galaxy, SBS 0335-072 (Houck et al. 2004b).

2. Observations

We chose SBS 0335-052, along with approximately 20 other well studied BCDs, to investigate the characteristics of star formation at very low metallicities using the IRS (Houck et al. 2004a) on Spitzer (Werner et al. 2004). Similar low metallicity objects may be detected at much higher luminosity and much greater redshifts in Spitzer discovery surveys.

SBS 0335-052 was observed using both IRS low resolution modules. The spectrum extends from 5.3 to 35 μm and was obtained on 6 Feb 2004. The red peak-up camera in medium-accuracy mode was used to locate the mid-IR centroid of the source and move it to the center of the spectrograph slits. The total integration time was 42 minutes with 28 minutes for the Short-Low module and 14 minutes for the Long-Low module. The total elapsed time including the telescope slew, target acquisition, settling, array conditioning, and integration was 61.3 minutes.

The basic processing of the data, such as ramp fitting, dark sky subtraction, removal of cosmic rays, droop and linearity correction, wavelength calibration, etc, was performed using the IRS pipeline at the Spitzer Science Center (version S9.1). The resulting spectral images were sky-subtracted and a one-dimensional spectrum then extracted. The peak-up images were also used to derive a photometric point at 22 μm (filter bandwidth 18.5–26.0 μm). As described in detail in chapter 7 of the Spitzer Observer's Manual, during IRS peak up we obtain 6 images of the science target. The on source time for the 22 μm peak-up images of our target was $6 \times 8 = 48$ s and each image was created by reading the array in double-correlated sample mode. We processed the data on the ground to remove cosmic rays and the residual noise of the electronics. The resulting image had a prominent diffraction ring and was indistinguishable from the image of a point source. The conversion to flux density was based on a number of calibration stars for which peak-up images, IRS spectra, and reliable templates are available (Cohen et al. 2003). We find that the 22 μm flux density of SBS 0335-052 is 70 ± 11 mJy.

[1] See http://ssc.spitzer.caltech.edu/documents/SOM/ or http://isc.astro.cornell.edu/

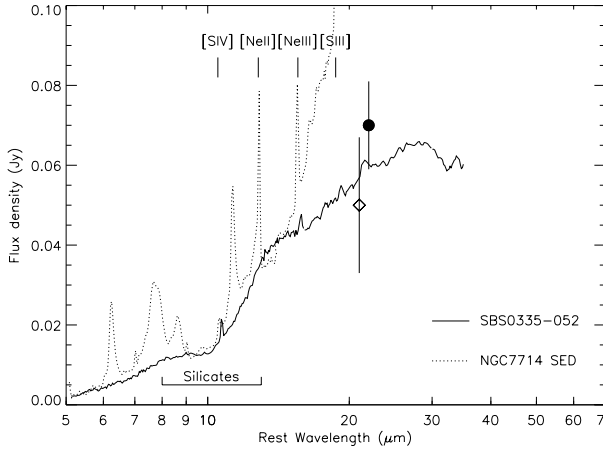

Figure 1. The IRS low resolution spectrum of SBS 0335-052 (solid line) along with the spectrum of NGC 7714 (dotted line) from Brandl et al. The spectrum of NGC 7714 has been divided by 9.53 so that its 14 μm flux density matches that of SBS 0335-052. Note the complete lack of PAHs in the spectrum of SBS 0335-052 as well as the spectrum peak at $\sim$30 μm. The solid circle is our 22 μm peak-up photometric point, while the diamond corresponds to the 21 μm Gemini point from Plante & Sauvage.

3. Interpretation

Figure 1 shows the 5.3–35 μm spectrum of SBS 0335-052 as observed by the IRS. Our data are in good agreement with the overall shape and intensity of the 5–15 μm ISO spectrum of Thuan et al. (1999), but our signal to noise is at least a factor of 10 higher. This enables us for the first time to directly detect a few mid-IR ionic lines, while placing strong upper limits on others. The 9.7 μm silicate absorption feature is clearly evident in our spectrum, and the 18 μm feature is probably present.

In Figure 1 we also present a scaled version of the IRS low-resolution spectrum for the prototype starburst nucleus of NGC 7714 (Brandl et al. 2004), normalizing its flux to the corresponding flux of SBS 0335-052 at 14 μm (the actual flux for NGC 7714 is $\sim$9.5 times larger than shown). As also noted by Thuan et al. (1999), a striking difference between the spectrum of SBS 0335-052 and that of a more typical starburst is the absence of polycyclic aromatic hydrocarbon (PAH) features and low excitation ionic lines. In starburst galaxies, emission from PAHs is thought to originate from the photodissociation envelopes bordering the H II regions produced by the ionizing starburst. How these features can be absent in a low-metallicity starburst is an important astrophysical question. One possibility is that the absence of PAHs is due to low

abundance of carbon and/or nucleating grains; another possibility is that PAHs are quickly destroyed.

Table 1. Mid-IR Line Fluxes of SBS 0335-052

Ion	$\lambda(\mu\mathrm{m})$	*Flux* ($\times 10^{-17}$ Wm^{-2})
[S IV]	10.51	1.62 ± 0.09
[S III]	18.71	< 0.54
[Ne II]	12.81	< 0.28
[Ne III]	15.55	1.40 ± 0.08
H_2 0–0 S(3)	9.67	< 0.37

Table 1 shows that the observed line ratios of $\log([\mathrm{S\,IV}]/[\mathrm{S\,III}]) > 0.48$, and $\log([\mathrm{Ne\,III}]/[\mathrm{Ne\,II}]) > 0.69$ are similar to the most extreme example of ultra-compact H II regions in our Galaxy. The ratios indicate that the radiation field is extremely hard and corresponds to an effective stellar temperature of $T_{\mathrm{eff}} \geq 4 \times 10^4$ K, assuming solar abundance (see Martin-Hernandez et al. 2002). This would suggest that the absence of PAHs results from their destruction by the hard UV photons and strong winds produced by the massive stars (i.e. Allain et al. 1996). Such a scenario is quite likely since in low metallicity systems the attenuation of UV photons is small and consequently their mean free path in the interstellar medium can be larger and photodissociation of PAHs may occur over considerably larger scales than those seen in typical Galactic H II regions. Whatever, the PAH life-cycle is in SBS 0335-052, the primary result is the well-defined absence of these features in the mid-IR. (Our recent results indicate a strong correlation between the PAH strength and the metallicity of the host BCD.)

Another major difference between the two spectra shown in Figure 1 is that in SBS 0335-052 the continuum shortward of $\sim$15 μm appears similar to that which underlies the emission features in NGC 7714. However, these continua depart dramatically at longer wavelengths. The continuum of NGC 7714 increases rapidly at longer wavelengths because of a massive cool dust component which characterizes many luminous infrared galaxies. Conversely, the spectrum of SBS 0335-052 peaks at 28 μm. In Figure 2 we have drawn an offset power-law, $f_\nu \sim \nu^{1.3}$, to the IRS spectrum to extrapolate to longer wavelengths. Using the non-thermal 1.46 GHz flux density of the galaxy measured by Hunt et al. (2004) and the radio to far-infrared correlation, we predict that the far-infrared luminosity is F_{FIR}(43–123 μm)$= 2 \times 10^{-15}$ Wm^{-2}. The corresponding average flux density over this wavelength range is $\sim$44 mJy. Even if the entire far-infrared luminosity originates from the 60 μm band, the corresponding flux density would be 58 mJy, well below the Plante & Sauvage (2002) 112 mJy measurement at 65 μm. However, the 58 mJy estimate is con-

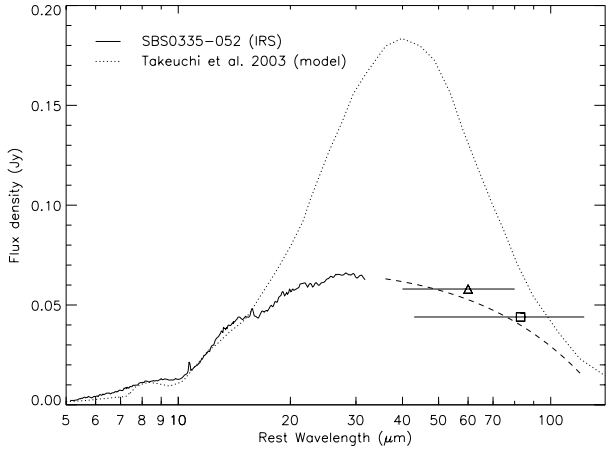

Figure 2. The IRS spectrum of SBS 0335-052 (solid line) along with the model of Takeuchi et al. (dotted line). Based on the observed 5–35 μm SED of the galaxy we can extrapolate to longer wavelengths (dashed line). The difference between the observed SED and the model has only a small effect in the infrared luminosity, but it substantially reduces the amount of cold dust in the galaxy. We also show estimates derived from the radio data of the average flux density over the far-infrared range and the upper limit at 60 μm (box and triangle, respectively).

sistent with the IRS spectrum which clearly decreases at wavelengths longer than 30 μm.

These two major differences, no PAH features and relatively flat continuum, provide an initial indication that the PAH criterion for identifying starbursts may not apply to systems of low metallicity. Mid-IR spectra of Active Galactic Nuclei (AGN) often display ionic lines and also lack PAH emission features, but the continua are typically even flatter between 5–20 μm than SBS 0335-052 (see ISO observations of Seyfert 1s by Clavel et al. 2000, or the nuclear spectrum of NGC 1068 by Sturm et al. 2000 and Le Floc'h et al. 2001 as well as Peeters et al. 2004). If metal poor galaxies such as SBS 0335-052 can be present at $z \sim 0.06$, it is likely that similar systems may exist not only as high-z primordial galaxies, but also at intermediate redshifts $0.5 < z < 1.5$ where moderate luminosity galaxies ($L_{\rm IR} < 10^{11}\ L_{\odot}$) are accessible with the deep infrared surveys performed by Spitzer. Far-infrared and submillimeter photometric methods for estimating redshifts based on spectral energy distributions (SEDs) of nearby metal rich systems, with continua peaking at $\sim$100 μm, would fail to identify metal poor systems with SEDs similar to that of SBS 0335-052, which peaks at $\sim$28 μm.

4. Conclusions

The very low metallicity Blue Compact Dwarf galaxy SBS 0335-052 is shown to have a very unusual spectrum which is quite different from the spectrum of typical starburst galaxies: the flux density, f_ν, peaks at $\sim$28 μm while the luminosity, νf_ν, peaks at $\sim$20 μm. There are no detectable PAH emission features. The spectrum is characterized by a warm ($\sim$150 K) dust component with a more massive cool ($\sim$65 K) dusty envelope. However, the mass of the cool region is far less than what had been previously estimated. Silicate absorption features are clearly present ($A_{9.7\mu\mathrm{m}} \geq 0.49$ mag). Preliminary analysis of the infrared ionic lines suggests that the young central cluster may have already polluted the cocoon enshrouding it, and its metallicity could be higher than that determined from optical observations alone. Upcoming mid-IR spectroscopy using the high resolution modules of IRS will provide higher sensitivity and more accurate line fluxes.

References

Allain, T., Leach, S., & Sedlmayr, E. 1996, A&A, 305, 602
Brandl, B. R., et al. 2004, ApJS, 154, 188
Clavel, J., et al. 2000, A&A, 357, 839
Cohen, M., Megeath, T.G., Hammersley, P.L., Martin-Luis, F., & Stauffer, J. 2003, AJ, 125, 2645
Houck, J. R., et al., 2004a, ApJS, 154, 18
Houck, J. R., et al., 2004b, ApJS, 154, 211
Hunt, L. K., Dyer K. K., Thuan, T. X., & Ulvestad, J. S. 2004, ApJ, 606, 853
Le Floc'h, E., Mirabel, I. F., Laurent, O., Charmandaris, V., Gallais, P., Sauvage, M., Vigroux, L., & Cesarsky, C. 2001, A&A, 367, 487
Martin-Hernandez, N. L., et al. 2002, A&A, 381, 606
Peeters, E., Spoon, H.W.W., & Tielens, A.G.G.M., 2004, ApJ, in press [astro-ph/ 0406183]
Plante, S. & Sauvage, M. 2002, AJ, 124, 1995
Rees, M. J. 1998, Space Science Reviews, 84, 43
Sturm, E., Lutz, D., Tran, D., Feuchtgruber, H., Genzel, R., Kunze, D., Moorwood, A. F. M., & Thornley, M. D. 2000, A&A, 358, 481
Thuan, T. X., Sauvage, M., & Madden, S. 1999, ApJ, 516, 783
Werner, M., et al. 2004, ApJS, 154, 1

FUTURE OBSERVATIONAL OPPORTUNITIES

Gary J. Melnick
Harvard-Smithsonian Center for Astrophysics, 60 Garden Street, Cambridge, MA 02138, USA
gmelnick@cfa.harvard.edu

Abstract The opportunities available to infrared, submillimeter, and millimeter wave astronomers are on the threshold of a revolution. Within the next 20 years, the number of new facilities coupled with their size, superb locations, and increased sensitivities will allow for markedly greater capabilities. This contribution will summarize the advances expected from those new telescopes operating between 30 μm and 1 cm.

1. Introduction

The infrared (~ 1 – 200 μm), submillimeter (~ 200 μm – 1 mm), and millimeter (1 – 10 mm) wavelength ranges are among the least explored windows into the cosmos. This is due to a combination of atmospheric interference and still-developing technology. Except for a set of relatively narrow bands, atmospheric H_2O, O_2, O_3, and CO_2 block a substantial fraction of the infrared and submillimeter and part of millimeter radiation reaching the earth. Overcoming this obstacle requires high dry sites for the millimeter and submillimeter and airborne or space-based facilities for the mid- and far-infrared. In addition, to achieve sensitivities limited only by the natural cosmic background, longward of a few microns and for spectral resolutions, $\lambda/\Delta\lambda$, less than a few $\times$ 10^4 it is necessary that telescopes be cooled to < 10 K. This can only be accomplished in the vacuum of space. Because the best high dry ground-based sites are often located in difficult-to-reach places, such as Antarctica and the Atacama desert, and because building telescopes with apertures $>$ 1-meter in diameter for use in aircraft and in space is challenging, the sensitivity and spatial resolution of the best infrared, submillimeter, and millimeter wavelength facilities are less than those of the premier facilities at neighboring optical and radio wavelengths.

Technologically, detectors for the infrared and the submillimeter have also lagged behind those at shorter and longer wavelengths. Large-format ($> 10^6$ pixels) detector arrays are only now becoming available in the near infrared while near-quantum-noise-limited heterodyne receivers are still only available

E. Corbelli et al. (eds.), The Initial Mass Function 50 Years Later, 533–538.

Table 1. Ground-Based, Airborne, & Space-Based Observatories: $50 \leq \nu \leq 10{,}000$ GHz (6 mm – 30 μm)

1980-1990	1990-2000	2000-2030	
FCRAO	FCRAO	FCRAO	Cornell/CIT
Yerbes	Yerbes	Yerbes	SKA
NRAO (12-m)	NRAO (12-m)	NRAO (12-m)	*SWAS*
KOSMA	KOSMA	KOSMA	*WMAP*
JCMT	JCMT	JCMT	*Odin*
SEST	SEST	CSO	*Spitzer*
CSO	CSO	IRAM (30-m)	*SOFIA*
IRAM (30-m)	IRAM (30-m)	Plateau de Burre	*Herschel*
Plateau de Burre	Plateau de Burre	Onsala	*SAFIR*
OVRO	OVRO	Nobeyama MM Array	*SPICA*
Onsala	Onsala	SMTO/HHT	*SPIRIT*
Nobeyama MM Array	Nobeyama MM Array	NANTEN	*SPECS*
IRAS	BIMA	Mt. Fuji	
Lear Jet	SMTO/HHT	NMA	
KAO	NANTEN	Delinga	
	Mt. Fuji	Taeduk	
	NMA	SMA	
	Astro	GBT	
	Delinga	CARMA	
NOTE: *Italics* denote airborne or space mission	*COBE*	APEX	
	KAO	LMT	
	ISO	S. Pole Telescope	
	SWAS	ALMA	

at wavelengths longward of ~ 200 μm. Between ~ 40 and 200 μm, neither large-format detector arrays nor heterodyne receivers operating near the quantum limit are currently available.

These limitations notwithstanding, many of the most important scientific questions of today – ranging from the early Universe to star and planet formation – require high sensitivity, high spatial resolution infrared, submillimeter, and millimeter wavelength capabilities. For this reason, the U.S. National Research Council in its Decadal Survey Report for both the 1990-2000 and 2000-2010 periods highlighted the importance of developing a number of new infrared-, submillimeter-, and millimeter-wave facilities. This paper will summarize briefly the new facilities that are likely to become operational in the next 10 to 20 years.

2. Motivation for New Infrared, Submillimeter, and Millimeter Wave Observatories

The wavelength range between 1 μm and 1 cm has emerged as the principal window for the study of a number of forefront astronomical problems. Among the problems of interest to star and planet formation are: locating embedded protostars (infrared and submillimeter photometry); the determination of a spectral excess indicative of the presence of an envelope or disk (infrared spectrophotometry); outflows (submillimeter and millimeter spectroscopy); protoplanetary disk properties (millimeter, submillimeter, and infrared spectroscopy); and, debris disk structure and inferred planets (infrared

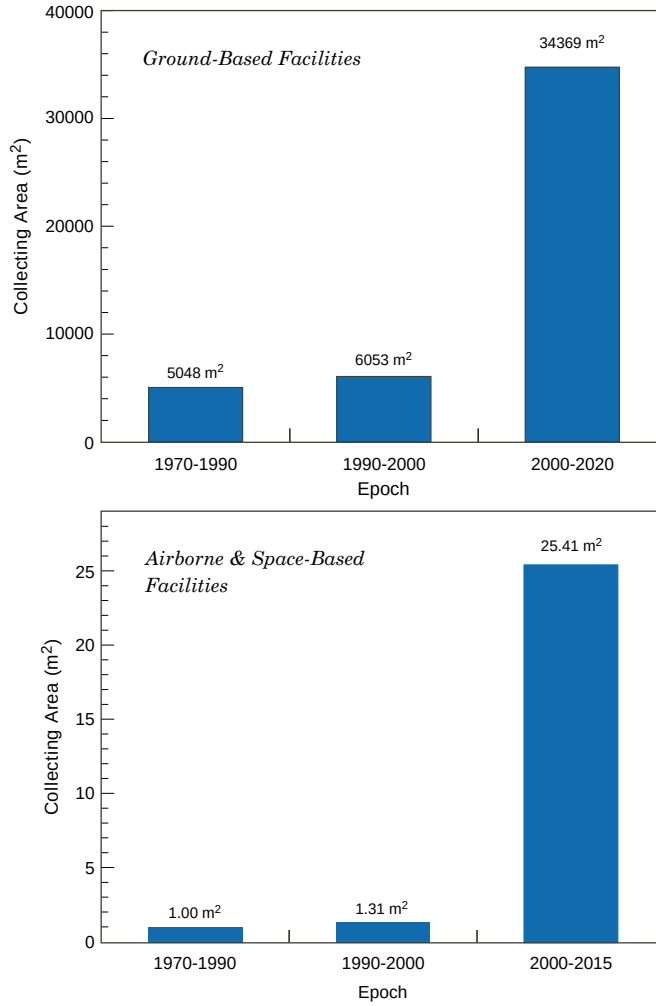

Figure 1. *Top panel*: Total collecting area of ground-based telescopes operating at frequencies between 100 and 1500 GHz (see Table 1). For the purpose of scale, the 2000-2030 epoch excludes the contribution from the Square Kilometer Array, with its estimated 500,000 m^2 of collecting area. *Bottom panel*: Total collecting area of airborne and space-based telescopes operating at frequencies between 300 and 10,000 GHz (1 mm and 30 μm; see Table 1).

and submillimeter high spatial resolution photometry). In addition to star and planet formation the IR, SMM, and MM wavelength range is becoming the premier spectral region for the study of highly-redshifted early Universe objects.

While it is now possible to reach the natural background over much of this wavelength range due to small aperture sizes and, until recently, the absence of

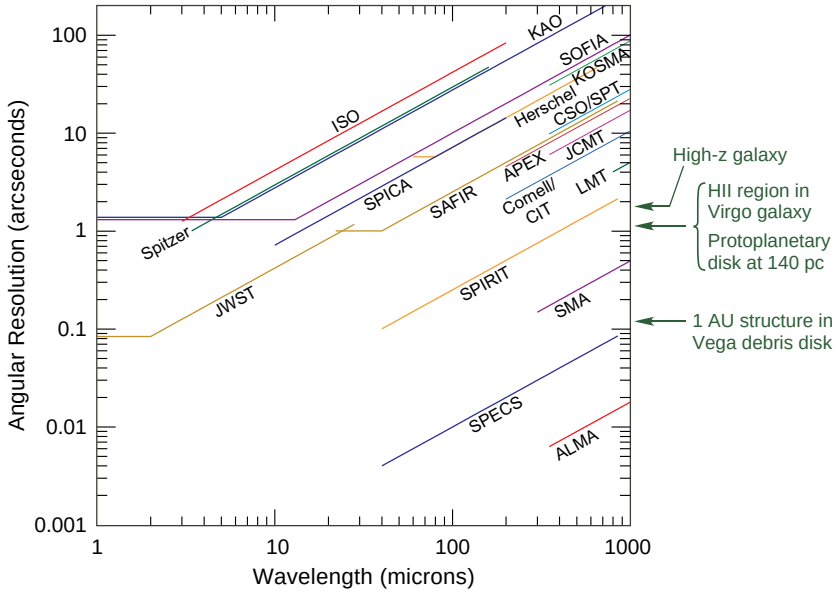

Figure 2. Angular resolution for existing and planned telescopes operating at infrared and submillimeter wavelengths.

large telescope arrays, the spatial resolution available at infrared and submillimeter wavelengths has lagged significantly behind that at optical and radio wavelengths. For the study of star and planet formation, this has meant that length scales of interest, such as 1 AU at the distance of the nearest star forming complex (~ 140 pc $\Leftrightarrow \sim 7$ milliarcseconds) are inaccessible by almost two orders of magnitude. However, even when the aperture size remains insufficient to spatially resolve structures of interest, a large collecting area is an asset. For example, much can be learned about the physical conditions in protoplanetary disks on spatially unresolved scales through the study of molecular line emission provided enough photons can be gathered.

For these reasons, major national and international efforts are in development or planned for a new generation of ground-based, airborne, and space-based telescopes. It is not possible to provide an in-depth discussion of each project here. Instead, I provide an overview of these advances as measured by the dramatic growth in overall collecting area, angular resolution, and sensitivity these facilities will provide.

3. The Roadmap for the Next 30 Years

Advances in infrared, submillimeter, and millimeter capabilities are proceeding along three main fronts. First, by continuing to develop and field larger

format, more sensitive detector arrays it is possible to greatly enhance the science output of even today's modest-sized telescopes. This approach allows the 85-cm diameter Spitzer Space Telescope, with its more than a quarter million detectors, to be orders of magnitude more capable than its comparably-sized predecessor, the 60-cm diameter Infrared Astronomical Satellite (IRAS) with its 64 detectors.

Second, new technologies are enabling larger single aperture telescopes to be developed. On the ground within the next few years, the Large Millimeter Array (LMA; 50 m), the Atacama Pathfinder Experiment (APEX; 12 m), and the South Pole Telescope (10 m) will extend both the size (in the case of the LMA) and the number of excellent sites from which millimeter and submillimeter telescopes will operate. The availability of a Boeing 747-SP aircraft is allowing the U.S. and Germany to replace the 0.91-cm diameter infrared/submillimeter telescope aboard the Kuiper Airborne Observatory (KAO) with a 2.5-m diameter telescope aboard the Stratospheric Observatory for Infrared Astronomy (SOFIA). SOFIA will conduct its first science flights in 2006. In space, passive cooling techniques, such as those demonstrated on the Spitzer Space Telescope, coupled with advances in mechanical coolers are freeing future space infrared/submillimeter telescopes from the size limitations (i.e., 60-cm) imposed by the types of full-telescope cryogen enclosures used on IRAS and ESA's Infrared Space Observatory (ISO). The ESA/NASA Herschel 3.5-m diameter infrared/submillimeter telescope, to be launched in 2007, will use passive cooling techniques to achieve a telescope temperature of < 80 K. Within the next decade, it is expected that the Japanese Space Infrared Telescope for Cosmology and Astrophysics (SPICA) will fly a comparably-sized telescope with optics cooled to ~ 4 K, allowing it to achieve even greater sensitivity than Herschel for all but the highest spectral resolutions. Currently, NASA is studying a follow-on mission to both Herschel and SPICA, the Single Aperture Far-Infrared (SAFIR) Telescope, a 10-m diameter telescope with optics cooled to ~ 4 K. On the ground, Cornell University and Caltech are studying a 25-m submillimeter telescope located at an exceptionally high, dry site in the Atacama desert that will allow it to operate at wavelengths as short as 200 μm.

Third, even the largest practical ground-based and space-borne far-infrared and submillimeter single aperture telescopes will be too small to spatially resolve sources within early-Universe objects and AU-scale structures within many of the closest debris disks. To accomplish this, interferometers are necessary. Building upon the success of several operating millimeter arrays, two arrays that cover the available submillimeter windows have been and will be built this decade – the Submillimeter Array (SMA; 8×6-m), which recently began operating on Mauna Kea, and the Atacama Large Millimeter Array (ALMA; 64×12-m), which is due to begin construction within the next few

years. Within the next decade, an international consortium plans to build the Square Kilometer Array (various configurations possible), with a total collecting area of $\sim$500,000 m^2 and operating at frequencies between 0.15 and 20 GHz.

Longer-term, i.e., beyond 2025, two projects are under study in the U.S to extend interferometric techniques to space – the Space Infrared Interferometric Telescope (SPIRIT), consisting of two 1-3 m cooled telescopes on a 30-50 m rigid boom and the Submillimeter Probe of the Evolution of Cosmic Structure (SPECS), consisting of three 3-10 m cooled telescopes connected with tethers and with an $\sim$ 1 km baseline.

The effect of these developments on the total collecting area, spatial resolution, and sensitivity available to astronomers are summarized in Figures 1-3. When these infrared, submillimeter and millimeter wave telescope projects are realized, this important but under-explored spectral range will have completed a giant stride toward maturity.

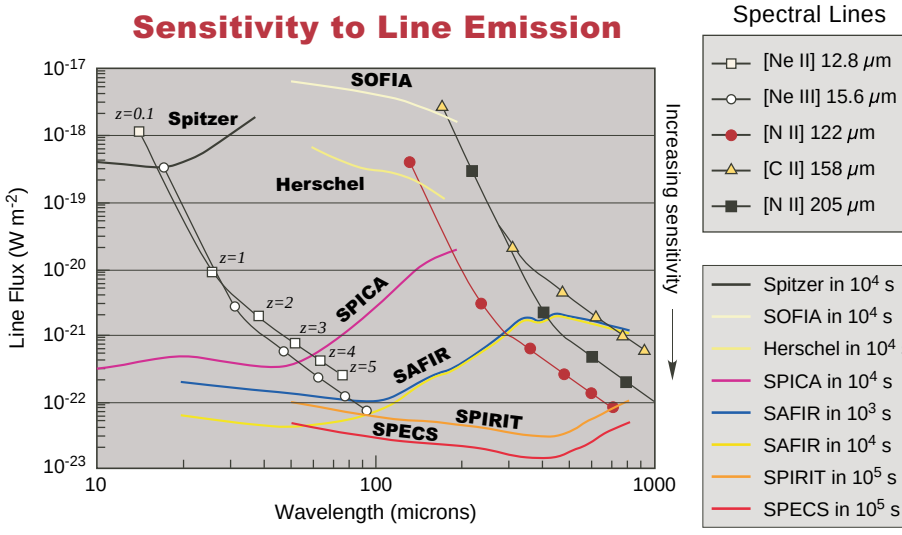

Figure 3. Expected line sensitivity for current and future airborne and space-based telescopes.

Author Index

Index of Astronomical Objects

Astrophysics and Space Science Library

Volume 324: ***Kristian Birkeland – The First Space Scientist,*** by A. Egeland, W.J. Burke. Hardbound ISBN 1-4020-3293-5, April 2005

Volume 323: ***Recollections of Tucson Operations,*** by M.A. Gordon. Hardbound ISBN 1-4020-3235-8, December 2004

Volume 322: ***Light Pollution Handbook,*** by K. Narisada, D. Schreuder Hardbound ISBN 1-4020-2665-X, November 2004

Volume 321: ***Nonequilibrium Phenomena in Plasmas***, edited by A.S. Shrama, P.K. Kaw. Hardbound ISBN 1-4020-3108-4, December 2004

Volume 320: ***Solar Magnetic Phenomena,*** edited by A. Hanslmeier, A. Veronig, M. Messerotti. Hardbound ISBN 1-4020-2961-6, December 2004

Volume 319: ***Penetrating Bars through Masks of Cosmic Dust***, edited by D.L. Block, I. Puerari, K.C. Freeman, R. Groess, E.K. Block. Hardbound ISBN 1-4020-2861-X, December 2004

Volume 318: ***Transfer of Polarized light in Planetary Atmospheres***, by J.W. Hovenier, J.W. Domke, C. van der Mee. Hardbound ISBN 1-4020-2855-5. Softcover ISBN 1-4020-2889-X, November 2004

Volume 317: ***The Sun and the Heliosphere as an Integrated System,*** edited by G. Poletto, S.T. Suess. Hardbound ISBN 1-4020-2830-X, November 2004

Volume 316: *Civic Astronomy - Albany's Dudley Observatory, 1852-2002,* by G. Wise
Hardbound ISBN 1-4020-2677-3, October 2004

Volume 315: ***How does the Galaxy Work*** *- A Galactic Tertulia with Don Cox and Ron Reynolds,* edited by E. J. Alfaro, E. Pérez, J. Franco
Hardbound ISBN 1-4020-2619-6, September 2004

Volume 314: ***Solar and Space Weather Radiophysics- Current Status and Future Developments,*** edited by D.E. Gary and C.U. Keller
Hardbound ISBN 1-4020-2813-X, August 2004

Volume 313: ***Adventures in Order and Chaos***, by G. Contopoulos. Hardbound ISBN 1-4020-3039-8, January 2005

Volume 312: ***High-Velocity Clouds,*** edited by H. van Woerden, U. Schwarz, B. Wakker
Hardbound ISBN 1-4020-2813-X, September 2004

Volume 311: ***The New ROSETTA Targets- Observations, Simulations and Instrument Performances***, edited by L. Colangeli, E. Mazzotta Epifani, P. Palumbo
Hardbound ISBN 1-4020-2572-6, September 2004

Volume 310: ***Organizations and Strategies in Astronomy 5,*** edited by A. Heck
Hardbound ISBN 1-4020-2570-X, September 2004

Volume 309: ***Soft X-ray Emission from Clusters of Galaxies and Related Phenomena***, edited by R. Lieu and J. Mittaz
Hardbound ISBN 1-4020-2563-7, September 2004

Volume 308: ***Supermassive Black Holes in the Distant Universe,*** edited by A.J. Barger
Hardbound ISBN 1-4020-2470-3, August 2004

Volume 307: ***Polarization in Spectral Lines***, by E. Landi Degl'Innocenti and M. Landolfi
Hardbound ISBN 1-4020-2414-2, August 2004

Volume 306: ***Polytropes – Applications in Astrophysics and Related Fields,*** by G.P. Horedt
Hardbound ISBN 1-4020-2350-2, September 2004

Volume 305: ***Astrobiology: Future Perspectives,*** edited by P. Ehrenfreund, W.M. Irvine, T. Owen, L. Becker, J. Blank, J.R. Brucato, L. Colangeli, S. Derenne, A. Dutrey, D. Despois, A. Lazcano, F. Robert
Hardbound ISBN 1-4020-2304-9, July 2004
Paperback ISBN 1-4020-2587-4, July 2004

Volume 304: ***Cosmic Gammy-ray Sources,*** edited by K.S. Cheng and G.E. Romero
Hardbound ISBN 1-4020-2255-7, September 2004

Volume 303: ***Cosmic rays in the Earth's Atmosphere and Underground***, by L.I, Dorman
Hardbound ISBN 1-4020-2071-6, August 2004

Volume 302:*Stellar Collapse,* edited by Chris L. Fryer
Hardbound, ISBN 1-4020-1992-0, April 2004

Volume 301: *Multiwavelength Cosmology*, edited by Manolis Plionis
Hardbound, ISBN 1-4020-1971-8, March 2004

Volume 300:*Scientific Detectors for Astronomy,* edited by Paola Amico, James W. Beletic, Jenna E. Beletic
Hardbound, ISBN 1-4020-1788-X, February 2004

Volume 299: *Open Issues in Local Star Fomation,* edited by Jacques Lépine, Jane Gregorio-Hetem
Hardbound, ISBN 1-4020-1755-3, December 2003

Volume 298: *Stellar Astrophysics - A Tribute to Helmut A. Abt,* edited by K.S. Cheng, Kam Ching Leung, T.P. Li
Hardbound, ISBN 1-4020-1683-2, November 2003

Volume 297: *Radiation Hazard in Space,* by Leonty I. Miroshnichenko
Hardbound, ISBN 1-4020-1538-0, September 2003

Volume 296: *Organizations and Strategies in Astronomy, volume 4,* edited by André Heck
Hardbound, ISBN 1-4020-1526-7, October 2003

Volume 295: *Integrable Problems of Celestial Mechanics in Spaces of Constant Curvature*, by T.G. Vozmischeva
Hardbound, ISBN 1-4020-1521-6, October 2003

Volume 294: *An Introduction to Plasma Astrophysics and Magnetohydrodynamics,* by Marcel Goossens
Hardbound, ISBN 1-4020-1429-5, August 2003
Paperback, ISBN 1-4020-1433-3, August 2003

Volume 293: *Physics of the Solar System,* by Bruno Bertotti, Paolo Farinella, David Vokrouhlický
Hardbound, ISBN 1-4020-1428-7, August 2003
Paperback, ISBN 1-4020-1509-7, August 2003

Volume 292: *Whatever Shines Should Be Observed,* by Susan M.P. McKenna-Lawlor
Hardbound, ISBN 1-4020-1424-4, September 2003

Volume 291: ***Dynamical Systems and Cosmology***, by Alan Coley
Hardbound, ISBN 1-4020-1403-1, November 2003

Volume 290: ***Astronomy Communication***, edited by André Heck, Claus Madsen
Hardbound, ISBN 1-4020-1345-0, July 2003

Volume 287/8/9: ***The Future of Small Telescopes in the New Millennium***, edited by Terry D. Oswalt
Hardbound Set only of 3 volumes, ISBN 1-4020-0951-8, July 2003

Volume 286: ***Searching the Heavens and the Earth: The History of Jesuit Observatories***, by Agustín Udías
Hardbound, ISBN 1-4020-1189-X, October 2003

Volume 285: ***Information Handling in Astronomy - Historical Vistas***, edited by André Heck
Hardbound, ISBN 1-4020-1178-4, March 2003

Volume 284: ***Light Pollution: The Global View***, edited by Hugo E. Schwarz
Hardbound, ISBN 1-4020-1174-1, April 2003

Volume 283: ***Mass-Losing Pulsating Stars and Their Circumstellar Matter***, edited by Y. Nakada, M. Honma, M. Seki
Hardbound, ISBN 1-4020-1162-8, March 2003

Volume 282: ***Radio Recombination Lines***, by M.A. Gordon, R.L. Sorochenko
Hardbound, ISBN 1-4020-1016-8, November 2002

Volume 281: ***The IGM/Galaxy Connection***, edited by Jessica L. Rosenberg, Mary E. Putman
Hardbound, ISBN 1-4020-1289-6, April 2003

Volume 280: ***Organizations and Strategies in Astronomy III***, edited by André Heck
Hardbound, ISBN 1-4020-0812-0, September 2002

Volume 279: ***Plasma Astrophysics , Second Edition***, by Arnold O. Benz
Hardbound, ISBN 1-4020-0695-0, July 2002

Volume 278: ***Exploring the Secrets of the Aurora***, by Syun-Ichi Akasofu
Hardbound, ISBN 1-4020-0685-3, August 2002

Volume 277: ***The Sun and Space Weather***, by Arnold Hanslmeier
Hardbound, ISBN 1-4020-0684-5, July 2002

Volume 276: ***Modern Theoretical and Observational Cosmology***, edited by Manolis Plionis, Spiros Cotsakis
Hardbound, ISBN 1-4020-0808-2, September 2002

Volume 275: ***History of Oriental Astronomy***, edited by S.M. Razaullah Ansari
Hardbound, ISBN 1-4020-0657-8, December 2002

Volume 274: ***New Quests in Stellar Astrophysics: The Link Between Stars and Cosmology***, edited by Miguel Chávez, Alessandro Bressan, Alberto Buzzoni,Divakara Mayya
Hardbound, ISBN 1-4020-0644-6, June 2002

Volume 273: ***Lunar Gravimetry***, by Rune Floberghagen
Hardbound, ISBN 1-4020-0544-X, May 2002

Volume 272:***Merging Processes in Galaxy Clusters***, edited by L. Feretti, I.M. Gioia, G. Giovannini
Hardbound, ISBN 1-4020-0531-8, May 2002

Volume 271: ***Astronomy-inspired Atomic and Molecular Physics***, by A.R.P. Rau
Hardbound, ISBN 1-4020-0467-2, March 2002

Volume 270: ***Dayside and Polar Cap Aurora***, by Per Even Sandholt, Herbert C. Carlson, Alv Egeland
Hardbound, ISBN 1-4020-0447-8, July 2002

Volume 269: ***Mechanics of Turbulence of Multicomponent Gases***, by Mikhail Ya. Marov, Aleksander V. Kolesnichenko
Hardbound, ISBN 1-4020-0103-7, December 2001

Volume 268: ***Multielement System Design in Astronomy and Radio Science***, by Lazarus E. Kopilovich, Leonid G. Sodin
Hardbound, ISBN 1-4020-0069-3, November 2001

Volume 267: ***The Nature of Unidentified Galactic High-Energy Gamma-Ray Sources,*** edited by Alberto Carramiñana, Olaf Reimer, David J. Thompson
Hardbound, ISBN 1-4020-0010-3, October 2001

Volume 266: *Organizations and Strategies in Astronomy II*, edited by André Heck
Hardbound, ISBN 0-7923-7172-0, October 2001

Volume 265: *Post-AGB Objects as a Phase of Stellar Evolution*, edited by R. Szczerba, S.K. Górny
Hardbound, ISBN 0-7923-7145-3, July 2001

Volume 264: *The Influence of Binaries on Stellar Population Studies*, edited by Dany Vanbeveren
Hardbound, ISBN 0-7923-7104-6, July 2001

Volume 262: *Whistler Phenomena - Short Impulse Propagation*, by Csaba Ferencz, Orsolya E. Ferencz, Dániel Hamar, János Lichtenberger
Hardbound, ISBN 0-7923-6995-5, June 2001

Volume 261: *Collisional Processes in the Solar System*, edited by Mikhail Ya. Marov, Hans Rickman
Hardbound, ISBN 0-7923-6946-7, May 2001

Volume 260: *Solar Cosmic Rays*, by Leonty I. Miroshnichenko
Hardbound, ISBN 0-7923-6928-9, May 2001

Volume 259: *The Dynamic Sun*, edited by Arnold Hanslmeier, Mauro Messerotti, Astrid Veronig
Hardbound, ISBN 0-7923-6915-7, May 2001

Volume 258: *Electrohydrodynamics in Dusty and Dirty Plasmas- Gravito-Electrodynamics and EHD*, by Hiroshi Kikuchi
Hardbound, ISBN 0-7923-6822-3, June 2001

Volume 257: *Stellar Pulsation - Nonlinear Studies*, edited by Mine Takeuti, Dimitar D. Sasselov
Hardbound, ISBN 0-7923-6818-5, March 2001

Volume 256: *Organizations and Strategies in Astronomy*, edited by André Heck
Hardbound, ISBN 0-7923-6671-9, November 2000

Volume 255: *The Evolution of the Milky Way- Stars versus Clusters*, edited by Francesca Matteucci, Franco Giovannelli
Hardbound, ISBN 0-7923-6679-4, January 2001

Volume 254: *Stellar Astrophysics*, edited by K.S. Cheng, Hoi Fung Chau, Kwing Lam Chan, Kam Ching Leung
Hardbound, ISBN 0-7923-6659-X, November 2000

Volume 253: *The Chemical Evolution of the Galaxy*, by Francesca Matteucci
Paperback, ISBN 1-4020-1652-2, October 2003
Hardbound, ISBN 0-7923-6552-6, June 2001

Volume 252: *Optical Detectors for Astronomy II*, edited by Paola Amico, James W. Beletic
Hardbound, ISBN 0-7923-6536-4, December 2000

Volume 251: *Cosmic Plasma Physics*, by Boris V. Somov
Hardbound, ISBN 0-7923-6512-7, September 2000

Volume 250: *Information Handling in Astronomy*, edited by André Heck
Hardbound, ISBN 0-7923-6494-5, October 2000

Volume 249: *The Neutral Upper Atmosphere*, by S.N. Ghosh
Hardbound, ISBN 0-7923-6434-1, July 2002

Volume 247: *Large Scale Structure Formation*, edited by Reza Mansouri, Robert Brandenberger
Hardbound, ISBN 0-7923-6411-2, August 2000

Volume 246: *The Legacy of J.C. Kapteyn*, edited by Piet C. van der Kruit, Klaas van Berkel
Paperback, ISBN 1-4020-0374-9, November 2001
Hardbound, ISBN 0-7923-6393-0, August 2000

Volume 245: *Waves in Dusty Space Plasmas,* by Frank Verheest
Paperback, ISBN 1-4020-0373-0, November 2001
Hardbound, ISBN 0-7923-6232-2, April 2000

Volume 244: *The Universe*, edited by Naresh Dadhich, Ajit Kembhavi
Hardbound, ISBN 0-7923-6210-1, August 2000

Volume 243: *Solar Polarization*, edited by K.N. Nagendra, Jan Olof Stenflo
Hardbound, ISBN 0-7923-5814-7, July 1999

Volume 242: *Cosmic Perspectives in Space Physics*, by Sukumar Biswas
Hardbound, ISBN 0-7923-5813-9, June 2000

Volume 241: ***Millimeter-Wave Astronomy: Molecular Chemistry & Physics in Space,*** edited by W.F. Wall, Alberto Carramiñana, Luis Carrasco, P.F. Goldsmith
Hardbound, ISBN 0-7923-5581-4, May 1999

Volume 240: ***Numerical Astrophysics,*** edited by Shoken M. Miyama, Kohji Tomisaka,Tomoyuki Hanawa
Hardbound, ISBN 0-7923-5566-0, March 1999

Volume 239: ***Motions in the Solar Atmosphere,*** edited by Arnold Hanslmeier, Mauro Messerotti
Hardbound, ISBN 0-7923-5507-5, February 1999

Volume 238: ***Substorms-4,*** edited by S. Kokubun, Y. Kamide
Hardbound, ISBN 0-7923-5465-6, March 1999

For further information about this book series we refer you to the following web site: www.springeronline.com

To contact the Publishing Editor for new book proposals:
Dr. Harry (J.J.) Blom: harry.blom@springer-sbm.com